

Electric Power Engineering Handbook
Second Edition

Power Systems



Edited by
LEONARD L. GRIGSBY

Electric Power Engineering Handbook

Second Edition

Edited by
Leonard L. Grigsby

Electric Power Generation, Transmission, and Distribution
Edited by Leonard L. Grigsby

Electric Power Transformer Engineering, Second Edition
Edited by James H. Harlow

Electric Power Substations Engineering, Second Edition
Edited by John D. McDonald

Power Systems
Edited by Leonard L. Grigsby

Power System Stability and Control
Edited by Leonard L. Grigsby

The Electrical Engineering Handbook Series

Series Editor

Richard C. Dorf

University of California, Davis

Titles Included in the Series

The Handbook of Ad Hoc Wireless Networks, Mohammad Ilyas

The Biomedical Engineering Handbook, Third Edition, Joseph D. Bronzino

The Circuits and Filters Handbook, Second Edition, Wai-Kai Chen

The Communications Handbook, Second Edition, Jerry Gibson

The Computer Engineering Handbook, Second Edition, Vojin G. Oklobdzija

The Control Handbook, William S. Levine

The CRC Handbook of Engineering Tables, Richard C. Dorf

The Digital Avionics Handbook, Second Edition Cary R. Spitzer

The Digital Signal Processing Handbook, Vijay K. Madisetti and Douglas Williams

The Electrical Engineering Handbook, Third Edition, Richard C. Dorf

The Electric Power Engineering Handbook, Second Edition, Leonard L. Grigsby

The Electronics Handbook, Second Edition, Jerry C. Whitaker

The Engineering Handbook, Third Edition, Richard C. Dorf

The Handbook of Formulas and Tables for Signal Processing, Alexander D. Pouliarikas

The Handbook of Nanoscience, Engineering, and Technology, Second Edition,

William A. Goddard, III, Donald W. Brenner, Sergey E. Lyshevski, and Gerald J. Iafrate

The Handbook of Optical Communication Networks, Mohammad Ilyas and

Hussein T. Mouftah

The Industrial Electronics Handbook, J. David Irwin

The Measurement, Instrumentation, and Sensors Handbook, John G. Webster

The Mechanical Systems Design Handbook, Osita D.I. Nwokah and Yidirim Hurmuzlu

The Mechatronics Handbook, Second Edition, Robert H. Bishop

The Mobile Communications Handbook, Second Edition, Jerry D. Gibson

The Ocean Engineering Handbook, Ferial El-Hawary

The RF and Microwave Handbook, Second Edition, Mike Golio

The Technology Management Handbook, Richard C. Dorf

The Transforms and Applications Handbook, Second Edition, Alexander D. Pouliarikas

The VLSI Handbook, Second Edition, Wai-Kai Chen

Electric Power Engineering Handbook
Second Edition

POWER SYSTEMS

Edited by
Leonard L. Grigsby



CRC Press is an imprint of the
Taylor & Francis Group, an Informa business

CRC Press
Taylor & Francis Group
6000 Broken Sound Parkway NW, Suite 300
Boca Raton, FL 33487-2742

© 2007 by Taylor & Francis Group, LLC
CRC Press is an imprint of Taylor & Francis Group, an Informa business

No claim to original U.S. Government works
Printed in the United States of America on acid-free paper
10 9 8 7 6 5 4 3 2 1

International Standard Book Number-10: 0-8493-9288-8 (Hardcover)
International Standard Book Number-13: 978-0-8493-9288-7 (Hardcover)

This book contains information obtained from authentic and highly regarded sources. Reprinted material is quoted with permission, and sources are indicated. A wide variety of references are listed. Reasonable efforts have been made to publish reliable data and information, but the author and the publisher cannot assume responsibility for the validity of all materials or for the consequences of their use.

No part of this book may be reprinted, reproduced, transmitted, or utilized in any form by any electronic, mechanical, or other means, now known or hereafter invented, including photocopying, microfilming, and recording, or in any information storage or retrieval system, without written permission from the publishers.

For permission to photocopy or use material electronically from this work, please access www.copyright.com (<http://www.copyright.com/>) or contact the Copyright Clearance Center, Inc. (CCC) 222 Rosewood Drive, Danvers, MA 01923, 978-750-8400. CCC is a not-for-profit organization that provides licenses and registration for a variety of users. For organizations that have been granted a photocopy license by the CCC, a separate system of payment has been arranged.

Trademark Notice: Product or corporate names may be trademarks or registered trademarks, and are used only for identification and explanation without intent to infringe.

Library of Congress Cataloging-in-Publication Data

Power systems / editor, Leonard Lee Grigsby.
p. cm.
Includes bibliographical references and index.
ISBN-13: 978-0-8493-9288-7 (alk. paper)
ISBN-10: 0-8493-9288-8 (alk. paper)
1. Electric power systems. I. Grigsby, Leonard L.

TK1001.P65 2007
621.31--dc22

2007005730

Visit the Taylor & Francis Web site at
<http://www.taylorandfrancis.com>

and the CRC Press Web site at
<http://www.crcpress.com>

Table of Contents

Preface

Editor

Contributors

I Power System Analysis and Simulation

1 The Per-Unit System

Charles A. Gross

2 Symmetrical Components for Power System Analysis

Tim A. Haskew

3 Power Flow Analysis

Leonard L. Grigsby and Andrew P. Hanson

4 Fault Analysis in Power Systems

Charles A. Gross

5 Computational Methods for Electric Power Systems

Mariesa L. Crow

II Power System Transients

6 Characteristics of Lightning Strokes

Francisco de la Rosa

7 Overvoltages Caused by Direct Lightning Strokes

Pritindra Chowdhuri

8 Overvoltages Caused by Indirect Lightning Strokes

Pritindra Chowdhuri

9 Switching Surges

Stephen R. Lambert

10 Very Fast Transients

Juan A. Martinez-Velasco

11 Transient-Voltage Response of Coils and Windings

Robert C. Degenef

12 Transmission System Transients—Grounding

William A. Chisholm

- 13 Surge Arresters**
Thomas E. McDermott
- 14 Insulation Coordination**
Stephen R. Lambert

III Power System Planning (Reliability)

- 15 Planning**
Gerald B. Sheblé
- 16 Short-Term Load and Price Forecasting with Artificial Neural Networks**
Alireza Khotanzad
- 17 Transmission Plan Evaluation—Assessment of System Reliability**
N. Dag Reppen and James W. Feltes
- 18 Power System Planning**
Hyde M. Merrill
- 19 Power System Reliability**
Richard E. Brown
- 20 Probabilistic Methods for Planning and Operational Analysis**
Gerald T. Heydt and Peter W. Sauer

IV Power Electronics

- 21 Power Semiconductor Devices**
Kaushik Rajashekara
- 22 Uncontrolled and Controlled Rectifiers**
Mahesh M. Swamy
- 23 Inverters**
Michael Giesselmann
- 24 Active Filters for Power Conditioning**
Hirofumi Akagi
- 25 FACTS Controllers**
Luis Morán, Juan Dixon, M. José Espinoza, and José Rodríguez

Preface

The generation, delivery, and utilization of electric power and energy remain one of the most challenging and exciting fields of electrical engineering. The astounding technological developments of our age are highly dependent upon a safe, reliable, and economic supply of electric power. The objective of *Electric Power Engineering Handbook*, 2nd Edition is to provide a contemporary overview of this far-reaching field as well as to be a useful guide and educational resource for its study. It is intended to define electric power engineering by bringing together the core of knowledge from all of the many topics encompassed by the field. The chapters are written primarily for the electric power engineering professional who is seeking factual information, and secondarily for the professional from other engineering disciplines who wants an overview of the entire field or specific information on one aspect of it.

The handbook is published in five volumes. Each is organized into topical sections and chapters in an attempt to provide comprehensive coverage of the generation, transformation, transmission, distribution, and utilization of electric power and energy as well as the modeling, analysis, planning, design, monitoring, and control of electric power systems. The individual chapters are different from most technical publications. They are not journal-type chapters nor are they textbook in nature. They are intended to be tutorials or overviews providing ready access to needed information while at the same time providing sufficient references to more in-depth coverage of the topic. This work is a member of the Electrical Engineering Handbook Series published by CRC Press. Since its inception in 1993, this series has been dedicated to the concept that when readers refer to a handbook on a particular topic they should be able to find what they need to know about the subject most of the time. This has indeed been the goal of this handbook.

This volume of the handbook is devoted to the subjects of power system analysis and simulation, power system transients, power system planning, and power electronics. If your particular topic of interest is not included in this list, please refer to the list of companion volumes seen at the beginning of this book.

In reading the individual chapters of this handbook, I have been most favorably impressed by how well the authors have accomplished the goals that were set. Their contributions are, of course, most key to the success of the work. I gratefully acknowledge their outstanding efforts. Likewise, the expertise and dedication of the editorial board and section editors have been critical in making this handbook possible. To all of them I express my profound thanks. I also wish to thank the personnel at Taylor & Francis who have been involved in the production of this book, with a special word of thanks to Nora Konopka, Allison Shatkin, and Jessica Vakili. Their patience and perseverance have made this task most pleasant.

Leo Grigsby
Editor-in-Chief

Editor

Leonard L. (“Leo”) Grigsby received his BS and MS in electrical engineering from Texas Tech University and his PhD from Oklahoma State University. He has taught electrical engineering at Texas Tech, Oklahoma State University, and Virginia Polytechnic Institute and University. He has been at Auburn University since 1984 first as the Georgia power distinguished professor, later as the Alabama power distinguished professor, and currently as professor emeritus of electrical engineering. He also spent nine months during 1990 at the University of Tokyo as the Tokyo Electric Power Company endowed chair of electrical engineering. His teaching interests are in network analysis, control systems, and power engineering.

During his teaching career, Professor Grigsby has received 13 awards for teaching excellence. These include his selection for the university-wide William E. Wine Award for Teaching Excellence at Virginia Polytechnic Institute and University in 1980, his selection for the ASEE AT&T Award for Teaching Excellence in 1986, the 1988 Edison Electric Institute Power Engineering Educator Award, the 1990–1991 Distinguished Graduate Lectureship at Auburn University, the 1995 IEEE Region 3 Joseph M. Beidenbach Outstanding Engineering Educator Award, the 1996 Birdsong Superior Teaching Award at Auburn University, and the IEEE Power Engineering Society Outstanding Power Engineering Educator Award in 2003.

Professor Grigsby is a fellow of the Institute of Electrical and Electronics Engineers (IEEE). During 1998–1999 he was a member of the board of directors of IEEE as director of Division VII for power and energy. He has served the Institute in 30 different offices at the chapter, section, regional, and international levels. For this service, he has received seven distinguished service awards, the IEEE Centennial Medal in 1984, the Power Engineering Society Meritorious Service Award in 1994, and the IEEE Millennium Medal in 2000.

During his academic career, Professor Grigsby has conducted research in a variety of projects related to the application of network and control theory to modeling, simulation, optimization, and control of electric power systems. He has been the major advisor for 35 MS and 21 PhD graduates. With his students and colleagues, he has published over 120 technical papers and a textbook on introductory network theory. He is currently the series editor for the Electrical Engineering Handbook Series published by CRC Press. In 1993 he was inducted into the Electrical Engineering Academy at Texas Tech University for distinguished contributions to electrical engineering.

Contributors

Hirofumi Akagi

Tokyo Institute of Technology
Tokyo, Japan

Richard E. Brown

InfraSource Technology
Raleigh, North Carolina

William A. Chisholm

Kinetrics/UQAC
Toronto, Ontario, Canada

Pritindra Chowdhuri

Tennessee Technological University
Cookeville, Tennessee

Mariesa L. Crow

University of Missouri-Rolla
Rolla, Missouri

Robert C. Degeneff

Rensselaer Polytechnic Institute
Troy, New York

Juan Dixon

Pontificia Universidad Católica de Chile
Santiago, Chile

M. José Espinoza

Universidad de Concepción
Concepción, Chile

James W. Feltes

Power Technologies
Schenectady, New York

Michael Giesselmann

Texas Tech University
Lubbock, Texas

Charles A. Gross

Auburn University
Auburn, Alabama

Andrew P. Hanson

PowerComm Engineering
Raleigh, North Carolina

Tim A. Haskew

University of Alabama
Tuscaloosa, Alabama

Gerald T. Heydt

Arizona State University
Tempe, Arizona

Alireza Khotanzad

Southern Methodist University
Dallas, Texas

Stephen R. Lambert

Shawnee Power Consulting, LLC
Williamsburg, Virginia

Juan A. Martinez-Velasco

Universitat Politècnica de Catalunya
Barcelona, Spain

Thomas E. McDermott

EnerNex Corporation
Pittsburgh, Pennsylvania

Hyde M. Merrill
Merrill Energy, LLC
Schenectady, New York

Luis Morán
Universidad de Concepción
Concepción, Chile

Mark Nelms
Auburn University
Auburn, Alabama

Kaushik Rajashekara
Delphi Automotive Systems
Kokomo, Indiana

N. Dag Reppen
Niskayuna Power Consultants, LLC
Schenectady, New York

José Rodríguez
Universidad Técnica Federico Santa María
Valparaíso, Chile

Francisco de la Rosa
Distribution Control Systems, Inc.
Hazelwood, Missouri

Peter W. Sauer
University of Illinois at Urbana-Champaign
Urbana, Illinois

Gerald B. Sheblé
Portland State University
Portland, Oregon

Mahesh M. Swamy
Yaskawa Electric America
Waukegan, Illinois

I

Power System Analysis and Simulation

Leonard L. Grigsby
Auburn University

Andrew P. Hanson
PowerComm Engineering

1	The Per-Unit System <i>Charles A. Gross</i>	1-1
	Impact on Transformers • Per-Unit Scaling Extended to Three-Phase Systems • Per-Unit Scaling Extended to a General Three-Phase System	
2	Symmetrical Components for Power System Analysis <i>Tim A. Haskew</i>	2-1
	Fundamental Definitions • Reduction to the Balanced Case • Sequence Network Representation in Per-Unit	
3	Power Flow Analysis <i>Leonard L. Grigsby and Andrew P. Hanson</i>	3-1
	Introduction • Power Flow Problem • Formulation of Bus Admittance Matrix • Formulation of Power Flow Equations • P - V Buses • Bus Classifications • Generalized Power Flow Development • Solution Methods • Component Power Flows	
4	Fault Analysis in Power Systems <i>Charles A. Gross</i>	4-1
	Simplifications in the System Model • The Four Basic Fault Types • An Example Fault Study • Further Considerations • Summary • Defining Terms	
5	Computational Methods for Electric Power Systems <i>Mariesa L. Crow</i>	5-1
	Power Flow • Optimal Power Flow • State Estimation	

1

The Per-Unit System

Charles A. Gross
Auburn University

1.1	Impact on Transformers	1-4
1.2	Per-Unit Scaling Extended to Three-Phase Systems	1-7
1.3	Per-Unit Scaling Extended to a General Three-Phase System	1-11

In many engineering situations, it is useful to scale or normalize quantities. This is commonly done in power system analysis, and the standard method used is referred to as the per-unit system. Historically, this was done to simplify numerical calculations that were made by hand. Although this advantage has been eliminated by using the computer, other advantages remain:

- Device parameters tend to fall into a relatively narrow range, making erroneous values conspicuous.
- The method is defined in order to eliminate ideal transformers as circuit components.
- The voltage throughout the power system is normally close to unity.

Some disadvantages are that component equivalent circuits are somewhat more abstract. Sometimes phase shifts that are clearly present in the unscaled circuit are eliminated in the per-unit circuit.

It is necessary for power system engineers to become familiar with the system because of its wide industrial acceptance and use and also to take advantage of its analytical simplifications. This discussion is limited to traditional AC analysis, with voltages and currents represented as complex phasor values. Per-unit is sometimes extended to transient analysis and may include quantities other than voltage, power, current, and impedance.

The basic per-unit scaling equation is

$$\text{Per-unit value} = \frac{\text{actual value}}{\text{base value}}. \quad (1.1)$$

The base value always has the same units as the actual value, forcing the per-unit value to be dimensionless. Also, the base value is always a real number, whereas the actual value may be complex. Representing a complex value in polar form, the angle of the per-unit value is the same as that of the actual value.

Consider complex power

$$S = VI^* \quad (1.2)$$

or

$$S\angle\theta = V\angle\alpha I\angle - \beta$$

where **V** = phasor voltage, in volts; **I** = phasor current, in amperes.

Suppose we arbitrarily pick a value S_{base} , a real number with the units of volt-amperes. Dividing through by S_{base} ,

$$\frac{S \angle \theta}{S_{\text{base}}} = \frac{V \angle \alpha I \angle - \beta}{S_{\text{base}}}.$$

We further define

$$V_{\text{base}} I_{\text{base}} = S_{\text{base}}. \quad (1.3)$$

Either V_{base} or I_{base} may be selected arbitrarily, but not both. Substituting Eq. (1.3) into Eq. (1.2), we obtain

$$\begin{aligned} \frac{S \angle \theta}{S_{\text{base}}} &= \frac{V \angle \alpha (I \angle - \beta)}{V_{\text{base}} I_{\text{base}}} \\ S_{\text{pu}} \angle \theta &= \left(\frac{V \angle \alpha}{V_{\text{base}}} \right) \left(\frac{I \angle - \beta}{I_{\text{base}}} \right) \\ S_{\text{pu}} &= V_{\text{pu}} \angle \alpha (I_{\text{pu}} \angle - \beta) \\ S_{\text{pu}} &= V_{\text{pu}} I_{\text{pu}}^* \end{aligned} \quad (1.4)$$

The subscript pu indicates per-unit values. Note that the form of Eq. (1.4) is identical to Eq. (1.2). This was not inevitable, but resulted from our decision to relate $V_{\text{base}} I_{\text{base}}$ and S_{base} through Eq. (1.3). If we select Z_{base} by

$$Z_{\text{base}} = \frac{V_{\text{base}}}{I_{\text{base}}} = \frac{V_{\text{base}}^2}{S_{\text{base}}}. \quad (1.5)$$

Convert Ohm's law:

$$Z = \frac{V}{I} \quad (1.6)$$

into per-unit by dividing by Z_{base} .

$$\begin{aligned} \frac{Z}{Z_{\text{base}}} &= \frac{V/I}{Z_{\text{base}}} \\ Z_{\text{pu}} &= \frac{V/V_{\text{base}}}{I/I_{\text{base}}} = \frac{V_{\text{pu}}}{I_{\text{pu}}}. \end{aligned}$$

Observe that

$$\begin{aligned} Z_{\text{pu}} &= \frac{Z}{Z_{\text{base}}} = \frac{R + jX}{Z_{\text{base}}} = \left(\frac{R}{Z_{\text{base}}} \right) + j \left(\frac{X}{Z_{\text{base}}} \right) \\ Z_{\text{pu}} &= R_{\text{pu}} + jX_{\text{pu}} \end{aligned} \quad (1.7)$$

Thus, separate bases for R and X are not necessary:

$$Z_{\text{base}} = R_{\text{base}} = X_{\text{base}}$$

By the same logic,

$$S_{\text{base}} = P_{\text{base}} = Q_{\text{base}}$$

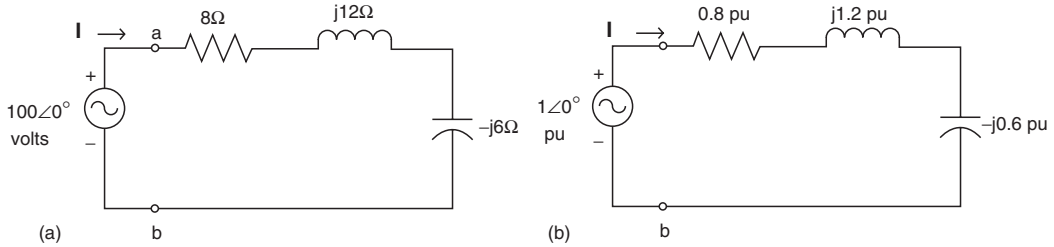


FIGURE 1.1 (a) Circuit with elements in SI units. (b) Circuit with elements in per-unit.

Example 1.1

- Solve for Z , I , and S at Port ab in Fig. 1.1a.
- Repeat (a) in per-unit on bases of $V_{base} = 100$ V and $S_{base} = 1000$ VA. Draw the corresponding per-unit circuit.

Solution

$$(a) Z_{ab} = 8 + j12 - j6 = 8 + j6 = 10 \angle 36.9^\circ \Omega$$

$$I = \frac{V_{ab}}{Z_{ab}} = \frac{100 \angle 0^\circ}{10 \angle 36.9^\circ} = 10 \angle -36.9^\circ \text{ amperes}$$

$$\begin{aligned} S &= V I^* = (100 \angle 0^\circ)(10 \angle -36.9^\circ)^* \\ &= 1000 \angle 36.9^\circ = 800 + j600 \text{ VA} \end{aligned}$$

$$P = 800 \text{ W} \quad Q = 600 \text{ var}$$

- On bases V_{base} and $S_{base} = 1000$ VA:

$$Z_{base} = \frac{V_{base}^2}{S_{base}} = \frac{(100)^2}{1000} = 10 \Omega$$

$$I_{base} = \frac{S_{base}}{V_{base}} = \frac{1000}{100} = 10 \text{ A}$$

$$V_{pu} = \frac{100 \angle 0^\circ}{100} = 1 \angle 0^\circ \text{ pu}$$

$$\begin{aligned} Z_{pu} &= \frac{8 + j12 - j6}{10} = 0.8 + j0.6 \text{ pu} \\ &= 1.0 \angle 36.9^\circ \text{ pu} \end{aligned}$$

$$I_{pu} = \frac{V_{pu}}{Z_{pu}} = \frac{1 \angle 0^\circ}{1 \angle 36.9^\circ} = 1 \angle -36.9^\circ \text{ pu}$$

$$\begin{aligned} S_{pu} &= V_{pu} I_{pu}^* = (1 \angle 0^\circ)(1 \angle -36.9^\circ)^* = 1 \angle 36.9^\circ \text{ pu} \\ &= 0.8 + j0.6 \text{ pu} \end{aligned}$$

Converting results in (b) to SI units:

$$I = (I_{pu}) I_{base} = (1 \angle -36.9^\circ)(10) = 10 \angle -36.9^\circ \text{ A}$$

$$Z = (Z_{pu}) Z_{base} = (0.8 + j0.6)(10) = 8 + j6 \Omega$$

$$S = (S_{pu}) S_{base} = (0.8 + j0.6)(1000) = 800 + j600 \text{ W, var}$$

The results of (a) and (b) are identical.

For power system applications, base values for S_{base} and V_{base} are arbitrarily selected. Actually, in practice, values are selected that force results into certain ranges. Thus, for V_{base} , a value is chosen such that the normal system operating voltage is close to unity. Popular power bases used are 1, 10, 100, and 1000 MVA, depending on system size.

1.1 Impact on Transformers

To understand the impact of pu scaling on transformer, consider the three-winding ideal device (see Fig. 1.2).

For sinusoidal steady-state performance:

$$\mathbf{V}_1 = \frac{N_1}{N_2} \mathbf{V}_2 \quad (1.8a)$$

$$\mathbf{V}_2 = \frac{N_2}{N_3} \mathbf{V}_3 \quad (1.8b)$$

$$\mathbf{V}_3 = \frac{N_3}{N_1} \mathbf{V}_1 \quad (1.8c)$$

and

$$N_1 \mathbf{I}_1 + N_2 \mathbf{I}_2 + N_3 \mathbf{I}_3 = 0 \quad (1.9)$$

Consider the total input complex power \mathbf{S} .

$$\begin{aligned} \mathbf{S} &= \mathbf{V}_1 \mathbf{I}_1^* + \mathbf{V}_2 \mathbf{I}_2^* + \mathbf{V}_3 \mathbf{I}_3^* \\ &= \mathbf{V}_1 \mathbf{I}_1^* + \frac{N_2}{N_1} \mathbf{V}_1 \mathbf{I}_2^* + \frac{N_3}{N_1} \mathbf{V}_1 \mathbf{I}_3^* \\ &= \frac{\mathbf{V}_1}{N_1} [N_1 \mathbf{I}_1 + N_2 \mathbf{I}_2 + N_3 \mathbf{I}_3]^* \\ &= 0 \end{aligned} \quad (1.10)$$

The interpretation to be made here is that the ideal transformer can neither absorb real nor reactive power. An example should clarify these properties.

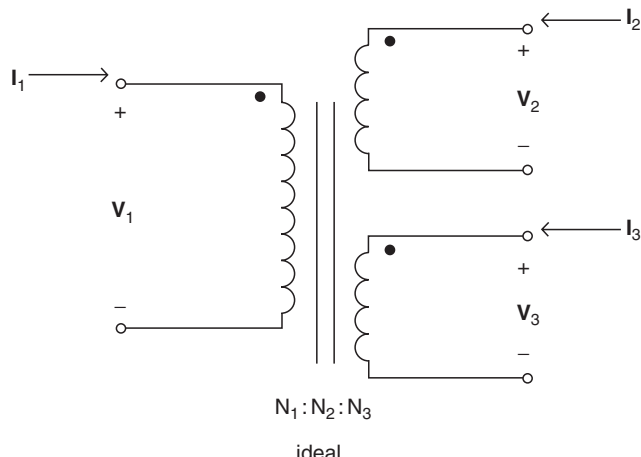


FIGURE 1.2 The three-winding ideal transformer.

Arbitrarily select two base values $V_{1\text{base}}$ and $S_{1\text{base}}$. Require base values for windings 2 and 3 to be:

$$V_{2\text{base}} = \frac{N_2}{N_1} V_{1\text{base}} \quad (1.11\text{a})$$

$$V_{3\text{base}} = \frac{N_3}{N_1} V_{1\text{base}} \quad (1.11\text{b})$$

and

$$S_{1\text{base}} = S_{2\text{base}} = S_{3\text{base}} = S_{\text{base}} \quad (1.12)$$

By definition,

$$I_{1\text{base}} = \frac{S_{\text{base}}}{V_{1\text{base}}} \quad (1.13\text{a})$$

$$I_{2\text{base}} = \frac{S_{\text{base}}}{V_{2\text{base}}} \quad (1.13\text{b})$$

$$I_{3\text{base}} = \frac{S_{\text{base}}}{V_{3\text{base}}} \quad (1.13\text{c})$$

It follows that

$$I_{2\text{base}} = \frac{N_1}{N_2} I_{1\text{base}} \quad (1.14\text{a})$$

$$I_{3\text{base}} = \frac{N_1}{N_3} I_{1\text{base}} \quad (1.14\text{b})$$

Recall that a per-unit value is the actual value divided by its appropriate base. Therefore:

$$\frac{V_1}{V_{1\text{base}}} = \frac{(N_1/N_2)V_2}{V_{1\text{base}}} \quad (1.15\text{a})$$

and

$$\frac{V_1}{V_{1\text{base}}} = \frac{(N_1/N_2)V_2}{(N_1/N_2)V_{2\text{base}}} \quad (1.15\text{b})$$

or

$$V_{1\text{pu}} = V_{2\text{pu}} \quad (1.15\text{c})$$

indicates per-unit values. Similarly,

$$\frac{V_1}{V_{1\text{base}}} = \frac{(N_1/N_3)V_3}{(N_1/N_3)V_{3\text{base}}} \quad (1.16\text{a})$$

or

$$V_{1\text{pu}} = V_{3\text{pu}} \quad (1.16\text{b})$$

Summarizing:

$$V_{1pu} = V_{2pu} = V_{3pu} \quad (1.17)$$

Divide Eq. (1.9) by N_1

$$I_1 + \frac{N_2}{N_1} I_2 + \frac{N_3}{N_1} I_3 = 0$$

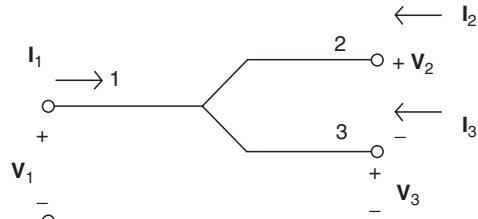


FIGURE 1.3 Single-phase ideal transformer.

Now divide through by I_{1base}

$$\frac{I_1}{I_{1base}} + \frac{(N_2/N_1)I_2}{I_{1base}} + \frac{(N_3/N_1)I_3}{I_{1base}} = 0$$

$$\frac{I_1}{I_{1base}} + \frac{(N_2/N_1)I_2}{(N_2/N_1)I_{2base}} + \frac{(N_3/N_1)I_3}{(N_3/N_1)I_{3base}} = 0$$

Simplifying to

$$I_{1pu} + I_{2pu} + I_{3pu} = 0 \quad (1.18)$$

Equations (1.17) and (1.18) suggest the basic scaled equivalent circuit, shown in Fig. 1.3. It is cumbersome to carry the pu in the subscript past this point: no confusion should result, since all quantities will show units, including pu.

Example 1.2

The 3-winding single-phase transformer of Fig. 1.1 is rated at 13.8 kV/138kV/4.157 kV and 50 MVA/40 MVA/10 MVA. Terminations are as followings:

- 13.8 kV winding: 13.8 kV Source
- 138 kV winding: 35 MVA load, pf = 0.866 lagging
- 4.157 kV winding: 5 MVA load, pf = 0.866 leading

Using $S_{base} = 10$ MVA, and voltage ratings as bases,

- (a) Draw the pu equivalent circuit.
- (b) Solve for the primary current, power, and power factor.

Solution

- (a) See Fig. 1.4.

$$(b,c) S_2 = \frac{35}{10} = 3.5 \text{ pu} \quad S_2 = 3.5 \angle +30^\circ \text{ pu}$$

$$S_3 = \frac{5}{10} = 0.5 \text{ pu} \quad S_3 = 0.5 \angle -30^\circ \text{ pu}$$

$$V_1 = \frac{13.8}{13.8} = 1.0 \text{ pu} \quad V_1 = V_2 = V_3 = 1.0 \angle 0^\circ \text{ pu}$$

$$I_2 = \left(\frac{S_2}{V_2} \right)^* = 3.5 \angle -30^\circ \text{ pu}$$

$$I_3 = \left(\frac{S_3}{V_3} \right)^* = 0.5 \angle +30^\circ \text{ pu}$$

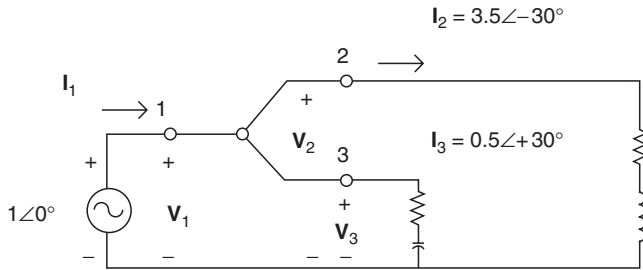


FIGURE 1.4 Per-unit circuit.

All values in Per-Unit Equivalent Circuit:

$$I_1 = I_2 + I_3 = 3.5\angle -30^\circ + 0.5\angle +30^\circ = 3.464 - j1.5 = 3.775\angle -23.4^\circ \text{ pu}$$

$$S_1 = V_1 I_1^* = 3.775\angle +23.4^\circ \text{ pu}$$

$$S_1 = 3.775(10) = 37.75 \text{ MVA; pf} = 0.9177 \text{ lagging}$$

$$I_1 = 3.775 \left(\frac{10}{0.0138} \right) = 2736 \text{ A}$$

1.2 Per-Unit Scaling Extended to Three-Phase Systems

The extension to three-phase systems has been complicated to some extent by the use of traditional terminology and jargon, and a desire to normalize phase-to-phase and phase-to-neutral voltage simultaneously. The problem with this practice is that it renders Kirchhoff's voltage and current laws invalid in some circuits. Consider the general three-phase situation in Fig. 1.5, with all quantities in SI units.

Define the complex operator:

$$\mathbf{a} = 1\angle 120^\circ$$

The system is said to be balanced, with sequence abc, if:

$$\begin{aligned} V_{bn} &= \mathbf{a}^2 V_{an} \\ V_{cn} &= \mathbf{a} V_{an} \end{aligned}$$

and

$$\begin{aligned} I_b &= \mathbf{a}^2 I_a \\ I_c &= \mathbf{a} I_a \\ -I_n &= I_a + I_b + I_c = 0 \end{aligned}$$

Likewise:

$$\begin{aligned} V_{ab} &= V_{an} - V_{bn} \\ V_{bc} &= V_{bn} - V_{cn} = \mathbf{a}^2 V_{ab} \\ V_{ca} &= V_{cn} - V_{an} = \mathbf{a} V_{ab} \end{aligned}$$

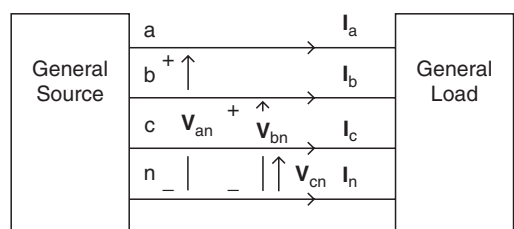


FIGURE 1.5 General three-phase system.

If the load consists of wye-connected impedance:

$$Z_y = \frac{V_{an}}{I_a} = \frac{V_{bn}}{I_b} = \frac{V_{cn}}{I_c}$$

The equivalent delta element is:

$$Z_\Delta = 3Z_y$$

To convert to per-unit, define the following bases:

$S_{3\phi\text{base}}$ = The three-phase apparent base at a specific location in a three-phase system, in VA.

$V_{L\text{base}}$ = The line (phase-to-phase) rms voltage base at a specific location in a three-phase system, in V.

From the above, define:

$$S_{\text{base}} = S_{3\phi\text{base}}/3 \quad (1.19)$$

$$V_{\text{base}} = V_{L\text{base}}/\sqrt{3} \quad (1.20)$$

It follows that:

$$I_{\text{base}} = S_{\text{base}}/V_{\text{base}} \quad (1.21)$$

$$Z_{\text{base}} = V_{\text{base}}/I_{\text{base}} \quad (1.22)$$

An example will be useful.

Example 1.3

Consider a balanced three-phase 60 MVA 0.8 pf lagging load, sequence abc operating from a 13.8 kV (line voltage) bus. On bases of $S_{3\phi\text{base}} = 100$ MVA and $V_{L\text{base}} = 13.8$ kV:

- (a) Determine all bases.
- (b) Determine all voltages, currents, and impedances, in SI units and per-unit.

Solution

$$(a) S_{\text{base}} = \frac{S_{3\phi\text{base}}}{3} = \frac{100}{3} = 33.33 \text{ MVA}$$

$$V_{\text{base}} = \frac{V_{L\text{base}}}{\sqrt{3}} = \frac{13.8}{\sqrt{3}} = 7.967 \text{ kV}$$

$$I_{\text{base}} = \frac{S_{\text{base}}}{V_{\text{base}}} = 4.184 \text{ kA}$$

$$Z_{\text{base}} = \frac{V_{\text{base}}}{I_{\text{base}}} = 1.904 \Omega$$

$$(b) V_{an} = 7.967 \angle 0^\circ \text{ kV} \quad (1.000 \angle 0^\circ \text{ pu})$$

$$V_{bn} = 7.967 \angle -120^\circ \text{ kV} \quad (1.000 \angle -120^\circ \text{ pu})$$

$$V_{cn} = 7.967 \angle +120^\circ \text{ kV} \quad (1.000 \angle +120^\circ \text{ pu})$$

$$S_a = S_b = S_c = \frac{S_{\text{base}}}{3} = \frac{60}{3} = 20 \text{ MVA} (0.60 \text{ pu})$$

$$S_a = S_b = S_c = 16 + j12 \text{ MVA} (0.48 + j0.36 \text{ pu})$$

$$I_a = \left(\frac{S_a}{V_{an}} \right) = 2.510 \angle -36.9^\circ \text{ kA} (0.6000 \angle -36.9^\circ \text{ pu})$$

$$I_b = 2.510 \angle -156.9^\circ \text{ kA} (0.6000 \angle -156.9^\circ \text{ pu})$$

$$I_c = 2.510 \angle 83.1^\circ \text{ kA} (0.6000 \angle 83.1^\circ \text{ pu})$$

$$Z_Y = \frac{V_{an}}{I_a} = 3.174 \angle +36.9^\circ = 2.539 + j1.904 \Omega (1.33 + j1.000 \text{ pu})$$

$$Z_\Delta = 3Z_Y = 7.618 + j5.713 \Omega (4 + j3 \text{ pu})$$

$$V_{ab} = V_{an} - V_{bn} = 13.8 \angle 30^\circ \text{ kV} (1.732 \angle 30^\circ \text{ pu})$$

$$V_{bc} = 13.8 \angle -90^\circ \text{ kV} (1.732 \angle -90^\circ \text{ pu})$$

$$V_{ca} = 13.8 \angle 150^\circ \text{ kV} (1.732 \angle 150^\circ \text{ pu})$$

Converting voltages and currents to symmetrical components:

$$\begin{bmatrix} V_0 \\ V_1 \\ V_2 \end{bmatrix} = \frac{1}{3} \begin{bmatrix} 1 & 1 & 1 \\ 1 & a & a^2 \\ 1 & a^2 & a \end{bmatrix} \begin{bmatrix} V_{an} \\ V_{bn} \\ V_{cn} \end{bmatrix} = \begin{bmatrix} 0 \text{ kV} & (0 \text{ pu}) \\ 7.967 \angle 0^\circ \text{ kV} & (1 \angle 0^\circ \text{ pu}) \\ 0 \text{ kV} & (0 \text{ pu}) \end{bmatrix}$$

$$I_0 = 0 \text{ kA} (0 \text{ pu})$$

$$I_1 = 2.510 \angle -36.9^\circ \text{ kA} (0.6 \angle -36.9^\circ \text{ pu})$$

$$I_2 = 0 \text{ kA} (0 \text{ pu})$$

Inclusion of transformers demonstrates the advantages of per-unit scaling.

Example 1.4

A 3φ 240 kV $\angle 15^\circ$ transformer supplies a 13.8 kV 60 MVA pf = 0.8 lagging load, and is connected to a 230 kV source on the HV side, as shown in Fig. 1.6.

- (a) Determine all base values on both sides for $S_{3\phi\text{base}} = 100\text{MVA}$. At the LV bus, $V_{L\text{base}} = 13.8 \text{ kV}$.
- (b) Draw the positive sequence circuit in per-unit, modeling the transformer as ideal.
- (c) Determine all currents and voltages in SI and per-unit.

Solution

- (a) Base values on the LV side are the same as in [Example 1.3](#). The turns ratio may be derived from the voltage ratings ratios:

$$\frac{N_1}{N_2} = \frac{240/\sqrt{3}}{15/\sqrt{3}} = 16$$

$$\therefore (V_{\text{base}})_{\text{HV side}} = \frac{N_1}{N_2} (V_{\text{base}})_{\text{LV side}} = 16.00(7.967) = 127.5 \text{ kV}$$

$$(I_{\text{base}})_{\text{HV side}} = \frac{S_{\text{base}}}{(V_{\text{base}})_{\text{HV side}}} = \frac{33.33}{0.1275} = 261.5 \text{ A}$$

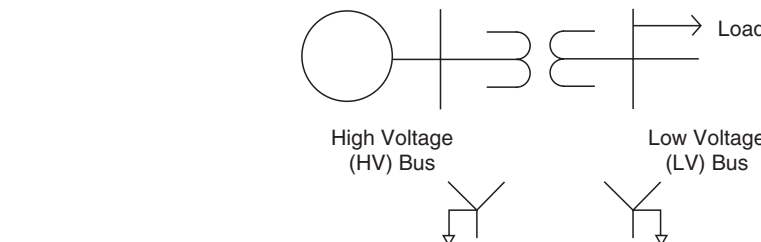


FIGURE 1.6 A three-phase transformer situation.



FIGURE 1.7 Positive sequence circuit.

Results are presented in the following chart.

Bus	S _{3phbase} MVA	V _{L base} kV	S _{base} MVA	I _{base} kA	V _{base} kV	Z _{base} ohm
LV	100	13.8	33.33	4.184	7.967	1.904
HV	100	220.8	33.33	0.2615	127.5	487.5

$$(b) V_{LV} = \frac{7.967\angle 0^\circ}{7.967} = 1\angle 0^\circ \text{ pu}$$

$$S_{1\phi} = \frac{60}{3} = 20 \text{ MVA}$$

$$S_{1\phi} = \frac{20}{33.33} = 0.6 \text{ pu}$$

The positive sequence circuit is shown as Fig. 1.7.

- (c) All values determined in pu are valid on both sides of the transformer! To determine SI values on the HV side, use HV bases. For example:

$$\mathbf{V}_{an} = (1\angle 0^\circ)127.5 = 127.5\angle 0^\circ \text{ kV}$$

$$\mathbf{V}_{ab} = (1.732\angle 30^\circ)(127.5) = 220.8\angle 30^\circ \text{ kV}$$

$$\mathbf{I}_a = (0.6\angle -36.9^\circ)(261.5) = 156.9\angle -36.9^\circ \text{ A}$$

Example 1.5

Repeat the previous example using a 3φ 240 kV:15 kV Δ

Solution

All results are the same as before. The reasoning is as follows.

The voltage ratings are interpreted as line (phase-to-phase) values *independent of connection* (wye or delta). Therefore the turns ratio remains:

$$\frac{N_1}{N_2} = \frac{240/\sqrt{3}}{15/\sqrt{3}} = 16$$

As before:

$$(V_{an})_{LV \text{ side}} = 7.967 \text{ kV}$$

$$(V_{an})_{HV \text{ side}} = 127.5 \text{ kV}$$

However, V_{an} is no longer in phase on both sides. This is a consequence of the transformer model, and not due to the scaling procedure. Whether this is important depends on the details of the analysis.

1.3 Per-Unit Scaling Extended to a General Three-Phase System

The ideas presented are extended to a three-phase system using the following procedure.

1. Select a three-phase apparent power base ($S_{3\text{ph}\ \text{base}}$), which is typically 1, 10, 100, or 1000 MVA. This base is valid at every bus in the system.
2. Select a line voltage base ($V_{L\ \text{base}}$), user defined, but usually the nominal rms line-to-line voltage at a user-defined bus (call this the “reference bus”).
3. Compute

$$S_{\text{base}} = (S_{3\text{ph}\ \text{base}})/3 \quad (\text{Valid at every bus}) \quad (1.23)$$

4. At the reference bus:

$$V_{\text{base}} = V_{L\ \text{base}}/\sqrt{3} \quad (1.24)$$

$$I_{\text{base}} = S_{\text{base}}/V_{\text{base}} \quad (1.25)$$

$$Z_{\text{base}} = V_{\text{base}}/I_{\text{base}} = V_{\text{base}}^2/S_{\text{base}} \quad (1.26)$$

5. To determine the bases at the remaining busses in the system, start at the reference bus, which we will call the “from” bus, and execute the following procedure:
Trace a path to the next nearest bus, called the “to” bus. You reach the “to” bus by either passing over (1) a line, or (2) a transformer.
 - (1) **The “line” case:** $V_{L\ \text{base}}$ is the same at the “to” bus as it was at the “from” bus. Use Eqs. (1.2), (1.3), and (1.4) to compute the “to” bus bases.
 - (2) **The “transformer” case:** Apply $V_{L\ \text{base}}$ at the “from” bus, and treat the transformer as ideal. Calculate the line voltage that appears at the “to” bus. This is now the new $V_{L\ \text{base}}$ at the “to” bus. Use Eqs. (1.2), (1.3), and (1.4) to compute the “to” bus bases.Rename the bus at which you are located, the “from” bus. Repeat the above procedure until you have processed every bus in the system.
6. We now have a set of bases for every bus in the system, which are to be used for every element terminated at that corresponding bus. Values are scaled according to:

$$\text{per-unit value} = \text{actual value}/\text{base value}$$

where actual value = the actual complex value of S , V , Z , or I , in SI units (VA, V, Ω , A); base value = the (user-defined) base value (real) of S , V , Z , or I , in SI units (VA, V, Ω , A); per-unit value = the per-unit complex value of S , V , Z , or I , in per-unit (dimensionless).

Finally, the reader is advised that there are many scaling systems used in engineering analysis, and, in fact, several variations of per-unit scaling have been used in electric power engineering applications. There is no standard system to which everyone conforms in every detail. The key to successfully using any scaling procedure is to understand how all base values are selected at every location within the power system. If one receives data in per-unit, one must be in a position to convert all quantities to SI units. If this cannot be done, the analyst must return to the data source for clarification on what base values were used.

2

Symmetrical Components for Power System Analysis

2.1	Fundamental Definitions.....	2-2
	Voltage and Current Transformation • Impedance Transformation • Power Calculations • System Load Representation • Summary of the Symmetrical Components in the General Three-Phase Case	
2.2	Reduction to the Balanced Case	2-9
	Balanced Voltages and Currents • Balanced Impedances • Balanced Power Calculations • Balanced System Loads • Summary of Symmetrical Components in the Balanced Case	
2.3	Sequence Network Representation in Per-Unit	2-14
	Power Transformers	

Tim A. Haskew
University of Alabama

Modern power systems are three-phase systems that can be balanced or unbalanced and will have mutual coupling between the phases. In many instances, the analysis of these systems is performed using what is known as “per-phase analysis.” In this chapter, we will introduce a more generally applicable approach to system analysis known as “symmetrical components.” The concept of symmetrical components was first proposed for power system analysis by C.L. Fortescue in a classic paper devoted to consideration of the general N-phase case (1918). Since that time, various similar modal transformations (Brogan, 1974) have been applied to a variety of power type problems including rotating machinery (Krause, 1986; Kundur, 1994).

The case for per-phase analysis can be made by considering the simple three-phase system illustrated in Fig. 2.1. The steady-state circuit response can be obtained by solution of the three loop equations presented in Eq. (2.1a) through (2.1c). By solving these loop equations for the three line currents, Eq. (2.2a) through (2.2c) are obtained. Now, if we assume completely balanced source operation (the impedances are defined to be balanced), then the line currents will also form a balanced three-phase set. Hence, their sum, and the neutral current, will be zero. As a result, the line current solutions are as presented in Eq. (2.3a) through (2.3c).

$$\bar{V}_a - \bar{I}_a(R_S + jX_S) - \bar{I}_a(R_L + jX_L) - \bar{I}_n(R_n + jX_n) = 0 \quad (2.1a)$$

$$\bar{V}_b - \bar{I}_b(R_S + jX_S) - \bar{I}_b(R_L + jX_L) - \bar{I}_n(R_n + jX_n) = 0 \quad (2.1b)$$

$$\bar{V}_c - \bar{I}_c(R_S + jX_S) - \bar{I}_c(R_L + jX_L) - \bar{I}_n(R_n + jX_n) = 0 \quad (2.1c)$$

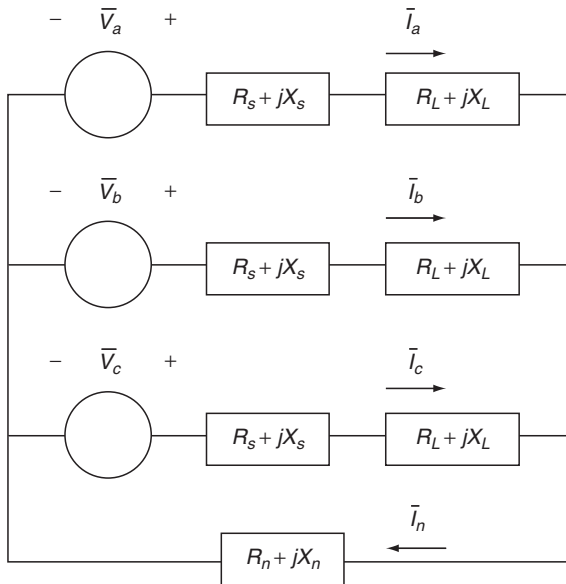


FIGURE 2.1 A simple three-phase system.

the other two phases. Thus, only one phase need be solved, and three-phase symmetry may be applied to determine the solutions for the other phases. This solution technique is the per-phase analysis method.

If one considers the introduction of an unbalanced source or mutual coupling between the phases in Fig. 2.1, then per-phase analysis will not result in three decoupled networks as shown in Fig. 2.2. In fact, in the general sense, no immediate circuit reduction is available without some form of reference frame transformation. The symmetrical component transformation represents such a transformation, which will enable decoupled analysis in the general case and single-phase analysis in the balanced case.

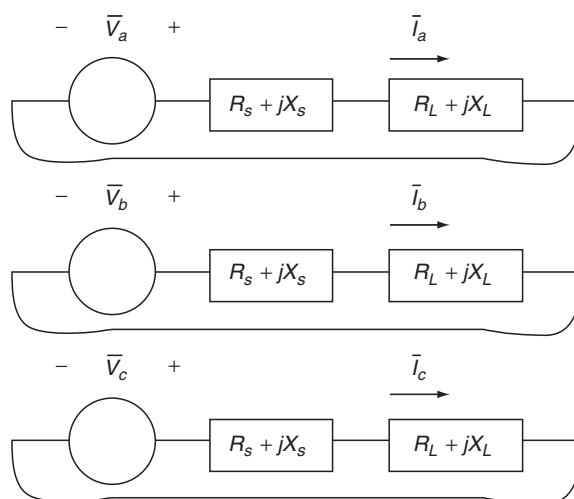


FIGURE 2.2 Decoupled phases of the three-phase system.

$$\bar{I}_a = \frac{\bar{V}_a - \bar{I}_n(R_n + jX_n)}{(R_s + R_n) + j(X_s + X_n)} \quad (2.2a)$$

$$\bar{I}_b = \frac{\bar{V}_b - \bar{I}_n(R_n + jX_n)}{(R_s + R_n) + j(X_s + X_n)} \quad (2.2b)$$

$$\bar{I}_c = \frac{\bar{V}_c - \bar{I}_n(R_n + jX_n)}{(R_s + R_n) + j(X_s + X_n)} \quad (2.2c)$$

$$\bar{I}_a = \frac{\bar{V}_a}{(R_s + R_n) + j(X_s + X_n)} \quad (2.3a)$$

$$\bar{I}_b = \frac{\bar{V}_b}{(R_s + R_n) + j(X_s + X_n)} \quad (2.3b)$$

$$\bar{I}_c = \frac{\bar{V}_c}{(R_s + R_n) + j(X_s + X_n)} \quad (2.3c)$$

The circuit synthesis of Eq. (2.3a) through (2.3c) is illustrated in Fig. 2.2. Particular notice should be taken of the fact the response of each phase is independent of

2.1 Fundamental Definitions

2.1.1 Voltage and Current Transformation

To develop the symmetrical components, let us first consider an arbitrary (no assumptions on balance) three-phase set of voltages as defined in Eq. (2.4a) through (2.4c). Note that we could just as easily be considering current for the purposes at hand, but voltage was selected arbitrarily. Each voltage is defined by a magnitude and phase angle. Hence, we have six degrees of freedom to fully define this arbitrary voltage set.

$$\bar{V}_a = V_a / \theta_a \quad (2.4a)$$

$$\bar{V}_b = V_b / \theta_b \quad (2.4b)$$

$$\bar{V}_c = V_c / \theta_c \quad (2.4c)$$

We can represent each of the three given voltages as the sum of three components as illustrated in Eq. (2.5a) through (2.5c). For now, we consider these components to be completely arbitrary except for their sum. The 0, 1, and 2 subscripts are used to denote the zero, positive, and negative sequence components of each phase voltage, respectively. Examination of Eq. (2.5a-c) reveals that 6 degrees of freedom exist on the left-hand side of the equations while 18 degrees of freedom exist on the right-hand side. Therefore, for the relationship between the voltages in the abc frame of reference and the voltages in the 012 frame of reference to be unique, we must constrain the right-hand side of Eq. (2.5).

$$\bar{V}_a = \bar{V}_{a_0} + \bar{V}_{a_1} + \bar{V}_{a_2} \quad (2.5a)$$

$$\bar{V}_b = \bar{V}_{b_0} + \bar{V}_{b_1} + \bar{V}_{b_2} \quad (2.5b)$$

$$\bar{V}_c = \bar{V}_{c_0} + \bar{V}_{c_1} + \bar{V}_{c_2} \quad (2.5c)$$

We begin by forcing the a_0 , b_0 , and c_0 voltages to have equal magnitude and phase. This is defined in Eq. (2.6). The zero sequence components of each phase voltage are all defined by a single magnitude and a single phase angle. Hence, the zero sequence components have been reduced from 6 degrees of freedom to 2.

$$\bar{V}_{a_0} = \bar{V}_{b_0} = \bar{V}_{c_0} \equiv \bar{V}_0 = V_0 \angle \theta_0 \quad (2.6)$$

Second, we force the a_1 , b_1 , and c_1 voltages to form a balanced three-phase set with positive phase sequence. This is mathematically defined in Eq. (2.7a-c). This action reduces the degrees of freedom provided by the positive sequence components from 6 to 2.

$$\bar{V}_{a_1} = \bar{V}_1 = V_1 \angle \theta_1 \quad (2.7a)$$

$$\bar{V}_{b_1} = V_1 \angle (\theta_1 - 120^\circ) = \bar{V}_1 \bullet 1 \angle -120^\circ \quad (2.7b)$$

$$\bar{V}_{c_1} = V_1 \angle (\theta_1 + 120^\circ) = \bar{V}_1 \bullet 1 \angle +120^\circ \quad (2.7c)$$

And finally, we force the a_2 , b_2 , and c_2 voltages to form a balanced three-phase set with negative phase sequence. This is mathematically defined in Eq. (2.8a-c). As in the case of the positive sequence components, the negative sequence components have been reduced from 6 to 2 degrees of freedom.

$$\bar{V}_{a_2} = \bar{V}_2 = V_2 \angle \theta_2 \quad (2.8a)$$

$$\bar{V}_{b_2} = V_2 \angle (\theta_2 + 120^\circ) = \bar{V}_2 \bullet 1 \angle +120^\circ \quad (2.8b)$$

$$\bar{V}_{c_2} = V_2 \angle (\theta_2 - 120^\circ) = \bar{V}_2 \bullet 1 \angle -120^\circ \quad (2.8c)$$

Now, the right- and left-hand sides of Eq. (2.5a) through (2.5c) each have 6 degrees of freedom. Thus, the relationship between the symmetrical component voltages and the original phase voltages is unique. The final relationship is presented in Eq. (2.9a) through (2.9c). Note that the constant "a" has been defined as indicated in Eq. (2.10).

$$\bar{V}_a = \bar{V}_0 + \bar{V}_1 + \bar{V}_2 \quad (2.9a)$$

$$\bar{V}_b = \bar{V}_0 + \bar{a}^2 \bar{V}_1 + \bar{a} \bar{V}_2 \quad (2.9b)$$

$$\bar{V}_c = \bar{V}_0 + \bar{a} \bar{V}_1 + \bar{a}^2 \bar{V}_2 \quad (2.9c)$$

$$\bar{a} = 1 \angle 120^\circ \quad (2.10)$$

Equation (2.9) is more easily written in matrix form, as indicated in Eq. (2.11) in both expanded and compact form. In Eq. (2.11), the [T] matrix is constant, and the inverse exists. Thus, the inverse

transformation can be defined as indicated in Eq. (2.12). The over tilde (\sim) indicates a vector of complex numbers.

$$\begin{bmatrix} \bar{V}_a \\ \bar{V}_b \\ \bar{V}_c \end{bmatrix} = \begin{bmatrix} 1 & 1 & 1 \\ 1 & \bar{a}^2 & \bar{a} \\ 1 & \bar{a} & \bar{a}^2 \end{bmatrix} \begin{bmatrix} \bar{V}_0 \\ \bar{V}_1 \\ \bar{V}_2 \end{bmatrix}$$

$$\tilde{V}_{abc} = [\bar{T}] \tilde{V}_{012} \quad (2.11)$$

$$\begin{bmatrix} \bar{V}_0 \\ \bar{V}_1 \\ \bar{V}_2 \end{bmatrix} = \frac{1}{3} \begin{bmatrix} 1 & 1 & 1 \\ 1 & \bar{a} & \bar{a}^2 \\ 1 & \bar{a}^2 & \bar{a} \end{bmatrix} \begin{bmatrix} \bar{V}_a \\ \bar{V}_b \\ \bar{V}_c \end{bmatrix}$$

$$\tilde{V}_{012} = [\bar{T}]^{-1} \tilde{V}_{abc} \quad (2.12)$$

Equations (2.13) and (2.14) define an identical transformation and inverse transformation for current.

$$\begin{bmatrix} \bar{I}_a \\ \bar{I}_b \\ \bar{I}_c \end{bmatrix} = \begin{bmatrix} 1 & 1 & 1 \\ 1 & \bar{a}^2 & \bar{a} \\ 1 & \bar{a} & \bar{a}^2 \end{bmatrix} \begin{bmatrix} \bar{I}_0 \\ \bar{I}_1 \\ \bar{I}_2 \end{bmatrix}$$

$$\tilde{I}_{abc} = [\bar{T}] \tilde{I}_{012} \quad (2.13)$$

$$\begin{bmatrix} \bar{I}_0 \\ \bar{I}_1 \\ \bar{I}_2 \end{bmatrix} = \frac{1}{3} \begin{bmatrix} 1 & 1 & 1 \\ 1 & \bar{a} & \bar{a}^2 \\ 1 & \bar{a}^2 & \bar{a} \end{bmatrix} \begin{bmatrix} \bar{I}_a \\ \bar{I}_b \\ \bar{I}_c \end{bmatrix}$$

$$\tilde{I}_{012} = [\bar{T}]^{-1} \tilde{I}_{abc} \quad (2.14)$$

2.1.2 Impedance Transformation

In order to assess the impact of the symmetrical component transformation on systems impedances, we turn to Fig. 2.3. Note that the balanced case has been assumed. Kirchhoff's Voltage Law for the circuit dictates equations Eq. (2.15a-c), which are written in matrix form in Eq. (2.16) and even more simply in Eq. (2.17).

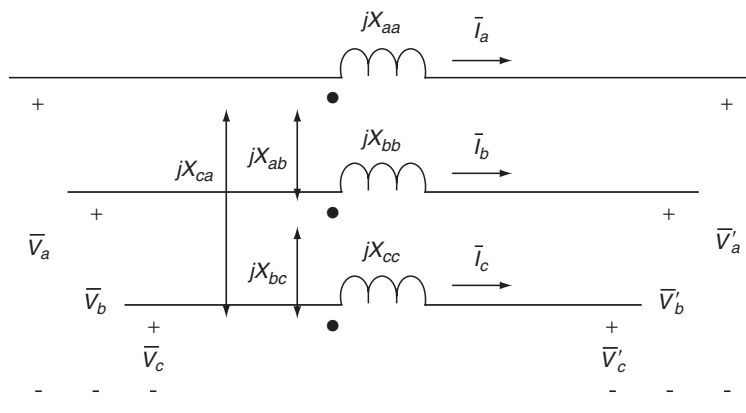


FIGURE 2.3 Mutually coupled series impedances.

$$\bar{V}_a - \bar{V}'_a = jX_{aa}\bar{I}_a + jX_{ab}\bar{I}_b + jX_{ca}\bar{I}_c \quad (2.15a)$$

$$\bar{V}_b - \bar{V}'_b = jX_{ab}\bar{I}_a + jX_{bb}\bar{I}_b + jX_{bc}\bar{I}_c \quad (2.15b)$$

$$\bar{V}_c - \bar{V}'_c = jX_{ca}\bar{I}_a + jX_{bc}\bar{I}_b + jX_{cc}\bar{I}_c \quad (2.15c)$$

$$\begin{bmatrix} \bar{V}_a \\ \bar{V}_b \\ \bar{V}_c \end{bmatrix} - \begin{bmatrix} \bar{V}'_a \\ \bar{V}'_b \\ \bar{V}'_c \end{bmatrix} = j \begin{bmatrix} X_{aa} & X_{ab} & X_{ca} \\ X_{ab} & X_{bb} & X_{bc} \\ X_{ca} & X_{bc} & X_{cc} \end{bmatrix} \begin{bmatrix} \bar{I}_a \\ \bar{I}_b \\ \bar{I}_c \end{bmatrix} \quad (2.16)$$

$$\tilde{V}_{abc} - \tilde{V}'_{abc} = [\bar{Z}_{abc}] \tilde{I}_{abc} \quad (2.17)$$

Multiplying both sides of Eq. (2.17) by $[\bar{T}]^{-1}$ yields Eq. (2.18). Then, substituting Eq. (2.12) and (2.13) into the result leads to the sequence equation presented in Eq. (2.19). The equation is written strictly in the 012 frame reference in Eq. (2.20) where the sequence impedance matrix is defined in Eq. (2.21).

$$[\bar{T}]^{-1} \tilde{V}_{abc} - [\bar{T}]^{-1} \tilde{V}'_{abc} = [\bar{T}]^{-1} [\bar{Z}_{abc}] \tilde{I}_{abc} \quad (2.18)$$

$$\tilde{V}_{012} - \tilde{V}'_{012} = [\bar{T}]^{-1} [\bar{Z}_{abc}] [\bar{T}] \tilde{I}_{012} \quad (2.19)$$

$$\tilde{V}_{012} - \tilde{V}'_{012} = [\bar{Z}_{012}] \tilde{I}_{012} \quad (2.20)$$

$$[\bar{Z}_{012}] = [\bar{T}]^{-1} [\bar{Z}_{abc}] [\bar{T}] = \begin{bmatrix} \bar{Z}_{00} & \bar{Z}_{01} & \bar{Z}_{02} \\ \bar{Z}_{10} & \bar{Z}_{11} & \bar{Z}_{12} \\ \bar{Z}_{20} & \bar{Z}_{21} & \bar{Z}_{22} \end{bmatrix} \quad (2.21)$$

2.1.3 Power Calculations

The impact of the symmetrical components on the computation of complex power can be easily derived from the basic definition. Consider the source illustrated in Fig. 2.4. The three-phase complex power supplied by the source is defined in Eq. (2.22). The algebraic manipulation to Eq. (2.22) is presented, and the result in the sequence domain is presented in Eq. (2.23) in matrix form and in Eq. (2.24) in scalar form.

$$\bar{S}_{3\phi} = \bar{V}_a \bar{I}_a^* + \bar{V}_b \bar{I}_b^* + \bar{V}_c \bar{I}_c^* = \tilde{V}_{abc}^T \tilde{I}_{abc}^* \quad (2.22)$$

$$\begin{aligned} \bar{S}_{3\phi} &= \tilde{V}_{abc}^T \tilde{I}_{abc}^* = \{[\bar{T}] \tilde{V}_{012}\}^T \{[\bar{T}] \tilde{I}_{012}\}^* \\ &= \tilde{V}_{012}^T [\bar{T}]^T [\bar{T}]^* \tilde{I}_{012}^* \\ [\bar{T}]^T [\bar{T}]^* &= \begin{bmatrix} 1 & 1 & 1 \\ 1 & \bar{a}^2 & \bar{a} \\ 1 & \bar{a} & \bar{a}^2 \end{bmatrix} \begin{bmatrix} 1 & 1 & 1 \\ 1 & \bar{a} & \bar{a}^2 \\ 1 & \bar{a}^2 & \bar{a} \end{bmatrix} \\ &= \begin{bmatrix} 3 & 0 & 0 \\ 0 & 3 & 0 \\ 0 & 0 & 3 \end{bmatrix} = 3 \begin{bmatrix} 1 & 0 & 0 \\ 0 & 1 & 0 \\ 0 & 0 & 1 \end{bmatrix} \\ \bar{S}_{3\phi} &= 3 \tilde{V}_{012}^T \tilde{I}_{012}^* \end{aligned} \quad (2.23)$$

$$\bar{S}_{3\phi} = 3 \{\bar{V}_0 \bar{I}_0^* + \bar{V}_1 \bar{I}_1^* + \bar{V}_2 \bar{I}_2^*\} \quad (2.24)$$

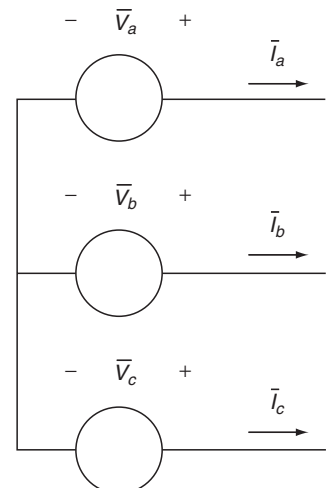


FIGURE 2.4 Three-phase wye-connected source.

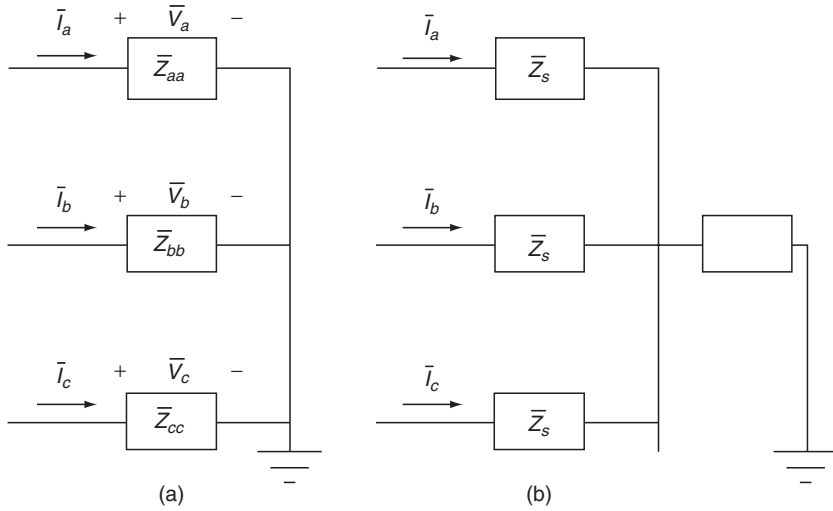


FIGURE 2.5 Three-phase impedance load model.

Note that the nature of the symmetrical component transformation is not one of power invariance, as indicated by the multiplicative factor of 3 in Eq. (2.24). However, this will prove useful in the analysis of balanced systems, which will be seen later. Power invariant transformations do exist as minor variations of the one defined herein. However, they are not typically employed, although the results are just as mathematically sound.

2.1.4 System Load Representation

System loads may be represented in the symmetrical components in a variety of ways, depending on the type of load model that is preferred. Consider first a general impedance type load. Such a load is illustrated in Fig. 2.5a. In this case, Eq. (2.17) applies with $\tilde{V}'_{abc} = 0$ due to the solidly grounded Y connection. Therefore, the sequence impedances are still correctly defined by Eq. (2.21). As illustrated in Fig. 2.5a, the load has zero mutual coupling. Hence, the off-diagonal terms will be zero. However, mutual terms may be considered, as Eq. (2.21) is general in nature. This method can be applied for any shunt-connected impedances in the system.

If the load is Δ -connected, then it should be converted to an equivalent Y-connection prior to the transformation (Irwin, 1996; Gross, 1986). In this case, the possibility of unbalanced mutual coupling will be excluded, which is practical in most cases. Then, the off-diagonal terms in Eq. (2.21) will be zero, and the sequence networks for the load will be decoupled. Special care should be taken that the zero sequence impedance will become infinite because the Δ -connection does not allow a path for a neutral current to flow, which is equivalent to not allowing a zero sequence current path as defined by the first row of matrix Eq. (2.14). A similar argument can be made for a Y-connection that is either ungrounded or grounded through an impedance, as indicated in Fig. 2.5b. In this case, the zero sequence impedance will be equal to the sum of the phase impedance and three times the neutral impedance, or, $\bar{Z}_{00} = \bar{Z}_Y + 3\bar{Z}_n$. Notice should be taken that the neutral impedance can vary from zero to infinity.

The representation of complex power load models will be left for the section on the application of balanced circuit reductions to the symmetrical component transformation.

2.1.5 Summary of the Symmetrical Components in the General Three-Phase Case

The general symmetrical component transformation process has been defined in this section. Table 2.1 is a short form reference for the utilization of these procedures in the general case (i.e., no assumption of

TABLE 2.1 Summary of the Symmetrical Components in the General Case

Quantity	Transformation Equations		
	abc \Rightarrow 012	012 \Rightarrow abc	
Voltage	$\begin{bmatrix} \bar{V}_0 \\ \bar{V}_1 \\ \bar{V}_2 \end{bmatrix} = \frac{1}{3} \begin{bmatrix} 1 & 1 & 1 \\ 1 & \bar{a} & \bar{a}^2 \\ 1 & \bar{a}^2 & \bar{a} \end{bmatrix} \begin{bmatrix} \bar{V}_a \\ \bar{V}_b \\ \bar{V}_c \end{bmatrix}$ $\tilde{V}_{012} = [\bar{T}]^{-1} \tilde{V}_{abc}$	$\begin{bmatrix} \bar{V}_a \\ \bar{V}_b \\ \bar{V}_c \end{bmatrix} = \begin{bmatrix} 1 & 1 & 1 \\ 1 & \bar{a}^2 & \bar{a} \\ 1 & \bar{a} & \bar{a}^2 \end{bmatrix} \begin{bmatrix} \bar{V}_0 \\ \bar{V}_1 \\ \bar{V}_2 \end{bmatrix}$ $\tilde{V}_{abc} = [\bar{T}] \tilde{V}_{012}$	
Current	$\begin{bmatrix} \bar{I}_0 \\ \bar{I}_1 \\ \bar{I}_2 \end{bmatrix} = \frac{1}{3} \begin{bmatrix} 1 & 1 & 1 \\ 1 & \bar{a} & \bar{a}^2 \\ 1 & \bar{a}^2 & \bar{a} \end{bmatrix} \begin{bmatrix} \bar{I}_a \\ \bar{I}_b \\ \bar{I}_c \end{bmatrix}$ $\bar{I}_{012} = [\bar{T}]^{-1} \bar{I}_{abc}$	$\begin{bmatrix} \bar{I}_a \\ \bar{I}_b \\ \bar{I}_c \end{bmatrix} = \begin{bmatrix} 1 & 1 & 1 \\ 1 & \bar{a}^2 & \bar{a} \\ 1 & \bar{a} & \bar{a}^2 \end{bmatrix} \begin{bmatrix} \bar{I}_0 \\ \bar{I}_1 \\ \bar{I}_2 \end{bmatrix}$ $\bar{I}_{abc} = [\bar{T}] \bar{I}_{012}$	
Impedance	$[\bar{Z}_{012}] = [\bar{T}]^{-1} [\bar{Z}_{abc}] [\bar{T}]$		
Power	$\bar{S}_{3\phi} = \bar{V}_a \bar{I}_a^* + \bar{V}_b \bar{I}_b^* + \bar{V}_c \bar{I}_c^* = \tilde{V}_{abc}^T \tilde{I}_{abc}$ $\bar{S}_{3\phi} = 3 \{ \bar{V}_0 \bar{I}_0^* + \bar{V}_2 \bar{I}_2^* + \bar{V}_3 \bar{I}_3^* \} = 3 \tilde{V}_{012}^T \tilde{I}_{012}$		

balanced conditions). Application of these relationships defined in Table 2.1 will enable the power system analyst to draw the zero, positive, and negative sequence networks for the system under study. These networks can then be analyzed in the 012 reference frame, and the results can be easily transformed back into the abc reference frame.

Example 2.1

The power system illustrated in Fig. 2.6 is to be analyzed using the sequence networks. Find the following:

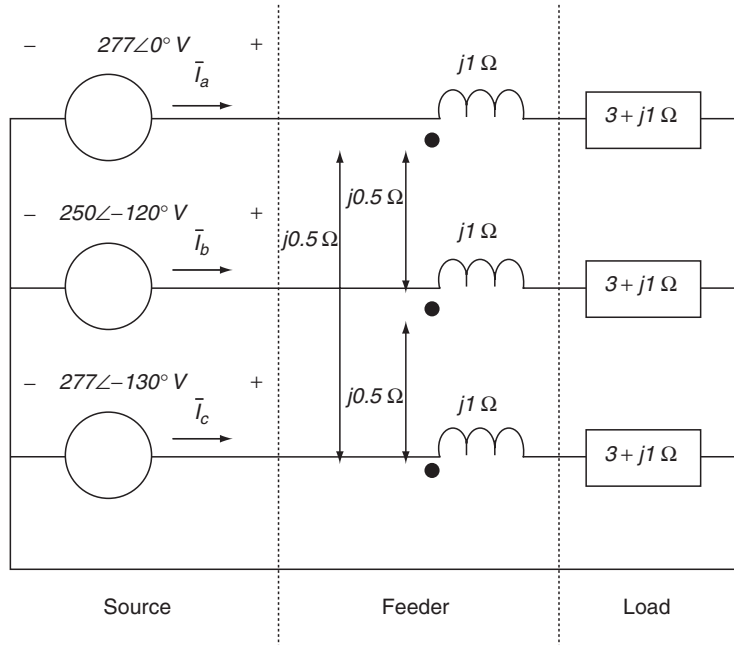


FIGURE 2.6 Power system for Example 2.1.

- (a) three line currents
- (b) line-to-neutral voltages at the load
- (c) three-phase complex power output of the source

Solution

The sequence voltages are computed in Eq. (2.25). The sequence impedances for the feeder and the load are computed in Eqs. (2.26) and (2.27), respectively. The sequence networks are drawn in Fig. 2.7.

$$\begin{bmatrix} \bar{V}_0 \\ \bar{V}_1 \\ \bar{V}_2 \end{bmatrix} = \frac{1}{3} \begin{bmatrix} 1 & 1 & 1 \\ 1 & \bar{a} & \bar{a}^2 \\ 1 & \bar{a}^2 & \bar{a} \end{bmatrix} \begin{bmatrix} 255\angle 0^\circ \\ 250\angle -120^\circ \\ 277\angle 130^\circ \end{bmatrix} = \begin{bmatrix} 8.8\angle -171^\circ \\ 267.1\angle 3^\circ \\ 24.0\angle -37^\circ \end{bmatrix} \text{ V} \quad (2.25)$$

$$[\bar{Z}_{012}] = [\bar{T}]^{-1} \begin{bmatrix} j1 & j0.5 & j0.5 \\ j0.5 & j1 & j0.5 \\ j0.5 & j0.5 & j1 \end{bmatrix} [\bar{T}] = \begin{bmatrix} j2 & 0 & 0 \\ 0 & j0.5 & 0 \\ 0 & 0 & j0.5 \end{bmatrix} \Omega \quad (2.26)$$

$$[\bar{Z}_{012}] = [\bar{T}]^{-1} \begin{bmatrix} 3+j1 & 0 & 0 \\ 0 & 3+j1 & 0 \\ 0 & 0 & 3+j1 \end{bmatrix} [\bar{T}] = \begin{bmatrix} 3+j1 & 0 & 0 \\ 0 & 3+j1 & 0 \\ 0 & 0 & 3+j1 \end{bmatrix} \Omega \quad (2.27)$$

The sequence currents are computed in Eq. (2.28a-c). In Eq. (2.29), the sequence currents and sequence load impedances are used to compute the zero, positive, and negative sequence load voltages.

$$\bar{I}_0 = \frac{8.8\angle -171^\circ}{3 + j(1 + 2)} = 2.1\angle 144^\circ \text{ A} \quad (2.28a)$$

$$\bar{I}_1 = \frac{267.1\angle 3^\circ}{3 + j(1 + 0.5)} = 79.6\angle -24^\circ \text{ A} \quad (2.28b)$$

$$\bar{I}_2 = \frac{24.0\angle -37^\circ}{3 + j(1 + 0.5)} = 7.2\angle -64^\circ \text{ A} \quad (2.28c)$$

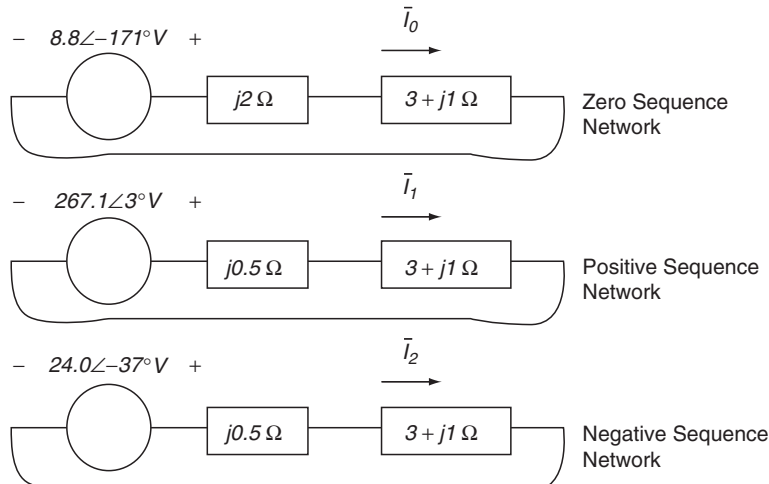


FIGURE 2.7 Sequence networks for [Example 2.1](#).

$$\begin{bmatrix} \bar{V}_0 \\ \bar{V}_1 \\ \bar{V}_2 \end{bmatrix} = [\bar{Z}_{012}] \tilde{I}_{012} = \begin{bmatrix} 3+j1 & 0 & 0 \\ 0 & 3+j1 & 0 \\ 0 & 0 & 3+j1 \end{bmatrix} \begin{bmatrix} 2.1\angle 144^\circ \\ 79.6\angle -24^\circ \\ 7.2\angle -64^\circ \end{bmatrix} \quad (2.29)$$

$$= \begin{bmatrix} 6.6\angle 162^\circ \\ 251.7\angle -6^\circ \\ 22.8\angle -46^\circ \end{bmatrix} V$$

The three line currents can be computed as illustrated in Eq. (2.30), and the line-to-neutral load voltages are computed in Eq. (2.31). The three-phase complex power output of the source is computed in Eq. (2.32).

$$\begin{bmatrix} \bar{I}_a \\ \bar{I}_b \\ \bar{I}_c \end{bmatrix} = \begin{bmatrix} 1 & 1 & 1 \\ 1 & \bar{a}^2 & \bar{a} \\ 1 & \bar{a} & \bar{a}^2 \end{bmatrix} \begin{bmatrix} 2.1\angle 144^\circ \\ 79.6\angle -24^\circ \\ 7.2\angle -64^\circ \end{bmatrix} = \begin{bmatrix} 83.2\angle -27^\circ \\ 73.6\angle -147^\circ \\ 82.7\angle 102^\circ \end{bmatrix} A \quad (2.30)$$

$$\begin{bmatrix} \bar{V}_a \\ \bar{V}_b \\ \bar{V}_c \end{bmatrix} = \begin{bmatrix} 1 & 1 & 1 \\ 1 & \bar{a}^2 & \bar{a} \\ 1 & \bar{a} & \bar{a}^2 \end{bmatrix} \begin{bmatrix} 6.6\angle 162^\circ \\ 251.7\angle -6^\circ \\ 22.8\angle -46^\circ \end{bmatrix} = \begin{bmatrix} 263.0\angle -9^\circ \\ 232.7\angle -129^\circ \\ 261.5\angle 120^\circ \end{bmatrix} V \quad (2.31)$$

$$\bar{S}_{3\phi} = 3\{\bar{V}_0\bar{I}_0^* + \bar{V}_1\bar{I}_1^* + \bar{V}_2\bar{I}_2^*\} = 57.3 + j29.2 \text{ kVA} \quad (2.32)$$

2.2 Reduction to the Balanced Case

When the power system under analysis is operating under balanced conditions, the symmetrical components allow one to perform analysis on a single-phase network in a manner similar to per-phase analysis, even when mutual coupling is present. The details of the method are presented in this section.

2.2.1 Balanced Voltages and Currents

Consider a balanced three-phase source operating with positive phase sequence. The voltages are defined below in Eq. (2.33). Upon computation of Eq. (2.12), one discovers that the sequence voltages that result are those shown in Eq. (2.34).

$$\tilde{V}_{abc} = \begin{bmatrix} V_a\angle\theta_a \\ V_a\angle(\theta_a - 120^\circ) \\ V_a\angle(\theta_a + 120^\circ) \end{bmatrix} \quad (2.33)$$

$$\tilde{V}_{012} = \begin{bmatrix} 0 \\ V_a\angle\theta_a \\ 0 \end{bmatrix} \quad (2.34)$$

In Eq. (2.35), a source is defined with negative phase sequence. The sequence voltages for this case are presented in Eq. (2.36).

$$\tilde{V}_{abc} = \begin{bmatrix} V_a\angle\theta_a \\ V_a\angle(\theta_a + 120^\circ) \\ V_a\angle(\theta_a - 120^\circ) \end{bmatrix} \quad (2.35)$$

$$\hat{V}_{012} = \begin{bmatrix} 0 \\ 0 \\ V_a \angle \theta_a \end{bmatrix} \quad (2.36)$$

These results are particularly interesting. For a balanced source with positive phase sequence, only the positive sequence voltage is non-zero, and its value is the a-phase line-to-neutral voltage. Similarly, for a balanced source with negative phase sequence, the negative sequence voltage is the only non-zero voltage, and it is also equal to the a-phase line-to-neutral voltage. Identical results can be shown for positive and negative phase sequence currents.

2.2.2 Balanced Impedances

In the balanced case, Eq. (2.16) is valid, but Eq. (2.37a-b) apply. Thus, evaluation of Eq. (2.21) results in the closed form expression of Eq. (2.38a). Equation (2.38b) extends the result of Eq. (2.38a) to impedance rather than just reactance.

$$X_{aa} = X_{bb} = X_{cc} \equiv X_s \quad (2.37a)$$

$$X_{ab} = X_{bc} = X_{ca} \equiv X_m \quad (2.37b)$$

$$\begin{aligned} [\bar{Z}_{012}] &= [\bar{T}]^{-1} [\bar{Z}_{abc}] [\bar{T}] = \begin{bmatrix} X_s + 2X_m & 0 & 0 \\ 0 & X_s - X_m & 0 \\ 0 & 0 & X_s - X_m \end{bmatrix} \\ &= \begin{bmatrix} Z_{00} & 0 & 0 \\ 0 & Z_{11} & 0 \\ 0 & 0 & Z_{22} \end{bmatrix} \end{aligned} \quad (2.38a)$$

$$[\bar{Z}_{012}] = \begin{bmatrix} \bar{Z}_s + 2\bar{Z}_m & 0 & 0 \\ 0 & \bar{Z}_s - \bar{Z}_m & 0 \\ 0 & 0 & \bar{Z}_s - \bar{Z}_m \end{bmatrix} = \begin{bmatrix} Z_{00} & 0 & 0 \\ 0 & Z_{11} & 0 \\ 0 & 0 & Z_{22} \end{bmatrix} \quad (2.38b)$$

2.2.3 Balanced Power Calculations

In the balanced case, Eq. (2.32) is still valid. However, in the case of positive phase sequence operation, the zero and negative sequence voltages and currents are zero. Hence, Eq. (2.39) results. In the case of negative phase sequence operation, the zero and positive sequence voltages and currents are zero. This results in Eq. (2.40).

$$\begin{aligned} \bar{S}_{3\phi} &= 3 \{ \bar{V}_0 \bar{I}_0^* + \bar{V}_1 \bar{I}_1^* + \bar{V}_2 \bar{I}_2^* \} \\ &= 3 \bar{V}_1 \bar{I}_1^* = 3 \bar{V}_a \bar{I}_a^* \end{aligned} \quad (2.39)$$

$$\begin{aligned} \bar{S}_{3\phi} &= 3 \{ \bar{V}_0 \bar{I}_0^* + \bar{V}_1 \bar{I}_1^* + \bar{V}_2 \bar{I}_2^* \} \\ &= 3 \bar{V}_2 \bar{I}_2^* = 3 \bar{V}_a \bar{I}_a^* \end{aligned} \quad (2.40)$$

Examination of Eqs. (2.39) and (2.40) reveals that the nature of complex power calculations in the sequence networks is identical to that performed using per-phase analysis (i.e., the factor of 3 is present). This feature of the symmetrical component transformation defined herein is the primary reason that power invariance is not desired.

2.2.4 Balanced System Loads

When the system loads are balanced, the sequence network representation is rather straightforward. We shall first consider the impedance load model by referring to Fig. 2.5a, imposing balanced impedances, and allowing for consideration of a neutral impedance, as illustrated in Fig. 2.5b. Balanced conditions are enforced by Eq. (2.41a-b). In this case, the reduction is based on Eq. (2.38). The result is presented in Eq. (2.42). Special notice should be taken that the mutual terms may be zero, as indicated on the figure, but have been included for completeness in the mathematical development.

$$\bar{Z}_{aa} = \bar{Z}_{bb} = \bar{Z}_{cc} \equiv \bar{Z}_s \quad (2.41a)$$

$$\bar{Z}_{ab} = \bar{Z}_{bc} = \bar{Z}_{ca} \equiv \bar{Z}_m \quad (2.41b)$$

$$[\bar{Z}_{012}] = \begin{bmatrix} \bar{Z}_s + 2\bar{Z}_m + 3\bar{Z}_n & 0 & 0 \\ 0 & \bar{Z}_s - \bar{Z}_m & 0 \\ 0 & 0 & \bar{Z}_s - \bar{Z}_m \end{bmatrix} = \begin{bmatrix} Z_{00} & 0 & 0 \\ 0 & Z_{11} & 0 \\ 0 & 0 & Z_{22} \end{bmatrix} \quad (2.42)$$

The balanced complex power load model is illustrated in Fig. 2.8. The transformation into the sequence networks is actually defined by the results presented in Eqs. (2.39) and (2.40). In positive phase sequence systems, the zero and negative sequence load representations absorb zero complex power; in negative phase sequence systems, the zero and positive sequence load representations absorb zero complex power. Hence, the zero complex power sequence loads are represented as short-circuits, thus forcing the sequence voltages to zero. The non-zero sequence complex power load turns out to be equal to the single-phase load complex power. This is defined for positive phase sequence systems in Eq. (2.43) and for negative phase sequence systems in Eq. (2.44).

$$\bar{S}_1 = \bar{S}_{1\phi} \quad (2.43)$$

$$\bar{S}_2 = \bar{S}_{1\phi} \quad (2.44)$$

2.2.5 Summary of Symmetrical Components in the Balanced Case

The general application of symmetrical components to balanced three-phase power systems has been presented in this section. The results are summarized in a quick reference form in Table 2.2. At this point, however, power transformers have been omitted from consideration. This will be rectified in the next few sections.

Example 2.2

Consider the balanced system illustrated by the one-line diagram in Fig. 2.9. Determine the line voltage magnitudes at buses 2 and 3 if the line voltage magnitude at bus 1 is 12.47 kV. We will assume positive phase sequence operation of the source. Also, draw the zero sequence network.

Solution

The two feeders are identical, and the zero and positive sequence impedances are computed in Eqs. (2.45a) and (2.45b), respectively. The zero and positive sequence impedances for the loads at buses 1 and 2 are computed in Eq. (2.46a-b) through (2.47a-b), respectively. The Δ -connected load at bus 3 is converted to an equivalent

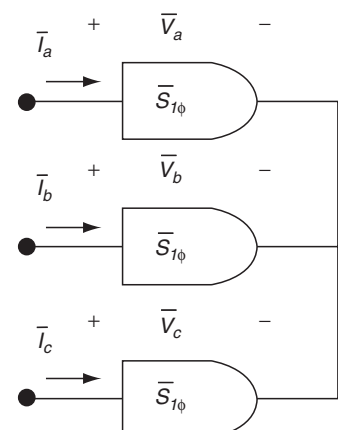


FIGURE 2.8 Balanced complex power load model.

TABLE 2.2 Summary of the Symmetrical Components in the Balanced Case

Transformation Equations		
Quantity	$abc \Rightarrow 012$	$012 \Rightarrow abc$
Voltage	Positive Phase Sequence: $\begin{bmatrix} \bar{V}_0 \\ \bar{V}_1 \\ \bar{V}_2 \end{bmatrix} = [\bar{T}]^{-1} \begin{bmatrix} \bar{V}_a \\ \bar{V}_b \\ \bar{V}_c \end{bmatrix} = \begin{bmatrix} 0 \\ \bar{V}_a \\ 0 \end{bmatrix}$ Negative Phase Sequence: $\begin{bmatrix} \bar{V}_0 \\ \bar{V}_1 \\ \bar{V}_2 \end{bmatrix} = [\bar{T}]^{-1} \begin{bmatrix} \bar{V}_a \\ \bar{V}_b \\ \bar{V}_c \end{bmatrix} = \begin{bmatrix} 0 \\ 0 \\ \bar{V}_a \end{bmatrix}$	Positive Phase Sequence: $\begin{bmatrix} \bar{V}_a \\ \bar{V}_b \\ \bar{V}_c \end{bmatrix} = [\bar{T}] \begin{bmatrix} \bar{V}_0 \\ \bar{V}_1 \\ \bar{V}_2 \end{bmatrix} = \begin{bmatrix} \bar{V}_1 \\ \bar{a}^2 \bar{V}_1 \\ \bar{a} \bar{V}_1 \end{bmatrix}$ Negative Phase Sequence: $\begin{bmatrix} \bar{V}_a \\ \bar{V}_b \\ \bar{V}_c \end{bmatrix} = [\bar{T}] \begin{bmatrix} \bar{V}_0 \\ \bar{V}_1 \\ \bar{V}_2 \end{bmatrix} = \begin{bmatrix} \bar{V}_2 \\ \bar{a} \bar{V}_2 \\ \bar{a}^2 \bar{V}_2 \end{bmatrix}$
Current	Positive Phase Sequence: $\begin{bmatrix} \bar{I}_0 \\ \bar{I}_1 \\ \bar{I}_2 \end{bmatrix} = [\bar{T}]^{-1} \begin{bmatrix} \bar{I}_a \\ \bar{I}_b \\ \bar{I}_c \end{bmatrix} = \begin{bmatrix} 0 \\ \bar{I}_a \\ 0 \end{bmatrix}$ Negative Phase Sequence: $\begin{bmatrix} \bar{I}_0 \\ \bar{I}_1 \\ \bar{I}_2 \end{bmatrix} = [\bar{T}]^{-1} \begin{bmatrix} \bar{I}_a \\ \bar{I}_b \\ \bar{I}_c \end{bmatrix} = \begin{bmatrix} 0 \\ 0 \\ \bar{I}_a \end{bmatrix}$	Positive Phase Sequence: $\begin{bmatrix} \bar{I}_a \\ \bar{I}_b \\ \bar{I}_c \end{bmatrix} = [\bar{T}] \begin{bmatrix} \bar{I}_0 \\ \bar{I}_1 \\ \bar{I}_2 \end{bmatrix} = \begin{bmatrix} \bar{I}_1 \\ \bar{a}^2 \bar{I}_1 \\ \bar{a} \bar{I}_1 \end{bmatrix}$ Negative Phase Sequence: $\begin{bmatrix} \bar{I}_a \\ \bar{I}_b \\ \bar{I}_c \end{bmatrix} = [\bar{T}] \begin{bmatrix} \bar{I}_0 \\ \bar{I}_1 \\ \bar{I}_2 \end{bmatrix} = \begin{bmatrix} \bar{I}_1 \\ \bar{a} \bar{I}_1 \\ \bar{a}^2 \bar{I}_1 \end{bmatrix}$
Impedance	$[\bar{Z}_{012}] = [\bar{T}]^{-1} [\bar{Z}_{abc}] [\bar{T}] = \begin{bmatrix} \bar{Z}_s + 2\bar{Z}_m + 3\bar{Z}_n & 0 & 0 \\ 0 & \bar{Z}_s - \bar{Z}_m & 0 \\ 0 & 0 & \bar{Z}_2 - \bar{Z}_m \end{bmatrix}$	
Power	$\bar{S}_{3\phi} = \bar{V}_a \bar{I}_a^* + \bar{V}_b \bar{I}_b^* + \bar{V}_c \bar{I}_c^* = 3\bar{V}_a \bar{I}_a^*$ $\bar{S}_{3\phi} = \{\bar{V}_0 \bar{I}_0^* + \bar{V}_1 \bar{I}_1^* + \bar{V}_2 \bar{I}_2^*\} = \begin{cases} 3\bar{V}_1 \bar{I}_1^* & \text{positive ph. seq} \\ 3\bar{V}_2 \bar{I}_2^* & \text{negative ph. seq} \end{cases}$	

Y-connection in Eq. (2.48a), and the zero and positive sequence impedances for the load are computed in Eq. (2.48b) and (2.48c), respectively.

$$\bar{Z}_{00_{feeder}} = \bar{Z}_s + 2\bar{Z}_m = j6 + 2(j2) = j10 \Omega \quad (2.45a)$$

$$\bar{Z}_{11_{feeder}} = \bar{Z}_s - \bar{Z}_m = j6 - j2 = j4 \Omega \quad (2.45b)$$

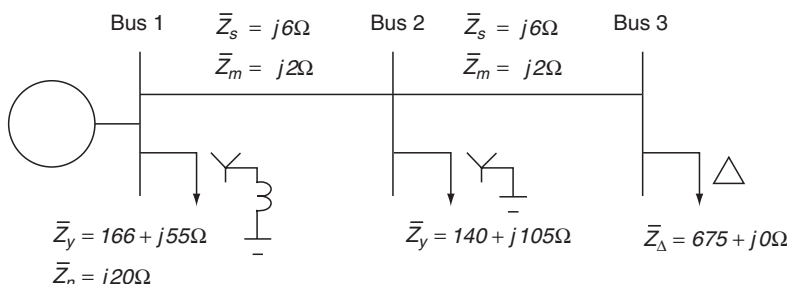


FIGURE 2.9 Balanced power system for Example 2.2.

$$\begin{aligned}\bar{Z}_{00_{bus1}} &= \bar{Z}_s + 2\bar{Z}_m + 3\bar{Z}_n \\ &= (166 + j55) + 2(0) + 3(j20) = 166 + j115\Omega\end{aligned}\quad (2.46a)$$

$$\bar{Z}_{11_{bus1}} = \bar{Z}_s - \bar{Z}_m = (166 + j55) - 0 = 166 + j55\Omega \quad (2.46b)$$

$$\begin{aligned}\bar{Z}_{00_{bus2}} &= \bar{Z}_s + 2\bar{Z}_m + 3\bar{Z}_n \\ &= (140 + j105) + 2(0) + 3(0) = 140 + j105\Omega\end{aligned}\quad (2.47a)$$

$$\bar{Z}_{11_{bus2}} = \bar{Z}_s - \bar{Z}_m = (140 + j105) - 0 = 140 + j105\Omega \quad (2.47b)$$

$$\bar{Z}_{Y_{bus3}} = \frac{\bar{Z}_\Delta}{3} = \frac{675 + j0}{3} = 225 + j0\Omega \quad (2.48a)$$

$$\bar{Z}_{00_{bus3}} = \bar{Z}_s + 2\bar{Z}_m + 3\bar{Z}_n = (225 + j0) + 2(0) + 3(\infty) \rightarrow \infty \quad (2.48b)$$

$$\bar{Z}_{11_{bus3}} = \bar{Z}_s - \bar{Z}_m = (225 + j0) - 0 = 225 + j0\Omega \quad (2.48c)$$

The zero and positive sequence networks for the system are provided in Figs. 2.10a and b. Note in the zero sequence network, that the voltage at bus 1 has been forced to zero by imposing a short-circuit to reference. For analysis, since the system is balanced, we need only concern ourselves with the positive sequence network. The source voltage at bus 1 is assumed to be the reference with a 0° phase angle. Note that the source voltage magnitude is the line-to-neutral voltage magnitude at bus 1. The positive sequence voltage at bus 2 can be found using the voltage divider, as shown in Eq. (2.49). Note here that the subscript numbers on the voltages denote the bus, not the sequence network. We assume that all voltages are in the positive sequence network. Again using the voltage divider, the positive sequence voltage at bus 3 can be found, as shown in Eq. (2.50). The requested line voltage magnitudes at buses 2 and 3 can be computed from the positive sequence voltages as shown in [Eq. \(2.51a-b\)](#).

$$\bar{V}_2 = 7200\angle 0^\circ \frac{\{(140 + j105)/(225 + j4)\}}{j4 + \{(140 + j105)/(225 + j4)\}} = 7095.9\angle -2^\circ V \quad (2.49)$$

$$\bar{V}_3 = 7095.9\angle -2^\circ \frac{225}{225 + j4} = 7094.8\angle -3^\circ V \quad (2.50)$$

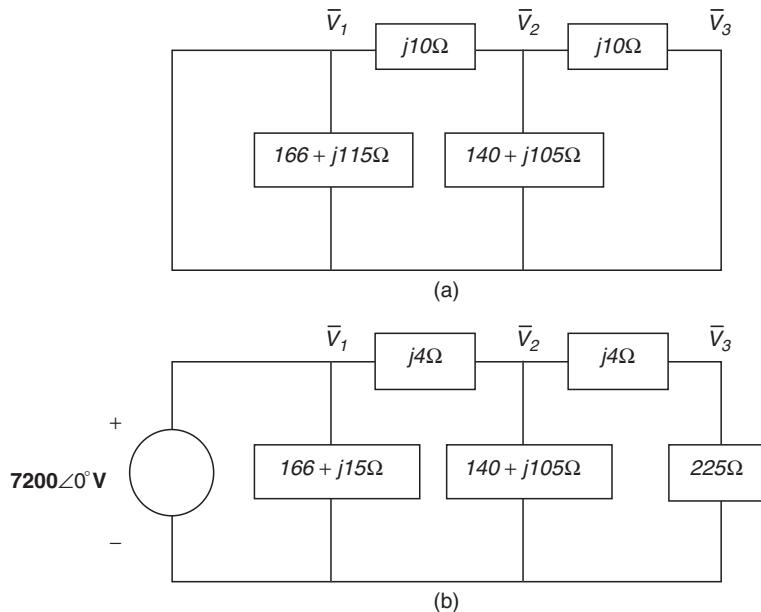


FIGURE 2.10 (a) Zero and (b) positive sequence networks for [Example 2.2](#).

$$V_{L_2} = \sqrt{3}|\bar{V}_2| = \sqrt{3}(7095.9) = 12,290.5V \quad (2.51a)$$

$$V_{L_3} = \sqrt{3}|\bar{V}_3| = \sqrt{3}(7094.8) = 12,288.6V \quad (2.51b)$$

2.3 Sequence Network Representation in Per-Unit

The foregoing development has been based on the inherent assumption that all parameters and variables were expressed in SI units. Quite often, large-scale power system analyses and computations are performed in the per-unit system of measurement (Gross, 1986; Grainger and Stevenson, 1994; Glover and Sarma, 1989). Thus, we must address the impact of per-unit scaling on the sequence networks. Such a conversion is rather straightforward because of the similarity between the positive or negative sequence network and the a-phase network used in per-phase analysis (the reader is cautioned not to confuse the concepts of per-phase analysis and per-unit scaling). The appropriate bases are the same for each sequence network, and they are defined in Table 2.3. Note that the additional subscript “pu” has been added to denote a variable in per-unit; variables in SI units do not carry the additional subscripts.

2.3.1 Power Transformers

For the consideration of transformers and transformer banks, we will limit ourselves to working in the per-unit system. Thus, the ideal transformer in the transformer equivalent circuit can be neglected in the nominal case. The equivalent impedance of a transformer, whether it be single-phase or three-phase, is typically provided on the nameplate in percent, or test data may be available to compute equivalent winding and shunt branch impedances. Developing the sequence networks for these devices is not terribly complicated, but does require attention to detail in the zero sequence case. Of primary importance is the type of connection on each side of the transformer or bank.

The general forms of the per-unit sequence networks for the transformer are shown in Fig. 2.11. Notice should be taken that each transformer winding’s impedance and the shunt branch impedance are all modeled in the circuits. The sequence networks are of the presented form whether a

TABLE 2.3 Per-Unit Scaling of Sequence Network Parameters

Quantity	Base Value	Scaling Relationship		
		Zero Sequence	Positive Sequence	Negative Sequence
Voltage	Line-to-Neutral Voltage Base: $V_{LN_{base}} = \frac{V_{L_{base}}}{\sqrt{3}}$	$\bar{V}_{0_{pu}} = \frac{\bar{V}_0}{V_{LN_{base}}}$	$\bar{V}_{1_{pu}} = \frac{\bar{V}_1}{V_{LN_{base}}}$	$\bar{V}_{2_{pu}} = \frac{\bar{V}_2}{V_{LN_{base}}}$
Current	Line Current Base: $I_{L_{base}} = \frac{S_{3\phi_{base}}}{\sqrt{3}V_{L_{base}}}$	$\bar{I}_{0_{pu}} = \frac{\bar{I}_0}{I_{L_{base}}}$	$\bar{I}_{1_{pu}} = \frac{\bar{I}_1}{I_{L_{base}}}$	$\bar{I}_{2_{pu}} = \frac{\bar{I}_2}{I_{L_{base}}}$
Impedance	Y-Impedance Base: $Z_{Y_{base}} = \frac{V_{L_{base}}^2}{S_{3\phi_{base}}}$	$\bar{Z}_{00_{pu}} = \frac{Z_{00}}{Z_{Y_{base}}}$	$\bar{Z}_{11_{pu}} = \frac{Z_{11}}{Z_{Y_{base}}}$	$\bar{Z}_{22_{pu}} = \frac{Z_{22}}{Z_{Y_{base}}}$
Complex Power	Single-Phase Apparent Power Base: $S_{1\phi_{base}} = \frac{S_{3\phi_{base}}}{3}$		$\bar{S}_{1\phi_{pu}} = \frac{\bar{S}_{1\phi}}{S_{1\phi_{base}}} = \frac{\bar{S}_{3\phi}}{S_{3\phi_{base}}}$	

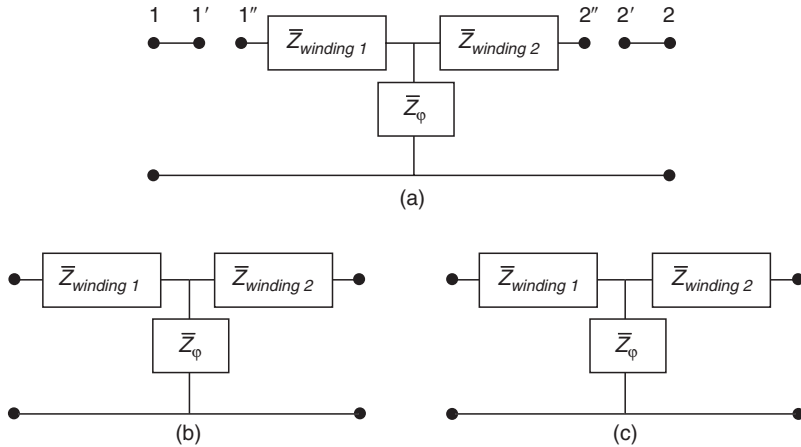


FIGURE 2.11 (a) Zero, (b) positive, and (c) negative sequence transformer networks.

three-phase transformer or a bank of three single-phase transformers is under consideration. Note that the positive and negative sequence networks are identical, and the zero sequence network requires some discussion. The “ i^{th} primed” terminals in the zero sequence network are terminated based on the type of connection that is employed for winding i . Details of the termination are presented in Table 2.4.

We must turn our attention to the calculation of the various impedances in the sequence networks as a function of the individual transformer impedances. The zero, positive, and negative sequence impedances are all equal for any transformer winding. Furthermore, the sequence impedances for any

TABLE 2.4 Power Transformer Zero Sequence Terminations

Winding “ i ” Connection	Connection of Terminals	Schematic Representation
	Leave i' and i'' unconnected.	
	Short i' to i'' .	
	Connect i' to i'' through $3\bar{Z}_n$.	
	Short i'' to reference.	

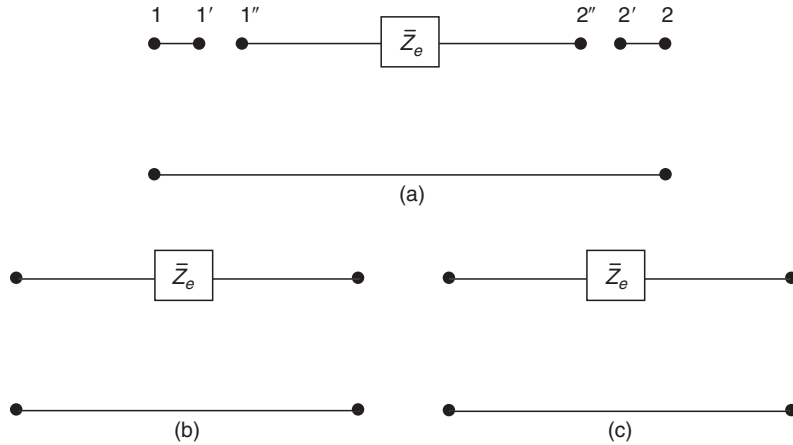


FIGURE 2.12 Reduced (a) zero, (b) positive, and (c) Negative sequence transformer networks.

transformer winding are equal to the winding impedance expressed in per-unit on the system (not device) ratings. This is independent of the winding connection (Y or Δ), because of the per-unit scaling. If the sequence networks are to be drawn in SI units, then the sequence impedances for a Δ connection would be $1/3$ of the transformer winding impedance. In the case of a three-phase transformer, where the phases may share a common magnetic path, the zero sequence impedance will be different from the positive and negative sequence impedances (Gross, 1986; Blackburn, 1993).

In many cases, a single equivalent impedance is provided on a transformer nameplate. Utilization of this value as a single impedance for the circuit model requires neglecting the shunt branch impedance, which is often justified. If open-circuit test data is not available, or just for the sake of simplicity, the shunt branch of the transformers may be neglected. This leads to the sequence networks illustrated in Fig. 2.12. Here again, care must be taken to place the equivalent transformer impedance in per-unit on the appropriate system bases. Derivation of the equivalent transformer impedance is most appropriately performed in a study focused on power transformers (Gross, 1986; Blackburn, 1993).

Example 2.3

Consider the simple power system, operating with positive phase sequence, described by the one-line diagram presented in Fig. 2.13. Compute the line voltage at bus 1, and draw the zero sequence network.

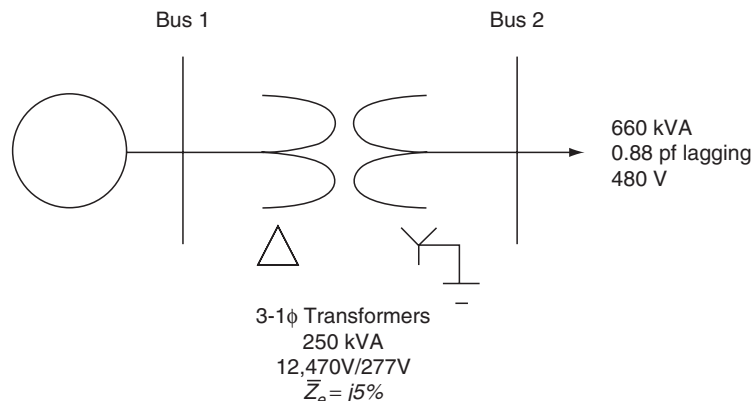


FIGURE 2.13 Power system with a transformer for Example 2.3.

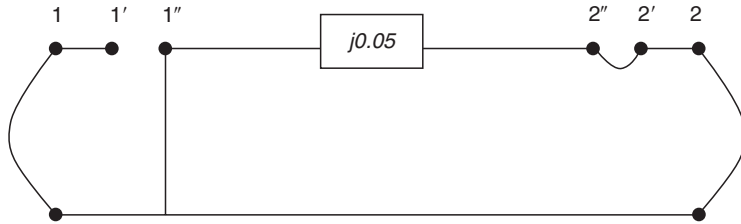


FIGURE 2.14 Zero sequence network for Example 2.3.

Solution

We begin by selecting system bases. For simplicity, we choose the system bases to be equal to the transformer ratings. In other words, the system apparent power base is chosen as 750 kVA (three times the single-phase transformer kVA rating), and the line voltage bases at buses 1 and 2 are chosen as 12,470 V (delta side) and 480 V (Y side), respectively. Thus, the transformer impedance provided for the transformer is unaltered when converted to the system bases, as illustrated in Eq. (2.52).

$$\bar{Z}_e = (j0.05) \frac{Z_{transformer_{base}}}{Z_{Y_{system_{base}}}} = (j0.05) \frac{\left(\frac{277^2}{250 \times 10^3}\right)}{\left(\frac{480^2}{750 \times 10^3}\right)} = j0.05 \quad (2.52)$$

Since balanced conditions are enforced, the load is a non-zero complex power in only the positive sequence network. The positive sequence load value is the single-phase load complex power. In per-unit, the three-phase and single-phase complex powers are equal, as indicated in Eq. (2.53).

$$\bar{S}_{1_{pu}} = \bar{S}_{1\phi_{pu}} = \bar{S}_{3\phi_{pu}} = \frac{\bar{S}_{3\phi}}{S_{3\phi_{base}}} = \frac{666/28.4^\circ}{750} = 0.88/28.4^\circ \quad (2.53)$$

The positive sequence load voltage is the a-phase line-to-neutral voltage at bus 2. If we assume this to be the reference voltage with a zero degree phase angle, then we get $277/0^\circ$ V. In per-unit, this corresponds to unity voltage.

The zero and positive sequence networks are provided in Figs. 2.14 and 2.15, respectively. The line voltage at bus 1 is found by solution of the positive sequence network. The load current is computed from the load voltage and complex power in Eq. (2.54). The positive sequence per-unit voltage at bus 1 is computed in Eq. (2.55). The line voltage at bus 1 is computed from the bus 1 positive sequence voltage in Eq. (2.56). The positive sequence voltage magnitude at bus 1 is the per-unit line-to-neutral voltage magnitude at bus 1. In per-unit, the line and line-to-neutral voltages are equal. Thus, multiplying the

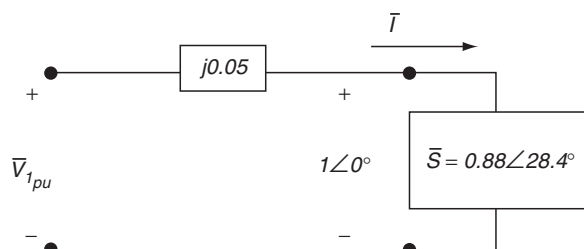


FIGURE 2.15 Positive sequence network for Example 2.3.

per-unit positive sequence voltage magnitude at bus 1 by the line voltage base at bus 1 produces the line voltage at bus 1.

$$\bar{I} = \left(\frac{0.88\angle 28.4^\circ}{1\angle 0^\circ} \right) = 0.88\angle -28.4^\circ \quad (2.54)$$

$$\bar{V}_{1_{pu}} = 1\angle 0^\circ + (0.88\angle -28.4^\circ)(j0.05) = 1.02\angle 2.2^\circ \quad (2.55)$$

$$V_L = |\bar{V}_{1_{pu}}| V_{L_{base}}(\text{bus1}) = 1.02(12,470) = 12,719 \text{ V} \quad (2.56)$$

References

- Blackburn, J.L., *Symmetrical Components for Power Systems Engineering*, Marcel Dekker, New York, 1993.
- Brogan, W.L., *Modern Control Theory*, Quantum Publishers, Inc., New York, 1974.
- Fortescue, C.L., Method of Symmetrical Coordinates Applied to the Solution of Polyphase Networks, *AIEE Transaction*, 37, part 2, 1918.
- Glover, J.D. and Sarma, M., *Power System Analysis and Design*, PWS-Kent Publishing Company, Boston, MA, 1989.
- Grainger, J.J. and Stevenson, Jr., W.D., *Power System Analysis*, McGraw-Hill, Inc., New York, 1994.
- Gross, C.A., *Power System Analysis*, 2nd ed., New York, John Wiley & Sons, New York, 1986.
- Irwin, J.D., *Basic Engineering Circuit Analysis*, 5th ed., Prentice-Hall, New Jersey, 1996.
- Krause, P.C., *Analysis of Electric Machinery*, McGraw-Hill, New York, 1986.
- Kundur, P., *Power System Stability and Control*, McGraw-Hill, Inc., New York, 1994.

3

Power Flow Analysis

Leonard L. Grigsby
Auburn University

Andrew P. Hanson
PowerComm Engineering

3.1	Introduction.....	3-1
3.2	Power Flow Problem	3-1
3.3	Formulation of Bus Admittance Matrix.....	3-3
3.4	Formulation of Power Flow Equations	3-3
3.5	P - V Buses.....	3-6
3.6	Bus Classifications	3-6
3.7	Generalized Power Flow Development.....	3-7
	Basic Power Flow Equations	
3.8	Solution Methods.....	3-7
	Newton–Raphson Method • Fast Decoupled	
	Power Flow Solution	
3.9	Component Power Flows.....	3-10

3.1 Introduction

The equivalent circuit parameters of many power system components are described in other sections of this handbook. The interconnection of the different elements allows development of an overall power system model. The system model provides the basis for computational simulation of the system performance under a wide variety of projected operating conditions. Additionally, “post mortem” studies, performed after system disturbances or equipment failures, often provide valuable insight into contributing system conditions. This chapter discusses one such computational simulation, the power flow problem.

Power systems typically operate under slowly changing conditions, which can be analyzed using steady-state analysis. Further, transmission systems operate under balanced or near-balanced conditions allowing per-phase analysis to be used with a high degree of confidence in the solution. Power flow analysis provides the starting point for most other analyses. For example, the small signal and transient stability effects of a given disturbance are dramatically affected by the “pre-disturbance” operating conditions of the power system. (A disturbance resulting in instability under heavily loaded system conditions may not have any adverse effects under lightly loaded conditions.) Additionally, fault analysis and transient analysis can also be impacted by the pre-disturbance operating point of the power system (although, they are usually affected much less than transient stability and small signal stability analysis).

3.2 Power Flow Problem

Power flow analysis is fundamental to the study of power systems; in fact, power flow forms the core of power system analysis. A power flow study is valuable for many reasons. For example, power flow analyses play a key role in the planning of additions or expansions to transmission and generation

facilities. A power flow solution is often the starting point for many other types of power system analyses. In addition, power flow analysis and many of its extensions are an essential ingredient of the studies performed in power system operations. In this latter case, it is at the heart of contingency analysis and the implementation of real-time monitoring systems.

The power flow problem (popularly known as the load flow problem) can be stated as follows:

For a given power network, with known complex power loads and some set of specifications or restrictions on power generations and voltages, solve for any unknown bus voltages and unspecified generation and finally for the complex power flow in the network components.

Additionally, the losses in individual components and the total network as a whole are usually calculated. Furthermore, the system is often checked for component overloads and voltages outside allowable tolerances.

Balanced operation is assumed for most power flow studies and will be assumed in this chapter. Consequently, the positive sequence network is used for the analysis. In the solution of the power flow problem, the network element values are almost always taken to be in per-unit. Likewise, the calculations within the power flow analysis are typically in per-unit. However, the solution is usually expressed in a mixed format. Solution voltages are usually expressed in per-unit; powers are most often given in kVA or MVA.

The “given network” may be in the form of a system map and accompanying data tables for the network components. More often, however, the network structure is given in the form of a one-line diagram (such as shown in Fig. 3.1).

Regardless of the form of the given network and how the network data is given, the steps to be followed in a power flow study can be summarized as follows:

1. Determine element values for passive network components.
2. Determine locations and values of all complex power loads.
3. Determine generation specifications and constraints.
4. Develop a mathematical model describing power flow in the network.
5. Solve for the voltage profile of the network.

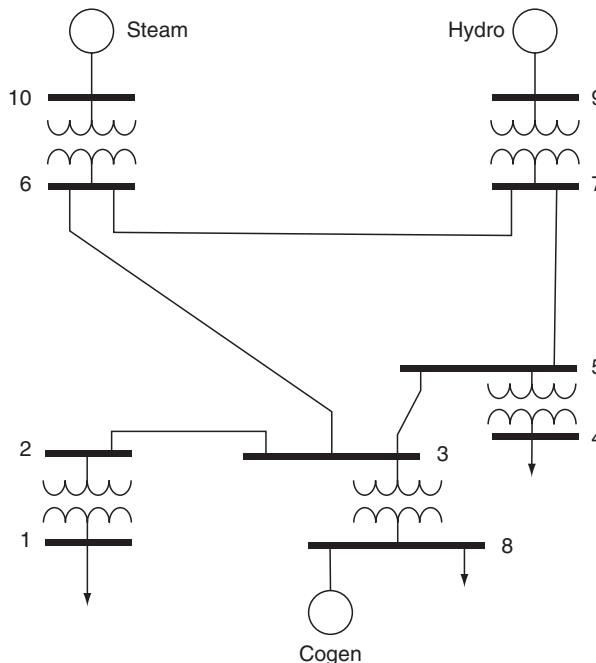


FIGURE 3.1 The one-line diagram of a power system.

6. Solve for the power flows and losses in the network.
7. Check for constraint violations.

3.3 Formulation of Bus Admittance Matrix

The first step in developing the mathematical model describing the power flow in the network is the formulation of the bus admittance matrix. The bus admittance matrix is an $n \times n$ matrix (where n is the number of buses in the system) constructed from the admittances of the equivalent circuit elements of the segments making up the power system. Most system segments are represented by a combination of shunt elements (connected between a bus and the reference node) and series elements (connected between two system buses). Formulation of the bus admittance matrix follows two simple rules:

1. The admittance of elements connected between node k and reference is added to the (k, k) entry of the admittance matrix.
2. The admittance of elements connected between nodes j and k is added to the (j, j) and (k, k) entries of the admittance matrix. The negative of the admittance is added to the (j, k) and (k, j) entries of the admittance matrix.

Off nominal transformers (transformers with transformation ratios different from the system voltage bases at the terminals) present some special difficulties. Figure 3.2 shows a representation of an off nominal turns ratio transformer.

The admittance matrix base mathematical model of an isolated off nominal transformer is

$$\begin{bmatrix} \bar{I}_j \\ \bar{I}_k \end{bmatrix} = \begin{bmatrix} \bar{Y}_e & -\bar{c}\bar{Y}_e \\ -\bar{c}^*\bar{Y}_e & |\bar{c}|^2\bar{Y}_e \end{bmatrix} \begin{bmatrix} \bar{V}_j \\ \bar{V}_k \end{bmatrix} \quad (3.1)$$

where

\bar{Y}_e is the equivalent series admittance (referred to node j)

\bar{c} is the complex (off nominal) turns ratio

\bar{I}_j is the current injected at node j

\bar{V}_j is the voltage at node j (with respect to reference)

Off nominal transformers are added to the bus admittance matrix by adding the corresponding entry of the isolated off nominal transformer admittance matrix to the system bus admittance matrix.

3.4 Formulation of Power Flow Equations

Considerable insight into the power flow problem and its properties and characteristics can be obtained by consideration of a simple example before proceeding to a general formulation of the problem. This simple case will also serve to establish some notation.

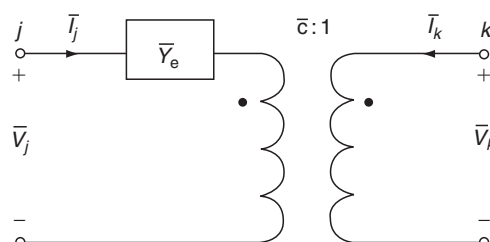


FIGURE 3.2 Off nominal turns ratio transformer.

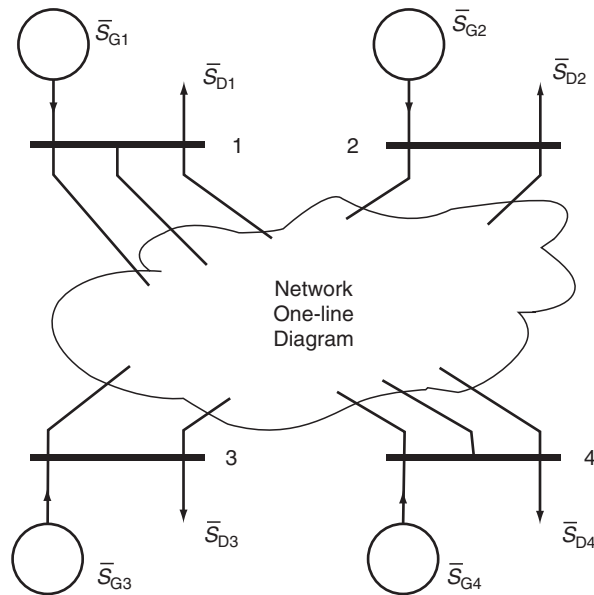


FIGURE 3.3 Conceptual one-line diagram of a four-bus power system.

A conceptual representation of a one-line diagram for a four-bus power system is shown in Fig. 3.3. For generality, we have shown a generator and a load connected to each bus. The following notation applies:

\bar{S}_{G1} = Complex power flow into bus 1 from the generator

\bar{S}_{D1} = Complex power flow into the load from bus 1

Comparable quantities for the complex power generations and loads are obvious for each of the three other buses.

The positive sequence network for the power system represented by the one-line diagram of Fig. 3.3 is shown in Fig. 3.4. The boxes symbolize the combination of generation and load. Network texts refer to

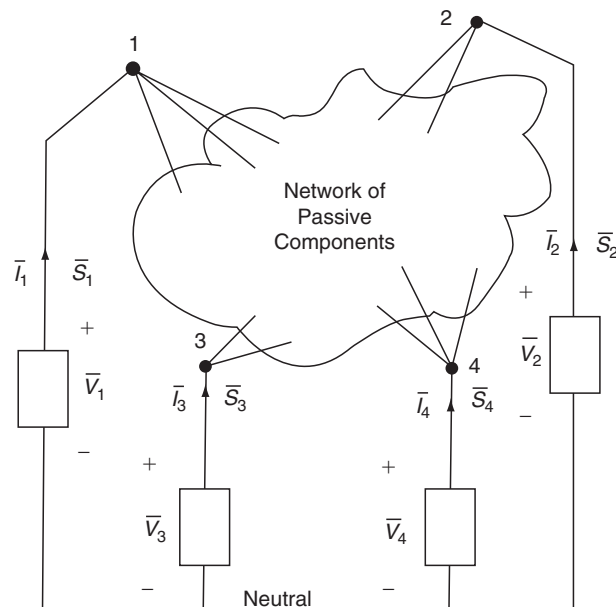


FIGURE 3.4 Positive sequence network for the system of Fig. 3.3.

this network as a five-node network. (The balanced nature of the system allows analysis using only the positive sequence network; reducing each three-phase bus to a single node. The reference or ground represents the fifth node.) However, in power systems literature it is usually referred to as a four-bus network or power system.

For the network of Fig. 3.4, we define the following additional notation:

$$\bar{S}_1 = \bar{S}_{G1} - \bar{S}_{D1} = \text{Net complex power injected at bus 1}$$

$$\bar{I}_1 = \text{Net positive sequence phasor current injected at bus 1}$$

$$\bar{V}_1 = \text{Positive sequence phasor voltage at bus 1}$$

The standard node voltage equations for the network can be written in terms of the quantities at bus 1 (defined above) and comparable quantities at the other buses:

$$\bar{I}_1 = \bar{Y}_{11}\bar{V}_1 + \bar{Y}_{12}\bar{V}_2 + \bar{Y}_{13}\bar{V}_3 + \bar{Y}_{14}\bar{V}_4 \quad (3.2)$$

$$\bar{I}_2 = \bar{Y}_{21}\bar{V}_1 + \bar{Y}_{22}\bar{V}_2 + \bar{Y}_{23}\bar{V}_3 + \bar{Y}_{24}\bar{V}_4 \quad (3.3)$$

$$\bar{I}_3 = \bar{Y}_{31}\bar{V}_1 + \bar{Y}_{32}\bar{V}_2 + \bar{Y}_{33}\bar{V}_3 + \bar{Y}_{34}\bar{V}_4 \quad (3.4)$$

$$\bar{I}_4 = \bar{Y}_{41}\bar{V}_1 + \bar{Y}_{42}\bar{V}_2 + \bar{Y}_{43}\bar{V}_3 + \bar{Y}_{44}\bar{V}_4 \quad (3.5)$$

The admittances in Eqs. (3.2)–(3.5), \bar{Y}_{ij} are the ij th entries of the bus admittance matrix for the power system. The unknown voltages could be found using linear algebra if the four currents $\bar{I}_1 \cdots \bar{I}_4$ were known. However, these currents are not known. Rather, something is known about the complex power and voltage, at each bus. The complex power injected into bus k of the power system is defined by the relationship between complex power, voltage, and current given by the following equation:

$$\bar{S}_k = \bar{V}_k \bar{I}_k^* \quad (3.6)$$

Therefore,

$$\bar{I}_k = \frac{\bar{S}_k^*}{\bar{V}_k^*} = \frac{\bar{S}_{Gk}^* - \bar{S}_{Dk}^*}{\bar{V}_k^*} \quad (3.7)$$

By substituting this result into the nodal equations and rearranging, the basic power flow equations (PFE) for the four-bus system are given as follows:

$$\bar{S}_{G1}^* - \bar{S}_{D1}^* = \bar{V}_1^* [\bar{Y}_{11}\bar{V}_1 + \bar{Y}_{12}\bar{V}_2 + \bar{Y}_{13}\bar{V}_3 + \bar{Y}_{14}\bar{V}_4] \quad (3.8)$$

$$\bar{S}_{G2}^* - \bar{S}_{D2}^* = \bar{V}_2^* [\bar{Y}_{21}\bar{V}_1 + \bar{Y}_{22}\bar{V}_2 + \bar{Y}_{23}\bar{V}_3 + \bar{Y}_{24}\bar{V}_4] \quad (3.9)$$

$$\bar{S}_{G3}^* - \bar{S}_{D3}^* = \bar{V}_3^* [\bar{Y}_{31}\bar{V}_1 + \bar{Y}_{32}\bar{V}_2 + \bar{Y}_{33}\bar{V}_3 + \bar{Y}_{34}\bar{V}_4] \quad (3.10)$$

$$\bar{S}_{G4}^* - \bar{S}_{D4}^* = \bar{V}_4^* [\bar{Y}_{41}\bar{V}_1 + \bar{Y}_{42}\bar{V}_2 + \bar{Y}_{43}\bar{V}_3 + \bar{Y}_{44}\bar{V}_4] \quad (3.11)$$

Examination of Eqs. (3.8)–(3.11) reveals that except for the trivial case where the generation equals the load at every bus, the complex power outputs of the generators cannot be arbitrarily selected. In fact, the complex power output of at least one of the generators must be calculated last since it must take up the unknown “slack” due to the, as yet, uncalculated network losses. Further, losses cannot be calculated until the voltages are known. These observations are the result of the principle of conservation of complex power (i.e., the sum of the injected complex powers at the four system buses is equal to the system complex power losses).

Further examination of Eqs. (3.8)–(3.11) indicates that it is not possible to solve these equations for the absolute phase angles of the phasor voltages. This simply means that the problem can only be solved to some arbitrary phase angle reference.

In order to alleviate the dilemma outlined above, suppose \bar{S}_{G4} is arbitrarily allowed to float or swing (in order to take up the necessary slack caused by the losses) and that \bar{S}_{G1} , \bar{S}_{G2} , and \bar{S}_{G3} are specified

(other cases will be considered shortly). Now, with the loads known, Eqs. (3.8)–(3.11) are seen as four simultaneous nonlinear equations with complex coefficients in five unknowns \bar{V}_1 , \bar{V}_2 , \bar{V}_3 , \bar{V}_4 , and \bar{S}_{G4} .

The problem of too many unknowns (which would result in an infinite number of solutions) is solved by specifying another variable. Designating bus 4 as the slack bus and specifying the voltage \bar{V}_4 reduces the problem to four equations in four unknowns. The slack bus is chosen as the phase reference for all phasor calculations, its magnitude is constrained, and the complex power generation at this bus is free to take up the slack necessary in order to account for the system real and reactive power losses.

The specification of the voltage \bar{V}_4 decouples Eq. (3.11) from Eqs. (3.8)–(3.10), allowing calculation of the slack bus complex power after solving the remaining equations. (This property carries over to larger systems with any number of buses.) The example problem is reduced to solving only three equations simultaneously for the unknowns \bar{V}_1 , \bar{V}_2 , and \bar{V}_3 . Similarly, for the case of n buses it is necessary to solve $n - 1$ simultaneous, complex coefficient, nonlinear equations.

Systems of nonlinear equations, such as Eqs. (3.8)–(3.10), cannot (except in rare cases) be solved by closed-form techniques. Direct simulation was used extensively for many years; however, essentially all power flow analyses today are performed using iterative techniques on digital computers.

3.5 P–V Buses

In all realistic cases, the voltage magnitude is specified at generator buses to take advantage of the generator's reactive power capability. Specifying the voltage magnitude at a generator bus requires a variable specified in the simple analysis discussed earlier to become an unknown (in order to bring the number of unknowns back into correspondence with the number of equations). Normally, the reactive power injected by the generator becomes a variable, leaving the real power and voltage magnitude as the specified quantities at the generator bus.

It was noted earlier that Eq. (3.11) is decoupled and only Eqs. (3.8)–(3.10) need be solved simultaneously. Although not immediately apparent, specifying the voltage magnitude at a bus and treating the bus reactive power injection as a variable result in retention of, effectively, the same number of complex unknowns. For example, if the voltage magnitude of bus 1 of the earlier four-bus system is specified and the reactive power injection at bus 1 becomes a variable, Eqs. (3.8)–(3.10) again effectively have three complex unknowns. (The phasor voltages \bar{V}_2 and \bar{V}_3 at buses 2 and 3 are two complex unknowns and the angle δ_1 of the voltage at bus 1 plus the reactive power generation Q_{G1} at bus 1 result in the equivalent of a third complex unknown.)

Bus 1 is called a *voltage controlled bus*, since it is apparent that the reactive power generation at bus 1 is being used to control the voltage magnitude. This type of bus is also referred to as a *P–V* bus because of the specified quantities. Typically, all generator buses are treated as voltage controlled buses.

3.6 Bus Classifications

There are four quantities of interest associated with each bus:

1. Real power, P
2. Reactive power, Q
3. Voltage magnitude, V
4. Voltage angle, δ

At every bus of the system two of these four quantities will be specified and the remaining two will be unknowns. Each of the system buses may be classified in accordance with which of the two quantities are specified. The following classifications are typical:

Slack bus—The slack bus for the system is a single bus for which the voltage magnitude and angle are specified. The real and reactive power are unknowns. The bus selected as the slack bus must have a source of both real and reactive power, since the injected power at this bus must “swing” to take up the

“slack” in the solution. The best choice for the slack bus (since, in most power systems, many buses have real and reactive power sources) requires experience with the particular system under study. The behavior of the solution is often influenced by the bus chosen. (In the earlier discussion, the last bus was selected as the slack bus for convenience.)

Load bus (P–Q bus)—A load bus is defined as any bus of the system for which the real and reactive powers are specified. Load buses may contain generators with specified real and reactive power outputs; however, it is often convenient to designate any bus with specified injected complex power as a load bus.

Voltage-controlled bus (P–V bus)—Any bus for which the voltage magnitude and the injected real power are specified is classified as a voltage controlled (or P–V) bus. The injected reactive power is a variable (with specified upper and lower bounds) in the power flow analysis. (A P–V bus must have a variable source of reactive power such as a generator or a capacitor bank.)

3.7 Generalized Power Flow Development

The more general (n bus) case is developed by extending the results of the simple four-bus example. Consider the case of an n -bus system and the corresponding $n + 1$ node positive sequence network. Assume that the buses are numbered such that the slack bus is numbered last. Direct extension of the earlier equations (writing the node voltage equations and making the same substitutions as in the four-bus case) yields the basic power flow equations in the general form.

3.7.1 Basic Power Flow Equations

$$\bar{S}_k^* = P_k - jQ_k = \bar{V}_k^* \sum_{i=1}^n \bar{Y}_{ki} \bar{V}_i \quad (3.12)$$

for $k = 1, 2, 3, \dots, n - 1$

and

$$P_n - jQ_n = \bar{V}_n^* \sum_{i=1}^n \bar{Y}_{ni} \bar{V}_i \quad (3.13)$$

Equation (3.13) is the equation for the slack bus. Equation (3.12) represents $n - 1$ simultaneous equations in $n - 1$ complex unknowns if all buses (other than the slack bus) are classified as load buses. Thus, given a set of specified loads, the problem is to solve Eq. (3.12) for the $n - 1$ complex phasor voltages at the remaining buses. Once the bus voltages are known, Eq. (3.13) can be used to calculate the slack bus power.

Bus j is normally treated as a P–V bus if it has a directly connected generator. The unknowns at bus j are then the reactive generation Q_{Gj} and δ_j , because the voltage magnitude, V_j , and the real power generation, P_{Gj} , have been specified.

The next step in the analysis is to solve Eq. (3.12) for the bus voltages using some iterative method. Once the bus voltages have been found, the complex power flows and complex power losses in all of the network components are calculated.

3.8 Solution Methods

The solution of the simultaneous nonlinear power flow equations requires the use of iterative techniques for even the simplest power systems. Although there are many methods for solving nonlinear equations, only two methods are discussed here.

3.8.1 Newton–Raphson Method

The Newton–Raphson algorithm has been applied in the solution of nonlinear equations in many fields. The algorithm will be developed using a general set of two equations (for simplicity). The results are easily extended to an arbitrary number of equations.

A set of two nonlinear equations are shown in the following equations:

$$f_1(x_1, x_2) = k_1 \quad (3.14)$$

$$f_2(x_1, x_2) = k_2 \quad (3.15)$$

Now, if $x_1^{(0)}$ and $x_2^{(0)}$ are inexact solution estimates and $\Delta x_1^{(0)}$ and $\Delta x_2^{(0)}$ are the corrections to the estimates to achieve an exact solution, Eqs. (3.14) and (3.15) can be rewritten as:

$$f_1(x_1^{(0)} + \Delta x_1^{(0)}, x_2^{(0)} + \Delta x_2^{(0)}) = k_1 \quad (3.16)$$

$$f_2(x_1^{(0)} + \Delta x_1^{(0)}, x_2^{(0)} + \Delta x_2^{(0)}) = k_2 \quad (3.17)$$

Expanding Eqs. (3.16) and (3.17) in a Taylor series about the estimate yields:

$$f_1\left(x_1^{(0)}, x_2^{(0)}\right) + \frac{\partial f_1}{\partial x_1}\Big|^{(0)} \Delta x_1^{(0)} + \frac{\partial f_1}{\partial x_2}\Big|^{(0)} \Delta x_2^{(0)} + \text{h.o.t.} = k_1 \quad (3.18)$$

$$f_2\left(x_1^{(0)}, x_2^{(0)}\right) + \frac{\partial f_2}{\partial x_1}\Big|^{(0)} \Delta x_1^{(0)} + \frac{\partial f_2}{\partial x_2}\Big|^{(0)} \Delta x_2^{(0)} + \text{h.o.t.} = k_2 \quad (3.19)$$

where the subscript, (0), on the partial derivatives indicates evaluation of the partial derivatives at the initial estimate and h.o.t. indicates the higher-order terms.

Neglecting the higher-order terms (an acceptable approximation if $\Delta x_1^{(0)}$ and $\Delta x_2^{(0)}$ are small) Eqs. (3.18) and (3.19) can be rearranged and written in matrix form:

$$\begin{bmatrix} \frac{\partial f_1}{\partial x_1}\Big|^{(0)} & \frac{\partial f_1}{\partial x_2}\Big|^{(0)} \\ \frac{\partial f_2}{\partial x_1}\Big|^{(0)} & \frac{\partial f_2}{\partial x_2}\Big|^{(0)} \end{bmatrix} \begin{bmatrix} \Delta x_1^{(0)} \\ \Delta x_2^{(0)} \end{bmatrix} \approx \begin{bmatrix} k_1 - f_1(x_1^{(0)}, x_2^{(0)}) \\ k_2 - f_2(x_1^{(0)}, x_2^{(0)}) \end{bmatrix} \quad (3.20)$$

The matrix of partial derivatives in Eq. (3.20) is known as the Jacobian matrix and is evaluated at the initial estimate. Multiplying each side of Eq. (3.20) by the inverse of the Jacobian matrix yields an approximation of the required correction to the estimated solution. Since the higher-order terms were neglected, addition of the correction terms to the original estimate will not yield an exact solution, but will often provide an improved estimate. The procedure may be repeated, obtaining successively better estimates until the estimated solution reaches a desired tolerance. Summarizing, correction terms for the ℓ th iterate are given in Eq. (3.21) and the solution estimate is updated according to Eq. (3.22):

$$\begin{bmatrix} \Delta x_1^{(\ell)} \\ \Delta x_2^{(\ell)} \end{bmatrix} = \begin{bmatrix} \frac{\partial f_1}{\partial x_1}\Big|^{(\ell)} & \frac{\partial f_1}{\partial x_2}\Big|^{(\ell)} \\ \frac{\partial f_2}{\partial x_1}\Big|^{(\ell)} & \frac{\partial f_2}{\partial x_2}\Big|^{(\ell)} \end{bmatrix}^{-1} \begin{bmatrix} k_1 - f_1(x_1^{(\ell)}, x_2^{(\ell)}) \\ k_2 - f_2(x_1^{(\ell)}, x_2^{(\ell)}) \end{bmatrix} \quad (3.21)$$

$$x^{(\ell+1)} = x^{(\ell)} + \Delta x^{(\ell)} \quad (3.22)$$

The solution of the original set of nonlinear equations has been converted to a repeated solution of a system of linear equations. This solution requires evaluation of the Jacobian matrix (at the current solution estimate) in each iteration.

The power flow equations can be placed into the Newton–Raphson framework by separating the power flow equations into their real and imaginary parts and taking the voltage magnitudes and phase angles as the unknowns. Writing Eq. (3.21) specifically for the power flow problem:

$$\begin{bmatrix} \Delta\underline{\delta}^{(\ell)} \\ \Delta\underline{V}^{(\ell)} \end{bmatrix} = \begin{bmatrix} \frac{\partial P}{\partial \underline{\delta}} \Big|^{(\ell)} & \frac{\partial P}{\partial \underline{V}} \Big|^{(\ell)} \\ \frac{\partial Q}{\partial \underline{\delta}} \Big|^{(\ell)} & \frac{\partial Q}{\partial \underline{V}} \Big|^{(\ell)} \end{bmatrix}^{-1} \begin{bmatrix} \underline{P}(\text{sched}) - \underline{P}^{(\ell)} \\ \underline{Q}(\text{sched}) - \underline{Q}^{(\ell)} \end{bmatrix} \quad (3.23)$$

The underscored variables in Eq. (3.23) indicate vectors (extending the two equation Newton–Raphson development to the general power flow case). The (sched) notation indicates the scheduled real and reactive powers injected into the system. $P^{(\ell)}$ and $Q^{(\ell)}$ represent the calculated real and reactive power injections based on the system model and the ℓ th voltage phase angle and voltage magnitude estimates. The bus voltage phase angle and bus voltage magnitude estimates are updated, the Jacobian reevaluated, and the mismatch between the scheduled and calculated real and reactive powers evaluated in each iteration of the Newton–Raphson algorithm. Iterations are performed until the estimated solution reaches an acceptable tolerance or a maximum number of allowable iterations is exceeded. Once a solution (within an acceptable tolerance) is reached, P – V bus reactive power injections and the slack bus complex power injection may be evaluated.

3.8.2 Fast Decoupled Power Flow Solution

The fast decoupled power flow algorithm simplifies the procedure presented for the Newton–Raphson algorithm by exploiting the strong coupling between real power and bus voltage phase angles and reactive power and bus voltage magnitudes commonly seen in power systems. The Jacobian matrix is simplified by approximating as zero the partial derivatives of the real power equations with respect to the bus voltage magnitudes. Similarly, the partial derivatives of the reactive power equations with respect to the bus voltage phase angles are approximated as zero. Further, the remaining partial derivatives are often approximated using only the imaginary portion of the bus admittance matrix. These approximations yield the following correction equations:

$$\Delta\underline{\delta}^{(\ell)} = [B']^{-1} [\underline{P}(\text{sched}) - \underline{P}^{(\ell)}] \quad (3.24)$$

$$\Delta\underline{V}^{(\ell)} = [B'']^{-1} [\underline{Q}(\text{sched}) - \underline{Q}^{(\ell)}] \quad (3.25)$$

where B' is an approximation of the matrix of partial derivatives of the real power flow equations with respect to the bus voltage phase angles and B'' is an approximation of the matrix of partial derivatives of the reactive power flow equations with respect to the bus voltage magnitudes. B' and B'' are typically held constant during the iterative process, eliminating the necessity of updating the Jacobian matrix (required in the Newton–Raphson solution) in each iteration.

The fast decoupled algorithm has good convergence properties despite the many approximations used during its development. The fast decoupled power flow algorithm has found widespread use, since it is less computationally intensive (requires fewer computational operations) than the Newton–Raphson method.

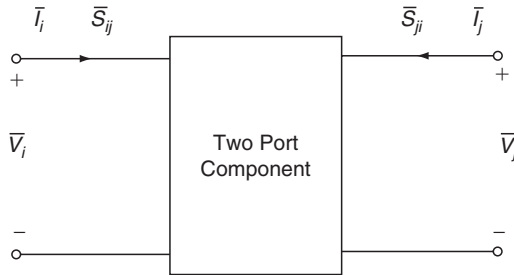


FIGURE 3.5 Typical power system component.

3.9 Component Power Flows

The positive sequence network for components of interest (connected between buses i and j) will be of the form shown in Fig. 3.5.

An admittance description is usually available from earlier construction of the nodal admittance matrix. Thus,

$$\begin{bmatrix} \bar{I}_i \\ \bar{I}_j \end{bmatrix} = \begin{bmatrix} \bar{Y}_a & \bar{Y}_b \\ \bar{Y}_c & \bar{Y}_d \end{bmatrix} \begin{bmatrix} \bar{V}_i \\ \bar{V}_j \end{bmatrix} \quad (3.26)$$

Therefore the complex power flows and the component loss are

$$\bar{S}_{ij} = \bar{V}_i \bar{I}_i^* = \bar{V}_i [\bar{Y}_a \bar{V}_i + \bar{Y}_b \bar{V}_j]^* \quad (3.27)$$

$$\bar{S}_{ji} = \bar{V}_j \bar{I}_j^* = \bar{V}_j [\bar{Y}_c \bar{V}_i + \bar{Y}_d \bar{V}_j]^* \quad (3.28)$$

$$\bar{S}_{\text{loss}} = \bar{S}_{ij} + \bar{S}_{ji} \quad (3.29)$$

The calculated component flows combined with the bus voltage magnitudes and phase angles provide extensive information about the power systems operating point. The bus voltage magnitudes may be checked to ensure operation within a prescribed range. The segment power flows can be examined to ensure no equipment ratings are exceeded. Additionally, the power flow solution may be used as the starting point for other analyses.

An elementary discussion of the power flow problem and its solution is presented in this section. The power flow problem can be complicated by the addition of further constraints such as generator real and reactive power limits. However, discussion of such complications is beyond the scope of this chapter. The references provide detailed development of power flow formulation and solution under additional constraints. The references also provide some background in the other types of power system analysis.

References

- Bergen, A.R. and Vital, V., *Power Systems Analysis*, 2nd ed., Prentice-Hall, Inc., Englewood Cliffs, NJ, 2000.
- Elgerd, O.I., *Electric Energy Systems Theory—An Introduction*, 2nd ed., McGraw-Hill, New York, NY, 1982.
- Glover, J.D. and Sarma, M., *Power System Analysis and Design*, 3rd ed., Brooks/Cole, Pacific Grove, CA, 2002.
- Grainger, J.J. and Stevenson, W.D., *Elements of Power System Analysis*, McGraw-Hill, New York, 1994.
- Gross, C.A. *Power System Analysis*, 2nd ed., John Wiley & Sons, New York, 1986.

Further Information

The references provide clear introductions to the analysis of power systems. An excellent review of many issues involving the use of computers for power system analysis is provided in July 1974, *Proceedings of the IEEE* (Special Issue on Computers in the Power Industry). The quarterly journal *IEEE Transactions on Power Systems* provides excellent documentation of more recent research in power system analysis.

4

Fault Analysis in Power Systems

4.1	Simplifications in the System Model.....	4-2
4.2	The Four Basic Fault Types..... The Balanced Three-Phase Fault • The Single Phase-to-Ground Fault • The Phase-to-Phase Fault • The Double Phase-to-Ground Fault	4-4
4.3	An Example Fault Study..... Balanced Three-Phase Fault • Single Phase-to-Ground Fault	4-7
4.4	Further Considerations.....	4-14
4.5	Summary.....	4-15
4.6	Defining Terms	4-16

Charles A. Gross
Auburn University

A **fault** in an electrical power system is the unintentional and undesirable creation of a conducting path (a *short circuit*) or a blockage of current (an *open circuit*). The short-circuit fault is typically the most common and is usually implied when most people use the term *fault*. We restrict our comments to the short-circuit fault.

The causes of faults include lightning, wind damage, trees falling across lines, vehicles colliding with towers or poles, birds shorting out lines, aircraft colliding with lines, vandalism, small animals entering switchgear, and line breaks due to excessive ice loading. Power system faults may be categorized as one of four types: single line-to-ground, line-to-line, double line-to-ground, and balanced three-phase. The first three types constitute severe unbalanced operating conditions.

It is important to determine the values of system voltages and currents during faulted conditions so that protective devices may be set to detect and minimize their harmful effects. The time constants of the associated transients are such that sinusoidal steady-state methods may still be used. The method of symmetrical components is particularly suited to fault analysis.

Our objective is to understand how symmetrical components may be applied specifically to the four general fault types mentioned and how the method can be extended to any unbalanced three-phase system problem.

Note that phase values are indicated by subscripts, a , b , c ; sequence (symmetrical component) values are indicated by subscripts 0, 1, 2. The transformation is defined by

$$\begin{bmatrix} \bar{V}_a \\ \bar{V}_b \\ \bar{V} \end{bmatrix} = \begin{bmatrix} 1 & 1 & 1 \\ 1 & a^2 & a \\ 1 & a & a^2 \end{bmatrix} \begin{bmatrix} \bar{V}_0 \\ \bar{V}_1 \\ \bar{V}_2 \end{bmatrix} = [T] \begin{bmatrix} \bar{V}_0 \\ \bar{V}_1 \\ \bar{V}_2 \end{bmatrix}$$

4.1 Simplifications in the System Model

Certain simplifications are possible and usually employed in fault analysis.

- Transformer magnetizing current and core loss will be neglected.
- Line shunt capacitance is neglected.
- Sinusoidal steady-state circuit analysis techniques are used. The so-called **DC offset** is accounted for by using correction factors.
- Prefault voltage is assumed to be $1\angle 0^\circ$ per-unit. One per-unit voltage is at its nominal value prior to the application of a fault, which is reasonable. The selection of zero phase is arbitrary and convenient. Prefault load current is neglected.

For hand calculations, neglect series resistance is usually neglected (this approximation will not be necessary for a computer solution). Also, the only difference in the positive and negative sequence networks is introduced by the machine impedances. If we select the subtransient reactance X_d'' for the positive sequence reactance, the difference is slight (in fact, the two are identical for nonsalient machines). The simplification is important, since it reduces computer storage requirements by roughly one-third. Circuit models for generators, lines, and transformers are shown in Figs. 4.1, 4.2, and 4.3, respectively.

Our basic approach to the problem is to consider the general situation suggested in Fig. 4.4(a). The general terminals brought out are for purposes of external connections that will simulate faults. Note

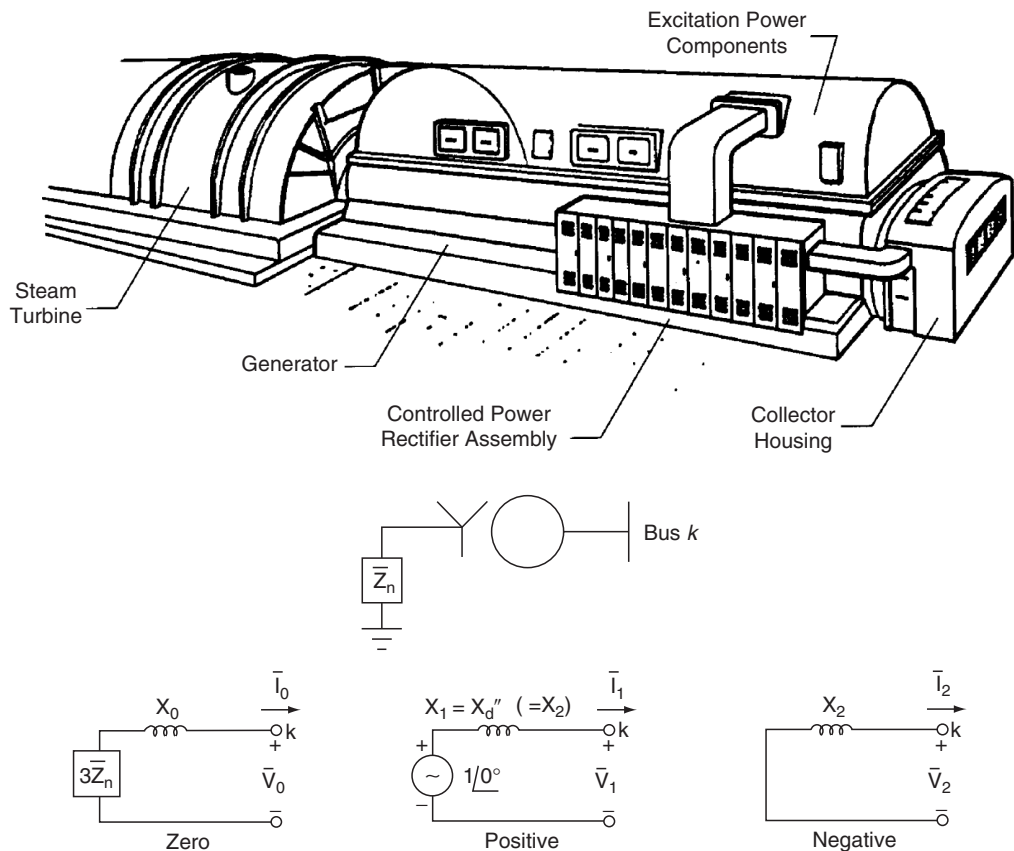


FIGURE 4.1 Generator sequence circuit models.

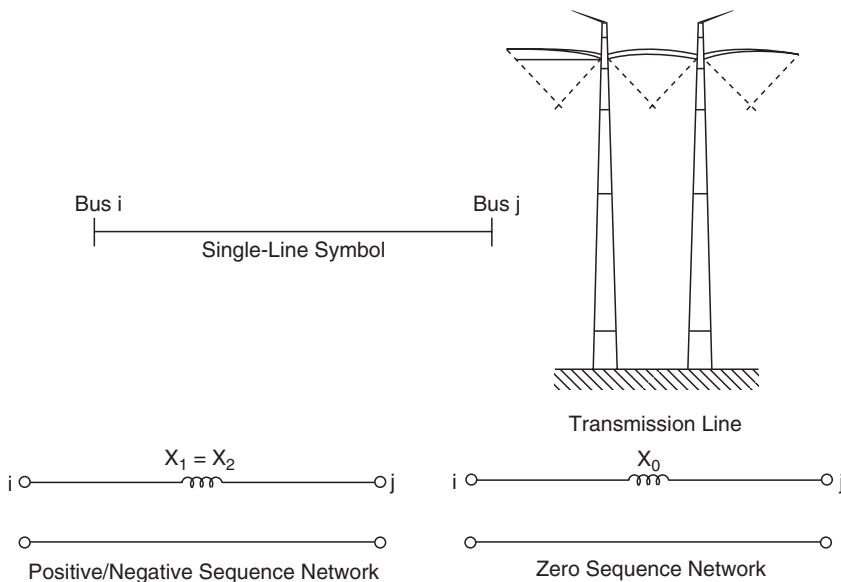


FIGURE 4.2 Line sequence circuit models.

carefully the positive assignments of phase quantities. Particularly note that the currents flow *out of* the system. We can construct general *sequence* equivalent circuits for the system, and such circuits are indicated in Fig. 4.4(b). The ports indicated correspond to the general three-phase entry port of Fig. 4.4(a). The positive sense of sequence values is compatible with that used for phase values.

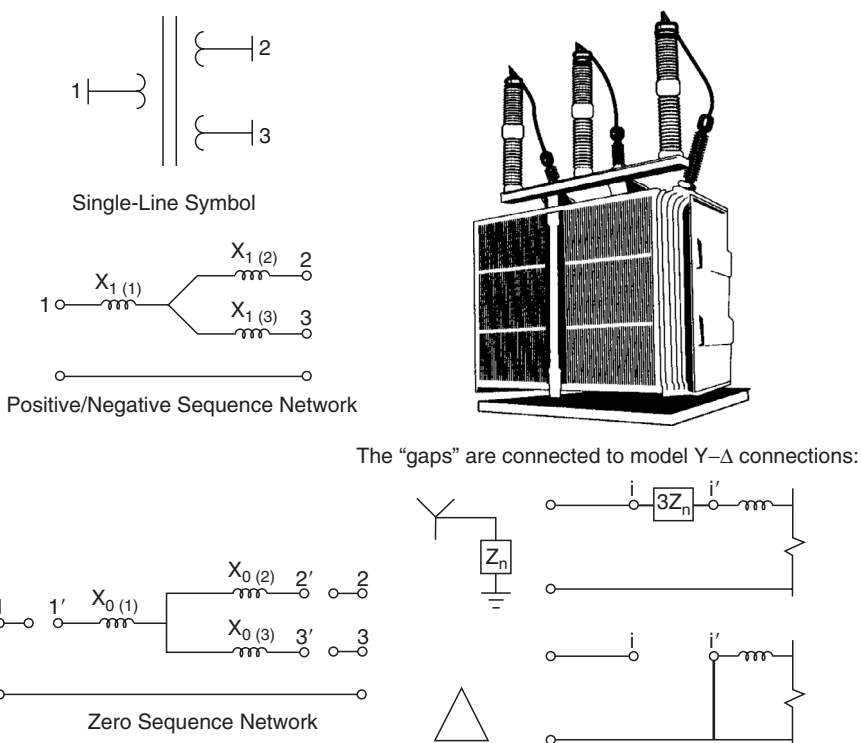


FIGURE 4.3 Transformer sequence circuit models.

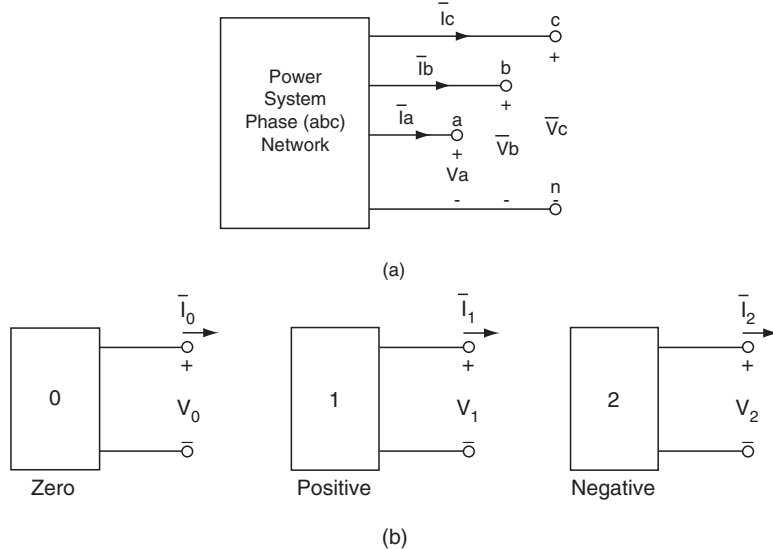


FIGURE 4.4 General fault port in an electric power system. (a) General fault port in phase (*abc*) coordinates; (b) corresponding fault ports in sequence (012) coordinates.

4.2 The Four Basic Fault Types

4.2.1 The Balanced Three-Phase Fault

Imagine the general three-phase access port terminated in a fault impedance (\bar{Z}_f) as shown in Fig. 4.5(a). The terminal conditions are

$$\begin{bmatrix} \bar{V}_a \\ \bar{V}_b \\ \bar{V}_c \end{bmatrix} = \begin{bmatrix} \bar{Z}_f & 0 & 0 \\ 0 & \bar{Z}_f & 0 \\ 0 & 0 & \bar{Z}_f \end{bmatrix} \begin{bmatrix} \bar{I}_a \\ \bar{I}_b \\ \bar{I}_c \end{bmatrix}$$

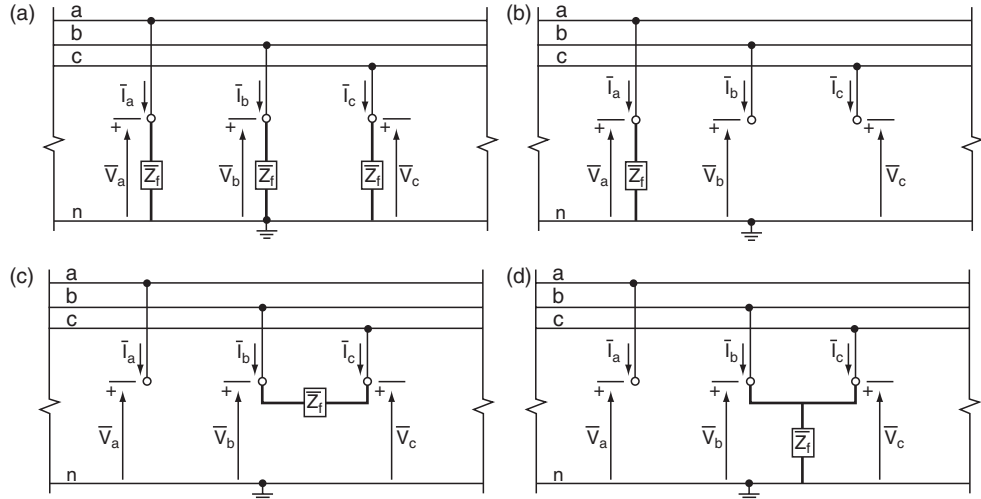


FIGURE 4.5 Fault types. (a) Three-phase fault; (b) single phase-to-ground fault; (c) phase-to-phase fault; (d) double phase-to-ground fault.

Transforming to $[Z_{012}]$,

$$[Z_{012}] = [T]^{-1} \begin{bmatrix} \bar{Z}_f & 0 & 0 \\ 0 & \bar{Z}_f & 0 \\ 0 & 0 & \bar{Z}_f \end{bmatrix} [T] = \begin{bmatrix} \bar{Z}_f & 0 & 0 \\ 0 & \bar{Z}_f & 0 \\ 0 & 0 & \bar{Z}_f \end{bmatrix}$$

The corresponding network connections are given in Fig. 4.6(a). Since the zero and negative sequence networks are passive, only the positive sequence network is nontrivial.

$$\bar{V}_0 = \bar{V}_2 = 0 \quad (4.1)$$

$$\bar{I}_0 = \bar{I}_2 = 0 \quad (4.2)$$

$$\bar{V}_1 = \bar{Z}_f \bar{I}_1 \quad (4.3)$$

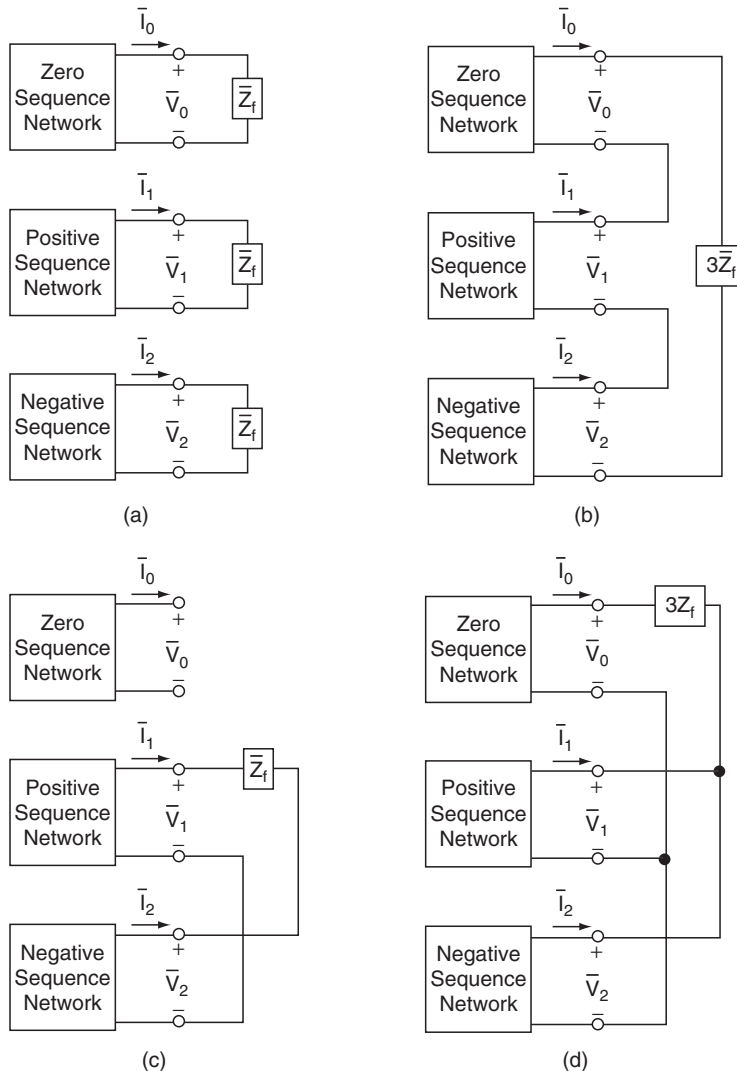


FIGURE 4.6 Sequence network terminations for fault types. (a) Balanced three-phase fault; (b) single phase-to-ground fault; (c) phase-to-phase fault; (d) double phase-to-ground fault.

4.2.2 The Single Phase-to-Ground Fault

Imagine the general three-phase access port terminated as shown in Fig. 4.5(b). The terminal conditions are

$$\bar{I}_b = 0 \quad \bar{I}_c = 0 \quad \bar{V}_a = \bar{I}_a \bar{Z}_f$$

Therefore,

$$\bar{I}_0 + a^2 \bar{I}_1 + a \bar{I}_2 = \bar{I}_0 + a \bar{I}_1 + a^2 \bar{I}_2 = 0$$

or

$$\bar{I}_1 = \bar{I}_2$$

Also,

$$\bar{I}_b = \bar{I}_0 + a^2 \bar{I}_1 + a \bar{I}_2 = \bar{I}_0 + (a^2 + a) \bar{I}_1 = 0$$

or

$$\bar{I}_0 = \bar{I}_1 = \bar{I}_2 \quad (4.2)$$

Furthermore, it is required that

$$\begin{aligned} \bar{V}_a &= \bar{Z}_f \bar{I}_a \\ \bar{V}_0 + \bar{V}_1 + \bar{V}_2 &= 3 \bar{Z}_f \bar{I}_1 \end{aligned} \quad (4.3)$$

In general then, Eqs. (4.2) and (4.3) must be simultaneously satisfied. These conditions can be met by interconnecting the sequence networks as shown in Fig. 4.6(b).

4.2.3 The Phase-to-Phase Fault

Imagine the general three-phase access port terminated as shown in Fig. 4.5(c). The terminal conditions are such that we may write

$$\bar{I}_0 = 0 \quad \bar{I}_b = -\bar{I}_c \quad \bar{V}_b = \bar{Z}_f \bar{I}_b + \bar{V}_c$$

It follows that

$$\bar{I}_0 + \bar{I}_1 + \bar{I}_2 = 0 \quad (4.4)$$

$$\bar{I}_0 = 0 \quad (4.5)$$

$$\bar{I}_1 = -\bar{I}_2 \quad (4.6)$$

In general then, Eqs. (4.4), (4.5), and (4.6) must be simultaneously satisfied. The proper interconnection between sequence networks appears in Fig. 4.6(c).

4.2.4 The Double Phase-to-Ground Fault

Consider the general three-phase access port terminated as shown in Fig. 4.5(d). The terminal conditions indicate

$$\bar{I}_a = 0 \quad \bar{V}_b = \bar{V}_c \quad \bar{V}_b = (\bar{I}_b + \bar{I}_c)\bar{Z}_f$$

It follows that

$$\bar{I}_0 + \bar{I}_1 + \bar{I}_2 = \bar{0} \quad (4.7)$$

$$\bar{V}_1 = \bar{V}_2 \quad (4.8)$$

and

$$\bar{V}_0 - \bar{V}_1 = 3\bar{Z}_f\bar{I}_0 \quad (4.9)$$

For the general double phase-to-ground fault, Eqs. (4.7), (4.8), and (4.9) must be simultaneously satisfied. The sequence network interconnections appear in Fig. 4.6(d).

4.3 An Example Fault Study

Case: EXAMPLE SYSTEM

Run:

System has data for 2 Line(s); 2 Transformer(s);
4 Bus(es); and 2 Generator(s)

Transmission Line Data

Line	Bus	Bus	Seq	R	X	B	Srat
1	2	3	pos	0.00000	0.16000	0.00000	1.0000
			zero	0.00000	0.50000	0.00000	
2	2	3	pos	0.00000	0.16000	0.00000	1.0000
			zero	0.00000	0.50000	0.00000	

Transformer Data

Transformer	HV Bus	LV Bus	Seq	R	X	C	Srat
1	2	1	pos	0.00000	0.05000	1.00000	1.0000
			zero	0.00000	0.05000		
2	3	4	pos	0.00000	0.05000	1.00000	1.0000
			zero	0.00000	0.05000		

Generator Data

No.	Bus	Rated	Ra	Xd''	Xo	Rn	Xn	Con
1	1	1.0000	0.0000	0.200	0.0500	0.0000	0.0400	Y
2	4	1.0000	0.0000	0.200	0.0500	0.0000	0.0400	Y

Zero Sequence {Z} Matrix

$0.0 + j(0.1144)$	$0.0 + j(0.0981)$	$0.0 + j(0.0163)$	$0.0 + j(0.0000)$
$0.0 + j(0.0981)$	$0.0 + j(0.1269)$	$0.0 + j(0.0212)$	$0.0 + j(0.0000)$
$0.0 + j(0.0163)$	$0.0 + j(0.0212)$	$0.0 + j(0.0452)$	$0.0 + j(0.0000)$
$0.0 + j(0.0000)$	$0.0 + j(0.0000)$	$0.0 + j(0.0000)$	$0.0 + j(0.1700)$

Positive Sequence [Z] Matrix

$0.0 + j(0.1310)$	$0.0 + j(0.1138)$	$0.0 + j(0.0862)$	$0.0 + j(0.0690)$
$0.0 + j(0.1138)$	$0.0 + j(0.1422)$	$0.0 + j(0.1078)$	$0.0 + j(0.0862)$
$0.0 + j(0.0862)$	$0.0 + j(0.1078)$	$0.0 + j(0.1422)$	$0.0 + j(0.1138)$
$0.0 + j(0.0690)$	$0.0 + j(0.0862)$	$0.0 + j(0.1138)$	$0.0 + j(0.1310)$

The single-line diagram and sequence networks are presented in Fig. 4.7.

Suppose bus 3 in the example system represents the fault location and $\bar{Z}_f = 0$. The positive sequence circuit can be reduced to its Thévenin equivalent at bus 3:

$$E_{T1} = 1.0 \angle 0^\circ \quad \bar{Z}_{T1} = j0.1422$$

Similarly, the negative and zero sequence Thévenin elements are:

$$\begin{aligned} \bar{E}_{T2} &= 0 & \bar{Z}_{T2} &= j0.1422 \\ \bar{E}_{T0} &= 0 & Z_{T0} &= j0.0452 \end{aligned}$$

The network interconnections for the four fault types are shown in Fig. 4.8. For each of the fault types, compute the currents and voltages at the faulted bus.

4.3.1 Balanced Three-Phase Fault

The sequence networks are shown in Fig. 4.8(a). Obviously,

$$\begin{aligned} \bar{V}_0 &= \bar{I}_0 = \bar{V}_2 = \bar{I}_2 = 0 \\ \bar{I}_1 &= \frac{1 \angle 0^\circ}{j0.1422} = -j7.032; \quad \text{also } \bar{V}_1 = 0 \end{aligned}$$

To compute the phase values,

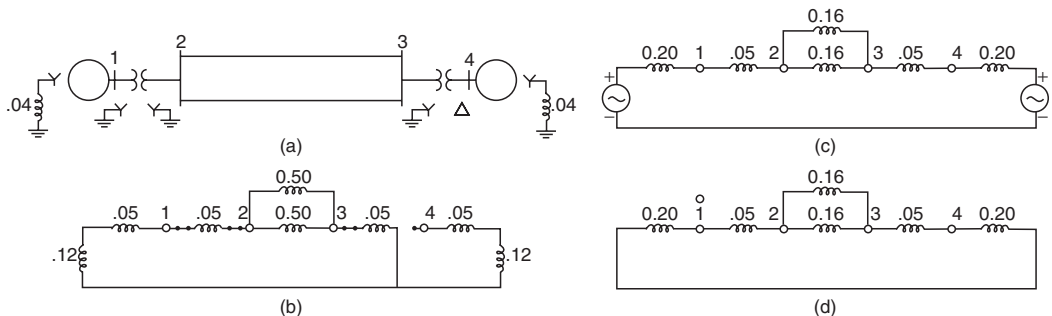


FIGURE 4.7 Example system. (a) Single-line diagram; (b) zero sequence network; (c) positive sequence network; (d) negative sequence network.

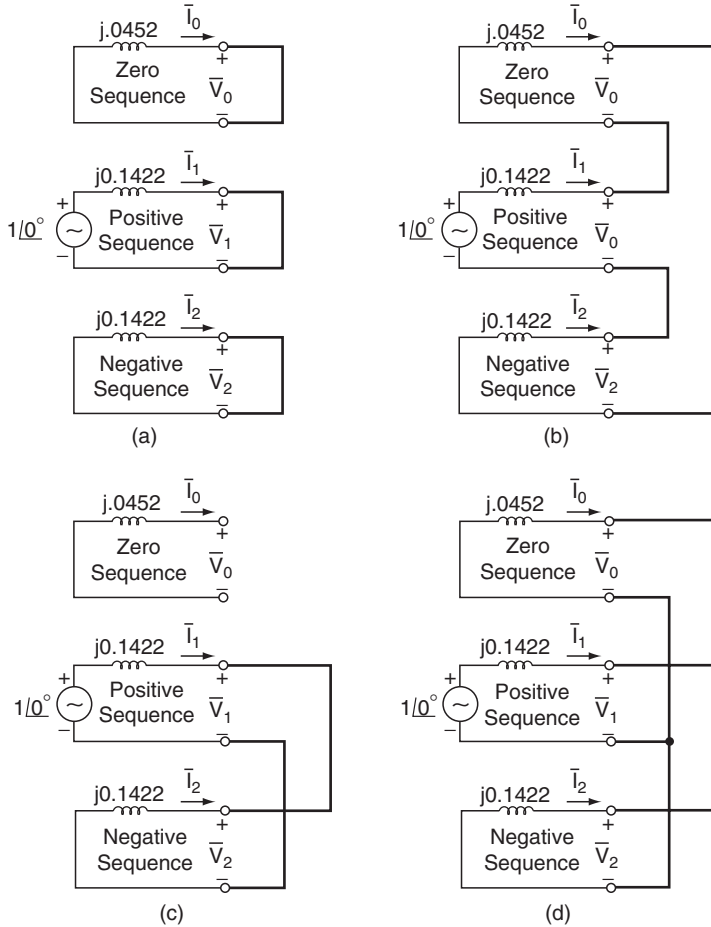


FIGURE 4.8 Example system faults at bus 3. (a) Balanced three-phase; (b) single phase-to-ground; (c) phase-to-phase; (d) double phase-to-ground.

$$\begin{bmatrix} \bar{I}_a \\ \bar{I}_b \\ \bar{I}_c \end{bmatrix} = [T] \begin{bmatrix} \bar{I}_0 \\ \bar{I}_1 \\ \bar{I}_2 \end{bmatrix} = \begin{bmatrix} 1 & 1 & 1 \\ 1 & a^2 & a \\ 1 & a & a^2 \end{bmatrix} \begin{bmatrix} 0 \\ -j7.032 \\ 0 \end{bmatrix} = \begin{bmatrix} 7.032 \angle -90^\circ \\ 7.032 \angle 150^\circ \\ 7.032 \angle 30^\circ \end{bmatrix}$$

$$\begin{bmatrix} \bar{V}_a \\ \bar{V}_b \\ \bar{V}_c \end{bmatrix} = [T] \begin{bmatrix} 0 \\ 0 \\ 0 \end{bmatrix} = \begin{bmatrix} 0 \\ 0 \\ 0 \end{bmatrix}$$

4.3.2 Single Phase-to-Ground Fault

The sequence networks are interconnected as shown in Fig. 4.8(b).

$$\bar{I}_0 = \bar{I}_1 = \bar{I}_2 = \frac{1 \angle 0^\circ}{j0.0452 + j0.1422 + j0.1422} = -j3.034$$

$$\begin{bmatrix} \bar{I}_a \\ \bar{I}_b \\ \bar{I}_c \end{bmatrix} = \begin{bmatrix} 1 & 1 & 1 \\ 1 & a^2 & a \\ 1 & a & a^2 \end{bmatrix} \begin{bmatrix} -j3.034 \\ -j3.034 \\ -j3.034 \end{bmatrix} = \begin{bmatrix} -j9.102 \\ 0 \\ 0 \end{bmatrix}$$

The sequence voltages are

$$\bar{V}_0 = -j0.0452(-j3.034) = -1371$$

$$\bar{V}_1 = 1.0 - j0.1422(-j3.034) = 0.5685$$

$$\bar{V}_2 = -j0.1422(-j3.034) = -0.4314$$

The phase voltages are

$$\begin{bmatrix} \bar{V}_a \\ \bar{V}_b \\ \bar{V}_c \end{bmatrix} = \begin{bmatrix} 1 & 1 & 1 \\ 1 & a^2 & a \\ 1 & a & a^2 \end{bmatrix} \begin{bmatrix} -0.1371 \\ 0.5685 \\ -0.4314 \end{bmatrix} = \begin{bmatrix} 0 \\ 0.8901 \angle -103.4^\circ \\ 0.8901 \angle -103.4^\circ \end{bmatrix}$$

Phase-to-phase and double phase-to-ground fault values are calculated from the appropriate networks [Figs. 4.8(c) and (d)]. Complete results are provided.

Faulted Bus	Phase a	Phase b	Phase c
3	G	G	G

Sequence Voltages

Bus	V0	V1	V2
1	0.0000/ 0.0	0.3939/ 0.0	0.0000/ 0.0
2	0.0000/ 0.0	0.2424/ 0.0	0.0000/ 0.0
3	0.0000/ 0.0	0.0000/ 0.0	0.0000/ 0.0
4	0.0000/ 0.0	0.2000/ -30.0	0.0000/ 30.0

Phase Voltages

Bus	Va	Vb	Vc
1	0.3939/ 0.0	0.3939/ -120.0	0.3939/ 120.0
2	0.2424/ 0.0	0.2424/ -120.0	0.2424/ 120.0
3	0.0000/ 6.5	0.0000/ -151.2	0.0000/ 133.8
4	0.2000/ -30.0	0.2000/ -150.0	0.2000/ 90.0

Sequence Currents

Bus to Bus	I0	I1	I2
1 2	0.0000/ 167.8	3.0303/ -90.0	0.0000/ 90.0
1 0	0.0000/ -12.2	3.0303/ 90.0	0.0000/ -90.0
2 3	0.0000/ 167.8	1.5152/ -90.0	0.0000/ 90.0
2 3	0.0000/ 167.8	1.5152/ -90.0	0.0000/ 90.0
2 1	0.0000/ -12.2	3.0303/ 90.0	0.0000/ -90.0
3 2	0.0000/ -12.2	1.5152/ 90.0	0.0000/ -90.0
3 2	0.0000/ -12.2	1.5152/ 90.0	0.0000/ -90.0
3 4	0.0000/ -12.2	4.0000/ 90.0	0.0000/ -90.0
4 3	0.0000/ 0.0	4.0000/ -120.0	0.0000/ 120.0
4 0	0.0000/ 0.0	4.0000/ 60.0	0.0000/ -60.0

Faulted Bus	Phase a	Phase b	Phase c
3	G	G	G

Phase Currents

Bus to Bus		Ia	Ib	Ic
1	2	3.0303/ -90.0	3.0303/ 150.0	3.0303/ 30.0
1	0	3.0303/ 90.0	3.0303/ -30.0	3.0303/ -150.0
2	3	1.5151/ -90.0	1.5151/ 150.0	1.5151/ 30.0
2	3	1.5151/ -90.0	1.5151/ 150.0	1.5151/ 30.0
2	1	3.0303/ 90.0	3.0303/ -30.0	3.0303/ -150.0
3	2	1.5151/ 90.0	1.5151/ -30.0	1.5151/ -150.0
3	2	1.5151/ 90.0	1.5151/ -30.0	1.5151/ -150.0
3	4	4.0000/ 90.0	4.0000/ -30.0	4.0000/ -150.0
4	3	4.0000/ -120.0	4.0000/ 120.0	4.0000/ -0.0
4	0	4.0000/ 60.0	4.0000/ -60.0	4.0000/ -180.0

Faulted Bus	Phase a	Phase b	Phase c
3	G	0	0

Sequence Voltages

Bus	V0	V1	V2
1	0.0496/ 180.0	0.7385/ 0.0	0.2615/ 180.0
2	0.0642/ 180.0	0.6731/ 0.0	0.3269/ 180.0
3	0.1371/ 180.0	0.5685/ 0.0	0.4315/ 180.0
4	0.0000/ 0.0	0.6548/ -30.0	0.3452/ 210.0

Phase Voltages

Bus	Va	Vb	Vc
1	0.4274/ 0.0	0.9127/ -108.4	0.9127/ 108.4
2	0.2821/ 0.0	0.8979/ -105.3	0.8979/ 105.3
3	0.0000/ 89.2	0.8901/ -103.4	0.8901/ 103.4
4	0.5674/ -61.8	0.5674/ -118.2	1.0000/ 90.0

Sequence Currents

Bus to Bus		I0	I1	I2
1	2	0.2917/ -90.0	1.3075/ -90.0	1.3075/ -90.0
1	0	0.2917/ 90.0	1.3075/ 90.0	1.3075/ 90.0
2	3	0.1458/ -90.0	0.6537/ -90.0	0.6537/ -90.0
2	3	0.1458/ -90.0	0.6537/ -90.0	0.6537/ -90.0
2	1	0.2917/ 90.0	1.3075/ 90.0	1.3075/ 90.0
3	2	0.1458/ 90.0	0.6537/ 90.0	0.6537/ 90.0
3	2	0.1458/ 90.0	0.6537/ 90.0	0.6537/ 90.0
3	4	2.7416/ 90.0	1.7258/ 90.0	1.7258/ 90.0
4	3	0.0000/ 0.0	1.7258/ -120.0	1.7258/ -60.0
4	0	0.0000/ 90.0	1.7258/ 60.0	1.7258/ 120.0

Faulted Bus	Phase a	Phase b	Phase c
3	G	0	0

Phase Currents

Bus to Bus	Ia	Ib	Ic
1 2	2.9066/ -90.0	1.0158/ 90.0	1.0158/ 90.0
1 0	2.9066/ 90.0	1.0158/ -90.0	1.0158/ -90.0
2 3	1.4533/ -90.0	0.5079/ 90.0	0.5079/ 90.0
2 3	1.4533/ -90.0	0.5079/ 90.0	0.5079/ 90.0
2 1	2.9066/ 90.0	1.0158/ -90.0	1.0158/ -90.0
3 2	1.4533/ 90.0	0.5079/ -90.0	0.5079/ -90.0
3 2	1.4533/ 90.0	0.5079/ -90.0	0.5079/ -90.0
3 4	6.1933/ 90.0	1.0158/ 90.0	1.0158/ 90.0
4 3	2.9892/ -90.0	2.9892/ 90.0	0.0000/ -90.0
4 0	2.9892/ 90.0	2.9892/ -90.0	0.0000/ 90.0

Faulted Bus	Phase a	Phase b	Phase c
3	0	C	B

Sequence Voltages

Bus	V0	V1	V2
1	0.0000/ 0.0	0.6970/ 0.0	0.3030/ 0.0
2	0.0000/ 0.0	0.6212/ 0.0	0.3788/ 0.0
3	0.0000/ 0.0	0.5000/ 0.0	0.5000/ 0.0
4	0.0000/ 0.0	0.6000/ -30.0	0.4000/ 30.0

Phase Voltages

Bus	Va	Vb	Vc
1	1.0000/ 0.0	0.6053/ -145.7	0.6053/ 145.7
2	1.0000/ 0.0	0.5423/ -157.2	0.5423/ 157.2
3	1.0000/ 0.0	0.5000/ -180.0	0.5000/ -180.0
4	0.8718/ -6.6	0.8718/ -173.4	0.2000/ 90.0

Sequence Currents

Bus to Bus	I0	I1	I2
1 2	0.0000/ -61.0	1.5152/ -90.0	1.5152/ 90.0
1 0	0.0000/ 119.0	1.5152/ 90.0	1.5152/ -90.0
2 3	0.0000/ -61.0	0.7576/ -90.0	0.7576/ 90.0
2 3	0.0000/ -61.0	0.7576/ -90.0	0.7576/ 90.0
2 1	0.0000/ 119.0	1.5152/ 90.0	1.5152/ -90.0
3 2	0.0000/ 119.0	0.7576/ 90.0	0.7576/ -90.0
3 2	0.0000/ 119.0	0.7576/ 90.0	0.7576/ -90.0
3 4	0.0000/ 119.0	2.0000/ 90.0	2.0000/ -90.0
4 3	0.0000/ 0.0	2.0000/ -120.0	2.0000/ 120.0
4 0	0.0000/ 90.0	2.0000/ 60.0	2.0000/ -60.0

Faulted Bus	Phase a	Phase b	Phase c
3	0	C	B

Phase Currents

Bus to Bus	Ia	Ib	Ic
1 2	0.0000/ 180.0	2.6243/ 180.0	2.6243/ 0.0
1 0	0.0000/ 180.0	2.6243/ 0.0	2.6243/ 180.0
2 3	0.0000/ -180.0	1.3122/ 180.0	1.3122/ 0.0
2 3	0.0000/ -180.0	1.3122/ 180.0	1.3122/ 0.0
2 1	0.0000/ 180.0	2.6243/ 0.0	2.6243/ 180.0
3 2	0.0000/ -180.0	1.3122/ 0.0	1.3122/ 180.0
3 2	0.0000/ -180.0	1.3122/ 0.0	1.3122/ 180.0
3 4	0.0000/ -180.0	3.4641/ 0.0	3.4641/ 180.0
4 3	2.0000/ -180.0	2.0000/ 180.0	4.0000/ 0.0
4 0	2.0000/ 0.0	2.0000/ 0.0	4.0000/ -180.0

Faulted Bus	Phase a	Phase b	Phase c
3	0	G	G

Sequence Voltages

Bus	V0	V1	V2
1	0.0703/ 0.0	0.5117/ 0.0	0.1177/ 0.0
2	0.0909/ 0.0	0.3896/ 0.0	0.1472/ 0.0
3	0.1943/ -0.0	0.1943/ 0.0	0.1943/ 0.0
4	0.0000/ 0.0	0.3554/ -30.0	0.1554/ 30.0

Phase Voltages

Bus	Va	Vb	Vc
1	0.6997/ 0.0	0.4197/ -125.6	0.4197/ 125.6
2	0.6277/ 0.0	0.2749/ -130.2	0.2749/ 130.2
3	0.5828/ 0.0	0.0000/ -30.7	0.0000/ -139.6
4	0.4536/ -12.7	0.4536/ -167.3	0.2000/ 90.0

Sequence Currents

Bus to Bus	I0	I1	I2
1 2	0.4133/ 90.0	2.4416/ -90.0	0.5887/ 90.0
1 0	0.4133/ -90.0	2.4416/ 90.0	0.5887/ -90.0
2 3	0.2067/ 90.0	1.2208/ -90.0	0.2943/ 90.0
2 3	0.2067/ 90.0	1.2208/ -90.0	0.2943/ 90.0
2 1	0.4133/ -90.0	2.4416/ 90.0	0.5887/ -90.0
3 2	0.2067/ -90.0	1.2208/ 90.0	0.2943/ -90.0
3 2	0.2067/ -90.0	1.2208/ 90.0	0.2943/ -90.0
3 4	3.8854/ -90.0	3.2229/ 90.0	0.7771/ -90.0
4 3	0.0000/ 0.0	3.2229/ -120.0	0.7771/ 120.0
4 0	0.0000/ -90.0	3.2229/ 60.0	0.7771/ -60.0

Faulted Bus	Phase a	Phase b	Phase c
3	0	G	G

Phase Currents

Bus to Bus		Ia	Ib	Ic
1	2	1.4396/ -90.0	2.9465/ 153.0	2.9465/ 27.0
1	0	1.4396/ 90.0	2.9465/ -27.0	2.9465/ -153.0
2	3	0.7198/ -90.0	1.4733/ 153.0	1.4733/ 27.0
2	3	0.7198/ -90.0	1.4733/ 153.0	1.4733/ 27.0
2	1	1.4396/ 90.0	2.9465/ -27.0	2.9465/ -153.0
3	2	0.7198/ 90.0	1.4733/ -27.0	1.4733/ -153.0
3	2	0.7198/ 90.0	1.4733/ -27.0	1.4733/ -153.0
3	4	1.4396/ -90.0	6.1721/ -55.9	6.1721/ -124.1
4	3	2.9132/ -133.4	2.9132/ 133.4	4.0000/ -0.0
4	0	2.9132/ 46.6	2.9132/ -46.6	4.0000/ -180.0

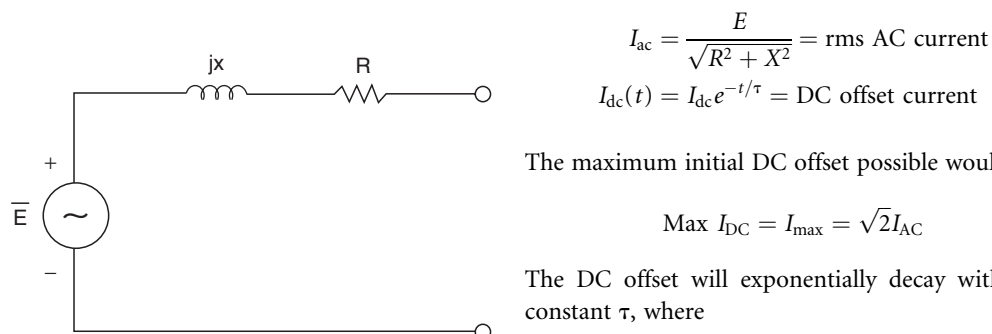
4.4 Further Considerations

Generators are not the only sources in the system. All rotating machines are capable of contributing to fault current, at least momentarily. Synchronous and induction motors will continue to rotate due to inertia and function as sources of fault current. The impedance used for such machines is usually the transient reactance X'_d or the subtransient X''_d , depending on protective equipment and speed of response. Frequently, motors smaller than 50 hp are neglected. Connecting systems are modeled with their Thévenin equivalents.

Although we have used AC circuit techniques to calculate faults, the problem is fundamentally transient since it involves sudden switching actions. Consider the so-called DC offset current. We model the system by determining its positive sequence Thévenin equivalent circuit, looking back into the positive sequence network at the fault, as shown in Fig. 4.9. The transient fault current is

$$i(t) = I_{ac}\sqrt{2} \cos(\omega t - \beta) + I_{dc}e^{-t/\tau}$$

This is a first-order approximation and strictly applies only to the three-phase or phase-to-phase fault. Ground faults would involve the zero sequence network also.



The maximum initial DC offset possible would be

$$\text{Max } I_{DC} = I_{max} = \sqrt{2}I_{AC}$$

The DC offset will exponentially decay with time constant τ , where

$$\tau = \frac{L}{R} = \frac{X}{\omega R}$$

FIGURE 4.9 Positive sequence circuit looking back into faulted bus.

The maximum DC offset current would be $I_{DC}(t)$

$$I_{DC}(t) = I_{DC}e^{-t/\tau} = \sqrt{2}I_{AC}e^{-t/\tau}$$

The *transient rms* current $I(t)$, accounting for both the AC and DC terms, would be

$$I(t) = \sqrt{I_{AC}^2 + I_{DC}^2(t)} = I_{AC}\sqrt{1 + 2e^{-2t/\tau}}$$

Define a multiplying factor k_i such that I_{AC} is to be multiplied by k_i to estimate the interrupting capacity of a breaker which operates in time T_{op} . Therefore,

$$k_i = \frac{I(T_{op})}{I_{AC}} = \sqrt{1 + 2e^{-2T_{op}/\tau}}$$

Observe that the maximum possible value for k_i is $\sqrt{3}$.

Example

In the circuit of Fig. 4.9, $E = 2400$ V, $X = 2$ Ω , $R = 0.1$ Ω , and $f = 60$ Hz. Compute k_i and determine the interrupting capacity for the circuit breaker if it is designed to operate in two cycles. The fault is applied at $t = 0$.

Solution

$$I_{ac} \cong \frac{2400}{2} = 1200 \text{ A}$$

$$T_{op} = \frac{2}{60} = 0.0333 \text{ s}$$

$$\tau = \frac{X}{\omega R} = \frac{2}{37.7} = 0.053$$

$$k_i = \sqrt{1 + 2e^{-2T_{op}/\tau}} = \sqrt{1 + 2e^{-0.0067/0.053}} = 1.252$$

Therefore,

$$I = k_i I_{ac} = 1.252(1200) = 1503 \text{ A}$$

The Thévenin equivalent at the fault point is determined by normal sinusoidal steady-state methods, resulting in a first-order circuit as shown in Fig. 4.9. While this provides satisfactory results for the steady-state component I_{AC} , the X/R value so obtained can be in serious error when compared with the rate of decay of $I(t)$ as measured by oscilloscopes on an actual faulted system. The major reasons for the discrepancy are, first of all, that the system, for transient analysis purposes, is actually high-order, and second, the generators do not hold constant impedance as the transient decays.

4.5 Summary

Computation of fault currents in power systems is best done by computer. The major steps are summarized below:

- Collect, read in, and store machine, transformer, and line data in per-unit on common bases.
- Formulate the sequence impedance matrices.

- Define the faulted bus and Z_f . Specify type of fault to be analyzed.
- Compute the sequence voltages.
- Compute the sequence currents.
- Correct for wye-delta connections.
- Transform to phase currents and voltages.

For large systems, computer formulation of the sequence impedance matrices is required. Refer to Further Information for more detail. Zero sequence networks for lines in close proximity to each other (on a common right-of-way) will be mutually coupled. If we are willing to use the same values for positive and negative sequence machine impedances,

$$[Z_1] = [Z_2]$$

Therefore, it is unnecessary to store these values in separate arrays, simplifying the program and reducing the computer storage requirements significantly. The error introduced by this approximation is usually not important. The methods previously discussed neglect the prefault, or load, component of current; that is, the usual assumption is that currents throughout the system were zero prior to the fault. This is almost never strictly true; however, the error produced is small since the fault currents are generally much larger than the load currents. Also, the load currents and fault currents are out of phase with each other, making their sum more nearly equal to the larger components than would have been the case if the currents were in phase. In addition, selection of precise values for prefault currents is somewhat speculative, since there is no way of predicting what the loaded state of the system is when a fault occurs. When it is important to consider load currents, a power flow study is made to calculate currents throughout the system, and these values are superimposed on (added to) results from the fault study.

A term which has wide industrial use and acceptance is the *fault level* or **fault MVA** at a bus. It relates to the amount of current that can be expected to flow out of a bus into a three-phase fault. As such, it is an alternate way of providing positive sequence impedance information. Define

$$\begin{aligned} \text{Fault level in MVA at bus } i &= V_{i_{\text{pu,nominal}}} I_{i_{\text{pu,fault}}} S_{3\phi_{\text{base}}} \\ &= (1) \frac{1}{Z_i^1} S_{3\phi_{\text{base}}} = \frac{S_{3\phi_{\text{base}}}}{Z_i^1} \end{aligned}$$

Fault study results may be further refined by approximating the effect of DC offset.

The basic reason for making fault studies is to provide data that can be used to size and set protective devices. The role of such protective devices is to detect and remove faults to prevent or minimize damage to the power system.

4.6 Defining Terms

DC offset—The natural response component of the transient fault current, usually approximated with a first-order exponential expression.

Fault—An unintentional and undesirable conducting path in an electrical power system.

Fault MVA—At a specific location in a system, the initial symmetrical fault current multiplied by the prefault nominal line-to-neutral voltage ($\times 3$ for a three-phase system).

Sequence (012) quantities—Symmetrical components computed from phase (*abc*) quantities. Can be voltages, currents, and/or impedances.

References

P.M. Anderson, *Analysis of Faulted Power Systems*, Ames: Iowa State Press, 1973.

M.E. El-Hawary, *Electric Power Systems: Design and Analysis*, Reston, Va.: Reston Publishing, 1983.

- M.E. El-Hawary, *Electric Power Systems*, New York: IEEE Press, 1995.
- O.I. Elgerd, *Electric Energy Systems Theory: An Introduction*, 2nd ed., New York: McGraw-Hill, 1982.
- General Electric, *Short-Circuit Current Calculations for Industrial and Commercial Power Systems*, Publication GET-3550.
- C.A. Gross, *Power System Analysis*, 2nd ed., New York: Wiley, 1986.
- S.H. Horowitz, *Power System Relaying*, 2nd ed, New York: Wiley, 1995.
- I. Lazar, *Electrical Systems Analysis and Design for Industrial Plants*, New York: McGraw-Hill, 1980.
- C.R. Mason, *The Art and Science of Protective Relaying*, New York: Wiley, 1956.
- J.R. Neuenwander, *Modern Power Systems*, Scranton, Pa.: International Textbook, 1971.
- G. Stagg and A.H. El-Abiad, *Computer Methods in Power System Analysis*, New York: McGraw-Hill, 1968.
- Westinghouse Electric Corporation, *Applied Protective Relaying*, Relay-Instrument Division, Newark, N.J., 1976.
- A.J. Wood, *Power Generation, Operation, and Control*, New York: Wiley, 1996.

Further Information

For a comprehensive coverage of general fault analysis, see Paul M. Anderson, *Analysis of Faulted Power Systems*, New York, IEEE Press, 1995. Also see Chapters 9 and 10 of *Power System Analysis* by C.A. Gross, New York: Wiley, 1986.

5

Computational Methods for Electric Power Systems

Mariesa L. Crow
University of Missouri-Rolla

5.1	Power Flow	5-1
	Admittance Matrix • Newton–Raphson Method	
5.2	Optimal Power Flow	5-13
	Steepest Descent Algorithm • Limitations on Independent Variables • Limitations on Dependent Variables	
5.3	State Estimation	5-24

Electric power systems are some of the largest human-made systems ever built. As with many physical systems, engineers, scientists, economists, and many others strive to understand and predict their complex behavior through mathematical models. The sheer size of the bulk power transmission system forced early power engineers to be among the first to develop computational approaches to solving the equations that describe them. Today's power system planners and operators rely very heavily on the computational tools to assist them in maintaining a reliable and secure operating environment.

The various computational algorithms were developed around the requirements of power system operation. The primary algorithms in use today are the power flow (also known as load flow), optimal power flow (OPF), and state estimation. These are all “steady-state” algorithms and are built up from the same basic approach to solving the nonlinear power balance equations. These particular algorithms do not explicitly consider the effects of time-varying dynamics on the system. The fields of transient and dynamic stability require a large number of algorithms that are significantly different from the power-flow-based algorithms and will therefore not be covered in this chapter.

5.1 Power Flow

The underlying principle of a power flow problem is that given the system loads, generation, and network configuration, the system bus voltages and line flows can be found by solving the nonlinear power flow equations. This is typically accomplished by applying Kirchoff's law at each power system bus throughout the system. In this context, Kirchoff's law can be interpreted as the sum of the powers entering a bus must be zero, or that the power at each bus must be conserved. Since power is comprised of two components, active power and reactive power, each bus gives rise to two equations—one for active power and one for reactive power. These equations are known as the *power flow equations*:

$$0 = \Delta P_i = P_i^{inj} - V_i \sum_{j=1} V_j Y_{ij} \cos(\theta_i - \theta_j - \phi_{ij}) \quad (5.1)$$

$$0 = \Delta Q_i = Q_i^{inj} - V_i \sum_{j=1}^N V_j Y_{ij} \sin(\theta_i - \theta_j - \phi_{ij})$$

$$i = 1, \dots, N \quad (5.2)$$

where P_i^{inj} and Q_i^{inj} are the active power and reactive power injected at the bus i , respectively. Loads are modeled by negative power injection. The values V_i and V_j are the voltage magnitudes at bus i and bus j , respectively. The values θ_i and θ_j are the corresponding phase angles. The value $Y_{ij} \angle \phi_{ij}$ is the (ij) th element of the network admittance matrix Y_{bus} . The constant N is the number of buses in the system. The updates ΔP_i and ΔQ_i of Eqs. (5.1) and (5.2) are called the *mismatch* equations because they give a measure of the power difference, or mismatch, between the calculated power values, as functions of voltage and phase angle, and the actual injected powers.

The formulation in Eqs. (5.1) and (5.2) is called the *polar* formulation of the power flow equations. If $Y_{ij} \angle \phi_{ij}$ is instead given by the complex sum $g_{ij} + j b_{ij}$, then the power flow equations may be written in *rectangular form* as

$$0 = \Delta P_i = P_i^{inj} - V_i \sum_{j=1}^N V_j (g_{ij} \cos(\theta_i - \theta_j) + b_{ij} \sin(\theta_i - \theta_j)) \quad (5.3)$$

$$0 = \Delta Q_i = Q_i^{inj} - V_i \sum_{j=1}^N V_j (g_{ij} \sin(\theta_i - \theta_j) - b_{ij} \cos(\theta_i - \theta_j))$$

$$i = 1, \dots, N \quad (5.4)$$

There are, at most, $2N$ equations to solve. This number is then further reduced by removing one power flow equation for each known voltage (at voltage controlled buses) and the swing bus angle. This reduction is necessary since the number of equations must equal the number of unknowns in a fully determined system. In either case, the power flow equations are a system of nonlinear equations. They are nonlinear in both the voltage and phase angle. Once the number and form of the nonlinear power flow equations have been determined, the Newton–Raphson method may be applied to numerically solve the power flow equations.

5.1.1 Admittance Matrix

The first step in solving the power flow equations is to obtain the admittance matrix Y for the system. The admittance matrix of a passive network (a network containing only resistors, capacitors, and inductors) may be found by summing the currents at every node in the system. An arbitrary bus i in the transmission network is shown in Fig. 5.1. The bus i can be connected to any number of other buses in the system through transmission lines. Each transmission line between buses i and j is represented by a π -circuit with series impedance $R_{ij} + jX_{ij}$ where R_{ij} is the per unit resistance of the transmission line. The per unit line reactance is $X_{ij} = \omega_s L_{ij}$ where ω_s is the system base frequency and L_{ij} is the inductance of the line. In the π -circuit, the line-charging capacitance is represented by two lumped admittances $j \frac{B_{ij}}{2}$ placed at each end of the transmission line. Note that although each transmission-line parameter is in per unit and therefore a unitless quantity, the impedance is given in Ω/Ω whereas the admittance is given as U/U . The series impedances can also be represented by their equivalent admittance value where

$$Y_{ij} \angle \phi_{ij} = \frac{1}{R_{ij} + jX_{ij}}$$

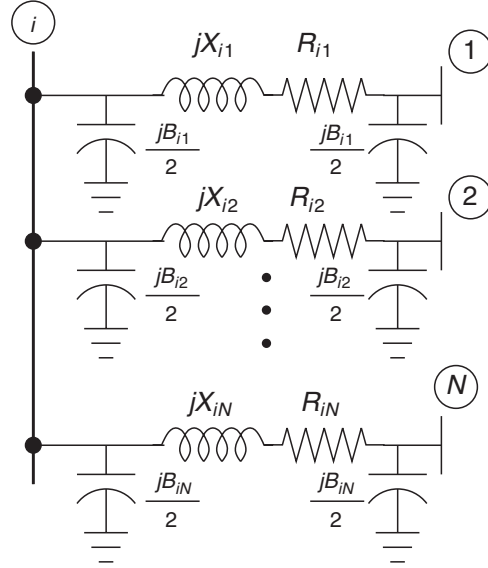


FIGURE 5.1 Bus i in a power transmission network.

Summing the currents at node i yields

$$I_{i,inj} = I_{i1} + I_{i2} + \dots + I_{iN} + I_{i10} + I_{i20} + \dots + I_{iN0} \quad (5.5)$$

$$= \frac{(\hat{V}_i - \hat{V}_1)}{R_{i1} + jX_{i1}} + \frac{(\hat{V}_i - \hat{V}_2)}{R_{i2} + jX_{i2}} + \dots + \frac{(\hat{V}_i - \hat{V}_N)}{R_{iN} + jX_{iN}}$$

$$+ \hat{V}_i \left(j \frac{B_{i1}}{2} + j \frac{B_{i2}}{2} + \dots + j \frac{B_{iN}}{2} \right) \quad (5.6)$$

$$= (\hat{V}_i - \hat{V}_1) y_{i1} \angle \phi_{i1} + (\hat{V}_i - \hat{V}_2) y_{i2} \angle \phi_{i2} + \dots + (\hat{V}_i - \hat{V}_N) y_{iN} \angle \phi_{iN}$$

$$+ \hat{V}_i \left(j \frac{B_{i1}}{2} + j \frac{B_{i2}}{2} + \dots + j \frac{B_{iN}}{2} \right) \quad (5.7)$$

where $\hat{V}_i = V_i \angle \theta_i$.

Gathering the voltages yields

$$I_{i,inj} = -\hat{V}_1 y_{i1} \angle \phi_{i1} - \hat{V}_2 y_{i2} \angle \phi_{i2} + \dots + \hat{V}_i \left(y_{i1} \angle \phi_{i1} + y_{i2} \angle \phi_{i2} Z + \dots + y_{iN} \angle \phi_{iN} \right. \\ \left. + j \frac{B_{i1}}{2} + j \frac{B_{i2}}{2} + \dots + j \frac{B_{iN}}{2} \right) + \dots - \hat{V}_N y_{iN} \angle \phi_{iN} \quad (5.8)$$

By noting that there are N buses in the system, there are N equations similar to Eq. (5.8). These can be represented in matrix form

$$\begin{bmatrix} I_{1,inj} \\ I_{2,inj} \\ \vdots \\ I_{i,inj} \\ \vdots \\ I_{N,inj} \end{bmatrix} = \begin{bmatrix} Y_{11} & -y_{12}/\phi_{12} & \dots & -y_{1i}/\phi_{1i} & \dots & -y_{1N}/\phi_{1N} \\ -y_{21}/\phi_{21} & Y_{22} & \dots & -y_{2i}/\phi_{2i} & \dots & -y_{2N}/\phi_{2N} \\ \vdots & \vdots & \ddots & \vdots & \vdots & \vdots \\ -y_{i1}/\phi_{i1} & -y_{i2}/\phi_{i2} & \dots & Y_{ii} & \dots & -y_{iN}/\phi_{iN} \\ \vdots & \vdots & \vdots & \vdots & \ddots & \vdots \\ -y_{N1}/\phi_{N1} & -y_{N2}/\phi_{N2} & \dots & -y_{Ni}/\phi_{Ni} & \dots & Y_{NN} \end{bmatrix} \begin{bmatrix} \hat{V}_1 \\ \hat{V}_2 \\ \vdots \\ \hat{V}_1 \\ \vdots \\ \hat{V}_N \end{bmatrix} \quad (5.9)$$

where

$$Y_{ii} = \left(y_{i1}/\phi_{i1} + y_{i2}/\phi_{i2} + \dots + y_{iN}/\phi_{iN} \right) + j \frac{B_{i1}}{2} + j \frac{B_{i2}}{2} + \dots + j \frac{B_{iN}}{2} \quad (5.10)$$

The matrix relating the injected currents vector to the bus voltage vector is known as the system *admittance matrix* and is commonly represented as Y . A simple procedure for calculating the elements of the admittance matrix is

$Y(i,j)$	negative of the admittance between buses i and j
$Y(i,i)$	sum of all admittances connected to bus i

noting that the line-charging values are shunt admittances and are included in the diagonal elements.

Example 5.1

Find the admittance matrix for the line data given by

i	j	R_{ij}	X_{ij}	B_{ij}
1	2	0.027	0.32	0.15
1	5	0.014	0.18	0.10
2	3	0.012	0.13	0.12
3	4	0.025	0.25	0.00
3	5	0.017	0.20	0.08

Solution

The first step in calculating the admittance matrix is to calculate the off-diagonal elements first. Note that in a passive network, the admittance matrix is symmetric and $Y(i,j) = Y(j,i)$.

The off-diagonal elements are calculated as the negative of the series admittance of each line. Therefore

$$\begin{aligned} Y(1,2) &= Y(2,1) = \frac{-1}{0.027 + j0.32} = 3.1139/94.82^\circ \\ Y(1,5) &= Y(5,1) = \frac{-1}{0.014 + j0.18} = 5.5388/94.45^\circ \\ Y(2,3) &= Y(3,2) = \frac{-1}{0.012 + j0.13} = 7.6597/95.27^\circ \\ Y(3,4) &= Y(4,3) = \frac{-1}{0.025 + j0.25} = 3.9801/95.71^\circ \\ Y(3,5) &= Y(5,3) = \frac{-1}{0.017 + j0.20} = 4.9820/94.86^\circ \end{aligned}$$

The diagonal elements are calculated as the sum of all admittances connected to each bus. Therefore

$$\begin{aligned}
 Y(1,1) &= \frac{1}{0.027 + j0.32} + \frac{1}{0.014 + j0.18} + j\frac{0.15}{2} + j\frac{0.10}{2} = 8.5281 \angle -85.35^\circ \\
 Y(2,2) &= \frac{1}{0.027 + j0.32} + \frac{1}{0.012 + j0.13} + j\frac{0.15}{2} + j\frac{0.12}{2} = 10.6392 \angle -84.79^\circ \\
 Y(3,3) &= \frac{1}{0.012 + j0.13} + \frac{1}{0.025 + j0.25} + \frac{1}{0.017 + j0.20} \\
 &\quad + j\frac{0.12}{2} + j\frac{0.08}{2} = 16.5221 \angle -84.71^\circ \\
 Y(4,4) &= \frac{1}{0.025 + j0.25} = 3.9801 \angle -84.29^\circ \\
 Y(5,5) &= \frac{1}{0.017 + j0.20} + j\frac{0.08}{2} = 10.4311 \angle -85.32^\circ
 \end{aligned}$$

5.1.2 Newton–Raphson Method

The most common approach to solving the power flow equations is to use the iterative Newton–Raphson method. The Newton–Raphson method is an iterative approach to solving continuous non-linear equations in the form

$$F(x) = \begin{bmatrix} f_1(x_1, x_2, \dots, x_n) \\ f_2(x_1, x_2, \dots, x_n) \\ \vdots \\ f_n(x_1, x_2, \dots, x_n) \end{bmatrix} = 0 \quad (5.11)$$

An iterative approach is one in which an initial guess (x^0) to the solution is used to create a sequence x^0, x^1, x^2, \dots that (hopefully) converges arbitrarily close to the desired solution vector x^* where $F(x^*) = 0$.

The Newton–Raphson method for n -dimensional systems is given as

$$x^{k+1} = x^k - [J(x^k)]^{-1} F(x^k) \quad (5.12)$$

where

$$\begin{aligned}
 x &= \begin{bmatrix} x_1 \\ x_2 \\ x_3 \\ \vdots \\ x_n \end{bmatrix} \\
 F(x^k) &= \begin{bmatrix} f_1(x^k) \\ f_2(x^k) \\ f_3(x^k) \\ \vdots \\ f_n(x^k) \end{bmatrix}
 \end{aligned}$$

and the Jacobian matrix $[J(x^k)]$ is given by

$$[J(x^k)] = \begin{bmatrix} \frac{\partial f_1}{\partial x_1} & \frac{\partial f_1}{\partial x_2} & \frac{\partial f_1}{\partial x_3} & \cdots & \frac{\partial f_1}{\partial x_n} \\ \frac{\partial f_2}{\partial x_1} & \frac{\partial f_2}{\partial x_2} & \frac{\partial f_2}{\partial x_3} & \cdots & \frac{\partial f_2}{\partial x_n} \\ \frac{\partial f_3}{\partial x_1} & \frac{\partial f_3}{\partial x_2} & \frac{\partial f_3}{\partial x_3} & \cdots & \frac{\partial f_3}{\partial x_n} \\ \vdots & \vdots & \vdots & \vdots & \vdots \\ \frac{\partial f_n}{\partial x_1} & \frac{\partial f_n}{\partial x_2} & \frac{\partial f_n}{\partial x_3} & \cdots & \frac{\partial f_n}{\partial x_n} \end{bmatrix}$$

Typically, the inverse of the Jacobian matrix $[J(x^k)]$ is not found directly, but rather through LU factorization. Convergence is typically evaluated by considering the norm of the function

$$\|F(x^k)\| < \varepsilon \quad (5.13)$$

Note that the Jacobian is a function of x^k and is therefore updated every iteration along with $F(x^k)$.

In this formulation, the vector $F(x)$ is the set of power flow equations and the unknown x is the vector of voltage magnitudes and angles. It is common to arrange the Newton–Raphson equations by phase angle followed by the voltage magnitudes as

$$\begin{bmatrix} J_1 & J_2 \\ J_3 & J_4 \end{bmatrix} \begin{bmatrix} \Delta\delta_1 \\ \Delta\delta_2 \\ \Delta\delta_3 \\ \vdots \\ \Delta\delta_N \\ \Delta V_1 \\ \Delta V_2 \\ \Delta V_3 \\ \vdots \\ \Delta Q_N \end{bmatrix} = - \begin{bmatrix} \Delta P_1 \\ \Delta P_2 \\ \Delta P_3 \\ \vdots \\ \Delta P_N \\ \Delta Q_1 \\ \Delta Q_2 \\ \Delta Q_3 \\ \vdots \\ \Delta Q_N \end{bmatrix} \quad (5.14)$$

where

$$\begin{aligned} \Delta\delta_i &= \delta_i^{k+1} - \delta_i^k \\ \Delta V_i &= V_i^{k+1} - V_i^k \end{aligned}$$

and ΔP_i and ΔQ_i are as given in Eqs. (5.1) and (5.2) and are evaluated at δ^k and V^k . The Jacobian is typically divided into four submatrices, where

$$\begin{bmatrix} J_1 & J_2 \\ J_3 & J_4 \end{bmatrix} = \begin{bmatrix} \frac{\partial \Delta P}{\partial \delta} & \frac{\partial \Delta P}{\partial V} \\ \frac{\partial \Delta Q}{\partial \delta} & \frac{\partial \Delta Q}{\partial V} \end{bmatrix} \quad (5.15)$$

Each submatrix represents the partial derivatives of each of the mismatch equations with respect to each of the unknowns. These partial derivatives yield eight types—two for each mismatch equation, where one is for the diagonal element and the other is for off-diagonal elements. The derivatives are summarized as

$$\frac{\partial \Delta P_i}{\partial \delta_i} = V_i \sum_{j=1}^N V_j Y_{ij} \sin(\delta_i - \delta_j - \phi_{ij}) + V_i^2 Y_{ii} \sin \phi_{ii} \quad (5.16)$$

$$\frac{\partial \Delta P_i}{\partial \delta_j} = -V_i V_j Y_{ij} \sin(\delta_i - \delta_j - \phi_{ij}) \quad (5.17)$$

$$\frac{\partial \Delta P_i}{\partial V_i} = - \sum_{i=1}^N V_j Y_{ij} \cos(\delta_i - \delta_j - \phi_{ij}) - V_i V_{ii} \cos \phi_{ii} \quad (5.18)$$

$$\frac{\partial \Delta P_i}{\partial V_j} = -V_i Y_{ij} \cos(\delta_i - \delta_j - \phi_{ij}) \quad (5.19)$$

$$\frac{\partial \Delta Q_i}{\partial \delta_i} = -V_i \sum_{j=1}^N V_j Y_{ij} \cos(\delta_i - \delta_j - \phi_{ij}) + V_i^2 Y_{ii} \cos \phi_{ii} \quad (5.20)$$

$$\frac{\partial \Delta Q_i}{\partial \delta_j} = V_i V_j Y_{ij} \cos(\delta_i - \delta_j - \phi_{ij}) \quad (5.21)$$

$$\frac{\partial \Delta Q_i}{\partial V_i} = - \sum_{j=1}^N V_j Y_{ij} \sin(\delta_i - \delta_j - \phi_{ij}) + V_i Y_{ii} \sin \phi_{ii} \quad (5.22)$$

$$\frac{\partial \Delta Q_i}{\partial V_j} = -V_i Y_{ij} \sin(\delta_i - \delta_j - \phi_{ij}) \quad (5.23)$$

A common modification to the power flow solution is to replace the unknown update ΔV_i by the normalized value $\frac{\Delta V_i}{V_i}$. This formulation yields a more symmetric Jacobian matrix as the Jacobian submatrices J_2 and J_4 are now multiplied by V_i to compensate for the scaling of ΔV_i by V_i . All partial derivatives of each submatrix then become quadratic in voltage magnitude.

The Newton–Raphson method for the solution of the power flow equations is relatively straightforward to program since both the function evaluations and the partial derivatives use the same expressions. Thus it takes little extra computational effort to compute the Jacobian once the mismatch equations have been calculated.

Example 5.2

Find the voltage magnitudes, phase angles, and line flows for the small power system shown in Fig. 5.2 with the following system:

Parameters in Per Unit

Bus	Type	V	P_{gen}	Q_{gen}	P_{load}	Q_{load}
1	swing	1.02	—	—	0.0	0.0
2	PV	1.00	0.5	—	0.0	0.0
3	PQ	—	0.0	0.0	1.2	0.5

I	j	R_{ij}	X_{ij}	B_{ij}
1	2	0.02	0.3	0.15
1	3	0.01	0.1	0.1
2	3	0.01	0.1	0.1

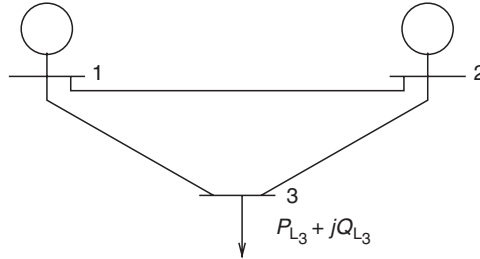


FIGURE 5.2 Example power system.

Solution

Calculating the admittance matrix for this system yields

$$Y_{\text{bus}} = \begin{bmatrix} 13.1505 \angle -84.7148^\circ & 3.3260 \angle 93.8141^\circ & 9.9504 \angle 95.7106^\circ \\ 3.326 \angle 95.7106^\circ & 13.1505 \angle -84.7148^\circ & 9.9504 \angle 95.7106^\circ \\ 9.9504 \angle 95.7106^\circ & 9.9504 \angle 95.7106^\circ & 19.8012 \angle 84.2606^\circ \end{bmatrix} \quad (5.24)$$

By inspection, this system has three unknowns: δ_2 , δ_3 , and V_3 ; thus, three power flow equations are required. These power flow equations are

$$0 = \Delta P_2 = 0.5 - V_2 \sum_{j=1}^3 V_j Y_{ij} \cos(\delta_2 - \delta_j - \theta_{ij}) \quad (5.25)$$

$$0 = \Delta P_3 = -1.2 - V_3 \sum_{j=1}^3 V_j Y_{ij} \cos(\delta_3 - \delta_j - \theta_{ij}) \quad (5.26)$$

$$0 = \Delta Q_3 = -0.5 - V_3 \sum_{j=1}^3 V_j Y_{ij} \sin(\delta_3 - \delta_j - \theta_{ij}) \quad (5.27)$$

Substituting the known quantities for $V_1 = 1.02$, $V_2 = 1.00$, and $\delta_1 = 0$ and the admittance matrix quantities yields

$$\Delta P_2 = 0.5 - (1.00) \begin{bmatrix} (1.02)(3.3260) \cos(\delta_2 - 0 - 93.8141^\circ) \\ +(1.00)(13.1505) \cos(\delta_2 - \delta_2 + 84.7148^\circ) \\ +(V_3)(9.9504) \cos(\delta_2 - \delta_3 - 95.7106^\circ) \end{bmatrix} \quad (5.28)$$

$$\Delta P_3 = -1.2 - (V_3) \begin{bmatrix} (1.02)(9.9504) \cos(\delta_2 - 0 - 95.7106^\circ) \\ +(1.00)(9.9504) \cos(\delta_3 - \delta_2 - 95.7106^\circ) \\ +(V_3)(19.8012) \cos(\delta_3 - \delta_3 - 84.2606^\circ) \end{bmatrix} \quad (5.29)$$

$$\Delta Q_3 = -0.5 - (V_3) \begin{bmatrix} (1.02)(9.9504) \sin(\delta_3 - 0 - 95.7106^\circ) \\ +(1.00)(9.9504) \sin(\delta_3 - \delta_2 - 95.7106^\circ) \\ +(V_3)(19.8012) \sin(\delta_3 - \delta_3 + 84.2606^\circ) \end{bmatrix} \quad (5.30)$$

The Newton–Raphson iteration for this system is then given by

$$\begin{bmatrix} \frac{\partial \Delta P_2}{\partial \delta_2} & \frac{\partial \Delta P_2}{\partial \delta_3} & \frac{\partial \Delta P_2}{\partial V_3} \\ \frac{\partial \Delta P_3}{\partial \delta_2} & \frac{\partial \Delta P_3}{\partial \delta_3} & \frac{\partial \Delta P_3}{\partial V_3} \\ \frac{\partial \Delta Q_3}{\partial \delta_2} & \frac{\partial \Delta Q_3}{\partial \delta_3} & \frac{\partial \Delta Q_3}{\partial V_3} \end{bmatrix} \begin{bmatrix} \Delta \delta_2 \\ \Delta \delta_3 \\ \Delta V_3 \end{bmatrix} = - \begin{bmatrix} \Delta P_2 \\ \Delta P_3 \\ \Delta Q_3 \end{bmatrix} \quad (5.31)$$

where

$$\begin{aligned} \frac{\partial \Delta P_2}{\partial \delta_2} &= 3.3925 \sin(\delta_2 - 93.8141^\circ) \\ &\quad + 9.9504 V_3 \sin(\delta_2 - \delta_3 - 94.7106^\circ) \\ \frac{\partial \Delta P_2}{\partial \delta_3} &= -9.9504 V_3 \sin(\delta_2 - \delta_3 - 95.7106^\circ) \\ \frac{\partial \Delta P_2}{\partial V_3} &= -9.9504 \cos(\delta_2 - \delta_3 - 95.7106^\circ) \\ \frac{\partial \Delta P_3}{\partial \delta_2} &= -9.9504 V_3 \sin(\delta_3 - \delta_2 - 95.7106^\circ) \\ \frac{\partial \Delta P_3}{\partial \delta_3} &= 10.1494 V_3 \sin(\delta_3 - 95.7106^\circ) \\ &\quad + 9.9504 V_3 \sin(\delta_3 - \delta_2 - 95.7106^\circ) \\ \frac{\partial \Delta P_3}{\partial V_3} &= -10.1494 \cos(\delta_3 - 95.7106^\circ) \\ &\quad - 9.9504 \cos(\delta_3 - \delta_2 - 95.7106^\circ) \\ &\quad - 39.6024 V_3 \cos(84.2606^\circ) \\ \frac{\partial \Delta Q_3}{\partial \delta_2} &= 9.9504 V_3 \cos(\delta_3 - \delta_2 - 95.7106^\circ) \\ \frac{\partial \Delta Q_3}{\partial \delta_3} &= -10.1494 V_3 \cos(\delta_3 - 95.7106^\circ) \\ &\quad - 9.9504 V_3 \cos(\delta_3 - \delta_2 - 95.7106^\circ) \\ \frac{\partial \Delta Q_3}{\partial V_3} &= -10.1494 \sin(\delta_3 - 95.7106^\circ) \\ &\quad - 9.9504 \sin(\delta_3 - \delta_2 - 95.7106^\circ) \\ &\quad - 39.6024 V_3 \sin(84.2606^\circ) \end{aligned}$$

One of the underlying assumptions of the Newton–Raphson iteration is that the higher order terms of the Taylor series expansion upon which the iteration is based are negligible only if the initial guess is sufficiently close to the actual solution to the nonlinear equations. Under most operating conditions, the voltages throughout the power system are within $\pm 10\%$ of the nominal voltage and therefore fall in the range $0.9 \leq V_i \leq 1.1$ per unit. Similarly, under most operating conditions the phase angle differences between adjacent buses are typically small. Thus if the swing bus angle is taken to be zero, then all phase angles throughout the system will also be close to zero. Therefore in initializing a power flow, it is common to choose a “flat start” initial condition. That is, all voltage magnitudes are set to 1.0 per unit and all angles are set to zero.

Iteration 1

Evaluating the Jacobian and the mismatch equations at the flat start initial conditions yields

$$[J^0] = \begin{bmatrix} -13.2859 & 9.9010 & 0.9901 \\ 9.9010 & -20.000 & -1.9604 \\ -0.9901 & 2.0000 & -19.4040 \end{bmatrix}$$

$$\begin{bmatrix} \Delta P_2^0 \\ \Delta P_3^0 \\ \Delta Q_3^0 \end{bmatrix} = \begin{bmatrix} 0.5044 \\ -1.1802 \\ -0.2020 \end{bmatrix}$$

Solving

$$[J^0] \begin{bmatrix} \Delta \delta_2^1 \\ \Delta \delta_3^1 \\ \Delta V_3^1 \end{bmatrix} = \begin{bmatrix} \Delta P_2^0 \\ \Delta P_3^0 \\ \Delta Q_3^0 \end{bmatrix}$$

by LU factorization yields

$$\begin{bmatrix} \Delta \delta_2^1 \\ \Delta \delta_3^1 \\ \Delta V_3^1 \end{bmatrix} = \begin{bmatrix} -0.0096 \\ -0.0621 \\ -0.0163 \end{bmatrix}$$

Therefore

$$\delta_2^1 = \delta_2^0 + \Delta \delta_2^1 = 0 - 0.0096 = -0.0096$$

$$\delta_3^1 = \delta_3^0 + \Delta \delta_3^1 = 0 - 0.0621 = -0.0621$$

$$V_3^1 = V_3^0 + \Delta V_3^1 = 1 - 0.0163 = 0.9837$$

Note that the angles are given in *radians* and not degrees. The error at the first iteration is the largest absolute value of the mismatch equations, which is

$$\varepsilon^1 = 1.1802$$

One quick check of this process is to note that the voltage update V_3^1 is slightly less than 1.0 per unit, which would be expected given the system configuration. Note also that the diagonals of the Jacobian are all equal or greater in magnitude than the off-diagonal elements. This is because the diagonals are summations of terms, whereas the off-diagonal elements are single terms.

Iteration 2

Evaluating the Jacobian and the mismatch equations at the updated values δ_2^1 , δ_3^1 , and V_3^1 yields

$$[J^1] = \begin{bmatrix} -13.1597 & 9.7771 & 0.4684 \\ 9.6747 & -19.5280 & -0.7515 \\ -1.4845 & 3.0929 & -18.9086 \end{bmatrix}$$

$$\begin{bmatrix} \Delta P_2^1 \\ \Delta P_3^1 \\ \Delta Q_3^1 \end{bmatrix} = \begin{bmatrix} 0.0074 \\ -0.0232 \\ -0.0359 \end{bmatrix}$$

Solving for the update yields

$$\begin{bmatrix} \Delta\delta_2^2 \\ \Delta\delta_3^2 \\ \Delta V_3^2 \end{bmatrix} = \begin{bmatrix} -0.0005 \\ -0.0014 \\ -0.0021 \end{bmatrix}$$

and

$$\begin{bmatrix} \delta_2^2 \\ \delta_3^2 \\ V_3^2 \end{bmatrix} = \begin{bmatrix} -0.0101 \\ -0.0635 \\ 0.9816 \end{bmatrix}$$

where

$$\varepsilon^2 = 0.0359$$

Iteration 3

Evaluating the Jacobian and the mismatch equations at the updated values δ_2^2 , δ_3^2 , and V_3^2 yields

$$[J^2] = \begin{bmatrix} -13.1392 & 9.7567 & 0.4600 \\ 9.6530 & -19.4831 & -0.7213 \\ -1.4894 & 3.1079 & -18.8300 \end{bmatrix}$$

$$\begin{bmatrix} \Delta P_2^0 \\ \Delta P_3^0 \\ \Delta Q_3^0 \end{bmatrix} = \begin{bmatrix} 0.1717 \\ -0.5639 \\ -0.9084 \end{bmatrix} \times 10^{-4}$$

Solving for the update yields

$$\begin{bmatrix} \Delta\delta_2^2 \\ \Delta\delta_3^2 \\ \Delta V_3^2 \end{bmatrix} = \begin{bmatrix} -0.1396 \\ -0.3390 \\ -0.5273 \end{bmatrix} \times 10^{-5}$$

and

$$\begin{bmatrix} \delta_2^3 \\ \delta_3^2 \\ V_3^3 \end{bmatrix} = \begin{bmatrix} -0.0101 \\ -0.0635 \\ 0.9816 \end{bmatrix}$$

where

$$\varepsilon^3 = 0.9084 \times 10^{-4}$$

At this point, the iterations have converged since the mismatch is sufficiently small and the values are no longer changing significantly.

The last task in power flow is to calculate the generated reactive powers, the swing bus active power output and the line flows. The generated powers can be calculated directly from the power flow equations:

$$P_i^{inj} = V_i \sum_{j=1}^N V_j Y_{ij} \cos(\theta_i - \theta_j - \phi_{ij})$$

$$Q_i^{inj} = V_i \sum_{j=1}^N V_j Y_{ij} \sin(\theta_i - \theta_j - \phi_{ij})$$

Therefore

$$P_{gen,1} = P_1^{inj} = 0.7087$$

$$Q_{gen,1} = Q_1^{inj} = 0.2806$$

$$Q_{gen,2} = Q_2^{inj} = -0.0446$$

The total active power losses in the system are the difference between the sum of the generation and the sum of the loads, in this case:

$$P_{loss} = \sum P_{gen} - \sum P_{load} = 0.7087 + 0.5 - 1.2 = 0.0087 \text{ pu} \quad (5.32)$$

The line losses for line $i-j$ are calculated at both the sending and receiving ends of the line. The apparent power leaving bus i to bus j on line $i-j$ is

$$S_{ij} = V_i \angle \delta_i \left(I_{ij} + j \frac{B_{ij}}{2} V_i \angle \theta_i \right)^* \quad (5.33)$$

$$= V_i \angle \delta_i \left(\left(\frac{V_i \angle \theta_i - V_j \angle \theta_j}{R_{ij} + j X_{ij}} \right) + j \frac{B_{ij}}{2} V_i \angle \theta_i \right)^* \quad (5.34)$$

and the power received at bus j from bus i on line $i-j$ is

$$S_{ji} = V_j \angle \delta_j \left(I_{ji} - j \frac{B_{ij}}{2} V_j \angle \theta_j \right)^* \quad (5.35)$$

Thus

$$P_{ij} = \operatorname{Re}\{S_{ij}\} = V_i V_j Y_{ij} \cos(\delta_i - \delta_j - \phi_{ij}) - V_i^2 Y_{ij} \cos \phi_{ij} \quad (5.36)$$

$$Q_{ij} = \operatorname{Im}\{S_{ij}\} = V_i V_j Y_{ij} \sin(\delta_i - \delta_j - \phi_{ij}) + V_i^2 \left(Y_{ij} \sin \phi_{ij} - \frac{B_{ij}}{2} \right) \quad (5.37)$$

Similarly, the powers P_{ji} and Q_{ji} can be calculated. The active power loss on any given line is the difference between the active power sent from bus i and the active power received at bus j . Calculating the reactive power losses is more complex since the reactive power generated by the line-charging (shunt capacitances) must also be included.

5.2 Optimal Power Flow

The basic objective of the OPF is to find the values of the system state variables and/or parameters that minimize some cost function of the power system. The types of cost functions are system dependent and can vary widely from application to application and are not necessarily strictly measured in terms of dollars. Examples of engineering optimizations can range from minimizing

- active power losses,
- particulate output (emissions),
- system energy, or
- fuel costs of generation

to name a few possibilities. The basic formulation of the OPF can be represented as minimizing a defined cost function subject to any physical or operational constraints of the system:
minimize

$$f(x,u) \quad x \in R^n \quad (5.38)$$

$$u \in R^n$$

subject to

$$g(x,u) = 0 \quad \text{equality constraints} \quad (5.39)$$

$$h(x,u) = 0 \quad \text{inequality constraints} \quad (5.40)$$

where x is the vector of system states and u is the vector of system parameters. The basic approach is to find the vector of system parameters that when substituted into the system model will result in the state vector x that minimizes the cost function $f(x,u)$.

In an unconstrained system, the usual approach to minimizing the cost function is to set the function derivatives to zero and then solve for the system states from the set of resulting equations. In the majority of applications, however, the system states at the unconstrained minimum will not satisfy the constraint equations. Thus, an alternate approach is required to find the constrained minimum. One approach is to introduce an additional set of parameters λ , frequently known as *Lagrange multipliers*, to impose the constraints on the cost function. The augmented cost function then becomes

$$\text{minimize } f(x,u) - \lambda g(x,u) \quad (5.41)$$

The augmented function in Eq. (5.41) can then be minimized by solving for the set of states that result from setting the derivatives of the augmented function to zero. Note that the derivative of Eq. (5.41) with respect to λ effectively enforces the equality constraint of Eq. (5.39).

Example 5.3

Minimize

$$C: \frac{1}{2}(x^2 + y^2) \quad (5.42)$$

subject to the following constraint:

$$2x - y = 5$$

Solution

Note that the function to be minimized is the equation for a circle. The unconstrained minimum of this function is the point at the origin with $x=0$ and $y=0$, which defines a circle with a radius of zero length. However, the circle must also intersect the line defined by the constraint equation; thus, the constrained circle must have a nonzero radius. The augmented cost function becomes

$$C^*: \frac{1}{2}(x^2 + y^2) - \lambda(2x - y - 5) \quad (5.43)$$

where λ represents the Lagrange multiplier. Setting the derivatives of the augmented cost function to zero yields the following set of equations:

$$\begin{aligned} 0 &= \frac{\partial C^*}{\partial x} = x - 2\lambda \\ 0 &= \frac{\partial C^*}{\partial y} = y + \lambda \\ 0 &= \frac{\partial C^*}{\partial \lambda} = 2x - y - 5 \end{aligned}$$

Solving this set of equations yields $[x \ y \ \lambda]^T = [2 \ -1 \ 1]^T$. The cost function of Eq. (5.42) evaluated at the minimum of the augmented cost function is

$$C: \frac{1}{2}[(2)^2 + (-1)^2] = \frac{5}{2}$$

If there is more than one equality constraint (i.e., if $g(x,u)$ of Eq. (5.39) is a vector of functions) then λ becomes a vector of multipliers and the augmented cost function becomes

$$C^*: f(x,u) - [\lambda]^T g(x,u) \quad (5.44)$$

where the derivatives of C^* become

$$\left[\frac{\partial C^*}{\partial \lambda} \right] = 0 = g(x,u) \quad (5.45)$$

$$\left[\frac{\partial C^*}{\partial x} \right] = 0 = \left[\frac{\partial f}{\partial x} \right] - \left[\frac{\partial g}{\partial x} \right]^T [\lambda] \quad (5.46)$$

$$\left[\frac{\partial C^*}{\partial u} \right] = 0 = \left[\frac{\partial f}{\partial u} \right] = \left[\frac{\partial g}{\partial u} \right]^T [\lambda] \quad (5.47)$$

Note that for any *feasible* solution, Eq. (5.45) is satisfied, but the feasible solution may not be the optimal solution that minimizes the cost function. In this case, $[\lambda]$ can be obtained from Eq. (5.46) and then only

$$\left[\frac{\partial C^*}{\partial u} \right] \neq 0$$

This vector can be used as a gradient vector $[\nabla C]$, which is orthogonal to the contour of constant values of the cost function C . Thus,

$$[\lambda] = \left[\begin{bmatrix} \frac{\partial g}{\partial x} \end{bmatrix}^T \right]^{-1} \begin{bmatrix} \frac{\partial f}{\partial x} \end{bmatrix} \quad (5.48)$$

which gives

$$\nabla C = \begin{bmatrix} \frac{\partial C^*}{\partial u} \end{bmatrix} = \begin{bmatrix} \frac{\partial f}{\partial u} \end{bmatrix} - \begin{bmatrix} \frac{\partial g}{\partial u} \end{bmatrix}^T [\lambda] \quad (5.49)$$

$$= \begin{bmatrix} \frac{\partial f}{\partial u} \end{bmatrix} - \begin{bmatrix} \frac{\partial g}{\partial u} \end{bmatrix}^T \left[\begin{bmatrix} \frac{\partial g}{\partial x} \end{bmatrix}^T \right]^{-1} \begin{bmatrix} \frac{\partial f}{\partial x} \end{bmatrix} \quad (5.50)$$

This relationship provides the foundation of the optimization method known as the *steepest descent* algorithm.

5.2.1 Steepest Descent Algorithm

1. Let $k = 0$. Guess an initial vector $u^k = u^0$.
2. Solve the (possibly nonlinear) system of Eq. (5.45) for a feasible solution x .
3. Calculate C^{k+1} and ∇C^{k+1} from Eq. (5.50). If $\|C^{k+1} - C^k\|$ is less than some predefined tolerance, stop.
4. Calculate the new vector $u^{k+1} = u^k - \gamma \nabla C$, where γ is a positive number, which is the user-defined “stepsize” of the algorithm.
5. $k = k + 1$. Go to step 2.

In the steepest descent method, the u vector update direction is determined at each step of the algorithm by choosing the direction of the greatest change of the augmented cost function C^* . The direction of steepest descent is perpendicular to the tangent of the curve of constant cost. The distance between adjustments is analogous to the stepsize γ of the algorithm. Thus the critical part of the steepest descent algorithm is the choice of γ . If γ is chosen small, then convergence to minimum value is more likely, but may require many iterations, whereas a large value of γ may result in oscillations about the minimum.

Example 5.4

Minimize

$$C: x_1^2 + 2x_2^2 + u^2 = f(x_1, x_2, u) \quad (5.51)$$

subject to the following constraints:

$$0 = x_1^2 - 3x_2 + u - 3 \quad (5.52)$$

$$0 = x_1 + x_2 - 4u - 2 \quad (5.53)$$

Solution

To find ∇C of Eq. (5.50), the following partial derivatives are required:

$$\left[\frac{\partial f}{\partial u} \right] = 2u$$

$$\left[\frac{\partial f}{\partial x} \right] = \begin{bmatrix} 2x_1 \\ 4x_2 \end{bmatrix}$$

$$\left[\frac{\partial g}{\partial u} \right]^T = [1 \ -4]$$

$$\left[\frac{\partial g}{\partial x} \right] = \begin{bmatrix} 2x_1 & -3 \\ 1 & 1 \end{bmatrix}$$

yielding

$$\begin{aligned} \nabla C &= \left[\frac{\partial f}{\partial u} \right] - \left[\frac{\partial g}{\partial u} \right]^T \left[\left[\frac{\partial g}{\partial x} \right]^T \right]^{-1} \left[\frac{\partial f}{\partial x} \right] \\ &= 2u - [1 \ -4] \left[\begin{bmatrix} 2x_1 & -3 \\ 1 & 1 \end{bmatrix}^T \right]^{-1} \begin{bmatrix} 2x_1 \\ 4x_2 \end{bmatrix} \end{aligned}$$

Iteration 1

Let $u = 1$, $\gamma = 0.05$, and choose a stopping criterion of $\varepsilon = 0.0001$. Solving for x_1 and x_2 yields two values for each with a corresponding cost function:

$$\begin{aligned} x_1 &= 1.7016 & x_2 &= 0.2984 & f &= 4.0734 \\ x_1 &= -4.7016 & x_2 &= 6.7016 & f &= 23.2828 \end{aligned}$$

The first set of values leads to the minimum cost function, so they are selected as the operating solution. Substituting $x_1 = 1.7016$ and $x_2 = 0.2984$ into the gradient function yields $\nabla C = 10.5705$ and the new value of u becomes

$$\begin{aligned} u^{(2)} &= u^{(1)} - \gamma \Delta C \\ &= 1 - (0.05)(10.5705) \\ &= 0.4715 \end{aligned}$$

Iteration 2

With $u = 0.4715$, solving for x_1 and x_2 again yields two values for each with a corresponding cost function:

$$\begin{aligned} x_1 &= 0.6062 & x_2 &= -0.7203 & f &= 1.6276 \\ x_1 &= -3.6062 & x_2 &= 3.4921 & f &= 14.2650 \end{aligned}$$

The first set of values again leads to the minimum cost function, so they are selected as the operating solution. The difference in cost functions is

$$|C^{(1)} - C^{(2)}| = |4.0734 - 1.6276| = 2.4458$$

which is greater than the stopping criterion. Substituting these values into the gradient function yields $\nabla C = 0.1077$ and the new value of u becomes

$$\begin{aligned} u^{(3)} &= u^{(2)} - \gamma \Delta C \\ &= 0.4715 - (0.05)(0.1077) \\ &= 0.4661 \end{aligned}$$

Iteration 3

With $u = 0.4661$, solving for x_1 and x_2 again yields two values for each with a corresponding cost function:

$$\begin{aligned} x_1 &= 0.5921 & x_2 &= -0.7278 & f &= 1.6271 \\ x_1 &= 3.5921 & x_2 &= 3.4565 & f &= 14.1799 \end{aligned}$$

The first set of values again leads to the minimum cost function, so they are selected as the operating solution. The difference in cost functions is

$$|C^{(2)} - C^{(3)}| = |1.6276 - 1.6271| = 0.005$$

which is greater than the stopping criterion. Substituting these values into the gradient function yields $\nabla C = 0.0541$ and the new value of u becomes

$$\begin{aligned} u^{(4)} &= u^{(3)} - \gamma \Delta C \\ &= 0.4661 - (0.05)(0.0541) \\ &= 0.4634 \end{aligned}$$

Iteration 4

With $u = 0.4634$, solving for x_1 and x_2 again yields two values for each with a corresponding cost function:

$$\begin{aligned} x_1 &= 0.5850 & x_2 &= -0.7315 & f &= 1.6270 \\ x_1 &= 3.5850 & x_2 &= 3.4385 & f &= 14.1370 \end{aligned}$$

The first set of values again leads to the minimum cost function, so they are selected as the operating solution. The difference in cost functions is

$$|C^{(3)} - C^{(4)}| = |1.6271 - 1.6270| = 0.001$$

which satisfies the stopping criterion. Thus, the values $x_1 = 0.5850$, $x_2 = -0.7315$, and $u = 0.4634$ yield the minimum cost function $f = 1.6270$.

Many power system applications, such as the power flow, offer only a snapshot of the system operation. Frequently, the system planner or operator is interested in the effect that making adjustments to the system parameters will have on the power flow through lines or system losses. Rather than making the adjustments in a random fashion, the system planner will attempt to optimize the adjustments according to some objective function. This objective function can be chosen to minimize generating costs, reservoir water levels, or system losses, among others. The OPF problem is to formulate the power flow problem to find system voltages and generated powers within the framework of the objective function. In this application, the inputs to the power flow are systematically adjusted to maximize

(or minimize) a scalar function of the power flow state variables. The two most common objective functions are minimization of generating costs and minimization of active power losses.

The time frame of OPF is on the order of minutes to one hour; therefore it is assumed that the optimization occurs using only those units that are currently on-line. The problem of determining whether or not to engage a unit, at what time, and for how long is part of the *unit commitment* problem and is not covered here. The minimization of active transmission losses saves both generating costs and creates a higher generating reserve margin.

Example 5.5

Consider again the three machine system of [Example 5.2](#) except that bus 3 has been converted to a generator bus with a voltage magnitude of 1.0 pu. The cost functions of the generators are

$$\begin{aligned} C_1 &: P_1 + 0.0625P_1^2 \text{ \$/h} \\ C_2 &: P_2 + 0.0125P_2^2 \text{ \$/h} \\ C_3 &: P_3 + 0.0250P_3^2 \text{ \$/h} \end{aligned}$$

Find the optimal generation scheduling of this system.

Solution

Following the steepest descent procedure, the first step is to develop an expression for the gradient ∇C , where

$$\nabla C = \left[\frac{\partial f}{\partial u} \right] - \left[\frac{\partial g}{\partial u} \right]^T \left[\left[\frac{\partial g}{\partial x} \right]^T \right]^{-1} \left[\frac{\partial f}{\partial x} \right] \quad (5.54)$$

where f is the sum of the generator costs:

$$f: C_1 + C_2 + C_3 = P_1 + 0.0625P_1^2 + P_2 + 0.0125P_2^2 + P_3 + 0.0250P_3^2$$

g is the set of load flow equations:

$$\begin{aligned} g_1: 0 &= P_2 - P_{L2} - V_2 \sum_{i=1}^3 V_i Y_{2i} \cos(\delta_2 - \delta_i - \phi_{2i}) \\ g_2: 0 &= P_3 - P_{L3} - V_3 \sum_{i=1}^3 V_i Y_{3i} \cos(\delta_3 - \delta_i - \phi_{3i}) \end{aligned}$$

where P_{Li} denotes the active power load at bus i , the set of inputs u is the set of independent generation settings:

$$u = \begin{bmatrix} P_2 \\ P_3 \end{bmatrix}$$

and x is the set of unknown states

$$x = \begin{bmatrix} \delta_2 \\ \delta_3 \end{bmatrix}$$

The generator setting P_1 is not an input because it is the slack bus generation and cannot be independently set. From these designations, the various partial derivatives required for ∇C can be derived:

$$\left[\frac{\partial g}{\partial u} \right] = \begin{bmatrix} 1 \\ 1 \end{bmatrix} \quad (5.55)$$

$$\left[\frac{\partial g}{\partial x} \right] = \begin{bmatrix} \frac{\partial g_1}{\partial \delta_2} & \frac{\partial g_1}{\partial \delta_3} \\ \frac{\partial g_2}{\partial \delta_2} & \frac{\partial g_2}{\partial \delta_3} \end{bmatrix} \quad (5.56)$$

where

$$\frac{\partial g_1}{\partial \delta_2} = V_2(V_1 Y_{12} \sin(\delta_2 - \delta_1 - \phi_{21}) + V_3 Y_{13} \sin(\delta_2 - \delta_3 - \phi_{23})) \quad (5.57)$$

$$\frac{\partial g_1}{\partial \delta_3} = V_2 V_3 Y_{32} \sin(\delta_2 - \delta_3 - \phi_{23}) \quad (5.58)$$

$$\frac{\partial g_2}{\partial \delta_2} = V_3 V_2 Y_{23} \sin(\delta_3 - \delta_2 - \phi_{32}) \quad (5.59)$$

$$\frac{\partial g_2}{\partial \delta_3} = V_3(V_1 Y_{13} \sin(\delta_3 - \delta_1 - \phi_{31}) + V_2 Y_{23} \sin(\delta_3 - \delta_2 - \phi_{32})) \quad (5.60)$$

and

$$\left[\frac{\partial f}{\partial u} \right] = \begin{bmatrix} 1 + 0.025P_2 \\ 1 + 0.050P_3 \end{bmatrix} \quad (5.61)$$

Finding the partial derivative $[\partial f / \partial x]$ is slightly more difficult since the cost function is not written as a direct function of x . Recall, however, that P_1 is not an input, but is actually a quantity that depends on x , i.e.,

$$P_1 = V_1(V_1 Y_{11} \cos(\delta_1 - \delta_1 - \phi_{11}) + V_2 Y_{12} \cos(\delta_1 - \delta_2 - \phi_{12}) + V_3 Y_{13} \cos(\delta_1 - \delta_3 - \phi_{13})) \quad (5.62)$$

Thus, using the chain rule,

$$\left[\frac{\partial f}{\partial x} \right] = \left[\frac{\partial f}{\partial P_1} \right] \left[\frac{\partial P_1}{\partial x} \right] \quad (5.63)$$

$$= (1 + 0.125P_1) \begin{bmatrix} V_1 V_2 Y_{12} \sin(\delta_1 - \delta_2 - \phi_{12}) \\ V_1 V_3 Y_{13} \sin(\delta_1 - \delta_3 - \phi_{13}) \end{bmatrix} \quad (5.64)$$

If the initial values of $P_2 = 0.56$ pu and $P_3 = 0.28$ pu are used as inputs, then the power flow yields the following states: $[\delta_2 \quad \delta_3] = [0.0286 \quad -0.0185]$ in radians and $P_1 = 0.1152$. Converting the generated powers to megawatt and substituting these values into the partial derivatives yields

$$\left[\frac{\partial g}{\partial u} \right] = \begin{bmatrix} 1 & 0 \\ 0 & 1 \end{bmatrix} \quad (5.65)$$

$$\left[\begin{array}{c} \frac{\partial g}{\partial x} \\ \end{array} \right] = \left[\begin{array}{cc} -13.3267 & 9.9366 \\ 9.8434 & -19.9219 \\ \end{array} \right] \quad (5.66)$$

$$\left[\begin{array}{c} \frac{\partial f}{\partial u} \\ \end{array} \right] = \left[\begin{array}{c} 15.0000 \\ 15.0000 \\ \end{array} \right] \quad (5.67)$$

$$\left[\begin{array}{c} \frac{\partial f}{\partial x} \\ \end{array} \right] = 15.4018 \left[\begin{array}{c} -52.0136 \\ 155.8040 \\ \end{array} \right] \quad (5.68)$$

which yields

$$\nabla C = \left[\begin{array}{c} -0.3256 \\ -0.4648 \\ \end{array} \right] \quad (5.69)$$

Thus, the new values for the input generation are

$$\left[\begin{array}{c} P_2 \\ P_3 \\ \end{array} \right] = \left[\begin{array}{c} 560 \\ 280 \\ \end{array} \right] - \gamma \left[\begin{array}{c} -0.3256 \\ -0.4648 \\ \end{array} \right] \quad (5.70)$$

With $\gamma = 1$, the updated generation is $P_2 = 560.3$ and $P_3 = 280.5$ MW.

Proceeding with more iterations until the gradient is reduced to less than a user-defined value yields the final generation values for all of the generators:

$$\left[\begin{array}{c} P_1 \\ P_2 \\ P_3 \\ \end{array} \right] = \left[\begin{array}{c} 112.6 \\ 560.0 \\ 282.7 \\ \end{array} \right] \text{ MW}$$

which yields a cost of \$7664/MW h.

Often the steepest descent method may indicate that either states or inputs lie outside of their physical constraints. For example, the algorithm may result in a power generation value that exceeds the physical maximum output of the generating unit. Similarly, the resulting bus voltages may lie outside of the desired range (usually $\pm 10\%$ of unity). These are violations of the *inequality constraints* of the problem. In these cases, the steepest descent algorithm must be modified to reflect these physical limitations. There are several approaches to account for limitations and these approaches depend on whether or not the limitation is on the input (independent) or on the state (dependent).

5.2.2 Limitations on Independent Variables

If the application of the steepest descent algorithm results in an updated value of input that exceeds the specified limit, then the most straightforward method of handling this violation is simply to set the input state equal to its limit and continue with the algorithm except with one less degree of freedom.

Example 5.6

Repeat Example 5.5 except that the generators must satisfy the following limitations:

$$80 \leq P_1 \leq 1200 \text{ MW}$$

$$450 \leq P_2 \leq 750 \text{ MW}$$

$$150 \leq P_3 \leq 250 \text{ MW}$$

Solution

From the solution of [Example 5.5](#), the output of generator 3 exceeds the maximum limit of 0.25 pu. Therefore after the first iteration in the previous example, P_3 is set to 0.25 pu. The new partial derivatives become

$$\left[\frac{\partial g}{\partial u} \right] = \begin{bmatrix} 0 \\ 1 \end{bmatrix} \quad (5.71)$$

$$\left[\frac{\partial g}{\partial x} \right] = \text{same} \quad (5.72)$$

$$\left[\frac{\partial f}{\partial u} \right] = [1 + 0.025P_2] \quad (5.73)$$

$$\left[\frac{\partial f}{\partial x} \right] = \text{same} \quad (5.74)$$

From the constrained steepest descent, the new values of generation become

$$\begin{bmatrix} P_1 \\ P_2 \\ P_3 \end{bmatrix} = \begin{bmatrix} 117.1 \\ 588.3 \\ 250.0 \end{bmatrix} \text{ MW}$$

with a cost of \$7703/MW h, which is higher than the unconstrained cost of generation of \$7664/MW h. As more constraints are added to the system, the system is moved away from the optimal operating point, increasing the cost of generation.

5.2.3 Limitations on Dependent Variables

In many cases, the physical limitations of the system are imposed upon states that are dependent variables in the system description. In this case, the inequality equations are functions of x and must be added to the cost function. Examples of limitations on dependent variables include maximum line flows or bus voltage levels. In these cases, the value of the states cannot be independently set, but must be enforced indirectly. One method of enforcing an inequality constraint is to introduce a *penalty function* into the cost function. A penalty function is a function that is small when the state is far away from its limit, but becomes increasingly larger the closer the state is to its limit. Typical penalty functions include

$$p(h) = e^{kh} \quad k > 0 \quad (5.75)$$

$$p(h) = x^{2n}e^{kh} \quad n,k > 0 \quad (5.76)$$

$$p(h) = ax^{2n}e^{kh} + be^{kh} \quad n,k,a,b > 0 \quad (5.77)$$

and the cost function becomes

$$C^*: C(u,x) + \lambda^T g(u,x) + p(h(u,x)) - h^{\max} \quad (5.78)$$

This cost equation is then minimized in the usual fashion by setting the appropriate derivatives to zero. This method not only has the advantage of simplicity of implementation, but also has several disadvantages. The first disadvantage is that the choice of penalty function is often a heuristic choice and

can vary by application. A second disadvantage is that this method cannot enforce *hard* limitations on states, i.e., the cost function becomes large if the maximum is exceeded, but the state is allowed to exceed its maximum. In many applications this is not a serious disadvantage. If the power flow on a transmission line slightly exceeds its maximum, it is reasonable to assume that the power system will continue to operate, at least for a finite length of time. If, however, the physical limit is the height above ground for an airplane, then even a slightly negative altitude will have dire consequences. Thus the use of penalty functions to enforce limits must be used with caution and is not applicable for all systems.

Example 5.7

Repeat Example 5.5, except use penalty functions to limit the power flow across line 2–3 to 0.4 pu.

Solution

The power flow across line 2–3 in Example 5.5 is given by

$$\begin{aligned} P_{23} &= V_2 V_3 Y_{23} \cos(\delta_2 - \delta_3 - \phi_{23}) - V_2^2 Y_{23} \cos \phi_{23} \\ &= 0.467 \text{ pu} \end{aligned} \quad (5.79)$$

If P_{23} exceeds 0.4 pu, then the penalty function

$$p(h) = [1000V_2 V_3 Y_{23} \cos(\delta_2 - \delta_3 - \phi_{23}) - 1000V_2^2 Y_{23} \cos \phi_{23} - 400]^2 \quad (5.80)$$

will be appended to the cost function. The partial derivatives remain the same with the exception of $[\partial f / \partial x]$, which becomes

$$\left[\frac{\partial f}{\partial x} \right] = \left[\frac{\partial f}{\partial P_1} \right] \left[\frac{\partial P_1}{\partial x} \right] + \left[\frac{\partial f}{\partial P_{23}} \right] \left[\frac{\partial P_{23}}{\partial x} \right] \quad (5.81)$$

$$\begin{aligned} &= (1 + 0.125P_1) \begin{bmatrix} V_1 V_2 Y_{12} \sin(\delta_1 - \delta_2 - \phi_{1,2}) \\ V_1 V_3 Y_{13} \sin(\delta_1 - \delta_3 - \phi_{1,3}) \end{bmatrix} \\ &\quad + 2(P_{23} - 400) \begin{bmatrix} -V_2 V_3 Y_{23} \sin(\delta_2 - \delta_3 - \phi_{23}) \\ V_2 V_3 Y_{23} \sin(\delta_2 - \delta_3 - \phi_{23}) \end{bmatrix} \end{aligned} \quad (5.82)$$

Proceeding with the steepest gradient algorithm iterations yields the final constrained optimal generation scheduling:

$$\begin{bmatrix} P_1 \\ P_2 \\ P_3 \end{bmatrix} = \begin{bmatrix} 128.5 \\ 476.2 \\ 349.9 \end{bmatrix} \text{ MW}$$

and $P_{23} = 400$ MW. The cost for this constrained scheduling is \$7882/MW h, which is slightly greater than the nonconstrained cost.

In the case where hard limits must be imposed, an alternate approach to enforcing the inequality constraints must be employed. In this approach, the inequality constraints are added as additional equality constraints with the inequality set equal to the limit (upper or lower) that is violated. This in essence introduces an additional set of Lagrangian multipliers. This is often referred to as the dual-variable approach, because each inequality has the potential of resulting in two equalities: one for the upper limit and one for the lower limit. However, the upper and lower limit cannot be simultaneously violated; thus, out of the possible set of additional Lagrangian multipliers only one of the two will be included at any given operating point and thus the dual limits are mutually exclusive.

Example 5.8

Repeat Example 5.7 using the dual-variable approach.

Solution

By introducing the additional equation

$$P_{23} = V_2 V_3 Y_{23} \cos(\delta_2 - \delta_3 - \phi_{23}) - V_2^2 Y_{23} \cos \phi_{23} = 0.400 \text{ pu} \quad (5.83)$$

to the equality constraints, an additional equation gets added to the set of $g(x)$. Therefore an additional unknown must be added to the state vector x to yield a solvable set of equations (three equations in three unknowns). Either P_{G2} or P_{G3} can be chosen as the additional unknown. In this example, P_{G3} will be chosen. The new system Jacobian becomes

$$\begin{bmatrix} \partial g \\ \partial x \end{bmatrix} = \begin{bmatrix} \frac{\partial g_1}{\partial x_1} & \frac{\partial g_1}{\partial x_2} & \frac{\partial g_1}{\partial x_3} \\ \frac{\partial g_2}{\partial x_1} & \frac{\partial g_2}{\partial x_2} & \frac{\partial g_2}{\partial x_3} \\ \frac{\partial g_3}{\partial x_1} & \frac{\partial g_3}{\partial x_2} & \frac{\partial g_3}{\partial x_3} \end{bmatrix} \quad (5.84)$$

where

$$\begin{aligned} \frac{\partial g_1}{\partial x_1} &= V_2(V_1 Y_{12} \sin(\delta_2 - \delta_1 - \phi_{21}) + V_3 Y_{13} \sin(\delta_2 - \delta_3 - \phi_{23})) \\ \frac{\partial g_1}{\partial x_2} &= -V_2 V_3 Y_{32} \sin(\delta_2 - \delta_3 - \phi_{23}) \\ \frac{\partial g_1}{\partial x_3} &= 0 \\ \frac{\partial g_2}{\partial x_1} &= -V_3 V_2 Y_{23} \sin(\delta_3 - \delta_2 - \phi_{32}) \\ \frac{\partial g_2}{\partial x_2} &= V_3(V_1 Y_{13} \sin(\delta_3 - \delta_1 - \phi_{31}) + V_2 Y_{23} \sin(\delta_3 - \delta_2 - \phi_{32})) \\ \frac{\partial g_2}{\partial x_3} &= 1 \\ \frac{\partial g_3}{\partial x_1} &= -V_2 V_3 Y_{23} \sin(\delta_2 - \delta_3 - \phi_{23}) \\ \frac{\partial g_3}{\partial x_2} &= V_2 V_3 Y_{23} \sin(\delta_2 - \delta_3 - \phi_{23}) \\ \frac{\partial g_3}{\partial x_3} &= 0 \end{aligned}$$

and

$$\begin{bmatrix} \partial g \\ \partial u \end{bmatrix} = \begin{bmatrix} 1 \\ 0 \\ 0 \end{bmatrix}; \quad \begin{bmatrix} \partial f \\ \partial u \end{bmatrix} = [1 + 0.025 P_{G2}]$$

Similar to [Example 5.5](#), the chain rule is used to obtain $[\partial f / \partial x]$:

$$\left[\frac{\partial f}{\partial x} \right] = \left[\frac{\partial C}{\partial P_{G1}} \right] \left[\frac{\partial P_{G1}}{\partial x} \right] + \left[\frac{\partial C}{\partial P_{G3}} \right] \left[\frac{\partial P_{G3}}{\partial x} \right] \quad (5.85)$$

$$= (1 + 0.125P_{G1}) \begin{bmatrix} V_1 V_2 Y_{12} \sin(\delta_1 - \delta_2 - \phi_{12}) \\ V_1 V_3 Y_{13} \sin(\delta_1 - \delta_3 - \phi_{13}) \\ 0 \end{bmatrix} + \\ (1 + 0.050P_{G3}) \begin{bmatrix} V_3 V_2 Y_{32} \sin(\delta_3 - \delta_2 - \phi_{32}) \\ -V_3 (V_1 Y_{13} \sin(\delta_3 - \delta_1 - \phi_{31}) + V_2 Y_{23} \sin(\delta_3 - \delta_2 - \phi_{32})) \\ 0 \end{bmatrix} \quad (5.86)$$

Substituting these partial derivatives into the expression for ∇C of [Eq. \(5.54\)](#) yields the same generation scheduling as [Example 5.7](#).

5.3 State Estimation

In many physical systems, the system operating condition cannot be determined directly by an analytical solution of known equations using a given set of known, dependable quantities. More frequently, the system operating condition is determined by the measurement of system states at different points throughout the system. In many systems, more measurements are made than are necessary to uniquely determine the operating point. This redundancy is often purposely designed into the system to counteract the effect of inaccurate or missing data due to instrument failure. Conversely, not all of the states may be available for measurement. High temperatures, moving parts, or inhospitable conditions may make it difficult, dangerous, or expensive to measure certain system states. In this case, the missing states must be estimated from the rest of the measured information of the system. This process is often known as *state estimation* and is the process of estimating unknown states from measured quantities. State estimation gives the “best estimate” of the state of the system in spite of uncertain, redundant, and/or conflicting measurements. A good state estimation will smooth out small random errors in measurements, detect and identify large measurement errors, and compensate for missing data. This process strives to minimize the error between the (unknown) true operating state of the system and the measured states.

The set of measured quantities can be denoted by the vector z , which may include measurements of system states (such as voltage and current) or quantities that are functions of system states (such as power flows). Thus,

$$z^{\text{true}} = Ax \quad (5.87)$$

where x is the set of system states and A is usually not square. The error vector is the difference between the measured quantities z and the true quantities:

$$e = z - z^{\text{true}} = z - Ax \quad (5.88)$$

Typically, the minimum of the square of the error is desired to negate any effects of sign differences between the measured and true values. Thus, a state estimator endeavors to find the minimum of the squared error, or a *least squares minimization*:

$$\text{minimize} \|e\|^2 = e^T \cdot e = \sum_{i=1}^m \left[z_i - \sum_{j=1}^m a_{ij} x_j \right]^2 \quad (5.89)$$

The squared error function can be denoted by $U(x)$ and is given by

$$U(x) = e^T \cdot e = (z - Ax)^T(z - Ax) \quad (5.90)$$

$$= (z^T - x^T A^T)(z - Ax) \quad (5.91)$$

$$= (z^T z - z^T Ax - x^T A^T z + x^T A^T Ax) \quad (5.92)$$

Note that the product $z^T Ax$ is a scalar and so it can be equivalently written as

$$z^T Ax = (z^T Ax)^T = x^T A^T z$$

Therefore the squared error function is given by

$$U(x) = z^T z - 2x^T A^T z + x^T A^T Ax \quad (5.93)$$

The minimum of the squared error function can be found by an unconstrained optimization where the derivative of the function with respect to the states x is set to zero:

$$\frac{\partial U(x)}{\partial x} = 0 - 2A^T z + 2A^T z + 2A^T Ax \quad (5.94)$$

Thus,

$$A^T Ax = A^T z \quad (5.95)$$

Thus, if $b = A^T z$ and $\hat{A} = A^T A$, then

$$\hat{A}x = b \quad (5.96)$$

This state vector x is the best estimate (in the squared error) to the system operating condition from which the measurements z were taken. The measurement error is given by

$$e = z^{\text{meas}} - Ax \quad (5.97)$$

In power system state estimation, the estimated variables are the voltage magnitudes and the voltage phase angles at the system buses. The input to the state estimator is the active and reactive powers of the system, measured either at the injection sites or on the transmission lines. The state estimator is designed to give the best estimates of the voltages and phase angles minimizing the effects of the measurement errors. All instruments add some degree of error to the measured values, but the problem is how to quantify this error and account for it during the estimation process.

If all measurements are treated equally in the least squares solution, then the less accurate measurements will affect the estimation as significantly as the more accurate measurements. As a result, the final estimation may contain large errors due to the influence of inaccurate measurements. By introducing a weighting matrix to emphasize the more accurate measurements more heavily than the less accurate measurements, the estimation procedure can then force the results to coincide more closely with the measurements of greater accuracy. This leads to the weighted least squares estimation:

$$\text{minimize} \|e\|^2 = e^T \cdot e = \sum_{i=1}^m w_i \left[z_i - \sum_{j=1}^m a_{ij} x_j \right]^2 \quad (5.98)$$

where w_i is a weighting factor reflecting the level of confidence in the measurement z_i .

In general, it can be assumed that the introduced errors have normal (Gaussian) distribution with zero mean and that each measurement is independent of all other measurements. This means that each measurement error is as likely to be greater than the true value as it is to be less than the true value. A zero mean Gaussian distribution has several attributes. The standard deviation of a zero mean Gaussian distribution is denoted by σ . This means that 68% of all measurements will fall within $\pm\sigma$ of the expected value, which is zero in a zero mean distribution. Further, 95% of all measurements will fall within $\pm 2\sigma$ and 99% of all measurements will fall within $\pm 3\sigma$. The variance of the measurement distribution is given by σ^2 . This implies that if the variance of the measurements is relatively small, then the majority of measurements are close to the mean. One interpretation of this is that accurate measurements lead to small variance in the distribution.

This relationship between accuracy and variance leads to a straightforward approach from which a weighting matrix for the estimation can be developed. With measurements taken from a particular meter, the smaller the variance of the measurements (i.e., the more consistent they are), the greater the level of confidence in that set of measurements. A set of measurements that have a high level of confidence should have a higher weighting than a set of measurements that have a larger variance (and therefore less confidence). Therefore, a plausible weighting matrix that reflects the level of confidence in each measurement set is the inverse of the covariance matrix. Thus, measurements that come from instruments with good consistency (small variance) will carry greater weight than measurements that come from less accurate instruments (high variance). Thus, one possible weighting matrix is given by

$$W = R^{-1} = \begin{bmatrix} \frac{1}{\sigma_1^2} & 0 & \dots & 0 \\ 0 & \frac{1}{\sigma_2^2} & \dots & 0 \\ \vdots & \vdots & \ddots & \vdots \\ 0 & 0 & \dots & \frac{1}{\sigma_m^2} \end{bmatrix} \quad (5.99)$$

where R is the covariance matrix for the measurements.

As in the linear least squares estimation, the nonlinear least squares estimation attempts to minimize the square of the errors between a known set of measurements and a set of weighted nonlinear functions:

$$\text{minimize } f = \|e\|^2 = e^T \cdot e = \sum_{i=1}^m \frac{1}{\sigma_i^2} [z_i - h_i(x)]^2 \quad (5.100)$$

where $x \in R^n$ is the vector of unknowns to be estimated, $z \in R^m$ is the vector of measurements, σ_i^2 is the variance of the i th measurement, and $h(x)$ is the nonlinear function vector relating x to z , where the measurement vector z can be a set of geographically distributed measurements, such as voltages and power flows.

In state estimation, the unknowns in the nonlinear equations are the state variables of the system. The state values that minimize the error are found by setting the derivatives of the error function to zero:

$$F(x) = H_x^T R^{-1} [z - h(x)] = 0 \quad (5.101)$$

where

$$H_x = \begin{bmatrix} \frac{\partial h_1}{\partial x_1} & \frac{\partial h_1}{\partial x_2} & \dots & \frac{\partial h_1}{\partial x_n} \\ \frac{\partial h_2}{\partial x_1} & \frac{\partial h_2}{\partial x_2} & \dots & \frac{\partial h_2}{\partial x_n} \\ \vdots & \vdots & \ddots & \vdots \\ \frac{\partial h_m}{\partial x_1} & \frac{\partial h_m}{\partial x_2} & \dots & \frac{\partial h_m}{\partial x_n} \end{bmatrix} \quad (5.102)$$

Note that Eq. (5.101) is a set of nonlinear equations that must be solved using Newton–Raphson or another iterative numerical solver. In this case, the Jacobian of $F(x)$ is

$$J_F(x) = H_x^T(x)R^{-1} \frac{\partial}{\partial x} [z - h(x)] \quad (5.103)$$

$$= -H_x^T(x)R^{-1}H_x(x) \quad (5.104)$$

and the Newton–Raphson iteration becomes

$$[H_x^T(x^k)R^{-1}H_x(x^k)][x^{k+1} - x^k] = H_x^T(x^k)R^{-1}[z - h(x^k)]. \quad (5.105)$$

At convergence, x^{k+1} is equal to the set of states that minimize the error function f of Eq. (5.100).

Example 5.9

The SCADA system for the power network shown in Fig. 5.3 reports the following measurements and variances:

z_i	State	Measurement	Variance (s^2)
1	V_3	0.975	0.010
2	P_{13}	0.668	0.050
3	Q_{21}	-0.082	0.075
4	P_3	-1.181	0.050
5	Q_2	-0.086	0.075

Estimate the power system states.

Solution

The first step in the estimation process is to identify and enumerate the unknown states. In this example, the unknowns are $[x_1 \ x_2 \ x_3]^T = [\delta_2 \ \delta_3 \ V_3]^T$. After the states are identified, the next step in the estimation process is to identify the appropriate functions $h(x)$ that correspond to each of the measurements. The nonlinear function that is being driven to zero to minimize the weighted error is

$$F(x) = H_x^T R^{-1} [z - h(x)] = 0 \quad (5.106)$$

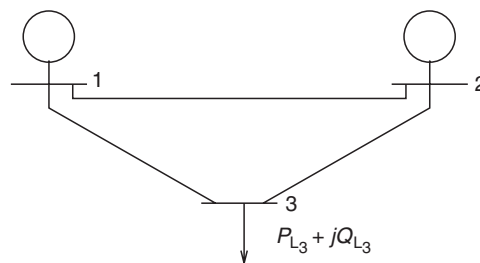


FIGURE 5.3 Example power system.

where the set of $z - h(x)$ is given by

$$\begin{aligned}
z_1 - h_1(x) &= V_3 - x_3 \\
z_2 - h_2(x) &= P_{13} - (V_1 x_3 Y_{12} \cos(-x_2 - \phi_{13}) - V_1^2 Y_{13} \cos \phi_{13}) \\
z_3 - h_3(x) &= Q_{21} - (V_2 V_1 Y_{21} \sin(x_1 - \phi_{21}) + V_2^2 Y_{21} \sin \phi_{21}) \\
z_4 - h_4(x) &= P_3 - (x_3 V_1 Y_{31} \cos(x_2 - \phi_{31}) + x_3 V_2 Y_{32} \cos(x_2 - x_1 - \phi_{32}) \\
&\quad + x_3^2 Y_{33} \cos \phi_{33}) \\
z_5 - h_5(x) &= Q_2 - \left[\begin{array}{l} V_2 V_1 Y_{21} \sin(x_1 - \phi_{21}) - V_2^2 Y_{22} \sin \phi_{22} \\ + V_2 x_3 Y_{23} \sin(x_1 - x_2 - \phi_{23}) \end{array} \right]
\end{aligned}$$

and the matrix of partial derivatives for the set of functions in Eq. (5.106) is

$$H_x = \left[\begin{array}{ccc} 0 & 0 & 0 \\ 0 & V_1 x_3 Y_{13} \sin(-x_2 - \phi_{13}) & 0 \\ V_1 V_2 Y_{21} \cos(x_1 - \phi_{21}) & 0 & -x_3 V_1 Y_{31} \sin(x_2 - \phi_{31}) - x_3 V_2 Y_{32} \sin(x_2 - x_1 - \phi_{32}) \\ x_3 V_2 Y_{32} \sin(x_2 - x_1 - \phi_{32}) & -x_3 V_1 Y_{31} \sin(x_2 - \phi_{31}) - x_3 V_2 Y_{32} \sin(x_2 - x_1 - \phi_{32}) & -V_2 x_3 Y_{23} \cos(x_1 - x_2 - \phi_{23}) \\ V_1 V_2 Y_{21} \cos(x_1 - \phi_{21}) + V_2 x_3 Y_{23} \cos(x_1 - x_2 - \phi_{23}) & -V_2 x_3 Y_{23} \cos(x_1 - x_2 - \phi_{23}) & \end{array} \right] \quad (5.107)$$

The covariance matrix of the measurements is

$$R = \left[\begin{array}{cccc} \frac{1}{0.010^2} & & & \\ & \frac{1}{0.050^2} & & \\ & & \frac{1}{0.075^2} & \\ & & & \frac{1}{0.050^2} \\ & & & & \frac{1}{0.075^2} \end{array} \right] \quad (5.108)$$

The Newton–Raphson iteration to solve for the set of states x that minimize the weighted errors is

$$[H_x^T(x^k) R^{-1} H_x(x^k)] [x^{k-1} - x^k] = H_x^T(x^k) R^{-1} [z - h(x^k)] \quad (5.109)$$

Iteration 1

The initial condition for the state estimation solution is the same flat start as for the power flow equations; namely, all angles are set to zero and all unknown voltage magnitudes are set to unity. The measurement functions $h(x)$ evaluated at the initial conditions are

$$h(x^0) = \begin{bmatrix} 1.0000 \\ 0.0202 \\ -0.0664 \\ -0.0198 \\ -0.1914 \end{bmatrix}$$

The matrix of partials evaluated at the initial condition yields

$$H_x^0 = \begin{bmatrix} 0 & 0 & 1.0000 \\ 0 & -10.0990 & -1.0099 \\ -0.2257 & 0 & 0 \\ -9.9010 & 20.0000 & 1.9604 \\ -1.2158 & 0.9901 & -9.9010 \end{bmatrix}$$

The nonlinear functions in Eq. (5.106) are

$$F(x^0) = \begin{bmatrix} 0.5655 \\ -1.4805 \\ -0.2250 \end{bmatrix}$$

The incremental updates for the states are

$$\Delta x^1 = \begin{bmatrix} -0.0119 \\ -0.0625 \\ -0.0154 \end{bmatrix}$$

leading to the updated states

$$\begin{bmatrix} \delta_2^1 \\ \delta_3^1 \\ V_3^1 \end{bmatrix} = \begin{bmatrix} -0.0119 \\ -0.0625 \\ -0.9846 \end{bmatrix}$$

where δ_2 and δ_3 are in radians. The error at iteration 0 is

$$\varepsilon^0 = 1.4805$$

Iteration 2

The updated values are used to recalculate the Newton–Raphson iterations:

$$h(x^1) = \begin{bmatrix} 0.9846 \\ 0.6585 \\ -0.0634 \\ -1.1599 \\ -0.724 \end{bmatrix}$$

The matrix of partials is

$$H_x^1 = \begin{bmatrix} 0 & 0 & 1.0000 \\ 0 & -9.9858 & -0.3774 \\ -0.2660 & 0 & 0 \\ -9.6864 & 19.5480 & 0.7715 \\ -0.7468 & 0.4809 & -9.9384 \end{bmatrix}$$

The nonlinear function evaluated at the updated values yields

$$F(x^1) = \begin{bmatrix} 0.0113 \\ -0.0258 \\ 0.0091 \end{bmatrix}$$

The incremental updates for the states are

$$\Delta x^2 = \begin{bmatrix} 0.0007 \\ -0.0008 \\ 0.0013 \end{bmatrix}$$

leading to the updated states

$$\begin{bmatrix} \delta_2^2 \\ \delta_3^2 \\ V_3^2 \end{bmatrix} = \begin{bmatrix} -0.0113 \\ -0.0633 \\ 0.9858 \end{bmatrix}$$

The error at Iteration 1 is

$$\varepsilon^1 = 0.0258$$

The iterations are obviously converging. At convergence, the states that minimize the weighted measurement errors are

$$x = \begin{bmatrix} -0.0113 \\ -0.0633 \\ 0.9858 \end{bmatrix}$$

This concludes the discussion of the most commonly used computational methods for power system analysis. This chapter describes only the basic approaches to power flow, optimal power flow, and state estimation. These methods have been utilized for several decades, yet improvements in accuracy and speed are constantly being proposed in the technical literature.

II

Power System Transients

Pritindra Chowdhuri
Tennessee Technological University

6	Characteristics of Lightning Strokes	<i>Francisco de la Rosa</i>	6-1
Introduction • Lightning Generation Mechanism • Parameters of Importance for Electric Power Engineering • Incidence of Lightning to Power Lines • Conclusions			
7	Overtvoltages Caused by Direct Lightning Strokes	<i>Pritindra Chowdhuri</i>	7-1
Direct Strokes to Unshielded Lines • Direct Strokes to Shielded Lines • Significant Parameters • Outage Rates by Direct Strokes • Effects of Induction for Direct Strokes			
8	Overtvoltages Caused by Indirect Lightning Strokes	<i>Pritindra Chowdhuri</i>	8-1
Inducing Voltage • Induced Voltage • Green's Function • Induced Voltage of a Doubly Infinite Single-Conductor Line • Induced Voltages on Multiconductor Lines • Effects of Shield Wires on Induced Voltages • Stochastic Characteristics of Lightning Strokes • Estimation of Outage Rates Caused by Nearby Lightning Strokes • Estimation of Total Outage Rates • Appendix A Voltage Induced by Linearly Rising and Falling Return-Stroke Current			
9	Switching Surges	<i>Stephen R. Lambert</i>	9-1
Transmission Line Switching Operations • Series Capacitor Bank Applications • Shunt Capacitor Bank Applications • Shunt Reactor Applications			
10	Very Fast Transients	<i>Juan A. Martinez-Velasco</i>	10-1
Origin of VFT in GIS • Propagation of VFT in GIS • Modeling Guidelines and Simulation • Effects of VFT on Equipment			
11	Transient-Voltage Response of Coils and Windings	<i>Robert C. Degenneff</i>	11-1
Transient-Voltage Concerns • Surges in Windings • Determining Transient Response • Resonant Frequency Characteristic • Inductance Model • Capacitance Model • Loss Model • Winding Construction Strategies • Models for System Studies			
12	Transmission System Transients—Grounding	<i>William A. Chisholm</i>	12-1
General Concepts • Material Properties • Electrode Dimensions • Self-Capacitance of Electrodes • Initial Transient Response from Capacitance • Ground Electrode Impedance: Wire over Perfect Ground • Ground Electrode Impedance: Wire over Imperfect Ground • Analytical Treatment of Complex Electrode Shapes • Numerical Treatment of Complex Electrode Shapes • Treatment of Multilayer Soil Effects • Layer of Finite Thickness over Insulator • Treatment of Soil Ionization • Design Process • Design Recommendations • Appendix A Relevant IEEE Grounding Standards			

13	Surge Arresters <i>Thomas E. McDermott</i>	13-1
	Arrester Types and Auxiliary Equipment • Ratings and Tests • Selection by TOV •	
	Selection by Energy Rating • Arrester Modeling • Applications	
14	Insulation Coordination <i>Stephen R. Lambert</i>	14-1
	Insulation Coordination • Insulation Characteristics • Probability of Flashover •	
	Flashover Characteristics of Air Insulation	

6

Characteristics of Lightning Strokes

6.1	Introduction.....	6-1
6.2	Lightning Generation Mechanism	6-1
	First Strokes • Subsequent Strokes	
6.3	Parameters of Importance for Electric Power Engineering	6-4
	Ground Flash Density • Current Peak Value • Correlation between Current and Other Parameters of Lightning	
6.4	Incidence of Lightning to Power Lines	6-7
6.5	Conclusions.....	6-8

Francisco de la Rosa
Distribution Control Systems, Inc.

6.1 Introduction

Lightning, one of the most spectacular events of Mother Nature, started to appear significantly demystified after Franklin showed its electric nature with his famous electrical kite experiment in 1752. Although a great deal of research on lightning followed Franklin's observation, lightning continues to be a topic of considerable interest for investigation (Uman, 1969, 1987). This is particularly true for the improved design of electric power systems, since lightning-caused interruptions and equipment damage during thunderstorms stand as the leading causes of failures in the electric utility industry.

On a worldwide scale most lightning currents (over 90%) are of negative polarity. However, it has to be acknowledged that in some parts of the world, mostly over the Northern Hemisphere, the fraction of positive lightning currents can be substantial. A formal assessment of the effects of positive lightning on electric power systems will require using the corresponding parameters, since they may show large deviations from negative flashes in peak current, charge, front duration and flash duration, etc., as it will be described.

6.2 Lightning Generation Mechanism

6.2.1 First Strokes

The wind updrafts and downdrafts that take place in the atmosphere create a charging mechanism that separates electric charges, leaving negative charge at the bottom and positive charge at the top of the cloud. As charge at the bottom of the cloud keeps growing, the potential difference between cloud and ground, which is positively charged, grows as well. This process will continue until air breakdown occurs. See Fig. 6.1.

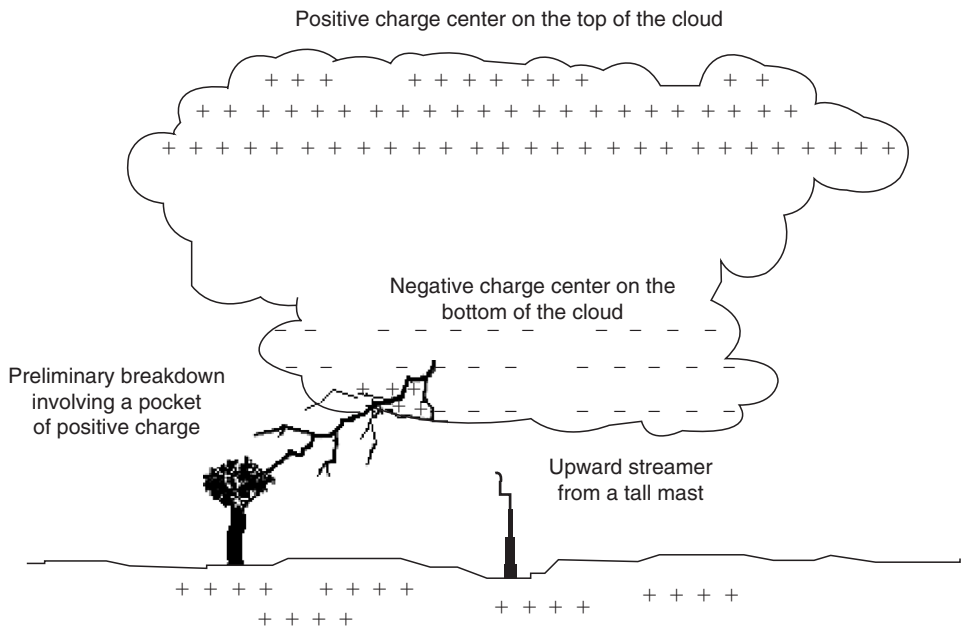


FIGURE 6.1 Separation of electric charge within a thundercloud.

The way in which a cloud-to-ground flash develops involves a stepped leader that starts traveling downward following a preliminary breakdown at the bottom of the cloud. This involves a positive pocket of charge, as illustrated in Fig. 6.1. The stepped leader travels downward in steps several tens of meters in length and pulse currents of at least 1 kA in amplitude (Uman, 1969). When this leader is near ground, the potential to ground can reach values as large as 100 MV before the attachment process with one of the upward streamers is completed. Figure 6.2 illustrates the final step when the upward streamer developing from a transmission line tower intercepts the downward leader.

The connection point-to-ground is not decided until the downward leader is some tens of meters above the ground plane. The downward leader will be attached to one of the growing upward streamers developing from elevated objects such as trees, chimneys, power lines, telecommunication towers, etc. It is actually under this principle that lightning protection rods work, i.e., they have to be strategically located so that they can trigger upward streamers that can develop into attachment points to downward leaders approaching the protected area. For this to happen, upward streamers developing from protected objects within the shielded area have to compete unfavorably with those developing from the tip of the lightning rods, which are positioned at a higher elevation.

Just after the attachment process takes place, the charge that is lowered from the cloud base through the leader channel is conducted to ground as a breakdown current pulse, known as the return stroke, travels

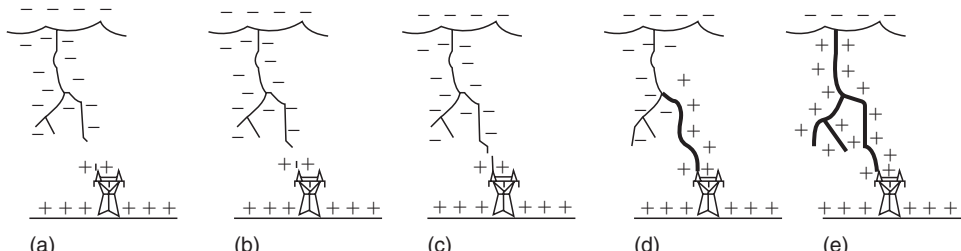


FIGURE 6.2 Attachment between downward and upward leaders in a cloud-to-ground flash.

TABLE 6.1 Lightning Current Parameters for Negative Flashes

Parameters	Units	Sample Size	Value Exceeding in 50% of the Cases
<i>Peak current (minimum 2 kA)</i>	kA		
First strokes		101	30
Subsequent strokes		135	12
<i>Charge (total charge)</i>	C		
First strokes		93	5.2
Subsequent strokes		122	1.4
Complete flash		94	7.5
<i>Impulse charge (excluding continuing current)</i>	C		
First strokes		90	4.5
Subsequent strokes		117	0.95
<i>Front duration (2 kA to peak)</i>	μs		
First strokes		89	5.5
Subsequent strokes		118	1.1
Maximum di/dt	kA/μs		
First strokes		92	12
Subsequent strokes		122	40
<i>Stroke duration (2 kA to half peak value on the tail)</i>	μs		
First strokes		90	75
Subsequent strokes		115	32
<i>Action integral ($\int i^2 dt$)</i>	A ²		
First strokes	s	91	5.5×10^4
Subsequent strokes		88	6.0×10^3
Time interval between strokes	ms	133	33
<i>Flash duration</i>	ms		
All flashes		94	13
Excluding single-stroke flashes		39	180

Source: Adapted from Berger et al., Parameters of lightning flashes, *Electra No. 41*, 23–37, July 1975.

upward along the channel. The return stroke velocity is around one-third the speed of light. The median peak current value associated to the return stroke is reported to be of the order of 30 kA, with rise time and time to half values around 5 and 75 μs, respectively. See Table 6.1 adapted from Berger et al. (1975).

Associated to this charge-transfer mechanism (an estimated 5 C total charge is lowered to ground through the stepped leader) are the electric and magnetic field changes that can last several milliseconds. These fields can be registered at remote distances from the channel and it is under this principle that lightning sensors work to produce the information necessary to monitor cloud-to-ground lightning.

6.2.2 Subsequent Strokes

After the negative charge from the cloud base has been transferred to ground, additional charge can be made available on the top of the channel when discharges known as J and K processes take place within the cloud (Uman, 1969). This can lead to some three to five strokes of lightning following the first stroke. A so-called dart leader develops from the top of the channel lowering charges, typically of 1 C, until recently believed to follow the same channel of the first stroke. Studies conducted in the past few years, however, suggest that around half of all lightning discharges to earth, both single- and multiple-stroke flashes, may strike ground at more than one point, with separation between channel terminations on ground varying from 0.3 to 7.3 km and a geometric mean of 1.3 km (Thottappillil et al., 1992).

Generally, dart leaders develop no branching, and travel downward at velocities of around 3×10^6 m/s. Subsequent return strokes have peak currents usually smaller than first strokes but faster zero-to-peak rise times. The mean interstroke interval is about 60 ms, although intervals as large as a few tenths of a second can be involved when a so-called continuing current flows between strokes (this happens in 25–50% of all cloud-to-ground flashes). This current, which is of the order of 100 A, is associated to charges of around 10 C and constitutes a direct transfer of charge from cloud to ground (Uman, 1969).

The percentage of single-stroke flashes presently suggested by CIGRE of 45% (Anderson and Eriksson, 1980) is considerably higher than the following figures recently obtained from experimental results: 17% in Florida (Rakov et al., 1994), 14% in New Mexico Florida (Rakov et al., 1994), 21% in Sri Lanka (Cooray and Jayaratne, 1994), and 18% in Sweden (Cooray and Perez, 1994).

6.3 Parameters of Importance for Electric Power Engineering

6.3.1 Ground Flash Density

Ground flash density, frequently referred to as GFD or N_g , is defined as the number of lightning flashes striking ground per unit area and per year. Usually it is a long-term average value and ideally it should take into account the yearly variations that take place within a solar cycle—believed to be the period within which all climatic variations that produce different GFD levels occur.

A 10-year average GFD map of the continental U.S. obtained by and reproduced here with permission from Vaisala, Inc. of Tucson, Arizona, is presented in Fig. 6.3. Note the considerable large GFD levels affecting remarkably the state of Florida, as well as all the southern states along the Gulf of Mexico (Alabama, Mississippi, Louisiana, and Texas). High GFD levels are also observed in the southeastern states of Georgia and South Carolina. To the west side, Arizona is the only state with GFD levels as high as 8 flashes/km²/year. The lowest GFD levels (<0.5 flashes/km²/year) are observed in the western states, notably in California, Oregon, and Washington on the Pacific Ocean, in a spot area of Colorado and in the Northeastern state of Maine on the Atlantic Ocean.

It is interesting to mention that a previous (a 5-year average) version of this map showed levels of around 6 flashes/km²/year also in some areas of Illinois, Iowa, Missouri, and Indiana, not seen in the present version. This is often the result of short-term observations that do not reflect all climatic variations that take place in a longer time-frame.

The low incidence of lightning does not necessarily mean an absence of lightning-related problems. Power lines, for example, are prone to failures even if GFD levels are low when they pass through

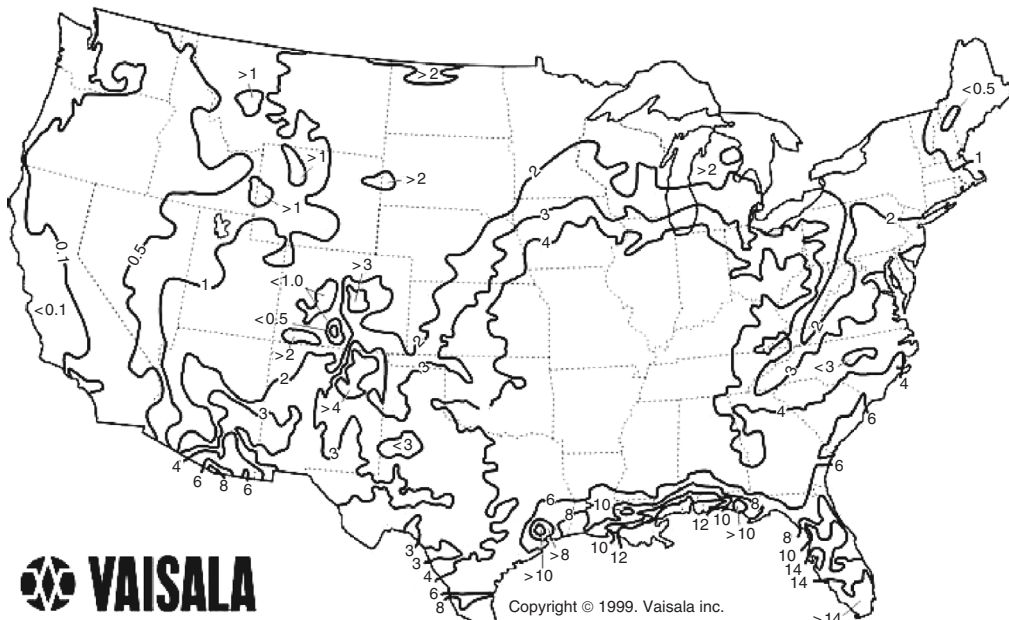


FIGURE 6.3 Ten-year average GFD map of the U.S. (Reproduced from Vaisala, Inc. of Tucson, AZ., Standards Information Network, "How to Protect Your House and its Contents from Lightning." IEEE Guide for Surge Protection of Equipment Connected to AC Power and Communication Circuits, IEEE Press, 2005. With permission.)

high-resistivity soils like deserts or when lines span across hills or mountains, where ground wire or lightning arrester earthing becomes difficult.

The GFD level is an important parameter to consider for the design of electric power and telecommunication facilities. This is due to the fact that power line performance and damage to power and telecommunication equipment are considerably affected by lightning. Worldwide, lightning accounts for most of the power supply interruptions in distribution lines and it is a leading cause of failures in transmission systems. In the U.S. alone, an estimated 30% of all power outages are lightning-related on annual average, with total costs approaching \$1 billion (Kithil, 1998).

In De la Rosa et. al. (1998), it is discussed how to determine GFD as a function of TD (thunder days or keraunic level) or TH (thunder-hours). This is important where GFD data from lightning location systems are not available. Basically, any of these parameters can be used to get a *rough* approximation of ground flash density. Using the expressions described in Anderson et al. (1984) and MacGorman et al. (1984), respectively:

$$N_g = 0.04TD^{1.25} \text{ flashes/km}^2/\text{year} \quad (6.1)$$

$$N_g = 0.054TH^{1.1} \text{ flashes/km}^2/\text{year} \quad (6.2)$$

6.3.2 Current Peak Value

Regarding current peak values, first strokes are associated with peak currents around 2 to 3 times larger than subsequent strokes. According to De la Rosa et al. (1998), electric field records, however, suggest that subsequent strokes with higher electric field peak values may be present in one out of three cloud-to-ground flashes. These may be associated with current peak values greater than the first stroke peak.

Tables 6.1 and 6.2 are summarized and adapted from Berger et al. (1975) for negative and positive flashes, respectively. They present statistical data for 127 cloud-to-ground flashes, 26 of them positive, measured in Switzerland. These are the types of lightning flashes known to hit flat terrain and structures of moderate height. This summary, for simplicity, shows only the 50% or statistical value, based on the log-normal approximations to the respective statistical distributions. These data are amply used as primary reference in the literature on both lightning protection and lightning research.

The action integral is an interesting concept, i.e., the energy that would be dissipated in a $1\text{-}\Omega$ resistor if the lightning current were to flow through it. This is a parameter that can provide some insight on the understanding of forest fires and on damage to power equipment, including surge arresters, in power line installations. All the parameters presented in Tables 6.1 and 6.2 are estimated from current oscilloscopes with the shortest measurable time being $0.5 \mu\text{s}$ (Berger and Garbagnati, 1984). It is thought that the distribution of front duration might be biased toward larger values and the distribution of di/dt toward smaller values (De la Rosa et al., 1998).

TABLE 6.2 Lightning Current Parameters for Positive Flashes

Parameters	Units	Sample Size	Value Exceeding in 50% of the Cases
Peak current (minimum 2 kA)	kA	26	35
Charge (total charge)	C	26	80
Impulse charge (excluding continuing current)	C	25	16
Front duration (2 kA to peak)	μs	19	22
Maximum di/dt	$\text{kA}/\mu\text{s}$	21	2.4
Stroke duration (2 kA to half peak value on the tail)	μs	16	230
Action integral ($\int i^2 dt$)	A^2s	26	6.5×10^5
Flash duration	ms	24	85

Source: Adapted from Berger et al., Parameters of lightning flashes, *Electra No. 41*, 23–37, July 1975.

6.3.3 Correlation between Current and Other Parameters of Lightning

Lightning parameters are sometimes standardized for the purpose of assessment of lighting performance of specific power line designs (IEEE Std 1410-1997, 1997). Although this can be adequately used to determine effectiveness of different lightning protection methods in a comparative basis, it is important to understand the limitations that this approach may encompass: Lightning parameters may show considerable deviations often caused by spatial and temporal variations (Torres, 1998). On the other hand, gathering data on lightning parameters other than current makes it an impossible task. Among the parameters which can be associated with lightning damage are lightning peak current (i_p), rate-of-rise (T_{front} and peak dI/dt), charge transfer (Q_{imp} and Q_{flash}), and energy (action integral), as described in De la Rosa et al. (2000). Unfortunately, contemporary lightning-detection systems are not able to provide accurate estimates of many of these parameters, including the current, since they are designed only to sense and record radiated electric and magnetic fields at hundreds of kilometers from the source. Nevertheless, it seems tangible to envision that even with the limited accuracy of lightning current derived from lightning detection systems (LDS), it will be possible to infer other lightning parameters directly linked to lightning damage. This will allow us to continue assessing the efficacy of lightning mitigation methods based on records of lightning current and other parameters obtained from LDSs.

Table 6.3 shows an interesting correlation study conducted by Dellera (1997) where he found moderate-to-high correlation coefficients between lightning peak current with other parameters measured in a number of research experiments that involved lightning strikes to instrumented towers. This work presented a way to obtain estimates of the total probability of a specific range of simultaneous values (e.g., $I > I_o$ and $Q > Q_o$), thereby refining the probability estimates for the conditions under which a lightning-related failure may occur. Table 6.3 comprises relevant findings for positive flashes, negative first strokes, and negative subsequent strokes. The table entries for parameters in negative discharges

TABLE 6.3 Correlation between Lightning Parameters

Positive Flashes		
Lightning Parameter	Correlation (Corr. Coeff)	Data Source
Front time (T_{front})	Low (0.18)	Berger and Garbagnati, 1984
Peak rate-of-rise (dI/dt)	Moderate (0.55)	Berger and Garbagnati, 1984
Impulse charge (Q_{imp})	High (0.77)	Berger and Garbagnati, 1984
Flash charge (Q_{flash})	Moderate (0.59)	Berger and Garbagnati, 1984
Impulse action integral (W_{imp})	—	
Flash action integral (W_{flash})	High (0.76)	Berger and Garbagnati, 1984
Negative First Strokes		
Lightning Parameter	Correlation (Corr. Coeff)	Data Source
Front time (T_{front})	Low (—)	Weidman and Krider, 1984 ^a
Peak rate-of-rise (dI/dt)	Moderate/high (—)	Weidman and Krider, 1984 ^a
Impulse charge (Q_{imp})	High (0.75)	Berger and Garbagnati, 1984
Flash charge (Q_{flash})	Low (0.29)	Berger and Garbagnati, 1984
Impulse action integral (W_{imp})	High (0.86)	Berger and Garbagnati, 1984
Flash action integral (W_{flash})	—	
Negative Subsequent Strokes		
Lightning Parameter	Correlation (Corr. Coeff)	Data Source
Front time (T_{front})	Low (0.13)	Fisher et al., 1993
Peak rate-of-rise (dI/dt)	High (0.7–0.8)	Fisher et al., 1993; Leteinturier et al., 1991 ^b
Impulse charge (Q_{imp})	—	
Impulse action integral (W_{imp})	—	

Source: Adapted from Dellera, L., Lightning Parameters for Protection: An Updated Approach, CIGRE 97 SC33, WG33.01, 17 IWD, August 1997.

^aInferred from measurements of electric fields propagated over salt water.

^b30–90% slope, which corresponds to an “average” dI/dt (triggered lightning studies).

provide more accurate results, due to broader bandwidth (higher frequency) recording instruments. Table entries that are not filled in (—) were not analyzed by Deller.

To illustrate the interpretation of the table, we observe that a moderate-to-high correlation is found between lightning current and all but peak rate of rise in positive flashes. Therefore, extreme heating should be expected in arcing or transient currents conducted through protective devices following insulation flashover produced by positive lightning flashes. Note that lightning parameters associated with heat are charge and action integral and that rate-of-change of lightning current is connected with inductive effects, which do not show strong from the correlation table.

Similarly, overvoltages from negative lightning strokes should be associated with peak current producing large inductive overvoltages especially due to subsequent strokes. Heating effects, however, are loosely correlated with peak current, since correlation coefficient for the total charge (Q_{flash}) is poor. It is possible that consideration of all stroke peak currents and interstroke intervals in negative flashes, which are available in some modern lightning detection systems, will prove a more deterministic means to infer heating due to negative flashes.

6.4 Incidence of Lightning to Power Lines

One of the most accepted expressions to determine the number of direct strikes to an overhead line in an open ground with no nearby trees or buildings is that described by Eriksson (1987):

$$N = N_g \left(\frac{28h^{0.6} + b}{10} \right) \quad (6.3)$$

where

h is the pole or tower height (m)—negligible for distribution lines;

b is the structure width (m);

N_g is the ground flash density (flashes/km²/year);

N is the number of flashes striking the line/100 km/year. For unshielded distribution lines this is comparable to the fault index due to direct lightning hits. For transmission lines, this is an indicator of the exposure of the line to direct strikes. (The response of the line being a function of overhead ground wire shielding angle on one hand and on conductor-tower surge impedance and footing resistance on the other hand.)

Note the dependence of the incidence of strikes to the line with height of the structure. This is important since transmission lines are several times taller than distribution lines, depending on their operating voltage level.

Also important is that in the real world, power lines are to different extents shielded by nearby trees or other objects along their corridors. This will decrease the number of direct strikes estimated by Eq. (6.3) to a degree determined by the distance and height of the objects. In IEEE Std. 1410-1997, a shielding factor is proposed to estimate the shielding effect of nearby objects to the line. An important aspect of this reference work is that objects within 40 m from the line, particularly if equal or higher than 20 m, can attract most of the lightning strikes that would otherwise hit the line. Likewise, the same objects would produce insignificant shielding effects if located beyond 100 m from the line. On the other hand, sectors of lines extending over hills or mountain ridges may increase the number of strikes to the line.

The above-mentioned effects may in some cases cancel each other so that the estimation obtained from Eq. (6.3) can still be valid. However, it is recommended that any assessment of the incidence of lightning strikes to a power line be performed by taking into account natural shielding and orographic conditions (terrain undulations) along the line route. This also applies when identifying troubled sectors of the line for the installation of metal oxide surge arresters to improve its lightning performance. For example, those parts of a distribution feeder crossing over hills with little natural shielding would greatly benefit from surge arrester protection.

Finally, although meaningful only for distribution lines, the inducing effects of lightning, also described in De la Rosa et al. (1998) and Anderson et al. (1984), have to be considered to properly understand their lightning performance or when dimensioning the outage rate improvement after application of any mitigation action. Under certain conditions, like in circuits without grounded neutral, with low critical flashover voltages, high GFD levels, or located on high-resistivity terrain, the number of outages produced by close lightning can considerably surpass those due to direct strikes to the line.

6.5 Conclusions

Parameters that are important for the assessment of lightning performance of power transmission and distribution lines or for evaluation of different protection methods are lightning current and ground flash density. The former provides a means to appraise the impact of direct hits on power lines or substations and the latter provides an indication of how often this phenomenon may occur. There are, however, other lightning parameters that can be related to the probability of insulation flashover and heating effects in surge protective devices, which are difficult to obtain from conventional lightning detection equipment. Some correlation coefficients observed between lightning peak current and other parameters obtained from experiments in instrumented towers are portrayed in this review.

Aspects like the different methods available to calculate shielding failures and back flashovers in transmission lines, or the efficacy of remedial measures are not covered here. Among these, overhead ground wires, metal oxide surge arresters, increased insulation, or use of wood as an arc-quenching device, can only be mentioned. The reader is encouraged to further look at the suggested references or to get experienced advice for a more comprehensive understanding on the subject.

References

- Anderson, R.B. and Eriksson, A.J., Lightning parameters for engineering applications, *Electra*, 69, 65–102, March 1980.
- Anderson, R.B., Eriksson, A.J., Kroninger, H., Meal, D.V., and Smith, M.A., Lightning and thunderstorm parameters, *IEE Lightning and Power Systems Conf. Publ. No. 236*, London, 1984.
- Berger, K., Anderson, R.B., and Kroninger, H., Parameters of lightning flashes, *Electra*, 41, 23–37, July 1975.
- Berger, K. and Garbagnati, E., Lightning current parameters, results obtained in Switzerland and in Italy, in *Proceedings of URSI Conference*, Florence, Italy, 1984.
- Cooray, V. and Jayaratne, K.P.S., Characteristics of lightning flashes observed in Sri Lanka in the tropics, *J. Geophys. Res.*, 99, 21,051–21,056, 1994.
- Cooray, V. and Perez, H., Some features of lightning flashes observed in Sweden, *J. Geophys. Res.*, 99, 10,683–10,688, 1994.
- De la Rosa, F., Nucci, C.A., and Rakov, V.A., Lightning and its impact on power systems, in *Proceedings of International Conference on Insulation Coordination for Electricity Development in Central European Countries*, Zagreb, Croatia, 1998.
- De la Rosa, F., Cummins, K., Dellera, L., Diendorfer, G., Galvan, A., Huse, J., Larsen, V., Nucci, C.A., Rachidi, F., Rakov, V., Torres, H., and Uman, M., Characterization of Lightning for Applications in Electric Power Systems, *CIGRE Report#172*, TF33.01.02, December 2000.
- Dellera, L., Lightning Parameters for Protection: An Updated Approach, *CIGRE 97 SC33*, WG33.01, 17 IWD, August 1997.
- Eriksson, A.J., The incidence of lighting strikes to power lines, *IEEE Trans. Power Delivery*, 2(2), 859–870, July 1987.
- Fisher, R.J., Schnetzer, G.H., Thottappillil, R., Rakov, V.A., Uman, M.A., and Goldberg, J.D., Parameters of triggered-lightning flashes in Florida and Alabama, *J. Geophys. Res.*, 98(D12), 22,887–22,902, 1993.

- IEEE Std 1410-1997, IEEE Guide for Improving the Lightning Performance of Electric Power Distribution Lines, *IEEE PES*, December, 1997, Section 5.
- Kithil, R., Lightning protection codes: Confusion and costs in the USA, in *Proceedings of the 24th International Lightning Protection Conference*, Birmingham UK, Sept 16, 1998.
- Leteinturier, C., Weidman, C., and Hamelin, J., Current and electric field derivatives in triggered lightning return strokes, *J. Geophys. Res.*, 95(D1) 811–828, 1990.
- MacGorman, D.R., Maier, M.W., and Rust, W.D., Lightning strike density for the contiguous United States from thunderstorm duration records, *NUREG/CR-3759, Office of Nuclear Regulatory Research, U.S. Nuclear Regulatory Commission*, 44, Washington, D.C., 1984.
- Rakov, M.A., Uman, M.A., and Thottappillil, R., Review of lightning properties from electric field and TV observations, *J. Geophys. Res.* 99, 10,745–10,750, 1994.
- Thottappillil, R., Rakov, V.A., Uman, M.A., Beasley, W.H., Master, M.J., and Shelukhin, D.V., Lightning subsequent stroke electric field peak greater than the first stroke and multiple ground terminations, *J. Geophys. Res.*, 97, 7503–7509, 1992.
- Torres, H., Variations of lightning parameter magnitudes within space and time, in *24th International Conference on Lightning Protection*, Birmingham, UK, Sept 1998.
- Uman, M.A. *Lightning*, Dover, New York, 1969, Appendix E.
- Uman, M.A., *The Lightning Discharge*, International Geophysics Series, Vol. 39, Academic Press, Orlando, FL, Chapter 1, 1987.
- Weidman, C.D. and Krider, E.P., Variations à l'Échelle Submicroconde des Champs Électromagnétiques Rayonnés par la Foudre, *Ann. Telecommun.*, 39, 165–174, 1984.

7

Overvoltages Caused by Direct Lightning Strokes

7.1	Direct Strokes to Unshielded Lines	7-1
7.2	Direct Strokes to Shielded Lines	7-3
	Shielding Design	
7.3	Significant Parameters.....	7-8
7.4	Outage Rates by Direct Strokes.....	7-10
	Unshielded Lines • Shielded Lines	
7.5	Effects of Induction for Direct Strokes	7-13

Pritindra Chowdhuri
Tennessee Technological University

A lightning stroke is defined as a direct stroke if it hits either the tower or the shield wire or the phase conductor. This is illustrated in Fig. 7.1. When the insulator string at a tower flashes over by direct hit either to the tower or to the shield wire along the span, it is called a backflash; if the insulator string flashes over by a strike to the phase conductor, it is called a shielding failure for a line shielded by shield wires. Of course, for an unshielded line, insulator flashover is caused by backflash when the stroke hits the tower or by direct contact with the phase conductor. In the analysis of performance and protection of power systems, the most important parameter that must be known is the insulation strength of the system. It is not a unique number. It varies according to the type of the applied voltage, e.g., DC, AC, lightning, or switching surges. For the purpose of lightning performance, the insulation strength has been defined in two ways: basic impulse insulation level (BIL) and critical flashover voltage (CFO or V_{50}). BIL has been defined in two ways. The statistical BIL is the crest value of a standard (1.2/50- μ s) lightning impulse voltage, which the insulation will withstand with a probability of 90% under specified conditions. The conventional BIL is the crest value of a standard lightning impulse voltage, which the insulation will withstand for a specific number of applications under specified conditions. CFO or V_{50} is the crest value of a standard lightning impulse voltage, which the insulation will withstand during 50% of the applications. In this chapter, we will use the conventional BIL as the insulation strength under lightning impulse voltages. Analysis of direct strokes to overhead lines can be divided into two classes: unshielded lines and shielded lines. The first discussion involves the unshielded lines.

7.1 Direct Strokes to Unshielded Lines

If lightning hits one of the phase conductors, the return-stroke current splits into two equal halves, each half traveling in either direction of the line. The traveling current waves produce traveling voltage waves, which are given by

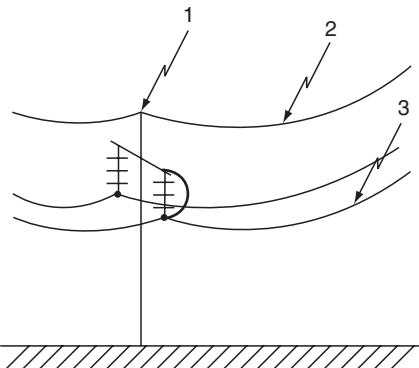


FIGURE 7.1 Illustration of direct lightning strokes to line (1) backflash caused by direct stroke to tower; (2) backflash caused by direct stroke to shield wire; (3) insulator flashover by direct stroke to phase conductor (shielding failure).

current, I_c , of the line for the specified BIL. Thus, following Eq. (7.1):

$$I_c = \frac{2\text{BIL}}{Z_o} \quad (7.2)$$

Lightning may hit one of the towers. The return-stroke current then flows along the struck tower and over the tower-footing resistance before being dissipated in the earth. The estimation of the insulator voltage in that case is not simple, especially because there has been no consensus about the modeling of the tower in estimating the insulator voltage. In the simplest assumption, the tower is neglected. Then, the tower voltage, including the voltage of the cross arm from which the insulator is suspended, is the voltage drop across the tower-footing resistance given by $V_{tf} = IR_{tf}$, where R_{tf} is the tower-footing resistance. Neglecting the power-frequency voltage of the phase conductor, this is then the voltage across the insulator. It should be noted that this voltage will be of opposite polarity to that for stroke to the phase conductor for the same polarity of the return-stroke current.

Neglecting the tower may be justified for short towers. The effect of the tower for transmission lines must be included in the estimation of the insulator voltage. For these cases, the tower has also been represented as an inductance. Then the insulator voltage is given by $V_{ins} = V_{tf} + L(dI/dt)$, where L is the inductance of the tower.

However, it is known that voltages and currents do travel along the tower. Therefore, the tower should be modeled as a vertical transmission line with a surge impedance, Z_t , where the voltage and current waves travel with a velocity, v_t . The tower is terminated at the lower end by the tower-footing resistance, R_{tf} , and at the upper end by the lightning channel that can be assumed to be another transmission line of surge impedance, Z_{ch} . Therefore, the traveling voltage and current waves will be repeatedly reflected at either end of the tower while producing voltage at the cross arm, V_{ca} . The insulator from which the phase conductor is suspended will then be stressed at one end by V_{ca} (to ground) and at the other end by the power-frequency phase-to-ground voltage of the phase conductor. Neglecting the power-frequency voltage, the insulator voltage, V_{ins} , will be equal to the cross-arm voltage, V_{ca} . This is schematically shown in Fig. 7.2a. The initial voltage traveling down the tower, V_{to} , is $V_{to}(t) = Z_t I(t)$, where $I(t)$ is the initial tower current that is a function of time, t . The voltage reflection coefficients at the two ends of the tower are given by

$$a_{r1} = \frac{R_{tf} - Z_t}{R_{tf} + Z_t} \quad \text{and} \quad a_{r2} = \frac{Z_{ch} - Z_t}{Z_{ch} + Z_t} \quad (7.3)$$

Figure 7.2b shows the lattice diagram of the progress of the multiply reflected voltage waves along the tower. The lattice diagram, first proposed by Bewley (1951), is the space-time diagram that shows

$$V = \frac{Z_o I}{2} \quad (7.1)$$

where I is the return-stroke current and Z_o is the surge impedance of the line given by $Z_o = (L/C)^{1/2}$, and L and C are the series inductance and capacitance to ground per meter length of the line. These traveling voltage waves stress the insulator strings from which the line is suspended as these voltages arrive at the succeeding towers. The traveling voltages are attenuated as they travel along the line by ground resistance and mostly by the ensuing corona enveloping the struck line. Therefore, the insulators of the towers adjacent to the struck point are most vulnerable. If the peak value of the voltage, given by Eq. (7.1), exceeds the BIL of the insulator, then it might flash over causing an outage. The minimum return-stroke current that causes an insulator flashover is called the critical

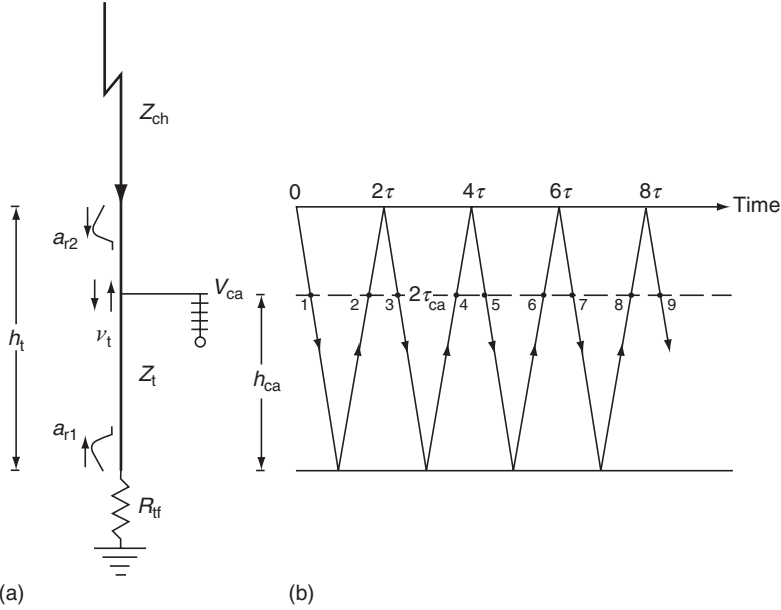


FIGURE 7.2 Lightning channel striking tower top: (a) schematic of struck tower; (b) voltage lattice diagram.

the position and direction of motion of every incident, reflected, and transmitted wave on the system at every instant of time. In Fig. 7.2, if the heights of the tower and the cross arm are h_t and h_{ca} , respectively, and the velocity of the traveling wave along the tower is v_t , then the time of travel from the tower top to its foot is $\tau_t = h_t/v_t$, and the time of travel from the cross arm to the tower foot is $\tau_{ca} = h_{ca}/v_t$. In Fig. 7.2b, the two solid horizontal lines represent the positions of the tower top and the tower foot, respectively. The broken horizontal line represents the cross-arm position. It takes $(\tau_t - \tau_{ca})$ seconds for the traveling wave to reach the cross arm after lightning hits the tower top at $t=0$. This is shown by point 1 on Fig. 7.2b. Similarly, the first reflected wave from the tower foot (point 2 in Fig. 7.2b) reaches the cross arm at $t=(\tau_t + \tau_{ca})$. The first reflected wave from the tower top (point 3 in Fig. 7.2b) reaches the cross arm at $t=(3\tau_t - \tau_{ca})$. The downward-moving voltage waves will reach the cross arm at $t=(2n-1)\tau_t - \tau_{ca}$, and the upward-moving voltage waves will reach the cross arm at $t=(2n-1)\tau_t + \tau_{ca}$, where $n=1, 2, \dots, n$. The cross-arm voltage, $V_{ca}(t)$, is then given by

$$V_{ca}(t) = \sum_{n=1}^n (a_{r1} a_{r2})^{n-1} V_{to}(t - (2n-1)\tau_t + \tau_{ca}) u(t - (2n-1)\tau_t + \tau_{ca}) \\ + a_{r1} \sum_{n=1}^n (a_{r1} a_{r2})^{n-1} V_{to}(t - (2n-1)\tau_t - \tau_{ca}) u(t - (2n-1)\tau_t - \tau_{ca}) \quad (7.4)$$

The voltage profiles of the insulator voltage, $V_{ins}(= V_{ca})$ for two values of tower-footing resistances, R_{tf} , are shown in Fig. 7.3. It should be noticed that the V_{ins} is higher for higher R_{tf} and that it approaches the voltage drop across the tower-footing resistance (IR_{tf}) with time. However, the peak of V_{ins} is significantly higher than the voltage drop across R_{tf} . Higher peak of V_{ins} will occur for (i) taller tower and (ii) shorter front time of the stroke current (Chowdhuri, 2004).

7.2 Direct Strokes to Shielded Lines

One or more conductors are strung above and parallel to the phase conductors of single- and double-circuit overhead power lines to shield the phase conductors from direct lightning strikes. These shield

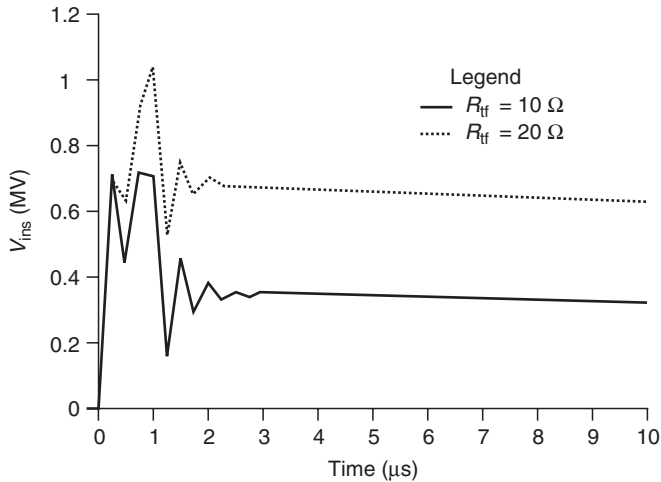


FIGURE 7.3 Profiles of insulator voltage for an unshielded line for a lightning stroke to tower. Tower height = 30 m; cross-arm height = 27 m; phase-conductor height = 25 m; cross-arm width = 2 m; return-stroke current = 30 kA at 1/50- μ s; $Z_t = 100 \Omega$; $Z_{ch} = 500 \Omega$.

wires are generally directly attached to the towers so that the return-stroke currents are safely led to ground through the tower-footing resistances. Sometimes, the shield wires are insulated from the towers by short insulators to prevent power-frequency circulating currents from flowing in the closed-circuit loop formed by the shield wires, towers, and the earth return. When lightning strikes the shield wire, the short insulator flashes over connecting the shield wire directly to the grounded towers.

For a shielded line, lightning may strike either a phase conductor or the shield wire or the tower. If it strikes a phase conductor but the magnitude of the current is below the critical current level, then no outage occurs. However, if the lightning current is higher than the critical current of the line, then it will precipitate an outage, which is called the shielding failure. In fact, sometimes, shielding is so designed that a few outages are allowed, the objective being to reduce excessive cost of shielding. However, the critical current for a shielded line is higher than that for an unshielded line because the presence of the grounded shield wire reduces the effective surge impedance of the line. The effective surge impedance of a line shielded by one shield wire is given by (Chowdhuri, 2004)

$$Z_{eq} = Z_{11} - \frac{Z_{12}^2}{Z_{22}} \quad (7.5)$$

where

$$Z_{11} = 60\ell n \frac{2h_p}{r_p}; \quad Z_{22} = 60\ell n \frac{2h_s}{r_s}; \quad Z_{12} = 60\ell n \frac{d_{ps}}{d_{ps}} \quad (7.6)$$

h_p and r_p are the height and radius of the phase conductor, h_s and r_s are the height and radius of the shield wire, d_{ps} is the distance from the shield wire to the image of the phase conductor in the ground, and d_{ps} is the distance from the shield wire to the phase conductor. Z_{11} is the surge impedance of the phase conductor in the absence of the shield wire, Z_{22} is the surge impedance of the shield wire, and Z_{12} is the mutual surge impedance between the phase conductor and the shield wire.

It can be shown that either for strokes to tower or for strokes to shield wire, the insulator voltage will be the same if the attenuation caused by impulse corona on the shield wire is neglected (Chowdhuri, 2004). For a stroke to tower, the return-stroke current will be divided into three parts; two parts going to the shield wire in either direction from the tower and the third part to the tower. Thus, lower voltage will

be developed along the tower of a shielded line than that for an unshielded line for the same return-stroke current, because lower current will penetrate the tower. This is another advantage of a shield wire. The computation of the cross-arm voltage, V_{ca} , is similar to that for the unshielded line, except for the following modifications in Eqs. (7.3) and (7.4):

1. The initial tower voltage is equal to $I Z_{eq}$, instead of $I Z_t$ as for the unshielded line, where Z_{eq} is the impedance as seen from the striking point, i.e.,

$$Z_{eq} = \frac{0.5 Z_s Z_t}{0.5 Z_s + Z_t} \quad (7.7)$$

where $Z_s = 60 \ell n(2h_s/r_s)$ is the surge impedance of the shield wire.

2. The traveling voltage wave moving upward along the tower, after being reflected at the tower foot, encounters three parallel branches of impedances, the lightning-channel surge impedance, and the surge impedances of the two halves of the shield wire on either side of the struck tower. Therefore, Z_{ch} in Eq. (7.3) should be replaced by $0.5 Z_s Z_{ch} / (0.5 Z_s + Z_{ch})$.

The insulator voltage, V_{ins} , for a shielded line is not equal to V_{ca} , as for the unshielded line. The shield-wire voltage, which is the same as the tower-top voltage, V_{tt} , induces a voltage on the phase conductor by electromagnetic coupling. The insulator voltage is, then, the difference between V_{ca} and this coupled voltage:

$$V_{ins} = V_{ca} - k_{sp} V_{tt} \quad (7.8)$$

where $k_{sp} = Z_{12}/Z_{22}$. It can be seen that the electromagnetic coupling with the shield wire reduces the insulator voltage. This is another advantage of the shield wire. To compute V_{tt} , we go back to Fig. 7.2. As the cross arm is moved towards the tower top, τ_{ca} approaches τ_t , and naturally, at tower top $\tau_{ca} = \tau_t$. Then, except the wave 1, the pairs of upward-moving and downward-moving voltages (e.g., 2 and 3, 4 and 5, etc.) arrive at the tower top at the same time. Substituting $\tau_{ca} = \tau_t$ in Eq. (7.4), and writing $a_{t2} = 1 + a_{r2}$, we get V_{tt} :

$$V_{tt}(t) = V_{to} u(t) + a_{t2} a_{r1} \sum_{n=1}^{\infty} (a_{r1} a_{r2})^{n-1} V_{to}(t - 2n\tau_t) u(t - 2n\tau_t) \quad (7.9)$$

From Eq. (7.3)

$$a_{t2} = 1 + a_{r2} = \frac{2 Z_{ch}}{Z_{ch} + Z_t} \quad (7.10)$$

The coefficient, a_{t2} , is called the coefficient of voltage transmission.

When lightning strikes the tower, equal voltages ($I Z_{eq}$) travel along the tower as well as along the shield wire in both directions. The voltages on the shield wire are reflected at the subsequent towers and arrive back at the struck tower at different intervals as voltages of opposite polarity (Chowdhuri, 2004). Generally, the reflections from the nearest towers are of any consequence. These reflected voltage waves lower the tower-top voltage. The tower-top voltage remains unaltered until the first reflected waves arrive from the nearest towers. The profiles of the insulator voltage for the same line as in Fig. 7.3 but with a shield wire are shown in Fig. 7.4. Comparing Figs. 7.3 and 7.4, it should be noticed that the insulator voltage is significantly reduced for a shielded line for a stroke to tower. This reduction is possible because (i) a part of the stroke current is diverted to the shield wire, thus reducing the initial tower-top voltage ($V_{to} = I_t Z_t$, $I_t < I$) and (ii) the electromagnetic coupling between the shield wire and the phase conductor induces a voltage on the phase conductor, thus lowering the voltage difference across the insulator ($V_{ins} = V_{ca} - k_{sp} V_{tt}$).

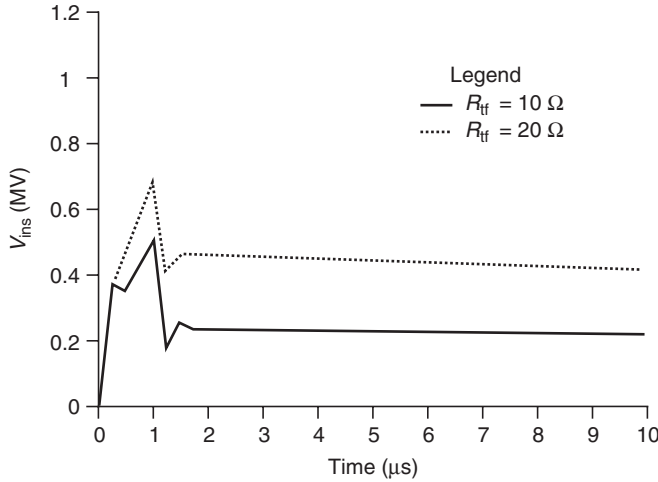


FIGURE 7.4 Profiles of insulator voltage for a shielded line for lightning stroke to tower. Tower height = 30 m; cross-arm height = 27 m; phase-conductor height = 25 m; cross-arm width = 2 m; return-stroke current = 30 kA at 1/50-μs; $Z_t = 100 \Omega$; $Z_{ch} = 500 \Omega$.

7.2.1 Shielding Design

Striking distance of the lightning stroke plays a crucial role in the design of shielding. Striking distance is defined as the distance through which a descending stepped leader will strike a grounded object. Armstrong and Whitehead (1968) and Brown and Whitehead (1969) proposed a simple relation between the striking distance, r_s , and the return-stroke current, I (in kA) of the form:

$$r_s = aI^b \text{ (m)} \quad (7.11)$$

where a and b are constants. The most frequently used value of a is 8 or 10, and that of b is 0.65. Let us suppose that a stepped leader with prospective return-stroke current of I_s is descending near a horizontal conductor, P (Fig. 7.5a). Its striking distance, r_s , will be given by Eq. (7.11). It will hit the surface of the earth when it penetrates a plane which is r_s meters above the earth. The horizontal conductor will be struck if the leader touches the surface of an imaginary cylinder of radius, r_s , with its center at the center of the conductor. The attractive width of the horizontal conductor will be ab in Fig. 7.5a. It is given by

$$ab = 2\omega_p = 2\sqrt{r_s^2 - (r_s - h_p)^2} = 2\sqrt{h_p(2r_s - h_p)} \quad \text{for } r_s > h_p \quad (7.12a)$$

and

$$ab = 2\omega_p = 2r_s \quad \text{for } r_s \leq h_p \quad (7.12b)$$

where h_p is the height of the conductor. For a multiconductor line with a separation distance, d_p , between the outermost conductors, the attractive width will be $2\omega_p + d_p$.

Now, if a second horizontal conductor, S , is placed near P , the attractive width of S will be cd (Fig. 7.5b). If S is intended to completely shield P , then the cylinder around S and the r_s -plane above the earth's surface must completely surround the attractive cylinder around P . However, as Fig. 7.5b shows, an unprotected width, db , remains. Stepped leaders falling through db will strike P . If S is repositioned to S' so that the point d coincides with b , then P is completely shielded by S .

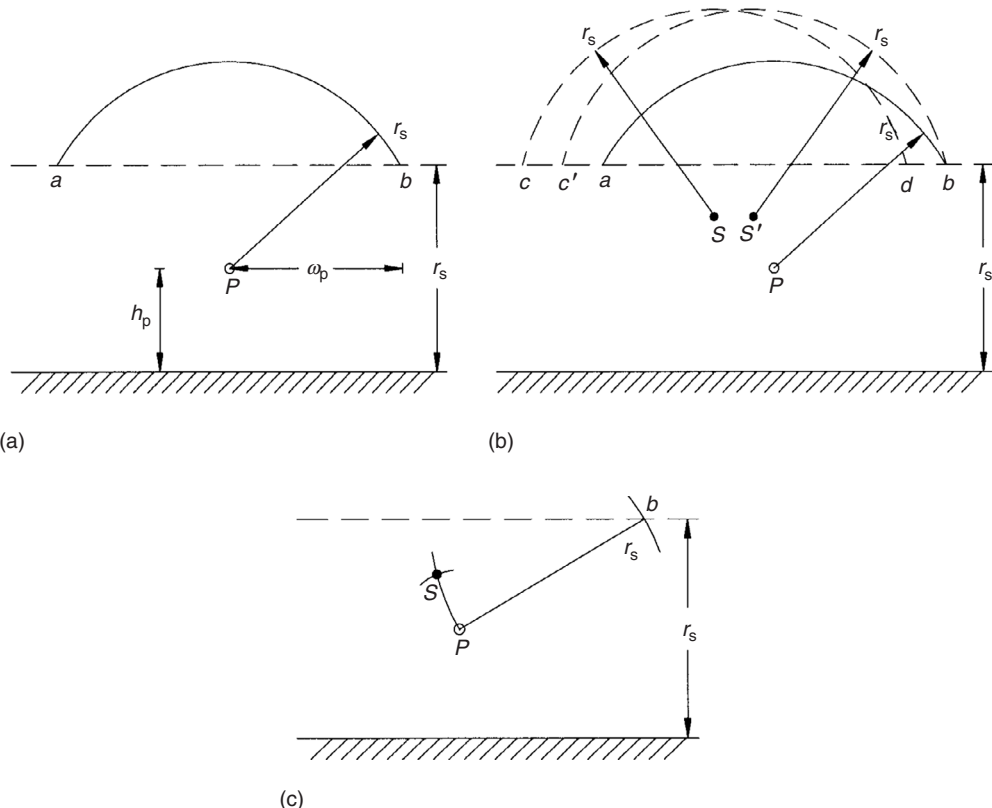


FIGURE 7.5 Principle of shielding: (a) electrogeometric model; (b) shielding principle; (c) placement of shield wire for perfect shielding.

The procedure to place the conductor, S , for perfect shielding of P is shown in Fig. 7.5c. Knowing the critical current, I_c , from Eq. (7.2), the corresponding striking distance, r_s , is computed from Eq. (7.11). A horizontal straight line is drawn at a distance, r_s , above the earth's surface. An arc of radius, r_s , is drawn with P as center, which intersects the r_s -line above earth at b . Then, an arc of radius, r_s , is drawn with b as center. This arc will go through P . Now, with P as radius another arc is drawn of radius r_{sp} , where r_{sp} is the minimum required distance between the phase conductor and a grounded object. This arc will intersect the second arc at S , which is the position of the shield wire for perfect shielding of P .

Figure 7.6 shows the placement of a single shield wire above a three-phase horizontally configured line for shielding. In Fig. 7.6a, the attractive cylinders of all three phase conductors are contained within the attractive cylinder of the shield wire and the r_s -plane above the earth. However, in Fig. 7.6b where the critical current is lower, the single shield wire at S cannot perfectly shield the two outer phase conductors. Raising the shield wire helps in reducing the unprotected width; but, in this case, it cannot completely eliminate shielding failure. As the shield wire is raised, its attractive width increases until the shield-wire height reaches the r_s -plane above earth, where the attractive width is the largest, equal to the diameter of the r_s -cylinder of the shield wire. Raising the shield-wire height further will not help. In this case, either the insulation strength of the line should be increased (i.e., the critical current increased) or two shield wires should be used.

Figure 7.7 shows the use of two shield wires. In Fig. 7.7a, all three phase conductors are completely shielded by the two shield wires. However, for smaller I_c (i.e., smaller r_s), part of the attractive cylinder of the middle phase conductor is left exposed (Fig. 7.7b). This shows that the middle phase conductor may experience shielding failure even when the outer phase conductors are perfectly shielded. In that case, either the insulation strength of the line should be increased or the height of the shield wires raised or both.

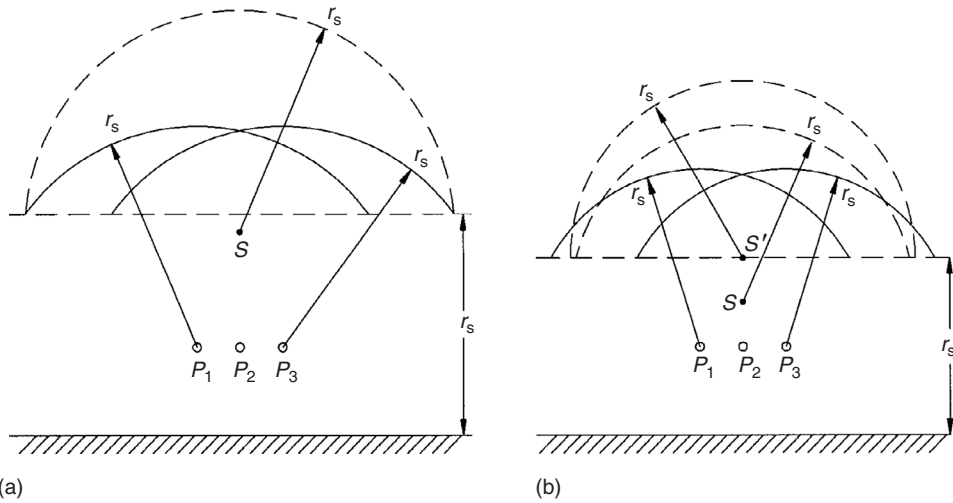


FIGURE 7.6 Shielding of three-phase horizontally configured line by single shield wire: (a) perfect shielding; (b) imperfect shielding.

7.3 Significant Parameters

The most significant parameter in estimating the insulator voltage is the return-stroke current, i.e., its peak value, waveshape, and statistical distributions of the amplitude and waveshape. The waveshape of the return-stroke current is generally assumed to be double exponential where the current rapidly rises to its peak exponentially, and subsequently decays exponentially:

$$I(t) = I_0(e^{-a_1 t} - e^{-a_2 t}) \quad (7.13)$$

The parameters, I_0 , a_1 , and a_2 are determined from the given peak, I_p , the front time, t_b , and the time to half value, t_h , during its subsequent decay. However, the return-stroke current can also be simulated as a linearly rising and linearly falling wave:

$$I(t) = \alpha_1 t u(t) - \alpha_2 (t - t_f) u(t - t_f) \quad (7.14)$$

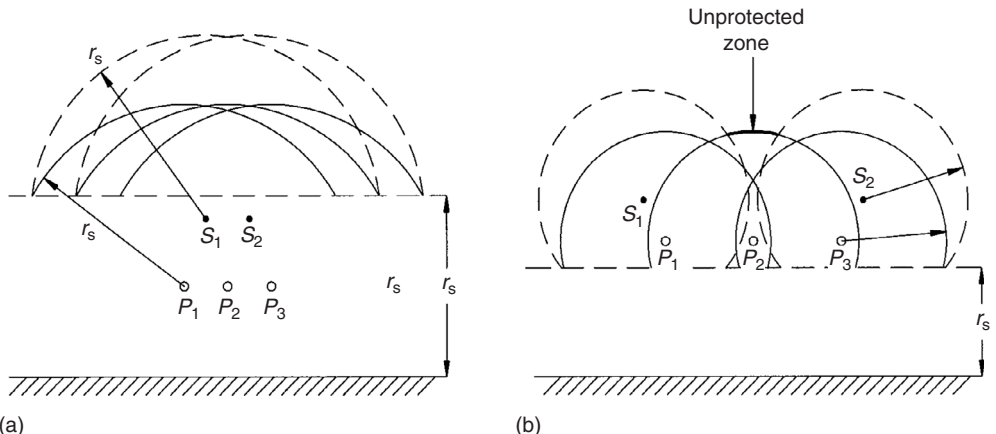


FIGURE 7.7 Shielding of three-phase horizontally configured line by two shield wires: (a) perfect shielding; (b) imperfect shielding.

where

$$\alpha_1 = \frac{I_p}{t_f} \quad \text{and} \quad \alpha_2 = \frac{2t_h - t_f}{2t_f(t_h - t_f)} I_p \quad (7.15)$$

I_o , a_1 , and a_2 of the double exponential function in Eq. (7.13) are not very easy to evaluate. In contrast, α_1 and α_2 of the linear function in Eq. (7.14) are easy to evaluate as given in Eq. (7.15). The results from the two waveshapes are not significantly different, particularly for lightning currents where t_f is on the order of a few microseconds and t_h is several tens of microseconds. As t_h is very long compared to t_f , the influence of t_h on the insulator voltage is not significant. Therefore, any convenient number can be assumed for t_h (e.g., 50 μs) without loss of accuracy.

The statistical variations of the peak return-stroke current, I_p , fit the log-normal distribution (Popolansky, 1972). The probability density function of I_p , $p(I_p)$, can then be expressed as

$$p(I_p) = \frac{1}{\sqrt{2\pi} I_p \sigma_{\ell n I_p}} e^{-0.5 \left(\frac{\ell n I_p - \ell n I_{pm}}{\sigma_{\ell n I_p}} \right)^2} \quad (7.16)$$

where $\sigma_{\ell n I_p}$ is the standard deviation of $\ell n I_p$ and I_{pm} is the median value of the return-stroke current, I_p . The cumulative probability, P_c , that the peak current in any lightning flash will exceed I_p kA can be determined by integrating Eq. (7.16) as follows:

Substituting,

$$u = \frac{\ell n I_p - \ell n I_{pm}}{\sqrt{2} \sigma_{\ell n I_p}} \quad (7.17)$$

$$P_c(I_p) = \frac{1}{\sqrt{\pi}} \int_u^{\infty} e^{-u^2} du = 0.5 \operatorname{erfc}(u) \quad (7.18)$$

The probability density function, $p(t_f)$, of the front time, t_f , can be similarly determined by replacing I_{pm} and $\sigma_{\ell n I_p}$ by the corresponding t_{fm} and $\sigma_{\ell n t_f}$ in Eqs. (7.17) and (7.18). Assuming no correlation between I_p and t_f , the joint probability density function of I_p and t_f is $p(I_p, t_f) = p(I_p)p(t_f)$. The equation for $p(I_p, t_f)$ becomes more complex if there is a correlation between I_p and t_f (Chowdhuri, 2004). The joint probability density function is then given by

$$p(I_p, t_f) = \frac{e^{\frac{0.5}{1-\rho^2}(f_1 - 2\rho\sqrt{f_1 \cdot f_2} + f_2)}}{2\pi(I_p \cdot t_f)(\sigma_{\ell n I_p} \cdot \sigma_{\ell n t_f})\sqrt{1-\rho^2}} \quad (7.19)$$

where

$$f_1 = \left(\frac{\ell n I_p - \ell n I_{pm}}{\sigma_{\ell n I_p}} \right)^2; \quad f_2 = \left(\frac{\ell n t_f - \ell n t_{fm}}{\sigma_{\ell n t_f}} \right)^2$$

and ρ = coefficient of correlation. The statistical parameters (I_{pm} , $\sigma_{\ell n I_p}$, t_{fm} , and $\sigma_{\ell n t_f}$) have been analyzed in Anderson and Eriksson (1980) and Eriksson (1986) and are given in Chowdhuri (2004) and IEEE/PES Task Force 15.09 (2005):

$$t_{fm} = 3.83 \text{ } \mu\text{s}; \sigma_{\ell ntf} = 0.553$$

$$\text{For } I_p < 20 \text{ kA: } I_{pm} = 61.1 \text{ kA; } \sigma_{\ell nlp} = 1.33$$

$$\text{For } I_p > 20 \text{ kA: } I_{pm} = 33.3 \text{ kA; } \sigma_{\ell nlp} = 0.605$$

Besides I_p and t_b the ground flash density, n_g , is the third significant parameter in estimating the lightning performance of power systems. The ground flash density is defined as the average number of lightning flashes per square kilometer per year in a geographic region. It should be borne in mind that the lightning activity in a particular geographic region varies by a large margin from year to year. Generally, the ground flash density is averaged over ten years. In the past, the index of lightning severity was the keraunic level, i.e., the number of thunder days in a region, because that was the only parameter available. Several empirical equations have been used to relate keraunic level with n_g . However, there has been a concerted effort in many parts of the world to measure n_g directly, and the measurement accuracy has also been improved in recent years.

7.4 Outage Rates by Direct Strokes

The outage rate is the ultimate gauge of lightning performance of a transmission line. It is defined as the number of outages caused by lightning per 100 km of line length per year. One needs to know the attractive area of the line in order to estimate the outage rate. The line is assumed to be struck by lightning if the stroke falls within the attractive area. The electrical shadow method has been used to estimate the attractive area. According to the electrical shadow method, a line of height, h_p meters, will attract lightning from a distance of $2h_p$ m from either side. Therefore, for a 100-km length, the attractive area will be $0.4h_p \text{ km}^2$. This area is then a constant for a specific overhead line of given height, and is independent of the severity of the lightning stroke (i.e., I_p). The electrical shadow method has been found to be unsatisfactory in estimating the lightning performance of an overhead power line. Now, the electrogeometric model is used in estimating the attractive area of an overhead line. The attractive area is estimated from the striking distance, which is a function of the return-stroke current, I_p , as given by Eq. (7.11). Although it has been suggested that the striking distance should also be a function of other variables (Chowdhuri and Kotapalli, 1989), the striking distance as given by Eq. (7.11) is being universally used.

The first step in the estimation of outage rate is the determination of the critical current. If the return-stroke current is less than the critical current, then the insulator will not flash over if the line is hit by the stepped leader. If one of the phase conductors is struck, such as for an unshielded line, then the critical current is given by Eq. (7.2). However, for strikes either to the tower or to the shield wire of a shielded line, the critical current is not that simple to compute if the multiple reflections along the tower are considered as in Eq. (7.4) or Eq. (7.9). For these cases, it is best first to compute the insulator voltage by Eq. (7.4) or by Eq. (7.9) for a return-stroke current of 1 kA, then estimate the critical current by taking the ratio between the insulation strength and the insulator voltage caused by 1 kA of return-stroke current of the specified front time, t_f , bearing in mind that the insulator voltage is a function of t_f .

Methods of estimation of the outage rate for unshielded and shielded lines will be somewhat different. Therefore, they are discussed separately.

7.4.1 Unshielded Lines

The vertical towers and the horizontal phase conductors coexist for an overhead power line. In that case, there is a race between the towers and the phase conductors to catch the lightning stroke. Some lightning strokes will hit the towers and some will hit the phase conductors. Figure 7.8 illustrates how to estimate the attractive areas of the towers and the phase conductors.

The tower and the two outermost phase conductors are shown in Fig. 7.8. In the cross-sectional view, a horizontal line is drawn at a height r_s from the earth's surface, where r_s is the striking distance corresponding to the return-stroke current, I_s . A circle (cross-sectional view of a sphere) is drawn with

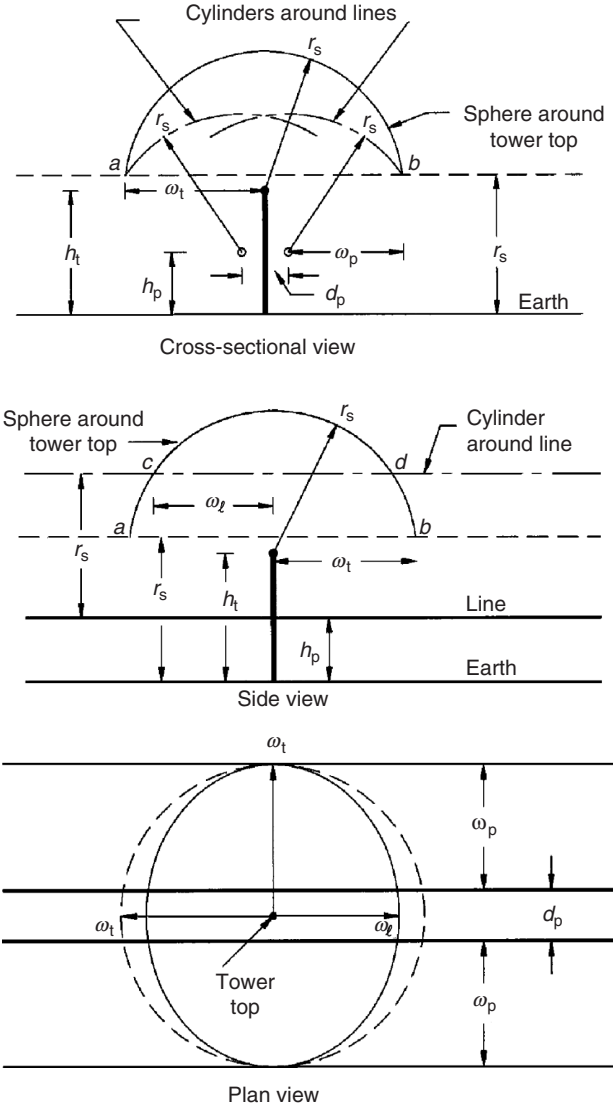


FIGURE 7.8 Attractive areas of tower and horizontal conductors.

radius, r_s , and center at the tip of the tower, cutting the line above the earth at a and b . Two circles (representing cylinders) are drawn with radius, r_s , and centers at the outermost phase conductors, cutting the line above the earth again at a and b . The horizontal distance between the tower tip and either a or b is ω_t . The side view of Fig. 7.8 shows where the sphere around the tower top penetrates both the r_s -plane (a and b) above ground and the cylinders around the outermost phase conductors (c and d). The projection of the sphere around the tower top on the r_s -plane is a circle of radius, ω_t , given by

$$\omega_t = \sqrt{r_s^2 - (r_s - h_t)^2} = \sqrt{h_t(2r_s - h_t)} \quad (7.20)$$

The projection of the sphere on the upper surface of the two cylinders around the outer phase conductors will be an ellipse with its minor axis, $2\omega_\ell$, along a line midway between the two outer

phase conductors and parallel to their axes; the major axis of the ellipse will be $2\omega_t$, as shown in the plan view of Fig. 7.8. ω_ℓ is given by

$$\omega_\ell = \sqrt{r_s^2 - (r_s - h_t + h_p)^2} \quad (7.21)$$

If a lightning stroke with return-stroke current, I_s or greater, falls within the ellipse, then it will hit the tower. It will hit one of the phase conductors if it falls outside the ellipse but within the width $(2T_p + d_p)$; it will hit the ground if it falls outside the width $(2\omega_p + d_p)$. Therefore, for each span length, ℓ_s , the attractive areas for the tower (A_t) and for the phase conductors (A_p) will be

$$A_t = \pi\omega_t\omega_\ell \quad (7.22a)$$

and

$$A_p = (2\omega_p + d_p)\ell_s - A_t \quad (7.22b)$$

The above analysis was performed for the shielding current of the overhead line when the sphere around the tower top and the cylinders around the outer phase conductors intersect the r_s -plane above ground at the same points (points a and b in Fig. 7.8). In this case, $2\omega_t = 2\omega_p + d_p$. The sphere and the cylinders will intersect the r_s -plane at different points for different return-stroke currents; their horizontal segments (widths) can be similarly computed. The equation for ω_t is given in Eq. (7.20). The equation for ω_p is given in Eq. (7.12). Due to conductor sag, the effective height of a conductor is lower than that at the tower. The effective height is generally assumed as

$$h_p = h_{pt} - \frac{2}{3}(\text{midspan sag}) \quad (7.23)$$

where h_{pt} is the height of the conductor at tower.

The critical current, i_{cp} , for stroke to a phase conductor is computed from Eq. (7.2). It should be noted that i_{cp} is independent of the front time, t_f , of the return-stroke current. The critical current, i_{ct} , for stroke to tower is a function of t_f . Therefore, starting with a short t_f , such as 0.5 μ s, the insulator voltage is determined with 1 kA of tower injected current; then, the critical tower current for the selected t_f is determined by the ratio of the insulation strength (e.g., BIL) to the insulator voltage determined with 1 kA of tower injected current. The procedure for estimating the outage rate is started with the lower of the two critical currents (i_{cp} or i_{ct}). If i_{cp} is the lower one, which is usually the case, the attractive areas, A_p and A_t , are computed for that current. If $i_{cp} < i_{ct}$, then this will not cause any flashover if it falls within A_t . In other words, the towers act like partial shields to the phase conductors. However, all strokes with i_{cp} and higher currents falling within A_p will cause flashover. The cumulative probability, $P_c(i_{cp})$, for strokes with currents i_{cp} and higher is given by Eq. (7.18). If there are n_{sp} spans per 100 km of the line, then the number of outages for lightning strokes falling within A_p along the 100-km stretch of the line will be

$$nfp = n_g P_c(i_{cp}) p(t_f) \Delta t_f n_{sp} A_p \quad (7.24)$$

where $p(t_f)$ is the probability density function of t_f , and Δt_f is the front step size. The stroke current is increased by a small step (e.g., 500 A), Δi ($i = i_{cp} + \Delta i$), and the enlarged attractive area, A_{p1} , is calculated. All strokes with currents i and higher falling within A_{p1} will cause outages. However, outage rate for strokes falling within A_p for strokes i_{cp} and greater has already been computed in Eq. (7.24). Therefore, only the additional outage rate, Δnfp , should be added to Eq. (7.24):

$$\Delta nfp = n_g P_c(i)p(t_f)\Delta t_f n_{sp} \Delta A_p \quad (7.25)$$

where $\Delta A_p = A_{p1} - A_p$. The stroke current is increased in steps of Δi and the incremental outages are added until the stroke current is very high (e.g., 200 kA) when the probability of occurrence becomes acceptably low. Then, the front time, t_f is increased by a small step, Δt_f , and the computations are repeated until the probability of occurrence of higher t_f is low (e.g., $t_f = 10.5 \mu s$). In the mean time, if the stroke current becomes equal to i_{ct} , then the outages due to strokes to the tower should be added to the outages caused by strokes to the phase conductors. The total outage rate is then given by (Chowdhuri et al., 2002):

$$nfo = nfp + nft \quad (7.26a)$$

$$nfp = nfp_0 + n_g n_{sp} \sum_{t_f} \sum_i P_c(i) p(t_f) \Delta t_f \Delta A_p \quad (7.26b)$$

and

$$nft = nft_0 + n_g n_t \sum_{t_f} \sum_i P_c(i) p(t_f) \Delta t_f \Delta A_t \quad (7.26c)$$

With digital computers, the total outage rates can be computed within a few seconds.

7.4.2 Shielded Lines

For strokes to the shield wire, the voltage at the adjacent towers will be the same as that for stroke to the tower for the same stroke current. Therefore, there will be only one critical current for strokes to shielded lines, unlike the unshielded lines. The critical current for shielded lines can be computed similar to that for the unshielded lines, except that Eq. (7.8) is now used instead of Eq. (7.4).

Otherwise, the computation for shielded lines is similar to that for unshielded lines. h_p and d_p for the phase conductors are replaced by h_s and d_s , which are the shield-wire height and the separation distance between the shield wires, respectively. For a line with a single shield wire, $d_s = 0$. Generally, shield wires are attached to the tower at its top. However, the effective height of the shield wire is lower than that of the tower due to sag. The effective height of the shield wire, h_s , can be computed from Eq. (7.23) by replacing h_{pt} by h_{st} , the shield-wire height at tower.

The backflash rates of a horizontally configured three-phase overhead line with two shield wires were computed. The dimensions of the line are shown in Table 7.1. The backflashover rates with and without shield wires are plotted in Fig. 7.9 as function of the insulation withstand voltage. It should be noted that the outage rate of the unshielded line decreases much slower than that for the shielded line. This happens because the phase conductor is struck by lightning more often than the towers, and the critical current for strikes to the phase conductor is significantly smaller than that for strike to a tower.

7.5 Effects of Induction for Direct Strokes

In the analysis of the insulator-string voltage, V_{ins} , it was assumed that V_{ins} has two components: (i) one due to the cross-arm voltage, V_{ca} , caused by the multiply reflected traveling voltage waves along the struck tower and (ii) the other due to electromagnetic coupling of the phase conductor to the shield

TABLE 7.1 Dimensions of a Horizontally Configured Distribution Line

Cross-Arm Height, m	Phase-Conductor Height, m	Phase-Conductor Separation, m	Shield-Wire Height, m	Shield-Wire Separation, m	Span Length, m
9.72	10.00	3.66	13.05	3.66	100.0

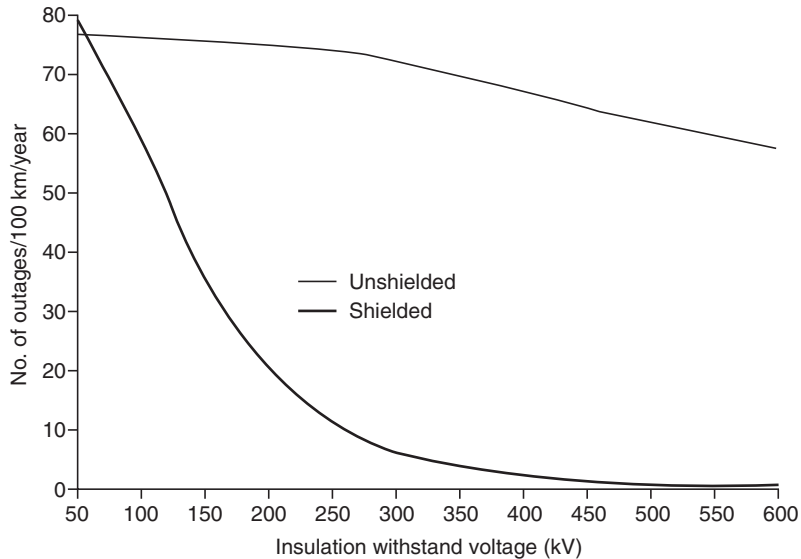


FIGURE 7.9 Outage rates of the horizontally configured three-phase overhead line of Table 7.1 (shielded and unshielded) caused by direct strokes to the line.

Tower surge impedance = 100Ω ; tower-footing resistance = 10Ω ; return-stroke surge impedance = 500Ω ; ground flash density = $10/\text{km}^2/\text{year}$; correlation coefficient = 0.47.

wire for a shielded line. However, two other component voltages contribute to the total voltage across the insulator string (Chowdhuri et al., 2002; Chowdhuri, 2004). The third voltage component is induced by the electromagnetic fields of the charge and current of the return-stroke channel (Fig. 7.10). The stroke channel being only a few meters from the phase conductors, the induction effect should not be ignored. The fourth voltage component is induced across the insulator string by the multiply reflected traveling current waves along the struck tower (Fig. 7.10). The voltage induced across the insulator string by the rapid change of the tower current can be significant because of the proximity of the tower to the insulators.

The third voltage component can be computed by the analysis shown in Chapter 8, with the difference that, in the present case, the stroke hits the tower top instead of the ground. This

difference is manifested in the inducing voltage, V_i , which is given in Eqs. (8.2) and (8.3) of Chapter 8. The scalar potential, φ , and the vector potential, A , in Eq. (8.3) of Chapter 8 in this book can be computed from Chapter 8 of *Electromagnetic Transients in Power Systems* (Chowdhuri, 2004) with the difference that the lower and the upper limits of z' (height of a specified point along the stepped leader) are the tower height, h_t , and the cloud height, h_c , for strike to the tower top. Therefore, the voltage induced on the phase conductor for a tower strike is computed for two cloud heights (h_c and h_t), and then the second induced voltage (for h_t) is subtracted from the first induced voltage (due to h_c).

The fourth voltage component, i.e., the induced voltage due to the traveling current along the tower, can be computed similar to the normal case for stroke to ground, with the following modifications:

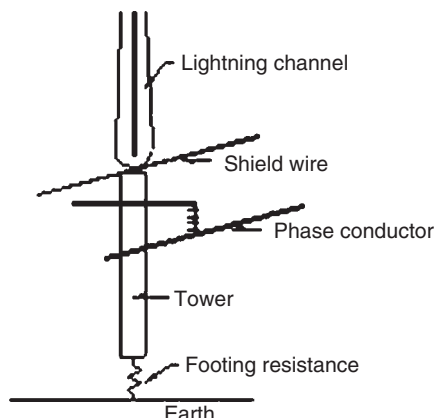


FIGURE 7.10 Direct stroke to a tower.

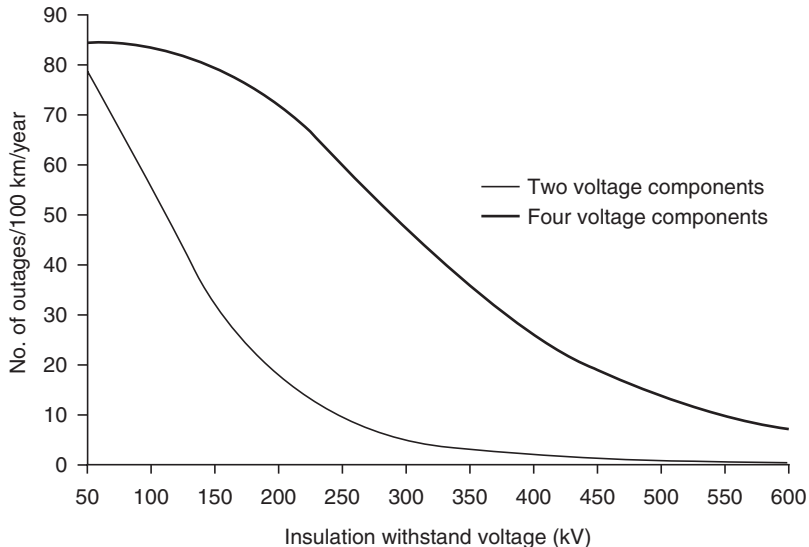


FIGURE 7.11 Outage rates by direct strokes of the horizontally configured three-phase overhead line of Table 7.1 considering two and four voltage components across insulator string.

Tower surge impedance = 100Ω ; tower-footing resistance = 10Ω ; velocity of traveling-wave current in tower = 0.8 p.u.; cloud height = 3 km; return-stroke surge impedance = 500Ω ; ground flash density = $10/\text{km}^2/\text{year}$; correlation coefficient = 0.47.

1. In the computation of the inducing voltage for a strike to ground, both the electrostatic component of the upper charge column and the magnetic component of the lower current column are considered. For the traveling current waves along the tower, only the magnetic component of the electromagnetic field is considered.
2. After each reflection at either end of the struck tower, both the magnitude and the direction of travel change for the traveling current waves. Therefore, new computations must be superimposed on the initial computation after each reflection.

The effects of the third and fourth voltage components on the estimation of outage rates are shown in Fig. 7.11 for a horizontally configured three-phase distribution line with two shield wires.

References

-
- Anderson, R.B. and Eriksson, A.J., Lightning parameters for engineering applications, *Electra*, 69, 65–102, 1980.
- Armstrong, H.R. and Whitehead, E.R., Field and analytical studies of transmission line shielding, *IEEE Trans. Power Apparatus Systems*, PAS-87, 270–281, 1968.
- Bewley, L.V., *Traveling Waves on Transmission Systems*, 2nd ed., John Wiley, New York, 1951.
- Brown, G.W. and Whitehead, E.R., Field and analytical studies of transmission line shielding: Part II, *IEEE Trans. Power Apparatus Systems*, PAS-88, 617–626, 1969.
- Chowdhuri, P. and Kotapalli, A.K., Significant parameters in estimating the striking distance of lightning strokes to overhead lines, *IEEE Trans. Power Delivery*, 4, 1970–1981, 1989.
- Chowdhuri, P., Li, S., and Yan, P., Rigorous analysis of back-flashover outages caused by direct lightning strokes to overhead power lines, *IEE Proc.—Generation, Transmission, Distribution*, 149, 58–65, 2002.
- Chowdhuri, P., *Electromagnetic Transients in Power Systems*, 2nd ed., Research Studies Press, Baldock, Hertfordshire, U.K., 2004.

- Eriksson, A.J., Notes on lightning parameters, CIGRE Note 33–86 (WG33-01) IWD, 15 July 1986.
- IEEE/PES Task Force 15.09, Parameters of lightning strokes: A review, *IEEE Trans. Power Delivery*, 20, 346–358, 2005.
- Popolansky, F., Frequency distribution of amplitudes of lightning currents, *Electra*, 22, 139–147, 1972.

8

Overvoltages Caused by Indirect Lightning Strokes

8.1	Inducing Voltage	8-2
8.2	Induced Voltage.....	8-4
8.3	Green's Function.....	8-5
8.4	Induced Voltage of a Doubly Infinite Single-Conductor Line.....	8-5
	Evaluation of Green's Function • Induced Voltage Caused by Return-Stroke Current of Arbitrary Waveshape	
8.5	Induced Voltages on Multiconductor Lines.....	8-10
8.6	Effects of Shield Wires on Induced Voltages	8-11
8.7	Stochastic Characteristics of Lightning Strokes.....	8-12
8.8	Estimation of Outage Rates Caused by Nearby Lightning Strokes	8-13
8.9	Estimation of Total Outage Rates	8-15
	Appendix A Voltage Induced by Linearly Rising and Falling Return-Stroke Current.....	8-17

Pritindra Chowdhuri
Tennessee Technological University

A direct stroke is defined as a lightning stroke when it hits a shield wire, a tower, or a phase conductor. An insulator string is stressed by very high voltages caused by a direct stroke. An insulator string can also be stressed by high transient voltages when a lightning stroke hits the nearby ground. An indirect stroke is illustrated in Fig. 8.1.

The voltage induced on a line by an indirect lightning stroke has four components:

1. The charged cloud above the line induces bound charges on the line while the line itself is held electrostatically at ground potential by the neutrals of connected transformers and by leakage over the insulators. When the cloud is partially or fully discharged, these bound charges are released and travel in both directions on the line giving rise to the traveling voltage and current waves.
2. The charges lowered by the stepped leader further induce charges on the line. When the stepped leader is neutralized by the return stroke, the bound charges on the line are released and thus produce traveling waves similar to that caused by the cloud discharge.
3. The residual charges on the upper part of the return stroke induce an electrostatic field in the vicinity of the line and hence an induced voltage on it.
4. The rate of change of current in the return stroke produces a magnetically induced voltage on the line.

If the lightning has subsequent strokes, then the subsequent components of the induced voltage will be similar to one or the other of the four components discussed above.

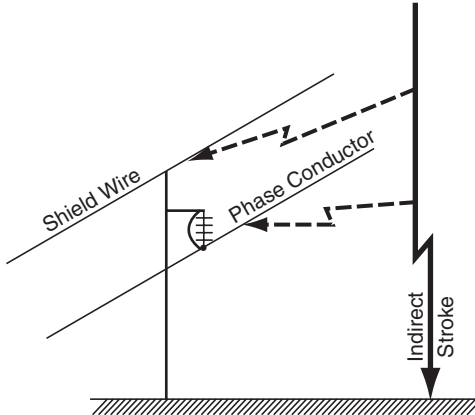


FIGURE 8.1 Illustration of direct and indirect lightning strokes.

a column of residual charge that is neutralized by the rapid upward movement of the return-stroke current in the lower part of the channel.

Figure 8.3 shows a rectangular system of coordinates where the origin of the system is the point where lightning strikes the surface of the earth. The line conductor is located at a distance y_0 meters from the origin, having a mean height of h_p meters above ground and running along the x -direction. The origin of time ($t=0$) is assumed to be the instant when the return stroke starts at the earth level.

8.1 Inducing Voltage

The total electric field created by the charge and the current in the lightning stroke at any point in space is

$$E_i = E_{ei} + E_{mi} = -\nabla\varphi - \frac{\partial A}{\partial t} \quad (8.1)$$

where φ is the *inducing* scalar potential created by the residual charge at the upper part of the return stroke and A is the *inducing* vector potential created by the upward-moving return-stroke current (Fig. 8.2). φ and A are called the retarded potentials, because these potentials at a given point in space and time are determined by the charge and current at the source (i.e., the lightning channel) at an earlier time; the difference in time (i.e., the retardation) is the time required to travel the distance between the source and the field point in space with a finite velocity, which in air is $c=3\times 10^8$ m/s. These electromagnetic potentials can be deduced from the distribution of the charge and the current in the return-stroke channel. The next step is to find the inducing electric field (Eq. 8.1). The *inducing* voltage, V_i , is the line integral of E_i :

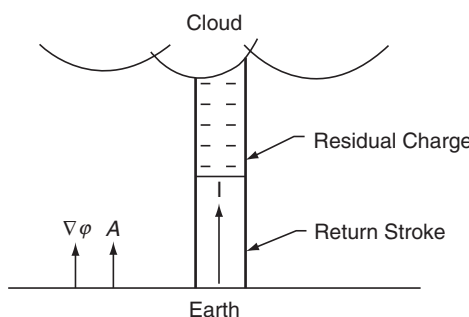


FIGURE 8.2 Return stroke with residual charge column.

The magnitudes of the voltages induced by the release of the charges bound either by the cloud or by the stepped leader are small compared with the voltages induced by the return stroke. Therefore, only the electrostatic and the magnetic components induced by the return stroke are considered in the following analysis. The initial computations are performed with the assumption that the charge distribution along the leader stroke is uniform, and that the return-stroke current is rectangular. However, the result with the rectangular current wave can be transformed to that with currents of any other waveshape by the convolution integral (Duhamel's theorem). It was also assumed that the stroke is vertical and that the overhead line is lossfree and the earth is perfectly conducting. The vertical channel of the return stroke is shown in Fig. 8.2, where the upper part consists of

$$V_i = - \int_0^{h_p} E_i \cdot dz = - \int_0^{h_p} E_{ei} \cdot dz - \int_0^{h_p} E_{mi} \cdot dz = V_{ei} + V_{mi} \quad (8.2)$$

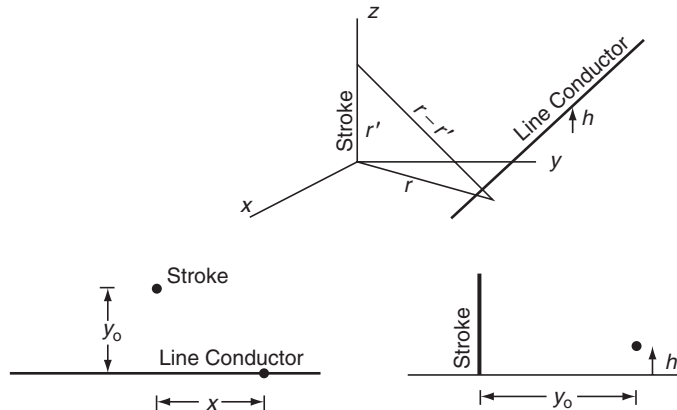


FIGURE 8.3 Coordinate system of line conductor and lightning stroke.

As the height, h_p , of the line conductor is small compared with the length of the lightning channel, the inducing electric field below the line conductor can be assumed to be constant and equal to that on the ground surface:

$$V_i = \left(\nabla \varphi + \frac{\partial A}{\partial t} \right) \cdot h_p \quad (8.3)$$

The inducing voltage will act on each point along the length of the overhead line. However, because of the retardation effect, the earliest time, t_o , the disturbance from the lightning channel will reach a point on the line conductor would be

$$t_o = \frac{\sqrt{x^2 + y_0^2}}{c} \quad (8.4)$$

Therefore, the inducing voltage at a point on the line remains zero until $t = t_o$. Hence

$$V_i = \psi(x, t) u(t - t_o) \quad (8.5)$$

where $u(t - t_o)$ is the shifted unit step function. The continuous function, $\psi(x, t)$, is the same as Eq. (8.3), and is given, for a negative stroke with uniform charge density along its length, by (Rusck, 1958)

$$\psi(x, t) = -\frac{60I_o h_p}{\beta} \left[\frac{1 - \beta^2}{\sqrt{\beta^2 c^2 (t - t_o)^2 + (1 - \beta^2)r^2}} - \frac{1}{\sqrt{h_c^2 + r^2}} \right] \quad (8.6)$$

where

I_o = step-function return-stroke current (A)

h_p = height of line above ground (m)

$\beta = v/c$

v = velocity of return stroke (m/s)

r = distance of point x on line from point of strike (m)

h_c = height of cloud charge center above ground (m)

The inducing voltage is the voltage at a field point in space with the same coordinates as a corresponding point on the line conductor, but without the presence of the line conductor. The inducing voltage at different points along the length of the line conductor will be different. In the overhead line these

differences will tend to be equalized by the flow of current, as it is a good conductor of electricity. Therefore, the actual voltage between a point on the line and the ground below it will be different from the inducing voltage at that point. This voltage, which can actually be measured on the line conductor, is defined as the *induced* voltage. The calculation of the induced voltage is the primary objective.

8.2 Induced Voltage

Neglecting losses, an overhead line may be represented as consisting of distributed series inductance L (H/m) and distributed shunt capacitance C (F/m). The effect of the inducing voltage will then be equivalent to connecting a voltage source along each point of the line (Fig. 8.4). The partial differential equation for such a configuration will be

$$-\frac{\partial V}{\partial x} \Delta x = L \Delta x \frac{\partial I}{\partial t} \quad (8.7)$$

and

$$-\frac{\partial I}{\partial x} \Delta x = C \Delta x \frac{\partial}{\partial t} (V - V_i) \quad (8.8)$$

Differentiating Eq. (8.7) with respect to x , and eliminating I , the equation for the induced voltage can be written as

$$\frac{\partial^2 V}{\partial x^2} - \frac{1}{c^2} \frac{\partial^2 V}{\partial t^2} = -\frac{1}{c^2} \frac{\partial^2 V_i}{\partial t^2} = F(x,t) \quad (8.9)$$

where

$$c = \frac{1}{\sqrt{LC}} = \frac{1}{\sqrt{\mu_0 \epsilon_0}} = 3 \times 10^8 \text{ m/s} \quad (8.10)$$

In Laplace transform,

$$\frac{\partial^2 V(x,s)}{\partial x^2} - \frac{s^2}{c^2} V(x,s) = -\frac{s^2}{c^2} V_i(x,s) = F(x,s) \quad (8.11)$$

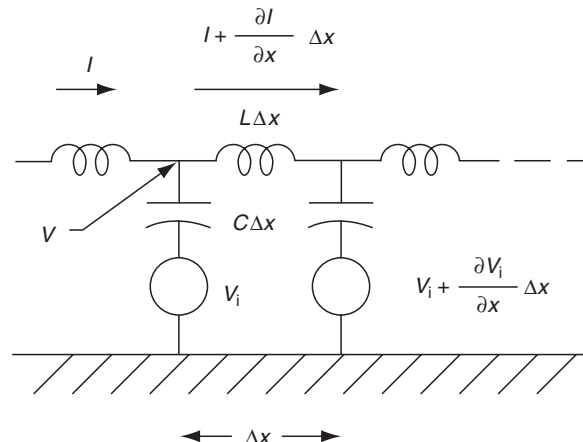


FIGURE 8.4 Equivalent circuit of transmission line with inducing voltage.

[Equation \(8.9\)](#) is an inhomogeneous wave equation for the induced voltage along the overhead line. It is valid for any charge distribution along the leader channel and any waveshape of the return-stroke current. Its solution can be obtained by assuming $F(x,t)$ to be the superposition of impulses that involves the definition of Green's function (Morse and Feshbach, 1950).

8.3 Green's Function

To obtain the voltage caused by a distributed source, $F(x)$, the effects of each elementary portion of the source are calculated and then integrated for the whole source. If $G(x;x')$ is the voltage at a point x along the line caused by a unit impulse source at a source point x' , the voltage at x caused by a source distribution $F(x')$ is the integral of $G(x;x')F(x')$ over the whole domain (a,b) of x' occupied by the source, provided that $F(x')$ is a piecewise continuous function in the domain $a \leq x' \leq b$:

$$V(x) = \int_a^b G(x;x')F(x') dx' \quad (8.12)$$

The function $G(x;x')$, called Green's function, is, therefore, a solution for a case that is homogeneous everywhere except at one point. Green's function, $G(x;x')$, has the following properties:

1. $G(x;x' + 0) - G(x;x' - 0) = 0$, (8.13)

2. $\left(\frac{dG}{dx}\right)_{x'+0} - \left(\frac{dG}{dx}\right)_{x'-0} = 1$, (8.14)

3. $G(x;x')$ satisfies the homogeneous equation everywhere in the domain, except at the point $x = x'$, and

4. $G(x;x')$ satisfies the prescribed homogeneous boundary conditions.

Green's function can be found by converting [Eq. \(8.11\)](#) to a homogeneous equation and replacing $V(x,s)$ by $G(x;x',s)$:

$$\frac{\partial^2 G(x;x',s)}{\partial x^2} - \frac{s^2}{c^2} G(x;x',s) = 0 \quad (8.15)$$

The general solution of Eq. (8.15) is given by

$$G(x;x',s) = Ae^{sx/c} + Be^{-sx/c} \quad (8.16)$$

The constants A and B are found from the boundary conditions and from the properties of Green's function.

8.4 Induced Voltage of a Doubly Infinite Single-Conductor Line

The induced voltage at any point, x , on the line can be determined by invoking Eq. (8.12), where $G(x;x') \cdot F(x')$ is the integrand. $F(x')$ is a function of the amplitude and waveshape of the inducing voltage, V_i ([Eq. \[8.5\]](#)), whereas Green's function, $G(x;x')$, is dependent on the boundary conditions of the line and the properties of Green's function. In other words, it is a function of the line configuration and is independent of the lightning characteristics. Therefore it is appropriate to determine Green's function first.

8.4.1 Evaluation of Green's Function

As Green's function is finite for $x \rightarrow -\infty$ and $x \rightarrow +\infty$,

$$G_1 = Ae^{sx/c} \text{ for } x < x'; \quad G_2 = Be^{-sx/c} \text{ for } x > x'$$

From Eq. (8.13),

$$Ae^{sx'/c} = Be^{-(sx'/c)}, \quad \text{i.e., } B = Ae^{2sx'/c}$$

From Eq. (8.14),

$$A = -\frac{c}{2s}e^{-sx/c}$$

Hence

$$\begin{aligned} B &= -\frac{c}{2s}e^{sx/c} \\ G_1(x; x', s) &= -\frac{c}{2s} \exp\left(-\frac{s(x' - x)}{c}\right) \quad \text{for } x < x' \end{aligned} \quad (8.17)$$

and

$$G_2(x; x', s) = -\frac{c}{2s} \exp\left(\frac{s(x' - x)}{c}\right) \quad \text{for } x > x' \quad (8.18)$$

By applying Eq. (8.12),

$$V(x, s) = -\frac{c}{2s} \int_{-\infty}^x e^{\frac{s(x' - x)}{c}} F(x', s) dx' - \frac{c}{2s} \int_x^\infty e^{-\frac{s(x' - x)}{c}} F(x', s) dx' = V_1(x, s) + V_2(x, s) \quad (8.19)$$

8.4.2 Induced Voltage Caused by Return-Stroke Current of Arbitrary Waveshape

The induced voltage caused by return-stroke current, $I(t)$, of arbitrary waveshape can be computed from Eq. (8.11) by several methods. In method I, the inducing voltage, V_i , due to $I(t)$ is found by applying Duhamel's integral (Halder and Liew, 1988):

$$V_i = \frac{d}{dt} \int_0^t I(t - \tau) V_{istep}(x', \tau) d\tau \quad (8.20)$$

where V_{istep} is the inducing voltage caused by a unit step-function current. In other words,

$$V_{istep}(x', \tau) = \psi_o(x', \tau) u(\tau - t_o) \quad (8.21)$$

where

$$\psi_o(x', \tau) = \psi(x', \tau) / I_o$$

and $\psi(x', \tau)$ is given in Eq. (8.6). Inserting Eq. (8.21) in Eq. (8.20), and taking Laplace transform of V_i in Eq. (8.20):

$$V_i(x', s) = sI(s)\psi_o(x', s)e^{-st_0} \quad (8.22)$$

and

$$F(x', s) = -\frac{s^2}{c^2} V_i(x', s) = -\frac{s^2}{c^2} I(s)\psi_o(x', s)e^{-st_0} \quad (8.23)$$

Replacing $F(x', s)$ in Eq. (8.19) by Eq. (8.23), the induced voltage, $V(x, s)$, is

$$V(x, s) = \frac{1}{2c} \left[sI(s) \left\{ s \int_{-\infty}^x \psi_o(x', s) e^{-s(t_0 - \frac{x'-x}{c})} dx' + s \int_x^\infty \psi_o(x', s) e^{-s(t_0 + \frac{x'-x}{c})} dx' \right\} \right] \quad (8.24)$$

Inverting to time domain by convolution integral:

$$\begin{aligned} V(x, t) &= \frac{1}{2c} \int_0^t \frac{d}{dt} I(t - \tau) \left[\frac{d}{d\tau} \int_{-\infty}^x \psi_o\left(x', \tau + \frac{x' - x}{c}\right) u\left(\tau - t_0 + \frac{x' - x}{c}\right) dx' \right] d\tau \\ &\quad + \frac{1}{2c} \int_0^t \frac{d}{dt} I(t - \tau) \left[\frac{d}{d\tau} \int_x^\infty \psi_o\left(x', \tau - \frac{x' - x}{c}\right) u\left(\tau - t_0 - \frac{x' - x}{c}\right) dx' \right] d\tau = V_1(x, t) + V_2(x, t) \end{aligned} \quad (8.25)$$

Because of the shifted unit-step function in $V_1(x, t)$

$$\tau \geq t_0 - \frac{x' - x}{c}$$

In the limit,

$$\tau = t_0 - \frac{x_{o1} - x}{c} = \frac{\sqrt{x_{o1}^2 + y_{o1}^2}}{c} - \frac{x_{o1} - x}{c}$$

or

$$x_{o1} = \frac{y_{o1}^2 - (c\tau - x)^2}{2(c\tau - x)} \quad (8.26)$$

Similarly,

$$\text{for } V_2(x, t): x_{o2} = \frac{(c\tau + x)^2 - y_{o1}^2}{2(c\tau + x)} \quad (8.27)$$

Replacing $-\infty$ by x_{o1} in $V_1(x, t)$, and $+\infty$ by x_{o2} in $V_2(x, t)$ in Eq. (8.25):

$$V_1(x, t) = \frac{1}{2c} \int_0^t \frac{d}{dt} I(t - \tau) \frac{d}{d\tau} \left\{ \int_{x_{o1}}^x \psi_o\left(x, \tau + \frac{x' - x}{c}\right) dx' \right\} u(\tau - t_0) d\tau \quad (8.28)$$

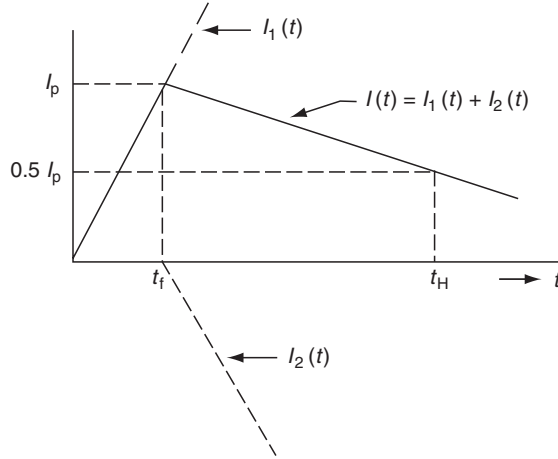


FIGURE 8.5 A linearly rising and falling lightning return-stroke current.

and

$$V_2(x,t) = \frac{1}{2c} \int_0^t \frac{d}{dt} I(t-\tau) \frac{d}{d\tau} \left\{ \int_x^{x_{o2}} \psi_o \left(x, \tau - \frac{x' - x}{c} \right) dx' \right\} u(\tau - t_o) d\tau \quad (8.29)$$

A lightning return-stroke current can be represented by a linearly rising and linearly falling wave with sufficient accuracy (Fig. 8.5) (Chowdhuri, 2004):

$$I(t) = \alpha_1 t u(t) - \alpha_2 (t - t_f) u(t - t_f) \quad (8.30)$$

where

$$\alpha_1 = \frac{I_p}{t_f} \quad \text{and} \quad \alpha_2 = \frac{2t_H - t_f}{2t_f(t_H - t_f)} I_p \quad (8.31)$$

It will be evident from Eq. (8.30) that $V_1(x,t)$ in Eq. (8.28) will have two components; one component, $V_{11}(x,t)$, will be a function of $I_1(t)$, and the other component, $V_{21}(x,t)$, will be a function of $I_2(t)$, i.e., $V_1(x,t) = V_{11}(x,t) + V_{21}(x,t)$. Similarly, $V_2(x,t) = V_{12}(x,t) + V_{22}(x,t)$. After integration and simplifying Eq. (8.28), $V_{11}(x,t)$ can be written as

$$V_{11}(x,t) = -\frac{\alpha_1 h_p}{\beta} \times 10^{-7} u(t - t_o) \left[(1 - \beta^2) \ell n \frac{f_{11}(\tau = t) f_{21}(\tau = t_o)}{f_{11}(\tau = t_o) f_{21}(\tau = t)} + \ell n \frac{f_{31}(\tau = t)}{f_{31}(\tau = t_o)} \right] \quad (8.32)$$

where

$$f_{11}(\tau) = m_{11} + \sqrt{m_{11}^2 + a_{11}^2}; \quad f_{21}(\tau) = m_{21} + \sqrt{m_{21}^2 + a_{11}^2}; \quad f_{31} = x_{o1} + \sqrt{x_{o1}^2 + y_o^2 + h_c^2}; \\ m_{11} = x + \beta^2(c\tau - x); \quad m_{21} = x_{o1} + \beta^2(c\tau - x); \quad a_{11}^2 = (1 - \beta^2)[y_o^2 + \beta^2(c\tau - x)^2]$$

The expression for $V_{21}(x,t)$ is similar to Eq. (8.32), except that α_1 is replaced by $(-\alpha_2)$, and t is replaced by $(t - t_f)$. The computation of $V_2(x,t)$ is similar; namely,

$$V_{12}(x,t) = -\frac{\alpha_1 h_p}{\beta} \times 10^{-7} u(t - t_o) \left[(1 - \beta^2) \ell n \frac{f_{12}(\tau = t) f_{22}(\tau = t_o)}{f_{12}(\tau = t_o) f_{22}(\tau = t)} - \ell n \frac{f_{32}(\tau = t)}{f_{32}(\tau = t_o)} \right] \quad (8.33)$$

where

$$f_{12}(\tau) = m_{12} + \sqrt{m_{12}^2 + a_{12}^2}; \quad f_{22} = m_{22} + \sqrt{m_{22}^2 + a_{12}^2}; \quad f_{32} = x_{o2} + \sqrt{x_{o2}^2 + y_o^2 + h_c^2}; \\ m_{12} = x_{o2} - \beta^2(c\tau + x); \quad m_{22} = x - \beta^2(c\tau + x); \quad a_{12}^2 = (1 - \beta^2)[y_o^2 + \beta^2(c\tau + x)^2]$$

$V_{22}(x,t)$ can similarly be determined by replacing α_1 in Eq. (8.33) by $(-\alpha_2)$, and replacing t by $(t - t_f)$.

The second method of determining the induced voltage, $V(x,t)$, is to solve Eq. (8.19), for a unit step-function return-stroke current, then find the induced voltage for the given return-stroke current waveshape by applying Duhamel's integral (Chowdhuri and Gross, 1967; Chowdhuri, 1989a). The solution of Eq. (8.19) for a unit step-function return-stroke current is given by (Chowdhuri, 1989a):

$$V_{\text{step}}(x,t) = (V_{11} + V_{12} + V_{21} + V_{22})u(t - t_0) \quad (8.34)$$

where

$$V_{11} = \frac{30h_p(1 - \beta^2)}{\beta^2(ct - x)^2 + y_o^2} \left[\beta(ct - x) + \frac{(ct - x)x - y_o^2}{\sqrt{c^2t^2 + \frac{1 - \beta^2}{\beta^2}(x^2 + y_o^2)}} \right] \quad (8.35)$$

$$V_{12} = -\frac{30h_p}{\beta} \left[1 - \frac{1}{\sqrt{k_1^2 + 1}} - \beta^2 \right] \frac{1}{ct - x} \quad (8.36)$$

$$V_{21} = \frac{30h_p(1 - \beta^2)}{\beta^2(ct + x)^2 + y_o^2} \left[\beta(ct + x) - \frac{(ct + x)x + y_o^2}{\sqrt{c^2t^2 + \frac{1 - \beta^2}{\beta^2}(x^2 + y_o^2)}} \right] \quad (8.37)$$

$$V_{22} = -\frac{30h_p}{\beta} \left[1 - \frac{1}{\sqrt{k_2^2 + 1}} - \beta^2 \right] \frac{1}{ct + x} \quad (8.38)$$

$$k_1 = \frac{2h_c(ct - x)}{y_o^2 + (ct - x)^2} \quad (8.39)$$

and

$$k_2 = \frac{2h_c(ct + x)}{y_o^2 + (ct + x)^2} \quad (8.40)$$

The expressions for the induced voltage, caused by a linearly rising and falling return-stroke current, are given in Appendix A.

The advantage of method II is that once the induced voltage caused by a step-function return-stroke current is computed, then it can be used as the reference in computing the induced voltage caused by currents of any given waveshape by applying Duhamel's integral, thus avoiding the mathematical manipulations for every given waveshape. However, the mathematical procedures are simpler for method I than that for method II.

A third method to solve Eq. (8.9) is to apply numerical method, which bypasses all mathematical complexities (Agrawal et al., 1980). However, the accuracy of the numerical method strongly depends

upon the step size of computation. Therefore, the computation of the induced voltage of long lines, greater than 1 km, becomes impractical.

8.5 Induced Voltages on Multiconductor Lines

Overhead power lines are usually three-phase lines. Sometimes several three-phase circuits are strung from the same tower. Shield wires and neutral conductors are part of the multiconductor system. The various conductors in a multiconductor system interact with each other in the induction process for lightning strokes to nearby ground. The equivalent circuit of a two-conductor system is shown in Fig. 8.6. Extending to an n -conductor system, the partial differential equation for the induced voltage, in matrix form, is (Chowdhuri and Gross, 1969; Cinieri and Fumi, 1979; Chowdhuri, 1990, 2004):

$$\frac{\partial^2 [V]}{\partial x^2} - \frac{1}{c^2} \frac{\partial^2 [V]}{\partial t^2} = -[L][C_g] \frac{\partial^2 [V_i]}{\partial t^2} = -[M] \frac{\partial^2 [V_i]}{\partial t^2} \quad (8.41)$$

where $[L]$ is an $n \times n$ matrix whose elements are

$$L_{rr} = 2 \times 10^{-7} \ell n \frac{2h_r}{r_r}; \quad L_{rs} = 2 \times 10^{-7} \ell n \frac{d_{rs}}{d_{rs}}$$

$[C_g]$ is an $n \times n$ diagonal matrix whose elements are $C_{jg} = C_{j1} + C_{j2} + \dots + C_{jn}$ where C_{jr} is an element of an $n \times n$ matrix, $[C] = [p]^{-1}$ and

$$p_{rr} = 18 \times 10^9 \ell n \frac{2h_r}{r_r}; \quad p_{rs} = 18 \times 10^9 \ell n \frac{d_{rs}}{d_{rs}}$$

h_r and r_r are the height above ground and radius of the r -th conductor, d_{rs} is the distance between the image of the r -th conductor below earth and the s -th conductor, d_{rs} is the distance between the r -th and s -th conductors. From Eq. (8.41), for the j -th conductor

$$\frac{\partial^2 V_j}{\partial x^2} - \frac{1}{c^2} \frac{\partial^2 V_j}{\partial t^2} = - \left(M_{j1} \frac{\partial^2 V_{j1}}{\partial t^2} + \dots + M_{jj} \frac{\partial^2 V_{jj}}{\partial t^2} + \dots + M_{jn} \frac{\partial^2 V_{jn}}{\partial t^2} \right) \quad (8.42)$$

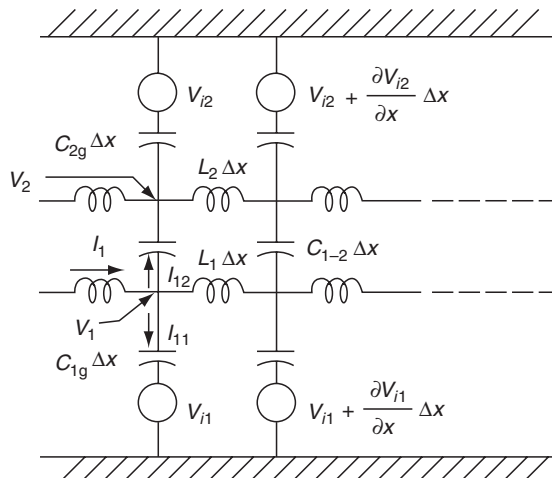


FIGURE 8.6 Equivalent circuit of a two-conductor system.

If the ratio of the inducing voltage of the m -th conductor to that of the j -th conductor is k_{mj} ($m = 1, 2, \dots, n$), then

$$\frac{\partial^2 V_j}{\partial x^2} - \frac{1}{c^2} \frac{\partial^2 V_j}{\partial t^2} = -c^2(M_{j1}k_{1j} + \dots + M_{jj} + \dots + M_{jn}k_{nj}) \frac{1}{c^2} \frac{\partial^2 V_{ij}}{\partial t^2} = (c^2 M_j) F_j(x, t) \quad (8.43)$$

where

$$M_j = M_{j1}k_{1j} + \dots + M_{jj} + \dots + M_{jn}k_{nj} \quad \text{and} \quad F_j(x, t) = \frac{1}{-c^2} \frac{\partial^2 V_{ij}}{\partial t^2} \quad (8.44)$$

If the j -th conductor in its present position existed alone, the partial differential equation of its induced voltage, V_{js} , would have been the same as Eq. (8.9), i.e.,

$$\frac{\partial^2 V_{js}}{\partial x^2} - \frac{1}{c^2} \frac{\partial^2 V_{js}}{\partial t^2} = F_j(x, t) \quad (8.45)$$

Therefore, the ratio of the induced voltage of the j -th conductor in an n -conductor system to that of a single conductor at the same position would be

$$\frac{V_j}{V_{js}} = M_j c^2 \quad (8.46)$$

The inducing voltage being nearly proportional to the conductor height, and the lateral distance of the stroke point being significantly larger than the separation distance between phase conductors, the presence of other conductors in a horizontally configured line will be minimal. On the other hand, for a vertically configured line, the induced voltage of the highest conductor will be lower than that for the same conductor without any neighboring conductors. Similarly, the lowest conductor voltage will be pulled up by the presence of the neighboring conductors of higher elevation, and the middle conductor will be the least affected by the presence of the other conductors (Chowdhuri, 2004).

8.6 Effects of Shield Wires on Induced Voltages

If there are $(n+r)$ conductors, of which r conductors are grounded (r shield wires), then the partial differential equation for the induced voltages of the n number of phase conductors is given by Chowdhuri and Gross (1969), Cinieri and Fumi (1979), and Chowdhuri (1990, 2004):

$$\frac{\partial^2 [V_n]}{\partial x^2} - \frac{1}{c^2} \frac{\partial^2 [V_n]}{\partial t^2} = -[L'][C_{gn}] \frac{\partial^2 [V_{in}]}{\partial t^2} = -[M_g] \frac{\partial^2 [V_{in}]}{\partial t^2} \quad (8.47)$$

The matrix $[L']$ is obtained by partitioning the $(n+r) \times (n+r)$ inductance matrix of the $(n+r)$ conductors, and putting $[L'] = [L_{nn}] - [L_{nr}][L_{rr}]^{-1}[L_{rn}]$, where

$$[L]_{(n+r), (n+r)} = \begin{bmatrix} L_{nn} & L_{nr} \\ L_{rn} & L_{rr} \end{bmatrix} \quad (8.48)$$

$[C_{gn}]$ is an $n \times n$ diagonal matrix each element of which is the sum of the elements of the corresponding row, upto the n -th row, of the original $(n+r) \times (n+r)$ capacitance matrix of the $(n+r)$ conductors,

$[C] = [p]^{-1}$, where $[p]$ is the matrix of the potential coefficients of the $(n+r)$ conductors. The j -th element of $[C_{gn}]$ is given by

$$C_{jgn}(j \leq n) = \sum_{k=1}^{n+r} C_{jk} \quad (8.49)$$

From Eq. (8.47), the induced voltage of the j -th conductor is

$$\frac{\partial^2 V_j}{\partial x^2} - \frac{1}{c^2} \frac{\partial^2 V_j}{\partial t^2} = -c^2(M_{gj1}k_{1j} + \dots + M_{gjj} + \dots + M_{gnj}k_{nj}) \frac{1}{c^2} \frac{\partial^2 V_{ij}}{\partial t^2} = -(c^2 M_{gj}) F_j(x, t) \quad (8.50)$$

Defining the protective ratio as the ratio of the induced voltages on the j -th conductor with and without the shield wires in place:

$$\text{Protective ratio} = \frac{M_{gj}}{M_j} \quad (8.51)$$

where M_j is given by Eq. (8.44).

8.7 Stochastic Characteristics of Lightning Strokes

The voltage induced on an overhead line is caused by the interaction between various lightning return-stroke parameters and the parameters of the line. The most important return-stroke parameters are: (a) peak current, I_p , (b) current front time, t_f , (c) return-stroke velocity, v , and (d) ground flash density, n_g . These parameters are stochastic in nature.

Analysis of field data shows that the statistical variation of the peak, I_p , and the time to crest, t_f , of the return-stroke current fit lognormal distribution (Anderson and Eriksson, 1980). The probability density function, $p(I_p)$ of I_p then can be expressed as

$$p(I_p) = \frac{e^{-0.5f_1}}{I_p \cdot \sigma_{\ell n I_p} \cdot \sqrt{2\pi}} \quad (8.52)$$

where

$$f_1 = \left(\frac{\ell n I_p - \ell n I_{pm}}{\sigma_{\ell n I_p}} \right)^2 \quad (8.53)$$

and $\sigma_{\ell n I_p}$ = standard deviation of $\ell n I_p$, and I_{pm} = median value of I_p . Similarly, the probability density function of t_f can be expressed as

$$p(t_f) = \frac{e^{-0.5f_2}}{t_f \cdot \sigma_{\ell n t_f} \cdot \sqrt{2\pi}} \quad (8.54)$$

where

$$f_2 = \left(\frac{\ell n t_f - \ell n t_{fm}}{\sigma_{\ell n t_f}} \right)^2 \quad (8.55)$$

The joint probability density function, $p(I_p, t_f)$, is given by

$$p(I_p, t_f) = \frac{e^{-\frac{0.5}{1-\rho^2}(f_1 - 2\rho\sqrt{f_1 \cdot f_2} + f_2)}}{2\pi(I_p \cdot t_f)(\sigma_{\ell n I_p} \cdot \sigma_{\ell n t_f})\sqrt{1-\rho^2}} \quad (8.56)$$

where ρ = coefficient of correlation. The statistical parameters of return-stroke current are as follows (Anderson and Eriksson, 1980; Eriksson, 1986; IEEE/PES Task Force 15.09, 2005):

Median time to crest, $t_{fm} = 3.83 \mu s$; Log (to base e) of standard deviation, $\sigma(\ell n t_f) = 0.553$

For $I_p < 20$ kA: Median peak current, $I_{pm1} = 61.1$ kA; Log (to base e) of standard deviation,

$$\sigma(\ell n I_{p1}) = 1.33$$

For $I_p > 20$ kA: Median peak current, $I_{pm2} = 33.3$ kA; Log (to base e) of standard deviation,

$$\sigma(\ell n I_{p2}) = 0.605$$

Correlation coefficient, $\rho = 0.47$.

Field data on the return-stroke velocity is limited. Lundholm (1957) and Rusck (1958) proposed the following empirical relationship between the return-stroke peak current and its velocity from the available field data:

$$\nu = \frac{c}{\sqrt{1 + \frac{500}{I_p}}} \text{ (m/s)} \quad (8.57)$$

where c = velocity of electromagnetic fields in free space = 3×10^8 m/s, and I_p = return-stroke peak current, kA.

The ground flash density, n_g (number of flashes to ground per km^2 per year), varies regionally and seasonally. However, the average ground flash density maps around the globe are available to estimate lightning-caused outages.

8.8 Estimation of Outage Rates Caused by Nearby Lightning Strokes

The knowledge of the basic impulse insulation level (BIL) is essential for estimating the outage rate of an overhead power line. With this knowledge, the electrogeometric model is constructed to estimate the attractive area (Fig. 8.7). According to the electrogeometric model, the striking distance of a lightning stroke is proportional to the return-stroke current. The following relation is used to estimate this striking distance, r_s :

$$r_s = 8I_p^{0.65} \text{ (m)} \quad (8.58)$$

where I_p in kA is the peak of the return-stroke current. In the cross-sectional view of Fig. 8.7, a horizontal line (representing a plane) is drawn at a distance of r_s meters from the ground plane corresponding to the return-stroke current, I_p . A circular arc is drawn with its center on the conductor, P , and r_s as radius. This represents a cylinder of attraction above the line conductor. The circular arc and the horizontal line intersect at points A and B . The strokes with $I = I_p$ falling between A and B will strike

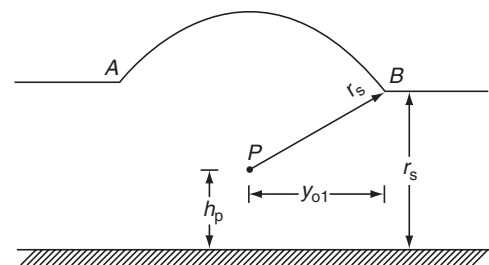


FIGURE 8.7 Electrogeometric model for estimating the least distance of ground strike.

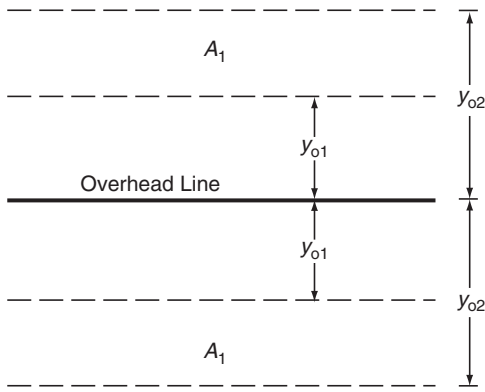


FIGURE 8.8 Attractive area of lightning ground flash to cause line flashover. $A = 2A_1 = 0.2(y_{o2} - y_{o1}) \text{ km}^2$.

front time, t_f is varied from 0.5 to 10.5 μs in steps of 0.5 μs . At each current level, the shortest possible distance of the stroke, y_{o1} , is computed from Eq. (8.59). Starting at $t_f=0.5 \mu\text{s}$, the induced voltage is calculated as a function of time and compared with the given BIL of the line. If the BIL is not exceeded then the next higher level of current is chosen. If the BIL is exceeded, then the lateral distance of the stroke from the line, y , is increased by Δy (e.g., 1 m), the induced voltage is recalculated and compared with the BIL of the line. The lateral distance, y , is progressively increased until the induced voltage does not exceed BIL. This distance is called y_{o2} . For the selected I_p and t_f the induced voltage will then exceed the BIL of the line and cause line flashover, if the lightning stroke hits the ground between y_{o1} and y_{o2} along the length of the line. For a 100-km sector of the line, the attractive area, A , will be (Fig. 8.8)

$$A = 0.2(y_{o2} - y_{o1}) \text{ km}^2 \quad (8.60)$$

The joint probability density function, $p(I_p, t_f)$, is then computed from Eq. (8.56) for the selected $I_p - t_f$ combination. If n_g is the ground flash density of the region, the expected number of flashovers per 100 km per year for that particular $I_p - t_f$ combination will be

$$\text{nfo} = p(I_p, t_f) \cdot \Delta I_p \cdot \Delta t_f \cdot n_g \cdot A \quad (8.61)$$

where ΔI_p = current step and Δt_f = front-time step.

The front time, t_f , is then increased by $\Delta t_f=0.5 \mu\text{s}$ to the next step, and nfo for the same current but with the new t_f is computed and added to the previous nfo. Once $t_f=10.5 \mu\text{s}$ is reached, the return-stroke current is increased by $\Delta I_p=0.5 \text{ kA}$, and the whole procedure repeated until the limits $I_p=200 \text{ kA}$ and $t_f=10.5 \mu\text{s}$ are reached. The cumulative nfo will then give the total number of expected line flashovers per 100 km per year for the selected BIL.

The lightning-induced outage rates of the horizontally configured three-phase overhead line of Chapter 7 are plotted in Fig. 8.9. The effectiveness of the shield wire, as shown in the figure, is optimistic, bearing in mind that the shield wire was assumed to be held at ground potential. The shield wire will not be held at ground potential under transient conditions. Therefore, the effectiveness of the shield wire will be less than the idealized case shown in Fig. 8.9.

the conductor resulting in direct strokes; those falling outside AB will hit the ground, inducing voltages on the line. The horizontal projection of A or B is y_{o1} , which is given by

$$y_{o1} = r_s \quad \text{for } r_s \leq h_p \quad (8.59a)$$

$$y_{o1} = \sqrt{r_s^2 - (r_s - h_p)^2} \quad \text{for } r_s > h_p \quad (8.59b)$$

and y_{o1} is the shortest distance of a lightning stroke of given return-stroke current from the overhead line, which will result in a flash to ground.

To compute the outage rate, the return-stroke current, I_p , is varied from 1 to 200 kA in steps of 0.5 kA (Chowdhuri, 1989b, 2004). The current

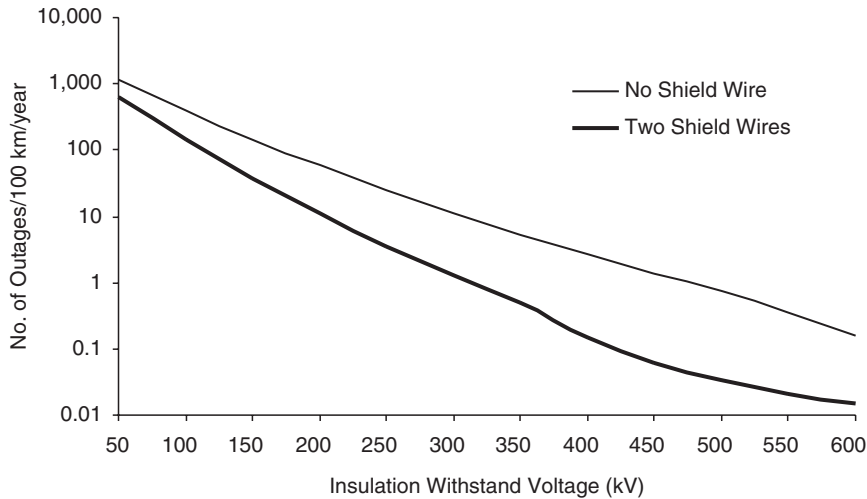


FIGURE 8.9 Outage rates of overhead line by indirect strokes vs. BIL.

8.9 Estimation of Total Outage Rates

Outages of an overhead power line may be caused by both direct and indirect lightning strokes, especially if the voltage withstand level of the line is low, e.g., power distribution lines. Outages caused by direct strokes are caused by either backflash (i.e., lightning hitting the tower or the shield wire), or by shielding failure if lightning hits one of the phase conductors. Outages caused by direct strokes were discussed in Chapter 7. Outages caused by indirect strokes are caused by lightning strokes hitting the nearby ground, which is discussed in this chapter. Therefore, information from both these chapters will be required to estimate the total outage rates of overhead lines caused by lightning. The outage rates of the three-phase horizontally configured overhead line of Chapter 7 are shown in Fig. 8.10a for the unshielded line and in Fig. 8.10b for the shielded line.

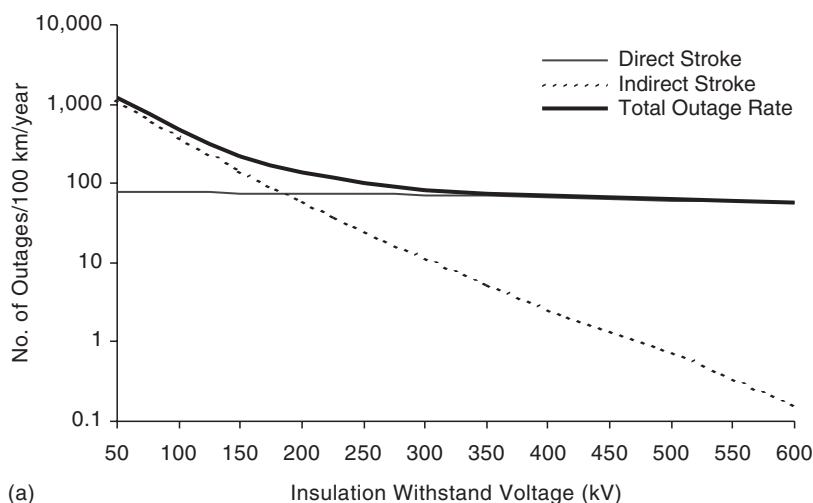


FIGURE 8.10 Total outage rates of overhead line vs. BIL

(continued)

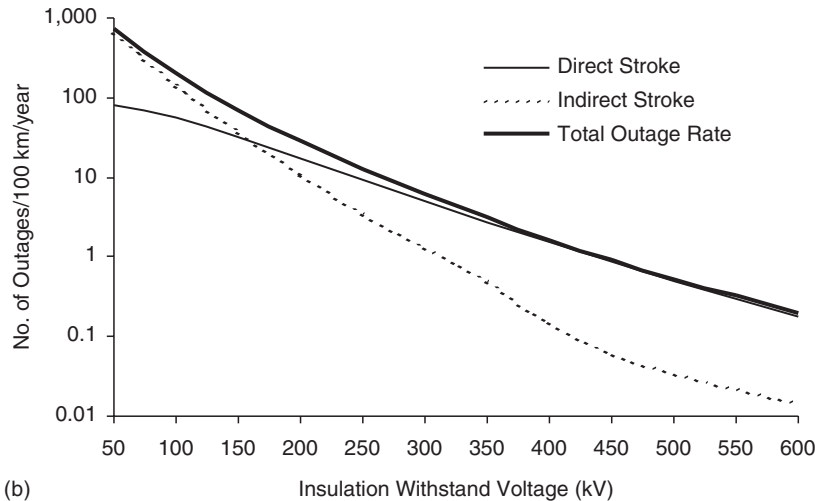


FIGURE 8.10 (continued)

References

- Agrawal, A.K., Price, H.J., and Gurbaxani, S.H., Transient response of multiconductor transmission lines excited by a nonuniform electromagnetic field, *IEEE Trans. Electromagnetic Compatibility*, EMC-22, 119–129, 1980.
- Anderson, R.B. and Eriksson, A.J., Lightning parameters for engineering applications, *Electra*, 69, 65–102, 1980.
- Chowdhuri, P., Analysis of lightning-induced voltages on overhead lines, *IEEE Trans. Power Delivery*, 4, 479–492, 1989a.
- Chowdhuri, P., Estimation of flashover rates of overhead power distribution lines by lightning strokes to nearby ground, *IEEE Trans. Power Delivery*, 4, 1982–1989, 1989b.
- Chowdhuri, P., Lightning-induced voltages on multiconductor overhead lines, *IEEE Trans. Power Delivery*, 5, 658–667, 1990.
- Chowdhuri, P., *Electromagnetic Transients in Power Systems*, 2nd ed., Research Studies Press, Baldock, Hertfordshire, U.K., 2004.
- Chowdhuri, P. and Gross, E.T.B., Voltage surges induced on overhead lines by lightning strokes, *Proc. IEE (U.K.)*, 114, 1899–1907, 1967.
- Chowdhuri, P. and Gross, E.T.B., Voltages induced on overhead multiconductor lines by lightning strokes, *Proc. IEE (U.K.)*, 116, 561–565, 1969.
- Cinieri, E. and Fumi, A., The effect of the presence of multiconductors and ground wires on the atmospheric high voltages induced on electrical lines (in Italian), *L'Energia Elettrica*, 56, 595–601, 1979.
- Eriksson, A.J., Notes on lightning parameters for system performance estimation, CIGRE Note 33–86 (WG33-01) IWD, 15 July 1986.
- Haldar, M.K. and Liew, A.C., Alternative solution for the Chowdhuri-Gross model of lightning-induced voltages on power lines, *Proc. IEE (U.K.)*, 135, 324–329, 1988.
- IEEE/PES Task Force 15.09, Parameters of lightning strokes: A review, *IEEE Trans. Power Delivery*, 20, 346–358, 2005.
- Lundholm, R., Induced overvoltage-surges on transmission lines and their bearing on the lightning performance at medium voltage networks, *Trans. Chalmers Univ. Technol.*, Gothenburg, Sweden, 188, 1–117, 1957.

Morse, P.M. and Feshbach, H., *Methods of Theoretical Physics*, Vol. 1, McGraw-Hill, New York, 1950, Chap. 7.

Rusck, S., Induced lightning over-voltages on power-transmission lines with special reference to the over-voltage protection of low-voltage networks, *Trans. Royal Inst. Tech.*, Stockholm, Sweden, 120, 1–118, 1958.

Appendix A Voltage Induced by Linearly Rising and Falling Return-Stroke Current

$$V(x,t) = V_1(x,t)u(t - t_o) + V_2(x,t)u(t - t_{of})$$

where

$$\begin{aligned}
 V_1(x,t) &= \frac{30\alpha_1 h_p}{\beta c} \left[b_o \cdot \ell n \frac{f_{12}}{f_{11}} + 0.5 \ell n(f_{13}) \right]; \quad V_2(x,t) = -\frac{30\alpha_2 h_p}{\beta c} \left[b_o \cdot \ell n \frac{f_{12a}}{f_{11a}} + 0.5 \ell n(f_{13a}) \right] \\
 b_o &= 1 - \beta^2; \quad t_{of} = t_o + t_f; \quad t_{tf} = t - t_f \\
 f_1 &= m_1 + (ct - x)^2 - y_o^2; \quad f_2 = m_1 - (ct - x)^2 + y_o^2 \\
 f_3 &= m_0 + (ct - x)^2 + y_o^2; \quad f_4 = m_0 + (ct_o - x)^2 - y_o^2 \\
 f_5 &= n_1 + (ct + x)^2 - y_o^2; \quad f_6 = n_1 - (ct + x)^2 + y_o^2 \\
 f_7 &= n_o - (ct_o + x)^2 + y_o^2; \quad f_8 = n_o + (ct_o + x)^2 - y_o^2 \\
 f_9 &= b_o(\beta^2 x^2 + y_o^2) + \beta^2 c^2 t^2(1 + \beta^2); \quad f_{10} = 2\beta^2 ct \sqrt{\beta^2 c^2 t^2 + b_o(x^2 + y_o^2)} \\
 f_{11} &= \frac{c^2 t^2 - x^2}{y_o^2}; \quad f_{12} = \frac{f_9 - f_{10}}{b_o y_o^2}; \quad f_{13} = \frac{f_1 \cdot f_3 \cdot f_5 \cdot f_7}{f_2 \cdot f_4 \cdot f_6 \cdot f_8} \\
 f_{1a} &= m_{1a} + (ct_{tf} - x)^2 - y_o^2; \quad f_{2a} = m_{1a} - (ct_{tf} - x)^2 + y_o^2 \\
 f_{3a} &= f_3; \quad f_{4a} = f_4; \quad f_{7a} = f_7; \quad f_{8a} = f_8 \\
 f_{5a} &= n_{1a} + (ct_{tf} + x)^2 - y_o^2; \quad f_{6a} = n_{1a} - (ct_{tf} + x)^2 + y_o^2 \\
 f_{9a} &= b_o(\beta^2 x^2 + y_o^2) + \beta^2 c^2 t_{tf}^2(1 + \beta^2); \quad f_{10a} = 2\beta^2 ct_{tf} \sqrt{\beta^2 c^2 t_{tf}^2 + b_o(x^2 + y_o^2)} \\
 f_{11a} &= \frac{c^2 t_{tf}^2 - x^2}{y_o^2}; \quad f_{12a} = \frac{f_{9a} - f_{10a}}{b_o y_o^2}; \quad f_{13a} = \frac{f_{1a} \cdot f_{3a} \cdot f_{5a} \cdot f_{7a}}{f_{2a} \cdot f_{4a} \cdot f_{6a} \cdot f_{8a}} \\
 m_0 &= \sqrt{[(ct_o - x)^2 + y_o^2]^2 + 4h_c^2(ct_o - x)^2}; \quad m_1 = \sqrt{[(ct - x)^2 + y_o^2]^2 + 4h_c^2(ct - x)^2} \\
 n_0 &= \sqrt{[(ct_o + x)^2 + y_o^2]^2 + 4h_c^2(ct_o + x)^2}; \quad n_1 = \sqrt{[(ct + x)^2 + y_o^2]^2 + 4h_c^2(ct + x)^2} \\
 m_{1a} &= \sqrt{[(ct_{tf} - x)^2 + y_o^2]^2 + 4h_c^2(ct_{tf} - x)^2}; \quad n_{1a} = \sqrt{[(ct_{tf} + x)^2 + y_o^2]^2 + 4h_c^2(ct_{tf} + x)^2}
 \end{aligned}$$

9

Switching Surges

Stephen R. Lambert
Shawnee Power Consulting, LLC

9.1	Transmission Line Switching Operations.....	9-1
9.2	Series Capacitor Bank Applications.....	9-4
9.3	Shunt Capacitor Bank Applications	9-4
9.4	Shunt Reactor Applications.....	9-5

Switching surges occur on power systems as a result of instantaneous changes in the electrical configuration of the system, and such changes are mainly associated with switching operations and fault events. These overvoltages generally have crest magnitudes which range from about 1 per unit to 3 pu for phase-to-ground surges and from about 2.0 to 4 pu for phase-to-phase surges (in pu on the phase to ground crest voltage base) with higher values sometimes encountered as a result of a system resonant condition. Waveshapes vary considerably with rise times ranging from 50 μ s to thousands of μ s and times to half-value in the range of hundreds of μ s to thousands of μ s. For insulation testing purposes, a waveshape having a time to crest of 250 μ s with a time to half-value of 2000 μ s is often used.

The following addresses the overvoltages associated with switching various power system devices. Possible switching surge magnitudes are indicated, and operations and areas of interest that might warrant investigation when applying such equipment are discussed.

9.1 Transmission Line Switching Operations

Surges associated with switching transmission lines (overhead, SF₆, or cable) include those that are generated by line energizing, reclosing (three phase and single phase operations), fault initiation, line dropping (deenergizing), fault clearing, etc. During an energizing operation, for example, closing a circuit breaker at the instant of crest system voltage results in a 1 pu surge traveling down the transmission line and being reflected at the remote, open terminal. The reflection interacts with the incoming wave on the phase under consideration as well as with the traveling waves on adjacent phases. At the same time, the waves are being attenuated and modified by losses. Consequently, it is difficult to accurately predict the resultant waveshapes without employing sophisticated simulation tools such as a transient network analyzer (TNA) or digital programs such as the Electromagnetic Transients Program (EMTP).

Transmission line overvoltages can also be influenced by the presence of other equipment connected to the transmission line—shunt reactors, series or shunt capacitors, static var systems, surge arresters, etc. These devices interact with the traveling waves on the line in ways that can either reduce or increase the severity of the overvoltages being generated.

When considering transmission line switching operations, it can be important to distinguish between “energizing” and “reclosing” operations, and the distinction is made on the basis of whether the line’s inherent capacitance retains a trapped charge at the time of line closing (reclosing operation) or whether no trapped charge exists (an energizing operation). The distinction is important as the magnitude of the switching surge overvoltage can be considerably higher when a trapped charge is present; with higher

magnitudes, insulation is exposed to increased stress, and devices such as surge arresters will, by necessity, absorb more energy when limiting the higher magnitudes. Two forms of trapped charges can exist—DC and oscillating. A trapped charge on a line with no other equipment attached to the line exists as a DC trapped charge, and the charge can persist for some minutes before dissipating (Beehler, 1964). However, if a transformer (power or wound potential transformer) is connected to the line, the charge will decay rapidly (usually in less than 0.5 sec) by discharging through the saturating branch of the transformer (Marks, 1969). If a shunt reactor is connected to the line, the trapped charge takes on an oscillatory waveshape due to the interaction between the line capacitance and the reactor inductance. This form of trapped charge decays relatively rapidly depending on the Q of the reactor, with the charge being reduced by as much as 50% within 0.5 seconds.

Figures 9.1 and 9.2 show the switching surges associated with reclosing a transmission line. In Fig. 9.1 note the DC trapped charge (approximately 1.0 pu) that exists prior to the reclosing operation (at 20 μ s). Figure 9.2 shows the same case with an oscillating trapped charge (a shunt reactor was present on the line) prior to reclosing. Maximum surges were 3.0 for the DC trapped charge case and 2.75 pu for the oscillating trapped charge case (both occurred on phase c).

The power system configuration behind the switch or circuit breaker used to energize or reclose the transmission line also affects the overvoltage characteristics (shape and magnitude) as the traveling wave interactions occurring at the junction of the transmission line and the system (i.e., at the circuit breaker) as well as reflections and interactions with equipment out in the system are important. In general, a stronger system (higher short circuit level) results in somewhat lower surge magnitudes than a weaker system, although there are exceptions. Consequently, when performing simulations to predict overvoltages, it is usually important to examine a variety of system configurations (e.g., a line out of service or contingencies) that might be possible and credible.

Single phase switching as well as three phase switching operations may also need to be considered. On EHV transmission lines, for example, most faults (approximately 90%) are single phase in nature, and

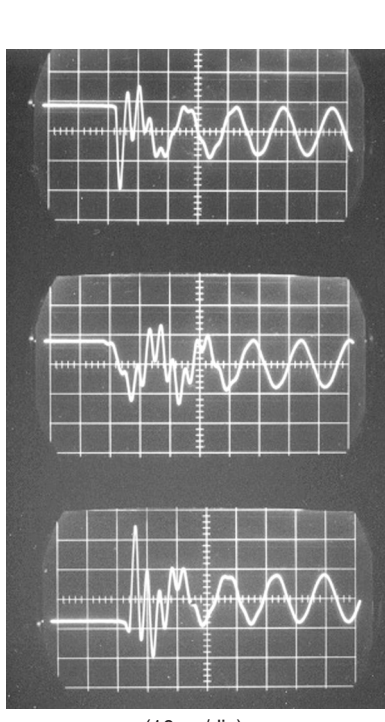


FIGURE 9.1 DC trapped charge.

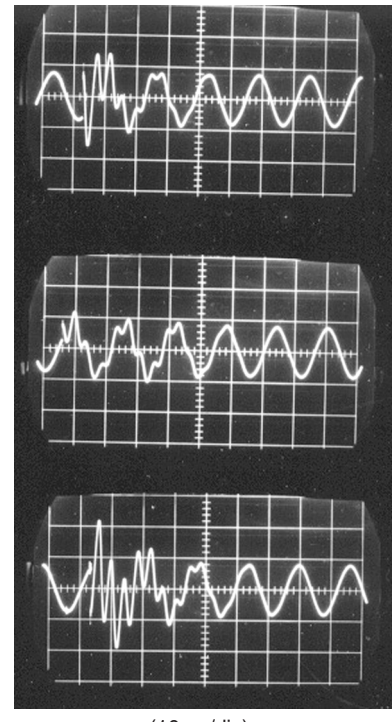


FIGURE 9.2 Oscillating trapped charge.

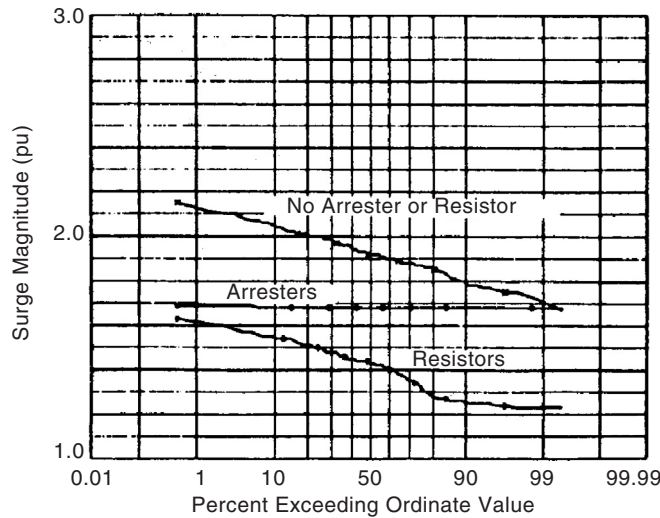


FIGURE 9.3 Phase-to-ground overvoltage distribution.

opening and reclosing only the faulted phase rather than all three phases, reduces system stresses. Typically, the overvoltages associated with single phase switching have a lower magnitude than those that occur with three phase switching (Koschik et al., 1978).

Switching surge overvoltages produced by line switching are statistical in nature—that is, due to the way that circuit breaker poles randomly close (excluding specially modified switchgear designed to close on or near voltage zero), the instant of electrical closing may occur at the crest of the system voltage, at voltage zero, or somewhere in between. Consequently, the magnitude of the switching surge varies with each switching event. For a given system configuration and switching operation, the surge voltage magnitude at the open end of the transmission line might be 1.2 pu for one closing event and 2.8 pu for the next (Johnson et al., 1964; Hedman et al., 1964), and this statistical variation can have a significantly impact on insulation design (see Chapter 14 on insulation coordination).

Typical switching surge overvoltage statistical distributions (160 km line, 100 random closings) are shown in Figs. 9.3 and 9.4 for phase-to-ground and phase-to-phase voltages (Lambert, 1988), and

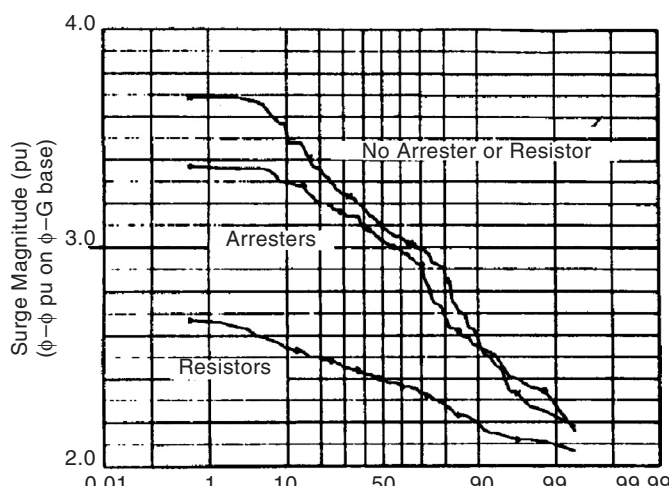


FIGURE 9.4 Phase-to-phase overvoltage distribution.

the surge magnitudes indicated are for the highest that occurred on any phase during each closing. With no surge limiting action (by arresters or circuit breaker preinsertion resistors), phase-to-ground surges varied from 1.7 to 2.15 pu with phase-to-phase surges ranging from 2.2 to 3.7 pu. Phase-to-phase surges can be important to line-connected transformers and reactors as well as to transmission line phase-to-phase conductor separation distances when line uprating or compact line designs are being considered.

[Figure 9.3](#) also demonstrates the effect of the application of surge arresters on phase-to-ground surges, and shows the application of resistors preinserted in the closing sequence of the circuit breaker (400Ω for 5.56 ms) is even more effective than arresters in reducing surge magnitude. The results shown on [Fig. 9.4](#), however, indicate that while resistors are effective in limiting phase-to-phase surges, arresters applied line to ground are generally not very effective at limiting phase-to-phase overvoltages.

Line dropping (deenergizing) and fault clearing operations also generate surges on the system, although these typically result in phase-to-ground overvoltages having a maximum value of 2 to 2.2 pu. Usually the concern with these operations is not with the phase-to-ground or phase-to-phase system voltages, but rather with the recovery voltage experienced by the switching device. The recovery voltage is the voltage which appears across the interrupting contacts of the switching device (a circuit breaker for example) following current extinction, and if this voltage has too high a magnitude, or in some instances rises to its maximum too quickly, the switching device may not be capable of successfully interrupting.

The occurrence of a fault on a transmission line also can result in switching surge type overvoltages, especially on parallel lines. These voltages usually have magnitudes on the order of 1.8–2.2 pu and are usually not a problem (Kimbark and Legate, 1968; Madzarevic et al., 1977).

9.2 Series Capacitor Bank Applications

Installation of a series capacitor bank in a transmission line (standard or thyristor controlled) has the potential for increasing the magnitude of phase-to-ground and phase-to-phase switching surge overvoltages due to the trapped charges that can be present on the bank at the instant of line reclosing. In general, surge arresters limit the phase-to-ground and phase-to-phase overvoltages to acceptable levels; however, one problem that can be serious is the recovery voltage experienced by circuit breakers when clearing faults on a series compensated line. Depending the bank's characteristics and on fault location with respect to the bank's location, a charge can be trapped on the bank, and this trapped charge can add to the surges already being generated during the fault clearing operation (Wilson, 1972). The first circuit breaker to clear is sometimes exposed to excessive recovery voltages under such conditions.

9.3 Shunt Capacitor Bank Applications

Energizing a shunt capacitor bank typically results in maximum overvoltages of about 2 pu or less. However, there are two conditions where significant overvoltages can be generated. One involves

a configuration (shown on Fig. 9.5) where two banks are separated by a significant inductance (e.g., a transformer) (Schultz et al., 1959). When one bank is switched, if the system inductance and bank 1 capacitance has the same natural frequency as that of the transformer leakage inductance and the bank 2 capacitance, then a voltage magnification can take place.

Another configuration that can result in damaging overvoltages involves energizing a

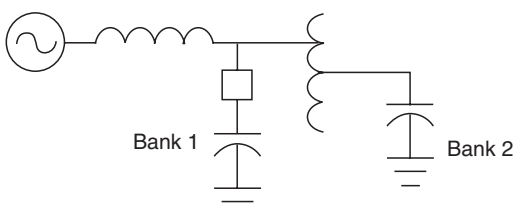


FIGURE 9.5 Voltage magnification circuit.

capacitor bank with a transformer terminated transmission line radially fed from the substation at which the capacitor bank is located (Jones and Fortson, 1985). During bank switching, phase-to-phase surges are imposed on the transformer, and because these are not very well suppressed by the usual phase-to-ground application of surge arresters, transformer failures have been known to result. Various methods to reduce the surge magnitude have included the application of controlled circuit breaker closing techniques (closing near voltage zero), and resistors or reactors preinserted in the closing sequence of the switching devices.

Restriking of the switching device during bank deenergizing can result in severe line-to-ground overvoltages of 3 pu to 5 pu or more (rarely) (Johnson et al., 1955; Greenwood, 1971). Surge arresters are used to limit the voltages to acceptable levels, but at higher system voltages, the energy discharged from the bank into the arrester can exceed the arrester's capability.

9.4 Shunt Reactor Applications

Switching of shunt reactors (and other devices characterized as having small inductive currents such as transformer magnetizing currents, motor starting currents, etc.) can generate high phase-to-ground overvoltages as well as severe recovery voltages (Greenwood, 1971), especially on lower voltage equipment such as reactors applied on the tertiary of transformers. Energizing the devices seldom generates high overvoltages, but overvoltages generated during deenergizing, as a result of current chopping by the switching device when interrupting the small inductive currents, can be significant. Neglecting damping, the phase-to-ground overvoltage magnitude can be estimated by:

$$V = i\sqrt{\frac{L}{C}} \quad (9.1)$$

where i is the magnitude of the chopped current (0 to perhaps as high as 10 A or more), L is the reactor's inductance, and C is the capacitance of the reactor (on the order of a few thousand picofarads). When C is small, especially likely with dry-type reactors often used on transformer tertiaries, the surge impedance term can be large, and hence the overvoltage can be excessive.

To mitigate the overvoltages, surge arresters are sometimes useful, but the application of a capacitor on the terminals of the reactor (or other equipment) have a capacitance on the order of 0.25–0.5 μF is very helpful. In the equation above, note that if C is increased from pF to μF , the surge impedance term is dramatically reduced, and hence the voltage is reduced.

References

- Beehler, J.E., Weather, corona, and the decay of trapped energy on transmission lines, *IEEE Trans. on Power Appar. and Syst.* 83, 512, 1964.
- Greenwood, A., *Electrical Transients in Power Systems*, John Wiley & Sons, New York, 1971.
- Hedman, D.E., Johnson, I.B., Titus, C.H., and Wilson, D.D., Switching of extra-high-voltage circuits, II—surge reduction with circuit breaker resistors, *IEEE Trans. on Power Appar. and Syst.* 83, 1196, 1964.
- Johnson, I.B., Phillips, V.E., and Simmons, Jr., H.O., Switching of extra-high-voltage circuits, I—system requirements for circuit breakers, *IEEE Trans. on Power Appar. and Syst.* 83, 1187, 1964.
- Johnson, I.B., Schultz, A.J., Schultz, N.R., and Shores, R.R., Some fundamentals on capacitance switching, *AIEE Trans. on Power Appar. and Syst.* PAS-74, 727, 1955.
- Jones, R.A. and Fortson, Jr., H.S., Considerations of phase-to-phase surges in the application of capacitor banks, IEEE PES Summer Meeting, 1985, 85 SM 400–7.
- Kimbark, E.W. and Legate, A.C., Fault surge versus switching surge: A study of transient overvoltages caused by line-to-ground faults, *IEEE Trans. on Power Appar. and Syst.* PAS-87, 1762, 1968.

- Koschik, V., Lambert, S.R., Rocamora, R.G., Wood, C.E., and Worner, G., Long line single-phase switching transients and their effect on station equipment, *IEEE Trans. on Power Appar. and Syst.* PAS-97, 857, 1978.
- Lambert, S.R., Effectiveness of zinc oxide surge arresters on substation equipment probabilities of flashover, *IEEE Trans. on Power Delivery* 3(4), 1928, 1988.
- Madzarevic, V., Tseng, F.K., Woo, D.H., Niebuhr, W.D., and Rocamora, R.G., Overvoltages on ehv transmission lines due to fault and subsequent bypassing of series capacitors, IEEE PES Winter Meeting, January 1977, F77 237–1.
- Marks, L.W., Line discharge by potential transformers, *IEEE Trans. on Power Appar. and Syst.* PAS-88, 293, 1969.
- Schultz, A.J., Johnson, J.B., and Schultz, N.R., Magnification of switching surges, *AIEE Trans. on Power Appar. and Syst.* 77, 1418, 1959.
- Wilson, D.D., Series compensated lines—voltages across circuit breakers and terminals caused by switching, *IEEE PES Summer Meeting*, 1972, T72 565–0.

10

Very Fast Transients

10.1	Origin of VFT in GIS.....	10-1
10.2	Propagation of VFT in GIS Internal Transients • External Transients	10-3
10.3	Modeling Guidelines and Simulation..... Computation of Internal Transients • Computation of TEV • Statistical Calculation • Validation	10-6
10.4	Effects of VFT on Equipment..... SF ₆ Insulation • Transformers • Disconnectors and Breakers • Enclosure • Bushings • Secondary Equipment	10-12

Juan A. Martinez-Velasco
Universitat Politecnica de Catalunya

Transient phenomena in power systems are caused by switching operations, faults, and other disturbances, such as lightning strokes. They may appear with a wide range of frequencies that vary from DC to several MHz. A distinction is usually made between slow electromechanical transients and faster electromagnetic transients. The latter type of transients can occur on a time scale that goes from microseconds to several cycles. Due to frequency-dependent behavior of power components and difficulties for developing models accurate enough for a wide frequency range, the frequency ranges are classified into groups, with overlapping between them. An accurate mathematical representation of each power component can generally be developed for a specific frequency range (CIGRE, 1990).

Very Fast Transients (VFT), also known as Very Fast Front Transients, belong to the highest frequency range of transients in power systems. According to the classification proposed by the CIGRE Working Group 33-02, VFT may vary from 100 kHz up to 50 MHz (1990). According to IEC 71-1, the shape of a very fast front overvoltage is “usually unidirectional with time to peak < 0.1 μs, total duration < 3 ms, and with superimposed oscillations at frequency 30 kHz < f < 100 MHz” (1993). In practice, the term VFT is restricted to transients with frequencies above 1 MHz. Several causes can originate these transients in power systems: disconnector operations and faults within gas insulated substations (GIS), switching of motors and transformers with short connections to the switchgear, certain lightning conditions (IEC 71-2, 1996).

This section is exclusively dedicated to explaining the origin, and to analyze the propagation and the effects of VFT in GIS. These transients have a rise time in the range of 4 to 100 ns, and are normally followed by oscillations ranging from 1 to 50 MHz. Their magnitude is in the range of 1.5 to 2 per unit of the line-to-neutral voltage crest, but they can also reach values higher than 2.5 per unit. These values are generally below the BIL of the GIS and connected equipment of lower voltage classes. VFT in GIS are of greater concern at the highest voltages, for which the ratio of the BIL to the system voltage is lower (Yamagata et al., 1996). External VFT can be dangerous for secondary and adjacent equipment.

10.1 Origin of VFT in GIS

VFT within a gas-insulated substation (GIS) are usually generated by disconnect switch operations, although other events, such as the closing of a grounding switch or a fault, can also cause VFT.

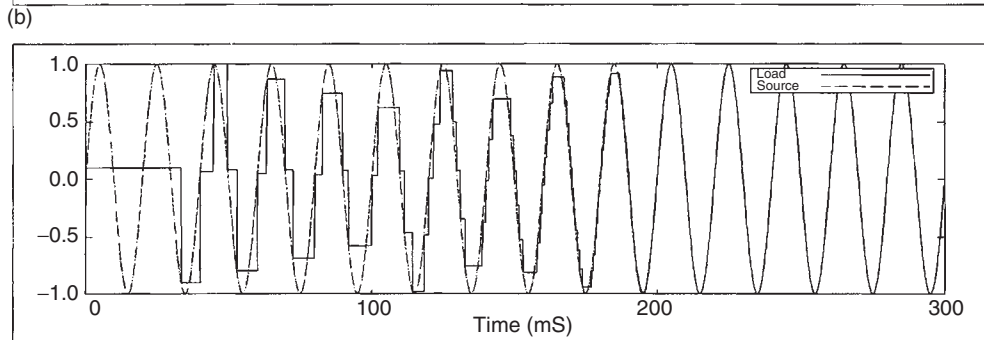
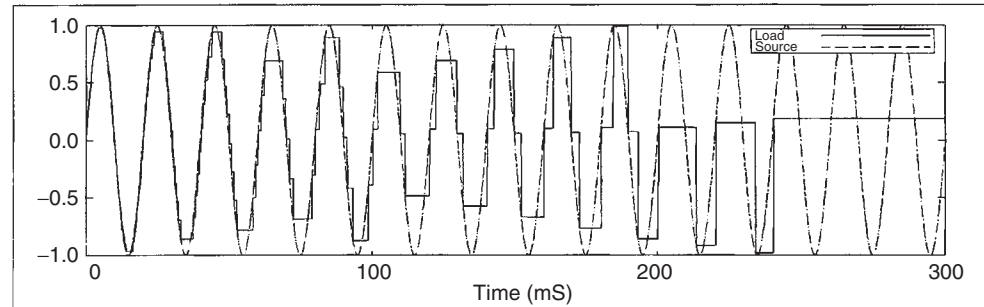
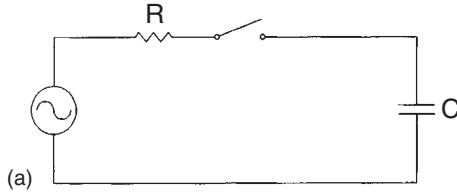


FIGURE 10.1 Variation of load and source side voltages during disconnector switching: (a) scheme of the circuit, (b) opening operation; (c) closing operation.

A large number of pre- or restrikes can occur during a disconnector operation due to the relatively slow speed of the moving contact (Ecklin et al., 1980). Figure 10.1 shows a very simple configuration used to explain the general switching behavior and the pattern of voltages on opening and closing of a disconnector at a capacitive load (Boggs et al., 1982). During an opening operation, sparking occurs as soon as the voltage between the source and the load exceeds the dielectric strength across contacts. After a restrike, a high-frequency current will flow through the spark and equalize the capacitive load voltage to the source voltage. The potential difference across the contacts will fall and the spark will extinguish. The subsequent restrike occurs when the voltage between contacts reaches the new dielectric strength level that is determined by the speed of the moving contact and other disconnector characteristics. The behavior during a closing operation is very similar, and the load side voltage will follow the supply voltage until the contact-make. For a discussion of the physics involved in the restrikes and prestrikes of a disconnect switch operation see (Boggs et al., 1982).

The scheme shown in Fig. 10.2 will be very useful to illustrate the generation of VFT due to a disconnector operation. The breakdown of a disconnector when it is closing originates two surges V_L and V_S which travel outward in the bus duct and back into the source side respectively. The magnitude of both traveling surges is given by

$$V_L = \frac{Z_L}{Z_S + Z_L} (V_1 - V_2) \quad V_S = -V_L \quad (10.1)$$

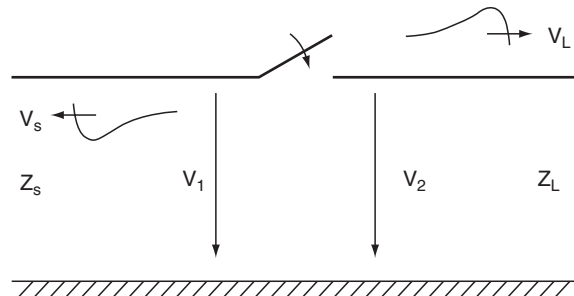


FIGURE 10.2 Generation of very fast transients.

where Z_s and Z_L are the surge impedances on the source and on the load side respectively. V_1 is the intercontact spark voltage, while V_2 is the trapped charge voltage at the load side.

Steep fronted traveling surges can also be generated in case of a line-to-ground fault, as the voltage collapse at the fault location occurs in a similar way as in the disconnector gap during striking.

10.2 Propagation of VFT in GIS

VFT in GIS can be divided into internal and external. Internal transients can produce overvoltages between the inner conductor and the enclosure, while external transients can cause stress on secondary and adjacent equipment. A summary about the propagation and main characteristics of both types of phenomena follows.

10.2.1 Internal Transients

Breakdown phenomena across the contacts of a disconnector during a switch operation or a line-to-ground fault generate very short rise time traveling waves which propagate in either direction from the breakdown location. As a result of the fast rise time of the wave front, the propagation throughout a substation must be analyzed by representing GIS sections as low-loss distributed parameter transmission lines, each section being characterized by a surge impedance and a transit time. Traveling waves are reflected and refracted at every point where they encounter a change in the surge impedance. The generated transients depend on the GIS configuration and on the superposition of the surges reflected and refracted on line discontinuities like breakers, "T" junctions, or bushings. As a consequence of multiple reflections and refractions, traveling voltages can increase above the original values and very high-frequency oscillations occur.

The internal damping of the VFT influencing the highest frequency components is determined by the spark resistance. Skin effects due to the aluminum enclosure can be generally neglected. The main portion of the damping of the VFT occurs by outcoupling at the transition to the overhead line. Due to the traveling wave behavior of the VFT, the overvoltages caused by disconnector switches show a spatial distribution. Normally the highest overvoltage stress is reached at the open end of the load side.

Overvoltages are dependent on the voltage drop at the disconnector just before striking, and on the trapped charge that remains on the load side of the disconnector. For a normal disconnector with a slow speed, the maximum trapped charge reaches 0.5 pu resulting in a most unfavorable voltage collapse of 1.5 pu. For these cases, the resulting overvoltages are in the range of 1.7 pu and reach 2 pu for very specific cases. For a high-speed disconnector, the maximum trapped charge could be 1 pu and the highest overvoltages reach values up to 2.5 pu. Although values larger than 3 pu have been reported, they have been derived by calculation using unrealistic simplified simulation models. The main frequencies depend on the length of the GIS sections affected by the disconnector operation and are in the range of 1 to 50 MHz.

The following examples will be useful to illustrate the influence of some parameters on the frequency and magnitude of VFT in GIS. [Figure 10.3](#) shows two very simple cases, a single bus duct and a “T” junction in which GIS components are modeled as lossless distributed parameter transmission lines. The source side is represented as a step-shaped source in series with a resistance. This is a simplified modeling of an infinite length bus duct. The surge impedance of all bus sections is 50Ω . For the simplest configuration, the reflections of the traveling waves at both terminals of the duct will produce, when the source resistance is neglected, a pulse-shaped transient of constant magnitude—2 pu—and constant frequency at the open terminal. The frequency of this pulse can be calculated from the following expression

$$f = \frac{1}{4\tau} \quad (10.2)$$

where τ is the transit time of the line. If the propagation velocity is close to that of light, the frequency, in MHz, of the voltage generated at the open terminal will be

$$f \approx \frac{75}{d} \quad (10.3)$$

where d is the duct length, in meters. When a more realistic representation of the source is used, $R = 40 \Omega$, the maximum overvoltage at the open terminal will depend on the voltage at the disconnector just before striking, and on the trapped charge which remains on the load side.

Overtvoltages can reach higher values in more complex GIS configurations. The simulations performed for the “T” configuration shown in [Fig. 10.3](#) gave in all cases higher values than in the previous case, where node 4 is the location where the highest overvoltages were originated.

10.2.2 External Transients

Internally generated VFT propagate throughout the GIS and reach bushings where they cause transient enclosure voltages and traveling waves that propagate along the overhead transmission line. An explanation about the generation of external transients and some comments on their main characteristics follow.

10.2.2.1 Transient Enclosure Voltages

Transient enclosure voltages (TEV), also known as transient ground potential rises (TGPR), are short-duration high-voltage transients that appear on the enclosure of the GIS through the coupling of internal transients to enclosure at enclosure discontinuities. The simplified circuit shown in [Fig. 10.4](#) is used to explain the generation of TEV (Meppelink et al., 1989). At the GIS-air interface, three transmission lines can be distinguished: the coaxial GIS transmission line, the transmission line formed by the bushing conductor and the overhead line, and the GIS enclosure-to-ground transmission line. When an internal wave propagates to the gas-to-air bushing, a portion of the transient is coupled onto the overhead transmission line, and a portion is coupled onto the GIS enclosure-to-ground transmission line. The wave that propagates along the enclosure-to-ground transmission line is the TEV. The usual location for these voltages is the transition GIS-overhead line at an air bushing, although they can also emerge at visual inspection ports, insulated spacers for CTs, or insulated flanges at GIS/cables interfaces.

TEV waveforms have at least two components; the first one has a short initial rise time and is followed by high-frequency oscillations, in the range of 5 to 10 MHz, determined by the lengths of various sections of the GIS. The second component is of lower frequency, hundreds of kHz, and is often associated with the discharge of capacitive devices with the earthing system. Both components are damped quickly as a result of the lossy nature of the enclosure-to-ground plane transmission mode. TEV generally persists for a few microseconds. The magnitude varies along the enclosure; it can be in the range of 0.1 to 0.3 pu of the system voltage, and reaches the highest magnitude near the GIS-air interface. Mitigation methods include short length leads, low impedance grounding, and the installation of metal-oxide arresters across insulating spacers.

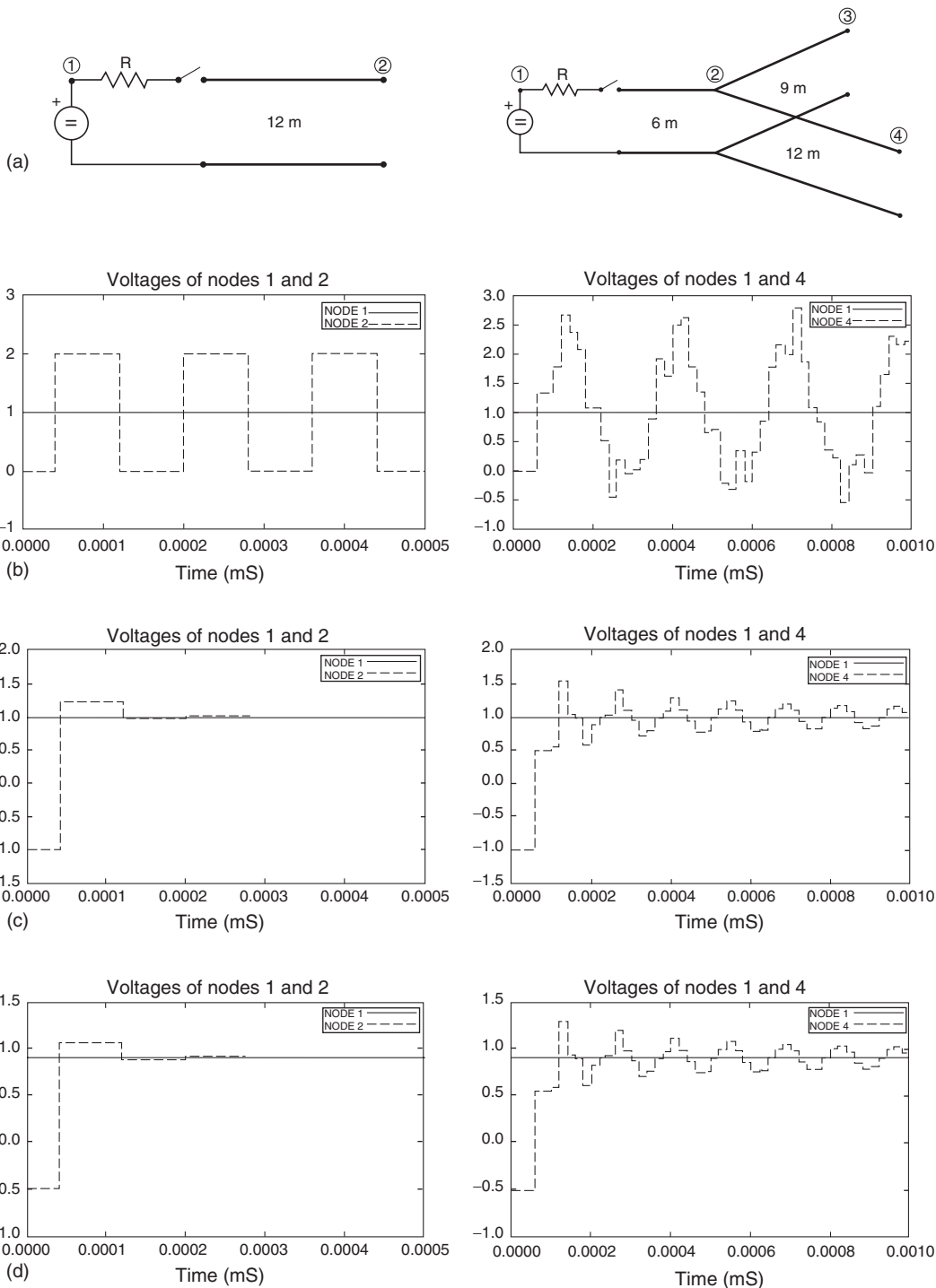


FIGURE 10.3 VFT overvoltages in GIS: (a) scheme of the network, (b) $R = 0$; $V_1 = 1$ pu; $V_2 = 0$, (c) $R = 40 \Omega$; $V_1 = 1$ pu; $V_2 = -1$ pu, (d) $R = 40 \Omega$; $V_1 = 0.9$ pu; $V_2 = -0.5$ pu.

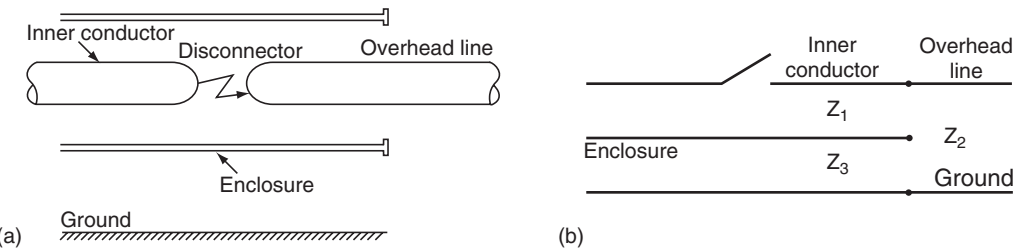


FIGURE 10.4 Generation of TEV: (a) GIS-air transition, (b) single-line diagram.

10.2.2.2 Transients on Overhead Connections

A portion of the VFT traveling wave incident at a gas-air transition is coupled onto the overhead connection and propagates to other components. This propagation is lossy and results in some increase of the waveform rise time. In general, external waveforms have two different characteristics: the overall waveshape that is dictated by lumped circuit parameters, such as the capacitance of voltage transformers or line and earthing inductance, with a rise time in the range of a few hundred nanoseconds; and a fast front portion that is dictated by transmission line effects, with a rise time in the range of 20 ns. A fast rise time of the initial portion is possible as capacitive components, such as bushings, are physically long and distributed and cannot be treated as lumped elements; the magnitude is generally lower than that of internal VFT, it is usually reduced by discontinuities in the transmission path, with a voltage rate-of-rise in the range of 10–30 kV/μs.

10.2.2.3 Transient Electromagnetic Fields

These fields are radiated from the enclosure and can cause some stress on secondary equipment. Their frequency depends on the GIS arrangement, but are typically in the range of 10 to 20 MHz.

10.3 Modeling Guidelines and Simulation

Due to the origin and the traveling nature of VFT, modeling of GIS components makes use of electrical equivalent circuits composed of lumped elements and distributed parameter lines. At very high frequencies, the skin losses can produce an important attenuation; however, these losses are usually neglected, which produces conservative results. Only the dielectric losses in some components (e.g., capacitively graded bushing) need be taken into account. The calculation of internal transients may be performed using distributed parameter models for which only an internal mode (conductor-enclosure) is taken into account, and assuming that the external enclosure is perfectly grounded. If TEV is a concern, then a second mode (enclosure-ground) is to be considered.

The next two sections present modeling guidelines to represent GIS equipment in computation of internal and external transients (Fujimoto et al., 1986; Ogawa et al., 1986; Witzmann, 1987; CIGRE, 1988; Povh, 1996; Fujimoto et al., 1982; Dick et al., 1982). They make use of single-phase models and very simple representations. Depending on the substation layout and the study to be performed, three-phase models for inner conductors (Miri and Binder, 1995) or the outer enclosures (Dick et al., 1982) should be considered. More advanced guidelines have been analyzed and proposed in by Haznadar et al. (1992).

10.3.1 Computation of Internal Transients

A short explanation about the representation of the most important GIS components follows.

10.3.1.1 Bus Ducts

For frequencies lower than 100 MHz, a bus duct can be represented as a lossless transmission line. The surge impedance and the travel time are calculated from the physical dimensions of the duct.

The inductance and the capacitance per unit length of a horizontal single-phase coaxial cylinder configuration, as that shown in Fig. 10.5, are given by the following expressions

$$L'_1 = \frac{\mu_0}{2\pi} \ln \frac{R}{r} \quad (10.4)$$

$$C'_1 = \frac{2\pi\epsilon}{\ln \frac{R}{r}} \quad (\epsilon \approx \epsilon_0) \quad (10.5)$$

from where the following form for the surge impedance is derived

$$Z_1 = \sqrt{\frac{L'_1}{C'_1}} = \frac{\sqrt{\mu_0\epsilon}}{2\pi} \ln \frac{R}{r} \approx 60 \ln \frac{R}{r} \quad (10.6)$$

A different approach should be used for vertically oriented bus sections (Miri and Binder, 1995). As for the propagation velocity, empirical corrections are usually needed to adjust its value. Experimental results show that the propagation velocity in GIS ducts is close to 0.95–0.96 of the speed of light (Fujimoto et al., 1986).

Other equipment, such as elbows, can also be modeled as lossless transmission lines.

10.3.1.2 Surge Arresters

Experimental results have shown that if switching operations in GIS do not produce voltages high enough to cause metal-oxide surge arrester to conduct, then the arrester can be modeled as a capacitance-to-ground. However, when the arrester conducts, the model should take into account the steep front wave effect, since the voltage developed across the arrester for a given discharge current increases as the time to crest of the current increases, but reaches crest prior to the crest of the current. A detailed model must represent each internal shield and block individually, and include the travel times along shield sections, as well as capacitances between these sections, capacitances between blocks and shields, and the blocks themselves.

10.3.1.3 Circuit Breakers

A closed breaker can be represented as a lossless transmission line whose electrical length is equal to the physical length, with the propagation velocity reduced to 0.95–0.96 of the speed of light. The representation of an open circuit breaker is more complicated due to internal irregularities. In addition, circuit breakers with several chambers contain grading capacitors, which are not arranged symmetrically. The electrical length must be increased above the physical length due to the effect of a longer path through the grading capacitors, while the speed of progression must be decreased due to the effects of the higher dielectric constant of these capacitors.

10.3.1.4 Gas-to-Air Bushings

A bushing gradually changes the surge impedance from that of the GIS to that of the line. A simplified model may consist of several transmission lines in series with a lumped resistor representing losses; the surge impedance of each line section increases as the location goes up the bushing. If the bushing is distant from the point of interest, the resistor can be neglected and a single line section can be used. A detailed model must consider the coupling between the conductor and shielding electrodes, and include the representation of the grounding system connected to the bushing (Fujimoto and Boggs, 1988; Ardito et al., 1992).

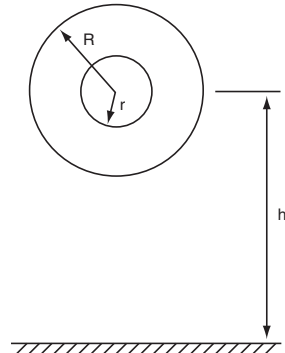


FIGURE 10.5 Coaxial bus duct cross section.

10.3.1.5 Power Transformers

At very high frequencies, a winding of a transformer behaves like a capacitive network consisting of series capacitances between turns and coils, and shunt capacitances between turns and coils to the grounded core and transformer tank; the saturation of the magnetic core can be neglected, as well as leakage impedances. When voltage transfer has to be calculated, interwinding capacitances and secondary capacitance-to-ground must also be represented. If voltage transfer is not a concern, an accurate representation can be obtained by developing a circuit that matches the frequency response of the transformer at its terminals. Details on the computation of equivalent capacitances have been covered by Chowdhuri (1996).

10.3.1.6 Spark Dynamics

The behavior of the spark in disconnector operations can be represented by a dynamically variable resistance with a controllable collapse time. In general, this representation does not affect the magnitude of the maximum VFT overvoltages, but it can introduce a significant damping on internal transients (Yanabu et al., 1990).

10.3.2 Computation of TEV

At very high frequencies, currents are constrained to flow along the surface of the conductors and do not penetrate through them. The inside and the outside of a GIS enclosure are distinct, so that transients generated within the substation do not appear on the outside surface of the enclosure until discontinuities in the sheath are encountered. These discontinuities occur at gas-to-air terminations, GIS-cable transitions, or external core current transformers. The modeling of the GIS for computation of TEV must include the effects of the enclosure, the representation of ground straps, and the earthing grid.

10.3.2.1 Enclosures

A GIS-air termination can be modeled as a junction of three transmission lines, each with its own surge impedance (Fig. 10.4). This equivalent network can be analyzed using lossless transmission line models to determine reflected and transmitted waves. The surge impedance of the enclosure-to-ground transmission line (Fig. 10.4) is derived from the following forms

$$L'_3 \approx \frac{\mu_0}{2\pi} \ln \frac{2h}{R} \quad (10.7)$$

$$C'_3 \approx \frac{2\pi\epsilon_0}{\ln \frac{2h}{R}} \quad (10.8)$$

$$Z_3 = \sqrt{\frac{L'_3}{C'_3}} = \frac{\sqrt{\mu_0\epsilon_0}}{2\pi} \ln \frac{2h}{R} \approx 60 \ln \frac{2h}{R} \quad (10.9)$$

The basic mechanism of TEV is defined by the refraction of waves from the internal coaxial bus duct to the enclosure sheath-to-ground system. Figure 10.6 shows the scattering coefficients involved in an air-SF6 transition, and the equivalent circuit to be used for calculating these coefficients. The coefficients S_{ji} represent the refraction of waves from line “i” into line “j”.

The coefficient S_{11} , which is also the reflection coefficient at the transition, is given by

$$S_{11} = \frac{(Z_2 + Z_3) - Z_1}{Z_1 + Z_2 + Z_3} \quad (10.10)$$

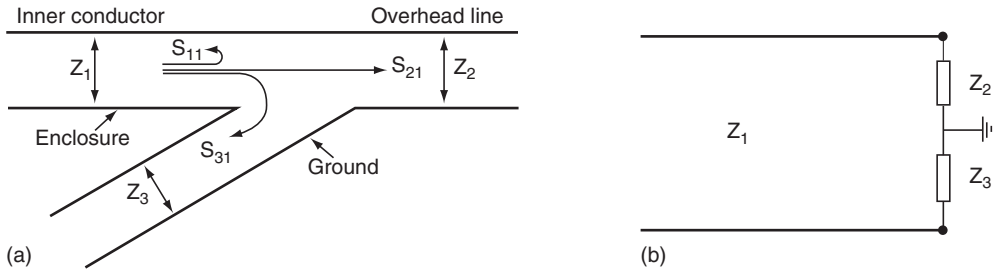


FIGURE 10.6 GIS-air transition. Scattering coefficients: (a) schematic diagram; (b) equivalent circuit.

The refraction coefficient at the transition is then

$$r_t = 1 + S_{11} = \frac{2(Z_2 + Z_3)}{Z_1 + Z_2 + Z_3} \quad (10.11)$$

The magnitude of the transmitted wave onto the outside of the enclosure sheath is given by following scattering coefficient

$$S_{31} = r_t \frac{-Z_3}{Z_2 + Z_3} = -\frac{2Z_3}{Z_1 + Z_2 + Z_3} \quad (10.12)$$

The negative sign means that there is an inversion of the waveform with respect to the internal transient.

10.3.2.2 Ground Straps

TEV propagates back from the gas-to-air termination into the substation on the transmission line defined by the enclosure and the ground plane. The first discontinuity in the propagation is generally a ground strap. For TEV rise times, most ground straps are too long and too inductive for effective grounding. Ground leads may have a significant effect on the magnitude and waveshape of TEV. This effect can be explained by considering two mechanisms (Fujimoto et al., 1982). First, the ground lead may be seen as a vertical transmission line whose surge impedance varies with height; when the transient reaches the ground strap, a reflected wave is originated that reduces the magnitude of the transmitted wave, with the reduction expressed by the coefficient

$$\frac{2Z_g}{2Z_g + Z_3} \quad (10.13)$$

where Z_g is the surge impedance of the ground strap. As Z_g is usually much larger than Z_3 , the attenuation produced by the ground strap will usually be small. Second, when the portion of the wave that propagates down the ground strap meets the low impedance of the ground grid, a reflected wave is produced that propagates back to the enclosure where it will tend to reduce the original wave.

The representation of a ground lead as a constant surge impedance is not strictly correct. It has a continuously varying surge impedance, so that a continuous reflection occurs as a wave propagates down the lead. The ground strap can be divided into sections, each one represented by a surge impedance calculated from the following expression

$$Z_s = 60 \ln \frac{2\sqrt{2} h}{r} \quad (10.14)$$

where r is the lead radius and h is the average height of the section (Fujimoto et al., 1982). However, a constant inductor model may be adequate for straps with travel time less than the surge rise time, while a nonuniform impedance model may be necessary for very long straps.

10.3.2.3 Earthing Grid

The representation of the earthing grid at TEV frequencies is a very complex task. Furthermore, this grid may not be designed to carry very high frequency currents, as no standards for very high frequency earthing systems are currently available. A simplified modeling may be used by representing the earthing grid as a low value constant resistance.

Advanced models for GIS components in computation of TEV might consider a frequency-dependent impedance for ground straps, a frequency-dependent model for the enclosure-to-ground line (which could take into account earth losses), and the propagation of phase-to-phase modes on the three enclosures (Fujimoto et al., 1982).

10.3.3 Statistical Calculation

The largest VFT stresses under normal operating conditions originate from disconnector operations. The level reached by overvoltages is random by nature. The maximum overvoltage produced by a disconnector breakdown depends on the geometry of the GIS, the measuring point, the voltage prior to the transient at the load side (trapped charge), and the intercontact voltage at the time of the breakdown, as shown in the section on Internal Transients.

Several works have been performed to determine the statistical distribution of VFT overvoltages in a GIS (Boggs et al., 1982; Yanabu et al., 1990; Boggs et al., 1984; Fujimoto et al., 1988). A very simple expression can be used to calculate the transient overvoltages as a function of time t and position s (Boggs et al., 1984; Fujimoto et al., 1988)

$$V(t,s) = V_b * K(t,s) + V_q \quad (10.15)$$

where $K(t,s)$ is the normalized response of the GIS, V_b is the intercontact spark voltage, and V_q the voltage prior to the transient at the point of interest. As V_b and V_q are random variables, $V(t,s)$ is also random. This equation can be used to estimate worst-case values (Fujimoto et al., 1988).

The performance of a disconnector during an opening operation can be characterized by the pattern of arcing on a capacitive load (Fig. 10.1). A difference in breakdown voltages for the two polarities indicates a dielectric asymmetry. When the asymmetry is large compared to the statistical variance in breakdown voltage, a systematic pattern is originated near the end of the arcing sequence (Boggs et al., 1984). The final trapped charge voltage has a distribution which is very dependent on the asymmetry in the intercontact breakdown voltage.

The dielectric asymmetry of a disconnector is usually a function of contact separation. A disconnector may show a different performance at different operating voltages. A consequence of this performance is that very different stresses will be originated as a result of different operational characteristics.

From the results presented in the literature, the following conclusions may be derived (Boggs et al., 1982; Yanabu et al., 1990; Boggs et al., 1984; Fujimoto et al., 1988):

- The value of the trapped charge is mainly dependent on the disconnect switch characteristics: the faster the switch, the greater the mean value that the trapped charge voltage can reach.
- For slow switches, the probability of a re-/prestrike with the greatest breakdown voltage, in the range 1.8–2 pu, is very small; however, due to the great number of re/prestrikes that are produced with one operation, this probability should not always be neglected.
- The asymmetry of the intercontact breakdown voltage can also affect the trapped charge distribution; in general, both the magnitude and the range of values are reduced if there is a difference in the breakdown voltage of the gap for positive and negative values.

10.3.4 Validation

The results presented in Figs. 10.7 and 10.8 illustrate the accuracy which can be obtained by means of a digital simulation. Figure 10.7 shows a good match between a direct measurement in an actual GIS and a computer result. The simulation was performed including the effects of spacers, flanges, elbows, and other

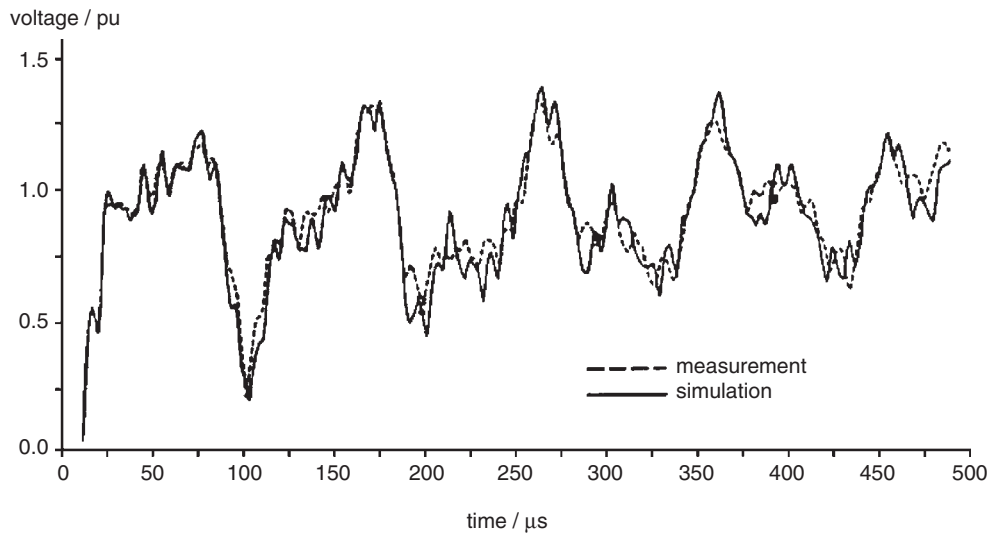


FIGURE 10.7 Comparison of simulation and measurement of disconnect switch induced overvoltages in a 420 kV GIS. (Copyright 1999 IEEE.)

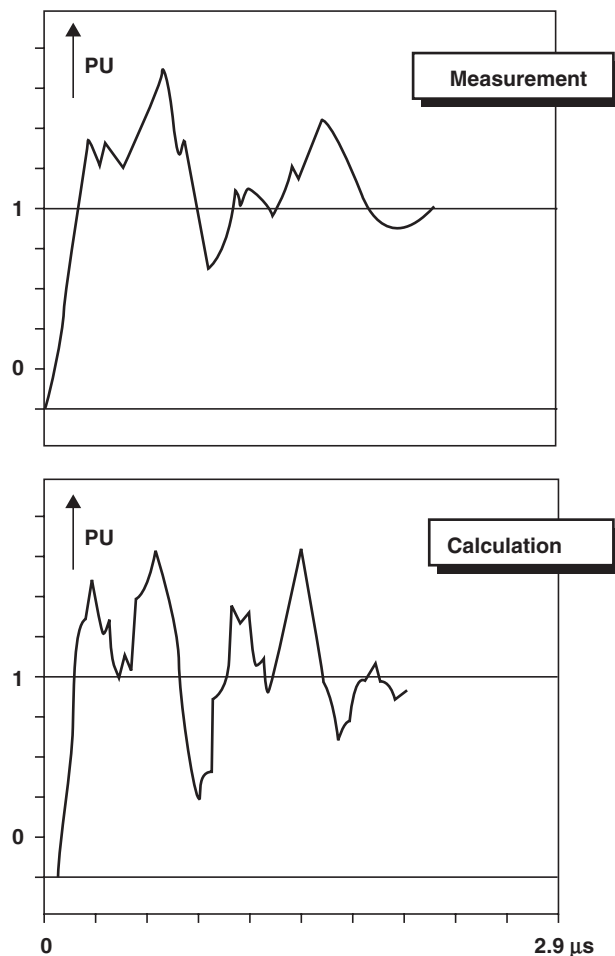


FIGURE 10.8 Measurement and simulation of overvoltages in a 420 kV GIS at closing a switch. (Copyright 1999 IEEE.)

hardware, but neglecting propagation losses (Witzmann, 1987). [Figure 10.8](#) shows that important differences could occur when comparing a measurement and a digital simulation result, although a detailed representation of the GIS was considered. The differences were due to use of low damping equivalent circuits and to limitation of measuring instruments that did not capture very high frequencies (IEEE, 1996).

10.4 Effects of VFT on Equipment

The level reached by VFT overvoltages originated by disconnector switching or line-to-ground faults inside a GIS are below the BIL of substation and external equipment (Boersma, 1987). However, aging of the insulation of external equipment due to frequent VFT must be considered. TEV is a low energy phenomenon and it is not considered dangerous to humans; the main concern is in the danger of the surprise-shock effect. External transients can cause interference with or even damage to the substation control, protection, and other secondary equipment (Meppelink et al., 1989; Boersma, 1987). The main effects caused by VFT to equipment and the techniques that can be used to mitigate these effects are summarized below (CIGRE, 1988).

10.4.1 SF₆ Insulation

Breakdown caused by VFT overvoltages is improbable in a well-designed GIS insulation system during normal operations. The breakdown probability increases with the frequency of the oscillations. In addition, breakdown values can be reduced by insulation irregularities like edges and fissures. However, at ultra high voltage systems, more than 1000 kV, for which the ratio of BIL to the system voltage is lower, breakdown is more likely to be caused. At these levels, VFT overvoltages can be reduced by using resistor-fitted disconnectors (Yamagata et al., 1996).

10.4.2 Transformers

Due to steep fronted wave impulses, direct connected transformers can experience an extremely non-linear voltage distribution along the high-voltage winding, connected to the oil-SF₆ bushings, and high resonance voltages due to transient oscillations generated within the GIS. Transformers can generally withstand these stresses; however, in critical cases, it may be necessary to install varistors to protect tap changers.

10.4.3 Disconnectors and Breakers

The insulation system of breakers and switches is not endangered by VFT overvoltages generated in adjacent GIS equipment. Ground faults induced by VFT overvoltages have been observed in disconnectors operations, as residual leader branches can be activated by enhanced field gradient to ground. These faults can be avoided by a proper disconnector design.

10.4.4 Enclosure

TEV can cause sparking across insulated flanges and to insulated busbars of CTs, and can puncture insulation that is intended to limit the spread of circulating currents within the enclosure. TEV can be minimized with a proper design and arrangement of substation masts, keeping ground leads as short and straight as possible in order to minimize the inductance, increasing the number of connections to ground, introducing shielding to prevent internally generated VFT from reaching the outside of the enclosure, and installing voltage limiting varistors where spacers must be employed.

10.4.5 Bushings

Very few problems have been reported with capacitively graded bushings. High impedances in the connection of the last graded layer to the enclosure should be avoided.

10.4.6 Secondary Equipment

TEV may interfere with secondary equipment or damage sensitive circuits by raising the housing potential if they are directly connected, or via cable shields to GIS enclosure by emitting free radiation which may induce currents and voltages in adjacent equipment. Correct cable connection procedures may minimize interference. The coupling of radiated energy may be reduced by mounting control cables closely along the enclosure supports and other grounded structures, grounding cable shields at both ends by leads as short as possible, or using optical coupling services. Voltage limiting devices may have to be installed.

References

- Ardito, A., Iorio, R., Santagostino, G., and Porrino, A., Accurate modeling of capacitively graded bushings for calculation of fast transient overvoltages in GIS, *IEEE Trans. on Power Delivery*, 7, 1316, 1992.
- Boersma, R., Transient ground potential rises in gas-insulated substations with respect to earthing systems, *Electra*, 110, 47, 1987.
- Boggs, S.A., Chu, F.Y., Fujimoto, N., Krenicky, A., Plessl, A., and Schlicht, D., Disconnect switch induced transients and trapped charge in gas-insulated substations, *IEEE Trans. on Power Appar. and Syst.*, 101, 3593, 1982.
- Boggs, S.A., Fujimoto, N., Colloid, M., and Thuries, E., The modeling of statistical operating parameters and the computation of operation-induced surge waveforms for GIS disconnectors, *CIGRE*, Paper No. 13-15, Paris, 1984.
- Chowdhuri, P., *Electromagnetic Transients in Power Systems*, RSP-John Wiley, 1996, Chap. 12.
- CIGRE Working Group 33/13-09, Very fast transient phenomena associated with gas insulated substations, *CIGRE*, Paper 33-13, Paris, 1988.
- CIGRE Joint WG 33/23-12, Insulation co-ordination of GIS: Return of experience, on site tests and diagnostic techniques, *Electra*, 176, 66, 1998.
- CIGRE Working Group 33.02, *Guidelines for representation of networks elements when calculating transients*, CIGRE Brochure, 1990.
- Dick, E.P., Fujimoto, N., Ford, G.L., and Harvey, S., Transient ground potential rise in gas-insulated substations—problem identification and mitigation, *IEEE Trans. on Power Appar. and Syst.*, 101, 3610, 1982.
- Ecklin, A., Schlicht, D., and Plessl, A., Overvoltages in GIS caused by the operation of isolators, in *Surges in High-Voltage Networks*, Ragaller, K., Ed., Plenum Press, New York, 1980, chap. 6.
- Fujimoto, N., and Boggs, S.A., Characteristics of GIS disconnector-induced short risetime transients incident on externally connected power system components, *IEEE Trans. on Power Delivery*, 3, 961, 1988.
- Fujimoto, N., Chu, F.Y., Harvey, S.M., Ford, G.L., Boggs, S.A., Tahiliani, V.H., and Colloid, M., Developments in improved reliability for gas-insulated substations, *CIGRE*, Paper No. 23-11, Paris, 1988.
- Fujimoto, N., Dick, E.P., Boggs, S.A., and Ford, G.L., Transient ground potential rise in gas-insulated substations—experimental studies, *IEEE Trans. on Power Appar. and Syst.*, 101, 3603, 1982.
- Fujimoto, N., Stuckless, H.A., and Boggs, S.A., Calculation of disconnector induced overvoltages in gas-insulated substations, in *Gaseous Dielectrics IV*, Pergamon Press, 1986, 473.
- Haznadar, Z., Carsimamovic, S., and Mahmutcehajic, R., More accurate modeling of gas insulated substation components in digital simulations of very fast electromagnetic transients, *IEEE Trans. on Power Delivery*, 7, 434, 1992.
- IEC 71-1, *Insulation Co-ordination—Part 1: Definitions, Principles and Rules*, 1993.
- IEC 71-2, *Insulation Co-ordination—Part 2: Application Guide*, 1996.
- IEEE TF on Very Fast Transients (Povh, D., Chairman), Modelling and analysis guidelines for very fast transients, *IEEE Trans. on Power Delivery*, 11, 2028, 1996.

- Meppelink, J., Diederich, K., Feser, K., and Pfaff, W., Very fast transients in GIS, *IEEE Trans. on Power Delivery*, 4, 223, 1989.
- Miri, A.M. and Binder, C., Investigation of transient phenomena in inner- and outer systems of GIS due to disconnector operation, in *Proc. Int. Conf. Power Systems Transients*, Lisbon, 1995, 71.
- Ogawa, S., Haginomori, E., Nishiwaki, S., Yoshida, T., and Terasaka, K., Estimation of restriking transient overvoltage on disconnecting switch for GIS, *IEEE Trans. on Power Delivery* 1, 95, 1986.
- Witzmann, R., Fast transients in gas insulated substations. Modelling of different GIS components, in *Proc. 5th Int. Symp. HV Engineering*, Braunschweig, 1987.
- Yamagata, Y., Tanaka, K., Nishiwaki, S., Takahashi, N., Kokumai, T., Miwa, I., Komukai, T., and Imai, K., Suppression of VFT in 1100 kV GIS by adopting resistor-fitted disconnector, *IEEE Trans. on Power Delivery* 11, 872, 1996.
- Yanabu, S., Murase, H., Aoyagi, H., Okubo, H., and Kawaguchi, Y., Estimation of fast transient overvoltage in gas-insulated substation, *IEEE Trans. on Power Delivery*, 5, 1875, 1990.

11

Transient-Voltage Response of Coils and Windings

11.1	Transient-Voltage Concerns.....	11-1
	Normal System Operation • Sources and Types of Transient-Voltage Excitation • Addressing Transient-Voltage Performance • Complex Issue to Predict	
11.2	Surges in Windings	11-3
	Response of a Simple Coil • Initial Voltage Distribution • Steady-State Voltage Distribution • Transient-Voltage Distribution	
11.3	Determining Transient Response	11-6
	History • Lumped-Parameter Model • Frequency-Domain Solution • Solution in the Time Domain • Accuracy vs. Complexity	
11.4	Resonant Frequency Characteristic.....	11-9
	Definitions • Impedance vs. Frequency • Amplification Factor	
11.5	Inductance Model.....	11-12
	Definition of Inductance • Transformer Inductance Model • Inductance Model Validity	
11.6	Capacitance Model.....	11-14
	Definition of Capacitance • Series and Shunt Capacitance • Equivalent Capacitance for Disk Windings • Initial Voltage Distribution	
11.7	Loss Model	11-16
	Copper Losses • Core Losses • Dielectric Losses	
11.8	Winding Construction Strategies.....	11-19
	Design • Core-Form • Shell-Form • Proof of Design Concept • Standard Winding Tests • Design Margin • Insulation Coordination • Additional System Considerations	
11.9	Models for System Studies	11-24
	Model Requirements • Reduced Order Model	

Robert C. Degeneff
Rensselaer Polytechnic Institute

11.1 Transient-Voltage Concerns

11.1.1 Normal System Operation

Transformers are normally used in systems to change power from one voltage (or current) to another. This is often driven by a desire to optimize the overall system characteristics, e.g., economics, reliability, and/or performance. To achieve these system goals, a purchaser must specify and a designer must

configure the transformer to meet a desired impedance, voltage and power rating, thermal characteristic, short-circuit strength, sound level, physical size, and voltage withstand capability. Obviously, many of these goals will produce requirements that are in conflict and prudent compromise is required. Failure to achieve an acceptable characteristic for any of these makes the overall transformer design unacceptable. Transformer characteristics and the concomitant design process are outlined in Blume et al. (1951), Bean et al. (1959), MIT (1943), and Franklin (1983).

Normally a transformer operates under steady voltage excitation. Occasionally a transformer (in fact, all electrical equipment) experiences dynamic and/or transient overvoltages. Often, these infrequent transient voltages that establish design constraints for the transformer's insulation system have far-reaching effects on the overall equipment design. The transformer must be configured to withstand any abnormal voltages covered in the design specification and realistically expected in service. Often, these constraints have great impact on other design issues and, as such, have significant effect on the overall transformer cost, performance, and configuration. In recent years, engineers have explored the adverse effect of transient voltages on the reliability of transformers (Working group 05, 1983; Kogan et al., 1988, 1990), and found it to be a major cause of transformer failure.

11.1.2 Sources and Types of Transient-Voltage Excitation

The voltages applied to a transformer's terminals can be broadly classed as steady state and "transient." Normally, the "transient" voltages a transformer experiences are commonly referred to as dynamic, transient, and very fast transients.

The majority of voltages a transformer experiences during its operational life are steady state, e.g., the voltage is within $\pm 10\%$ of nominal and the frequency is within 1% of rated. As power quality issues grow, the effect of harmonic voltages and currents on performance becomes more of an issue. These harmonics are effectively reduced magnitude, steady-state voltages, and currents at harmonic frequencies (say 2nd to the 50th). These are addressed in great detail in reference IEEE Std. 519 (1999). Strictly speaking, all other voltage excitation are transients, e.g., dynamic, transient, and very fast transient voltages.

Dynamic voltages refer to relatively low frequency (60 to 1500 Hz), damped oscillatory voltage. Magnitudes routinely observed are from 1 to 3 times the systems peak nominal voltage. Transient voltage refers to the class of excitation caused by events like lightning surges, switching events, and line faults causing voltages of the chopped waveform (Degenef et al., 1982). Normally, these are aperiodic waves. Occasionally, the current chopping of a vacuum breakers will produce transient periodic excitation in the 10 to 200 kHz range (Greenwood, 1994). The term very fast transient encompasses voltage excitation with rise times in the range of 50–100 ns and frequencies from 0.5 to 30 MHz. These types of voltages are encountered in gas-insulated stations. The voltages produced within the transformer-winding structure by the system is a part of, must be addressed and understood if a successful insulation design is to be achieved (Narang et al., 1998). Since transient voltages affect system reliability, and that, in turn, system safety and economics, a full understanding of the transient characteristic of a transformer is warranted.

11.1.3 Addressing Transient-Voltage Performance

Addressing the issue of transient-voltage performance can be divided into three activities: recognition, prediction, and mitigation. By 1950 over 1000 papers had been written to address these issues (Abetti, 1959a,b, 1962, 1964). The first is to appreciate that transient-voltage excitation can produce equipment responses different than one would anticipate at first glance. For example, the addition of more insulation around a conductor may in fact make the transient-voltage distribution worse and the insulation integrity of the design weaker. Another example would be the internal voltage amplification a transformer experiences when excited near one of its resonant frequencies. The transient-voltage distribution is a function of the applied voltage excitation and the transformer's physical shape and material content. The capability of the winding to withstand the transient voltage is a function of the specific winding shape, the

materials voltage vs. time characteristic, the past history of the structure, and the statistical nature of the structure's voltage withstand characteristic.

The second activity is to assess or predict the transient voltage within the coil or winding. Today this is generally accomplished using a lumped-parameter model of the winding structure and some form of computer solution method that allows the internal transient response of the winding to be computed. Once this voltage distribution is known, its effect on the insulation structure can be computed with a two- or three-dimensional finite element method (FEM). The resultant voltages, stresses, and creeps are examined in light of the known material and geometrical capability of the system in light of desired performance margins.

The third activity is to establish a transformer structure or configuration that, in light of the anticipated transient-voltage excitation and material capability, variability, and statistics nature, will provide acceptable performance margins. Occasionally, nonlinear resistors are used as part of the insulation system to achieve a cost-effective, reliable insulation structure. Additionally, means of limiting the transient excitation include modifying the system configuration and/or the use of nonlinear resistors, capacitors, or snubbers.

11.1.4 Complex Issue to Predict

The accurate prediction of the transient-voltage response of coils and winding has been of interest for almost 100 years. The problem is complex for several reasons. The form of excitation varies greatly. Most large power transformers are unique designs, and as such, each transformer's transient response characteristic is unique. Each has its own impedance vs. frequency characteristic. As such, the transient response characteristic of each transformer is different. Generally, the problem is addressed by building a large lumped-parameter model of inductances, capacitances, and resistances. Constructing the lumped-parameter model is challenging. The resultant mathematical model is ill-conditioned, e.g., the resultant set of differential equations is difficult to solve. The following sections outline how these challenges are currently addressed.

It should be emphasized that the voltage distribution within the winding is only the first component of the insulation design process. The spatial distribution of the voltages within the winding must be determined and finally the ability of the winding configuration to withstand this voltage in view of its voltage vs. time characteristic must be assessed.

11.2 Surges in Windings

11.2.1 Response of a Simple Coil

Transformer windings are complex structures of conductors and insulation. This is the result of many contradictory requirements levied during the design process. In an effort to introduce the basic concepts of transient response, a very simple disk coil was modeled and the internal transient response computed. The coil consisted of 100 identical continuous disk sections of 24 turns each. The inside radius of the coil is 12.55 in., the space between each disk coil is 0.220 in., and the coil was assumed to be in air with no iron core. Each turn was made of copper 0.305 in. in height, 0.1892 in. in the radial direction, with 0.0204 in. of insulation between the turns. For this example, the coil was subjected to a full wave with a 1.0 per unit voltage. [Figure 11.1](#) provides a sketch of the coil and the node numbers associated with the calculation. For this example, the coil has been subdivided into 50 equal subdivisions with each subdivision a section pair. [Figure 11.2](#) contains the response of the winding as a function of time for the first 200 μ s. It should be clear that the response is complex and a function of both the applied excitation voltage and the characteristics of the coil itself.

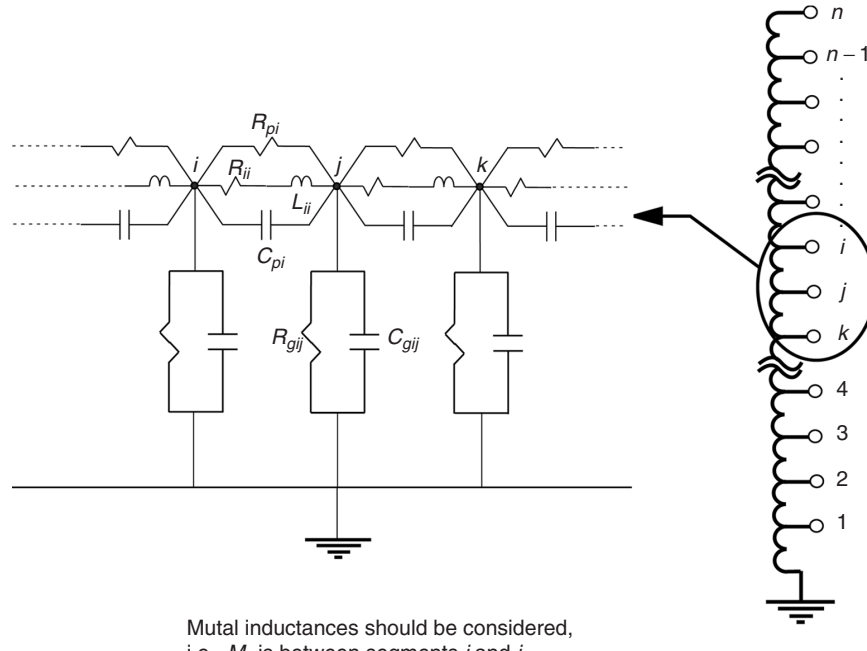


FIGURE 11.1 Sample of section used to model example coil.

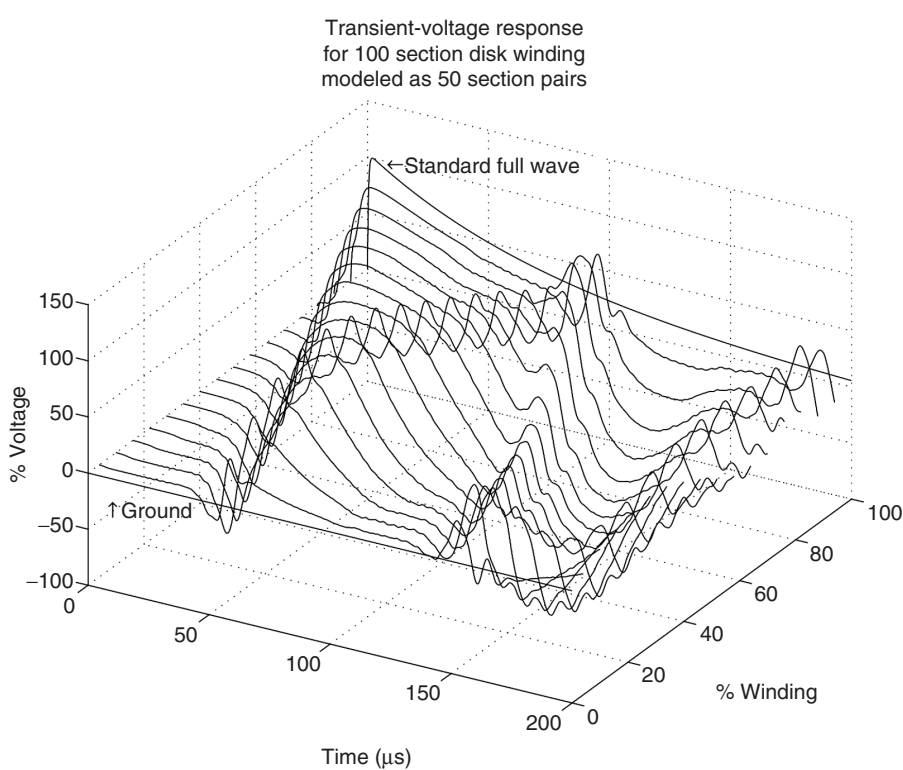


FIGURE 11.2 Voltage vs. time for helical winding.

11.2.2 Initial Voltage Distribution

If the voltage distribution within the helical winding shown in Fig. 11.2 is examined at a time very close to zero, it is observed that the voltage distribution is highly nonuniform. For the first few tenths of a microsecond, the distribution is dominated by the capacitive structure of the coil. This distribution is often referred to as the initial (or short-time) distribution. This initial distribution is shown in Fig. 11.3. For example, examining the voltage gradient over the first 10% of the winding, one sees that the voltage is 82% rather than the anticipated 10% or a rather large enhancement or gradient in the initial portions of the winding.

The initial distribution shown in Fig. 11.3 is based on the assumption that the coil knows how it is connected, i.e., it requires some current to flow in the winding and this requires some few tenths of a microsecond. The initial distribution can be determined by evaluating the voltage distribution for the winding's capacitive network and ignoring both the inductive and resistive components of the transformer. This discussion is applicable for times greater than approximately 0.25 μs . This is the start of the transient response for the winding.

For times smaller than 0.25 μs , the distribution is still dictated by capacitance, but the transformer's capacitive network is unaware that it is connected. This is addressed in the chapter on very fast transients and in Narang et al. (1998).

11.2.3 Steady-State Voltage Distribution

The steady-state voltage distribution depends primarily on the inductance and resistance structure of the winding. This distribution, referred to by Abetti (1960) as the pseudofinal, is dominated primarily by the self- and mutual-inductance of the windings and the manner in which the winding is connected. This steady-state voltage distribution is very near (but not identical) to the turns ratio. For the simple winding shown in Fig. 11.1, the distribution is known by inspection and shown in Fig. 11.3, but for more complex windings it can be determined by finding the voltage distribution of the inductive network and ignoring the effect of winding capacitances.

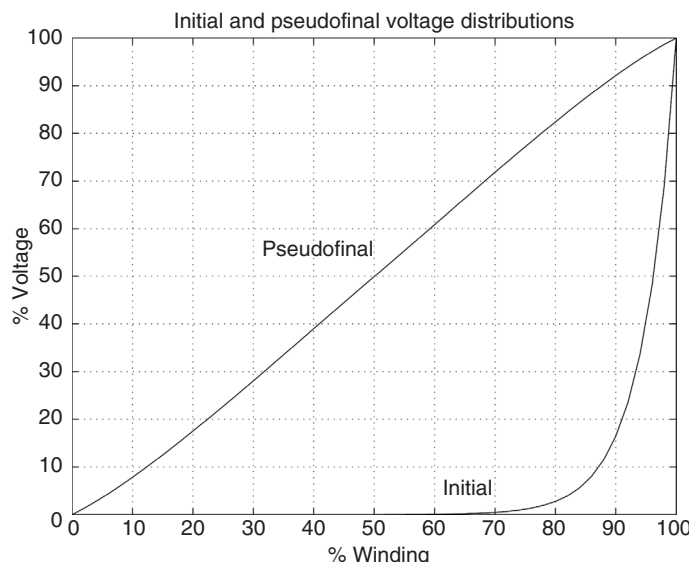


FIGURE 11.3 Initial and pseudofinal voltage distribution.

11.2.4 Transient-Voltage Distribution

Figure 11.2 shows the transient response for this simple coil when a 1.0 pu full wave has been applied. The transient response of the coil is the voltage the coil experiences as the coil transitions between the initial voltage distribution and the steady-state distribution. It is the very same idea as pulling a rubber band away from its stretched (but steady-state position) and then letting it go and monitoring its movement in space and time. What is of considerable importance is the magnitude and duration of these transient voltages and the ability of the transformer's insulation structure to consistently survive these voltages.

The coil shown in Fig. 11.1 is a very simple structure. The challenge facing transformer design engineers since the early 1900s has been to determine what this voltage distribution was for a complex winding structure of a commercial transformer design.

11.3 Determining Transient Response

11.3.1 History

Considerable research has been devoted to determining the transformer's internal transient-voltage distribution. These attempts started at the beginning of the 1900s and have continued at a steady pace for almost 100 years (Abetti, 1959a,b, 1962, 1964). The earliest attempts at using a lumped-parameter network to model the transient response were in 1915. Until the early 1960s, these efforts were of limited practical value due to computational limitations encountered when solving large numbers of coupled stiff differential equations. During this period, the problem was attacked in the time domain using either a standing-wave approach or the traveling wave method. The problem was also explored in the frequency domain and the individual frequency results combined to form the needed response in the time domain. Abetti introduced the idea of a physical scale model, or analog for each new design. Then, in the 1960s, with the introduction of the high-speed digital computer, major improvements in computational algorithms, detail, accuracy, and speed were obtained.

In 1956, Rouxel and Waldvogel used an analog computer to calculate the internal voltages in the transformer by solving a system of linear differential equations with constant coefficients resulting from a uniform, lossless, and linear lumped-parameter model of the winding where mutual- and self-inductances were calculated assuming an air core (Waldvogel and Rouxel, 1956). Later, McWhirter et al. (1956) developed a method of determining impulse voltage stresses within the transformer windings through the use of the digital and analog computers applicable to some extent for nonuniform windings. But it was not until 1958 that Dent et al. (1958) recognized the limitations of the analog models and developed a digital computer model in which any degree of nonuniformity in the windings could be introduced and any form of input voltage applied. During the mid-1970s, efforts at General Electric (White, 1977; Degenneff et al., 1980) focused on building a program to compute transients for core-form winding of completely general design. By the end of the 1970s, an adequate linear lossless model of the transformer was available to the industry. However, adequate representation of the effect of the nonlinear core and losses was not available. Additionally, the transformer models used in insulation design studies had little relationship with lumped-parameter transformer models used for system studies.

Wilcox improved the transformer model by including core losses in a linear-frequency-domain model where self- and mutual-impedances between winding sections were calculated considering a grain-oriented conductive core with permeability μ_r (Wilcox et al., 1988, 1992). In this work, Wilcox modeled the skin effect, the losses associated with the magnetizing impedance, and a loss mechanism associated with the effect of the radial component of flux on the transformer core during short-circuit conditions. Wilcox applied this modified modal theory to model the internal voltage response on practical transformers. Vakilian et al. (1995a,b) modified White's inductance model (1977) to include the core's saturable characteristics and established a system of ordinary differential equations (ODEs) for the

linearized lumped-parameter LRC network, then used Gear's method to solve for the internal voltage response in time domain. During the same period, Gutierrez and Degeneff (1993, 1994) presented a transformer model reduction technique as an effort to reduce the computational time required by linear and nonlinear detailed transformer models and to make these models small enough to fit into EMTP. In 1994, de Leon and Semlyen presented a nonlinear three-phase transformer model including core and winding losses. This was the first attempt to combine frequency dependency and nonlinearity in a detailed transformer model. The authors used the principle of duality to extend their model to three-phase transformers.

11.3.2 Lumped-Parameter Model

A device's transient response is a result of the flow of energy between the distributed electrostatic and electromagnetic structures of the device. For all practical transformer-winding structures, this interaction is quite complex and can only be realistically investigated by constructing a detailed model of the winding structure and then carrying out a numerical solution for the transient-voltage response. The most common approach is to subdivide the winding into a number of segments (or groups of turns) and build a lumped-parameter model. The method of subdividing the winding can be complex and, if not addressed carefully, affects the accuracy of the resultant model. The resultant lumped-parameter model is composed of inductances, capacitance, and losses. Starting with these inductances, capacitances, and resistive elements, equations reflecting the transformer's transient response can be written in numerous forms. Two of the most common are the basic admittance formulation of the differential equation and the state-variable formulation. The admittance formulation is given by Degeneff (1977):

$$[I(s)] = \left[\frac{1}{s} [\Gamma_n] + [G] + s[C] \right] [E(s)] \quad (11.1)$$

The general state-variable formulation is given by Vakilian (1993) describing the transformer's lumped-parameter network at time t :

$$\begin{bmatrix} [L] & 0 & 0 \\ 0 & [C] & 0 \\ 0 & 0 & [U] \end{bmatrix} \begin{bmatrix} [di_e/dt] \\ [de_n/dt] \\ [df_e/dt] \end{bmatrix} = \begin{bmatrix} -[r] & [T]^t \\ -[T] & -[G] \\ -[r] & [T]^t \end{bmatrix} \begin{bmatrix} [i_e] \\ [e_n] \end{bmatrix} - \begin{bmatrix} 0 \\ [I_s] \\ 0 \end{bmatrix} \quad (11.2)$$

where the variables in Eqs. (11.1) and (11.2)

$[i_e]$ = vector of currents in the winding segments

$[e_n]$ = model's nodal voltages vector

$[f_e]$ = windings' flux-linkages vector

$[r]$ = diagonal matrix of windings series resistance

$[T]$ = windings connection matrix

$[T]^t$ = transpose of $[T]$

$[C]$ = nodal capacitance matrix

$[U]$ = unity matrix

$[I(s)]$ = Laplace transform of current sources

$[E(s)]$ = Laplace transform of nodal voltages

$[\Gamma_n]$ = inverse nodal inductance matrix = $[T][L]^{-1}[T]^t$

$[L]$ = matrix of self- and mutual-inductances

$[G]$ = conductance matrix, for resistors connected between nodes

$[I_s]$ = vector of current sources

In a linear representation of an iron core transformer, the permeability of the core is assumed constant regardless of the magnitude of the core flux. This assumption allows the inductance model to remain

constant for the entire computation. Equations (11.1) and (11.2) are based on this assumption and that the various elements in the model are also not frequency-dependent. Work in the last decade has addressed both the nonlinear characteristics of the core and the frequency-dependent properties of the materials. Much progress has been made, but their inclusion adds considerably to the model's complexity and the computational difficulty. If the core is nonlinear, the permeability changes as a function of the material properties, past history, and instantaneous flux magnitude. Therefore, the associated inductance model is time-dependent. The basic strategy for solving the transient response of the nonlinear model in Eqs. (11.1) or (11.2) is to linearize the transformer's nonlinear magnetic characteristics at an instant of time based on the flux in the core at that instant.

Two other model formulations should be mentioned. de Leon addressed the transient problem using a model based on the idea of duality (de Leon and Semlyen, 1994). The FEM has found wide acceptance in solving for electrostatic and electromagnetic field distributions. In some instances, it is very useful in solving for the transient distribution in coils and windings of complex shape.

11.3.3 Frequency-Domain Solution

A set of linear differential equations representing the transient response of the transformer can be solved either in the time domain or in the frequency domain. If the model is linear, the resultant solution will be the same for either method. The frequency-domain solution requires that the components of the input waveform at each frequency be determined. These individual sinusoidal waves are then applied individually to the transformer and the resultant voltage response throughout the winding is determined. Finally, the total response in the time domain is determined by summing the component responses at each frequency by applying superposition. An advantage of this method is that it allows the recognition of frequency-dependent losses to be addressed easily. Disadvantages of this method are that it does not allow the modeling of time-dependent switches, nonlinear resistors like ZnO, or the recognition of nonlinear magnetic core characteristics.

11.3.4 Solution in the Time Domain

The following briefly discusses the solution of Eqs. (11.1) and (11.2). There are numerous methods to solve Eq. (11.1) but it has been found that when solving the stiff differential equation model of a transformer, a generalization of Dommel's method (Dommel, 1969; Degeneff, 1977) works very well. A lossless lumped-parameter transformer model containing n nodes has approximately $n(n+1)/2$ inductors and $3n$ capacitors. Since the total number of inductors far exceeds the number of capacitors in the network, this methodology reduces storage and computational time by representing each capacitor as an inductor in parallel with a current source. The following system of equations results:

$$[\hat{Y}][F(t)] = [I(t)] - [H(t)] \quad (11.3)$$

where

$[F(t)]$ = nodal integral of the voltage vector

$[I(t)]$ = nodal injected current vector

$[H(t)]$ = past history current vector

and

$$[\hat{Y}] = \frac{4}{\Delta t^2}[C] + \frac{2}{\Delta t}[G] + [\Gamma_n] \quad (11.4)$$

The lumped-parameter model is composed of capacitances, inductances, and losses computed from the winding geometry, permittivity of the insulation, iron core permeability, and the total number of sections into which the winding is divided. Then the matrix $[\hat{Y}]$ is computed using the integration

step size, Δt . At every time step, the above system of equations is solved for the unknowns in the integral of the voltage vector. The unknown nodal voltages, $[E(t)]$, are calculated by taking the derivative of $[F(t)]$. Δt is selected based on the detail of the model and the highest resonant frequency of interest. Normally, Δt is smaller than one-tenth the period of this frequency.

The state-variable formulation as shown in Eq. (11.2) can be solved using differential equation routines available in IMSL or others based on the work of Gear and Adams (1991). The advantage of these routines is that they are specifically written with the solution of stiff systems of equations in mind. The disadvantage of these routines is that they consume considerable time during the solution.

11.3.5 Accuracy vs. Complexity

Every model of a physical system is an approximation. Even the simplest transformer has a complex winding and core structure and as such possesses an infinite number of resonant frequencies. A lumped-parameter model, or for that matter, any model is at best an approximation of the actual device of interest. A lumped-parameter model containing a structure of inductances, capacitances, and resistances will produce a resonance frequency characteristic that contains the same number of resonant frequencies as nodes in the model. The transient behavior of a linear circuit (the lumped-parameter model) is determined by the location of the poles and zeros of its terminal impedance characteristic. It follows then that a detailed transformer model must possess two independent characteristics to faithfully reproduce the transient behavior of the actual equipment. First, it must include accurate values of R , L , and C , reflecting the transformer geometry. This fact is well appreciated and documented. Second, the transformer must be modeled with sufficient detail to address the bandwidth of the applied waveshape. In a valid model, the highest frequency of interest would have a period at least ten times larger than the travel time in the largest winding segment in the model. If this second characteristic is overlooked, a model can produce results that appear valid, but may have little physical basis. A final issue is the manner in which the transformer structure is subdivided. If care is not taken, the manner in which the model is constructed will itself introduce significant errors and the computation will be mathematically robust but an inaccurate approximation of the physical reality.

11.4 Resonant Frequency Characteristic

11.4.1 Definitions

The steady-state and transient behaviors of any circuit, for any applied voltage, are established by the location of the poles and zeros of the impedance function of the lumped-parameter model in the complex plane. The zeros of the terminal impedance coincide with the natural frequencies of the model, by definition. McNutt et al. (1974) define terminal resonance as the terminal current maximum and a terminal impedance minimum. In a physical system there are an infinite number of resonances. In a lumped-parameter model of a system, there are as many resonances as nodes in the model (or the order of the system). Terminal resonance is also referred to as series resonance (Abetti and Maginniss, 1954; Abetti, 1959a,b). Terminal antiresonance is defined as a terminal current minimum and a terminal impedance maximum (McNutt et al., 1974). This is also referred to as parallel resonance (Abetti and Maginniss, 1954; Abetti, 1959a,b). McNutt defines internal resonance as an internal voltage maximum and internal antiresonance as an internal voltage minimum.

11.4.2 Impedance vs. Frequency

The terminal resonances for a system can be determined by taking the square root of the eigenvalues of the system matrix, $[A]$, shown in the state-variable representation for the system shown as

$$\begin{aligned} [\dot{q}] &= [A][q] + [B][u] \\ [y] &= [C][q] + [D][u] \end{aligned} \tag{11.5}$$

where

- [A] = state matrix
- [B] = input matrix
- [C] = output matrix
- [D] = direct transmission matrix
- [q] = vector of state variables for system
- [\dot{q}] = first derivative of [q]
- [u] = vector of input variables
- [y] = vector of output variables

Determining the impedance vs. frequency characteristic requires a little more effort. In light of the previous definitions, terminal resonance may be defined as occurring when the reactive component of the terminal impedance is zero. Equivalently, terminal resonance occurs when the imaginary component of the quotient of the terminal voltage divided by the injected terminal current is zero. Recalling that in the Laplace domain, that s is equivalent to $j\omega$ with a system containing n nodes with the excited terminal code j , one can rewrite Eq. (11.1) to obtain

$$\begin{bmatrix} e_1(s) \\ e_2(s) \\ \vdots \\ e_j(s) \\ \vdots \\ e_n(s) \end{bmatrix} = \begin{bmatrix} Z_{1j}(s) \\ Z_{2j}(s) \\ \vdots \\ Z_{jj}(s) \\ \vdots \\ Z_{nj}(s) \end{bmatrix} \begin{bmatrix} i_j(s) \end{bmatrix} \quad (11.6)$$

The voltage at the primary (node j) is in operation form. Rearranging the terminal impedance is given by

$$Z_t(\omega) = Z_{jj}(j\omega) = Z_{jj}(s) = \frac{e_j(s)}{i_j(s)} \quad (11.7)$$

In these equations the unknown quantities are the voltage vector and the frequency. It is a simple matter to assume a frequency and solve for the corresponding voltage vector. Solving Eq. (11.7) over a range of frequencies results in the well-known impedance vs. frequency plot. Figure 11.4 contains the impedance vs. frequency for the example used in Figs. 11.1 and 11.2.

11.4.3 Amplification Factor

The amplification factor or gain function is defined as

$$[N_{lm,j}] = \frac{\text{Voltage between points } l \text{ and } m \text{ at frequency } \omega}{\text{Voltage applied at input node } j \text{ at frequency } \omega} \quad (11.8)$$

Degenef (1977) shows that this results in

$$N_{lm,j} = \frac{Z_{l1}(j\omega) - Z_{mj}(j\omega)}{Z_{jj}(j\omega)} \quad (11.9)$$

If one is interested in the voltage distribution within a coil at one of the resonant frequencies, this can be found from the eigenvector of the coil at the frequency of interest. If one is interested in the distribution at any other frequency, Eq. (11.9) can be utilized. This is shown in Fig. 11.5.

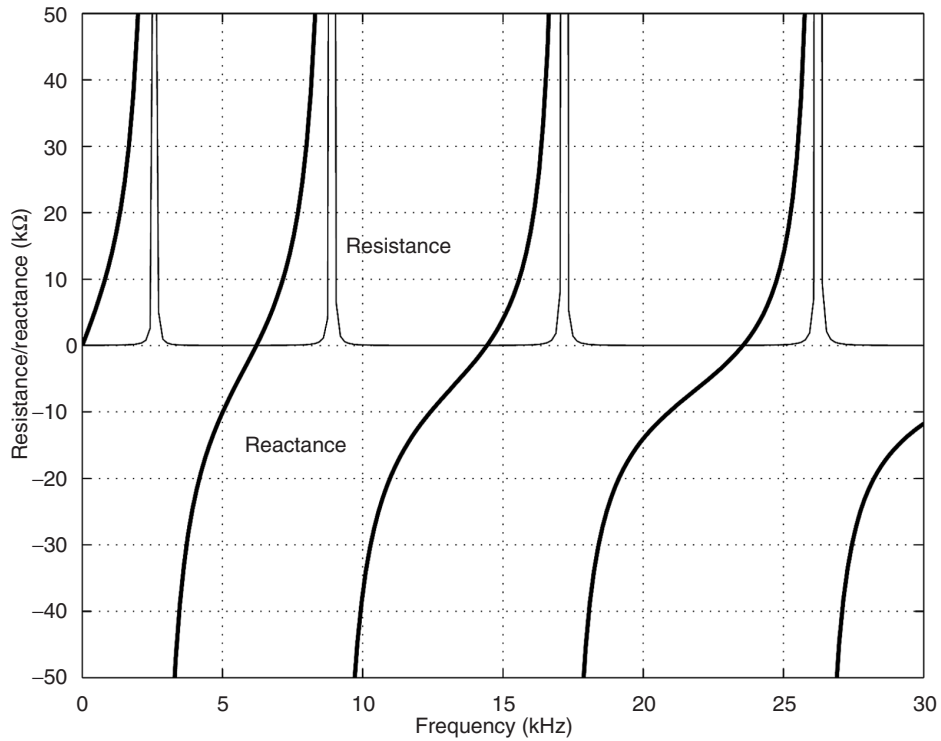


FIGURE 11.4 Terminal impedance for a helical winding.

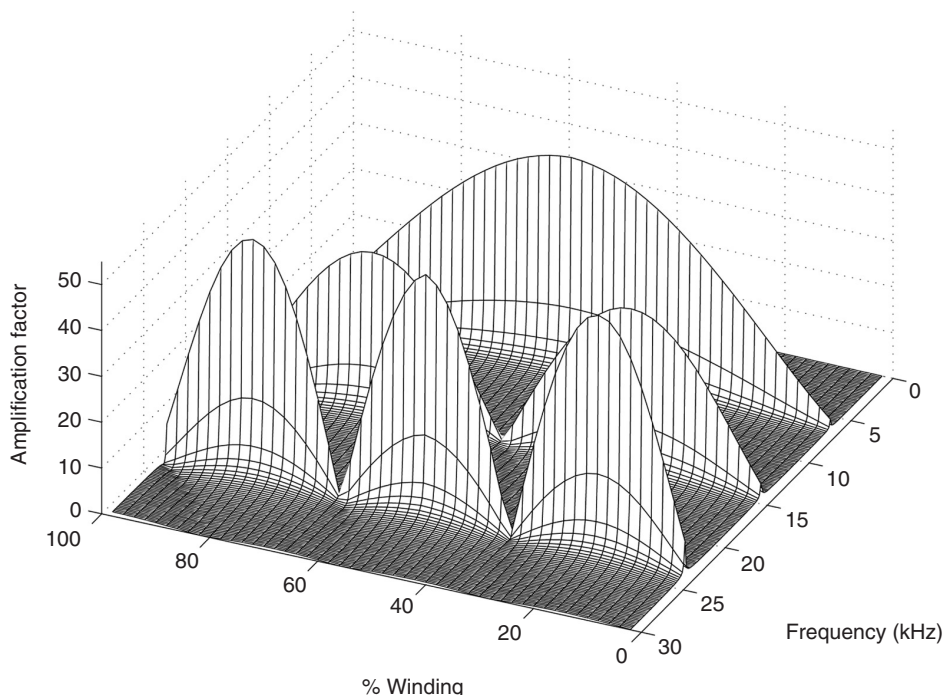


FIGURE 11.5 Amplification factor at 5 from 0 to 30 kHz.

11.5 Inductance Model

11.5.1 Definition of Inductance

Inductance is defined as

$$L = \frac{d\lambda}{dI} \quad (11.10)$$

and if the system is linear:

$$L = \frac{\lambda}{I} \quad (11.11)$$

where

- L = inductance (H)
- λ = flux linkage caused by current I (Wb) turns
- I = current producing flux linkages (A)
- $d\lambda$ = first derivative of λ
- dI = first derivative of I

L is referred to as self-inductance if the current producing the flux is the same current being linked. L is referred to as mutual-inductance if the current producing the flux is other than the current being linked (MIT, 1943). Grover (1962) published an extensive work providing expressions to compute the self- and mutual-inductances in air for a large number of practical conductor and winding shapes.

One of the most difficult phenomena to model is the magnetic flux interaction involving the different winding sections and the iron core. Historically, this phenomenon has been modeled by dividing the flux into two components: the common and leakage flux. The common flux dominates when the transformer behavior is studied under open-circuit conditions and the leakage flux dominates the transient response when the winding is shorted or loaded heavily. Developing a transformer model capable of representing the magnetic flux behavior for all conditions the transformer will see in factory test and in service requires the accurate calculation of the self- and mutual-inductances.

11.5.2 Transformer Inductance Model

Until the introduction of the computer there was a lack of practical analytical formulae to compute the self- and mutual-inductances of coils with an iron core. Rabins (1956) developed expressions to calculate self- and mutual-inductances for a coil on an iron core based on the assumption of a round core leg and infinite core yokes both of infinite permeability. Fergestad and Henriksen (1974) improved Rabins' inductance model in 1974 by assuming an infinitely permeable core except for the core leg. In their approach, a set of state-variable equations was derived from the classic lumped-parameter model of the winding.

White (1977, 1978) derived an expression to calculate the self- and mutual-inductances in the presence of an iron core with finite permeability under the assumption of an infinitely long iron core. White's inductance model had the advantage that the open-circuit inductance matrix could be inverted (White, 1978). White derived an expression for the self- and mutual-inductances between sections of a transformer winding by solving a two-dimensional problem in cylindrical coordinates for the magnetic vector potential assuming a nonconductive and infinitely long open core. He assumed that the leakage inductance of an open-core configuration is the same as that of the closed core.

Starting from the definition of the magnetic vector potential $\vec{B} = \nabla \times \vec{A}$ and $\nabla \cdot \vec{A} = 0$ and using Ampere's law in differential form, $\vec{J}_f = \nabla \times \vec{H}$, White solved the following equation:

$$\nabla^2 \vec{A}(r,z) = -\mu_0 \vec{J}(r,z) \quad (11.12)$$

The solution is divided into two parts: the air core solution and the change in the solution due to the insertion of the iron core as shown in the following equations:

$$\vec{A}(r,z) = \begin{cases} \vec{A}_0(r,z) + \vec{A}_1(r,z), & 0 \leq r \leq R_c \\ \vec{A}_0(r,z) + \vec{A}_2(r,z), & r > R_c \end{cases}$$

$\vec{A}_0(r,z)$ is the solution when the core is present and $\vec{A}_1(r,z)$ and $\vec{A}_2(r,z)$ are the solutions when the iron core is added. Applying Fourier series to Eq. (11.12), the solution for $\vec{A}_0(r,z)$ was found first and then $\vec{A}_2(r,z)$.

Knowing the magnetic vector potential allows the flux linking a filamentary turn at (r,z) to be determined by recalling $\phi(r,z) = \oint \vec{A}(r,z) \cdot d\vec{l}$. The flux for the filamentary turn is given by

$$\phi(r,z) = 2\pi r \{ \vec{A}_0(r,z) + \vec{A}_2(r,z) \} = \phi_0(r,z) + 2\pi r \vec{A}_2(r,z) \quad (11.13)$$

The flux in air, $\phi_0(r,z)$, can be obtained from known formulae for filaments in air (Grover, 1962); therefore, it is only necessary to obtain the change in the flux linking the filamentary turn due to the iron core. If the mutual-inductance, L_{ij} , between two coil sections is going to be calculated, then the average flux linking section i needs to be calculated. This average flux is given by

$$\phi_{ave} = \frac{\int_{R_i}^{\bar{R}_i} \int_{Z_i}^{\bar{Z}_i} \phi(r,z) dz dr}{H_i(R_i - \bar{R}_i)} \quad (11.14)$$

Knowing the average flux, the mutual-inductance can be calculated using the following expression:

$$L_{ij} = \frac{N_i N_j \phi_{ave}}{I_j} \quad (11.15)$$

White's final expression for the mutual-inductance between two coil segments is

$$L_{ij} = L_{ijo} + 2N_i N_j (1 - \nu_r) \mu_0 R_c \int_0^\infty \frac{I_0(\omega R_c) I_1(\omega R_c) F(\omega)}{\nu_r + (1 - \nu_r) \omega R_c I_1(\omega R_c) K_0(\omega R_c)} d\omega \quad (11.16)$$

where

$$F(\omega) = \frac{1}{\omega} \left[\frac{1}{\omega(\bar{R}_i - R_i)} \int_{\omega R_i}^{\omega \bar{R}_i} x K_1(x) dx \right] \frac{2}{\omega H_i} \sin\left(\frac{\omega H_i}{2}\right) \\ \left[\frac{1}{\omega(\bar{R}_j - R_j)} \int_{\omega R_j}^{\omega \bar{R}_j} x K_1(x) dx \right] \frac{2}{\omega H_j} \sin\left(\frac{\omega H_j}{2}\right) \cos(\omega d_{ij}) \quad (11.17)$$

L_{ijo} is the air core inductance, $\nu_r = 1/\mu_r$ is the relative reluctivity. $I_0(\omega R_c)$, $I_1(\omega R_c)$, $K_0(\omega R_c)$, and $K_1(\omega R_c)$ are modified Bessel functions of first and second kind.

11.5.3 Inductance Model Validity

The ability of the inductance model to accurately represent the magnetic characteristic of the transformer can be assessed by the accuracy with which it reproduces the transformer electrical characteristics, e.g., the short- and open-circuit inductances, and the pseudofinal (turns ratio) voltage distribution. The short- and open-circuit inductances of a transformer can be determined by several methods, but the simplest is to obtain the inverse of the sum of all the elements in the inverse nodal

inductance matrix, Γ_n . This has been verified (Degenef and Kennedy, 1975; Degenef, 1978). The pseudofinal voltage distribution is defined by Abetti (1960). It is very nearly the turns ratio distribution and must match whatever voltage distribution the winding arrangement and number of turns dictate. An example of this is contained in Degenef and Kennedy (1975).

11.6 Capacitance Model

11.6.1 Definition of Capacitance

Capacitance is defined as

$$C = \frac{Q}{V} \quad (11.18)$$

where

C = capacitance between the two plates (F)

Q = charge on one of the capacitor plates (C)

V = voltage between the capacitor plates (V)

Snow (1954) published an extensive work on computing the capacitance for unusually shaped conductors. Practically, however, most lumped-parameter models of windings are created by subdividing the winding into segments with small radial and axial dimensions and large radii where a simple parallel-plate formula can be used Degenef et al. (1980) to compute both the series and shunt capacitances for a segment. For example

$$C = \epsilon_0 \epsilon_r \frac{\text{RadCir}}{nD} \quad (11.19)$$

where

ϵ_0 = permittivity of freespace, 8.9×10^{-12} C/m

ϵ_r = relative permittivity between turns

Rad = radial build of the segment turns (m)

Cir = circumference of the mean turn within segment (m)

n = number of turns with the segment

D = separation between turns (m)

In computing these capacitances, the relative permittivity, ϵ_r , of the materials must be recognized. This is a function of the material, moisture content, temperature, and effective age of the material. Clark (1962) and Von Hippel (1954) provide a large database of this type of information. Since most lumped-parameter models assume the topology to be of circular symmetry, if the geometry is unusually complex it may be appropriate to model the system with a three-dimensional FEM. It should be emphasized that all of the above are based on the assumption that the capacitive structure of the transformer is frequency invariant. If the transient model is required to be valid over a very large bandwidth, then the frequency characteristic of the dielectric structure must be taken into account.

11.6.2 Series and Shunt Capacitance

In order to construct a lumped-parameter model, the transformer is subdivided into segments (or groups of turns). Each of these segments contains a beginning node and an exit node. Between these two nodes there will generally be associated a capacitance, traditionally called the series capacitance. These are the intrasection capacitances. In most cases they are computed using the simple parallel plate capacitance given in Eq. (11.19). An exception to this is the series capacitance of disk-winding segments. Expressions for the series capacitance of the disk-winding section are given in the next section.

Additionally, each segment will have associated with it, capacitances between adjacent sections of turns or to a shield or earth. These are the intersection capacitances. These capacitances are generally referred to as shunt capacitances and are normally divided in half and connected to each end of the appropriate segments. This is an approximation, but if the winding is subdivided into relatively small segments, the approximation is acceptable and the error introduced by the model is small.

11.6.3 Equivalent Capacitance for Disk Windings

This section presents simplified expressions to compute the series capacitance for disk-winding section pairs. Since most lumped-parameter models are not turn-to-turn models, an electrostatic equivalent of the disk section is used for the series capacitance. It is well known that as the series capacitance of disk-winding sections becomes larger with respect to the capacitances to ground, the initial distribution becomes more linear (straight line) and the transient response in general more benign. Therefore, since it is possible to arrange the turns within a disk section in many ways without affecting the section's inductance characteristic or the space or material it requires, the industry has offered many different disk arrangements in an effort to increase this effective series capacitance.

The effective series capacitance of a disk winding is a capacitance, which when connected between the input and output of the disk-winding section pair would store the same electrostatic energy the disk section pair would store (between all turns) if the voltage were distributed linearly within the section. This modeling strategy is discussed in detail by Scheich (1965) and Degeneff and Kennedy (1975). Figure 11.6 illustrates the cross-section of three common disk-winding configurations. The series capacitance of the continuous disk is given by

$$C_{\text{continuous}} = \frac{2}{3} C_s + \left[\frac{n-2}{n^2} \right] C_t \quad (11.20)$$

The series capacitance of the interleaved disk section pair is given by

$$C_{\text{interleaved}} = 1.128 C_s + \left[\frac{n-4}{4} \right] C_t \quad (11.21)$$

The interleaved disk provides a greater series capacitance than the continuous disk but is more difficult to manufacture. A winding that has a larger series capacitance than the continuous disk but simpler to manufacture than the interleave is the internally shielded winding. Its series capacitance is given by

$$C_{\text{internal shield}} = \frac{2}{3} C_s + \left[\frac{n-2-2n_s}{n^2} \right] C_t + 4C_{ts} \sum_{i=1}^{n_s} \left[\frac{n_i}{n} \right]^2 \quad (11.22)$$

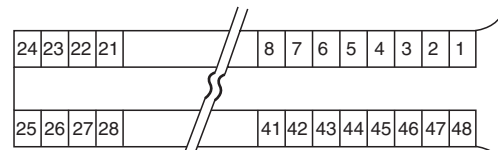
where

C_s = capacitance between sections

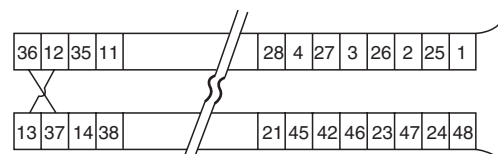
C_t = capacitance between turns

C_{ts} = capacitance between turn and internal shield

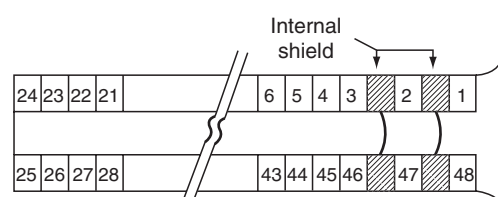
n = turns in section pair



(A) Continuous disk winding



(B) Interleaved disk winding



(C) Internally shielded disk winding
2 per section

FIGURE 11.6 Common disk-winding section pairs:
(A) continuous; (B) interleaved; and (C) internal shield.

n_i =location of shield within section

n_s =internal shields within section pair

The method of selecting a disk-winding section is often a compromise of electrical performance, economics, and manufacturing preference for a given firm.

11.6.4 Initial Voltage Distribution

The initial voltage distribution can be determined experimentally by applying a voltage wave with a fairly fast rise time (say 0.5 μs) and measuring the normalized distribution within the winding structure at an intermediate time (say 0.3 μs). The initial distribution can be computed analytically by injecting a current into the excited node and determining the normalized voltage throughout the transformer-winding structure. This computational method is outlined in detail by Degenef and Kennedy (1975). If one is considering a single coil, it is common practice to determine the gradient of the transient voltage near the excited terminal (which is the most severe). This gradient is referred to as α and is found by Greenwood (1991):

$$\alpha = \sqrt{\frac{C_g}{C_s}} \quad (11.23)$$

where

α =winding gradient

C_g =capacitance to ground (F)

C_s =effective series capacitance (F)

For the coil shown in Fig. 11.3, the α is on the order of 12.

11.7 Loss Model

At steady state, losses are a costly and unwanted characteristic of physical systems. At high frequency, losses produce a beneficial effect in that they reduce the transient-voltage response of the transformer by reducing the transient-voltage oscillations. In general, the oscillations are underdamped. The effect of damping on the resonant frequency is to reduce the natural frequencies slightly. Losses within the transformer are a result of a number of sources, each source with a different characteristic.

11.7.1 Copper Losses

The losses caused by the current flowing in the winding conductors are referred to as series losses. Series losses are composed of three components: DC losses, skin effect, and proximity effect.

11.7.1.1 DC Resistance

The conductor's DC resistance is given by

$$R_{dc} = \rho \frac{l}{A} \quad (11.24)$$

with

ρ =conductor resistivity ($\Omega \text{ m}$)

l =length of conductor (m)

A =conductor area (m^2)

ρ is a function of the conductor material and its temperature.

11.7.1.2 Skin Effect

Lammerer and Stafl (1966) give an expression for the skin effect in a rectangular conductor. The impedance per unit length of the conductor is given by

$$Z = \frac{k}{4h\sigma} \coth kb \quad \Omega/m \quad (11.25)$$

where

$$k = \frac{1+j}{a} \quad (11.26)$$

with

$$a = \sqrt{\frac{2}{\omega\sigma\mu}} \quad (11.27)$$

h = half the conductor height (m)

b = half the conductor thickness (m)

σ = conductivity of the conductor (S/m)

μ = permeability of the material (H/m)

ω = frequency (rad/s)

Defining

$$\xi = b\sqrt{j\omega\sigma\mu} \quad (11.28)$$

and Eq. (11.25) is expressed as

$$Z_{\text{skin}} = R_{\text{dc}}\xi \coth \xi \quad \Omega/m \quad (11.29)$$

where R_{dc} is the DC resistance per unit length of the conductor. Equation (11.29) is used to calculate the impedance due to the skin effect as a function of frequency.

11.7.1.3 Proximity Effect

Proximity effect is the increase in losses in one conductor due to currents in other conductors produced by a redistribution of the current in the conductor of interest by the currents in the other conductors. A method of finding the proximity effect losses in the transformer winding consists of finding a mathematical expression for the impedance in terms of the flux cutting the conductors of an open-winding section due to an external magnetic field. Since windings in large power transformers are mainly built using rectangular conductors, the problem reduces to the study of eddy current losses in a packet of laminations. Lammerer and Stafl (1966) provide an expression for the flux as a function of frequency in a packet of laminations. It is given in the following equation:

$$\Phi = \frac{2al\mu}{1+j} H_0 \tanh(1+j) \frac{b}{a} \quad (11.30)$$

where l is the conductor length, H_0 is the rms value of the magnetic flux intensity, and the remaining variables are the same as defined in Eq. (11.27).

Assuming H_0 in Eq. (11.30) represents the average value of the magnetic field intensity inside the conductive region represented by the winding section i and defining L_{ijo} as

$$L_{ijo} = N_i N_j \phi_{ijo} \quad (11.31)$$

where ϕ_{ijo} is the average flux cutting each conductor in section i due to the current I_j , and N is the number of turns in each section, the inductance L_{ij} as a function of frequency is

$$L_{ij} = \frac{L_{ijo}}{(1+j)b/a} \tanh(1+j)\frac{b}{a} H \quad (11.32)$$

The impedance $Z_{\text{prox}_{ij}}$ is obtained by multiplying the inductance by the complex variable s . Using the same notation as in Eq. (11.29), the impedance of the conductor due to the proximity effect is given as

$$Z_{\text{prox}_{ij}} = s \frac{L_{ijo}}{\xi} \tanh \xi \quad \Omega \quad (11.33)$$

11.7.2 Core Losses

The effect of eddy currents in the core has been represented in Avila-Rosales and Alvarado (1982), Tarasiewicz et al. (1993), and de Leon and Semlyen (1994) by the well-tested formula:

$$Z = \frac{4N^2 A}{ld^2 \sigma} x \tanh x \quad (11.34)$$

where

$$x = \frac{d \sqrt{j \omega \mu \sigma}}{2} \quad (11.35)$$

and

l = length of the core limb in meters (axial direction) (m)

d = thickness of the lamination (m)

μ = permeability of the material (H/m)

N = number of turns in the coil

A = total cross-sectional area of all laminations

ω = frequency (rad/s)

This formula represents the equivalent impedance of a coil wound around a laminated iron core limb. The expression was derived by Avila-Rosales and Alvarado (1982) by solving Maxwell's equations assuming the electromagnetic field distribution is identical in all laminations and an axial component of the magnetic flux.

The total hysteresis loss in core volume, V , in which the flux density is uniform everywhere and varying cyclically at a frequency of ω , can be expressed as

$$P_h = 2\pi\omega\eta V \beta_{1\max}^n \quad (11.36)$$

with

P_h = total hysteresis loss in core (W/m^3)

η = constant a function of material ($\text{m A}/\text{V}^2 \text{ s}$)

V = core volume (m^3)

β = flux density

n = exponent dependent upon material (1.6–2.0)

ω = frequency (rad/s)

11.7.3 Dielectric Losses

The capacitive structure of a transformer has parallel losses associated with it. At low frequency, the effect of capacitance on the internal voltage distribution can be ignored. As such, the effect of the losses in the dielectric structure can be ignored. However, at higher frequencies the losses in the dielectric system can have a significant effect on the transient response. Batruni et al. (1996) explore the effect of dielectric losses on the impedance vs. frequency characteristic of the materials in power transformers.

These losses are frequency-dependent and are shown in Fig. 11.7.

11.8 Winding Construction Strategies

11.8.1 Design

The successful design of a commercial transformer requires the selection of a simple structure so that the core and coils are easy to manufacture. At the same time, the structure should be as compact as possible to reduce required materials, shipping concerns, and base dimensions. The form of construction should allow convenient removal of heat, sufficient mechanical strength to withstand forces generated during system faults, acceptable noise characteristics, and an electrical insulation system that meets the system steady-state and transient requirements. There are two common power transformer structures in use

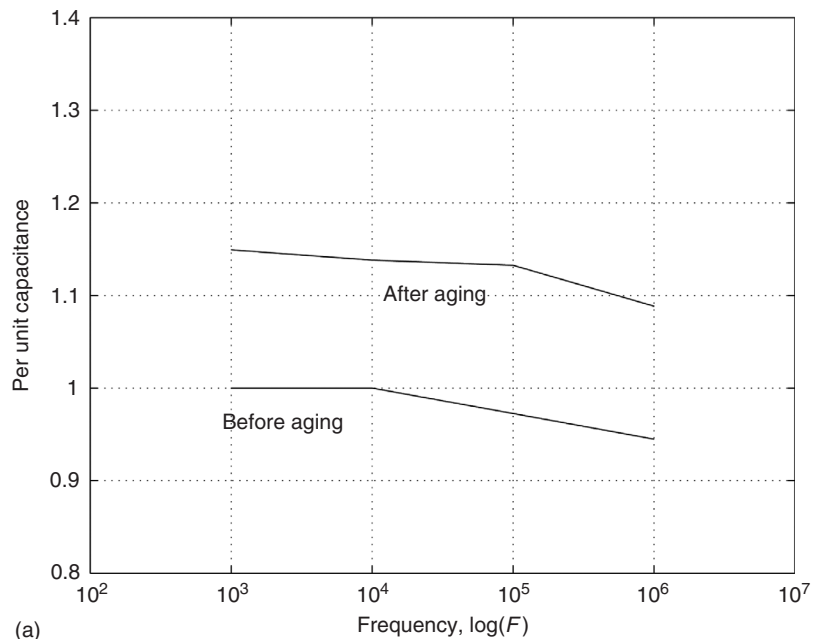


FIGURE 11.7 Oil-soaked paper capacitance and conductance as a function of frequency.

(continued)

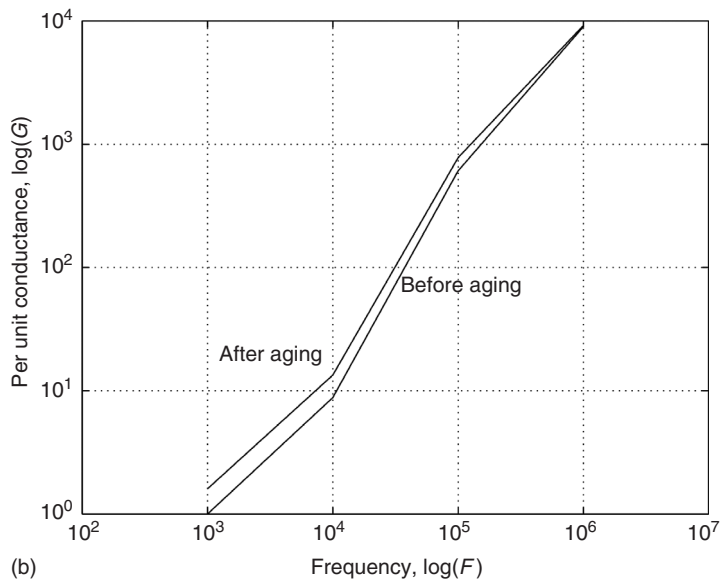


FIGURE 11.7 (continued)

today. When the magnetic circuit is encircled by two or more windings of the primary and secondary, the transformer is referred to as a core-type transformer. When the primary and secondary windings are encircled by the magnetic material, the transformer is referred to as a shell-type transformer.

11.8.2 Core-Form

Characteristics of the core-form transformer are a long magnetic path and a shorter mean length of turn. Commonly used core-form magnetic circuits are single-phase transformers with a two-legged magnetic path with turns wound around each leg, a three-legged magnetic path with the center leg wound with conductor, and a four-legged magnetic path with the two interior legs wound with conductors (MIT, 1943; Bean et al., 1959). Three-phase core-form designs are generally three-legged magnetic cores with all three legs possessing windings and a five-legged core arrangement with the three center legs possessing windings. The simplest winding arrangement has the low-voltage winding near the core and the high-voltage winding wound on top of the low. Normally in the core-form construction, the winding system is constructed from helical-, layer-, or disk-type windings. Often the design requirements call for a winding arrangement that is a more complex arrangement, e.g., interleaving high- and low-voltage windings, interwound taps, windings that are bifurcated and have entry and exit points other than the top or bottom of the coil. All of these variations have, to one degree or another, an effect on the transformer's transient-voltage response. To insure an adequate insulation structure, each possible variation must be explored during the design stage to evaluate its effect on the transient overvoltages.

11.8.3 Shell-Form

Shell-form transformer construction features a short magnetic path and a longer mean length of electrical turn. Fink and Beaty (1987) point out that this results in the shell-form transformer having a larger core area and a smaller number of winding turns than the core-form of the same output and performance. Additionally, the shell-form will generally have a larger ratio of steel to copper than an

equivalently rated core-form transformer. The most common winding structure for shell-form windings is the primary–secondary–primary (P–S–P) but it is not uncommon to encounter shell-form windings of P–S–P–S–P. The winding structure for both the primary and secondary windings is normally of the pancake-type winding structure (Bean et al., 1959).

11.8.4 Proof of Design Concept

The desire of the purchaser is to obtain a transformer at a reasonable price that will achieve the required performance for an extended period of time. The desire of the manufacturer is to construct and sell a product, at a profit, that meets the customer's goals. The specification and purchase contract is the document that combines both the purchaser's requirements and the manufacturer's commitment in a legal format. The specification will typically address the transformer's service condition, rating, general construction, control and protection, design and performance review, testing requirements, and transportation and handling. Since it is impossible to address all issues in a specification, the industry uses standards that are acceptable to purchaser and supplier. In the case of power transformers, the applicable standards would include IEEE C57, IEC 76, and NEMA TR-1.

11.8.5 Standard Winding Tests

ANSI/IEEE C57.12.00 (1993) defines routine and optional tests and testing procedures for power transformers. The following are listed as routine tests for transformers larger than 501 kVA:

1. Winding resistance
2. Winding turns ratio
3. Phase-relationship tests: polarity, angular displacements, phase sequence
4. No-load loss and exciting current
5. Load loss and impedance voltage
6. Low-frequency dielectric tests (applied voltage and induced voltage)
7. Leak test on transformer tank

The following are listed as tests to be performed on only one of a number of units of similar design for transformers 501 kVA and larger:

1. Temperature rise tests
2. Lightning-impulse tests (full and chopped wave)
3. Audible sound test
4. Mechanical test from lifting and moving of transformer
5. Pressure tests on tank

Other tests are listed in ANSI/IEEE C57.12.00 (1993) which include, for example, short-circuit forces and switching-surge impulse tests. Additionally, specific tests may be required by the purchaser based on their applications or field experience.

The variety of transient voltages a transformer may see in its normal useful life is virtually unlimited (Degenoff et al., 1982). It is impractical to proof test each transformer for all conceivable combinations of transient voltage. However, the electrical industry has found that it is possible, in most instances, to assess the integrity of the transformer's insulation systems to withstand transient voltages with the application of a few specific aperiodic voltage waveforms. [Figure 11.8](#) illustrates the full, chopped, and switching-surge waveforms. IEEE C57 contains the specific wave characteristics, relationships, and acceptable methods and connections required for these standard tests. Each of these tests is designed to test the insulation structure for a different transient condition. The purpose of applying this variety of

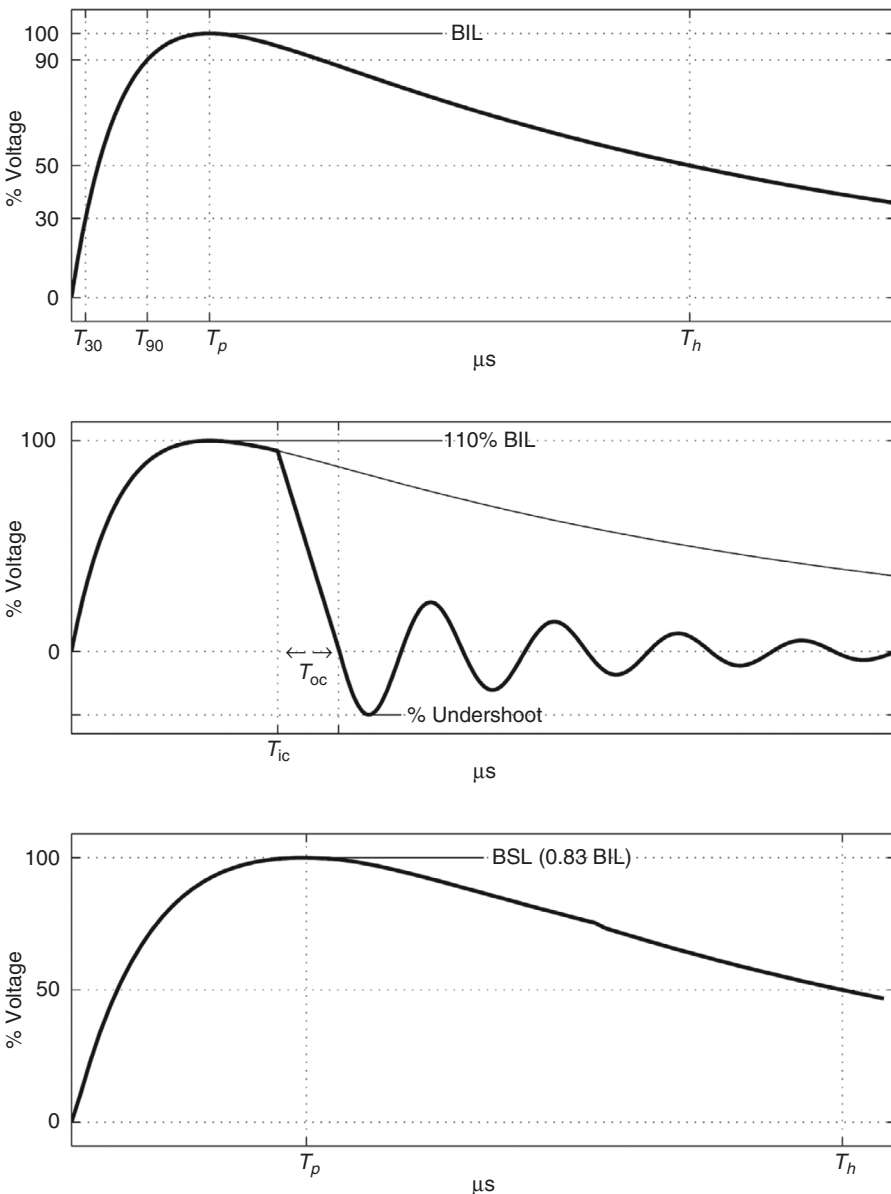


FIGURE 11.8 Standard voltage waveforms for impulse tests: full, chopped, switching surge.

tests is to substantiate adequate performance of the total insulation system for all the various transient voltages it may see in service.

The insulation integrity for steady state and for dynamic voltages is also assessed by factory tests called out in ANSI/IEEE C57.12.00 (1993). One should not be lulled into thinking that a transformer that has passed all factory voltage tests (both impulse and low frequency) can withstand all transient voltages to which the system may subject it. One should always assess the environment the transformer is applied in and determine if there may be unusual transient-voltage excitation present in an application that is not covered in the standards (see McNutt et al., 1974; Degenneff et al., 1982; Greenwood, 1991).

11.8.6 Design Margin

The actual level of insulation requested, e.g., BIL/BSL, is determined by recognizing the system within which the transformer will operate, and the arrester protective level. Normally, a minimum protective margin of 15 to 20% between the arrester peak voltage and the transformer capability at three (σ) is established. This is illustrated in Fig. 11.9 for a 230 kV transformer with a 750 kV BIL protected with a 180 kV rated arrester (Balma et al., 1996). The curve designated A in Fig. 11.9 is used to represent the transformer's insulation coordination characteristic (insulation capability) when subjected to aperiodic and oscillatory waveforms. The curve to be used to represent the transformer voltage-time insulation coordination characteristic when subjected to aperiodic waveforms with a time to failure between 0.1 and 2000 μ s is to be based on five points (IEEE C62.22-1991). The five points are:

1. Front of wave voltage plotted at its time of crest (about 0.5 μ s). If the front of wave voltage is not available, a value of 1.3 times the BIL should be plotted at 0.5 μ s.
2. Chopped wave voltage at its time of crest (about 3.0 μ s).
3. Full wave voltage (or BIL) plotted about 8 μ s.
4. Switching-surge voltage (or BSL) plotted about 300 μ s.
5. A point at 2000 μ s where its magnitude is established with the following expression:

$$\log V_{2000} = \frac{\log T_{\text{BSL}} - \log T_{2000}}{m} + \log V_{\text{BSL}} = \frac{\log 300/2000}{m} + \log V_{\text{BSL}}$$

V_{2000} is the voltage at 2000 μ s, T_{2000} , V_{BSL} is the BSL voltage (or 0.83 the BIL), and T_{BSL} equal to 300 μ s. The value of m is established as the inverse of the slope of a straight line drawn on log-log paper from the BSL point to a point established by the peak of the 1 h induced test voltage plotted at a time the induced voltage exceeds 90% of its peak value (this would be 28.7% of 3600 s or 1033.2 s).

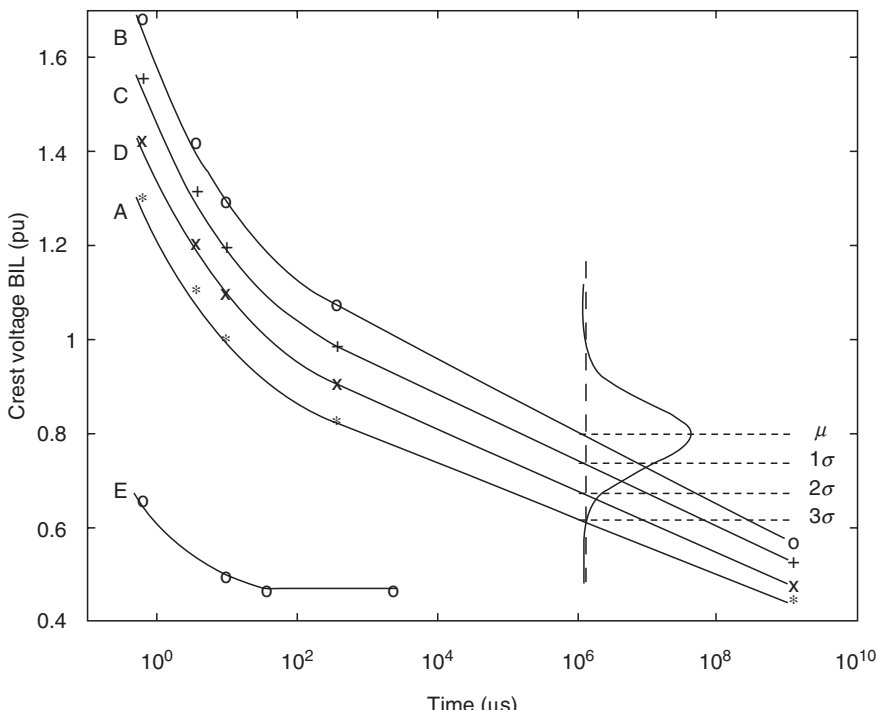


FIGURE 11.9 Voltage-time curve for insulation coordination.

The connection between all points is made with a smooth continuous curve. The first four points in the curve establish an approximate level of insulation voltage capability for which one would anticipate only one insulation failure out of 1000 applications of that voltage level, e.g., at 3σ the probability of failure is 1.0–0.99865 or approximately 0.001. Experience has shown that the standard deviation for transformer insulation structures is on the order of 10 to 15%. Figure 11.9 assumes that σ is 10%. Curve B, or the 50% failure rate curve, is established by increasing the voltage in curve A by 30%. Therefore, for curve B, on average the unit would be expected to fail one out of two times if it were subjected to this level of voltage. Curves C and D establish 1 and 2σ curves, or 16 and 2.3% failure rate curves, respectively. The inserted normal distribution on the right of Fig. 11.9 illustrates this concept. All of this assumes the transformer is new.

11.8.7 Insulation Coordination

In a field installation, an arrester is normally placed directly in front of the transformer to afford it protection from transient voltages produced on the system. Curve E in Fig. 11.9 is a metal oxide arrester protective curve established in a manner similar to that described in IEEE standard C62.2. The curve is specified by three points:

1. The front-of-wave voltage held by the arrester plotted at 0.5 μ s
2. The 8×20 μ s voltage plotted at 8.0 μ s
3. The switching-surge voltage plotted in straight line from 30 to 2000 μ s

The protective ratio is established by dividing the transformer insulation capability by the arrester protective level for the waveshape of interest. For example, in Fig. 11.9, the protective level for a switching surge is on the order of 177% or $(0.83/0.47) \times 100$.

11.8.8 Additional System Considerations

The standards reflect the growing and learning within the industry and each year they expand in breadth, addressing issues that are of concern to the industry. However, at present the standards are silent with regard to the effects of system voltage on transient response, multiphase surges, aging or mechanical movements of insulation structures, oscillatory voltage excitation, temperature variations, movement of oil, and loading history. A prudent user will seek similar users and explore their experience base.

11.9 Models for System Studies

11.9.1 Model Requirements

The behavior of large power transformers under transient conditions is of interest to both transformer designers and power engineers. The transformer designer employs detailed electrical models to establish a reliable and cost-effective transformer insulation structure. The power engineer models not only the transformer, but also the system, in order to investigate the effects of power system transients.

Considerable effort has been devoted to computing the transformer's internal transient response. Models of this type may contain several hundred nodes for each phase. This detail is necessary in order to compute the internal response in enough detail to establish an adequate transformer insulation design. The utility engineer usually is not interested in the internal response, but is concerned only with the transformer's terminal response. Even if the transformer's detailed models were available, their use would create system models too large to be effectively used in system studies. Normal practice has been to create a reduced order model of the transformer that represents the terminal response of the transformer. Experience has shown that great care must be taken to obtain a terminal model that provides a reasonable representation of the transformer over the frequency range of interest (Degenef, 1977; Gutierrez et al., 1993).

The challenge in creating a high fidelity reduced model lies in the fact that as the size of the model is reduced, the number of valid eigenvalues must also decrease. In effect, any static reduction technique will produce a model which is intrinsically less accurate than the more detailed lumped-parameter model (de Leon and Semlyen, 1992; Morched et al., 1992).

11.9.2 Reduced Order Model

McNutt et al. (1974) suggested a method of obtaining a reduced order transformer model by starting with the detailed model and appropriately combining series and shunt capacitances. This suggestion was extended by de Leon and Semlyen (1992). This method is limited to linear models and cannot be used to eliminate large proportions of the detailed models without affecting the resulting model's accuracy. Degenneff (1978) proposed a terminal model developed from information from the transformer's nameplate and capacitance measured among the terminals. This model is useful below the first resonant frequency but lacks the necessary accuracy at higher frequencies for system. Dommel et al. (1982) proposed a reduced model for EMTP described by branch impedance or admittance matrix calculated from open- and short-circuit tests. TRELEG and BCTRAN matrix models for EMTP can be applied only for very low-frequency studies. Morched et al. (1992) proposed a terminal transformer model, composed of a synthesized LRC network, where the nodal admittance matrix approximates the nodal admittance matrix of the actual transformer over the frequency range of interest. This method is appropriate only for linear models.

Gutierrez et al. (1993) and Degenneff et al. (1994) present a method for reducing both a detailed linear and nonlinear lumped-parameter model to a terminal model with no loss of accuracy. The work starts with Eq. (11.1), then progresses to Eq. (11.4), and then applies Kron reduction to obtain a terminal model of the transformer that retains all the frequency fidelity of the initial transformer lumped-parameter model. Gutierrez et al. (1993) and Degenneff et al. (1994) present all the appropriate equations to apply this technique within EMTP.

References

- Abetti, P.A., Correlation of forced and free oscillations of coils and windings, *IEEE PAS*, 986–996, December 1959a.
- Abetti, P.A., Survey and classification of published data on the surge performance of transformers and rotating machines, *AIEE Trans.*, 78, 1403–1414, 1959b.
- Abetti, P.A., Pseudo-final voltage distribution in impulsed coils and windings, *Trans. AIEE*, 87–91, 1960.
- Abetti, P.A., First supplement to reference (12), *AIEE Trans.*, 81, 213, 1962.
- Abetti, P.A., Second supplement to reference (12), *AIEE Trans.*, 83, 855, 1964.
- Abetti, P.A. and Maginniss, F.J., Fundamental oscillations of coils and windings, *IEEE PAS*, 1–10, February 1954.
- Avila-Rosales, J. and Alvarado, L., Nonlinear frequency dependent transformer model for electromagnetic transient studies in power systems, *IEEE Trans. PAS*, 101(11), 4281–4288, November 1982.
- Balma, P.M., Degenneff, R.C., Moore, H.R., and Wagenaar, L.B., The effects of long term operation and system conditions on the dielectric capability and insulation coordination of large power transformers, Paper No. 96 SM 406-9 PWRD, presented at the Summer Meetings of IEEE/PES, Denver, CO, 1996.
- Batruni, R., Degenneff, R., and Lebow, M., Determining the effect of thermal loading on the remaining useful life of a power transformer from its impedance versus frequency characteristics, *IEEE Trans. Power Deliv.*, 11(3), 1385–1390, July 1996.
- Bean, R.L., Crackan, N., Moore, H.R., and Wentz, E., *Transformers for the Electric Power Industry*, Westinghouse Electric Corporation, McGraw-Hill, New York, 1959.
- Blume, L.F., Boyajian, A., Camilli, G., Lennox, T.C., Minneci, S., and Montsinger, V.M., *Transformer Engineering*, 2nd ed., John Wiley & Sons, New York, 1951, pp. 416–423.

- Clark, F.M., *Insulating Materials for Design and Engineering Practice*, Wiley, New York, 1962.
- Degeneff, R.C., Simplified Formulas to Calculate Equivalent Series Capacitances for Groups of Disk Winding Sections, General Electric, TIS 75PTD017, August 16, 1976.
- Degeneff, R.C., A general method for determining resonances in transformer windings, *IEEE Trans. PAS*, 96(2), 423–430, March/April 1977.
- Degeneff, R.C., Reducing storage and saving computational time with a generalization of the Dommel (BPA) solution method, in *IEEE PICA Conference Proceedings*, Toronto, Canada, May 24–27, 1977, pp. 307–313.
- Degeneff, R.C., A Method for Constructing Terminal Models for Single-Phase n -Winding Transformers, IEEE Paper A78 539-9, Summer Power Meeting, Los Angeles, 1978.
- Degeneff, R.C. and Kennedy, W.N., Calculation of Initial, Pseudo-Final, and Final Voltage Distributions in Coils Using Matrix Techniques, Paper A75-416-8, Summer Power Meeting, San Francisco, CA, 1975.
- Degeneff, R.C., Blalock, T.J., and Weissbrod, C.C., Transient Voltage Calculations in Transformer Windings, General Electric Technical Information Series, No. 80PTD006, 1980.
- Degeneff, R.C., Neugebaur, W., Panek, J., McCallum, M.E., and Honey, C.C., Transformer response to system switching voltages, *IEEE Trans. PAS*, 101(6), 1457–1465, June 1982.
- Degeneff, R.C., Gutierrez, M., and Vakilian, M., Nonlinear, Lumped Parameter Transformer Model Reduction Technique, IEEE Paper No. 94 SM 409-3 PWRD, 1994.
- Dent, B.M., Hartill, E.R., and Miles, J.G., A method of analysis of transformer impulse voltage distribution using a digital computer, *IEE Proc.*, 105(Pt. A), 445–459, 1958.
- Dommel, H.W., Digital computer solution of electromagnetic transients in single and multiphase networks, *IEEE Trans. PAS*, 388–399, April 1969.
- Dommel, H.W., Dommel, I.I., and Brandwajn, V., Matrix representation of three-phase n -winding transformers for steady state and transient studies, *IEEE Trans.*, PAS-101(6), 1369–1378, June 1982.
- Fergestad, P.I. and Henriksen, T., Transient oscillations in multiwinding transformers, *IEEE Trans. PAS*, PAS-93, 500–507, 1974.
- Fink, D.G. and Beaty, H.W., *Standard Handbook for Electrical Engineers*, 12th ed., McGraw-Hill, New York, 1987.
- FORTRAN Subroutines for Mathematical Applications, Version 2.0, September 1991, MALB-USM-PERFCT-EN9109-2.0.
- Franklin, A.C., *The J & P Transformer Book*, 11th ed., chap. 15, 1983, pp. 351–367.
- Greenwood, A., *Electrical Transients in Power Systems*, John Wiley & Sons, New York, 1991.
- Greenwood, A., *Vacuum Switchgear*, Institute of Electrical Engineers, Short Run Press Ltd., Exeter, 1994.
- Grover, F.W., *Inductance Calculations—Working Formulas and Tables*, Dover Publications, New York, 1962.
- Gutierrez, M., Degeneff, R.C., McKenny, P.J., and Schneider, J.M., Linear, Lumped Parameter Transformer Model Reduction Technique, IEEE Paper No. 93 SM 394-7 PWRD, 1993.
- IEEE C62.22-1991, *IEEE Guide for the Application of Metal-Oxide Surge Arrester for Alternating-Current Systems*.
- IEEE Std. 519, *IEEE Recommended Practices and Requirements for Harmonic Control in Electrical Power Systems*, IEEE Industry Applications Society and Power Engineering Society, April 12, 1999.
- IEEE C57.12.00, *IEEE Guide and Standards for Distribution, Power, and Regulating Transformers*, 1993.
- Kogan, V.I., Fleeman, J.A., Provanzana, J.H., and Shih, C.H., Failure analysis of EHV transformers, *IEEE Trans. Power Deliv.*, 672–683, April 1988.
- Kogan, V.I., Fleeman, J.A., Provanzana, J.H., Yanucci, D.A., and Kennedy, W.N., Rationale and implementation of a new 765 kV generator step-up transformer specification, CIGRE Paper 12-202, August 1990.
- Lammeraner, J. and Stafl, M., *Eddy Currents*, CRC Press, Cleveland, OH, 1966.

- de Leon, F. and Semlyen, A., Reduced order model for transformer transients, *IEEE Trans. PWRD*, 7(1), 361–369, January 1992.
- de Leon, F. and Semlyen, A., Complete transformer model for electromagnetic transients, *IEEE Trans. Power Deliv.*, 9(1), 231–239, January 1994.
- Massachusetts Institute of Technology, Department of Electrical Engineering, *Magnetic Circuits and Transformers*, John Wiley & Sons, New York, 1943.
- McNutt, W.J., Blalock, T.J., and Hinton, R.A., Response of transformer windings to system transient voltages, *IEEE Trans. PAS*, 93, 457–467, 1974.
- McWhirter, J.H., Fahrnkopf, C.D., and Steele, J.H., Determination of impulse stresses within transformer windings by computers, *AIEE Transactions*, pt. III, 75, 1267–1273, 1956.
- Morched, A., Marti, L., and Ottavangers, J., A High Frequency Transformer Model for EMTP, Paper No. 925M 359-0 IEEE 1992 Summer Meeting, Seattle, WA, July 12–16, 1992.
- Narang, A., Wisenden, D., and Boland, M., Characteristics of Stress on Transformer Insulation Subjected to Very Fast Transient Voltages, CEA No. 253 T 784, Canadian Electricity Association, July 1998.
- Rabins, L., Transformer reactance calculations with digital computers, *AIEE Trans.*, 75(1), 261–267, July 1956.
- Scheich, A., Behavior of partially interleave transformer windings subject to impulse voltages, *Bulletin Oerlikon*, 389/390, 41–52, 1965.
- Snow, C., *Formulas for Computing Capacitance and Inductances*, National Bureau of Standards, Circular 544, September 10, 1954.
- Tarasiewicz, E.J., Morched, A.S., Narang, A., and Dick, E.P., Frequency dependent eddy current models for the nonlinear iron cores, *IEEE Trans. PAS*, 8(2), 588–597, May 1993.
- Vakilian, M., A Nonlinear Lumped Parameter Model for Transient Studies of Single Phase Core Form Transformers, Ph.D. Thesis, Rensselaer Polytechnic Institute, Troy, New York, 1993.
- Vakilian, M., Degeneff, R., and Kupferschmid, M., Computing the internal transient voltage response of a transformer with a nonlinear core using Gear's method—Part 2: Verification, *IEEE Trans. Power Deliv.*, 10(2), 702–708, May 1995a.
- Vakilian, M., Degeneff, R., and Kupferschmid, M., Computing the internal transient voltage response of a transformer with a nonlinear core using Gear's method—Part 1: Theory, *IEEE Trans. Power Deliv.*, 10(4), 1836–1841, October 1995b.
- Von Hippel, A., *Dielectric Materials and Applications*, MIT Press, Cambridge, 1954.
- Waldvogel, P. and Rouxel, R., A new method of calculating the electric stresses in a winding subjected to a surge voltage, *Brown Boveri Rev.*, 43(6), 206–213, June 1956.
- White, W.N., An Examination of Core Steel Eddy Current Reaction Effect on Transformer Transient Oscillatory Phenomena, General Electric Technical Information Series, No. 77PTD012, April 1977.
- White, W.N., Inductance Models of Power Transformers, General Electric Technical Information Series, No. 78PTD003, April 1978.
- White, W.N., Numerical Transient Voltage Analysis of Transformers and LRC Networks Containing Nonlinear Resistive Elements, 1977 PICA Conference, pp. 288–294.
- Wilcox, D.J., Conlon, M., and Hurley, W.G., Calculation of self and mutual impedances for coils on ferromagnetic cores, *IEE Proc.*, 135, A7, 470–476, September 1988.
- Wilcox, D.J., Hurley, W.G., McHale, T.P., and Conlon, M., Application of modified modal theory in the modeling of practical transformers, *IEE Proc.-C*, 139, 6, November 1992.
- An international survey on failures in large power transformers in service, Final Report of Working Group 05 of Study Committee 12 (Transformers), *Electra*, 88, May 1983.

12

Transmission System Transients— Grounding

12.1	General Concepts	12-1
12.2	Material Properties.....	12-2
12.3	Electrode Dimensions	12-3
12.4	Self-Capacitance of Electrodes	12-3
12.5	Initial Transient Response from Capacitance	12-5
12.6	Ground Electrode Impedance: Wire over Perfect Ground	12-6
12.7	Ground Electrode Impedance: Wire over Imperfect Ground	12-7
12.8	Analytical Treatment of Complex Electrode Shapes....	12-7
12.9	Numerical Treatment of Complex Electrode Shapes.....	12-8
12.10	Treatment of Multilayer Soil Effects	12-10
12.11	Layer of Finite Thickness over Insulator.....	12-10
12.12	Treatment of Soil Ionization	12-11
12.13	Design Process	12-13
12.14	Design Recommendations	12-13
	Appendix A Relevant IEEE Grounding Standards	12-15

William A. Chisholm
Kinetrics/UQAC

12.1 General Concepts

Electric power systems are often grounded, that is to say “intentionally connected to earth through a ground connection or connections of sufficiently low impedance and having sufficient current-carrying capacity to prevent the buildup of voltages which may result in undue hazard to connected equipment or to persons” (IEEE Std 100). Grounding affects the dynamic power-frequency voltages of unfaulted phases, and influences the choice of surge protection. Also, the tower-footing impedance is an important specification for estimating the severity of insulator-string transient voltage for a lightning flash to an overhead groundwire, tower or phase conductor with surge arrester.

To mitigate AC fault conditions, systems can be grounded by any of three means (IEEE Std 100):

- *Inductance grounded*, such that the system zero-sequence reactance is much higher than the positive-sequence reactance, and is also greater than the zero-sequence resistance. The ground-fault current then becomes more than 25% of the three-phase fault current.

- *Resistance grounded*, either directly to ground, or indirectly through a transformer winding. The low-resistance-grounded system permits a higher ground-fault current (on the order of 25 A to several kiloampere) for selective relay performance.
- *Resonant grounded*, through a reactance with a value of inductive current that balances the power-frequency capacitive component of the ground-fault current during a single line-to-ground fault. With resonant grounding of a system, the net current is limited so that the fault arc will extinguish itself.

Power system transients have a variety of waveshapes, with spectral energy ranging from the power-frequency harmonics up to broadband content in the 300-kHz range, associated with 1- μ s rise and fall times of lightning currents and insulator breakdown voltages. With the wide frequency content of transient waveshapes, resonant grounding techniques offer no direct benefit in preventing arcing flash-over from the grounding system to the insulated phases. Also, resistance grounds that may be effective for power frequency can have an additional inductive voltage rise (LdI/dt with $dt=1\ \mu$ s) that dominates the transient response. Both resistive and inductive aspects must be considered in the selection of an appropriate ground electrode for adequate performance during transients such as lightning.

12.2 Material Properties

The earth resistivity (ρ , units of $\Omega\text{ m}$) dominates the potential rise on ground systems at low frequencies and currents. Near the surface, resistivity changes as a function of moisture, temperature, frequency, and electric field stress. Figure 12.1 shows that this variation can be quite large.

Reconnaissance of earth resistivity, from traditional four-terminal resistance measurements, is a classic tool in geological prospecting (Keller and Frishknecht, 1982). A current I is injected at the outer two locations in a line of four equally spaced probes. A potential difference U then appears

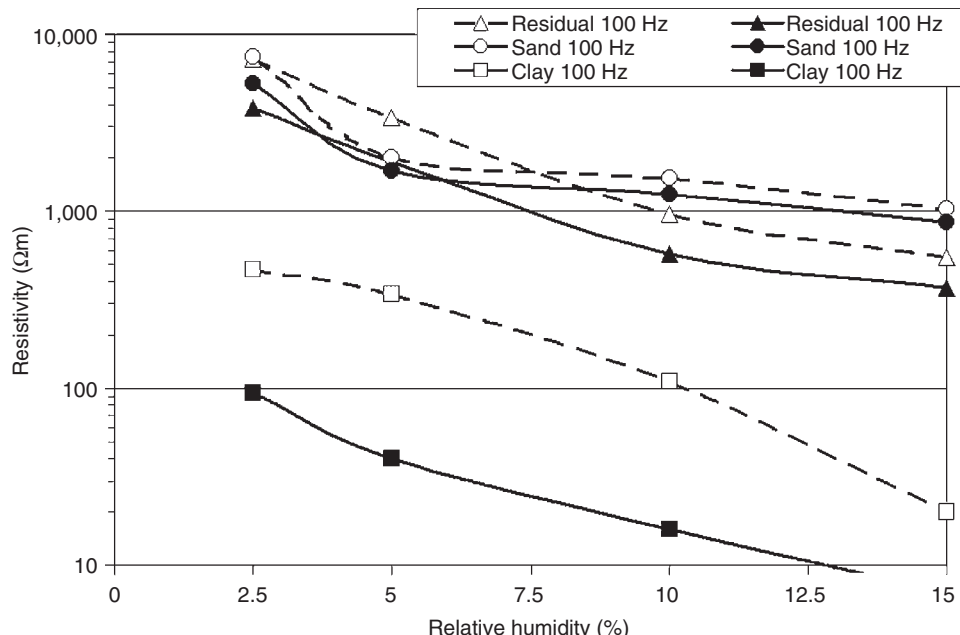


FIGURE 12.1 Change in resistivity with relative humidity and frequency for three typical surface materials. (From Visacro, S. and Portela, C.M., *Proceedings of 5th ISH*, Paper 93.06, 1987.)

between the inner two probes, which are separated by a distance a . The apparent resistivity ρ_a is then defined as

$$\rho_a = 2\pi a \frac{U}{I}$$

At a given location, several measurements of ρ_a are taken at geometrically spaced values of a , such as $a=1, 3, 9, 27, 81$ m or $a=2, 6, 18, 54$ m so that the outer probes from one measurement become the inner probes on the next. When ρ_a is constant with distance, the assumption of a uniform soil model is justified, and the effective resistivity ρ_e for any electrode size is simply ρ_a . However, in many cases, there are two or more layers of contrasting soil. The most difficult case tends to be a thin conducting top layer (clay, till, sand) over a thick, poorly conducting rock layer ($\rho_1 < \rho_2$). This case will have an increasing value of ρ_a with distance. A simplified interpretation in this case can be given for a practical range of resistivity values: For flat electrodes, the effective resistivity, ρ_e , equals the value of ρ_a observed at a probe spacing of ($a=2s$), where s is the maximum extent (for example the radius of a ring electrode). A Wenner probe separation a equal to the diagonal dimension of the legs of a tower is also appropriate.

12.3 Electrode Dimensions

Four dimensions are relevant for analysis of electrode response under steady-state and transient conditions. In order of decreasing importance, these are:

s — s is the three-dimensional distance from the center of the electrode to its outermost point. For a spheroid in a conducting half-plane, $s = \text{MAX}(a,b)$ where a is the maximum cross-section radius and b is the length in the axis of symmetry. Table 12.1 adapts equations for surface area of a cylinder, spheroid, and box to typical electrodes. Different dimensions dominate the s , g , and A terms, depending on the electrode shape. Table 12.1 shows that the three-dimensional extent s of cylinders and prisms is slightly larger than the s for a prolate spheroid of the same depth. The propagation time $\tau = s/c$, calculated from speed-of-light propagation at $c = 3 \times 10^8$ m/s, is used to estimate transient electrode impedance.

g —The geometric radius of the electrode, $g = (r_x^2 + r_y^2 + r_z^2)^{1/2}$ is used to estimate capacitance. For long, thin, or rectangular shapes, $g = s$; for a disc, $g = \sqrt{2}s$; for a hemisphere, $g = \sqrt{3}s$.

A —The surface area in contact with soil. Electrodes with large surface area will have lower resistance, lower impedance, and less susceptibility to unpredictable effects of soil ionization. For objects with concave features, the area of the smallest convex body that can envelop it is determined. With this model, a tube has the same area as a solid cylinder of the same dimensions. Disk electrodes have two sides. Buried horizontal wires expose area on both sides of the narrow trench. Table 12.1 provides further interpretations.

L —The total length of wire in a wire frame approximation to a three-dimensional solid, L , is used to correct for the contact resistance, typically with $R_{\text{contact}} \leq \rho_1/L$ as described in Laurent (IEEE Std 100). Contact resistance tends to be much smaller than the geometric resistance for most electrodes.

12.4 Self-Capacitance of Electrodes

Electrode capacitance is easily calculated (Chow and Yovanovich, 1982; Chow and Srivastava, 1988) and offers elegant description of grounding response to transients. Also, the self-capacitance C_{self} to infinity of an arbitrary conducting object in full space has a useful dual relation to its steady-state resistance R in a half-space of conducting medium, given by (Weber, 1950):

$$R = \frac{2\epsilon_0\rho}{C_{\text{self}}} \quad (12.1)$$

where ϵ_0 is the permittivity constant, 8.854×10^{-12} F/m and ρ is the earth resistivity, in $\Omega \cdot \text{m}$.

TABLE 12.1 Values of A , s , g , and L for Typical Ground Electrodes in Half-Plane

Geometry	Surface Area, A	Maximum Extent, s	$g = \sqrt{r_x^2 + r_y^2 + r_z^2}$	Wire Frame, L
Vertical cylindrical rod length l , radius r	$2\pi rl + \pi r^2 \approx 2\pi rl$	$\sqrt{l^2 + r^2} \approx l$	$\sqrt{l^2 + r^2 + r^2} \approx l$	∞
Solid cylinder length l , radius r	$2\pi rl + \pi r^2$	$\sqrt{l^2 + r^2}$	$\sqrt{l^2 + 2r^2}$	∞
Buried circular disk at depth h with radius r	$2\pi rh + \pi r^2$	$\sqrt{h^2 + r^2}$	$\sqrt{h^2 + 2r^2}$	∞
Buried circular ring at depth h with radius r				$2\pi r$
Circular disc on surface thickness t , radius r	$2\pi rt + \pi r^2 \approx \pi r^2$	$\sqrt{t^2 + r^2} \approx r$	$\sqrt{t^2 + 2r^2} \approx \sqrt{2}r$	∞
Oblate (disk-like) half spheroid radius $a >$ thickness b , $\varepsilon = \sqrt{1 - b^2/a^2}$	$\pi a^2 + \frac{\pi b^2}{2\varepsilon} \ln\left(\frac{1+\varepsilon}{1-\varepsilon}\right)$	a	$\sqrt{2a^2 + b^2}$	∞
Hemisphere of radius r	$2\pi r^2$	r	$\sqrt{3}r$	∞
prolate (tube-like) half spheroid radius $a <$ length b , $\varepsilon = \sqrt{1 - a^2/b^2}$	$\pi a^2 + \frac{\pi ab}{\varepsilon} \sin^{-1}(\varepsilon)$	b	$\sqrt{2a^2 + b^2}$	∞
Vertical solid plate, l long, w wide, and t thick	$wt + 2(t+w)l \approx 2lw$	$s = g = \sqrt{t^2/4 + w^2/4 + l^2}$		∞
Two or more vertical rods in straight line of length l , driven to depth h , rod thickness w	$lw + 2(l+w)h \approx 2lh$	$s = g = \sqrt{\frac{l^2}{4} + \frac{w^2}{4} + h^2}$		nh , $n = \#$ of rods
Buried counterpoise of length l at depth h , wire diameter w				$h + l$
Conducting box l long by w wide at depth h	$lw + 2(l+w)h$			∞
Buried rectangle plate, l long by w wide at depth h				∞
Buried rectangular grid l long by w wide at depth h				$nl + mw$ where $n, m = \#$ of grids
Buried rectangular loop l long by w wide at depth h				$h + 2(l+w)$
Four wires from center to corners of rectangle, l long by w wide at depth h				$h + 2\sqrt{w^2 + l^2}$
Four vertical rods on corners of rectangle, l long by w wide by h deep				$4h$
Surface plate, l long by w wide by t thick	$lw + 2(l+w)t \approx lw$	$s = g = \sqrt{l^2/4 + w^2/4 + t^2}$		∞

The transient impedance of the same arbitrary conducting object can be modeled using the time (τ) it takes to charge up its self-capacitance C_{self} . This time cannot be less than the maximum dimension of the electrode, s , divided by the speed of light. An average surge impedance Z , given by the ratio τ/C , can then be used to relate voltages and currents during any initial surge. The capacitance of an object is approximately (Chow and Yovanovich, 1982)

$$C_{\text{self}} = \epsilon_0 c_f \sqrt{4\pi A} \quad (12.2)$$

where A is the total surface area of the object, including both sides of disk-like objects, c_f is a correction factor between the capacitance of the object and the capacitance of a sphere with the same surface area. For a wide range of objects, $0.9 < c_f < 1.2$ using $c_f \approx \sqrt{2\gamma}/\ln(4\gamma)$ where γ is the ratio of length to width of the object.

A close estimate of c_f for spheroids is given by the following expression:

$$c_f = \frac{4\pi g}{\sqrt{4\pi A \ln\left(\frac{4\pi e^{\sqrt{3}} g^2}{3A}\right)}} \approx \frac{3.54 g}{\sqrt{A} \ln\left(\frac{23.7 g^2}{A}\right)} \quad (12.3)$$

Again, $g = \sqrt{r_x^2 + r_y^2 + r_z^2}$, the geometric radius. Equation (12.3) is exact for a sphere, and remains valid for a wide range of electrode shapes, from disk to rod.

A surprisingly large amount of the surface area of a solid can be removed without materially affecting its self-capacitance. For example, the capacitance of a solid box of dimensions $1 \times 1 \times 0.4$ m and a surface area of 3.6 m^2 is 56 pF. The capacitance of two parallel loops filling out the same space is 50 pF, even though the loops have only 20% of the surface area of the box (Chow and Srivastava, 1988). The equivalent correction from wire frame approximations to solid objects in ground resistance calculations is known as a “contact resistance.”

12.5 Initial Transient Response from Capacitance

Once the capacitance of a conducting electrode and its minimum charging time τ have been estimated, its average transient impedance can be computed from the relation $Z = \tau/C_{\text{self}}$ obtained from the use of open-circuit stub transmission lines for tuning radio antennas. The charging time τ of the conducting electrode in free space is the maximum three-dimensional extent s , divided by the velocity of light in free space, c . This transient impedance of the ground electrode will be seen only during the charging time from the center of the electrode to its full extent, and the impedance will reduce with increasing time as the electromagnetic fields start to interact with the surroundings, including soil, towers, and overhead groundwires.

The following graph (Fig. 12.2) gives the initial transient response of conducting spheroid electrodes. The main observation from Fig. 12.2 is that wide, flat electrodes will have inherently better initial transient response than long, thin electrodes. This includes electrodes in both horizontal and vertical planes, giving a physical reason why long leads to remote ground electrodes are not effective under transient conditions.

Chisholm and Janischewskyj (1989) confirmed an initial transient impedance of about 60Ω for a perfectly conducting ground plane (infinite circular disk) that reduced as a function of time, with a rate of reduction depending on the electromagnetic travel time from tower top to tower base. For compact electrodes, the response can be lumped into an inductance element ($L_{\text{self}} = \tau^2/C_{\text{self}}$). The potential rise on the earth electrode can then be estimated from the simple circuit model:

$$U_{\text{electrode}} = RI + \left(\frac{\tau^2}{C_{\text{self}}}\right) \frac{dI}{dt} \quad (12.4)$$

A numerical example for Eq. (12.4) is useful. For $\rho = 100 \Omega\text{m}$, and a disk electrode of 5 m radius, the resistance to remote ground will be 3.2Ω and $\tau^2/C_{\text{self}} = 0.8 \mu\text{H}$. For a typical (median) lightning stroke with $I = 30 \text{ kA}$ and $dI/dt = 24 \text{ kA}/\mu\text{s}$ at the peak, the two terms of the peak potential rise will be

$$(30 \text{ kA})(3.2 \Omega) + (24 \text{ kA}/\mu\text{s})(0.8 \mu\text{H}) = 96 \text{ kV} + 19 \text{ kV}.$$

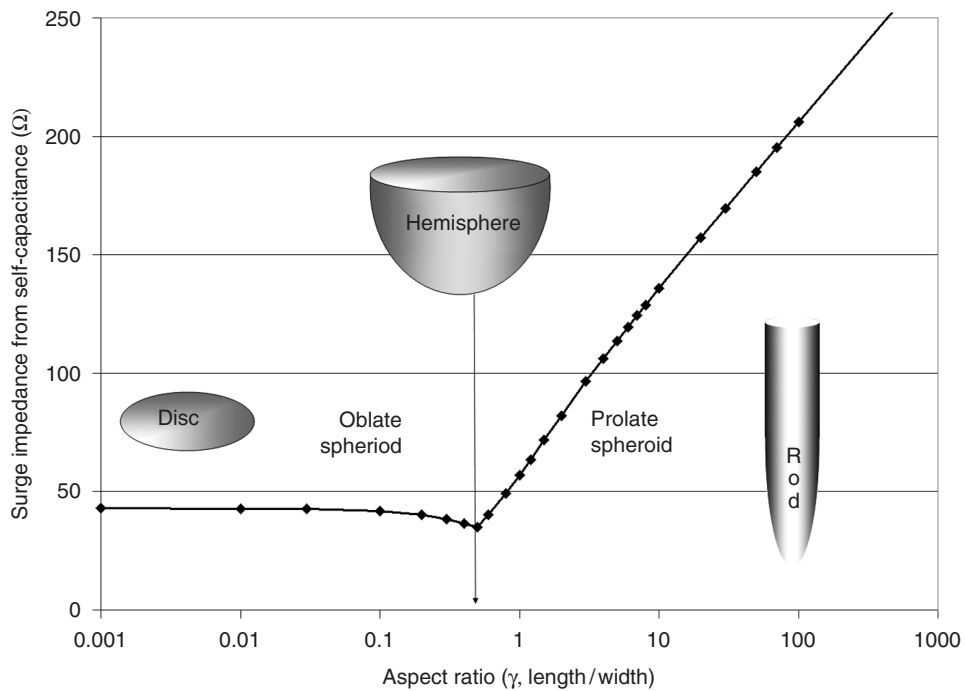


FIGURE 12.2 Relation between transient impedance and aspect ratio: spheroid electrodes in half space.

The inductive term is desirably low in the example, but it can dominate the response of long, thin electrodes as shown in Table 12.2. For distributed electrodes, however, the circuit approximation in Eq. (12.4) eventually fails as rate of current rise (dI/dt) increases and surge impedance models must be used as developed next.

12.6 Ground Electrode Impedance: Wire over Perfect Ground

The inductance L per unit length of a distributed grounding connection over a conducting plane can be calculated from the surge impedance Z of the wire and its travel time τ :

$$L = Z\tau = \left(\frac{\tau^2}{C_{\text{self}}} \right) \quad Z = 60 \ln\left(\frac{2h}{r}\right) \quad (12.5)$$

where Z is the surge impedance (Ω) of a wire of radius r over a ground plane at a height h , $\tau = s/c$, the wire length or electrode extent (m) divided by the speed of light (3.0×10^8 m/s).

TABLE 12.2 Transient Impedance of Conducting Electrodes

Shape	Surface Area	3-D Extent, s	Capacitance (Equation 12.2)	Travel Time	Transient Impedance
Circular disc	$2\pi s^2$	s	$0.9\pi\epsilon s\sqrt{8}$	s/c	47Ω
Hemisphere	$3\pi s^2$	s	$1.0\pi\epsilon s\sqrt{12}$	s/c	35Ω
Long cylinder	$2\pi rs$	s	$3.3\pi\epsilon\sqrt{4rs}$ $7.8\pi\epsilon\sqrt{4rs}$ $20\pi\epsilon\sqrt{4rs}$	s/c $s/r = 100: 210 \Omega$ $s/r = 1000: 270 \Omega$ $s/r = 10000: 340 \Omega$	

12.7 Ground Electrode Impedance: Wire over Imperfect Ground

When the electrode is placed over imperfect ground, the effective return depth of current will increase. Bewley (1963) suggests that the plane for image currents, in his tests of buried horizontal wires, was 61 m (200') below the earth surface. Some analytical indication of the increase in return depth is given by the normal skin depth, $\delta = 1/\sqrt{\pi f \mu_0 / \rho}$, which decreases from 460 m (60 Hz) to 11 m (100 kHz) for resistivity of $\rho = 50 \Omega \text{ m}$. Deri et al. (1981) propose a more complete approach, replacing the height h in Eq. (12.5) with $(h + p)$ where with the depth p to an equivalent perfectly conducting plane is a complex number given by

$$p = \sqrt{\frac{\rho}{j\omega\mu_0}} \quad (12.6)$$

where ω is 2π times the frequency (Hz), μ_0 is $4\pi \times 10^{-7} \text{ H/m}$, and ρ is the resistivity in $\Omega \text{ m}$.

For good soil with a resistivity of $\rho = 50 \Omega \text{ m}$, the complex depth is $230(1-j)$ m at 60 Hz and $5.6(1-j)$ m at 100 kHz. The complex depth is related to the normal skin depth by the relation $1/p = (1+j)1/\delta$. The velocity of propagation will also reduce as the wire is brought close to, or buried in, imperfectly conducting ground.

12.8 Analytical Treatment of Complex Electrode Shapes

Simple analytical expressions are documented for a variety of regular electrode shapes, (see, e.g., Smythe, 1950; Weber, 1950; Keller and Frischknecht, 1982; Sunde, 1949). However, grounding of electrical systems often exists of several interconnected components, making estimation of footing resistance more difficult. The tower foundation can be a single or (more typically) four concrete cylinders, often reinforced with steel. In the preferred case, the steel is bonded electrically, and a grounding connection is brought out of the form before the concrete is poured. In areas with low soil resistivity, four concrete footings can often provide a low tower resistance without supplemental electrodes.

In some cases on both transmission and distribution systems, a metal grillage (or pole butt-wrap) is installed at the base after excavation. This deep electrode is more effective than a surface electrode of the same area. Also, grillage and pole-wrap electrodes are protected from vandalism and frost damage.

Supplemental grounding electrodes are often installed during line construction or upgrade. The following approaches are used:

- Horizontal conductors are bonded to the tower, then buried at a practical depth.
- Vertical rods are driven into the soil at some distance from the tower, then bonded to the tower base, again using bare wires, buried at a practical depth.
- Supplemental guy wires are added to the tower (often for higher mechanical rating) and then grounded using rock or soil anchors at some distance away.

Supplemental grounding should be considered to have a finite lifetime of 5 to 20 years, especially in areas where the soil freezes in winter. Also, auxiliary electrodes such as rock anchors should be designed to carry their share of impulse current and to withstand the associated traverse forces.

The resistance of an electrode that envelops all contacts can be used to obtain a good estimate of the combined resistance of a complex, interconnected electrode. From Chisholm and Janischewskyj (1989), the resistance of a solid rectangular electrode is approximately

$$R_{\text{Geometric}} = \frac{\rho}{2\pi s} \ln\left(\frac{2\pi es^2}{A}\right) \cong \frac{\rho}{2\pi s} \ln\left(\frac{17s^2}{A}\right) \quad (12.7)$$

where

s is the three-dimensional distance from the center to the furthest point on the electrode

A is the convex surface area that would be exposed if the electrode were excavated

e is the exponential constant, 2.718

The resistance can also be estimated using the geometric radius g rather than the maximum dimension s :

$$R_{\text{Geometric}} \cong \frac{\rho}{2\pi g} \ln\left(\frac{11.8g^2}{A}\right) \quad (12.8)$$

where

$g = \sqrt{r_x^2 + r_y^2 + r_z^2}$ the geometric radius of the electrode

$r_{x,y,z}$ = maximum x , y , and z dimensions

$11.8 = (2\pi e^{\sqrt{3}})/3$

If the electrode is a wire frame, rather than a solid, then a correction for contact resistance should be added to the geometric resistance:

$$R_{\text{Wire Frame}} = R_{\text{Geometric}} + R_{\text{Contact}} = R_{\text{Geometric}} + K \frac{\rho_1}{L} \quad (12.9)$$

where

L is the total length of the wire frame

ρ_1 is the resistivity of the upper layer of soil (the layer next to the wire)

K is a constant that varies from $0.5 \leq K \leq 1.3$ for most electrode shapes, depending on fill ratio

Many examples of contact resistance can be found in the literature on grounding (e.g., Sunde, 1949; IEEE Std 80/1986). Consider for example the resistance of a surface disk of radius s compared to a ring of the same radius, made from wire with a diameter d :

$$\begin{aligned} R_{\text{Disc}} &= \frac{\rho}{4s}; \quad R_{\text{Ring}} = \frac{\rho}{2\pi^2 s} \ln\left(\frac{4s}{d}\right) \\ g &= \sqrt{s^2 + s^2 + d^2} \approx \sqrt{2}s; \quad A = \pi s^2; \quad R_{\text{Geometric}} = \frac{\rho}{2\pi g} \ln\left(\frac{11.8g^2}{A}\right) = \frac{\rho}{4.4s} \\ R_{\text{Contact}} &= R_{\text{Ring}} - R_{\text{Disk}} \end{aligned} \quad (12.10)$$

The difference between the resistance of a ring of $d=13$ mm wire and a disk of the same radius s can be described using a value of K in Eq. (12.9) that ranges from $K=0.48$ for $s=2$ m, to $K=0.99$ for $s=10$ m ring, to $K=1.33$ for $s=30$ m, depending on the logarithm of the ratio of overall to wire surface areas.

12.9 Numerical Treatment of Complex Electrode Shapes

Solving for the combined resistance of a number of individual electrode elements, such as four foundations of a transmission tower along with some horizontal wires and ground rods, can take several approaches.

The geometric resistance of the entire electrode can be computed and the contact resistance correction for a wire frame approximation can be added as in Eq. (12.9). However, in some cases such as solid cylinders of concrete, the “length” of wire to use is not obvious, and also, the value of K varies depending on whether the electrode is horizontal or vertical.

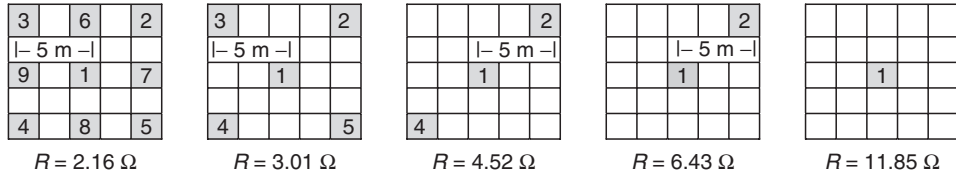


FIGURE 12.3 Numerical solutions of resistance for 10-m rods at 5-m grid spacing. (IEEE Guide 80.)

A second possibility is to develop a matrix of self- and mutual-resistance values of each solid, conducting element. The geometric resistances defined in Eq. (12.8) give the self-resistance R_{ij} . The mutual resistance between the centroids of two objects is calculated from their separation d_{ij} :

$$R_{ij} = \frac{\rho}{2\pi d_{ij}} \quad (12.11)$$

A symmetrical matrix of self- and mutual-resistances is multiplied by a vector of current values to obtain the potentials at each electrode. The matrix can be built, inverted, and solved in Excel™ as follows.

In our case, we will consider five, 3-m long rods of 5-mm radius in $\rho = 320 \Omega \text{ m}$ soil, on a 5×5 m grid as shown in Fig. 12.3. The self-resistance is calculated from $g = 10 \text{ m}$, $A = 2\pi rl = 0.4 \text{ m}^2$ in Eq. (12.8) as 119Ω . The distance between the center rod and all others is $d_{1j} = 7.07 \text{ m}$, $d_{23} = d_{34} = d_{45} = d_{25} = 10 \text{ m}$ and $d_{24} = d_{35} = 14.1 \text{ m}$. The mutual resistances are given by $R_{ij} = \rho / (2\pi d_{ij})$ from Eq. (12.11) as follows.

Distance, d_{ij} (m)					Resistances, R_{ij} (Ω) ($\rho = 320 \Omega \text{ m}$)				
0.01	7.07	7.07	7.07	7.07	119.30	7.20	7.20	7.20	7.20
7.07	0.01	10.00	14.14	10.00	7.20	119.30	5.09	3.60	5.09
7.07	10.00	0.01	10.00	14.14	7.20	5.09	119.30	5.09	3.60
7.07	14.14	10.00	0.01	10.00	7.20	3.60	5.09	119.30	5.09
7.07	10.00	14.14	10.00	0.01	7.20	5.09	3.60	5.09	119.30

In Excel™, a square matrix can be inverted by highlighting a blank space of the same size (5×5 cells in this case), typing in the formula = MINVERSE(A1:E5) where the original R_{ij} matrix resides in cells A1:E5 and pressing the F2 key, then <Ctrl><Shift><Enter> at the same time.

The inverted matrix can be multiplied by a vector of unit potentials (1s) to obtain the currents in each electrode. The unit potential divided by the sum of these currents gives the resistance of the combined electrode, including self and mutual effects. The following table completes the numerical example.

Inverse of R_{ij} Matrix ($\times 1000$)					Potential	Current = MMULT([R_{ij}], V_i)
8.49	-0.46	-0.46	-0.46	-0.46	1 V	6.65 mA
-0.46	8.44	-0.31	-0.20	-0.31	1 V	7.15 mA
-0.46	-0.31	8.44	-0.31	-0.20	1 V	7.15 mA
-0.46	-0.20	-0.31	8.44	-0.31	1 V	7.15 mA
-0.46	-0.31	-0.20	-0.31	8.44	1 V	7.15 mA
					Sum	35.27 mA $1/.03527 = 28.4 \Omega$

To multiply the inverted resistance matrix (say in locations A10:E15) by a vector of unit potentials (say in locations G10:G15), the cells I10:I15 would be highlighted, the formula = MMULT(A10:E15,

G10:G15) would be entered, the *F2* key would be pressed then *<Ctrl><Shift><Enter>* pressed at the same time.

The currents are summed to a total of 35.27 mA, giving a resistance of 28.4 Ω . The five resistances in parallel, ignoring mutual effects, would have a resistance of 23.9 Ω , so the effect at a separation of 5 m is still significant.

A series of numerical calculations are found for a similar set of electrodes in (IEEE Guide 80/2000, p. 183), 10-m rods on 5-m grid spacing in 100- Ω m soil.

The relative reduction in resistance is largest when the second electrode is added, and additional nearby rods are seen to be less effective.

12.10 Treatment of Multilayer Soil Effects

Generally, the treatment of footing resistance in lightning calculations considers a homogeneous soil with a finite conductivity. This treatment, however, seldom matches field observations, particularly in areas where grounding is difficult. Under these conditions, a thin “overburden” layer of conducting clay, till, or gravel often rests on top of insulating rock. The distribution of resistivity values for a particular overburden material and condition can be narrow, with standard deviations usually less than 10%. However, the variation of overburden depth with distance can be large. Airborne electromagnetic survey techniques at multiple frequencies in the 10–100 kHz range offer an inexpensive new method of reconnaissance of the overburden parameters of resistivity and depth.

Once a resistivity survey has established an upper-layer resistivity ρ_1 , a layer depth d , and a lower-layer resistivity ρ_2 , the equivalent resistivity ρ_e can be computed. For a disk-like electrode buried just below the surface, ρ_e from the elliptic-integral solutions of Zaborsky (1955) can be approximated with better than 5% accuracy by the following empirical equations:

$$\rho_e = \rho_1 \frac{1 + C \frac{\rho_2}{\rho_1} \frac{r}{d}}{1 + C \frac{r}{d}}$$

$$C = \begin{cases} \rho_1 \geq \rho_2, & \frac{1}{1.4 + \left(\frac{\rho_2}{\rho_1}\right)^{0.8}} \\ \rho_1 < \rho_2, & \frac{1}{1.4 + \left(\frac{\rho_2}{\rho_1}\right)^{0.8} + \left(\frac{\rho_2}{\rho_1} \frac{r}{d}\right)^{0.5}} \end{cases} \quad (12.12)$$

The ratio of effective resistivity to upper-layer resistivity varies with the ratio of electrode radius s to upper-layer depth d , with a small ratio of s/d giving a ratio of unity as shown in Fig. 12.4.

Normally, electrode penetration through an upper layer would only be desirable in extreme examples of Case 1 ($\rho_1 \gg \rho_2$). Rather than recomputing the effective resistivity with revised image locations, the effects of the upper layer can be neglected, with the connection through ρ_1 providing only series self-inductance.

12.11 Layer of Finite Thickness over Insulator

A simpler two-layer soil treatment is appropriate for Case 2 when $\rho_2 \gg \rho_1$, or equivalently the reflection coefficient from upper to lower layer Γ_{12} approaches 1. Under these conditions, the following summation in Eq. (12.13) (e.g., Keller and Frischknecht, 1982) describes the resistance of a single hemisphere of radius s in a finitely conducting slab with resistivity ρ_1 and thickness d :

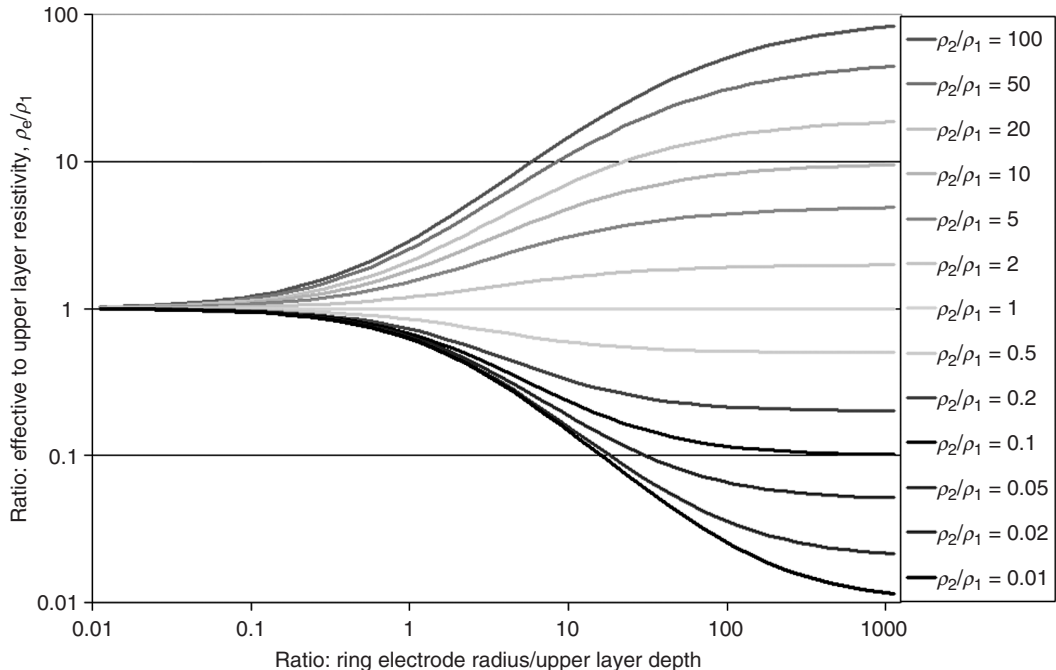


FIGURE 12.4 Relative effective resistivity vs. ratio of electrode radius to upper layer depth, with resistivity ratio as a parameter.

$$\Gamma_{12} = \frac{\rho_2 - \rho_1}{\rho_2 + \rho_1} \approx 1 \quad \text{for } \rho_2 \gg \rho_1 \quad R_{\text{Keller}} = \frac{\rho_1}{2\pi s} \left(1 + 2 \sum_{n=1}^{\infty} \frac{\Gamma_{12}^n}{\sqrt{1 + \left(\frac{2nd}{s}\right)^2}} \right)$$

$$R_{\text{Loyka}} \approx \frac{\rho_1}{2\pi s} \left[1 + \frac{s}{d} \ln \left(\frac{1 + \sqrt{1 + \left(\frac{10^5 d}{2d}\right)^2}}{1 + \sqrt{1 + \left(\frac{s}{2d}\right)^2}} \right) \right] \approx \frac{\rho_1}{2\pi s} \left[1 + \frac{s}{d} \ln \left(\frac{50,000}{1 + \sqrt{1 + \left(\frac{s}{2d}\right)^2}} \right) \right] \quad (12.13)$$

For a reflection coefficient $\Gamma_{12}=1$, the Keller series in Eq. (12.13) becomes the harmonic series and converges slowly. Loyka (1999) offers a convenient approximation to the sum, developed using the potential from a second hemisphere, located sufficiently far away (e.g., $10^5 d$, where d is the layer thickness) to have no influence. Figure 12.5 shows that the Loyka approximation to the Keller series is good for a wide range of transmission line grounding applications, and that finite upper layer depth has a strong influence on the resistance of the electrodes.

12.12 Treatment of Soil Ionization

Under high electric fields, air will ionize and become effectively a conductor. The transient electric fields needed to ionize air in small volumes of soil, or to flashover across the soil surface, are typically between 100 and 1000 kV/m (Korsuncev, 1958; Liew and Darveniza, 1974; Oettle, 1988). Considering that the potential rise on a small ground electrode can reach 1 MV, the origins of 10-m furrows around small (inadequate) ground electrodes after lightning strikes become clear. Surface arcing activity is unpredictable and may

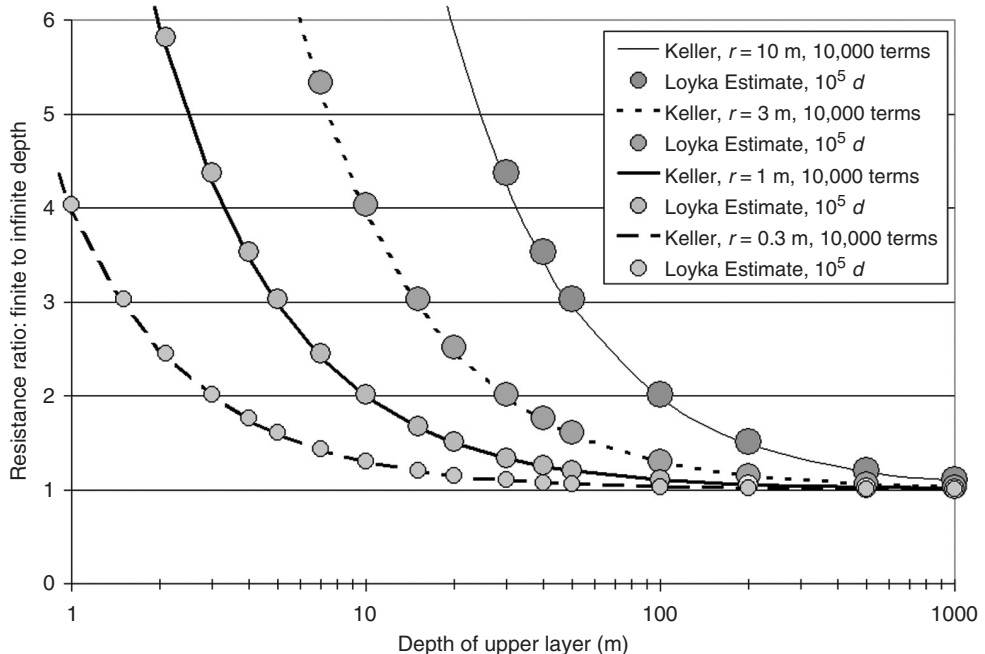


FIGURE 12.5 Asymptotic behavior of hemispherical electrode in conducting layer over insulator.

transfer lightning surge currents to unprotected facilities. Thus, power system ground electrodes for lightning protection should have sufficient area and multiplicity to limit ionization.

Korsuncev used similarity analysis to relate dimensionless ratios of s , ρ , resistance R , current I , and critical breakdown gradient E_o as follows:

$$\Pi_1 = \frac{Rs}{\rho} \quad \text{with } \Pi_1^0 = \frac{1}{2\pi} \ln\left(\frac{2\pi es^2}{A}\right) \quad (12.14)$$

$$\Pi_2 = \frac{\rho I}{E_o s^2} \quad (12.15)$$

$$\Pi_1 = \text{MIN}(\Pi_1^0, 0.26 \cdot \Pi_2^{-0.31}) \quad (12.16)$$

$$R = \frac{\rho \Pi_1}{s} \quad (12.17)$$

where

s is the three-dimensional distance from the center to the furthest point on the electrode, m

I is the electrode current, A

ρ is the resistivity, Ω m

E_o is the critical breakdown gradient of the soil, usually 300–1000 kV/m

R is the resistance of the ground electrode under ionized conditions

The calculation of ionized electrode resistance proceeds as follows:

- A value of Π_1^0 is calculated from Eq. (12.14). This un-ionized value will range from $\Pi_1^0 = 0.159$ (for a hemisphere) to 1.07 for a 3-m long, 0.01-m radius cylinder.
- A value of Π_2 is calculated from Eq. (12.15). For a 3-m rod at 100 kA in 100 Ω m soil, with $E_o = 300$ kV/m, the value of $\Pi_2 = 3.7$ is obtained.

- A value of Π_1 is computed from Π_2 using $0.26 \Pi_2^{-0.31}$. This value, from Eq. (12.16), represents the fully ionized sphere with the gradient of E_o at the injected current; for the rod example, $\Pi_1 = 0.173$.
- If the ionized value of Π_1 is not greater than Π_1^0 , then there is not enough current to ionize the footing, so the un-ionized resistance from Π_1^0 will be seen for the calculation of resistance in Eq. (12.17). For the 3-m rod, ionization reduces the low-current resistance of 36 to 6Ω at 100 kA.

In two-layer soils with sparse electrodes, ionization effects will tend to reduce the contact resistance [from Eq. (12.9)] without altering the surface area A or characteristic dimension s . This will tend to reduce the influence of ionization, since the geometric resistance of the electrode is unchanged.

12.13 Design Process

The inputs to the design process are the prospective lightning surge current, the local soil resistivity, and the dimensions of the tower base or trial electrode. The low-frequency geometric resistance of the electrode is computed from Eq. (12.8) and double-checked with the estimate from Eqs. (12.14) and (12.17).

If the electrode is compact (for example a driven rod) then the ionization effects should be estimated using Eqs. (12.15) and (12.16), with the reduced resistance under high-current conditions being given by Eq. (12.17).

If the electrode is distributed (for example a buried wire) then the ionized resistance will only reduce the contact resistance term in Eq. (12.9), and for practical purposes it will be sufficient to disregard this term and consider only the geometric resistance from Eq. (12.8).

In each case, an apparent transient impedance of the ground electrode should be modeled as an equivalent inductance in series with the resistive rise associated with the geometric resistance.

The fraction of surge current absorbed by a given electrode will change as its size is adjusted, making the design process iterative.

12.14 Design Recommendations

It is prudent where possible to select an electrode size that does not rely on ionization for adequate transient performance. This can be achieved by inverting the design process as follows:

- Establish Π_1^0 , the shape coefficient of the electrode (0.16 for a hemisphere, 0.26 for a cube, 0.27 for a disk).
- Establish the value of Π_2^0 that will just cause ionization (Chisholm and Janischewskyj, 1989), inverting Eq. (12.16) to obtain

$$\Pi_2^0 = 0.0131 (\Pi_1^0)^{-3.24} \quad (12.18)$$

- For the example of a disc electrode, the value of $\Pi_2^0 = 0.92$ is obtained.
- The extent (in this case radius) of the electrode s needed to prevent ionization in soil of resistivity ρ in $\Omega \text{ m}$ with current I in kA and voltage gradient E_o in kV/m is given by

$$s = \sqrt{\frac{\rho I}{E_o \Pi_2^0}} \quad (12.19)$$

- For $\rho = 300 \Omega \text{ m}$, $I = 30 \text{ kA}$, and E_o of 400 kV/m a disk or ring radius of $s = 9.1 \text{ m}$ will be sufficient to prevent ionization. The geometric resistance of this electrode from Eq. (12.17) is 8.9Ω .

The following advice is especially relevant for transmission towers or other tall structures, where a low-impedance ground is needed to limit lightning-transient overvoltages.

- Choose a wide, flat electrode shape rather than a long, thin shape. Four radial counterpoise wires of 60 m will be two to eight times more effective than a single counterpoise of 240 m under lightning surge conditions.
- Take advantage of natural elements in the structure grounding, such as foundations and guy anchors, by planning for electrical connections and by extending radial wires outward from these points.
- In rocky areas, use modern airborne techniques to survey resistivity and layer depth using several frequencies up to 100 kHz. Place towers where conductive covering material is deep.
- Provide grounding staff with the tools and techniques to pre-estimate the amount of wire required for target footing impedance values, using simple interpretation of two-layer soil data.
- Near areas where transferred lightning potentials could be dangerous to adjacent objects or systems, use sufficient electrode dimensions to limit ionization, that is, to remain on the Π_1^0 characteristic.

References

- ANSI/IEEE Std 80-1986, *IEEE Guide for Safety in Substation Grounding*, IEEE Press, Piscataway, NJ, 1986.
- ANSI/IEEE Std 80-2000, *IEEE Guide for Safety in Substation Grounding*, IEEE Press, Piscataway, NJ, 2000.
- Bewley, L.V., *Traveling Waves on Transmission Systems*, Dover, New York, 1963.
- Chisholm, W.A. and Janischewskyj, W., Lightning surge response of ground electrodes, *IEEE Trans. Power Delivery*, 4(2), April 1989.
- Chow, Y.L. and Yovanovich, M.M., The shape factor of the capacitance of a conductor, *J. Appl. Phys.*, 52, December 1982.
- Chow, Y.L. and Srivastava, K.D., Non-uniform electric field induced voltage calculations, Final Report for Canadian Electrical Association Contract 117 T 317, February 1988.
- Deri, A., Tevan, G., Semlyen, A. and Castanheira, A., The complex ground return plane—a simplified model for homogeneous and multilayer earth return, *IEEE Trans. Power Apparatus Systems*, PAS-100(8), August 1981.
- IEEE Standard 100, *The Authoritative Dictionary of IEEE Standard Terms*, 7th ed., IEEE, Piscataway, NJ, 2000.
- IEEE Standard 80-2000, *IEEE Guide for Safety in AC Substation Grounding*, IEEE, Piscataway, NJ, 2000.
- Keller, G.G. and Frischknecht, F.C., *Electrical Methods in Geophysical Prospecting*, Pergamon, New York, 1982.
- Korsuncev, A.V., Application on the theory of similarity to calculation of impulse characteristics of concentrated electrodes, *Elektrichestvo*, 5, 1958.
- Liew, A.C. and Darveniza, M., Dynamic model of impulse characteristics of concentrated earths, *IEE Proc.*, 121(2), Feb. 1974.
- Loyka, S.L., A simple formula for the ground resistance calculation, *IEEE Trans. EMC*, 41(2), 152–154, May 1999.
- Oettle, E.E., A new general estimation curve for predicting the impulse impedance of concentrated earth electrodes, *IEEE Trans. Power Delivery*, 3(4), October 1988.
- Smythe, W.R., *Static and Dynamic Electricity*, McGraw-Hill, New York, 1950.
- Sunde, E.D., *Earth Conduction Effects in Transmission Systems*, Van Nostrand, Toronto, 1949.
- Visacro, S. and Portela, C.M., Soil permittivity and conductivity behavior on frequency range of transient phenomena in electric power systems, in *Proceedings of 5th ISH*, Paper 93.06, August 1987.
- Weber, E., *Electromagnetic Fields Theory and Applications Volume 1—Mapping of Fields*, Wiley, New York, 1950.
- Zaborsky, J., Efficiency of grounding grids with nonuniform soil, *AIEE Trans.*, 1230–1233, December 1955.

Appendix A Relevant IEEE Grounding Standards

ANSI/IEEE Std 80-1986: IEEE Guide for Safety in AC Substation Grounding

Presents essential guidelines for assuring safety through proper grounding at AC substations at all voltage levels. Provides design criteria to establish safe limits for potential differences within a station, under fault conditions, between possible points of contact. Uses a step-by-step format to describe test methods, design and testing of grounding systems. Provides English translations of three fundamental papers on grounding by Rudenberg, Laurent, and Zeitschrift that are not available in Std 80-2000.

ANSI/IEEE Std 80-2000: IEEE Guide for Safety in AC Substation Grounding

Provides an improved methodology for interpreting two-layer soil resistivity and using the values in the design of AC substations. Provides methods for determining the maximum grid current at substations, some of which also predict the maximum fault currents available on lines close by. Provides a number of new worked-examples in appendices.

IEEE Std 81-1983: IEEE Guide for Measuring Earth Resistivity, Ground Impedance, and Earth Surface Potentials of a Ground System

The present state of the technique of measuring ground resistance and impedance, earth resistivity, and potential gradients from currents in the earth, and the prediction of the magnitude of ground resistance and potential gradients from scale-model tests are described and discussed. Factors influencing the choice of instruments and the techniques for various types of measurements are covered. These include the purpose of the measurement, the accuracy required, the type of instruments available, possible sources of error, and the nature of the ground or grounding system under test. The intent is to assist the engineer or technician in obtaining and interpreting accurate, reliable data. The test procedures described promote the safety of personnel and property and prevent interference with the operation of neighboring facilities. The standard is under revision as of September 2005.

IEEE Std 81.2-1991: IEEE Guide for Measurement of Impedance and Safety Characteristics of Large, Extended, or Interconnected Grounding Systems

Practical instrumentation methods are presented for measuring the AC characteristics of large, extended, or interconnected grounding systems. Measurements of impedance to remote earth, step and touch potentials, and current distributions are covered for grounding systems ranging in complexity from small grids (less than 900 m²) with only a few connected overhead or direct-burial bare concentric neutrals, to large grids (greater than 20,000 m²) with many connected neutrals, overhead ground wires (sky wires), counterpoises, grid tie conductors, cable shields, and metallic pipes. This standard addresses measurement safety; earth-return mutual errors; low-current measurements; power-system staged faults; communication and control cable transfer impedance; current distribution (current splits) in the grounding system; step, touch, mesh, and profile measurements; the foot-equivalent electrode earth resistance; and instrumentation characteristics and limitations.

IEEE Std 367-1996: IEEE Recommended Practice for Determining the Electric Power Station Ground Potential Rise and Induced Voltage from a Power Fault

Information for the determination of the appropriate values of fault-produced power station ground potential rise (GPR) and induction for use in the design of protection systems is provided. Included are the determination of the appropriate value of fault current to be used in the GPR calculation; taking into account the waveform, probability, and duration of the fault current; the determination of inducing

currents, the mutual impedance between power and telephone facilities, and shield factors; the vectorial summation of GPR and induction; considerations regarding the power station GPR zone of influence; and communications channel time requirements for noninterruptible services. Guidance for the calculation of power station GPR and longitudinal induction (LI) voltages is provided, as well as guidance for their appropriate reduction from worst-case values, for use in metallic telecommunication protection design.

IEEE Std 524a-1993: IEEE Guide to Grounding During the Installation of Overhead Transmission Line Conductors—Supplement to IEEE Guide to the Installation of Overhead Transmission Line Conductors

General recommendations for the selection of methods and equipment found to be effective and practical for grounding during the stringing of overhead transmission line conductors and overhead ground wires are provided. The guide is directed to transmission voltages only. The aim is to present in one document sufficient details of present day grounding practices and equipment used in effective grounding and to provide electrical theory and considerations necessary to safeguard personnel during the stringing operations of transmission lines.

IEEE Std 789-1988 (R1994): IEEE Standard Performance Requirements for Communications and Control Cables for Application in High-Voltage Environments

Requirements are set forth for wires and cables used principally for power system communications and control purposes that are located within electric power stations, installed within the zone of influence of the power station GPR, or buried adjacent to electric power transmission and distribution lines. The cables can be subjected to high voltages either by conduction or induction coupling, or both. Cable specifications that ensure overall reliability in high-voltage environments are provided. Environmental considerations, operating service conditions, installation practices, and cable-design requirements are covered. Design tests, routine production tests, and physical and electrical tests are included.

IEEE Std 837-1989 (R1996): IEEE Standard for Qualifying Permanent Connections Used in Substation Grounding

Directions and methods for qualifying permanent connections used for substation grounding are provided. Particular attention is given to the connectors used within the grid system, connectors used to join ground leads to the grid system, and connectors used to join the ground leads to equipment and structures. The purpose is to give assurance to the user that connectors meeting the requirements of this standard will perform in a satisfactory manner over the lifetime of the installation provided, that the proper connectors are selected for the application, and that they are installed correctly. Parameters for testing grounding connections on aluminum, copper, steel, copper-clad steel, galvanized steel, stainless steel, and stainless-clad steel are addressed. Performance criteria are established, test procedures are provided, and mechanical, current-temperature cycling, freeze-thaw, corrosion, and fault-current tests are specified.

IEEE Std 1048-1990: IEEE Guide for Protective Grounding of Power Lines

Guidelines are provided for safe protective grounding methods for persons engaged in de-energized overhead transmission and distribution line maintenance. They comprise state-of-the-art information on protective grounding as currently practiced by power utilities in North America. The principles of protective grounding are discussed. Grounding practices and equipment, power-line construction, and ground electrodes are covered.

IEEE Std 1050-1996: IEEE Guide for Instrumentation and Control Equipment Grounding in Generating Stations

Information about grounding methods for generating station instrumentation and control (I & C) equipment is provided. The identification of I & C equipment grounding methods to achieve both a suitable level of protection for personnel and equipment is included, as well as suitable noise immunity for signal ground references in generating stations. Both ideal theoretical methods and accepted practices in the electric utility industry are presented.

IEEE Std 1243-1997: IEEE Guide for Improving the Lightning Performance of Transmission Lines

Procedures for evaluating the lightning outage rate of overhead transmission lines at voltage levels of 69 kV or higher are described. Effects of improved insulation, shielding, coupling and grounding on backflashover, and shielding failure rates are then discussed.

IEEE Std 1313.1-1996: IEEE Standard for Insulation Coordination—Definitions, Principles, and Rules

The procedure for selection of the withstand voltages for equipment phase-to-ground and phase-to-phase insulation systems is specified. A list of standard insulation levels, based on the voltage stress to which the equipment is being exposed, is also identified. This standard applies to three-phase AC systems above 1 kV.

IEEE Std 1410-2004: IEEE Guide for Improving the Lightning Performance of Distribution Lines

Procedures for evaluating the lightning outage rate of overhead distribution lines at voltage levels below 69 kV are described. Effects of improved insulation, shielding, coupling and grounding for direct strokes, and induced over-voltage are then discussed.

13

Surge Arresters

13.1	Arrester Types and Auxiliary Equipment.....	13-1
13.2	Ratings and Tests.....	13-3
13.3	Selection by TOV	13-6
13.4	Selection by Energy Rating.....	13-7
13.5	Arrester Modeling	13-8
13.6	Applications	13-11

Thomas E. McDermott
EnerNex Corporation

Surge arresters are shunt, nonlinear resistive devices that are installed to limit transient overvoltages, thereby protecting equipment insulation. Sometimes they have been called “lightning arresters,” and this may be due to the fact that many years ago, surge arresters were tailored to protect against the surge front times typical of lightning. They were much less effective against steeper-fronted overvoltages, or against slow-front switching surges. However, the proper term is “surge arresters,” and the modern generation of metal oxide surge arresters is effective against both lightning and switching surges.

The rest of this chapter summarizes metal oxide surge arrester ratings and application principles, which may suffice for educational purposes. For actual design work, the use of time-domain simulation in an electromagnetic transients program would be highly recommended. The designer should also have access to one of the standard application guides (IEEE C62.22, IEC 60099-5) or the text on insulation coordination by Hileman (1999).

13.1 Arrester Types and Auxiliary Equipment

Nearly 100 years ago, electrode gaps (rod, sphere, or pipe) were used to limit overvoltages on equipment (Sakshaug, 1991). Some of these systems, particularly pipe gaps, may still be in service today. However, the characteristic of gap sparkover voltage vs. surge front time does not match up well with the strength vs. front characteristics of most insulation; that is, it is difficult to coordinate. The next evolutionary step was to add a resistive element in series with the gap, in order to limit the power follow current after an arrester discharge operation. The current limiting would hopefully allow the arrester to clear this power follow current, instead of relying on a nearby breaker or fuse. At the same time, the resistor voltage during a discharge must be low enough that it does not allow an excessive voltage to appear on the protected equipment. These competing requirements led to the use of expensive and complicated nonlinear resistive elements, some involving both solid and liquid materials with high maintenance burdens.

Beginning around 1930, silicon carbide (SiC) was used for the nonlinear resistive elements, leading to much better protective characteristics. Because the SiC would conduct significant current at nominal voltage, it was necessary to provide a sparkover gap that prevents conduction at nominal voltage. After an arrester discharge, these gaps must reseal against the power follow current, otherwise, the arrester

would fail thermally. In the mid 1950s, active gaps were developed for SiC arresters. These active gaps contain auxiliary elements that would

1. pre-ionize the sparkover gap to obtain better surge protective levels and
2. elongate the power follow arc, and move its attachment points, to obtain better interruption performance.

SiC arresters were successfully applied on transmission systems up to 345 kV, but some limitations appeared with regard to switching surge protection, energy discharge capability, and pressure relief capability. Having both gaps and SiC blocks, the arrester height increased to the point where it was difficult to vent the pressure built-up during a fault, which limited the arrester's pressure relief rating. Due to their discharge characteristics vs. frequency or front time, the SiC surge arresters were optimized for lightning. They were less effective for steeper-fronted surges and slow-fronted switching surges.

In the mid 1970s, metal oxide surge arresters were developed into commercial products (Sakshaug, et al., 1977). The metal oxide blocks are much more nonlinear than silicon carbide, so that they conduct only a few milliamperes at nominal AC voltage. It eventually became possible to dispense with gaps completely, although earlier designs made some use of gaps (see Fig. 13.1). Metal oxide surge arresters have several major advantages over the earlier silicon carbide arresters:

1. Active gaps are not necessary, leading to improved reliability
2. Metal oxide can discharge much more energy per unit volume than silicon carbide
3. Metal oxide provides better protection across the range of surge wavefronts than silicon carbide, and in fact, protects effectively against switching surges
4. The decrease in arrester height, caused by eliminating sparkover gaps, leads to higher pressure relief ratings

Virtually all new applications will use metal oxide surge arresters. Metal oxide has enabled some new applications, like series capacitor protection and overhead line switching surge control that were not possible with silicon carbide. However, many silicon carbide arresters are still in service. Some investigators have noted high silicon carbide arrester failure rates, due to moisture ingress, after several years of service on medium-voltage distribution systems. This experience does not necessarily apply to surge arresters in substations. If such problems arise, it would make sense to systematically replace silicon carbide arresters on a system. Otherwise, assuming that the original application was proper, the older silicon carbide arresters could remain in service.

Figure 13.1 shows the general use of gaps in surge arresters. The gapped design (13.1a) applies to silicon carbide, whereas the gapless design (13.1d) applies to the latest generation of metal oxide. One manufacturer used the shunt gap (13.1b) in early metal oxide arresters. At steady state, both nonlinear elements would support the nominal voltage, somewhat reducing the current. During a surge discharge,

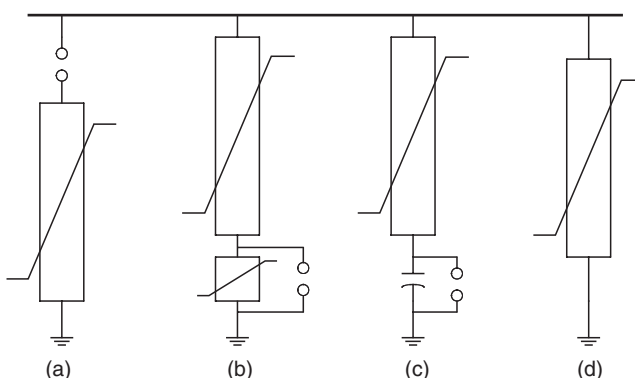


FIGURE 13.1 Use of gaps in metal oxide surge arresters.

the shunt gap would sparkover to bypass the smaller section of metal oxide, thereby reducing the discharge voltage and providing somewhat better protection. Another manufacturer used the series gap with capacitive grading (13.1c) in early metal oxide arresters. At steady state, this decreases the voltage on the metal oxide. During a surge discharge, the gap sparks over “immediately” due to the capacitive grading. The latest generations of metal oxide do not need these gaps, although there is some consideration for using gaps to achieve specific goals (e.g., coordinating arresters, withstanding temporary overvoltages).

The surge arrester must be installed on something, such as a transformer tank or a pedestal. It must also be connected to the protected system, typically through a wire or lead. Later, it will be shown that these connections have important effects on the overall protection, especially for steep surges. The pedestal and lead, both length and location, must be considered as part of the overall arrester installation.

On distribution systems, a ground lead disconnector is often used with the surge arrester. If the arrester fails and then conducts current on a steady-state basis, the disconnector will detonate and disconnect the base of the arrester from ground. This should happen in approximately 1 sec, or faster. The arrester may then remain connected to the system until maintenance personnel have a chance to replace it. No breaker or fuse need operate to isolate the failed arrester; if the arrester is the only thing that failed, no customers need to lose their electric service. Of course, the arrester is not providing any surge protection during this period with its ground lead disconnected. There would be a clear visual indication that the ground lead has been disconnected; it will be “hanging down” below the arrester. Regular visual inspections are necessary to maintain surge protection whenever ground-lead disconnectors are used.

Many surge arresters in substations or industrial facilities have been installed with “surge counters.” These are accessories to be installed in the surge arrester’s ground-lead connection. Two functions may be provided:

1. A steady-state current meter, calibrated in mA. If this current increases over time, it may indicate thermal damage to the surge arrester. However, the presence of harmonics or external leakage currents would complicate the assessment.
2. A counter indicates the number of surge current discharges above a certain threshold, which may depend on frequency or front time. Even if the count is accurate, it does not mean that the discharge voltage reached any particular level during those events.

To use surge counters effectively, it is important to track the readings on a regular basis, beginning at the time of commissioning.

13.2 Ratings and Tests

Surge arresters have both a voltage rating and a class, or type. For metal oxide, the important voltage rating is the maximum continuous operating voltage (MCOV), which is the steady-state voltage the arrester could support indefinitely. This rating is most important for metal oxide, because most of these arresters are now gapless and carry a few milliamperes at all times. The MCOV should be at least 1.05 times the system’s nominal line-to-ground voltage. There are some cases like distribution feeders with poor voltage regulation, which might require a higher MCOV. As discussed later, short-term temporary overvoltages (TOV) also play an important role in selecting the arrester rating, but still the basic rating is MCOV.

Historically, the SiC arresters had a voltage rating that corresponded to the duty cycle test, with no direct link to MCOV. Given that SiC arresters were always gapped, MCOV was not an important concern. In IEEE standards, the old SiC numerical schedule of voltage ratings has been carried over to metal oxide arresters, and the MCOV is usually about 84% of the arrester voltage rating. For example, a typical 108-kV arrester has an MCOV of 84 kV. Only the MCOV number is important.

The IEC standard defines the voltage rating to be the TOV capability at 10 sec, and again the MCOV is about 84% of this value. [Table 13.1](#) shows the schedule of IEC voltage rating steps, and in general these

TABLE 13.1 Schedule of IEC Voltage Rating Steps

Range of Rated Voltage (kV rms)	Step Size (kV rms)
3–30	1
30–54	3
54–96	6
96–288	12
288–396	18
396–756	24

line up with the schedule of IEEE voltage ratings. This table could be used to choose the preliminary arrester-rating for some application. However, all surge arrester manufacturers now have their catalog information readily available on the Web, and it is better to use their actual data.

The IEEE specifies a set of withstand tests for surge arresters, each of them followed by a period of operation at MCOV. These tests are

1. High current, short duration: Two $4 \times 10 \mu\text{s}$ current surges are discharged through the arrester. The peak current is 65 kA for station, intermediate, and distribution normal-duty arresters. It is 100 kA for distribution heavy-duty and 40 kA for distribution light-duty arresters. Followed by 30 minutes at MCOV.
2. Low current, long duration: For station and intermediate arresters, a transmission pi section is discharged 20 times through the arrester. The switching surge voltage ranges from 2.0 to 2.6 pu and the equivalent line length ranges from 160 to 320 km, depending on the arrester class and voltage rating. For distribution arresters, a 2000 ms square wave of current is discharged 20 times, with a peak current of 250 A for heavy-duty and 75 A for normal-duty or light-duty arresters. Followed by 30 minutes at MCOV.
3. Duty cycle test: While energized at the voltage rating, which is higher than MCOV, discharge an $8 \times 20 \mu\text{s}$ lightning impulse 20 times, with peak ranging from 5 to 20 kA, followed by two discharges without power frequency voltage, followed by 30 minutes at MCOV.
4. Pressure relief test: An rms current of 40–80 kA is applied for station class, or 16.1 kA for intermediate class, so that the arrester fails. The pressure must vent well enough that any components lie no farther away than the arrester height. Polymer housings tend to have better pressure relief ratings than porcelain housings.
5. Contamination test: Energized for 1 hour at MCOV under contaminated conditions, followed by 30 minutes at MCOV.
6. Temporary overvoltages: Verifies the TOV capability over a range from 0.02 to 1000 sec.
7. Switching surge energy: This is an optional supplement to the low current, long-duration test, which carries an implied energy discharge duty. The manufacturer typically provides a value for energy capability in kJ per kV of MCOV, which is meant to cover multiple discharges within a period of about 1 minute.

The test results for TOV and switching surge energy capability are often used in application studies.

The manufacturer also conducts tests of the arrester protective characteristics. These are always directly useful in modeling and application studies:

1. $8 \times 20 \mu\text{s}$ discharge voltage: Current surges are applied with peak magnitudes of 1.5, 3, 5, 10, and 20 kA, with the resulting peak discharge voltages tabulated. Due to various frequency-dependent effects, the peak voltage occurs before the peak current. For some ratings, the 15- and 40-kA discharge voltages are also tabulated.
2. Front-of-wave (FOW) protective level: This is the voltage having a $0.5-\mu\text{s}$ time to crest, for a current surge of 5, 10, 15, or 20 kA depending on the rating. To get this value, it is necessary to apply different front times for the current surge and interpolate or extrapolate the results.

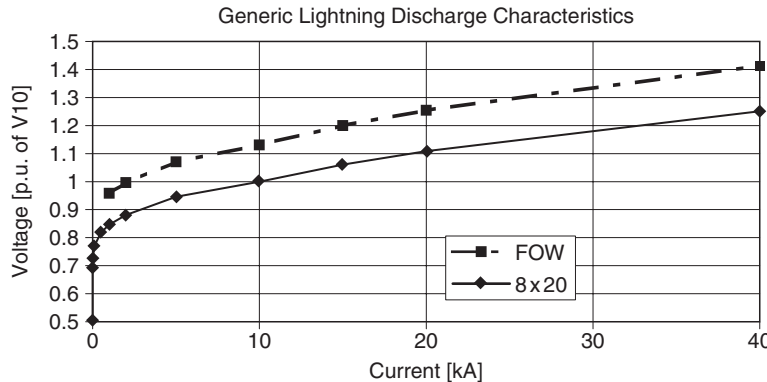


FIGURE 13.2 Metal oxide surge arrester lightning discharge characteristics, for voltage ratings from 54 to 360 kV. V_{10} is the arrester's $8 \times 20 \mu\text{s}$ discharge voltage at 10 kA.

3. Switching surge protective level: The peak arrester voltage for a current surge having 45–60 μs front time and a peak of 500–2000 A depending on the rating.

Many vendors provide more detailed information about protective levels as a function of the surge front time, which is helpful in modeling.

Figure 13.2 shows typical maximum $8 \times 20 \mu\text{s}$ discharge voltage and FOW discharge characteristics for station class metal oxide surge arresters, rated 54 kV and above. There is a manufacturing variation within each product line, and the minimum discharge voltage could be a few percent lower than these values. In most cases, the maximum values would be used for application studies. Figure 13.3 shows a typical maximum switching surge discharge characteristic. All of these are normalized to the published $8 \times 20 \mu\text{s}$ discharge voltage at 10 kA.

The IEEE standards define several classes of surge arresters, based on the withstand test levels discussed earlier. In substations and many transmission line applications, the station class arresters are most common. The intermediate class arresters are used for lightning protection of transmission line towers and for some of the smaller substations. The choice of distribution arrester class depends mainly on how severe the local lightning environment is. Although purchased in significant quantities, the surge arresters are typically not a significant cost item in a single substation.

Among the IEEE standards, C62.11 defines the metal oxide arrester tests and ratings, whereas C62.2 provides the application guidance. The older standards for silicon carbide arresters, C62.1 and C62.2, are still available. These apply to the U.S.; whereas, in most other parts of the world, the International

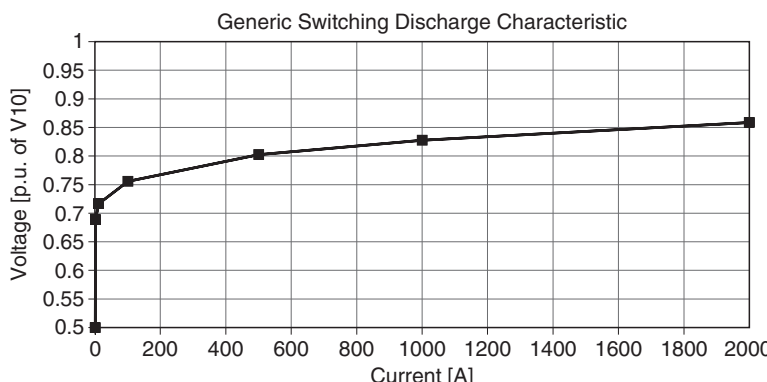


FIGURE 13.3 Metal oxide surge arrester switching discharge characteristic, for voltage ratings from 54 to 360 kV. V_{10} is the arrester's $8 \times 20 \mu\text{s}$ discharge voltage at 10 kA.

Electrotechnical Committee (IEC) standards are used. These are denoted IEC 60099 parts 1 through 7, except that there is no part 2 and part 7 is a glossary. For gapless metal oxide arresters, part 4 defines the tests and ratings, while part 5 presents the application guidelines. For gapped arresters, including silicon carbide, part 1 applies. The IEEE standards may be found through www.ieee.org, and the IEC standards through www.iec.ch.

Both IEEE and IEC standards define the discharge characteristics in similar ways. The same applies to MCOV and TOV capabilities. In IEC standards, the rated voltage is actually the TOV capability at 10 sec and also the duty cycle test voltage. These differences generally will not concern the user. The main difference is that IEC standards classify arresters by nominal discharge current (1.5, 2.5, 5, 10, or 20 kA) and line discharge class (1–5, or none). An IEEE station class arrester is roughly comparable to an IEC 10-kA arrester, whereas the intermediate and distribution class arresters are roughly comparable to IEC 5-kA arresters. At 500 kV and above, the IEEE classifying current is 15 or 20 kA, roughly corresponding to the IEC nominal discharge current of 20 kA used at these voltage levels. The appropriate standard should be consulted for details, but Osterhout (1992) and Hamel and St. Jean (1992) provide overviews of the differences.

13.3 Selection by TOV

As discussed earlier, the first choice of arrester voltage rating is based on MCOV. That would be the lowest and best choice because it minimizes the arrester discharge voltage for any particular surge, thereby maximizing protective margins. However, it may be necessary to increase the arrester voltage rating to withstand either temporary overvoltages or surge energy content.

The TOVs come from several sources, most commonly

1. During ground faults, voltage on the unfaulted phases will rise above nominal unless the system is solidly grounded. The duration of this overvoltage depends on protective relaying system response, usually less than 1 sec, but up to several hours for delta systems or ungrounded systems.
2. When first energizing a long line or cable, the voltage at the open end will rise above nominal due to the Ferranti effect. The duration depends on how long it takes to switch on shunt compensation or to close the other end of the line. A similar effect occurs after load rejection when only one end of the line opens.
3. Harmonics, ferroresonance, and transformer inrush currents can produce dynamic overvoltages that last for several cycles.

Usually the ground fault TOVs are most important, but there are special cases where simulation of other TOVs should be considered. Given the zero sequence and positive sequence impedances at the point of a fault, the per-unit unfaulted phase voltage, often called the earth-fault factor (EFF) may be estimated for a single-line-to-ground fault:

$$\begin{aligned} \text{EFF} &= -\frac{\sqrt{3}}{2} \left[\frac{\sqrt{3}K}{2+K} \pm j1 \right] \\ K &= \frac{Z_0 + R_f}{Z_1 + R_f} \\ Z_0 &= R_0 + jX_0 \\ Z_1 &= R_1 + jX_1 \end{aligned} \quad (13.1)$$

Note that there are two unfaulted phases to evaluate, for the positive and negative $j1$ terms. That voltage should be further increased by a factor of 1.05 to account for above-nominal operating voltage. In most cases, the fault resistance, R_f , should be considered zero as it maximizes EFF. For distribution systems, R_f should be equal to the design level of fault resistance that relaying will detect; this is really a matter of policy. For double-line-to-ground faults, the per-unit voltage on the unfaulted phase would be

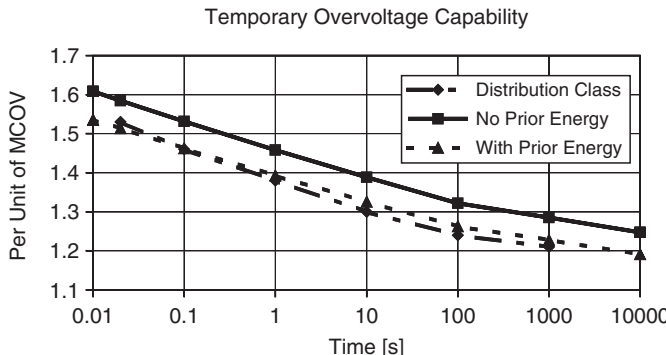


FIGURE 13.4 Temporary overvoltage (TOV) capability.

$$\text{EFF} = \frac{3K}{2K + 1}$$

$$K = \frac{Z_0 + 2R_f}{Z_1 + 2R_f} \quad (13.2)$$

Again, this voltage should be further increased by a factor of 1.05 to account for above-nominal prefault voltage.

The TOV duties from various sources must be compared to the arrester's TOV capability, which may be obtained from the manufacturer's catalog, or taken from Fig. 13.4 to use typical data. Some data includes TOV capability both with and without earlier surge discharges; the capability with prior discharge, which is always lower, should be used. If the TOV duty exceeds the arrester capability, then a higher voltage rating must be chosen for the arrester, accepting lower protective margins. It is difficult to mitigate TOVs as they typically arise from high-level system design choices.

13.4 Selection by Energy Rating

Surge arresters have a switching surge energy discharge capability higher than implied by the low-current, long-duration discharge test. The vendor may provide this value as kJ per kV of MCOV, or rated voltage with footnotes that specify the number, shape, and interval between surges. For example, if the capability is given as 8 kJ per kV of MCOV for a single discharge, then a 108-kV arrester with an MCOV of 84 kV has a switching surge discharge capability of 672 kJ .

The energy capability may be increased by using two or more columns of metal oxide in parallel. The manufacturer has to match the disks to achieve this and typically two parallel columns provide a bit less than double the energy rating. Note that increasing the arrester voltage rating will not help much, because even though the energy rating increases, the discharge voltage also increases resulting in higher surge energy discharge. Parallel columns will not help with TOV, as TOV is a sustained phenomena supported by the system voltage.

There is some evidence that these energy ratings are actually the point at which failure probability becomes nonzero. Hileman (1999) estimated the probability of failure from several reported tests, assuming a Weibull function to model the failure probability:

$$P_F = 1 - 0.5 \left(\frac{Z}{4} + 1 \right)^5$$

$$Z = \frac{W_C / W_R - 2.5}{0.375} \quad (13.3)$$

In Eq. (13.3), W_R is the energy rating and W_C is the calculated energy duty. Under this model, P_F reaches 50% only at 2.5 times the energy rating. Note that standards and vendors do not address this point yet, but consideration of the actual failure probability may avoid overdesign for switching surge energy discharge.

A conservative estimate of the switching surge energy discharge, W_C , is

$$W_C = \frac{1}{2} CE^2 \quad (13.4)$$

For energy in joules, C is the total capacitance in μF and E is the peak voltage in kV. The peak voltage ranges from 2 to 2.5 pu of the peak line-to-neutral voltage, although it may be higher for cases like capacitor bank restrikes and line reclosing. The total capacitance may come from an overhead line, a cable, or a shunt capacitor bank. Better estimates may be obtained through time-domain simulation.

Lightning surge discharge also poses a significant energy duty on surge arresters. However, the switching surge energy rating does not apply directly and the duty might be better described as a charge duty. In either case, the lightning discharge current may be represented as a decaying exponential with total area equal to the stroke charge. Details of the wave front are unimportant for this evaluation. If one arrester discharges all of the lightning stroke current, a conservative estimate of the energy duty would be

$$W_C = QE_d \quad (13.5)$$

In Eq. (13.5), Q is the total stroke charge in coulombs and E_d is the arrester discharge voltage at the peak lightning stroke current. The actual energy discharge is reduced by nonlinear arrester characteristics and by sharing from nearby arresters. Even though nearby arresters will not have matched characteristics, they still share a significant portion of the energy because of inductances between the arresters and also because the characteristics are more linear at lightning discharge current levels than at switching discharge current levels. Time-domain simulation helps to quantify these effects.

13.5 Arrester Modeling

Surge arresters are both nonlinear and frequency-dependent devices. The only strictly correct model would be a time-domain simulation at the level of material physics. In most practical cases, one must use a nonlinear resistance with a separate linear circuit to represent frequency-dependent effects. Surge arresters also interact with other equipment that has distributed parameters. Usually the other system nonlinearities are not important, but in special cases some of these effects (e.g., corona) may become significant. In general, arrester application studies need to be done with time-domain simulation in the Electromagnetic Transients Program (EMTP) or one of its variants like the Alternative Transients Program (ATP).

In the absence of EMTP or ATP, the arrester discharge voltage may be approximated for a given surge current peak and waveshape. First, choose the FOW, $8 \times 20 \mu\text{s}$, or switching surge characteristic that best matches the waveshape. If manufacturer's data is not available, Figs. 13.2 and 13.3 may be used with a normalizing value (10-kA discharge) of 2.3 times MCOV. In cases where the discharge current peak is "known," interpolate with this value to estimate the peak discharge voltage.

More often, though, a voltage surge arrives at the arrester location and the discharge current peak is not known in advance. In the simplest case, the arrester is at the end of a line with known surge impedance, Z , incoming surge magnitude, E , and power frequency offset, V_{pf} . The arrester current and voltage may then be estimated as

$$\begin{aligned} I_A &= \frac{2E - E_0 - V_{pf}}{Z + R_A} \\ E_d &= E_0 + I_A R_A \\ E_A &= E_d + V_{pf} \end{aligned} \quad (13.6)$$

This approximates the arrester discharge characteristic, E_d , with a straight line having slope R_A and intercept E_0 , as determined by interpolation on either the manufacturer's data, or on Figs. 13.2 and 13.3. The actual arrester voltage, E_A , is the discharge voltage, E_d , plus the power frequency offset voltage, V_{pf} . To use Eq. (13.6), make the first guess at I_A and determine the corresponding E_0 and R_A parameters from

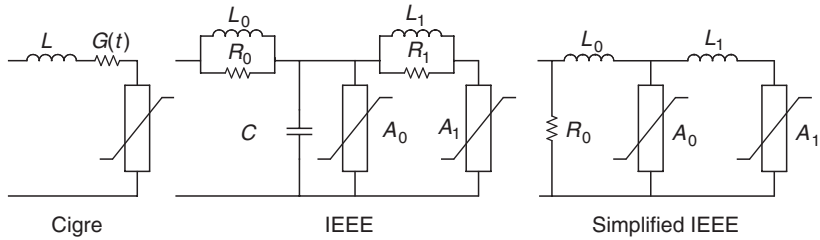


FIGURE 13.5 Frequency-dependent surge arrester models.

the discharge characteristic. Then solve for I_A using the first equation; if it falls outside the linear segment used to estimate R_A and E_0 , iterate until convergence on I_A . Then E_d and E_A may be determined directly. Hileman (1999) presents more detailed estimating methods for other situations, but in those cases it may be easier to use EMTP or ATP.

Figure 13.5 shows three frequency-dependent surge arrester models. The Cigre model (Hileman et. al., 1990) works well, but it requires the user to program a time-dependent conductance to simulate the arrester turn-on characteristics. It is not directly applicable to EMTP or ATP. The IEEE model (IEEE PES Task Force) uses high-frequency and low-frequency discharge characteristics represented by A_0 and A_1 , respectively, with a two-stage RL filter connecting them. At nominal voltage, the arrester current is primarily capacitive, represented by the shunt C component. Both IEEE and Cigre models require iteration of the parameters to represent a particular arrester, before it can be used in application studies. A simplified version of the IEEE model (Magro et al., 2004) has been developed for use “out of the box;” it ignores the capacitive effect.

In the Cigre model, the turn-on conductance begins at zero and increases with time. A reasonable approximation for distribution arresters is

$$\begin{aligned} \frac{dG}{dt} &= \frac{G_{\text{ref}}}{T} \left(1 + \frac{G}{G_{\text{ref}}} \right) \left(1 + \frac{G}{G_{\text{ref}}} \left(\frac{I}{I_{\text{ref}}} \right)^2 \right) \exp \left(\frac{U}{U_{\text{ref}}} \right) \\ G_0 &= 0 \\ T &= 80 \\ G_{\text{ref}} &= \frac{34}{U_{10}} \\ I_{\text{ref}} &= 5.4 \\ U_{\text{ref}} &= kU_{10} \end{aligned} \tag{13.7}$$

where U_{10} is the 10-kA discharge voltage in kV, U is the arrester voltage in kV, I is the arrester current in kA, and k is a constant ranging between 0.03 and 0.05, depending on the manufacturer. The series inductance, L , is approximately 1 μH per meter of arrester height for outdoor arresters, and one-third of that for gas-insulated substation (GIS) arresters.

The following are starting values for the IEEE model parameters:

$$\begin{aligned} L_1 &= 15 \frac{d}{n} \\ R_1 &= 65 \frac{d}{n} \\ L_0 &= 0.2 \frac{d}{n} \\ R_0 &= 100 \frac{d}{n} \\ C &= 100 \frac{n}{d} \end{aligned} \tag{13.8}$$

where d is the arrester height in meters, n is the number of metal oxide columns in parallel, L is in μH , R is in Ω , and C is in pF . Parameters for the simplified model are

$$\begin{aligned} R_0 &= 1e6 \\ L_0 &= \frac{1}{12} \frac{V_{\text{FOW}} - V_{10}}{V_{10}} V_n \\ L_1 &= \frac{1}{4} \frac{V_{\text{FOW}} - V_{10}}{V_{10}} V_n \end{aligned} \quad (13.9)$$

The inductance values L_0 and L_1 are in μH , V_{FOW} is the front-of-wave discharge voltage in kV, V_{10} is the $8 \times 20 \mu\text{s}$ discharge voltage in kV, and V_n is the arrester voltage rating (not the MCOV), also in kV. R_0 is present for numerical stability and may not be required for some time-domain simulators. R_0 may also be increased by one or two orders of magnitude for extra high voltage (EHV) levels. Whenever V_{FOW} is not available or when the ratio V_{FOW}/V_{10} is more than 1.18, the simplified inductance parameters become

$$\begin{aligned} L_0 &= 0.01 V_n \\ L_1 &= 0.03 V_n \end{aligned} \quad (13.10)$$

For both versions of the IEEE model, Table 13.2 provides A_0 and A_1 in pu of the 10-kA discharge voltage.

All of the frequency-dependent models include built-in arrester inductance. The arrester lead and pedestal should also be modeled, along with bus, line, or cable lengths to the nearby protected equipment. The lead and pedestal may be represented either as lumped inductance, approximately 1 μH per meter, or with traveling wave lines having surge impedance of about 300 Ω .

The separation effect may be approximated for an open-end termination, at which traveling wave reflections will cause doubling before the arrester's limiting effect is seen. The peak voltage at the open end is

$$E_T = E_d + 2S\tau \quad (13.11)$$

where E_d is the arrester discharge voltage in kV, S is the surge steepness in $\text{kV}/\mu\text{s}$, and τ is the travel time in μs to the open line end. For overhead lines or buswork, τ is approximately the distance in meters,

TABLE 13.2 IEEE Frequency Dependent Model
Discharge Characteristics

I (A)	A_0 (pu of V_{10})	A_1 (pu of V_{10})
0	0.000	0.000
0.002	0.813	0.651
10	0.875	0.748
100	0.963	0.800
1,000	1.050	0.885
2,000	1.088	0.931
4,000	1.125	0.963
6,000	1.138	0.976
8,000	1.169	0.996
10,000	1.188	1.009
12,000	1.206	1.015
14,000	1.231	1.028
16,000	1.250	1.035
18,000	1.281	1.041
20,000	1.313	1.048

divided by 300. For example, if the arrester discharge voltage is 297 kV, the surge steepness is 1000 kV/ μ s and the distance to the protected transformer is 10 m, then the peak transformer voltage, E_T , is approximately 364 kV. That is an increase of 22% from 297 kV, illustrating the importance of minimizing lead lengths. Note that this estimate ignores the effect of transformer capacitance and power frequency offset, both of which would further increase E_T .

In many cases, the ground resistance does not have to be included. The main exceptions occur when arresters are applied outside of the substation, such as riser poles, distribution transformers, and transmission line towers. In the riser pole application, a ground connection affects the differential-mode surge entering the cable. On distribution lines, the multigrounded neutral conductor allows current to circulate back through nearby arresters. The same thing happens with transmission line arresters installed with overhead shield wires. In all these cases, the ground resistances should be modeled, along with any conductors that are grounded periodically.

If it is necessary to model an older SiC arrester, the $8 \times 20 \mu$ s discharge characteristic is represented very well by a single exponential power law:

$$I_d = kV_d^\alpha \quad (13.12)$$

This must be connected in series with a gap, having a sparkover voltage ranging anywhere from 5% to 20% higher than V_{10} . The exponential power, α , ranges from 2 to 6, with higher values being more typical for SiC surge arresters. If the actual data is no longer available, it may be assumed that the 10-kA discharge voltage is approximately equal to the 10-kA, $8 \times 20 \mu$ s discharge voltage of a metal oxide arrester having the same voltage rating (Sakshaug, 1991). On that assumption, the value of k becomes, for units of kA and kV,

$$k = \frac{10}{V_{10}^\alpha} \quad (13.13)$$

Typical SiC data may also be found in Greenwood (1991). Both the FOW and switching surge protective levels for SiC arresters would be significantly higher than for metal oxide arresters of the same voltage rating, even when the V_{10} values are approximately equal. Conversely, the α parameter in metal oxide varies with current, so that a single exponential does not provide a good model. Piecewise exponential segments are often used for metal oxide surge arrester models in EMTP and ATP.

13.6 Applications

Perhaps the most important surge arrester application is to protect the equipment in a substation. After selecting the lowest possible arrester voltage rating, one typically applies an arrester as close as possible to each transformer terminal. Then given the transformer BIL, a protective margin is calculated using the $8 \times 20 \mu$ s discharge voltage at the “coordination current,” which is typically 10 kA:

$$M_{\text{pct}} = 100 \left(\frac{\text{BIL}}{V_{10}} - 1 \right) \quad (13.14)$$

where

M_{pct} is the protective margin, in percent

BIL is the transformer basic insulation level, in kV

V_{10} is the arrester’s 10-kA discharge voltage, in kV

The margin could also be calculated at a different coordination current, such as 5 or 20 kA, in which case V_5 or V_{20} would be used instead of V_{10} . One could also calculate a chopped wave protective

margin, using the chopped wave insulation level and FOW protective level in place of BIL and V_{10} . Finally, one could calculate a margin for switching surges using the BSL and the arrester's switching surge protective level. In all cases the principle applied is the same and 10%–20% should be considered the minimum acceptable margin. These margins are usually easy to obtain. For example, on a 138-kV system, the transformer BIL is at least 450 kV. If the system is effectively grounded, a 108-kV arrester might be used with a 10-kA discharge voltage of 263 kV, providing a margin of 71%. Using a 120-kV arrester with 297-kV discharge voltage, the margin is still 52%.

As discussed in [Chapter 14](#), many uncertainties and deviations complicate the use of margins. After a long time in service, the insulation strength may not really be at the original BIL and BSL levels. The actual surges also differ from laboratory test waves, so that the BIL and BSL do not describe the insulation strength perfectly. Furthermore, several important electrical circuit phenomena are not considered in the simple use of margins and Fig. 13.6 illustrates some of them.

The surge arrester's lead and pedestal connections should be added to the basic arrester model, either as lumped inductances or as very short distributed-parameter lines. As a result, the voltage to ground at the point of arrester connection will be somewhat higher than the pure arrester discharge voltage. The distances to protected equipment, L_B and L_T in Fig. 13.6, should also be represented with distributed-parameter lines. The arrester itself should be represented with a frequency-dependent model, as discussed earlier. At these high frequencies, the transformer should be represented as a capacitance ranging from 1 to 10 nF, with some sensitivity analysis of this parameter. The incoming surge itself is primarily described with a steepness, S , ranging from 1000 to 2000 kV/ μ s, depending on the transmission line characteristics, lightning environment, and design level of mean time between failures. The surge magnitude, E , is typically based on some percentage of the line insulation critical flashover (CFO) voltage. It arrives on top of an opposite-polarity power frequency offset, so the arriving surge voltage to ground is actually $E - V_{pf}$. All of these factors tend to increase the peak voltage appearing at the transformer, which decreases the protective margin. Note: when using EMTP, the margin is calculated from the simulated peak voltage at the transformer, instead of V_{10} .

If two or more lines enter the station, which is typically the case, the additional lines tend to increase protective margins. As an approximation, these lines may be represented with the line surge impedances to ground, connected in parallel at the point of arrester connection. This is shown in Fig. 13.6, where n is the total number of lines entering the station. A better representation would be to represent the bus sections with distributed-parameter lines, and connect the line entrances at points where they actually enter the station.

A further refinement is to represent the surge with a Thevenin equivalent. The simplest such equivalent is a surge voltage of $2E$ on top of a DC voltage equal to $-V_{pf}$, both behind a lumped resistance equal to the line surge impedance, Z . The next refinement would be to represent the line with distributed parameters back to the stroke point, with a tower footing resistance value in place of Z . Even with these refinements, a single-phase model is adequate for the simulation.

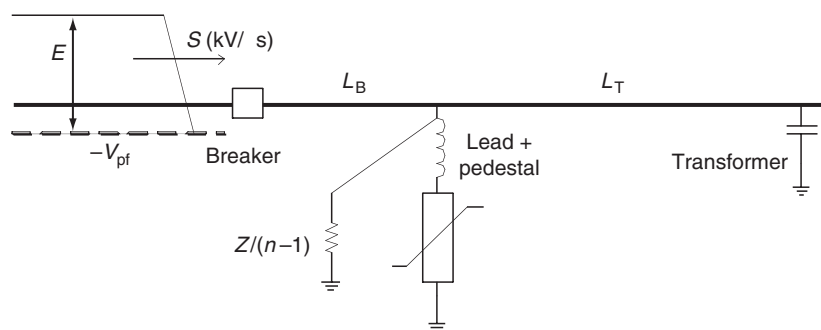


FIGURE 13.6 Station protection by surge arresters.

Sometimes, the switching surge energy discharge duty on a station arrester will exceed its rating. Typically this happens when large shunt capacitor banks, or long cables, are nearby. The arrester can be ordered with parallel columns, which are matched at the time of manufacturing to achieve effective sharing of the energy duty. If not matched, a small difference in the discharge characteristic could result in one column discharging virtually all of the energy. This would happen even with typical small manufacturing variations of 3% or less.

Once the model in Fig. 13.6 has been set up, the arrester rating and location will be finalized to adequately protect each transformer. Protective margins for other equipment will also be available, such as the circuit breaker in Fig. 13.6. For many stations, arresters at the transformer terminals will adequately protect all equipment in the station. If not, arresters can be added to protect equipment that is far away from the transformers. This process applies to each nominal voltage level in the substation.

As a further constraint, the arresters on two different voltage levels should be coordinated so that the high-side arrester always operates first for a surge impinging on the high side of the transformer. If the low-side arresters operate first, they might discharge all of the energy in the high-side surge, leading to possible failure. This coordination is achieved by ensuring 4% margin between the transformer turns ratio and the ratio of arrester protective levels. For example, a 345/138 transformer has a turns ratio of 2.5. The switching surge discharge voltage of the high-side arrester should be no more than $2.5/1.04$, or 2.4, times the switching surge discharge voltage of the low-side arrester.

Figure 13.7 shows how surge arresters may be used to protect overhead transmission lines. Arresters on the line side of a circuit breaker, shown to the left in Fig. 13.7, can protect the breaker from lightning surges traveling in from the line, while the breaker is open. If the breaker is open for maintenance, a disconnect switch would be opened to isolate it from the line. The need for protection would arise when the breaker opens to clear a lightning-induced fault during a storm, and then a subsequent lightning stroke to the line causes another surge while the breaker is still open. As this condition occurs rarely, some utilities may not use arresters to provide this protection.

On long EHV transmission lines, surge arresters may be applied at each end to mitigate switching surges during line energization and reclosing. A statistical switching study using either EMTP or a transient network analyzer (TNA) is required for this application. The overvoltages will be higher at intermediate points along the line, due to separation effects. The study results should include a profile of probabilistic switching overvoltage parameters vs. line length, to be used with a probabilistic evaluation of the switching surge flashover rate. Commonly used alternatives to these line-end arresters include pre-insertion resistors in the circuit breakers or controlled-closing circuit breakers. While often more expensive and more complicated, these alternatives typically produce a flatter overvoltage profile along the line length.

Some EHV transmission lines use series capacitors to reduce their electrical length, and during faults on the line, very high voltages would result on the capacitors. Metal oxide surge arresters typically protect these capacitor banks, as shown in Fig. 13.7. The energy dissipation requirements are severe and the manufacturer takes extra care to ensure that the parallel metal oxide columns are matched so that each column shares the energy and current duty. The blocks may also be larger than in typical station-class surge arresters. Although the transient phenomena is at power frequency and subsynchronous frequencies, these energy calculations are normally done using EMTP.

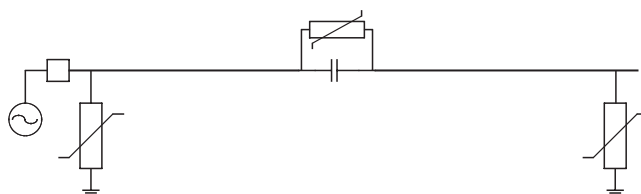


FIGURE 13.7 Transmission line protection by surge arresters.

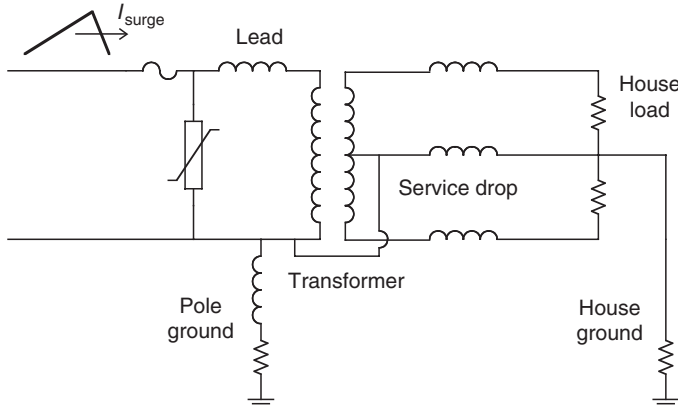


FIGURE 13.8 Distribution transformer protection by surge arresters.

Recently, arresters have been applied to transmission line towers to provide lightning protection of the line insulation. These may be used in place of, or in addition to, overhead shield wires. Some manufacturers have special-purpose line arresters, which are comparable to intermediate or distribution heavy-duty class. Arresters may be used in addition to a shield wire in areas where low footing resistance is difficult or in high-exposure areas like river crossings. In that case, the arrester energy duty is lessened because the shield wire and footing discharge most of the lightning stroke current. Without a shield wire, the energy duties will increase but are still mitigated by sharing from the arresters on nearby towers.

Surge arresters protect virtually all distribution transformers connected to overhead lines, as illustrated in Fig. 13.8. It is essential to keep the lead length short. The historical rules of thumb like “2 kV per foot” are grossly understated, because they were based on laboratory test waveshapes that do not represent natural lightning surges. If the arrester is installed between a small fuse and the transformer, then the arrester discharge current must also flow through the fuse, which may cause the fuse to melt unnecessarily. If this becomes a problem, larger fuses or completely self-protected transformers (CSPs), which have internal fuses, could help mitigate it.

Because the arrester is connected between the transformer tank and terminal, pole ground resistance and pole downlead inductance do not have a direct impact on the transformer’s protective margin. However, if the pole ground resistance is too high with respect to the house or customer ground resistance, higher surge currents will circulate in the secondary service drop and the customer load equipment. This may lead to failures due to surges in the transformer secondary, or damage to customer equipment, even when the transformer primary enjoys a comfortable protective margin. It has been suggested that transformers with interlaced secondary windings are less susceptible to these failures. In any case, the secondary surges should be limited by using triplex service drops rather than open-wire drops, and also by keeping the utility pole ground resistance to a reasonably low value.

Given the dispersed installation of transformers on a distribution feeder, surge arresters will be installed at relatively close spacings on the distribution line. Typical average spacings might be from 2 to 4 poles in built-up areas, although not necessarily on all phases. These arresters may be used to provide some protection from lightning flashovers of the line insulation. Because of the low insulation levels, typically 100 to 300 kV CFO, this protection will generally be more effective for induced voltages from nearby lightning strokes, which do not actually hit the line. For direct strokes to the line, energy duty on the arresters may be too high, although there is little field experience to indicate that arresters are failing at high rates due to lightning. If the arresters are not placed at every pole and on every phase, separation effects will be more significant than in a typical substation. Some trials have been done with arresters on just the topmost phase, reasoning that the arrester will convert that phase conductor into a shield wire during a lightning discharge. However, the topmost phase is typically not high enough to serve

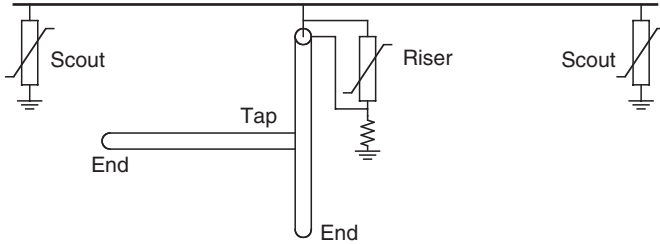


FIGURE 13.9 Riser pole and scout arresters on a distribution system.

as an effective shield wire for the two outside phase conductors. Many distribution engineers feel that a direct stroke to the line will result in either a line insulation flashover, or less often, an arrester failure.

Figure 13.9 shows the application of surge arresters at the riser pole, where an underground cable segment connects to an overhead primary distribution feeder. The riser pole arrester limits a surge entering the cable, but surge doubling may occur at the cable end and tap points. If the lightning surge is “bipolar,” the surge may even quadruple at the open cable ends (Barker, 1990). If the nominal voltage and cable lengths are low enough, and setting aside the small risk of voltage quadrupling, the riser pole arrester may be sufficient. For longer cables, it may be necessary to add arresters at some of the open cable ends or tap points. Before taking that step, the effect of “scout arresters,” shown at either end of the overhead feeder section in Fig. 13.9, should be included in the study. These arresters will mitigate most surges arriving at the riser pole.

References

- Barker, P.P., Voltage quadrupling on a UD cable, *IEEE Trans. Power Delivery*, 5(1), 498–501, January 1990.
- Greenwood, A.N., *Electrical Transients in Power Systems*, 2nd ed., John Wiley & Sons, 1991, pp. 533–534.
- Hamel, A. and St. Jean, G., Comparison of ANSI, IEC, and CSA standards’ durability requirements on station-type metal oxide surge arresters for EHV power systems, *IEEE Trans. Power Delivery*, 7(3), 1283–1298, July 1992.
- Hileman, A.R., *Insulation Coordination for Power Systems*, Marcel Dekker, Inc., 1999, pp. 497–675.
- Hileman, A.R., Roguin, J., and Weck, K.H., Metal oxide surge arresters in AC systems—part v: protection performance of metal oxide surge arresters, *Electra*, 133, 133–144, December 1990.
- IEC Standard 60099-1, Edition 3.1, *Surge Arresters—Part 1: Nonlinear Resistor Type Gapped Surge Arresters for A.C. Systems*, International Electrotechnical Commission, December 1999.
- IEC Standard 60099-3, Edition 1.0, *Surge Arresters—Part 3: Artificial Pollution Testing of Surge Arresters*, International Electrotechnical Commission, September 1990.
- IEC Standard 60099-4, Edition 2.0, *Surge Arresters—Part 4: Metal Oxide Surge Arresters without Gaps for AC Systems*, International Electrotechnical Commission, May 2004.
- IEC Standard 60099-5, Edition 1.1, *Surge Arresters—Part 5: Selection and Application Recommendations*, International Electrotechnical Commission, March 2000.
- IEC Standard 60099-6, Edition 1.0, *Surge Arresters—Part 6: Surge Arresters Containing both Series and Parallel Gapped Structures—Rated 52 kV and Less*, International Electrotechnical Commission, August 2002.
- IEEE PES Task Force on Data for Modeling System Transients, Parameter determination for modeling system transients—part v: surge arresters, *IEEE Trans. Power Delivery*, 20(3), 2073–2078, July 2005.
- IEEE Std. C62.11-1999, *IEEE Standard for Metal-Oxide Surge Arresters for AC Power Circuits (>1 kV)*, Institute of Electrical and Electronic Engineers, March 1999.

- IEEE Std. C62.22-1997, *IEEE Guide for the Application of Metal-Oxide Surge Arresters for Alternating-Current Systems*, Institute of Electrical and Electronic Engineers, December 1997.
- IEEE Std. C62.1-1989, *IEEE Standard for Gapped Silicon Carbide Surge Arresters for AC Power Circuits*, Institute of Electrical and Electronic Engineers, April 1990.
- IEEE Std. C62.2-1987, *IEEE Guide for the Application of Gapped Silicon-Carbide Surge Arresters for Alternating-Current Systems*, Institute of Electrical and Electronic Engineers, April 1989.
- Magro, M.C., Giannettini, M., and Pinceti, P., Validation of ZnO surge arrester model for overvoltage studies, *IEEE Trans. Power Delivery*, 19(4), 1692–1695, October 2004.
- Osterhout, J.C., Comparison of IEC and U.S. Standards for metal oxide surge arresters, *IEEE Trans. Power Delivery*, 7(4), 2002–2011, October 1992.
- Sakshaug, E.C., A brief history of AC surge arresters, *IEEE Power Eng. Rev.*, 40, 11–13, August 1991.
- Sakshaug, E.C., Kresge, J.S., and Miske, S.A., A new concept in arrester design, *IEEE Trans. Power Appar. Syst.*, 96(2), 647–656, March/April 1977.

14

Insulation Coordination

14.1	Insulation Coordination.....	14-1
14.2	Insulation Characteristics.....	14-2
14.3	Probability of Flashover..... Multiple Gaps per Phase • Multiple Gaps and Multiple Phases	14-2
14.4	Flashover Characteristics of Air Insulation Voltage Waveshape • Electrode Configuration • Effect of Insulator • Effect of Atmospheric Conditions on Air Insulation • Altitude • Insulator Contamination • Application of Surge Arresters • Examples of Surge Arrester Application (Nonself-Restoring Insulation)	14-3

Stephen R. Lambert
Shawnee Power Consulting, LLC

14.1 Insulation Coordination

The art of correlating equipment electrical insulation strengths with expected overvoltage stresses so as to result in an acceptable risk of failure while considering economics and operating criteria (McNutt and Lambert, 1992).

Insulation properties can be characterized as self-restoring and nonself-restoring. Self-restoring insulation has the ability to “heal” itself following a flashover, and such insulation media is usually associated with a gas—air, SF₆, etc. Examples include overhead line insulators, station buswork, external bushing surfaces, SF₆ buswork, and even switchgear insulation. With self-restoring insulation, some flashovers are often acceptable while in operation. An EHV transmission line, for example, is allowed to experience occasional line insulator flashovers during switching operations such as energizing or reclosing, or as a result of a lightning flash striking the tower, shield wires, or phase conductors.

Nonself-restoring insulation is assumed to have permanently failed following a flashover, and repairs must be effected before the equipment can be put back into service. Insulation such as oil, oil/paper, and solid dielectrics such as pressboard, cross-link polyethylene, butyl rubbers, etc. are included in this insulation class. Any flashover of nonself-restoring insulation, say within a transformer or a cable, is unacceptable as such events usually result in lengthy outages and costly repairs.

The performance level of self-restoring insulation is usually addressed and defined in terms of the probability of a flashover. Thus, for a specific voltage stress, a given piece of insulation has an expected probability of flashover (pfo), e.g., a 1-m conductor-to-conductor gap exposed to a 490-kV switching surge would be expected to have a 50% chance of flashover; with a 453-kV surge, the gap would be expected to have a 10% chance of flashover, etc. Consequently, when self-restoring insulation is applied, the procedure is to select a gap length that will give the overall desired performance (pfo) as a function of the stress (overvoltages) being applied.

For nonself-restoring insulation, however, any flashover is undesirable and unacceptable, and consequently for application of nonself-restoring insulation, a capability is selected such that the “100%” withstand level (effectively a 0% chance of flashover) of the insulation exceeds the highest expected stress by a suitable margin.

14.2 Insulation Characteristics

Self-restoring (as well as nonself-restoring) insulation has, when exposed to a voltage, a pfo which is dependent on

- dielectric material (air, SF₆, oil...)
- waveshape of the stress (voltage)
- electrode or gap configuration (rod–rod, conductor to structure...)
- gap spacing
- atmospheric conditions (for gases)

14.3 Probability of Flashover

Assuming the flashover characteristics of insulation follow a Gaussian distribution, and this is a good assumption for most insulation media (air, SF₆, oil, oil/paper), the statistical flashover characteristics of insulation can be described by the V_{50} or mean value of flashover, and a standard deviation. The V_{50} is a function of the rise time of the applied voltage, and when at a minimum, it is usually known as the CFO or critical flashover voltage.

Consequently, for a given surge level and insulation characteristic, the pfo of a single gap can be described by p , and can be determined by first calculating the number of standard deviations the stress level is above or below the mean:

$$\#\delta = \frac{V_{\text{stress}} - V_{50}}{\text{1 standard deviation}} \quad (14.1)$$

For air insulation, 1 standard deviation is either 3% of the V_{50} for fundamental frequency (50–60 Hz) voltages and for lightning impulses or 6% of the V_{50} for switching surge impulses. That the standard deviation is a fixed percentage of the V_{50} and is not a function of gap length is very fortuitous and simplifies the calculations. Once the number of standard deviations away from the mean has been found, then by calculation or by entering a table, the probability of occurrence associated with that number of standard deviations is found.

Example: Assume that an insulator has a V_{50} of 1100 kV with a standard deviation of 6%, and a switching overvoltage of 980 kV is applied to the insulation. The stress is 1.82 standard deviations below the mean:

$$\begin{aligned} \#\delta &= \frac{980 - 1100}{0.06 \times 1100} \\ &= -1.82 \text{ standard deviations below the mean} \end{aligned} \quad (14.2)$$

By calculation or table, the probability associated with –1.82 standard deviations below the mean (for a normal distribution) is 3.4%. Thus, there is a 3.4% chance of insulation flashover every time the insulation is exposed to a 980-kV surge.

The physics of the flashover mechanism precludes a breakdown or flashover below some stress level, and this is generally assumed to occur at 3.5–4 standard deviations below the mean.

14.3.1 Multiple Gaps per Phase

The pfo, P_n for n gaps in parallel (assuming the gaps have the same characteristics and are exposed to the same voltage) can be described by the following equation where p is the pfo of one gap. This mathematical expression defines the probability of one or more gaps flashing over, but practically only one gap of the group will flashover as the first gap to flashover reduces the voltage stress on the other gaps:

$$P_n = 1 - (1 - p)^n \quad (14.3)$$

14.3.2 Multiple Gaps and Multiple Phases

Analysis of some applications may not only require consideration of multiple gaps in a given phase but also of multiple phases. Consider the pfo analysis of a transmission line; during a switching operation for example, multiple towers are exposed to surges and at each tower, each of the three phases is stressed (typically by different surge magnitudes). Thus it is important to consider not only the multiple gaps associated with the multiple towers, but also all three phases often need to be considered to determine the overall line pfo. The overall pfo for a given surge, PFO, can be expressed as

$$\text{PFO} = 1 - (1 - \text{pfo}_{n,a})^g (1 - \text{pfo}_{n,b})^g (1 - \text{pfo}_{n,c})^g \quad (14.4)$$

where $\text{pfo}_{n,x}$ is the pfo of the x phase for the given surge, n , g is the number of towers (gaps in parallel).

The simultaneous analysis of all three phases can be important especially when various techniques are used to substantially suppress the surges (Lambert, 1988).

14.4 Flashover Characteristics of Air Insulation

14.4.1 Voltage Waveshape

Waveshapes used for testing and for determining the flashover response of insulation have been standardized by various groups and while there is not 100% agreement, the waveshapes used generally conform to the following:

Fundamental frequency	50 or 60 Hz sine wave (8000 μs rise time)
Switching impulse	200–250 μs by 2000 μs
Lightning impulse	1.2 μs by 50 μs

The impulse waveshapes are usually formed by a double exponential having the time to crest indicated by the first number and the time to 50% of the crest on the tail of the wave indicated by the second number. Thus, a lightning impulse would crest at 1.2 μs and following the crest would fall off to 50% of the crest at 50 μs .

Fundamental frequency characteristics have been published, and typical values are indicated on Fig. 14.1 (Aleksandrov et al., 1962; EPRI, 1982).

Equations have also been published or can be developed which define the typical responses to positive polarity switching and lightning impulses (see Fig. 14.2). Insulation usually has a lower withstand capability when exposed to positive polarity impulses than when exposed to negative impulses; thus, designs are usually based on positive magnitude impulses.

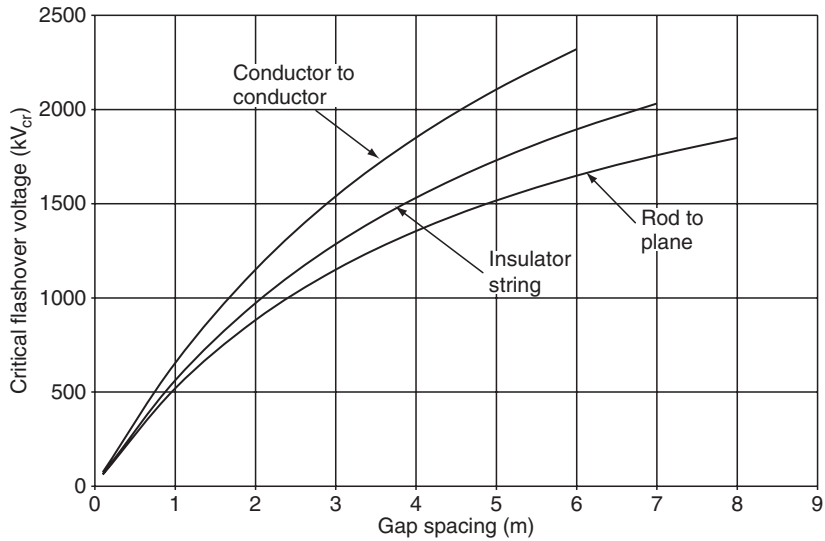


FIGURE 14.1 V_{50} for fundamental frequency waveshapes. (From *Transmission Line Reference Book, 345 kV and Above*, 2nd ed., Electric Power Research Institute, 1975.)

For switching surge impulses (gaps ≤ 15 m) (Gallet et al., 1976):

$$V_{50} = k \frac{3400}{8} \text{ kV} \quad (14.5)$$

$$1 + \frac{d}{d}$$

For lightning impulses, the following equation can be developed from EEI (1968):

$$V_{50} = k * 500 * d \text{ kV} \quad (14.6)$$

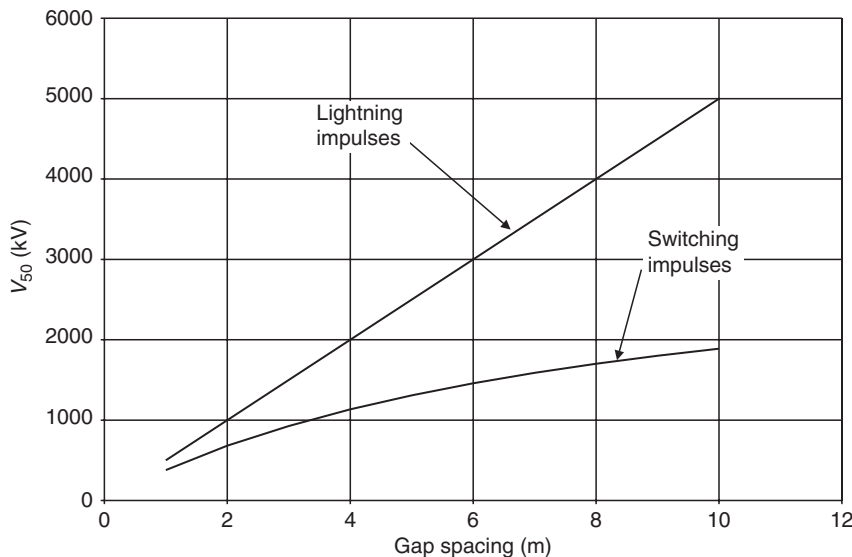


FIGURE 14.2 V_{50} for impulses—positive polarity, rod-plane gap. (From *EHV Transmission Line Reference Book*, Edison Electric Institute, New York, 1968; Gallet, G., Better, M. and Leroy, G., *IEEE T. Power Ap. Sys.*, PAS-95, 580, 1976.)

where k is an electrode factor reflecting the shape of the electrodes (Paris, 1967) and d is the electrode gap spacing in meters.

14.4.2 Electrode Configuration

Electrode configuration has a pronounced effect on the V_{50} characteristics, and this is reflected as a gap or electrode factor, k (Paris, 1967). Examples of k are:

Rod–plane	1.00
Conductor–structure	1.30
Rod–rod	1.30
Conductor–rope	1.40
Conductor–rod	1.65

14.4.3 Effect of Insulator

The presence of an insulator in a gap tends to reduce the gap factor from those given above, mainly due to the terminal electrode configuration (and intermediate flanges for multiunit column bus support insulators). The reduction increases with increased gap factor and typical correction values may be found on Fig. 14.3. Note that these corrections are subject to variations (Thione, 1984).

Rain has little effect on a gap without an insulator; however, rain does reduce the gap factor when an insulator is present. Reductions as high as 20% have been noted; but, in general a reduction of 4%–5% is typical (Thione, 1984).

14.4.4 Effect of Atmospheric Conditions on Air Insulation

V_{50} for gases is affected by temperature, atmospheric pressure, and humidity, and for air the correction can be expressed as

$$V_{50,\text{ambient}} = V_{50,\text{NTP}} \left(\frac{\delta}{H_0} \right)^n \quad (14.7)$$

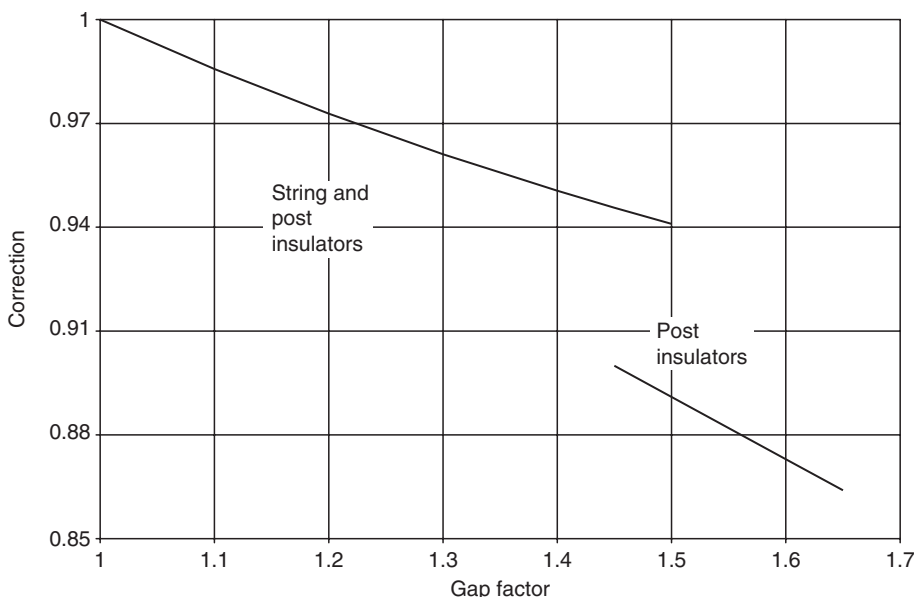


FIGURE 14.3 Gap factor correction for presence of insulator. (From Thione, L., *ELECTRA*, 94, 77, 1984.)

where

NTP is the normal temperature and pressure (20°C, 101.3 kPa)

H_o is the humidity correction factor

n is a gap length correction factor

δ is the relative air density correction factor

The correction for temperature and pressure, “ δ ,” is known as the RAD (relative air density) correction factor and is expressed by

$$\delta = \frac{0.386 H_{\text{mm of Hg}}}{273 + T} \quad (14.8)$$

where $H_{\text{mm of Hg}}$ is the atmospheric pressure in mm of Hg and T is the temperature in °C.

The humidity correction factor, “ H_o ,” is given in IEEE 4 (1978) and can be expressed approximately by

$$\begin{aligned} H_o &\cong 1.1 - 0.00820 * H_{AB} \\ &\cong 1.1 - 0.008071 * VP \end{aligned} \quad (14.9)$$

where H_{AB} is the absolute humidity in g/m³ and VP is the vapor pressure in mm of Hg.

For switching impulses (and fundamental frequency) the effect of the RAD and humidity on V_{50} is, however, a function of the gap length and has less effect on longer gap than on shorter gap lengths. For lengths of 0–1 m the “ n ” correction factor is 1.0; from 1 to 6 m, the correction decreases linearly from 1.0 to 0.4; and for lengths greater than 6 m, the factor is 0.4. There is no gap length correction for positive lightning impulses (EEI, 1968; EPRI, 1975, 1982). Other approaches for humidity corrections can be found in Menemenlis et al. (1988); Thione (1984); Feser and Pigini (1987).

14.4.5 Altitude

Corrections for altitude are also important as the insulation capability drops off about 10% per 1000 m as shown in Fig. 14.4. There are various equations for the altitude correction factor (ACF) and the following expression is representative of most in use (IEEE 1312, 1999):

$$ACF = \left(e^{-\frac{H_t}{8600}} \right)^n \quad (14.10)$$

where H_t is the altitude in meters and n is a gap length correction factor.

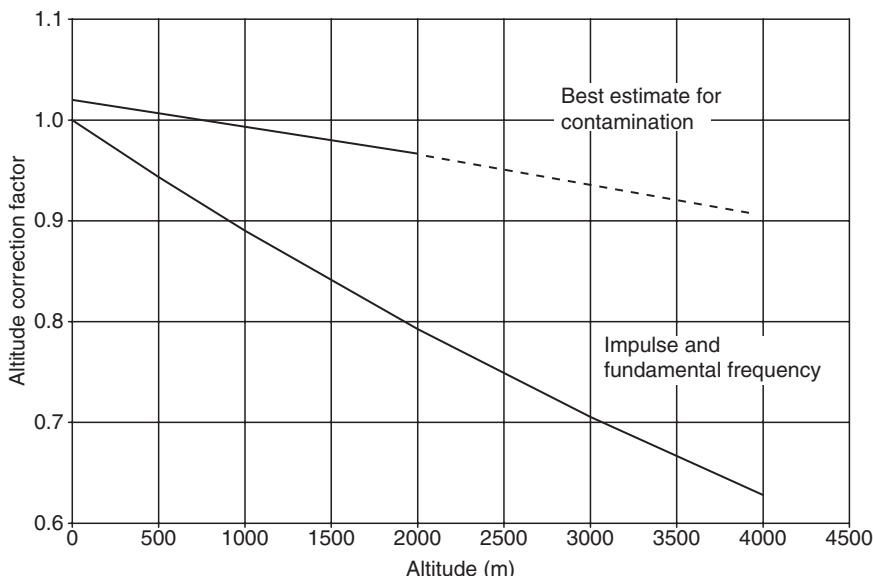


FIGURE 14.4 Altitude correction factors. (From Mizuno, Y., Kusada, H. and Naito, K., *IEEE T. Dielect El. In.*, 4, 286, 1997; *IEEE Standard for Insulation Coordination—Part 2, Application Guide*, Institute of Electrical and Electronic Engineers (IEEE), 1312, 1999.)

14.4.6 Insulator Contamination

Insulator contamination is an important issue for fundamental frequency voltage considerations, and the equivalent salt density, ESDD, approach is extensively used as a design tool. The contamination severity is defined by the ESDD in mg/cm^2 , and an insulator creepage distance, in terms of $\text{mm}/\text{kV}_{\text{rms}}$, phase to phase^a, can then be selected (IEC 815, 1986). Note that insulator/bushing shed/skirt design has a significant impact on the performance, and some past designs performed poorly due to skirt configuration even though they had large creepage distances. With the ESDD approach insulators are tested to define their expected performance. Table 14.1 shows the relationship between contamination level, ESDD, and recommended creepage distances.

Altitude also has an effect on the performance of contaminated insulation, and the degradation of capability as a function of altitude may be found in Fig. 14.4 (Mizuno et al., 1997).

Example 14.1

Assume 10 identical substation bus support insulators in parallel located in a 500-kV substation located at sea level; this configuration can be described as an air gap, conductor to rod configuration at standard atmospheric conditions. Assume that an overall pfo for the 10 gaps of 0.5% is desired when the configuration is exposed to a switching surge of 939 kV (2.3 pu on a 500-kV system). What is the required gap clearance in meters?

Solution

The desired pfo of one gap, p , then should be

$$\text{pfo}_{10 \text{ gaps}} = 0.005 = 1 - (1 - p)^{10}$$

and

$$\begin{aligned} p &= 1 - (1 - 0.005)^{1/10} \\ &= 0.0005011 \end{aligned}$$

From tables or calculations for a normal or Gaussian distribution, a probability of 0.0005011 corresponds to 3.29 standard deviations below the mean (V_{50}). Therefore, the desired V_{50} value is

$$939 \text{ kV} = V_{50}(1 - 3.29 * 0.06)$$

and

$$V_{50} = 1170 \text{ kV}$$

A standard deviation of 6% is often used for the air gap for switching surge stresses.

TABLE 14.1 Recommended Creepage Distances

Contamination Level	Example	ESDD (mg/cm^2)	Minimum Recommended Creepage Distance ($\text{mm}/\text{kV}_{\text{rms}}$, phase to phase)
Light	Low industrial activity	0.03–0.06	16
Medium	Industrial activity—some exposure to wind from the sea	0.1–0.2	20
Heavy	Industrial area and areas close to the sea	0.3–0.6	25
Very heavy	Heavy industrial or sea coast area	>0.6	31

With the V_{50} of 1170 kV and noting that a conductor to rod gap has a k factor of 1.65 assumed to be reduced to 1.42 due to the presence of the insulator, the desired gap spacing value can be calculated by

$$1170 \text{ kV} = 1.42 \frac{3400}{1 + \frac{8}{d}}$$

and

$$d = 2.56 \text{ m}$$

14.4.7 Application of Surge Arresters

Surge arresters are used to limit overvoltages and as a result, allow reductions in the clearances required for self-restoring gaps (e.g., transmission line towers) as well as the capability required for nonself-restoring insulation such as transformer windings. In most applications the proper approach is to determine the minimum arrester rating, which can be applied without resulting in damage to the arrester and then to define the insulation level required so as to result in an acceptable pfo or risk of failure.

For a transmission line application, for example, although the arrester reduces higher magnitude surges to lower levels, the line is still allowed to have a finite, albeit low, pfo for a specific switching operation. Thus, the arrester, by limiting the higher magnitude surges, allows smaller conductor to tower clearances.

However, when arresters are used to protect a transformer for example, an insulation level, which has a significantly higher capability than the maximum surge allowed by the arrester, is selected. This margin between the arrester protective levels (lightning or switching surge) is a function of various considerations as well as the conservatism of the person applying the arrester/insulation system.

Today, for new applications, only metal oxide (ZnO) arresters are being applied. Although there are certainly many of the gapped, silicon carbide type arresters still in service and which still perform effectively, in what follows, only metal oxide arresters will be considered to protect insulation. Successful application requires that the arrester survives the electrical environment in which it is placed, and the following arrester capabilities must be carefully considered:

MCOV—maximum fundamental frequency continuous operating voltage applied to the arrester

TOV—temporary fundamental frequency overvoltages to which the arrester may be exposed

Energy—the energy which must be absorbed by the arrester when limiting switching surges

14.4.7.1 MCOV

The highest system voltage, which can be continuously applied to the arrester, needs to be determined and the arrester capability, its MCOV rating, should at least be equal to and should usually exceed the highest continuous system voltage by some small margin. For example, if a nominal 345-kV system is never operated above 352 kV, then the maximum continuous voltage, which would be expected to be applied to a line to ground arrester, would be $352 \text{ kV}/\sqrt{3} = 203.2 \text{ kV}$. With today's typical arresters, the next highest available MCOV capability would be 209 kV and is associated with an arrester rated 258 kV.

14.4.7.2 TOV

On occasion, the fundamental frequency voltage applied to an arrester will exceed the expected MCOV. Examples include fault conditions during which line to ground voltages on unfaulted phases can rise significantly (as high as phase-to-phase voltage for ungrounded systems); rise in line voltage when energizing a transmission line (Ferranti effect) and voltages which occur during load rejection events—these are usually associated with voltages experienced on a radial transmission line emanating from a generating plant when the load terminal of the line opens unexpectedly.

14.4.7.3 Energy

When an arrester limits switching surges on a transmission line, it can absorb a significant amount of energy, and it can be important to examine events and determine the energy which could be absorbed. Exceeding the arrester's capability could result in immediate damage to the arrester and failure. It is also important to the arrester's TOV capability as absorbing energy heats the arrester material, and application of a significant temporary overvoltage immediately following absorption of a significant amount of energy could result in thermal runaway and arrester failure.

Following selection of an arrester which would be expected to survive the electrical environment (i.e., the minimum rated arrester), the protective levels of the arrester must be correlated with the insulation capability and acceptable margins between the protective levels and the insulation capability achieved.

The protective level or discharge voltage of an arrester is the voltage magnitude to which the arrester will limit the voltage while discharging a surge, and these levels are a function of the waveshape and rise time of the surge as well as the current magnitude of the discharge. In general, the discharge or protective levels considered for coordination with insulation capability are

- a 10-kA, $8 \times 20\text{-}\mu\text{s}$ discharge for coordination with the insulation full wave or lightning impulse (BIL) capability and
- a 0.5–2.0-kA, $36 \times 90\text{-}\mu\text{s}$ discharge for coordination with the switching impulse capability

There should always be margin between the protective level of the arrester and the insulation capability to allow for uncertainties in arrester protective levels due to surge rise times, discharge currents, and arrester separation distance (faster rise times, higher currents, and longer separation distance or lead lengths generate higher protective levels). Uncertainties in insulation capability include reduced insulation strength due to aging (especially for paper insulation in transformers for example) and limitations of the ability of laboratory dielectric testing to accurately relate to field conditions.

In the author's opinion, a margin of at least 40% is appropriate unless all the uncertainties and the risks are carefully evaluated.

14.4.8 Examples of Surge Arrester Application (Nonself-Restoring Insulation)

14.4.8.1 34.5-kV System Application

Surge arresters are to be applied line to ground at the terminals of a circuit breaker (38-kV rating, 150-kV BIL) used on a solidly grounded 34.5-kV system. The highest expected continuous system voltage is 37 kV, and during fault conditions, the phase to ground voltage can rise to 1.4 pu or 27.9 kV. Faults can persist for 20 cycles.

The maximum line to ground voltage is $37/\sqrt{3} = 21.4$ kV and the MCOV of the arrester must meet or exceed this value. An arrester rated 27 kV would be acceptable as it has an MCOV of 22.0 kV. The 1 s TOV capability of the arrester is 31.7 kV, and as this exceeds the 27.9 kV phase to ground voltage expected during faults, the 27-kV arrester meets the TOV criteria as well.

A 27-kV arrester has a 10-kA discharge level of 67.7 kV, and thus the margin between the discharge or protective level and the insulation BIL is $(150/67.7 \times 100 - 100)$ or 121%. This margin is obviously more than adequate, and selection of an arrester rated 27 kV would be appropriate.

14.4.8.2 500-kV System Application

A 500-kV shunt reactor (solidly grounded neutral) is being applied at the end of a 300 km, 500-kV transmission line, and arresters are to be applied line to ground on the terminals of the reactor to limit surges to reasonable levels. The reactor is solidly connected to the line and is switched with the line, and the substation at which the reactor resides is at an altitude of 1800 m. The highest expected continuous system voltage is 550 kV. During line switching operations, the circuit breaker at the reactor terminal may not be closed for some period following energizing of the line/reactor from the other terminal, and the phase to ground voltage at the reactor can be as high as 1.15 pu for as long as 5 min. Arrester energy

requirements were determined (by EMTP or TNA simulations of switching operations) to be well within the capability of an arrester rated 396 kV.

The minimum required MCOV is $550/\sqrt{3} = 317.5$ kV. The minimum required TOV is $1.15 \times 500/\sqrt{3} = 332$ kV for 300 s, and for most arresters, such a requirement would correlate with a 1 s TOV rating of 451 kV. An arrester rated 396 kV has a 318-kV MCOV and a 1 s TOV rating of 451 kV; thus, a 396-kV arrester would be the minimum rating that could be used. Of course any arrester rated higher than 396 kV could also be used. The 10-kA lightning ($8 \times 20 \mu\text{s}$ waveform) and switching surge (2 kA, $36 \times 90 \mu\text{s}$) discharge levels for a 396-kV and a 420-kV arrester are:

Discharge Levels		
Rating	10 kA	Switching surge
396 kV	872 kV	758 kV
420 kV	924 kV	830 kV

BIL values of 1300 and 1425 kV for the reactor's *internal insulation* (i.e., insulation not affected by altitude) could be considered as reasonable candidates for a specification. The corresponding switching impulse levels (SIL) would be 1080 and 1180 kV, respectively, and the following table indicates the margin between the arrester protective levels and the insulation level.

Arrester	1300-kV BIL		1425-kV BIL	
	396 kV	420 kV	396 kV	420 kV
SIL	42%	30%	56%	42%
BIL	49%	41%	63%	54%

Application of a 420-kV arrester for a 1300-kV BIL insulation level results in margins below 40%, and unless the application is very carefully considered from the point of view of arrester separation distance and lead length, expected maximum discharge current level, wave rise time, etc., a 396-kV arrester would be a better choice. For a 1425-kV BIL, either the 396-kV or the 420-kV arrester would result in sufficient margins.

For *external insulation*, i.e., the reactor bushings, the effect of altitude on the insulation capability needs to be considered. At 1800 m, the insulation has only 81% of the withstand capability demonstrated at sea level or 0 m. For example, the SIL of a 1425-kV bushing (1180 kV at sea level) would be reduced to 956 kV at 1800 m ($1180 \times 0.81 = 956$ kV), and application of even a 396-kV arrester would result in a margin of 26%—hardly acceptable.

Assume that a 420-kV arrester was selected to protect the reactor (the arrester itself is rated for application to 3000 m). The switching surge and 10 kA protective levels are 830 and 924 kV, respectively. With a desired minimum margin of 40%, and correcting for altitude, the minimum SIL and BIL at sea level (0 m) should be

$$\begin{aligned}\text{Minimum SIL} &= \frac{830 \times 1.4}{0.81} = 1435 \text{ kV} \\ \text{Minimum BIL} &= \frac{924 \times 1.4}{0.81} = 1597 \text{ kV}\end{aligned}$$

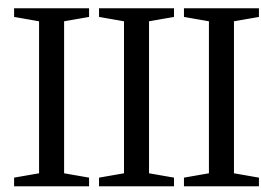
A 1550-kV BIL bushing would have a 1290-kV SIL, and even if one would accept the slightly less than a 36% margin for the BIL, the SIL margin would only be 26%. A 1675-kV BIL bushing would be expected to have a 1390-kV SIL capability, and so the SIL margin would be 36% with a BIL margin of 47%. The next higher rated bushing (1800-kV BIL) would mean applying 800-kV system class bushings, and their increased size and cost would likely not make for a reasonable design. Consequently, specifying a 1675-kV BIL bushing and accepting the slightly reduced SIL margin would be a reasonable compromise.

14.4.8.3 Effect of Surge Reduction Techniques on Overall PFO

Application of surge arresters to significantly reduce switching surge levels on transmission line and substation insulators can be effective, however, the designer should be aware that the overall PFO of all three phases needs to be considered as it will usually be higher than that found for a single phase by a factor often approaching three. Also for long transmission lines, application of arresters at the line terminals will certainly limit the surges at the terminals but will not limit the surges at other points on the line to the same level. Consequently, the surge distribution along the line may need to be considered (Lambert, 1988; Ribiero et al., 1991).

References

- Aleksandrov, G.N., Kizvetter, V.Y., Rudakova, V.M. and Tushnov, A.N., The AC flashover voltages of long air gaps and strings of insulators, *Elektrichestvo*, 6, 27–32, 1962.
- EHV Transmission Line Reference Book*, Edison Electric Institute, New York, 1968.
- Feser, K. and Pigini, A., Influence of atmospheric conditions on the dielectric strength of external insulation, *ELECTRA*, 112, 83–93, 1987.
- Gallet, G., Bettler, M. and Leroy, G., Switching impulse results obtained on the outdoor testing area at Renardieres, *IEEE Transactions on Power Apparatus and Systems*, PAS-95(2), 580–585, 1976.
- Guide for the Selection of Insulators in Respect of Polluted Conditions*, The International Electrotechnical Commission Publication 815, 1986.
- IEEE Standard for Insulation Coordination—Part 2, Application Guide*, Institute of Electrical and Electronic Engineers (IEEE) 1312-1999.
- IEEE Standard Techniques for High-Voltage Testing*, Institute of Electrical and Electronic Engineers (IEEE) 4-1978.
- Lambert, S.R., Effectiveness of zinc oxide surge arresters on substation equipment probabilities of flashover, *IEEE Transactions on Power Delivery*, 3(4), 1928–1934, 1988.
- McNutt, W.J. and Lambert, S.R., *Transformer Concepts and Applications Course*, Power Technologies, Inc., Schenectady, New York, 1992.
- Menemenlis, C., Carrara, G. and Lambeth, P.J., Application of insulators to withstand switching surges in substations, part I: switching impulse insulation strength, 88 WM 077-0, IEEE/PES Winter Meeting, New York, January 31–February 5, 1988.
- Mizuno, Y., Kusada, H. and Naito, K., Effect of climatic conditions on contamination flashover voltage of insulators, *IEEE Transactions on Dielectrics and Electrical Insulation*, 4(3), 286–289, 1997.
- Paris, L., Influence of air gap characteristics on line-to-ground switching surge strength, *IEEE Transactions on Power Apparatus and Systems*, PAS-86(8), 936–947, 1967.
- Ribeiro, J.R., Lambert, S.R. and Wilson, D.D., Protection of compact transmission lines with metal oxide arresters, CIGRE Leningrad Symposium, 400-6, S33–S91, 1991.
- Thione, L., Evaluation of the switching impulse strength of external insulation, *ELECTRA*, 94, 77–95, 1984.
- Transmission Line Reference Book, 345 kV and Above*, 1st ed., Electric Power Research Institute, 1975.
- Transmission Line Reference Book, 345 kV and Above*, 2nd ed., Electric Power Research Institute, 1982.



Power System Planning (Reliability)

Gerald B. Sheblé
Portland State University

15	Planning <i>Gerald B. Sheblé</i>	15-1
	Defining a Competitive Framework	
16	Short-Term Load and Price Forecasting with Artificial Neural Networks <i>Alireza Khotanzad</i>	16-1
	Artificial Neural Networks • Short-Term Load Forecasting • Short-Term Price Forecasting	
17	Transmission Plan Evaluation—Assessment of System Reliability <i>N. Dag Reppen and James W. Feltes</i>	17-1
	Bulk Power System Reliability and Supply Point Reliability • Methods for Assessing Supply Point Reliability • Probabilistic Reliability Assessment Methods • Application Examples	
18	Power System Planning <i>Hyde M. Merrill</i>	18-1
	Planning Entities • Arenas • The Planning Problem • Planning Processes	
19	Power System Reliability <i>Richard E. Brown</i>	19-1
	NERC Regions • System Adequacy Assessment • System Security Assessment • Probabilistic Security Assessment • Distribution System Reliability • Typical Sequence of Events after an Overhead Distribution Fault • Distribution Reliability Indices • Storms and Major Events • Component Reliability Data • Utility Reliability Problems • Reliability Economics • Annual Variations in Reliability	
20	Probabilistic Methods for Planning and Operational Analysis <i>Gerald T. Heydt and Peter W. Sauer</i>	20-1
	Uncertainty in Power System Engineering • Deterministic Power Flow Studies • Monte Carlo Power Flow Studies • Analytical Probabilistic Power Flow Studies • Applications for Available Transfer Capability • An Example of Stochastic Available Transfer Capability • An Example of Expected Financial Income from Transmission Tariffs • Conclusions	

15

Planning

15.1	Defining a Competitive Framework.....	15-2
	Preparing for Competition • Present View of Overall Problem • Economic Evolution • Market Structure • Fully Evolved Marketplace • Computerized Auction Market Structure • Capacity Expansion Problem Definition • Other Sections on Planning	

Gerald B. Sheblé
Portland State University

Capacity expansion decisions are made daily by government agencies, private corporations, partnerships, and individuals. Most decisions are small relative to the profit and loss sheet of most companies. However, many decisions are sufficiently large to determine the future financial health of the nation, company, partnership, or individual. Capacity expansion of hydroelectric facilities may require the commitment of financial capital exceeding the income of most small countries. Capacity expansion of thermal fossil fuel plants is not as severe, but does require a large number of financial resources including bank loans, bonds for long-term debt, stock issues for more working capital, and even joint-venture agreements with other suppliers or customers to share the cost and the risk of the expansion. This section proposes several mathematical optimization techniques to assist in this planning process. These models and methods are tools for making better decisions based on the uncertainty of future demand, project costs, loan costs, technology change, etc. Although the material presented in this section is only a simple model of the process, it does capture the essence of real capacity expansion problems.

This section relies on a definition of electric power industry restructuring presented in (Sheblé, 1999). The new environment within this work assumes that the vertically integrated utility has been segmented into a horizontally integrated system. Specifically, GENCOS, DISTCOs, and TRANSCOs exist in place of the old. This work does not assume that separate companies have been formed. It is only necessary that comparable services are available for anyone connected to the transmission grid.

As can be concluded, this description of a deregulated marketplace is an amplified version of the commodity market. It needs polishing and expanding. The change in the electric utility business environment is depicted generically below. The functions shown are the emerging paradigm. This work outlines the market organization for this new paradigm.

Attitudes toward restructuring still vary from state to state and from country to country. Many electric utilities in the U.S. have been reluctant to change the status quo. Electric utilities with high rates are very reluctant to restructure since the customer is expected to leave for the lower prices. Electric utility companies in regions with low prices are more receptive to change since they expect to pick up more customers. In 1998, California became the first state in the U.S. to adopt a competitive structure, and other states are observing the outcome. Several states on the eastern coast of the U.S. have also restructured. Some offer customer selection of supplier. Some offer markets similar to those established in the United Kingdom, Norway, and Sweden, but not Spain. Several countries have gone to the extreme competitive position of treating electricity as a commodity as seen in New Zealand and Australia. As these markets continue to evolve, governments in all areas of the world will continue to form opinions on what market, operational, and planning structures will suit them best.

15.1 Defining a Competitive Framework

There are many market frameworks that can be used to introduce competition between electric utilities. Almost every country embracing competitive markets for its electric system has done so in a different manner. The methods described here assume an electric marketplace derived from commodities exchanges like the Chicago Mercantile Exchange, Chicago Board of Trade, and New York Mercantile Exchange (NYMEX) where commodities (other than electricity) have been traded for many years. NYMEX added electricity futures to their offerings in 1996, supporting this author's previous predictions (Sheblé, 1991; 1992; 1993; 1994) regarding the framework of the coming competitive environment. The framework proposed has similarities to the Norwegian-Sweden electric systems. The proposed structure is partially implemented in New Zealand, Australia, and Spain. The framework is being adapted since similar structures are already implemented in other industries. Thus, it would be extremely expensive to ignore the treatment of other industries and commodities. The details of this framework and some of its major differences from the emerging power markets/pools are described in Sheblé (1999).

These methods imply that the ultimate competitive electric industry environment is one in which retail consumers have the ability to choose their own electric supplier. Often referred to as retail access, this is quite a contrast to the vertically integrated monopolies of the past. Telemarketers are contacting consumers, asking to speak to the person in charge of making decisions about electric service. Depending on consumer preference and the installed technology, it may be possible to do this on an almost real-time basis as one might use a debit card at the local grocery store or gas station. Real-time pricing, where electricity is priced as it is used, is getting closer to becoming a reality as information technology advances. Presently, however, customers in most regions lack the sophisticated metering equipment necessary to implement retail access at this level.

Charging rates that were deemed fair by the government agency, the average monopolistic electric utility of the old environment met all consumer demand while attempting to minimize their costs. During natural or man-made disasters, neighboring utilities cooperated without competitively charging for their assistance. The costs were always passed on to the rate payers. The electric companies in a country or continent were all members of one big happy family. The new companies of the future competitive environment will also be happy to help out in times of disaster, but each offer of assistance will be priced recognizing that the competitor's loss is gain for everyone else. No longer guaranteed a rate of return, the entities participating in the competitive electric utility industry of tomorrow will be profit driven.

15.1.1 Preparing for Competition

Electric energy prices recently rose to more than \$7500/MWh in the Midwest (1998) due to a combination of high demand and the forced outage of several units. Many midwestern electric utilities bought energy at that high price, and then sold it to consumers for the normal rate. Unless these companies thought they were going to be heavily fined, or lose all customers for a very long time, it may have been more fiscally responsible to terminate services.

Under highly competitive scenarios, the successful supplier will recover its incremental costs as well as its fixed costs through the prices it charges. For a short time, producers may sell below their costs, but will need to make up the losses during another time period. Economic theory shows that eventually, under perfect competition, all companies will arrive at a point where their profit is zero. This is the point at which the company can break even, assuming the average cost is greater than the incremental cost. At this ideal point, the best any producer can do in a competitive framework, ignoring fixed costs, is to bid at the incremental cost. Perfect competition is not often found in the real world for many reasons. The prevalent reason is *technology change*. Fortunately, there are things that the competitive producer can do to increase the odds of surviving and remaining profitable.

The operational tools used and decisions made by companies operating in a competitive environment are dependent on the structure and rules of the power system operation. In each of the

various market structures, the company goal is to maximize profit. Entities such as commodity exchanges are responsible for ensuring that the industry operates in a secure manner. The rules of operation should be designed by regulators prior to implementation to be complete and “fair.” *Fairness* in this work is defined to include noncollusion, open market information, open transmission and distribution access, and proper price signals. It could call for maximization of social welfare (i.e., maximize everyone’s happiness) or perhaps maximization of consumer surplus (i.e., make customers happy).

Changing regulations are affecting each company’s way of doing business and to remain profitable, new tools are needed to help companies make the transition from the old environment to the competitive world of the future. This work describes and develops methods and tools that are designed for the competitive component of the electric industry. Some of these tools include software to generate bidding strategies, software to incorporate the bidding strategies of other competitors, and updated common tools like economic dispatch and unit commitment to maximize profit.

15.1.2 Present View of Overall Problem

This work is motivated by the recent changes in regulatory policies of interutility power interchange practices. Economists believe that electric pricing must be regulated by free market forces rather than by public utilities commissions. A major focus of the changing policies is “competition” as a replacement for “regulation” to achieve economic efficiency. A number of changes will be needed as competition replaces regulation. The coordination arrangements presently existing among the different players in the electric market would change operational, planning, and organizational behaviors.

Government agencies are entrusted to encourage an open market system to create a competitive environment where generation and supportive services are bought and sold under demand and supply market conditions. The open market system will consist of generation companies (GENCOs), distribution companies (DISTCOs), transmission companies (TRANSCOs), a central coordinator to provide independent system operation (ISO), and brokers to match buyers and sellers (BROCOs). The interconnection between these groups is shown in Fig. 15.1.

The ISO is independent and a dissociated agent for market participants. The roles and responsibilities of the ISO in the new marketplace are yet not clear. This work assumes that the ISO is responsible for coordinating the market players (GENCOs, DISTCOs, and TRANSCOs) to provide a reliable power system functions. Under this assumption, the ISO would require a new class of optimization algorithms to perform price-based operation. Efficient tools are needed to verify that the system remains in operation with all contracts in place. This work proposes an energy brokerage model for all services as a novel framework for price-based optimization. The proposed foundation is used to develop analysis and simulation tools to study the implementation aspects of various contracts in a deregulated environment.

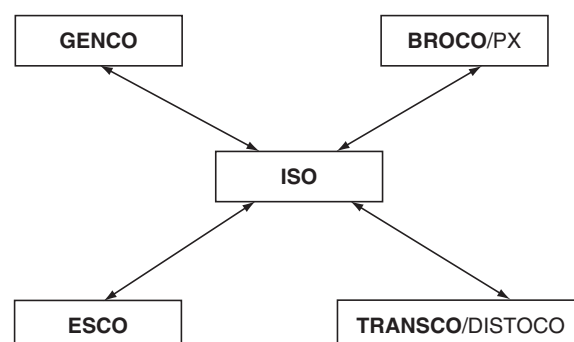


FIGURE 15.1 New organizational structure.

Although it is conceptually clean to have separate functions for the GENCOs, DISTCOs, TRANSCOs, and the ISO, the overall mode of real-time operation is still evolving. Presently, two possible versions of market operations are debated in the industry. One version is based on the traditional power pool concept (POOLCO). The other is based on transactions and bilateral transactions as presently handled by commodity exchanges in other industries. Both versions are based on the premise of price-based operation and market-driven demand. This work presents analytical tools to compare the two approaches. Especially with the developed auction market simulator, POOLCO, multilateral, and bilateral agreements can be studied.

Working toward the goal of economic efficiency, one should not forget that the reliability of the electric services is of the utmost importance to the electric utility industry in North America. In the words of the North American Electric Reliability Council (NERC), reliability in a bulk electric system indicates "*the degree to which the performance of the elements of that system results in electricity being delivered to customers within accepted standards and in the amount desired. The degree of reliability may be measured by the frequency, duration, and magnitude of adverse effects on the electric supply.*" The council also suggests that reliability can be addressed by considering the two basic and functional aspects of the bulk electric system—adequacy and security. In this work, the discussion is focused on the adequacy aspect of power system reliability, which is defined as the static evaluation of the system's ability to satisfy the system load requirements. In the context of the new business environment, market demand is interpreted as the system load. However, a secure implementation of electric power transactions concerns power system operation and stability issues:

1. *Stability issue*: The electric power system is a nonlinear dynamic system comprised of numerous machines synchronized with each other. Stable operation of these machines following disturbances or major changes in the network often requires limitations on various operating conditions, such as generation levels, load levels, and power transmission changes. Due to various inertial forces, these machines, together with other system components, require extra energy (reserve margins and load following capability) to safely and continuously actuate electric power transfer.
2. *Thermal overload issue*: Electrical network capacity and losses limit electric power transmission. Capacity may include real-time weather conditions as well as congestion management. The impact of transmission losses on market power is yet to be understood.
3. *Operating voltage issues*: Enough reactive power support must accompany the real power transfer to maintain the transfer capacity at the specified levels of open access.

In the new organizational structure, the services used for supporting a reliable delivery of electric energy (e.g., various reserve margins, load following capability, congestion management, transmission losses, reactive power support, etc.) are termed supportive services. These have been called "ancillary services" in the past. In this context, the term "ancillary services" is misleading since the services in question are not ancillary but *closely bundled* with the electric power transfer as described earlier. The open market system should consider all of these supportive services as an integral part of power transaction.

This work proposes that supportive services become a competitive component in the energy market. It is embedded so that no matter what reasonable conditions occur, the (operationally) centralized service will have the obligation and the authority to deliver and keep the system responding according to adopted operating constraints. As such, although competitive, it is burdened by additional goals of ensuring reliability rather than open access only. The proposed pricing framework attempts to become economically efficient by moving from cost-based to price-based operation and introduces a mathematical framework to enable all players to be sufficiently informed in decision-making when serving other competitive energy market players, including customers.

15.1.3 Economic Evolution

Some economists speculate that regional commodity exchanges within the U.S. would be oligopolistic in nature (having a limited numbers of sellers) due to the configuration of the transmission system.

Some postulate that the number of sellers will be sufficient to achieve near-perfect competition. Other countries have established exchanges with as few as three players. However, such experiments have reinforced the notion that collusion is all too tempting, and that market power is the key to price determination, as it is in any other market. Regardless of the actual level of competition, companies that wish to survive in the deregulated marketplace must change the way they do business. They will need to develop bidding strategies for trading electricity via an exchange.

Economists have developed theoretical results of how variably competitive markets are supposed to behave under varying numbers of sellers or buyers. The economic results are often valid only when aggregated across an entire industry and frequently require unrealistic assumptions. While considered sound in a macroscopic sense, these results may be less than helpful to a particular company (not fitting the industry profile) that is trying to develop a strategy that will allow it to remain competitive.

Generation companies (GENCOs), energy service companies (ESCOs), and distribution companies (DISTCOs) that participate in an energy commodity exchange must learn to place effective bids in order to win energy contracts. Microeconomic theory states that in the long term, a hypothetical firm selling in a competitive market should price its product at its marginal cost of production. The theory is based on several assumptions (e.g., all market players will behave rationally, all market players have perfect information) that may tend to be true industry-wide, but might not be true for a particular region or a particular firm. As shown in this work, the normal price offerings are based on average prices. Markets are very seldom perfect or in equilibrium.

There is no doubt that deregulation in the power industry will have many far-reaching effects on the strategic planning of firms within the industry. One of the most interesting effects will be the optimal pricing and output strategies generator companies (GENCOs) will employ in order to be competitive while maximizing profits. This case study presents two very basic, yet effective means for a single generator company (GENCO) to determine the optimal output and price of their electrical power output for maximum profits.

The first assumption made is that switching from a government regulated, monopolistic industry to a deregulated competitive industry will result in numerous geographic regions of oligopolies. The market will behave more like an oligopoly than a purely competitive market due to the increasing physical restrictions of transferring power over distances. This makes it practical for only a small number of GENCOs to service a given geographic region.

15.1.4 Market Structure

Although nobody knows the exact structure of the emerging deregulated industry, this research predicts that regional exchanges (i.e., electricity mercantile associations [EMAs]) will play an important role. Electricity trading of the future will be accomplished through bilateral contracts and EMAs where traders bid for contracts via a double auction. The electric marketplace used in this section has been refined and described by various authors. Fahd and Sheblé (1992a) demonstrated an auction mechanism. Sheblé (1994b) described the different types of commodity markets and their operation, outlining how each could be applied in the evolved electric energy marketplace. Sheblé and McCalley (1994e) outlined how spot, forward, future, planning, and swap markets can handle real-time control of the system (e.g., automatic generation control) and risk management. Work by Kumar and Sheblé (1996b) brought the above ideas together and demonstrated a power system auction game designed to be a training tool. That game used the double auction mechanism in combination with classical optimization techniques.

In several references (Kumar, 1996a, 1996b; Sheblé 1996b; Richter 1997a), a framework is described in which electric energy is only sold to distribution companies (DISTCOs), and electricity is generated by generation companies (GENCOs) ([see Fig. 15.2](#)). The North American Electric Reliability Council (NERC) sets the reliability standards. Along with DISTCOs and GENCOs, energy services companies (ESCOs), ancillary services companies (ANCILCOs), and transmission companies (TRANSCOs)

Level 1	FERC	SPUC	SPUC	SPUC
2			NERC		
3			ICA/ISO/RTO		
4	GENCO	ESCO	TRANSCO	DISTCO	EMA
5	MARKCO				BROCO

FIGURE 15.2 Business environmental model.

interact via contracts. The contract prices are determined through a double auction. Buyers and sellers of electricity make bids and offers that are matched subject to approval of the independent contract administrator (ICA), who ensures that the contracts will result in a system operating safely within limits. The ICA submits information to an independent system operator (ISO) for implementation. The ISO is responsible for physically controlling the system to maintain its security and reliability.

15.1.5 Fully Evolved Marketplace

The following sections outline the role of a horizontally integrated industry. Many curious acronyms have described generation companies (IPP, QF, Cogen, etc.), transmission companies (IOUTS, NUTS, etc.), and distribution companies (IOUDC, COOPS, MUNIES, etc.). The acronyms used in this work are described in the following sections.

15.1.5.1 Horizontally Integrated

The restructuring of the electric power industry is most easily visualized as a horizontally integrated marketplace. This implies that interrelationships exist between generation (GENCO), transmission (TRANSCO), and distribution (DISTCO) companies as separate entities. Note that independent power producers (IPP), qualifying facilities (QF), etc. may be considered as equivalent generation companies. Nonutility transmission systems (NUTS) may be considered as equivalent transmission companies. Cooperatives and municipal utilities may be considered as equivalent distribution companies. All companies are assumed to be coordinated through a regional Transmission Corporation (or regional transmission group).

15.1.5.2 Federal Energy Regulatory Commission (FERC)

FERC is concerned with the overall operation and planning of the national grid, consistent with the various energy acts and public utility laws passed by Congress. Similar federal commissions exist in other government structures. The goal is to provide a workable business environment while protecting the economy, the customers, and the companies from unfair business practices and from criminal behavior. GENCOs, ESCOs, and TRANSCOs would be under the jurisdiction of FERC for all contracts impacting interstate trade.

15.1.5.3 State Public Utility Commission (SPUC)

SPUCs protect the individual state economies and customers from unfair business practices and from criminal behavior. It is assumed that most DISTCOs would still be regulated by SPUCs under performance-based regulation and not by FERC. GENCOs, ESCOs, and TRANSCOs would be under the jurisdiction of SPUCs for all contracts impacting intrastate trade.

15.1.5.4 Generation Company (GENCO)

The goal for a generation company, which has to fill contracts for the cash and futures markets, is to package production at an attractive price and time schedule. One proposed method is similar to the classic decentralization techniques used by a vertically integrated company. The traditional power system approach is to use Dantzig-Wolfe decomposition. Such a proposed method may be compared with traditional operational research methods used by commercial market companies for a “make or buy” decision.

15.1.5.5 Transmission Company (TRANSCO)

The goal for transmission companies, which have to provide services by contracts, is to package the availability and the cost of the integrated transportation network to facilitate transportation from suppliers (GENCOs) to buyer (ESCOs). One proposed method is similar to oil pipeline networks and energy modeling. Such a proposed method can be compared to traditional network approaches using optimal power flow programs.

15.1.5.6 Distribution Company (DISTCO)

The goal for distribution companies, which have to provide services by contracts, is to package the availability and the cost of the radial transportation network to facilitate transportation from suppliers (GENCOs) to buyers (ESCOs). One proposed method is similar to distribution outlets. Such proposed methods can be compared to traditional network approaches using optimal power flow programs. The disaggregation of the transmission and the distribution system may not be necessary, as both are expected to be regulated as monopolies at the present time.

15.1.5.7 Energy Service Company (ESCO)

The goal for energy service companies, which may be large industrial customers or customer pools, is to purchase power at the least cost when needed by consumers. One proposed method is similar to the decision of a retailer to select the brand names for products being offered to the public. Such a proposed method may be compared to other retail outlet shops.

15.1.5.8 Independent System Operator (ISO)

The primary concern is the management of operations. Real-time control (or nearly real-time) must be completely secure if any amount of scheduling is to be implemented by markets. The present business environment uses a fixed combination of units for a given load level, and then performs extensive analysis of the operation of the system. If markets determine schedules, then the unit schedules may not be fixed sufficiently ahead of realtime for all of the proper analysis to be completed by the ISO.

15.1.5.9 Regional Transmission Organization (RTO)

The goal for a regional transmission group, which must coordinate all contracts and bids among the three major types of players, is to facilitate transactions while maintaining system planning. One proposed method is based on discrete analysis of a Dutch auction. Other auction mechanisms may be suggested. Such proposed methods are similar to a warehousing decision on how much to inventory for a future period. As shown later in this work, the functions of the RTG and the ISO could be merged. Indeed, this should be the case based on organizational behavior.

15.1.5.10 Independent Contract Administrator (ICA)

The goal for an Independent Contract Administrator is a combination of the goals for an ISO and an RTG. Northern States Power Company originally proposed this term. This term will be used in place of ISO and RTG in the following to differentiate the combined responsibility from the existing ISO companies.

15.1.5.11 Electric Markets

Competition may be enhanced through the various markets: cash, futures, planning, and swap. The cash market facilitates trading in spot and forward contracts. This work assumes that such trading would be on an hourly basis. Functionally, this is equivalent to the interchange brokerage systems implemented in several states. The distinction is that future time period interchange (forward contracts) are also traded.

The futures market facilitates trading of futures and options. These are financially derived contracts used to spread risk. The planning market facilitates trading of contracts for system expansion. Such a market has been proposed by a west coast electric utility. The swap market facilitates trading between all markets when conversion from one type of contract to another is desired. It should be noted that multiple markets are required to enable competition between markets.

Time Horizon (Months)						
0	1	2	12	18
Spot Market	Forward Market					360
Swap Market (Market to Market Contracts)						
	Futures Market				Planning Market	

FIGURE 15.3 Interconnection between markets.

The structure of any spot market auction must include the ability to schedule as far into the future as the industrial practice did before deregulation. This would require extending the spot into the future for at least six months, as proposed by this author (Sheblé, 1994). Future month production should be traded for actual delivery in forward markets. Future contracts should be implemented at least 18 months into the future if not 3 years. Planning contracts must be implemented for at least 20 years into the future, as recently offered by TVA, to provide an orderly, predictable expansion of the generation and transmission systems. Only then can timely addition of generation and transmission be assured. Finally, a swap market must be established to enable the transfer of contracts from one period (market) to another.

To minimize risk, the use of option contracts for each market should be implemented. Essentially, all of the players share the risk. This is why all markets should be open to the public for general trading and subject to all rules and regulations of a commodity exchange. Private exchanges, not subject to such regulations, do not encourage competition and open price discovery.

The described framework (Sheblé, 1996b) allows for cash (spot and forward), futures, and planning markets as shown in Fig. 15.3. The *spot market* is most familiar within the electric industry (Schweppie, 1988). A seller and a buyer agree (either bilaterally or through an exchange) upon a price for a certain amount of power (MW) to be delivered sometime in the near future (e.g., 10 MW from 1:00 p.m. to 4:00 p.m. tomorrow). The buyer needs the electricity, and the seller wants to sell. They arrange for the electrons to flow through the electrical transmission system and they are happy. A *forward contract* is a binding agreement in which the seller agrees to deliver an amount of a particular product in a specified quality at a specified time to the buyer. The forward contract is further into the future than is the spot market. In both the forward and spot contracts, the buyer and seller want physical goods (e.g., the electrons). A *futures contract* is primarily a financial instrument that allows traders to lock in a price for a commodity in some future month. This helps traders manage their risk by limiting potential losses or gains. Futures contracts exist for commodities in which there is sufficient interest and in which the goods are generic enough that it is not possible to tell one unit of the good from another (e.g., 1 MW of electricity of a certain quality, voltage level, etc.). A futures *option contract* is a form of insurance that gives the option purchaser the right, but not the obligation, to buy (sell) a futures contract at a given price. For each options contract, there is someone “writing” the contract who, in return for a premium, is obligated to sell (buy) at the strike price (see Fig. 15.3). Both the options and the futures contracts are financial instruments designed to minimize risk. Although provisions for delivery exist, they are not convenient (i.e., the delivery point is not located where you want it to be located). The trader ultimately cancels his position in the futures market, either with a gain or loss. The physicals are then purchased on the spot market to meet demand with the profit or loss having been locked in via the futures contract.

A *swap* is a customized agreement in which one firm agrees to trade its coupon payment for one held by another firm involved in the swap. Finally, a *planning market* is needed to establish a basis for financing long term projects like transmission lines and power plants (Sheblé, 1993).

15.1.6 Computerized Auction Market Structure

Auction market structure is a computerized market, as shown in Fig. 15.4. Each of the agents has a terminal (PC, workstation, etc.) connected to an auctioneer (auction mechanism) and a contract

ICA			
Auction Mechanism		Contract Evaluations	
Communication Player to Auction			
Player	Player	Player	Player

FIGURE 15.4 Computerized markets.

evaluator. Players generate bids (buy and sell) and submit the quotation to the auctioneer. A bid is a specified amount of electricity at a given price. The auctioneer binds bids (matching buyers and sellers) subject to approval of the contract evaluation. This is equivalent to the pool operating convention used in the vertically integrated business environment.

The contract evaluator verifies that the network can remain in operation with the new bid in place. If the network cannot operate, then the match is denied. The auctioneer processes all bids to determine which matches can be made. However, the primary problem is the complete specification of how the network can operate and how the agents are treated comparably as the network is operated closer to limits. The network model must include all constraints for adequacy and security.

The major trading objectives are hedging, speculation, and arbitrage. Hedging is a defense mechanism against loss and/or supply shortages. Speculation is assuming an investment risk with a chance for profit. Arbitrage is crossing sales (purchases) between markets for riskless profit. This work assumes that there are four markets commonly operated: forward, futures, planning, and swaps (Fig. 15.5).

Forward Market: The forward contracts reflect short term future system conditions. In the forward market, prices are determined at the time of the contract but the transactions occur at some future time. Optimization tools for short term scheduling problems can be enhanced to evaluate trading opportunities in the forward market. For example, short term dispatching algorithms, such as economic unit commitment dispatch, can be used to estimate and earn profit in the forward market.

Futures Market: A futures market creates competition because it unifies diverse and scattered local markets and stabilizes prices. The contracts in the futures market are risky because price movements over time can result in large gains or losses. There is a link between forward markets and futures markets that restricts price volatility. *Options* (options contracts) allow the agent to exercise the right to activate a contract or cancel it. Claims to buy are called “call” options. Claims to sell are called “put” options.

A more detailed discussion of an electric futures contract is discussed in Sheblé (1994b). The components include trading unit, trading hours, trading months, price quotation, minimum price fluctuation, maximum daily price fluctuation, last trading day, exercise of options, option strike prices, delivery, delivery period, alternate delivery procedure, exchange of futures for, or in connection with, physicals, quality specifications, and customer margin requirements.

Time Line Into Future (Hours)				Information Level
0.....			744	
GENCO	ESCO	MARKCO	BROCO	Player
Bids	Bids	Bids	Communication
Spot	Forward	Futures	Planning	Markets
		Swap		Market
		ICA/ISO/RTO		Coordination
GENCO	ESCO	MARKCO	BROCO	Players
...

FIGURE 15.5 Electric market.

Swap Market: In the swap market, contract position can be closed with an exchange of physical or financial substitutions. The trader can find another trader who will accept (make) delivery and end the trader's delivery obligation. The acceptor of the obligation is compensated through a price discount or a premium relative to the market rate.

The financial drain inflicted on traders when hedging their operations in the futures market is slightly higher than the one inflicted through direct placement in the forward market. An optimal mix of options, forward commitments, futures contracts, and physical inventories is difficult to assess and depends on hedging, constraints imposed by different contracts, and the cost of different contracts. A clearinghouse such as a swap market handles the exchange of various energy instruments.

Planning Market: The growth of transmission grid requires transmission companies to make contracts based on the expected usage to finance projects. The planning market would underwrite equipment usage subject to the long term commitments to which all companies are bound by the rules of network expansion to maintain a fair marketplace. The network expansion would have to be done to maximize the use of transmission grid for all agents. Collaboration would have to be overseen and prohibited with a sufficiently high financial penalty. The growth of the generation supply similarly requires such markets. However, such a market has been started with the use of franchise rights (options) as established in recent Tennessee Valley Authority connection contracts. This author has published several papers outlining the need for such a market. Such efforts are not documented in this work.

15.1.7 Capacity Expansion Problem Definition

The capacity expansion problem is different for an ESCO, GENCO, TRANSCO, DISTCO, and ANSILOCO. This section assumes that the ICA will not own equipment but will only administer the contracts between players. The capacity expansion problem is divided into the following areas: generation expansion, transmission expansion, distribution expansion, and market expansion. ESCOs are concerned with market expansion. GENCOs are concerned with generation expansion. TRANSCOs are concerned with transmission expansion. DISTCOs are concerned with distribution expansion. ANSILOCOs are concerned with supportive devices expansion. This author views ancillary services as a misnomer. Such services are necessary supportive services. Thus, the term "supportive" will be used instead of ancillary. Also, since supportive devices are inherently part and parcel of the transmission or distribution system, these devices will be assumed into the TRANSCO and DISTCO functions without loss of generality. Thus, ANSILOCOs are not treated separately.

Based on the above idealized view of the marketplace, the following generalizations are made. GENCOs are concerned with the addition of capacity to meet market demands while maximizing profit. Market demands include bilateral contracts with the EMA as well as bilateral contracts with ESCOs or with the ICA. ESCOs are concerned with the addition of capacity of supplying customers with the service desired to maintain market share. ESCOs are thus primarily concerned with the processing of information from marketplace to customer. However, ESCOs are also concerned with additional equipment supplied by DISTCOs or TRANSCOs to provide the level of service required by some customers. ESCOs are thus concerned with all aspects of customer contracts and not just the supply of "electrons."

The ICA is concerned with the operation of the overall system subject to the contracts between the buyers and the sellers and between all players with ICA. The overall goal of the ICA is to enable any customer to trade with any other customer with the quick resolution of contract enforcement available through mercantile associations. The ICA maintains the reliability of the network by resolving the unexpected differences between the contracts, real operation, and unplanned events. The ICA has the authority, through contracts, to buy generation services, supportive services, and/or transmission services, or to curtail contracts if the problems cannot be resolved with such purchases as defined in these contracts. Thus, the ICA has the authority to connect or disconnect generation and demand to protect the integrity of the system. The ICA has the authority to order new transmission or distribution expansion to maintain the system reliability and economic efficiency of the overall system. The economic

efficiency is determined by the price of electricity in the cash markets on a periodic basis. If the prices are approximately the same at all points in the network, then the network is not preventing customers from getting to the suppliers. Similarly, the suppliers can get to the buyers. Since all buyers and suppliers are protected from each other through the default clauses of the mercantile agreement, it does not matter which company deals with other companies as the quick resolution of disputes is guaranteed. This strictness of guarantee is the cornerstone of removing the financial uncertainty at the price of a transaction fee to cover the costs of enforcement.

The goal of each company is different but the tools are the same for each. First, the demand must be predicted for future time periods sufficiently into the future to maintain operation financially and physically. Second, the present worth of the expansion projects has to be estimated. Third, the risks associated with each project and the demand-forecast uncertainty must be estimated. Fourth, the acceptable value at risk acceptable for the company has to be defined. Fifth, the value at risk has to be calculated. Sixth, methods of reducing the value at risk have to be identified and evaluated for benefits. Seventh, the overall portfolio of projects, contracts, strategies, and risk has to be assessed. Only then can management decide to select a project for implementation.

The characteristics of expansion problems include:

1. The cost of equipment or facilities should exhibit economies of scale for the same risk level baring technology changes.
2. Time is a primary factor since equipment has to be in place and ready to serve the needs as they arise. Premature installation results in idle equipment. Delayed installation results in lost market share.
3. The risk associated with the portfolio of projects should decrease as time advances.
4. The portfolio has to be revalued at each point when new information is available that may change the project selection, change the strategy, or change the mix of contracts.

The capital expansion problem is often referred to as the “capital budgeting under uncertainty” problem (Aggarwal, 1993). Thus, capital expansion is an exercise in estimating the present net value of future cash flows and other benefits as compared to the initial investment required for the project given the risk associated with the project(s). The key concept is the uncertainty and thus the risk of all business ventures. Uncertainties may be due to estimation (forecasting) and measurement errors. Such uncertainties can be reduced by the proper application of better tools. Another approach is to investment in information technology to coordinate the dissemination of information. Indeed, information technology is one key to the appropriate application of capital expansion.

Another uncertainty factor is that the net present value depends on market imperfections. Market imperfections are due to competitor reactions to each other's strategies, technology changes, and market rule changes (regulatory changes). The options offered by new investment are very hard to forecast. Also the variances of the options to reduce the risk of projects are critical to proper selection of the right project. Management has to constantly revalue the project, change the project (including termination), integrate new information, or modify the project to include technology changes.

Estimates have often been biased by management pressure to move ahead, to not investigate all risks, or to maintain strategies that are not working as planned. Uncertainties in regulations and taxes are often critical for the decision to continue.

There are three steps to any investment plan: investment alternative identification, assessment, selection and management of the investment as events warrant.

The remaining sections outline the necessity of each step by simple models of the problem to be solved at each step. Since simple problems are given, linear programming solution techniques may be used to solve them. Indeed, the theory of optimization can yield valuable insight as to the importance of further investigations. The inclusion of such models is beyond the scope of this work.

Capacity expansion is one aspect of capital budgeting. Marketing and financial investments are also capital budgeting problems. Often, the capacity expansion has to be evaluated not only on the projects merits, but also the merits of the financing bundled with the project.

15.1.8 Other Sections on Planning

The following sections on planning deal with the overall approach as described by Dr. H. Merrill and include sections on forecasting, power system planning, transmission planning, and system reliability. Forecasting demand is a key issue for any business entity. Forecasting for a competitive industry is more critical than for a regulated industry. Transmission planning is discussed based on probabilistic techniques to evaluate the expected advantages and costs of present and future expansion plans. Reliability of the supply is covered, including transmission reliability. The most interesting aspect of the electric power industry is the massive changes presently occurring. It will be interesting to watch as the industry adapts to regulatory changes and as the various market players find their corporate niche in this new framework.

References

- R. Aggarwal, *Capital Budgeting Under Uncertainty*, Prentice-Hall, Englewood Cliffs, NJ, 1993.
- M.L. Baughman, J.W. Jones, and A. Jacob, Model for Evaluating the Economics of Cool Storage Systems, *IEEE Trans. Power Syst.*, 8(2), May 1993.
- W.G. Bently and J.C. Evelyn, "Customer Thermal Energy Storage: A Marketing Opportunity for Cooling Off Electric Peak Demand," *IEEE Trans. on Power Systems*, 1(4), 973–979, 1987.
- R. Billinton and G. Lian, "Monte Carlo Approach to Substation Reliability Evaluation," *IEE Proc.*, 140(2), 147–152, 1991.
- R. Billinton and L. Wenyuan, "Hybrid Approach for Reliability Evaluation of Composite Generation and Transmission Systems Using Monte-Carlo Simulation and Enumeration Technique," *IEE Proc.*, 138(3), 233–241, 1991.
- R. Billinton and W. Li, "A Monte Carlo Method for Multi-Area Generation System Reliability Assessment," *IEEE Trans. Power Syst.*, 7(4), 1487–1492, 1992.
- R. Billinton and L. Gan, "Monte Carlo Simulation Model for Multiarea Generation System Reliability Studies," *IEE Proc.*, 140(6), 532–538, 1993.
- B.R. Binger and E. Hoffman, *Microeconomics with Calculus*. Scott, Foresman and Company, Glenview, 1988.
- Lynn E. Bussey, *The Economic Analysis of Industrial Projects*, Prentice-Hall, Englewood Cliffs, NJ, 1981.
- H.P. Chao, "Peak Load Pricing and Capacity Planning with Demand and Supply Uncertainty," *Bell J. Econ.*, 14(1), 179–190, 1983.
- C.S. Chen and J.N. Sheen, "Cost Benefit Analysis of a Cooling Energy Storage System," *IEEE Trans. Power Syst.*, 8(4), 1993.
- W. Chu, B. Chen, and C. Fu, "Scheduling of Direct Load Control to Minimize Load Reduction for a Utility Suffering from Generation Shortage," *IEEE/PES Winter Meeting*, 1993, Columbus, OH.
- J.S. Clayton, S.R. Erwin, and C.A. Gibson, "Interchange Costing and Wheeling Loss Evaluation by Means of Incrementals," *IEEE Trans. Power Syst.*, 5(3), 759–765, 1990.
- R.E. Clayton and R. Mukerji, "System Planning Tools for the Competitive Market," *IEEE Computer Appl. Power*, 50, 1996.
- A.I. Cohen, J.W. Patmore, D.H. Oglevee, R.W. Berman, L.H. Ayers, and J.F. Howard, "An Integrated System for Load Control," *IEEE Trans. Power Syst.*, PWRS-2(3), 1987.
- H.G. Daellenbach, *Systems and Decision Making*, John Wiley & Sons, New York, 1994.
- B. Daryanian, R.E. Bohn, and R.D. Tabors, "Optimal Demand-side Response to Electricity Spot Prices for Storage-type Customers," *IEEE Trans. Power Syst.*, 4(3), 897–903, 1989.
- A.K. David and Y.Z. Li, "Effect of Inter-temporal Factors on the Real-time Pricing of Elasticity," *IEEE Trans. Power Syst.*, 8(1), 1993.
- J.T. Day, "Forecasting Minimum Production Costs with Linear Programming," *IEEE Trans. Power Apparatus Syst.*, PAS-90(2), 814–823, 1971.
- S. Dekrajangpetch and G.B. Sheblé, "Alternative Implementations of Electric Power Auctions," in *Proc. 60th Am. Power Conf.*, 60–1, 394–398, 1998.
- J.K. Delson, X. Feng, and W.C. Smith, "A Validation Process for Probabilistic Production Costing Programs," *IEEE Trans. Power Syst.*, 6(3), 1326–1336, 1991.

- G. Fahd and G. Sheblé, "Optimal Power Flow of Interchange Brokerage System Using Linear Programming," *IEEE Trans. Power Syst.*, T-PWRS, 7(2), 497–504, 1992.
- G. Fahd, Dan Richards, and Gerald B. Sheblé, "The Implementation of an Energy Brokerage System Using Linear Programming," *IEEE Trans. Power Syst.*, T-PWRS, 7(1), 90–96, 1992.
- George Fahd, "Optimal Power Flow Emulation of Interchange Brokerage Systems Using Linear Programming," Ph.D. dissertation, Auburn University, 1992.
- H.H. Happ, Report on Wheeling Costs, Case 88-E-238, The New York Public Service Commission, Feb. 1990.
- B.F. Hobbs and R.E. Schuler, "An Assessment of the Deregulation of Electric Power Generation Using Network Models of Imperfect Spatial Markets," *Papers of the Regional Science Association*, 57, 75–89, 1985.
- W.W. Hogan, "A Market Power Model with Strategic Interaction in Electricity Networks," *Energy J.*, 18(4), 107–141, 1997.
- S.R. Huang and S.L. Chen, "Evaluation and Improvement of Variance Reduction in Monte-Carlo Production Simulation," *IEEE Trans. Energy Conv.*, 8(4), 610–619, 1993.
- M. Ilic, F. Galiana, and L. Fink, *Power Systems Restructuring: Engineering and Economics*, Kluwer Academic Publishers, Norwell, MA, 1998.
- K. Kelley, S. Henderson, P. Nagler, and M. Eifert, Some Economic Principles for Pricing Wheeled Power. National Regulatory Research Institute, August 1987.
- B.A. Krause and J. McCalley "Bulk Power Transaction Selection in a Competitive Electric Energy System with Provision of Security Incentives," *Proc. 26th Ann. North Am. Power Symp.*, Manhattan, Kansas, September 1994, 126–136.
- J. Kumar and G.B. Sheblé, "A Decision Analysis Approach to Transaction Selection Problem in a Competitive Electric Market," *Electric Power Syst. Res. J.*, 1997.
- J. Kumar and G.B. Sheblé, "A Framework for Transaction Selection Using Decision Analysis Based upon Risk and Cost of Insurance," *Proc. 29th North Am. Power Symp.*, Kansas State University, KS, 1994, 548–557.
- J. Kumar and G.B. Sheblé, "Transaction Selection Using Decision Analysis Based Upon Risk and Cost of Insurance," *IEEE Winter Power Meeting*, 1996.
- J. Kumar Electric Power Auction Market Implementation and Simulation, Ph.D. dissertation, Iowa State University, 1996.
- C.N. Kurucz, D. Brandt, and S. Sim, "A Linear Programming Model for Reducing System Peak Through Customer Load Control Programs," *IEEE PES Winter Meeting*, 96 WM 239–9 PWRS, Baltimore, MD, 1996.
- K.D. Le, R.F. Boyle, M.D. Hunter, and K.D. Jones, "A Procedure for Coordinating Direct-Load-Control Strategies to Minimize System Production Cost," *IEEE Trans. Power App.. Syst.*, PAS-102(6), 1983.
- S.H. Lee and C.L. Wilkins, "A Practical Approach to Appliance Load Control Analysis: A Water Heater Case Study," *IEEE Trans. Power App. Syst.*, 7(4), 1992.
- F.N. Lee, "Three-Area Joint Dispatch Production Costing," *IEEE Trans. Power Syst.*, 3(1), 294–300, 1988.
- T.Y. Lee and N. Chen, "The Effect of Pumped Storage and Battery Energy Storage Systems on Hydrothermal Generation Coordination," *IEEE Trans. Energy Conv.*, 7(4), 631–637, 1992.
- T.Y. Lee and N. Chen, "Optimal Capacity of the Battery Storage System in a Power System," *IEEE Trans. Energy Conv.*, 8(4), 667–673, 1993.
- T.Y. Lee and N. Chen, "Effect of Battery Energy Storage System on the Time-of-Use Rates Industrial Customers," *IEE Proc.: Generator Transmission Distribution*, 141(5), 5521–528, 1994.
- A.P. Lerner, "Monopoly and the Measurement of Monopoly Power," *Rev. Econ. Stud.*, 1, 157–175, 1934.
- M. Lin, A. Breipohl, and F. Lee, "Comparison of Probabilistic Production Cost Simulation Methods" *IEEE Trans. Power Syst.*, 4(4), 1326–1333, 1989.
- J. McCalley and G.B. Sheblé, "Competitive Electric Energy Systems: Reliability of Bulk Transmission and Supply," tutorial paper presented at the *Fourth International Conference of Probabilistic Methods Applied to Power Systems*, 1994.

- J. McCalley, A. Fouad, V. Vittal, A. Irizarry-Rivera, R. Farmer, and B. Agarwal, "A Probabilistic Problem in Electric Power System Operation: The Economy-Security Tradeoff for Stability-Limited Systems," *Proc. Third Intl. Workshop on Rough Sets and Soft Computing*, November 10–12, 1994, San Jose, CA.
- H.M. Merrill and A.J. Wood, "Risk and Uncertainty in Power System Planning," *10th Power Syst. Comp. Conf.*, PSCC, Graz, Austria, August 1990.
- H.M. Merrill, "Have I Ever Got a Deal for You. Economic Principles in Pricing of Services," IEEE SP 91EH0345-9-PWR, pp. 1–8, 1991.
- V. Miranda, "Power System Planning and Fuzzy Sets: Towards a Comprehensive Model Including All Types of Uncertainties," *Proc. PMAPS'94*, Rio de Janeiro, Brazil, September 1994.
- V. Miranda and L.M. Proen  a, "A General Methodology for Distribution Planning Under Uncertainty, Including Genetic Algorithms and Fuzzy Models in a Multi-criteria Environment," *Proc. Stockholm Power Tech, SPT'95*, Stockholm, Sweden, June 18–22, 832–837, 1995.
- R.E. Mortensen, and K.P. Haggerty, "Dynamics of Heating and Cooling Loads: Models, Simulation, and Actual Utility Data," *IEEE Trans. Power Syst.*, 5(1), 253–248, 1990.
- K.-H. Ng and G.B. Shebl  , "Direct Load Control—A Profit-based Load Management Using Linear Programming," *IEEE Trans. Power Syst.*, 13(2), 1998.
- K.-H. Ng Reformulating Load Management Under Deregulation, Master's thesis, Iowa State University, Ames, May 1997.
- R.P. O'Neill and C.S. Whitmore, "Network Oligopoly Regulation: An Approach to Electric Federalism," *Electricity and Federalism Symp.*, June 24, 1993 (Revised March 16, 1994).
- S.S. Oren, P. Spiller, P. Variya, and F. Wu, "Nodal Prices and Transmission Rights: A Critical Appraisal," University of California at Berkeley Research Report, December 1994.
- S.S. Oren, "Economic Inefficiency of Passive Transmission Rights in Congested Electricity Systems with Competitive Generation," *Energy J.*, 18(1), 63–83, 1997.
- H.R. Outhred, "Principles of a Market-Based Electricity Industry and Possible Steps Toward Implementation in Australia," *Intl. Conf. Adv. Power Syst. Control, Operation and Management*, Hong Kong, December. 7–10, 1993.
- B.J. Parker, E. Denzinger, B. Porretta, G.J. Anders, and M.S. Mirsky, "Optimal Economic Power Transfers," *IEEE Trans. Power Syst.*, 4(3), 1167–1175, 1989.
- C. Parker and J. Strelmel, "A Smart Monte Carlo Procedure for Production Costing and Uncertainty Analysis," *Proc. Am. Power Conf.*, 58(II), 897–900, 1996.
- V. Pereira, B.G. Gorenstein, and Morozowski Fo, "Chronological Probabilistic Production Costing and Wheeling Calculations with Transmission Network Modeling," *IEEE Trans. Power Syst.*, 7(2), 885–891, 1992.
- D. Post, *Electric Power Interchange Transaction Analysis and Selection*, Master's thesis, Iowa State University, Ames, 1994.
- D. Post, S. Coppinger, and G. Shebl  , "Application of Auctions as a Pricing Mechanism for the Interchange of Electric Power," *IEEE Trans. Power Syst.*, 10(3), 1580–1584, 1995.
- M.V. Rakic and Z.M. Markovic, "Short Term Operation and Power Exchange Planning of Hydro-thermal Power Systems," *IEEE Trans. Power Syst.*, 9(1), 1994.
- N.S. Rau, "Certain Considerations in the Pricing of Transmission Service," *IEEE Trans. Power Syst.*, 4(3), 1133–1139, 1989.
- C. Richter and G. Shebl  , "Genetic Algorithm Evolution of Utility Bidding Strategies for the Competitive Marketplace," *1997 IEEE/PES Summer Meeting*, PE-752-PWRS-1-05-1997, New York: IEEE, 1997.
- C. Richter and G. Shebl  , "Building Fuzzy Bidding Strategies for the Competitive Generator," *Proc. 1997 North Am. Power Symp.*, 1997.
- C. Richter and G. Shebl  , "Bidding Strategies that Minimize Risk with Options and Futures Contracts," in *Proc. 1998 Am. Power Conf., Session 25, Open Access II-Power Marketing, Paper C*, 1998.
- S. Roy, "Goal-programming Approach to Optimal Price Determination for Inter-area Energy Trading," *Intl. J. Energy Res.*, 17, 847–862, 1993.

- P. Rupanagunta, M.L. Baughman, and J.W. Jones, "Scheduling of Cool Storage Using Non-linear Programming Techniques," *IEEE Trans. Power Syst.*, 10(3), 1995.
- T. Russel, "Working with an Independent Grid in the UK—A Generator's View," *Proc. 24th Ann. North Am. Power Symp.*, Manhattan, Kansas, 270–275, September 1992.
- F.C. Schweppe, M.C. Caramanis, R.D. Tabors, and R.E. Bohn, *Spot Pricing of Electricity*, Kluwer Academic Publishers, Boston, MA, 1988.
- G.B. Sheblé, "Electric Energy in a Fully Evolved Marketplace," *Proc. 26th Ann. North Am. Power Symp.*, Manhattan, Kansas, pp. 81–90, September 1994.
- G.B. Sheblé, "Simulation of Discrete Auction Systems for Power System Risk Management," *Proc. 27th Ann. Frontiers of Power Conf.*, Oklahoma State University, Stillwater, OK, pp. I.1–I.9, 1994.
- G. Sheblé and G. Fahd, "Unit Commitment Literature Synopsis," *IEEE Trans. Power Syst.*, 9, 128–135, 1994.
- G. Sheblé and J. McCalley, "Discrete Auction Systems for Power System Management," presented at the 1994 National Science Foundation Workshop, Pullman, WA, 1994.
- G. Sheblé, "Priced Based Operation in an Auction Market Structure," *IEEE Trans. on Power Systems*, 11(4), 1770–1777, 1996.
- Sheblé, G.B., *Computational Auction Methods for Restructured Power System Industry Operation*, Kluwer Academic Press, Boston, MA, 1999.
- D. Shirmohammadi, P.R. Gribik, T.K. Law, J.H. Malinowski, and R.E. O'Donnell, "Evaluation of Transmission Network Capacity Use for Wheeling Transactions," *IEEE Trans. Power Syst.*, 4(4), 1405–1413, 1989.
- J. Skeer, "Highlights of the International Energy Agency Conference on Advanced Technologies for Electric Demand-side Management," *Proc. Adv. Technol. Electric Demand-Side Management*, International Energy Agency, Sorrento, Italy, 1991.
- V.L. Smith, "Electric Power Deregulation: Background and Prospects," *Contemporary Policy Issues*, 6, 14–24, 1988.
- S. Smith, "Linear Programming Model for Real-time Pricing of Electric Power Service," *Operations Res.*, 41, 470–483, 1993.
- R.L. Sullivan, *Power System Planning*, McGraw-Hill, New York, 1977.
- A. Svoboda and S. Oren, "Integrating Price-based Resources in Short-term Scheduling of Electric Power Systems," *IEEE Trans. Energy Conv.*, 9, 760–769, 1994.
- R.D. Tabors, "Transmission System Management and Pricing: New Paradigms and International Comparisons," Paper WM110-7 presented at the *IEEE/PES Winter Meeting*, T-PWRS, February 1994.
- A. Vojdani, C. Imparto, N. Saini, B. Wollenberg, and H. Happ, "Transmission Access Issues," presented at the 1995 *IEEE/PES Winter Meeting*, 95 WM 121-4 PWRS, IEEE, New York, 1994.
- L. Wang, "Approximate Confidence Bounds on Monte Carlo Simulation Results for Energy Production," *IEEE Trans. Power Syst.*, 4(1), 69–74, 1989.
- C. Wang and J.R. McDonald, *Modern Power System Planning*, McGraw-Hill, New York, 1994.
- D.C. Wei and N. Chen, "Air-Conditioner Direct Load Control by Multi-pass Dynamic Programming," *IEEE Trans. Power Syst.*, 10(1), 1995.
- H.L. Willis, *Spatial Electric Load Forecasting*, Marcel Dekker, New York, 1996, 14–17.
- W.E. Winston and C.A. Gibson, "Geographical Load Shift and its Effect on Interchange Evaluation," *IEEE Trans. Power Syst.*, 3(3), 865–871, 1988.
- A.J. Wood and B.F. Wollenberg, *Power Generation, Operation, and Control*, 2nd ed., John Wiley & Sons, New York, 1996.
- F. Wu and P. Varaiya, "Coordinated Multi-lateral Trades For Electric Power Networks: Theory and Implementation," University of California at Berkeley Research Report, June 1995.

16

Short-Term Load and Price Forecasting with Artificial Neural Networks¹

Alireza Khotanzad
Southern Methodist University

16.1	Artificial Neural Networks.....	16-1
	Error Back-Propagation Learning Rule • Adaptive Update of the Weights During Online Forecasting	
16.2	Short-Term Load Forecasting.....	16-3
	ANNSTLF Architecture • Humidity and Wind Speed • Holidays and Special Days • Performance	
16.3	Short-Term Price Forecasting.....	16-8
	Architecture of Price Forecaster • Performance	

16.1 Artificial Neural Networks

Artificial neural networks (ANN) are systems inspired by research into how the brain works. An ANN consists of a collection of arithmetic computing units (nodes or neurons) connected together in a network of interconnected layers. A typical node of an ANN is shown in Fig. 16.1. At the input side, there are a number of so-called “connections” that have a weight of “ W_{ij} ” associated with them. The input denoted by X_i gets multiplied by W_{ij} before reaching node j via the respective connection. Inside the neuron, all the individual inputs are first summed up. The summed inputs are passed through a nonlinear single-input, single-output function “S” to produce the output of the neuron. This output in turn is propagated to other neurons via corresponding connections.

While there are a number of different ANN architectures, the most widely used one (especially in practical applications) is the multilayer feed-forward ANN, also known as a multilayer perceptron (MLP), shown in Fig. 16.2. An MLP consists of n input nodes, h so called “hidden layer” nodes (since they are not directly accessible from either input or output side), and m output nodes connected in a feed-forward fashion. The input layer nodes are simple data distributors whereas neurons in the hidden and output layers have an S-shaped nonlinear transfer function known as the “sigmoid activation function,” $f(z) = 1/(1 + e^{-z})$ where z is the summed inputs.

¹This work was supported in part by the Electric Power Research Institute and 1997 Advanced Technology Program of the State of Texas.

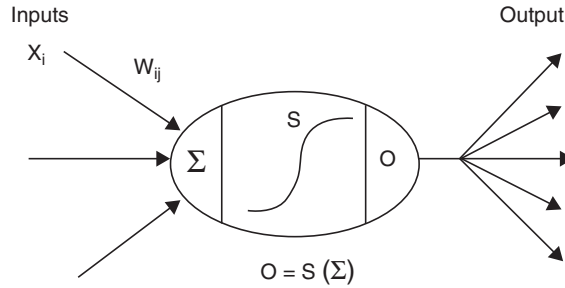


FIGURE 16.1 Model of one node of an ANN.

For hidden layer nodes, the output is:

$$H_j = \frac{1}{1 + \exp\left(-\sum_{i=1}^n W_{ij}X_i\right)}$$

where H_j is the output of the j th hidden layer node, $j = 1, \dots, h$, and X_i represents the i th input connected to this hidden node via W_{ij} with $i = 1, \dots, n$.

The output of the k th output node is given by

$$Y_k = \frac{1}{1 + \exp\left(-\sum_{j=1}^h W_{jk}H_j\right)}$$

where Y_k is the output of the k th output layer node with $k = h + 1, \dots, m$, and W_{jk} representing connection weights from hidden to output layer nodes.

One of the main properties of ANNs is the ability to model complex and nonlinear relationships between input and output vectors through a learning process with “examples.” During learning, known

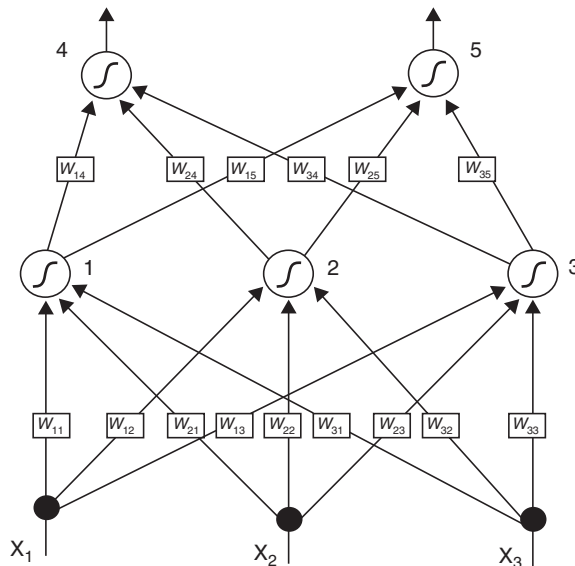


FIGURE 16.2 An example of an MLP with 3 input, 3 hidden, and 2 output nodes.

input-output examples, called the training set, are applied to the ANN. The ANN learns by adjusting or adapting the connection weights through comparing the output of the ANN to the expected output. Once the ANN is trained, the extracted knowledge from the process resides in the resulting connection weights in a distributed manner.

A trained ANN can generalize (i.e., produce the expected output) if the input is not exactly the same as any of those in the training set. This property is ideal for forecasting applications where some historical data exists but the forecast indicators (inputs) may not match up exactly with those in the history.

16.1.1 Error Back-Propagation Learning Rule

The MLP must be trained with historical data to find the appropriate values for W_{ij} and the number of required neurons in the hidden layer. The learning algorithm employed is the well-known error back-propagation (BP) rule (Rumelhart and McClelland, 1986). In BP, learning takes place by adjusting W_{ij} . The output produced by the ANN in response to inputs is repeatedly compared with the correct answer. Each time, the W_{ij} values are adjusted slightly in the direction of the correct answers by back-propagating the error at the output layer through the ANN according to a gradient descent algorithm.

To avoid overtraining, the cross-validation method is used. The training set is divided into two sets. For instance, if three years of data is available, it is divided into a two-year and a one-year set. The first set is used to train the MLP and the second set is used to test the trained model after every few hundred passes over the training data. The error on the validation set is examined. Typically this error decreases as the number of passes over the training set is increased until the ANN is overtrained, as signified by a rise in this error. Therefore, the training is stopped when the error on the validation set starts to increase. This procedure yields the appropriate number of epochs over the training set. The entire three years of data is then used to retrain the MLP using this number of epochs.

In a forecasting application, the number of input and output nodes is equal to the number of utilized forecast indicators and the number of desired outputs, respectively. However, there is no theoretical approach to calculate the appropriate number of hidden layer nodes. This number is determined using a similar approach for training epochs. By examining the error over a validation set for a varying number of hidden layer nodes, a number yielding the smallest error is selected.

16.1.2 Adaptive Update of the Weights During Online Forecasting

A unique aspect of the MLPs used in the forecasting systems described in this section is the adaptive update of the weights during online operation. In a typical usage of an MLP, it is trained with the historical data and the weights of the trained MLP are then treated as fixed parameters. This is an acceptable procedure for many applications. However, if the modeled process is a nonstationary one that can go through rapid changes, e.g., variations of electric load due to weather swings or seasonal changes, a tracking mechanism with sensitivity to the recent trends in the data can aid in producing better results.

To address this issue, an adaptive weight adjustment strategy that takes place during online operation is utilized. The MLP is initially trained using the BP algorithm; however, the trained weights are not treated as static parameters. During online operation, these weights are adaptively updated on a sample-by-sample basis. Before forecasting for the next instance, the forecasts of the past few samples are compared to the actual outcome (assuming that actual outcome for previous forecasts have become available) and a small scale error BP operation is performed with this data. This mini-training with the most recent data results in a slight adjustment of the weights and biases them toward the recent trend in data.

16.2 Short-Term Load Forecasting

The daily operation and planning activities of an electric utility requires the prediction of the electrical demand of its customers. In general, the required load forecasts can be categorized into short-term, mid-term, and long-term forecasts. The short-term forecasts refer to hourly prediction of the load for a lead

time ranging from one hour to several days out. The mid-term forecasts can either be hourly or peak load forecasts for a forecast horizon of one to several months ahead. Finally, the long-term forecasts refer to forecasts made for one to several years in the future.

The quality of short-term hourly load forecasts has a significant impact on the economic operation of the electric utility since many decisions based on these forecasts have significant economic consequences. These decisions include economic scheduling of generating capacity, scheduling of fuel purchases, system security assessment, and planning for energy transactions. The importance of accurate load forecasts will increase in the future because of the dramatic changes occurring in the structure of the utility industry due to deregulation and competition. This environment compels the utilities to operate at the highest possible efficiency, which, as indicated above, requires accurate load forecasts. Moreover, the advent of open access to transmission and distribution systems calls for new actions such as posting the available transmission capacity (ATC), which will depend on the load forecasts.

In the deregulated environment, utilities are not the only entities that need load forecasts. Power marketers, load aggregators, and independent system operators (ISO) will all need to generate load forecasts as an integral part of their operation.

This section describes the third generation of an artificial neural network (ANN) hourly load forecaster known as ANNSTLF (Artificial Neural Network Short-Term Load Forecaster). ANNSTLF, developed by Southern Methodist University and PRT, Inc. under the sponsorship of the Electric Power Research Institute (EPRI), has received wide acceptance by the electric utility industry and is presently being used by over 40 utilities across the U.S. and Canada.

Application of the ANN technology to the load forecasting problem has received much attention in recent years (Bakirtzis et al., 1996; Dillon et al., 1991; Ho et al., 1992; Khotanzad et al., 1998; Khotanzad et al., 1997; Khotanzad et al., 1996; Khotanzad et al., 1995; Lee et al., 1992; Lu et al., 1993; Mohammed et al., 1995; Papalexopoulos et al., 1994; Park et al., 1991; Peng et al., 1993). The function learning property of ANNs enables them to model the correlations between the load and such factors as climatic conditions, past usage pattern, the day of the week, and the time of the day, from historical load and weather data. Among the ANN-based load forecasters discussed in published literature, ANNSTLF is the only one that is implemented at several sites and thoroughly tested under various real-world conditions.

A noteworthy aspect of ANNSTLF is that a single architecture with the same input-output structure is used for modeling hourly loads of various size utilities in different regions of the country. The only customization required is the determination of some parameters of the ANN models. No other aspects of the models need to be altered.

16.2.1 ANNSTLF Architecture

ANNSTLF consists of three modules: two ANN load forecasters and an adaptive combiner (Khotanzad et al., 1998). Both load forecasters receive the same set of inputs and produce a load forecast for the same day, but they utilize different strategies to do so. The function of the combiner module is to mix the two forecasts to generate the final forecast.

Both of the ANN load forecasters have the same topology with the following inputs:

- 24 hourly loads of the previous day
- 24 hourly weather parameters of the previous day (temperatures or effective temperatures, as discussed later)
- 24 hourly weather parameters forecasts for the coming day
- Day type indices

The difference between the two ANNs is in their outputs. The first forecaster is trained to predict the regular (base) load of the next day, i.e., the 24 outputs are the forecasts of the hourly loads of the next day. This ANN will be referred to as the “Regular Load Forecaster (RLF).” On the other hand, the second

ANN forecaster predicts the *change* in hourly load from yesterday to today. This forecaster is named the “Delta Load Forecaster (DLF).”

The two ANN forecasters complement each other because the RLF emphasizes regular load patterns whereas the DLF puts stronger emphasis on yesterday’s load. Combining these two separate forecasts results in improved accuracy. This is especially true for cases of sudden load change caused by weather fronts. The RLF has a tendency to respond slowly to rapid changes in load. On the other hand, since the DLF takes yesterday’s load as the basis and predicts the changes in that load, it has a faster response to a changing situation.

To take advantage of the complimentary performance of the two modules, their forecasts are adaptively combined using the recursive least squares (RLS) algorithm (Proakis et al., 1992). The final forecast for each hour is obtained by a linear combination of the RLF and DLF forecasts as:

$$\hat{L}_{k+1}(i) = \alpha_B(i) \hat{L}_{k+1}^{RLF}(i) + \alpha_C(i) \hat{L}_{k+1}^{DLF}(i), i = 1, \dots, 24$$

The $\alpha_B(i)$ and $\alpha_C(i)$ coefficients are computed using the RLS algorithm. This algorithm produces coefficients that minimize the weighted sum of squared errors of the past forecasts denoted by J ,

$$J = \sum_{k=1}^N \beta^{N-k} [L_k(i) - \hat{L}_k(i)]^2$$

where $L_k(i)$ is the actual load at hour i , N is the number of previous days for which load forecasts have been made, and β is a weighting factor in the range of $0 < \beta \leq 1$ whose effect is to de-emphasize (forget) old data.

The block diagram of the overall system is shown in Fig. 16.3.

16.2.2 Humidity and Wind Speed

Although temperature (T) is the primary weather variable affecting the load, other weather parameters, such as relative humidity (H) and wind speed (W), also have a noticeable impact on the load. The

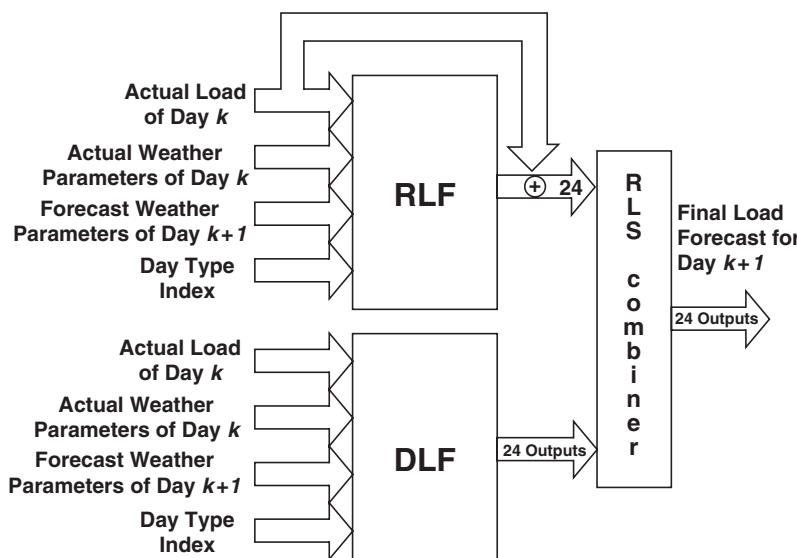


FIGURE 16.3 Block diagram of ANNSTLF.

effects of these variables are taken into account through transforming the temperature value into an effective temperature, T_{eff} , using the following transformation:

$$T_{eff} = T + \alpha * H$$

$$T_{eff} = T - \frac{W * (65^\circ - T)}{100}$$

16.2.3 Holidays and Special Days

Holidays and special days pose a challenge to any load forecasting program since the load of these days can be quite different from a regular workday. The difficulty is the small number of holidays in the historical data compared to the typical days. For instance, there would be three instances of Christmas Day in a training set of three years. The unusual behavior of the load for these days cannot be learned adequately by the ANNs since they are not shown many instances of these days.

It was observed that in most cases, the profile of the load forecast generated by the ANNs using the concept of designating the holiday as a weekend day, does resemble the actual load. However, there usually is a significant error in predicting the peak load of the day. The ANNSTLF package includes a function that enables the user to reshape the forecast of the entire day if the peak load forecast is changed by the user. Thus, the emphasis is placed on producing a better peak load forecast for holidays and reshaping the entire day's forecast based on it.

The holiday peak forecasting algorithm uses a novel weighted interpolation scheme. This algorithm will be referred to as "Reza algorithm" after the author who developed it (Khotanzad et al., 1998). The general idea behind the Reza algorithm is to first find the "close" holidays to the upcoming one in the historical data. The closeness criterion is the temperature at the peak-load hour. Then, the peak load of the upcoming holiday is computed by a novel weighted interpolation function described in the following.

The idea is best illustrated by an example. Let us assume that there are only three holidays in the historical data. The peak loads are first adjusted for any possible load growths. Let (t_i, p_i) designate the i -th peak-load hour temperature and peak load, respectively. Fig. 16.4 shows the plot of p_i vs. t_i for an example case.

Now assume that t_h represents the peak-load hour temperature of the upcoming holiday. t_h falls in between t_1 and t_2 with the implication that the corresponding peak load, p_h , would possibly lie in the range of $[p_1, p_2] = R_1 + R_2$. But, at the same time, t_h is also between t_1 and t_3 implying that p_h would lie in $[p_1, p_3] = R_1$. Based on this logic, p_h can lie in either R_1 or $R_1 + R_2$. However, note that R_1 is common in both ranges. The idea is to give twice as much weight to the R_1 range for estimating p_h since this range appears twice in pair-wise selection of the historical data points.

The next step is to estimate p_h for each nonoverlapping interval, R_1 and R_2 , on the y axis, i.e., $[p_1, p_3]$ and $[p_3, p_2]$.

For $R_1 = [p_1, p_3]$ interval:

$$\hat{p}_{h1} = \frac{p_3 - p_1}{t_3 - t_1} * (t_h - t_1) + p_1$$

For $R_2 = [p_3, p_2]$ interval:

$$\hat{p}_{h2} = \frac{p_2 - p_3}{t_2 - t_3} * (t_h - t_3) + p_3$$

If any of the above interpolation results in a value that falls outside the respective range, R_i , the closest p_i , i.e., maximum or minimum of the interval, is used instead.

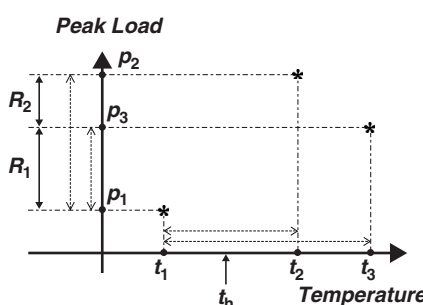


FIGURE 16.4 Example of peak load vs. temperature at peak load for a three-holiday database.

TABLE 16.1 Utility Information for Performance Study

Utility	No. Days in Testing Period	Weather Variable	Location
1	141	T	Canada
2	131	T	South
3	365	T,H,W	Northeast
4	365	T	East Coast
5	134	T	Midwest
6	365	T	West Coast
7	365	T,H	Southwest
8	365	T,H	South
9	174	T	North
10	275	T,W	Midwest

The final estimate of p_h is a weighted average of \hat{p}_{h1} and \hat{p}_{h2} with the weights decided by the number of overlaps that each pair-wise selection of historical datapoints creates. In this case, since R_1 is visited twice, it receives a weighting of two whereas the interval R_2 only gets a weighting coefficient of one.

$$\hat{p}_h = \frac{w_1 * \hat{p}_{h1} + w_2 * \hat{p}_{h2}}{w_1 + w_2} = \frac{2 * \hat{p}_{h1} + 1 * \hat{p}_{h2}}{2 + 1}$$

16.2.4 Performance

The performance of ANNSTLF is tested on real data from ten different utilities in various geographical regions. Information about the general location of these utilities and the length of the testing period are provided in Table 16.1.

In all cases, three years of historical data is used to train ANNSTLF. Actual weather data is used so that the effect of weather forecast errors do not alter the modeling error. The testing is performed in a blind fashion meaning that the test data is completely independent from the training set and is not shown to the model during its training.

One-to-seven-day-ahead forecasts are generated for each test set. To extend the forecast horizon beyond one day ahead, the forecast load of the previous day is used in place of the actual load to obtain the next day's load forecast.

The forecasting results are presented in Table 16.2 in terms of mean absolute percentage error (MAPE) defined as:

$$MAPE = \frac{100}{N} \sum_{i=1}^N \frac{|Actual(i) - Forecast(i)|}{Actual(i)}$$

with N being the number of observations. Note that the average MAPEs over ten utilities as reported in the last row of Table 16.3 indicate that the third-generation engine is quite accurate in forecasting both hourly and peak loads. In the case of hourly load, this average remains below 3% for the entire forecast horizon of seven days ahead, and for the peak load it reaches 3% on the seventh day. A pictorial example of one-to-seven-day-ahead load forecasts for utility 2 is shown in Fig. 16.5.

As pointed out earlier, all the weather variables (T or T_{eff}) used in these studies are the actual data. In online usage of the model, weather forecasts are used. The quality of these weather forecasts vary greatly from one site to another. In our experience, for most cases, the weather forecast errors introduce approximately 1% of additional error for one-to-two-days out load forecasts. The increase in the error for longer range forecasts is more due to less accurate weather forecasts for three or more days out.

TABLE 16.2 Summary of Performance Results in Terms of MAPE

Utility	MAPE OF	Days-Ahead						
		1	2	3	4	5	6	7
1	All hours	1.91	2.29	2.53	2.71	2.87	3.03	3.15
	Peak	1.70	2.11	2.39	2.62	2.73	2.94	3.10
2	All hours	2.72	3.44	3.63	3.77	3.79	3.83	3.80
	Peak	2.64	3.33	3.46	3.37	3.42	3.52	3.40
3	All hours	1.89	2.25	2.38	2.45	2.53	2.58	2.65
	Peak	1.96	2.26	2.41	2.49	2.60	2.69	2.82
4	All hours	2.02	2.37	2.51	2.58	2.61	2.65	2.69
	Peak	2.26	2.59	2.69	2.83	2.85	2.93	2.94
5	All hours	1.97	2.38	2.61	2.66	2.65	2.65	2.74
	Peak	2.03	2.36	2.49	2.37	2.49	2.51	2.55
6	All hours	1.57	1.86	1.99	2.08	2.14	2.17	2.18
	Peak	1.82	2.25	2.38	2.50	2.61	2.62	2.63
7	All hours	2.29	2.79	2.90	3.00	3.05	3.10	3.18
	Peak	2.42	2.78	2.90	2.98	3.07	3.17	3.28
8	All hours	2.22	2.91	3.15	3.28	3.39	3.45	3.50
	Peak	2.38	3.00	3.12	3.29	3.40	3.45	3.52
9	All hours	1.63	2.04	2.20	2.32	2.40	2.41	2.50
	Peak	1.83	2.25	2.36	2.51	2.54	2.64	2.78
10	All hours	2.32	2.97	3.25	3.38	3.44	3.52	3.56
	Peak	2.15	2.75	2.93	3.08	3.16	3.27	3.27
Average	All hours	2.05	2.53	2.72	2.82	2.89	2.94	2.99
	Peak	2.12	2.57	2.71	2.80	2.89	2.97	3.03

16.3 Short-Term Price Forecasting

Another forecasting function needed in a deregulated and competitive electricity market is prediction of future electricity prices. Such forecasts are needed by a number of entities such as generation and power system operators, wholesale power traders, retail market and risk managers, etc. Accurate price forecasts enable these entities to refine their market decisions and energy transactions leading to significant economic advantages. Both *long-term* and *short-term* price forecasts are of importance to the industry. The long-term forecasts are used for decisions on transmission augmentation, generation expansion, and distribution planning whereas the short-term forecasts are needed for daily operations and energy trading decisions. In this work, the emphasis will be on short-term hourly price forecasting with a horizon extending up to the next 24 hours.

In general, energy prices are tied to a number of parameters such as future demand, weather conditions, available generation, planned outages, system reserves, transmission constraints, market perception, etc. These relationships are nonlinear and complex and conventional modeling techniques cannot capture them accurately. In a similar manner to load forecasting, ANNs could be utilized to “learn” the appropriate relationships. Application of ANN technology to electricity price forecasting is relatively new and there are few published studies on this subject (Szkuta et al., 1998).

The adaptive BP MLP forecaster described in the previous section is used here to model the relationship of hourly price to relevant forecast indicators. The system is tested on data from two power pools with good performance.

TABLE 16.3 Training and Test Periods for the Price Forecaster Performance Study

Database	Training Period	Test Period	MAE of Day-Ahead Hourly Price Forecasts (\$)
CALPX	Apr 23, 98–Dec 31, 98	Jan 1, 99–Mar 3, 99	1.73
PJM	Apr 2, 97–Dec 31, 97	Jan 2, 98–Mar 31, 98	3.23

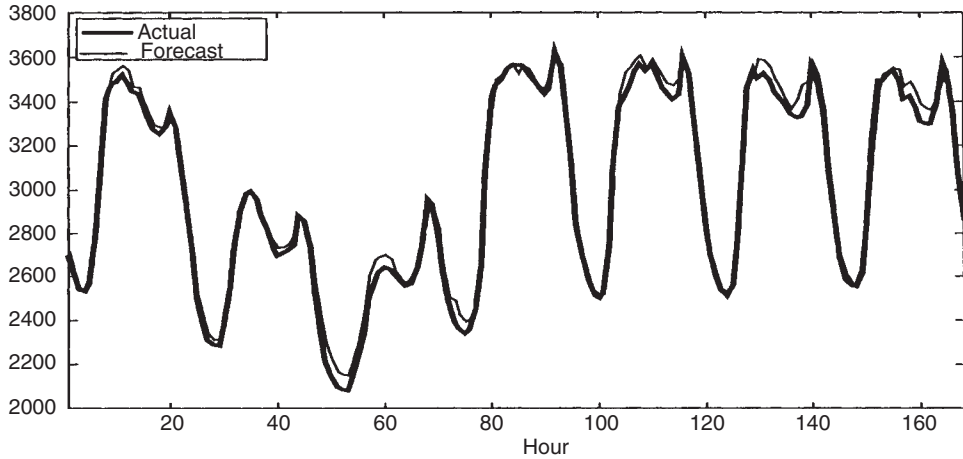


FIGURE 16.5 An example of a one-to-seven-day-ahead load forecast.

16.3.1 Architecture of Price Forecaster

The price forecaster consists of a single adaptive BP MLP with the following inputs:

- Previous day's hourly prices
- Previous day's hourly loads
- Next day's hourly load forecasts
- Next day's expected system status for each hour

The expected system status input is an indicator that is used to provide the system with information about unusual operating conditions such as transmission constraints, outages, or other subjective matters. A bi-level indicator is used to represent typical vs. atypical conditions. This input allows the user to account for his intuition about system condition and helps the ANN better interpret sudden jumps in price data that happen due to system constraints.

The outputs of the forecaster are the next day's 24 hourly price forecasts.

16.3.2 Performance

The performance of the hourly price forecaster is tested on data collected from two sources, the California Power Exchange (CALPX) and the Pennsylvania-New Jersey-Maryland Independent System Operator (PJM). The considered price data are the Unconstrained Market Clearing Price (UMCP) for CALPX, and Market Clearing Price (MCP) for PJM. The average of Locational Marginal Prices (LMP) uses a single MCP for PJM. The training and test periods for each database are listed in [Table 16.3](#). Testing is performed in a blind fashion, meaning that the test data is completely independent from the training set and is not shown to the model during its training. Also, actual load data is used in place of load forecast.

The day-ahead forecast results are presented in the first column of [Table 16.4](#) in terms of mean absolute error (*MAE*) expressed in dollars. This measure is defined as:

TABLE 16.4 Results of Performance Study for the Test Period

Database	MAE of Day-Ahead Hourly Price Forecasts (\$)	Sample Mean of Actual Hourly Prices (\$)	Sample Standard Deviation of Actual Hourly Prices (\$)
CALPX	1.73	19.98	5.45
PJM	3.23	17.44	7.67

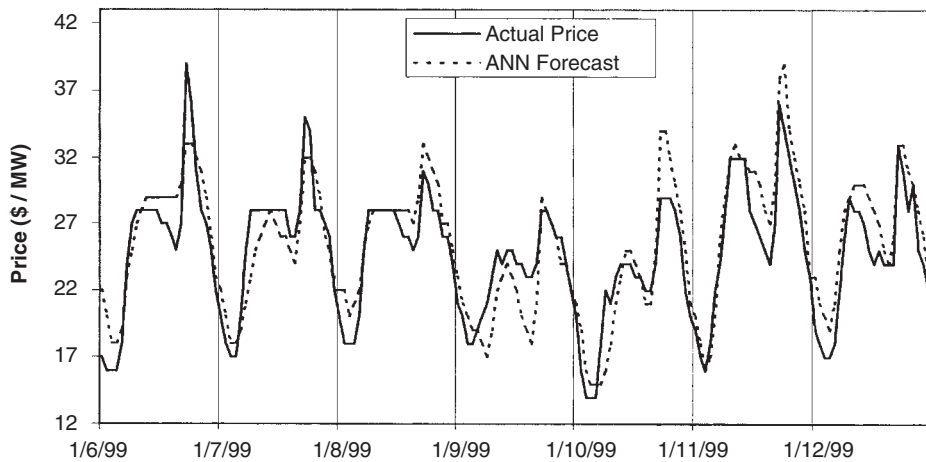


FIGURE 16.6 An example of the ANN price forecaster performance for CALPX price data.

$$MAE = \frac{100}{N} \sum_{i=1}^N |Actual\ Price(i) - Forecast\ Price(i)|$$

with N being the total number of hours in the test period.

To put these results in perspective, the sample mean and standard deviation of hourly prices in the test period are also listed in [Table 16.4](#). Note the correspondence between MAE and the standard deviation of data, i.e., the smaller standard deviation results in a lower MAE and vice versa.

Figures 16.6 and 16.7 show a representative example of the performance for each of the databases. It can be seen that the forecasts closely follow the actual data.

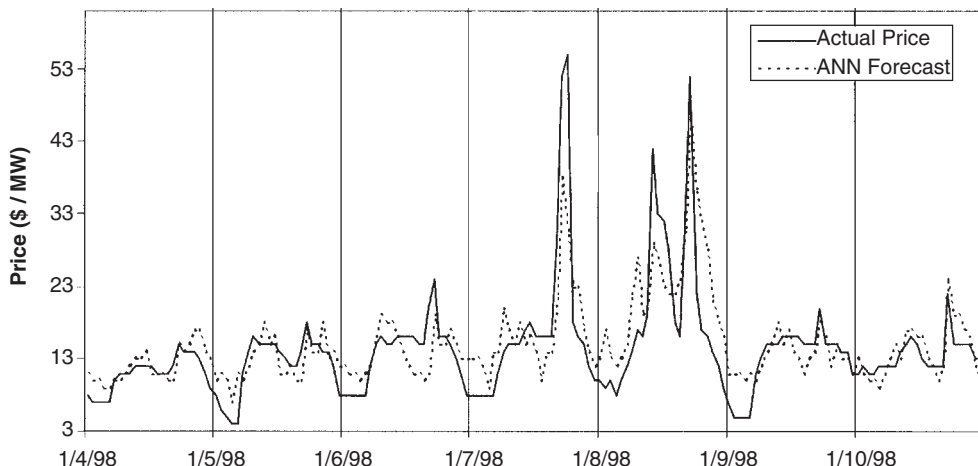


FIGURE 16.7 An example of the price forecaster performance for PJM price data.

References

- Bakirtzis, A.G., et. al., A neural network short term load forecasting model for the Greek power system, *IEEE Trans. PWRS*, 11, 2, 858–863, May, 1996
- Dillon, T.S., Sestito, S., and Leung, S., Short term load forecasting using an adaptive neural network, *Electrical Power and Energy Systems*, 13, 4, Aug. 1991.
- Ho, K., Hsu, Y., and Yang, C., Short term load forecasting using a multi-layer neural network with an adaptive learning algorithm, *IEEE Trans. PWRS*, 7, 1, 141–149, Feb. 1992.
- Khotanzad, A., Afkhami-Rohani, R., and Maratukulam, D., ANNSTLF—Artificial neural network short-term load forecaster-generation three, *IEEE Trans. on Power Syst.*, 13, 4, 1413–1422, November, 1998.
- Khotanzad, A., Afkhami-Rohani, R., Lu, T.L., Davis, M.H., Abaye, A., and Maratukulam, D.J., ANNSTLF—A neural network-based electric load forecasting system, *IEEE Trans. on Neural Networks*, 8, 4, 835–846, July, 97.
- Khotanzad, A., Davis, M.H., Abaye, A., and Martukulam, D.J., An artificial neural network hourly temperature forecaster with applications in load forecasting, *IEEE Trans. PWRS*, 11, 2, 870–876, May 1996.
- Khotanzad, A., Hwang, R.C., Abaye, A., and Maratukulam, D., An adaptive modular artificial neural network hourly load forecaster and its implementation at electric utilities, *IEEE Trans. PWRS*, 10, 3, 1716–1722, Aug. 1995.
- Lee, K.Y., Cha, Y.T., and Park, J.H., Short-term load forecasting using an artificial neural network, *IEEE Trans. PWRS*, 7, 1, 124–132, Feb. 1992.
- Lu, C.N., Wu, N.T., and Vemuri, S., Neural network based short term load forecasting, *IEEE Trans. PWRS*, 8, 1, 336–342, Feb. 1993.
- Mohammed, O., Park, D., Merchant, R., et. al, Practical experiences with an adaptive neural network short-term load forecasting system, *IEEE Trans. PWRS*, 10, 1, 254–265, Feb. 1995.
- Papalexopoulos, A.D., Hao, S., and Peng, T.M., An implementation of a neural network based load forecasting model for the EMS, *IEEE Trans. PWRS*, 9, 4, 1956–1962, Nov. 1994.
- Park, D.C., El-Sharkawi, M.A., Marks, R.J., Atlas, L.E., and Damborg, M.J., Electric load forecasting using an artificial neural network, *IEEE Trans. PWRS*, 442–449, May 1991.
- Peng, T.M., Hubele, N.F., and Karady, G.G., Advancement in the application of neural networks for short-term load forecasting, *IEEE Trans. PWRS*, 8, 3, 1195–1202, Feb. 1993.
- Proakis, J.G., Rader, C.M., Ling, F., and Nikias, C.L., *Advanced Digital Signal Processing*, Macmillan Publishing Company, New York, NY, 1992, 351–358.
- Rumelhart, D.E. and McClelland, J.L., *Parallel Distributed Processing*, Vol. 1, MIT Press, Cambridge, 1986.
- Szkuta, B.R., Sanabria, L.A., and Dillon, T.S., Electricity price short-term forecasting using artificial neural networks, *IEEE Trans. PWRS*, 14, 3, 851–857, Aug. 1999.

17

Transmission Plan Evaluation— Assessment of System Reliability

17.1	Bulk Power System Reliability and Supply Point Reliability	17-1
	Bulk Transmission Systems Reliability Is Evaluated Using Deterministic Reliability Criteria • Supply Point Reliability Is Evaluated Using Either Deterministic or Probabilistic Reliability Criteria	
17.2	Methods for Assessing Supply Point Reliability	17-4
	Reliability Measures—Reliability Indices • System Indices • Cost of Interruptions to Consumers • Outage Models	
17.3	Probabilistic Reliability Assessment Methods.....	17-7
	Contingency Enumeration Approach • Comparison of Contingency Enumeration and Monte Carlo Simulation	
17.4	Application Examples	17-10
	Calculation of the Reliability of Electric Power Supply to a Major Industrial Complex • Local Area Reliability	

N. Dag Reppen
Niskayuna Power Consultants, LLC

James W. Feltes
Power Technologies

17.1 Bulk Power System Reliability and Supply Point Reliability

Transmission systems must meet performance standards and criteria that ensure an acceptable level of quality of electric service. Service quality means continuity of supply and constancy of voltage waveform and power system frequency. Frequency is typically not an issue in large interconnected systems with adequate generation reserves. Similarly, voltage quality at the consumer connection is typically addressed at the distribution level and not by reinforcing the transmission system. This leaves continuity of power supply as the main criterion for acceptable transmission system performance.

Requirements for continuity of supply are traditionally referred to as power system reliability. Reliability criteria for transmission systems must address both local interruptions of power supply at points in the network as well as widespread interruptions affecting population centers or entire regions. Local and widespread interruptions are typically caused by different types of events and require different evaluation approaches.

Additional transmission facilities will virtually always increase reliability, but this remedy is constrained by the cost of new facilities and environmental impacts of new construction. Reliability

objectives, therefore, must be defined explicitly or implicitly in terms of the value of reliable power supply to the consumer and to society at large. Reflecting the different concerns of local interruptions and widespread interruptions, reliability objectives are different for the bulk transmission system than for the local area transmission or subtransmission systems supplying electric power to electric distribution systems. These two aspects of power system reliability will be referred to as bulk power system reliability (Endrenyi et al., 1982, Parts 1 and 2) and supply point reliability.

17.1.1 Bulk Transmission Systems Reliability Is Evaluated Using Deterministic Reliability Criteria

A distinguishing characteristic of bulk transmission systems is that severe disturbances arising in them can have widespread impact. Major failures of bulk transmission systems have resulted in interruption of thousands of MW of load and interruption of service to millions of customers. Three important characteristics of reliable bulk transmission system performance are:

1. Low risk of widespread shutdown of the bulk transmission system,
2. Confinement of the extent of bulk transmission system shutdown when it occurs, and
3. Rapid restoration of operation following shutdown of the bulk transmission system.

Most interconnected systems have reliability criteria and design standards that explicitly aim at limiting the risk of widespread shutdowns or blackouts. Such criteria may call for transmission reinforcements or limitations of power transfers across the system. The two other characteristics are addressed by sharpening operating command and control functions and improving control and communication facilities. Therefore, transmission system plans are typically evaluated with respect to reliability criteria that are aimed at limiting the risk of system shutdowns.

The U.S. National Electric Reliability Council (NERC), formed in response to the 1965 Northeast blackout, has developed basic design criteria aimed at reducing the risk of “instability and uncontrolled cascading” that may lead to system blackouts. The various regional reliability councils have interpreted these requirements in various ways and produced additional criteria and guides to address this problem (NERC, 1988). Deterministic criteria for bulk power systems will typically include the following requirements:

1. Test criteria for simulated tests aimed at avoiding overload cascading and instability, including voltage collapse. These test criteria specify in generic form:
 - a. the system conditions to be tested: e.g., peak load conditions, lines or generators assumed out on maintenance, transfer levels
 - b. the type of failure that initiates a disturbance: e.g., type and location of short circuit
 - c. assumptions to be applied regarding the operation of protection systems and other control systems
 - d. the allowable limits of system response: line and transformer loading limits, high and low voltage limits, and criteria for stable operation

The system must be reinforced to meet these criteria.

2. Requirements to test extreme contingencies such as the simultaneous outage of two or more parallel lines or the loss of entire substations. These tests are made to determine and understand the vulnerability of the system to such events. When critical extreme contingencies are identified, steps should be taken to minimize the risk of occurrence of such events.
3. Criteria and guides for protection system design to reduce the risk of critical protection initiated disturbances and for protection misoperation that may aggravate a serious system condition.

Evaluations of the system response to specified severe but rare types of failure events are labeled deterministic. The likelihood of the event specified is not considered, except in a qualitative way when the criteria were created. Since only a small subset of all potentially critical events can be tested, the tests

are sometimes referred to as “umbrella” tests. A system that passes these selected tests is believed to have a degree of resiliency that will protect it not only for the specific disturbances simulated, but also for a multitude of other disturbances of similar type and severity.

17.1.2 Supply Point Reliability Is Evaluated Using Either Deterministic or Probabilistic Reliability Criteria

Reliability objectives at the local area transmission or subtransmission level focus on the reliability of supply to specific supply points as shown in Fig. 17.1. Statistically, the reliability of supply may be expressed in terms of the frequency of occurrence of load interruptions, the amount of load interrupted, and the duration of the interruptions. Frequency of interruptions and MWh not served over a period such as a year are commonly used measures for the observed or predicted reliability of power supply to a particular node in a transmission system. Probabilistic reliability methods are required to predict reliability in these terms (Billinton and Allan, 1984; Endrenyi, 1978; Salvadori et al., 1990). These methods will typically consider more likely events rather than the more extreme and very rare events that can lead to system shutdown. This is justified since system shutdown occurrences are not frequent enough to significantly impact the reliability measures calculated.

While it is practical to perform probabilistic calculations to assess supply point reliability, deterministic simulation tests are also commonly used. As a minimum, deterministic criteria call for load flow testing of all single line and single transformer outages. This is referred to as single contingency testing or N-1 testing. For each of these outages, no line or transformer shall exceed its emergency rating, and no voltage shall violate specified high and low emergency voltage limits. Violation of these criteria calls for system reinforcements. Exceptions are typically made for supply points with low peak demand where it is judged to be too expensive to provide for redundant service. Some utilities use a peak load criterion such as 25 MW, above which redundant transmission connections to a supply point are called for.

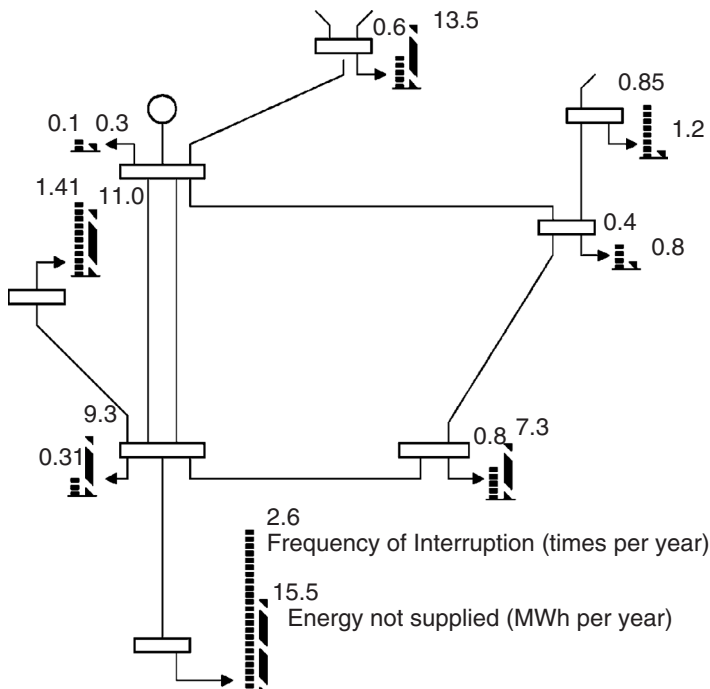


FIGURE 17.1 Prediction of supply point reliability.

17.2 Methods for Assessing Supply Point Reliability

Supply point reliability may be assessed in four different ways in order of increasing complexity:

1. **Deterministic:** System alternatives must meet criteria specifying allowable system response to specified contingencies.
2. **Probabilistic—System Trouble:** System alternatives must meet criteria specified in terms of probabilistic reliability indices reflecting risk of unacceptable system response.
3. **Probabilistic—Consumer Impact:** Same as (2), but criteria are specified in terms of consumer impact such as risk of supply interruption or risk of load curtailment.
4. **Cost/Benefit Analysis:** This approach is based on the concept that the proper level of service reliability should be defined by the balance of incremental worth of service reliability improvement and incremental cost of providing that improvement. The approach is also referred to as “effectiveness analysis” or “value based” reliability assessment.

The limitation of the deterministic approach (1) is that it considers only the initial system problems for a few contingencies. These contingencies have typically been selected by committee based on a mixture of judgment, tradition, and experience. If the selected contingencies do not cover all important reliability concerns, the resulting system may be unreliable. If the selected contingencies put undue emphasis on severe but rare events, an unnecessarily expensive system alternative may be selected.

The probabilistic approach (2) aims at eliminating the dependency on judgment in the selection of contingencies by attempting to look at all significant contingencies. In addition, it weighs the importance of the results for each contingency according to the severity of the system problems caused by each contingency and the frequency of occurrence of each contingency.

Approach (3) looks deeper into the problem, in that it is concerned with the impact on the consumer. However, the criteria used to define an acceptable level of reliability are still judgmental. For example, how many interruptions per year would be acceptable or what percentage of total MWh demand is it acceptable to interrupt or curtail? In the cost/benefit approach (4), the criterion for acceptable reliability is implicit in the methodology used.

17.2.1 Reliability Measures—Reliability Indices

Reliability can be measured by the frequency of events having unacceptable impacts on the system or on the consumer, and by the severity and duration of the unacceptable impacts. Thus, there are three fundamental components of reliability measures:

1. Frequency of unacceptable events,
2. Duration of unacceptable events, and
3. Severity of unacceptable events.

From these, other measures, such as probability of unacceptable events, can be derived. An expectation index, such as the loss of load expectation (LOLE) index commonly used to measure the reliability of a generating system is, in its nature, a probability measure. While probability measures have proved useful in generation reliability assessment, they may not be as meaningful in assessing the reliability of a transmission system or a combined generation/transmission system. It is, for example, important to differentiate between 100 events which last 1 sec and 1 event which lasts 100 sec. Since probability measures cannot provide such differentiation, it is often necessary to apply frequency and duration measures when assessing the reliability of transmission systems.

Probabilistic reliability measures or indices can express the reliability improvements of added resources and reinforcements quantitatively. However, several indices are required to capture various reliability aspects. There are two major types of indices: system indices and consumer or load indices (Guertin et al., 1978; Fong et al., 1989). The former concerns itself with system performance and system

effects, the latter with the impact on the consumer. The reliability cost measure used in cost/benefit analysis may be classified as a consumer index.

17.2.2 System Indices

Indices suitable for transmission system reliability evaluation may be divided into system problem indices and load curtailment indices.

System problem indices measure frequency, duration, probability, and severity of system problems. Some examples:

- Frequency of circuit overloads (overloads/year),
- Average duration of circuit overloads (hours), and
- Probability of circuit overloads.

Load curtailment indices measure severity in terms of load interrupted or curtailed. The salient characteristic of these indices is that the severity of any event, regardless of the system problems resulting from the event, is expressed in terms of load curtailment. From the three fundamental reliability measures (frequency, duration, and load curtailment), a series of derived reliability indices may be defined as illustrated by the following examples.

Basic Annual Indices

- Frequency of load curtailment $F = \sum_i F_i (\text{yr}^{-1})$
- Hours of load curtailment $D = \sum_i F_i D_i (\text{h yr}^{-1})$
- Power curtailed $C = \sum_i F_i C_i (\text{MW yr}^{-1})$
- Energy curtailed $E = \sum_i F_i D_i C_i (\text{MWh yr}^{-1})$

where

F_i = frequency of event i (yr^{-1})

D_i = duration of event i (h)

C_i = MW load curtailed for event i (MW)

i = all events for which $C_i > 0$

Energy curtailment (E), expressed in MWh not served, is often referred to as *Energy Not Served* (ENS), *Expected Energy Not Served* (EENS), or *Expected Unserved Energy* (EUE).

Load curtailment indices are sometimes normalized to system size. Two commonly used indices are:

- Power interruption index $C_N = C / CMX (\text{yr}^{-1})$
- Energy curtailment index $E_N = E / CMX (\text{h yr}^{-1})$

where CMX = peak load for system, area, or bus.

$E_N \times 60$ is referred to as system minutes, the equivalent number of minutes per year of total system shutdown during peak load conditions.

17.2.3 Cost of Interruptions to Consumers

The fact that a sudden interruption of very short duration can have a significant impact and that an outage of 4 h may have a significantly more severe impact than two outages of 2 h each, illustrates the limitations of simple aggregated reliability measures such as MWh not served. This is an important limitation since the various transmission reinforcement options considered may have dramatically different impacts as far as interruption durations are concerned. Since it is difficult to use a multi-parameter measure when comparing reinforcement alternatives, a single aggregate measure is much preferred as long as it includes the main reliability factors of concern. The concept of cost to consumers of unreliability expressed in dollars per year has emerged as a practical measure of reliability when comparing transmission reinforcement alternatives. As a measure, reliability cost has the additional

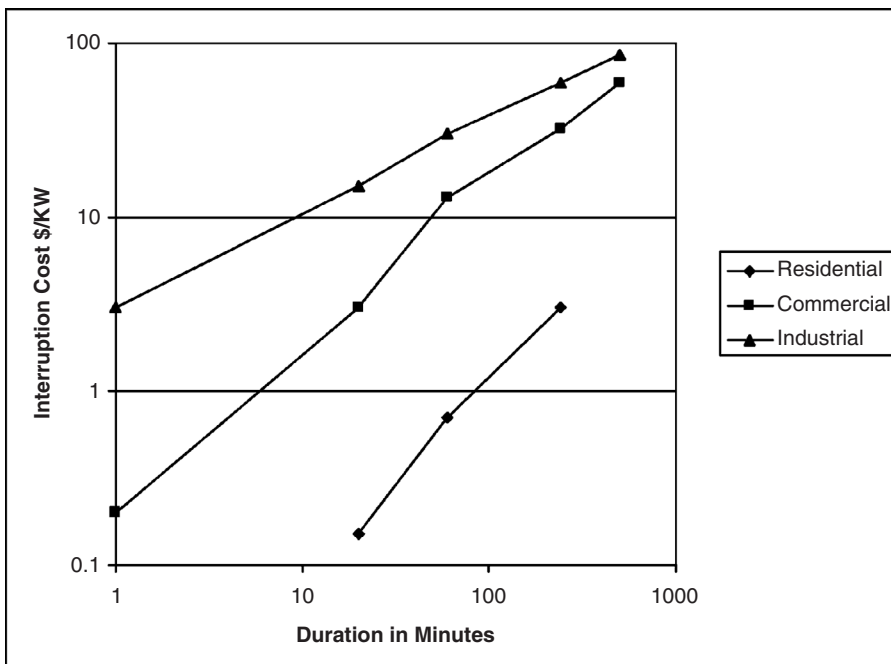


FIGURE 17.2 Illustration of customer damage functions for residential, commercial, and industrial load for process-oriented industrial load. The cost of very short duration outages may be much higher than shown here.

important advantage that it can be aggregated with installation cost and operating cost to arrive at a minimum “total cost” design in a cost/benefit analysis.

Conceptually, the annual reliability cost for a group of customers is the aggregated worth the customers put on avoiding load interruptions. In some cases the costs are tangible, allowing reliable dollar cost estimates; in other instances the impacts of interruptions are intangible and subjective, but still real in the eyes of the consumer. Surveys aimed at estimating what consumers would be willing to pay, either in increased rates or for backup service, have been used in the past to estimate the intangible costs of load interruptions. The results of these investigations may be expressed as *Customer Damage Functions*, (CDF), as illustrated in Fig. 17.2 (Mackay and Berk, 1978; Billinton et al., 1983).

Customer damage functions can be used to estimate the dollar cost of any particular load interruption given the amount of load lost and the duration of the interruption. If a customer damage function can be assigned for each supply point, then a cost of interrupted load may be determined.

17.2.4 Outage Models

Generation and transmission outages may be classified in two categories—forced outages and scheduled outages. While forced outages are beyond the control of the system operators, scheduled outages can usually be postponed if necessary to avoid putting the system in a precarious state. These two outage categories must, therefore, be treated separately (Forrest et al., 1985).

17.2.4.1 Forced Outage Models

The variety and characteristics of forced outage events may be illustrated with reference to Fig. 17.3. Transmission lines and transformers that can be isolated from the system by the opening of circuit breakers are referred to as “elements.”

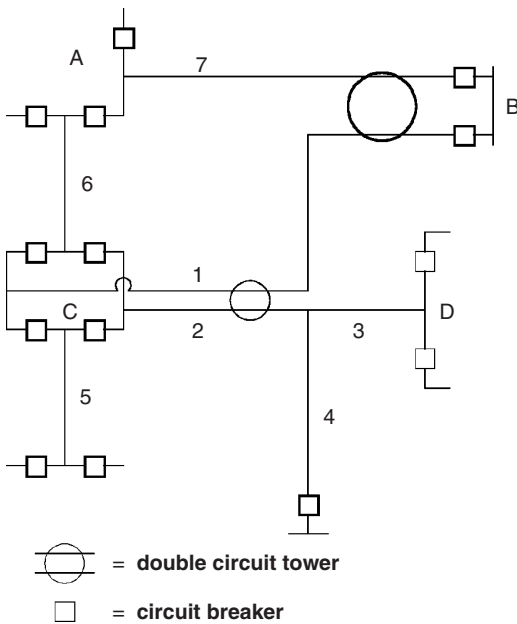


FIGURE 17.3 Sample system illustrating outage types.

Three categories of forced outage events are recognized:

1. **Single Component Outage Event**—The outage event involves only one element. For example, a fault on circuit 1, cleared by circuit breakers in a normal manner, would only affect circuit 1.
2. **Common Mode Outage Event**—This is a multiple element outage event where a single initiating cause results in multiple element outages where the outages are not consequences of each other. For example, a single lightning stroke taking out both circuits of the double circuit line exiting substation B would be a common mode outage. This event results in the simultaneous outage of circuits 1 and 7.
3. **Substation Related Outage Events**—This is a multiple element outage event that depends on the protection system response to a fault on a component in the substation or on an element connected to the substation. Examples of substation related outage events are:

- a. Stuck breaker—if the breaker common to circuits 1 and 6 is stuck, a fault on either circuits 1 and 6 would result in both circuits out.
- b. Tapped circuits—a fault on circuit 2 would result in circuits 2, 3 and 4 going out together.
- c. Breaker fault—if there is a fault on the breaker common to circuits 1 and 6, both circuits 1 and 6 would be outaged.
- d. Bus section fault—a fault on the bus section in substation B would outage circuits 1 and 7.

A common mode outage event may be combined with substation related outage events. For example, a common mode failure of circuits 1 and 2 would result in an outage event encompassing circuits 1, 2, 3, and 4. Two or more independent outage events from either of the three outage categories may overlap in time, creating more complex outages. Accurate tools for the prediction of reliability measures include most if not all of these outage types.

17.3 Probabilistic Reliability Assessment Methods

Probabilistic reliability assessment tools falls in one of two categories (Endrenyi et al., 1982):

1. The contingency enumeration method
2. The Monte Carlo method

In general, the contingency enumeration method is capable of looking at severe and rare events such as transmission events in great detail, but cannot practically look at many operating conditions. In contrast, the Monte Carlo methods are capable of looking at operating conditions in great detail (Noferi et al., 1975). However, from a computational standpoint, it is not possible to capture with precision, the impact of infrequent but severe transmission contingencies. Thus, the two methods are capturing different aspects of the reliability problem.

17.3.1 Contingency Enumeration Approach

The contingency enumeration approach to reliability analysis includes the systematic selection and evaluation of disturbances, the classification of each disturbance according to failure criteria, and the accumulation of reliability indices. Contingency enumeration techniques are structured so as to minimize the number of disturbances that need to be investigated in detail. This is achieved by testing, to the extent possible, only those disturbances that are sufficiently severe to cause trouble and sufficiently frequent to impact the risk indices to be computed.

The contingency enumeration approach is structured as shown in Fig. 17.4. For a specific predisruption condition, a contingency is selected and tested to determine whether the contingency causes any immediate system problem such as a circuit overload or a bus voltage out of limits. If it does not, a new contingency is selected and tested.

The occurrence of a system problem may by itself be logged as a failure. However, in many cases, it will be possible to adjust generation or phase shifters to relieve overloads and to adjust generator voltages or transformer taps to bring bus voltages back within range. It is, therefore, of interest to determine whether it is possible to eliminate a system problem by such corrective actions. A failure is logged when corrective actions, short of curtailing consumer loads, are insufficient to eliminate the system problems. The severity of such system problems may be assessed by computing the amount and location of load curtailment necessary to eliminate the problem. In this way, it is possible to compute supply point reliability indices that measure the frequency, duration, and amount of expected load curtailment.

17.3.1.1 Monte Carlo Approach

Monte Carlo methods (Oliveira et al., 1989) may be sequential or nonsequential. The sequential approach simulates the occurrences of random events through time, recognizing the statistical properties of the various types of events. Typically, the time functions of load and planned generation schedules are established for a period of a year. Starting at the beginning of the year, a sequence of forced shutdown and restoration of transmission and generating equipment is then determined based on random

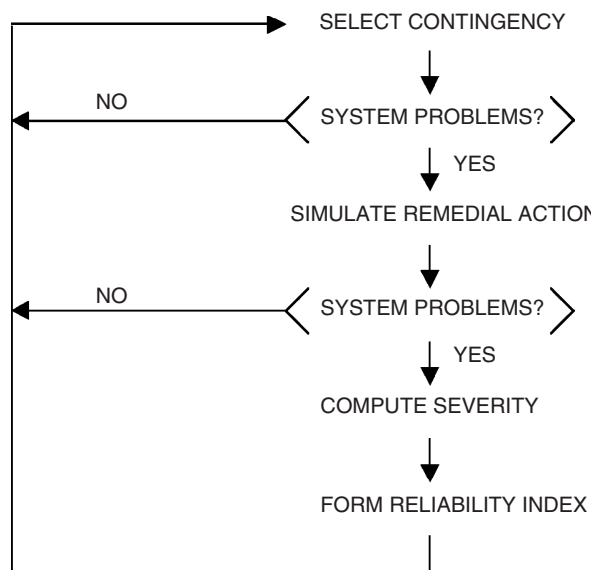


FIGURE 17.4 Contingency enumeration approach.

sampling in accordance with the statistical characteristics of the equipment failure processes. The response of the power system during equipment outages is simulated by power flow solutions. Whenever a system condition violating predefined failure criteria is encountered, the occurrence and characteristic of this failure is recorded. At the end of one year of simulation, parameters describing the “observed” reliability of the system can be determined. These parameters may include frequency of equipment overload, frequency of voltage violations, MWh not served, average duration and severity of specified types of failures, etc. This process is illustrated in Fig. 17.5.

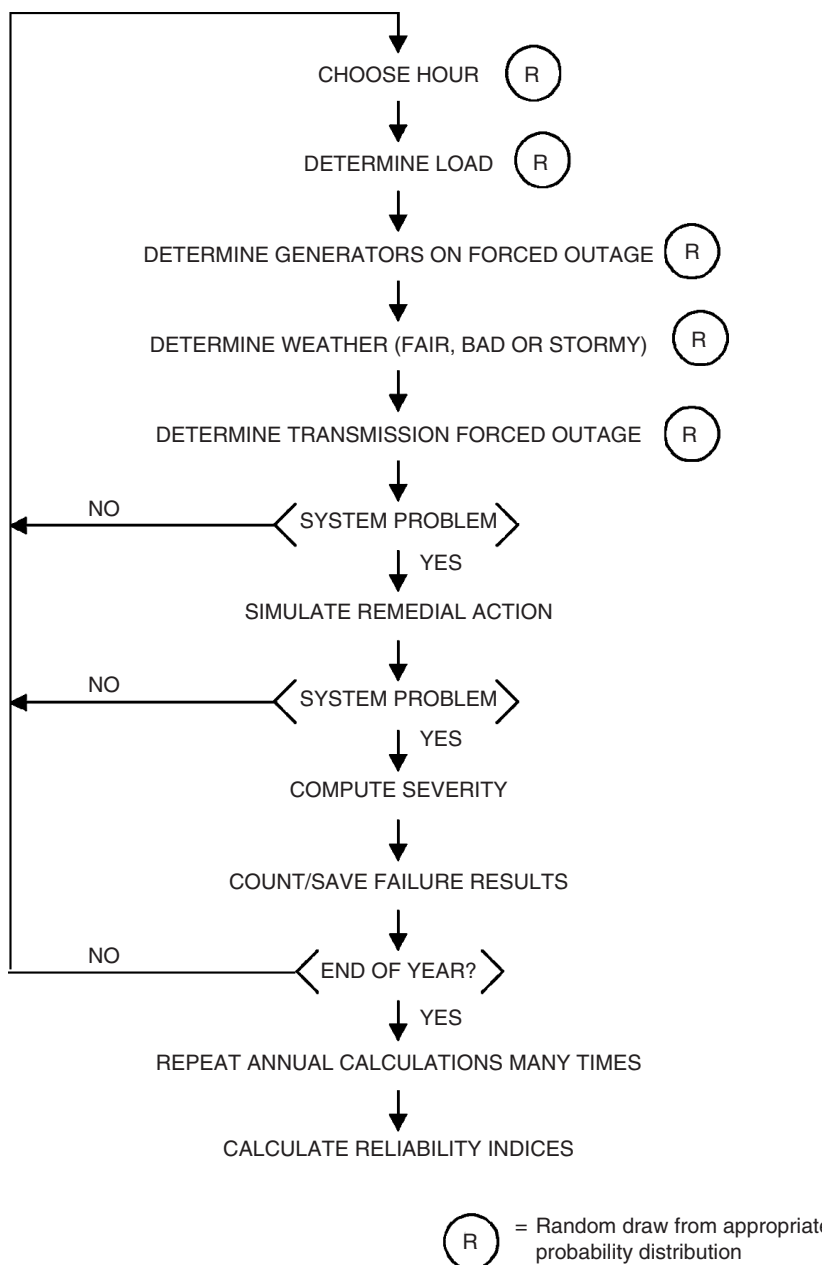


FIGURE 17.5 Possible computational sequence for Monte Carlo method.

One year of simulation constitutes one particular sample scenario governed by the random properties of equipment failure. In order to obtain a measure of the inherent reliability of the system, it is necessary to repeat the simulation over the annual period many times and calculate the reliability measures as the mean of the results obtained over the repeated annual simulations. For reliable systems, several hundred annual simulations may be required to obtain convergence in the reliability measures calculated.

When using the sequential approach, it is possible to model time dependencies between key variables. This allows elaborate modeling of energy limited resources such as hydro plants and pumped hydro. It is also possible to simulate environmental effects such as the occurrence of lightning storms that may impact the failure rate of transmission equipment. A brute-force sequential Monte Carlo simulation would be prohibitively time-consuming when applied to large systems. Practical techniques rely on special sampling techniques and acceptable approximations in power system modeling.

If time dependencies are not essential, the nonsequential approach may be used. In this case, hours of simulation may be selected at random rather than in sequence. For a specific hour, a precontingency state is established including bus loads and matching generation dispatch. When it can be used, the nonsequential approach is typically much faster than the sequential approach.

17.3.2 Comparison of Contingency Enumeration and Monte Carlo Simulation

From the preceding discussion, it is clear that the Monte Carlo method differs from the contingency enumeration method in the way power system states including load, generation dispatch, and component outages are selected. The actual network solution and corrective action models used may be the same or similar for both methods. The major advantage of the Monte Carlo method is the ease with which comprehensive statistics of power system states can be included. This makes the method suitable for computing period reliability indices such as annual indices (CIGRE, 1992).

The Monte Carlo method may not be suitable for estimating the probability or frequency of occurrence of infrequent events. The contingency enumeration method may, therefore, be a more practical approach in system design. In comparing system alternatives to strengthen a local area, the Contingency Enumeration approach will provide consistent and real differences in reliability indices computed for specific situations. Unless the reliability of the alternatives are far apart, it would be very time-consuming and perhaps impractical to obtain acceptable differences in reliability by means of the Monte Carlo method. One way to mitigate this problem is to remove time-consuming calculations from the inner loop of the Monte Carlo calculations. In one approach, which is used to assess the reliability of supply to load centers, the impact of rare transmission failures are obtained from precomputed look-up tables of transmission import limits. Using this approach and various sampling techniques, several thousand years of operation can be simulated in minutes.

17.4 Application Examples

The techniques described above are presently used for transmission planning by major utilities. The following examples illustrate some of these methods. The first example uses contingency enumeration while the second example uses Monte Carlo techniques.

17.4.1 Calculation of the Reliability of Electric Power Supply to a Major Industrial Complex

Contingency enumeration techniques were used to assess the reliability of the power supply to a major manufacturing complex (Reppen et al., 1990). In this analysis, the reliability concerns encompassed

system events and conditions that are capable of disturbing or shutting down all or portions of the manufacturing processes. The events of concern included initial interruptions, sustained interruptions, overloads, voltage violations, voltage collapse, and overload cascading. The reliability effects of possible system reinforcements in the immediate local power supply area and in the main grid supplying this area were evaluated by a comprehensive probabilistic reliability analysis.

The characteristics of the power system were radial feeds to the plant with provisions for automatic and manual switchover to alternative supply in case of loss of voltage on primary supply feeders, an extensive local 132 kV system, and a regional 300 kV and 420 kV transmission system. Contingency enumeration methods allow detailed modeling of the network, including the modeling of automatic responses of the power system to disturbances such as special relaying schemes for line tripping, generation runback, and load transfer.

Three typical categories of outages—single element outages, independent overlapping outages of multiple elements, and dependent multiple element outages—were considered in the reliability studies. The term “element” encompasses generating units as well as “transmission elements” such as transmission lines, transformers, capacitor banks, and static var devices. The reliability computations included network analysis of outages, classification of failure events according to type and severity, and calculation of reliability indices. Reliability indices representing the predicted frequency of each of the types of failure events were computed as well as load interruption and energy curtailment indices. The indices computed are referred to as annualized indices reflecting the reliability level that would be experienced if the precontingency condition considered should exist for an entire year.

The full analysis included assessment of existing power supply conditions, impact of system reconfiguration on the reliability of supply, reliability effects of system reinforcements, and impact of conditions in the main grid. Here we will concentrate on the reliability effects of system reinforcements. Two reinforcements were analyzed: construction of a new 132 kV line completing a loop at some distance from the plant and construction of a 300 kV ring connecting several of the power supply buses to the plant.

Figure 17.6 presents the results of the investigation using the energy curtailment index defined earlier. The energy curtailment index aggregates the expected loss of energy on an annualized basis. The results indicate that reinforcement A (the remote line) has no significant effect on the reliability of power supply to the plant. Reinforcement B (the 300 kV ring) provides a substantial overall improvement, although there is no significant improvement in the energy curtailment index for the winter case.

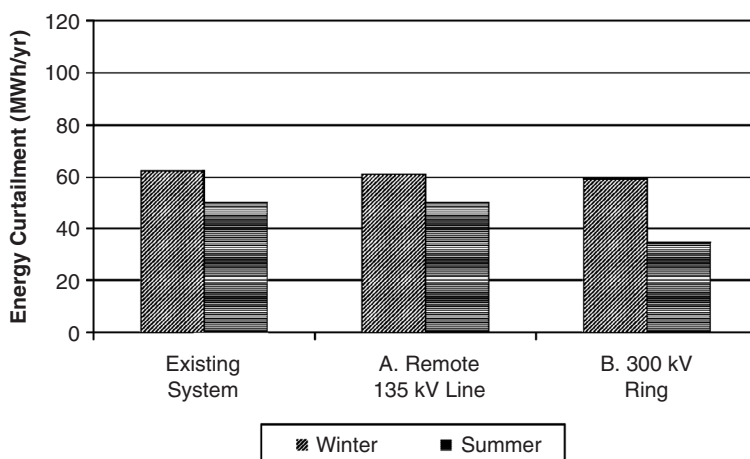


FIGURE 17.6 Benefit of system reinforcements. Annualized energy curtailment (MWh/yr). Sustained interruptions only.

While some of the suggested means of improving reliability could have been predicted prior to the analysis, the relative effectiveness of the various actions would not be apparent without a formal reliability analysis. Performing a reliability analysis of this type gives excellent insights into the dominating failure phenomena that govern system performance. The detailed contingency information available promotes understanding of the way systems fail, while the reliability indices computed provide the perspective necessary to make appropriate system design decisions.

17.4.2 Local Area Reliability

The second example considers the task of improving the reliability of electric power to a local area such as a city, major industrial complex, or other load center (Reppen, 1998). In simple terms, the reliability of the supply is a function of the following parameters:

- The load in the area as it fluctuates over time.
- The maximum amount of power that can be imported from the main grid. This import limit varies by maintenance and forced outage of transmission and generating equipment.
- Maximum available local generation at any particular time as it is affected by generation maintenance and forced outages.

At any particular time, load curtailment will occur if the load exceeds the maximum import capability into the area plus the maximum generation available in the area. Therefore, reliability of supply to consumers in the area can be measured in terms of statistics of load curtailment. Popular load curtailment measures include frequency of interruptions and energy not served (MWh/year). In addition, the expected annual customer interruption cost can be predicted using Monte Carlo techniques that simulate system conditions repeatedly over a time period to develop reliability measures by aggregating and averaging the impacts of individual load curtailment events. This allows the use of interruption cost functions (customer damage function) to estimate the expected annual cost of load interruptions.

Accepting calculated annual interruption costs as a realistic measure of the economic impact on the consumer, one might declare a system reinforcement alternative to be justified from a reliability standpoint if the reduction in interruption cost is greater than the net cost of investment and operation. While such a criterion may not necessarily be appropriate in all cases, it should provide a relevant benchmark in most environments.

[Figure 17.7](#) shows key components of the power supply picture for a small city with a peak load of 210 MW. The city is supplied by two generators totaling 150 MW, and by a 138 kV double circuit transmission line from the main grid. Prime reinforcement options are as follows:

1. Add a new single circuit transmission line as indicated in Fig. 17.7.
2. Add one gas turbine generator of size to be determined.
3. Add two identical gas turbine generators of size to be determined.

Key questions of interest are:

1. Can the line addition be justified on the basis of savings in customer interruption cost?
2. What generator capacities will produce the same reliability improvements as the line addition?
3. What size generators can be justified on the basis of customer interruption?

[Figure 17.8](#) shows results obtained from the Monte Carlo calculations along with the annual fixed charges for investment cost and net annual operating costs. Significant observations that can be made from Fig. 17.8 are:

- The additions of a new 138 kV line, a 50 MW generator, or two 25 MW generators have approximately the same interruption cost savings. However, the reason for this is that all three alternatives are an effective overkill, reducing the interruption cost to almost 0. If load is anticipated to grow, the line addition will be the better performer at a lower cost.

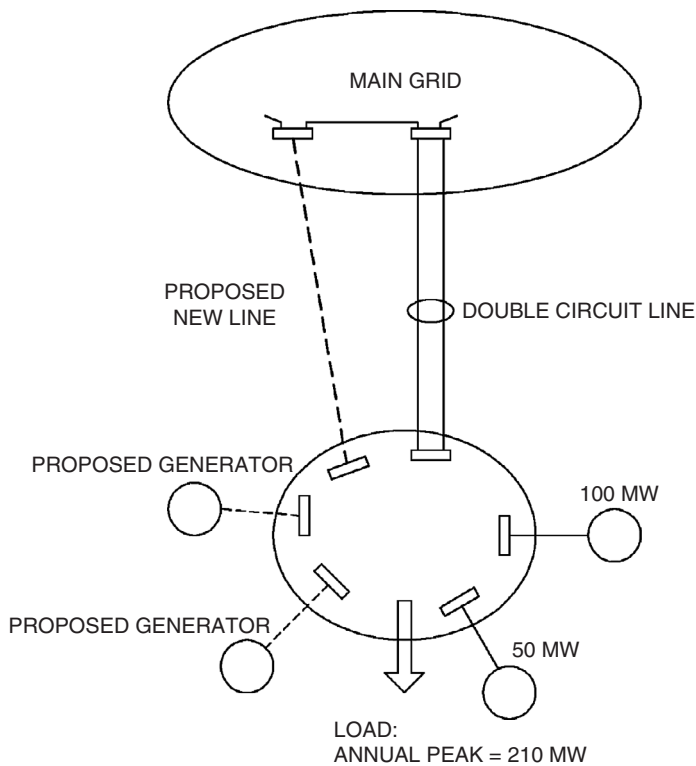


FIGURE 17.7 Power supply configuration for a small city.

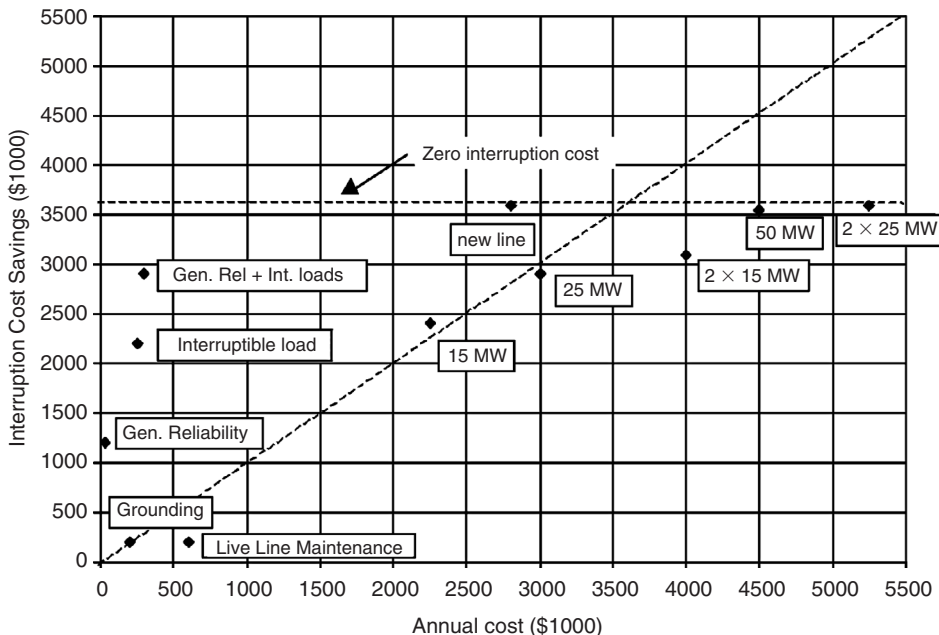


FIGURE 17.8 Annual savings in cost of interruption vs. annual combined investment and operating costs of transmission and generation reinforcements and short term measures. Measures in the upper left triangle can be justified on account of savings in interruption cost.

- One 15 MW to 25 MW generator would give much improved performance and at a cost which can be justified (marginally) based on reliability worth as expressed by the interruption cost curves.
- The line addition is clearly the most cost-effective alternative.

The first set of calculations compared the benefit of reinforcement by transmission or generation. While such additions are typically the most powerful reinforcements from the standpoint of improved reliability, they are typically also the most expensive. In addition, when dealing with small local systems, the natural or cost-effective line and generation additions are often more than what's needed to satisfy reliability needs for the next few years. This is particularly true for low load growth scenarios. Thus, there is a need for less expensive alternatives that typically will have smaller incremental reliability benefits than the addition of transmission lines and generators. The results of four such alternatives are shown in Fig. 17.8:

1. Improve reliability performance of existing generators.
2. Improve grounding of transmission lines.
3. Introduce live line maintenance.
4. Interruptible load contracts.

All of the short term measures except live line maintenance can be justified as the annual interruption cost is greater than the total expense associated with the reliability improvement. Also, live line maintenance and transmission line grounding have too small an impact to be of interest.

The most cost effective short term measure comes from improvements in the reliability performance of the 100 MW generator, closely followed by interruptible load contracts. If both of these short term measures are taken, the reliability improvement matches that obtainable from the addition of a 25 MW gas turbine generator and at a much lower cost.

This example illustrates how it is possible to use Monte Carlo reliability calculations to predict and compare the benefit-cost trade-off of transmission and generation reinforcements and various short term measures.

References

- Billinton, R., Allan, R.N., Power-system reliability in perspective, *IEE J. Electron. Power*, 30, 231–236, March 1984.
- Billinton, R., Wacker, G., Wojczynski, E., Comprehensive bibliography on electrical service interruption costs, *IEEE Trans. Power Appar. Syst.*, PAS-102, 6, 1831–1837, June 1983.
- CIGRE Task Force 38.03.10—1992, *Power System Reliability Analysis Volume 2 Composite Power System Reliability Evaluation*, 1992.
- Discussion of Regional Council Planning Reliability Criteria and Assessment Procedures*, A Reference Document by the North American Electric Reliability Council, June 1988.
- Endrenyi, J., *Reliability Modeling in Electric Power Systems*, John Wiley & Sons, Ltd., New York, 1978.
- Endrenyi, J., Albrecht, P.F., Billinton, R., Marks, G.E., Reppen, N.D., Salvadori, L., Bulk Power System Reliability Assessment—Why and How? Part 1: Why? IEEE Paper 82WM 147-7, presented at the *Winter Power Meeting*, New York, NY, February 1–5, 1982.
- Endrenyi, J., Albrecht, P.F., Billinton, R., Marks, G.E., Reppen, N.D., Salvadori, L., Bulk Power System Reliability Assessment—Why and How? Part 2: How? IEEE Paper 82WM 148-5, presented at the *Winter Power Meeting*, New York, NY, February 1–5, 1982.
- Fong, C.C., Billinton, R., Gunderson, R.O., O'Neill, P.M., Raksany, J., Schneider, Jr., A.W., Silverstein, B., Bulk system reliability—Measurement and indices, *IEEE Trans. Power Appar. Syst.*, 4, 3, 829–835, Aug. 1989.
- Forrest, D.W., Albrecht, P.F., Allan, R.N., Bhavaraju, M.P., Billinton, R., Landgren, G.L., McCory, M.F., Reppen, N.D., Proposed terms for reporting and analyzing outages of electrical transmission and distribution facilities, *IEEE Trans. Power Appar. Syst.*, PAS-104, 2, 337–348, Feb. 1985.

- Guertin, M.B., Albrecht, P.F., Bhavaraju, M.P., Billinton, R., Jorgensen, G.E., Karas, A.N., Masters, W.E.,
Patton, A.D., Reppen, N.D., Spence, R.P., Reliability indices for use in bulk power supply adequacy
evaluation, *IEEE Trans. Power Appar. Syst.*, PAS-97, 4, 1097–1103, July/Aug. 1978.
- Mackay, E.M., Berk, L.H., Costs of Power Interruptions to Industry Survey Results, CIGRE, Paper 3207,
Aug. 30–Sept. 7, 1978.
- Noferi, P.L., Paris, L., Salvaderi, L., Monte Carlo Methods for Power System Reliability Evaluations in
Transmission or Generation Planning, in *Proceedings, 1975 Reliability and Maintainability Symposium*,
Washington, 1975.
- Oliveira, G.C., Pereira, M.V.F., Cunha, S.H.F., A Technique for Reducing Computational Effort in
Monte-Carlo Based Composite Reliability Evaluation, IEEE 1989 WM 174-4 PWRS.
- Overview of Planning Reliability Criteria of the Regional Reliability Councils of NERC*, A Reference
Document by the North American Electric Reliability Council, 1988.
- Reppen, N.D., Balancing Investments and Operating Costs with Customer Interruption Costs to Give
Increased Reliability, presented at the IEE Colloquium on Tools and Techniques for Dealing with
Uncertainty, London, U.K., January 27, 1998.
- Reppen, N.D., Carlsen, T., Glende, I., Bostad, B., Lam, B.P., Calculation of the Reliability of Electric
Power Supply to a Major Industrial Complex, presented at the *10th Power Systems Computation
Conference (PSCC)*, Graz, Austria, August 19–24, 1990.
- Salvaderi, L., Allan, R., Billinton, R., Endrenyi, J., Mc Gillis, D., Lauby, M., Manning, P., Ringlee, R., State
of the Art of Composite-System Reliability Evaluation, CICRE Session, paper 38-104, Paris,
August 26–September 1, 1990.

18

Power System Planning

18.1	Planning Entities.....	18-2
18.2	Arenas	18-2
18.3	The Planning Problem.....	18-3
	Options • Uncertainties • Attributes	
18.4	Planning Processes.....	18-8
	Setting Standards or Criteria • Assessment • Generation Planning • Transmission Planning • Least-Cost Planning • Making Choices	

Hyde M. Merrill
Merrill Energy, LLC

Power system planning is the recurring process of studying and determining what facilities and procedures should be provided to satisfy and promote appropriate future demands for electricity. The electric power system as planned should meet or balance societal goals. These include availability of electricity to all potential users at the lowest possible cost, minimum environmental damage, high levels of safety and reliability, etc. Plans should be technically and financially feasible. Plans also should achieve the objectives of the entity doing the planning, including minimizing risk.

The *electric power system* is a force-at-a-distance energy-conversion system. It consists of three principal elements:

- Current- and voltage-producing, transmitting, and consuming hardware,
- Control and protective devices, and
- Planning, operating, commercial, and regulatory practices and procedures.

These definitions are very different from would have appeared on these pages 25 years ago. They no doubt will seem quaint 25 years hence. At this writing, the electric power industry worldwide is experiencing its most dramatic changes in two generations. These changes affect planning, but this section is intended as a practical exposition, not as a history lesson or a prophesy. We therefore will focus on how planning is or should be done today, avoiding flights of fantasy into the past or future (Sullivan, 1977; Stoll et al., 1989; Kahn, 1988; Ringlee, 1989).

Planning considers:

- Options,
- Uncertainties, and
- Attributes.

Options are the choices available to the planner. Uncertainties are parameters whose values are not known precisely or cannot be forecast without error. Attributes are measures of “goodness.” Stakeholder objectives are expressed in terms of attributes. Physical, economic, and institutional realities determine how different options and uncertainties affect the attributes.

The planning problem is to identify and choose among options, in the presence of uncertainties, so as to maximize or minimize (as the case may be) the attributes.

18.1 Planning Entities

Planners generally are trained as engineers, economists, civil servants, businessmen, or mathematicians. They do power system planning for the following entities:

- Vertically integrated utilities owning generation, transmission, and distribution systems.
- Transmission companies, independent system operators (ISO), and regional transmission organizations (RTO). Transmission companies own transmission assets; the latter do not, but may have some responsibility for their planning.
- Pools or combinations of vertically integrated utilities.

Other organizations do planning studies and higher-level power sector planning. A step removed from the operation and management of the power system, their interest is in seeing that it meets society's goals:

- Various levels of government.
- International development banks.

Still other organizations do power system planning studies, but without system responsibility. They wish to understand the market for various services and how they might compete in it—its economics and technical requirements for entry.

- Independent power producers (IPP) or nonutility generators (NUG). These include qualifying facilities (QF as defined by the U.S. Public Utilities Regulatory Policy Act of 1978) and exempt wholesale generators (EWG as defined by the U.S. Energy Policy Act of 1992). These are subject to less stringent regulation than are utilities. They neither enjoy monopoly protection nor have an obligation to provide electricity at cost-based tariffs.
- Large industrial users.
- Commercial middlemen who buy and sell electrical energy services.
- Investors.

All of these are supported by independent purveyors of planning information. Consultants with specialized analytic skills also do planning studies.

18.2 Arenas

Planning is done in several arenas, distinguished by the planning horizon and by the types of options under consideration. These arenas include:

- **Long-term vs. short-term planning.** Economists distinguish these by whether capital investment options are considered. For engineers, long-term planning has a distant horizon (perhaps 30 years for generation and half of that for transmission). Short-term planning considers about 5 years. Operations planning is for as short as a few hours and is not treated here.
- **Generation vs. transmission vs. least-cost planning.** Generation and transmission planning focus on supply options. Least-cost planning includes demand-side options for limiting or shaping load.
- **Products and services.** Some entities provide power (kW) and energy (kWh). Others plan the transmission system. Others provide for auxiliary services (voltage and power control, electrical reserves, etc.). Still others plan for diversified services like conservation and load management.

Other arenas require engineering and economic skills, but are within the purview of a book on business or policy rather than an engineering handbook.

- **Competitive markets.** Strategic planning is particularly concerned with financial and business plans in competitive markets.
- **Sector evolution.** Defining the form of the future power sector, including the relationships between competitive forces, regulation, and the broadest social objectives, is a particularly vital planning function.

18.3 The Planning Problem

18.3.1 Options

Power generation, transformer, transmission system, substation, protection, and operation and control options are discussed in other chapters of this handbook. Other options are discussed below.

18.3.1.1 Planning and Operating Standards or Criteria

Planning and operating criteria have a dual nature: they are both attributes and options. Here we will emphasize the fact that they are options, subject to change. Though they have no intrinsic value, standards or criteria are important for several reasons. Their consistent application allows independent systems to interconnect electrically in symmetrical relationships that benefit all. Criteria can also eliminate the need for planners to ask constantly, “How much reliability, controllability, etc., do I need to provide?” Criteria include:

- Maximum acceptable loss-of-load probability (LOLP) or expected unserved demand, minimum required reserve margins, and similar generation planning standards,
- What constitutes a single contingency (transmission systems are often designed to withstand “any” single contingency) and whether particular single contingencies are excluded because they are unlikely or expensive to forestall,
- Permissible operating ranges (voltages, power flows, frequency, etc.) in the normal or preventative state, the emergency state, and the restorative state, and
- How criteria are to be measured or applied.

Most power systems in industrialized nations are designed and operated so that:

1. With all elements in service, power flows, voltages, and other parameters are within normal ranges of the equipment,
2. The system remains stable after any single contingency, and
3. Power flows, voltages, and other operating parameters are within emergency ranges following any single contingency.

For financial and economic reasons, developing countries choose weaker criteria.

18.3.1.2 Demand Management

Demand-side planning often is tied to generation planning because it affects the power and energy that the power plants will need to provide. There is no perfect classification scheme for demand-side options. Some overlapping classifications are:

- Indirect load control vs. direct load control by the bulk system operator,
- Power (kW) or energy (kWh) modification or both, and
- Type of end-use targeted.

Table 18.1 shows the type of load under direct utility control in the U.S. early in the 1980s, when enthusiasm for demand-side options was especially high.

TABLE 18.1 Appliances and Sectors Under Direct Utility Control, U.S.—1983

Appliance or Sector	Number Controlled	Percent of Total Controlled
Electric water heaters	648,437	43%
Air conditioners	515,252	34%
Irrigation pumps	14,261	1%
Space heating	50,238	3%
Swimming pool pumps	258,993	17%
Other	13,710	1%
Total	1,500,891	100%
Residential	1,456,212	97%
Commercial	29,830	2%
Industrial	588	—
Agricultural	14,261	1%

Source: New Electric Power Technologies: Problems and Prospects for the 1990s, Washington, D.C.: U.S. Congress, Office of Technology Assessment, OTA-E-246, July 1985.

One of the most effective examples of load control was reported by a German utility. Typical off-peak winter demand was less than 70% of the peak for the same day. An indirect program promoted storage space heaters that use electricity at night, when demand is low, to heat ceramic bricks. During the day, air forced among the bricks transfers the heat to the living space. Within five years the program was so popular that direct control was added to avoid creating nighttime peaks. The winter daily load shape became practically flat.

18.3.1.3 Market and Strategic Options

Market and strategic options are also important. These range from buying a block of power from a neighboring utility to commodity trading in electricity futures to mergers, divestitures, and acquisitions.

18.3.2 Uncertainties

Uncertainty can seldom be eliminated. Planning and forecasting are linked so that even if the forecasts are wrong, the plans are right (Bjorkland, 1987).

18.3.2.1 Models of Uncertainty (Schwepppe, 1973)

Probabilistic models, where different outcomes are associated with different probabilities, are valid if the probability structure is known. The events involved must occur often enough for the law of large numbers to apply, or else the probabilities will have little relationship to the frequencies of the outcomes. Generation planners have excellent probabilistic reliability models. (Generation and transmission reliability evaluation are treated in more detail in a separate section.)

Unknown-but-bounded (set theoretic) models are used when one or both of the conditions above are not met. For instance, transmission planners design to withstand any of a set of single contingencies, usually without measuring them probabilistically.

18.3.2.2 Demand Growth

Planners forecast the use of energy (MWh) for a period (e.g., a year) first. They divide this by the hours in the period to calculate average demand, and divide again by the projected load factor (average MW demand/peak MW demand) to forecast peak demand. Three techniques are used most often to forecast energy.

Extrapolation—Exponential growth (e.g., 4%/year) appears as a straight line on semi-log paper. Planners plot past loads on semi-log paper and use a straight edge to extrapolate to the future.

Econometric models—Econometric models quantify relationships between such parameters as economic activity and population and use of electricity. The simplest models are linear or log-linear:

$$D_i = f(P, GDP, \text{etc.}) = k_1 D_{i-1} + k_2 P_i + k_3 GDP_i + \dots \quad (18.1)$$

D_i = Demand or log(demand) in period i

P_i = Population or log(population) in period i

GDP_i = Gross domestic product or log(gross domestic product) or some measure of local economic activity

k_1, k_2, k_3 , etc. are coefficients

Econometric models are *developed* in a trial-and-error process. Variants of Eq. (18.1) are hypothesized and least squares (regression) analysis is used to find values of coefficients that make Eq. (18.1) fit historical data. Econometric models are *used* by first forecasting population, economic activity, etc., and from them calculating future energy demand using Eq. (18.1).

End-use models—First, the number of households is forecast. Then the per-household penetration of various appliances is projected. The average kWh used by each appliance is estimated and is multiplied by the two previous numbers. The results are summed over all types of appliances.

Performance—Extrapolation became suspect after U.S. load forecasts in the 1970s were consistently too high. Econometric modeling is more work but is more satisfying. End-use modeling requires considerable effort but gives the most accurate forecasts of residential load.

Real drivers—One fundamental driver for per-capita load growth is the replacement by electricity of other forms of energy use. The second is the creation of new uses of energy that are uniquely satisfied by electricity.

During the decades when U.S. electric demand grew at over 7% per year, the demand for all forms of energy (of which electricity is a part) grew at about 2% per year. This obviously could not continue: the two cannot cross. The growth of electricity demand began to drop off about 1955, declining noticeably in the 1970s and thereafter. The drop in load growth was attributed to the oil crises of the 1970s. Post-1973 conservation played a part, but by then electricity had captured about all the market share it was going to get by replacement and creation of new demands for energy.

In developing countries, both fundamental drivers are limited by the ability of the electric companies to finance the necessary generation and distribution infrastructure, which is very expensive. Demand is also limited by their ability to generate. In industrialized countries, availability of capital and power plant performance are not constraining. In all countries, elasticity reduces demand if electricity is costly. This effect is much stronger in countries with low per-capita income and for energy-intensive industrial load.

18.3.2.3 Fuel and Water

In the near term, strikes, weather, and natural disasters can interrupt production or delivery. Fuel inventories and the ability to redispatch provide good hedges. In the intermediate term, government action can make fuel available or unavailable. For instance, in 1978, the U.S. Congress forbade burning natural gas by utilities, perceiving that there was a shortage. The shortage became a glut once the U.S. natural gas market was deregulated. In the long term, any single source of fuel is finite and will run out. British coal, which had fueled the industrial revolution, was shut down in the 1990s because it had been worked out.

The more important fuel uncertainties, however, are in price. For instance, Fig. 18.1 shows that the price of crude oil doubled in 1974 and again in 1979. Recognizing the high variability, in 1983 the U.S. Department of Energy forecast a fuzzy band instead of a single trajectory (U.S. Dept. of Energy, 1983). It is interesting that within a year of the publication of this projection, the price of

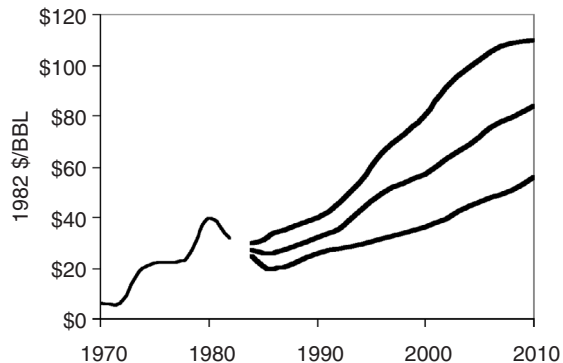


FIGURE 18.1 World oil price projections, 1983.

oil had dropped below the low limit of the band, and it has remained there until this writing. Planners must consider extreme possibilities for all uncertainties.

Brazil, Norway, the Pacific Northwest, Quebec, and a number of developing countries are highly dependent on hydropower. Systems usually are planned and operated so that there will not be a shortfall unless one of the worst hydrological years in recorded history recurs.

18.3.2.4 Construction

Three major construction uncertainties are: How long will it take to build? How much will it cost? Will the project be completed?

A World Bank study of 41 hydro projects revealed that 37% experienced a schedule slip of 30% or more, including 17% with schedule slips of 60%–100% (Crouseillat, 1989).

Figure 18.2 shows the range of actual versus budgeted cost for a number of World Bank-financed projects. The distribution is not symmetrical—overruns are much more frequent than under-budget projects. Some of the worst cases in Fig. 18.2 data occurred during periods of unexpected high inflation (Crouseillat, 1989). A 1983 report projected that the cost of some 40 U.S. nuclear plants scheduled for completion by 1990 would be close to normally distributed, with the least expensive costing a bit under \$2000/kW and the most expensive three times higher, at \$6000/kW (U.S. Dept. of Energy, 1989).

Possibly the most expensive nuclear plant ever built, the Shoreham Plant on Long Island, was completed at a cost of some \$16 billion U.S. It was shut down by the state before producing a single kWh of commercial energy.

18.3.2.5 Technology

New technologies are generally less certain than mature technologies in their cost, construction time, and performance.

Even mature technologies may have important uncertainties. For example, transmission transfer capability is an important measure of transmission system capability. It is usually expressed as a single number, but it is actually a time-varying random variable.

18.3.2.6 Demand Management

Demand management programs are risky, in part because of uncertainty in the public's response to them. The two major uncertainties are:

- What fraction of eligible customers will respond to a particular program?
- How much will the average customer change his use of electricity?

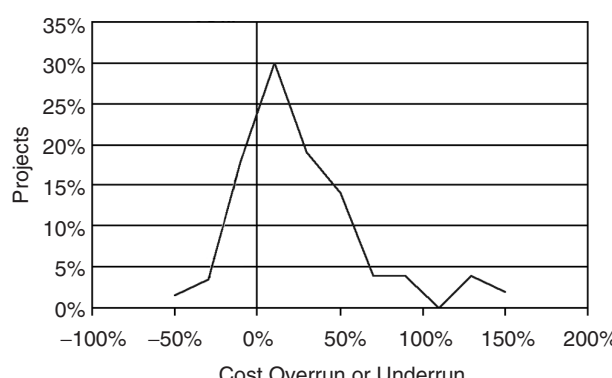


FIGURE 18.2 Budget vs. actual costs, power projects in developing countries.

These uncertainties are affected strongly by the design of the program, the incentives offered, how it is marketed, etc. Carrying out a carefully designed pilot program can reduce the uncertainty. The pilot program should be done in the region of the future commercial program.

18.3.2.7 Markets and Capital Recovery

For many years, vertically integrated utilities were guaranteed the recovery of all costs, including capital invested, plus a modest but sure profit. The customer paid this and absorbed the market uncertainties. At this writing,

the regulated monopoly, cost-recovery market is being replaced in many states and countries by a more competitive market. Some market risks are being transferred from customers to utilities, power marketers, generating companies, speculators, and others.

This creates new uncertainties. For example, in competitive generation markets it is not known which potential generating units will be built. This affects both transmission and generation planning.

18.3.2.8 Regulation

For the foreseeable future, government will play a key role. The uncertainty in what governments will do propagates into uncertainties in profitability of various players, in market entry, in prices, etc.

For example, in the 1980s, U.S. state and federal governments encouraged utilities to implement demand-side programs. Program costs, and in some cases costs of foregone sales, were recovered through tariffs. The government interest later switched to competitive markets. These markets do not have such a convenient mechanism for encouraging demand-side management. As a result, demand-side programs became less attractive.

18.3.2.9 Severe Events

High-risk, low-probability events usually are not considered by standard planning practices. For example, transmission planners design so that the system will withstand any single contingency. Planning procedures, criteria, and methods generally ignore several simultaneous or near-simultaneous contingencies. The power system is not designed to withstand them—whether or not it does is happenstance.

In January 1998 an ice storm of unprecedented magnitude struck the northeastern U.S. and Quebec. Ice on transmission lines greatly exceeded design standards. Many towers collapsed. All lines feeding Montreal, and all lines south and east of the city, were on the ground. The government later announced a high-risk, low-probability standard: the system should be designed and operated to prevent loss of more than half of the Montreal load should such an event recur.

18.3.3 Attributes

Attributes measure “goodness” in different ways, from different perspectives. Each stakeholder has objectives; they are expressed in terms of attributes.

Customers of various kinds (residential, commercial, industrial, etc.):

- Cost of electricity
- Other costs absorbed by the customer
- Quality of service (reliability, voltage control, etc.)

Investors in various providers of energy and services

- New capital required
- Net income, earnings per share, and other measures of income
- Cash flow, coverage ratios, and other measures of cash use and replacement

Employees

- Security
- Promotion opportunities
- Salaries
- Healthiness and safety of working conditions

Taxpayers

- Tax revenues
- Expenditures from public funds

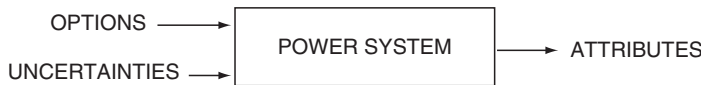


FIGURE 18.3 Options, uncertainties, and attributes.

Neighbors (environmentalists, visitors, local inhabitants, competitors, etc.)

- Emissions or thermal discharges
- Community disruption
- Employment opportunities
- Rights-of-way and other intrusions
- Flooding
- Measures of market power

The list of attributes given above is not complete, and different attributes are important for different studies. Deciding on the planning objectives and the attributes for a given study is an important initial step in power system planning.

Some attributes are measured using complex computer models. For others, approximate or ad hoc models may be adequate or may be the best that is available. The planner calculates how the options and the uncertainties (Fig. 18.3) affect the attributes.

Standards or criteria are surrogates for some attributes that are difficult or impossible to compute.

18.4 Planning Processes

18.4.1 Setting Standards or Criteria

Planning objectives often conflict. For example, maximizing reliability and minimizing environmental impacts generally conflict with minimizing costs.

Since all attributes cannot be measured in dollars, achieving the right trade-off can be a difficult socio-technico-economic-institutional problem. Doing this every day would burden the planning process. Having standards avoids having to revisit such judgments continually. For instance, once it is decided that (say) 20% generation reserve provides adequate reliability at an acceptable cost, the planner accepts 20% as a standard and designs to meet it. Testing whether a particular plan meets the reserve criterion is easy; the planner can concentrate on other issues.

Standards should be examined from time to time. If society becomes poorer or richer, its pocketbook may speak for lower or higher standards of service. Changes in technology may justify a change in standards—for instance, development of better scrubbers may make it reasonable to insist on reduced SO₂ or NO_x emissions. Increased reliance on electricity may require more reliability: a proposal to shut off the power throughout the U.S. for one minute to salute Edison's death was quashed. Had he died in 1900 instead of 1931, it might have been practical.

18.4.2 Assessment

18.4.2.1 Forecasts and Projections

Not all uncertainties create risk for every planning study. Those that do for a particular study are identified. Forecasts and projections are developed for these uncertainties.

18.4.2.2 System State

The state assessment begins with an evaluation of the technical and economic attributes of the present and future power system. Does it and will it satisfy established technical standards? Is it economical? Does it meet other objectives?

[Chapter 8](#) of this handbook, “Power System Analysis and Simulation,” describes the analytical tools available to planners. It also describes how these tools are used. The phenomena analyzed are described in [Chapters 10](#) through [12](#).

18.4.3 Generation Planning

[Chapter 2](#) of this handbook, “Electric Power Generation: Conventional Methods,” describes generation planning options and their characteristics. The generation planner does a preliminary selection from among them, recognizing any special features of his planning problem.

Planners measure how the various options would alleviate deficiencies discovered in the assessment step. The effects of various options or combinations of options and the effects of uncertainties on other attributes are also measured.

In particular, planners compute reserve margin or other measures of reliability. They simulate the operation of the system to measure operating cost and to determine if the operation is within acceptable ranges of other parameters.

18.4.4 Transmission Planning

Traditional transmission options and new technologies are described in [Chapters 3, 4, 11, 15](#), and [16](#) of this handbook. Like the generation planner, the transmission planner makes a preliminary selection based on the needs and development pattern of his system.

For instance, for technical and commercial reasons, a given system will use only a few distinct voltage classes. So a system whose existing transmission consists of 138-kV, 345-kV, and 765-kV equipment will rarely add new circuits at 230 kV or 400 kV, even though these may be popular elsewhere.

Transmission planners then identify a set of specific options and measure how these options in various combinations, along with the important uncertainties, affect the attributes. Load flow, short circuit, and stability analyses are performed to determine if voltages and currents are within acceptable bounds under various system states, and if the system will remain stable for all contingencies. How often and how much the operation of the generation system will be constrained by transmission limitations is an important consideration.

18.4.5 Least-Cost Planning

Least-cost planning is also known as integrated resource planning or integrated demand/supply planning. It considers supply-side options (generally generation options) on a level playing field with demand-side options (generally conservation, indirect load shifting, or direct load control). These options include incentives to encourage utilities and consumers to change energy consumption patterns.

As with generation planning and transmission planning, a preliminary selection weeds out options that are clearly not of interest in a particular area.

The least-cost planning process includes computing values of key attributes for various options and uncertainties.

18.4.6 Making Choices

A key question in generation, transmission, and least-cost planning is: How is one plan selected over another? A few distinctive approaches will be described.

18.4.6.1 Minimize Revenue Requirements

The planner selects the best option from the ratepayer’s perspective. He selects the plan that will minimize the ratepayer’s cost of electricity while satisfying reliability, environmental, and other criteria.

The ratepayer’s cost—an attribute—is the revenue that the utility will have to collect to recover all operating and capital costs and to earn a commission-approved return on unrecovered investor capital:

$$RR_i(\mathbf{O}, \mathbf{U}) = FC_i(\mathbf{O}, \mathbf{U}) + VC_i(\mathbf{O}, \mathbf{U}) \quad (18.2)$$

$RR_i(O, U)$ = Revenue requirements in period i

$FC_i(O, U)$ = Fixed costs in period i

$VC_i(O, U)$ = Variable costs in period i

O = A selection of the various options

U = Realizations or values of the various uncertainties

Fixed costs are independent of how much or how little a piece of equipment is used. Depreciation (recovery of investors' capital), interest on debt, and profit (return on unrecovered capital) are typical fixed costs.

Variable costs—fuel cost—for example, are related to how much a piece of equipment is used. These costs include all system costs, not just the cost of the individual option. For instance, old plants may run less when a new plant is built. The variable cost includes fuel cost for all plants.

To apply this traditional method, the planner must know his company's return rate, which is set by the regulator. In a closely related method, the market defines the cost of electricity and Eq. (18.2) is solved for the internal rate of return (IRR). The option selected is the one that maximizes the IRR, the investor's profit.

18.4.6.2 Cost-Benefit Analysis

If the benefits exceed the costs, a project is worth doing.

Typically, costs are incurred first, and benefits come later. A dollar of benefit later is not worth the same as a dollar of cost today. Present worth analysis is a way to compare dollars at different times. The basic equation is:

$$P = S / (1 + i)^n \quad (18.3)$$

In Eq. (18.3), P is the present worth or equivalent value today of an amount S, n years in the future, with i the discount rate or annual cost of capital.

Cost-benefit analysis is also used to rank mutually exclusive projects—the one with the highest benefit/cost ratio wins.

18.4.6.3 Multi-Objective Decision Analysis

18.4.6.3.1 Utility Function Methods

Table 18.2 compares two options for a new power plant in Utah (Keeney et al., 1981). Which choice is better? The attributes are combined in a utility function of the form:

$$U(x) = k_1 \text{Economics} + k_2 \text{Environment} + \dots + k_7 \text{Feasibility} \quad (18.4)$$

In Eq. (18.4), x takes on one of two values, "coal" or "nuclear." [The actual functional form for a particular study may be more complicated than Eq. (18.4).] The coefficients k_i reflect the relative

TABLE 18.2 Attributes: Nuclear Plant vs. Coal Plant

	Wellington Coal Plant	Green River Nuclear Plant
Economics (\$/MWh)	60.7	47.4
Environment (corridor-miles)	532.6	500.8
Public disbenefits (\$ × 000,000)	15.0	22.6
Tax revenues (\$ × 000,000/year)	3.5	1.0
Health lost (equivalent years)	446.7	6.3
Public attitudes	0.33	-1.0
Feasibility	60.0	37.0

Source: Keeney, R.L. et al., *Decision Framework for Technology Choice*, Report EA-2153, Electric Power Research Institute, Palo Alto, CA, 1981. With permission.

importance of each attribute. These coefficients convert the different attributes to a common measure. The choice that minimizes the utility function wins. In this study, for the values of coefficients selected $U(\text{coal})$ was \$131.4/MWh; $U(\text{nuclear})$ was \$162.9/MWh.

This approach has many variants. Uncertainties can be included, making $U(x)$ a random variable. Work has been done to develop methods for determining the decision-maker's values (the coefficients) and risk tolerance.

18.4.6.3.2 Trade-Off Analysis

Trade-off analysis measures each attribute in its natural units, without reducing them all to a common measure, and seeks reasonable compromises at points of saturation or diminishing return. A good compromise will not necessarily optimize any of the attributes, but will come close to optimizing all of them.

For example, Fig. 18.4 shows 22 plans examined in an energy strategy study. The plans in region A minimize SO_2 emissions, but are very costly. The plans in region B are cheap but have high emissions. The plans at the knee of the trade-off curve are at the point of diminishing returns for one attribute against the other. Significant reductions in emissions can be had at little cost by moving from B to the knee. Going beyond the knee toward A will not reduce SO_2 much more but will increase the cost significantly. The plans at the knee come close to minimizing both cost and emissions.

Trade-off analysis can be done graphically for two-attribute problems. More than two attributes cannot be graphed easily but can be analyzed mathematically (Croussillat, 1993).

18.4.6.4 Risk

Risk is the hazard due to uncertainty. Risk is also associated with decisions. Without uncertainties and alternatives, there is no risk.

System planning, engineering, and operating procedures have evolved to reduce the risks of widespread or local service interruptions. Another section of this handbook describes methods for modeling and enhancing reliability.

Not all risks are included in reliability analysis, however. Much talk about risk is directed to financial risks. Other important risks are not quantified in dollars.

One measure of risk is *robustness*, the likelihood that a particular decision will not be regretted. *Exposure* is the possible loss (in terms of an attribute) under adverse realizations of uncertainties. *Regret* is the difference between the value of an attribute for a particular set of decisions and realizations of uncertainties, and the value of the attribute for optimized decisions with perfect foreknowledge of the uncertainties.

Planners develop *hedges*, options that increase robustness or decrease exposure or regret. Building small generating units instead of large ones is an example; an insurance policy is another (De la Torre et al., 1999).

References

- Bjorklund, G.J., Planning for uncertainty at an electric utility, *Public Utilities Fortnightly*, October 15, 1987.
- Croussillat, E., *Incorporating Risk and Uncertainty in Power System Planning*, I&ED Energy Series paper # 17, The World Bank, Washington D.C., 1989.
- Croussillat, E.O., Dörfner, P., Alvarado, P., Merrill, H.M., Conflicting objectives and risk in power system planning, *IEEE Trans. Power Systems*, 8(3), Aug. 1993.
- Energy Projections to the Year 2010*, U.S. Dept of Energy, Office of Policy, Planning and Analysis, report DOE/PE-0029/2, October 1983.

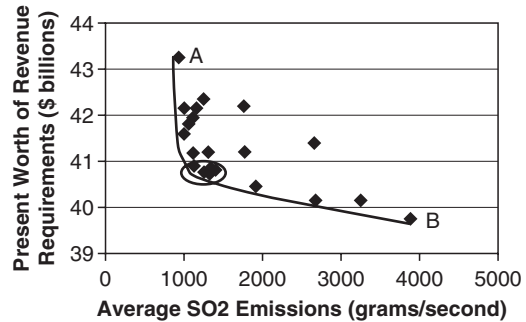


FIGURE 18.4 Trade-off: cost vs. SO_2 emissions.

The Future of Electric Power in America: Economic Supply for Economic Growth, U.S. Dept of Energy, Office of Policy, Planning and Analysis, report DOE/PE-0045, June 1983.

Kahn, E., *Electric Utility Planning & Regulation*, American Council for an Energy-Efficient Economy, Washington, 1988. This text presents power system planning in a broad social context and is close in spirit to this chapter.

Keeney, R.L., Beley, J.R., Fleischauer, P., Kirkwood, C.W., Sicherman, A., *Decision Framework for Technology Choice*, Report EA-2153, Electric Power Research Institute, Palo Alto, 1981.

Ringlee, R.J., Ed., special section on electric utility systems planning, *Proc. IEEE*, 77(6), June 1989. This special section contains several excellent papers on engineering issues in planning.

Schweppe, F.C., *Uncertain Dynamic Systems*, Prentice-Hall, Englewood Cliffs, NJ, 1973, chap. 3.

Stoll, H.G., Garver, L.J. (sic), Jordan, G.A., Price, W.H., Sigley, R.F., Jr., Szczepanski, R.S., Tice, J.B., *Least-Cost Electric Utility Planning*, John Wiley & Sons, New York, 1989. Its title notwithstanding, this is a general text on planning.

Sullivan, R.L., *Power System Planning*, McGraw-Hill, New York, 1977. This text covers some of the mechanics of planning.

De la Torre, T., Fertes, J.W., Gómez, T., and Merrill, H.M., Deregulation, privatization, and competition: transmission planning under uncertainty, *IEEE Trans. Power Systems*, 14(2), May 1999.

19

Power System Reliability

19.1	NERC Regions	19-2
19.2	System Adequacy Assessment	19-3
19.3	System Security Assessment	19-4
19.4	Probabilistic Security Assessment	19-6
19.5	Distribution System Reliability	19-6
19.6	Typical Sequence of Events after an Overhead Distribution Fault.....	19-7
19.7	Distribution Reliability Indices	19-7
19.8	Storms and Major Events	19-9
19.9	Component Reliability Data.....	19-10
19.10	Utility Reliability Problems	19-10
	Underground Cable • Transformer Failures • Lightning • Tree Contact • Birds • Squirrels • Snakes • Insects • Bears, Bison, and Cattle • Mice, Rats, and Gophers • Vandalism	
19.11	Reliability Economics.....	19-14
19.12	Annual Variations in Reliability.....	19-14

Richard E. Brown
InfraSource Technology

The electric power industry began in the late 1800s as a component of the electric lighting industry. At this time, lighting was the only application for electricity, and homes had other methods of illumination if the electricity supply was interrupted. Electricity was essentially a luxury item and reliability was not an issue.

As electricity became more common, new applications began to appear. Examples include electric motors, electric heating, irons, and phonographs. People began to grow accustomed to these new electric appliances, and their need for reliable electricity increased. This trend culminated with the invention of the radio. No nonelectrical appliance could perform the same function as a radio. If a person wanted to listen to the airwaves, electricity was required. As radio sales exploded in the 1920s, people found that reliable electricity was a necessity. By the late 1930s, electricity was regarded as a basic utility (Philipson and Willis, 1999).

As electric utilities expanded and increased their transmission voltage levels, they found that they could improve reliability by interconnecting their system to neighboring utilities. This allowed connected utilities to “borrow” electricity in case of an emergency. Unfortunately, a problem on one utility’s system could now cause problems to other utilities. This fact was made publicly evident on November 9, 1965. On this day, a major blackout left cities in the northeastern U.S. and parts of Ontario without power for several hours. Homes and businesses had become so dependent on electricity that this blackout was crippling. Action was needed to help prevent such occurrences from happening in the future.

19.1 NERC Regions

The North American Electric Reliability Council (NERC) was formed in 1968 as a response to the 1965 blackout. By this time, reliability assessment was already a mature field and was being applied to many types of engineered systems (Billinton and Allan, 1988; Ramakumar, 1993). NERC's mission is to promote the reliability of the North America's bulk power system (generation and transmission). It reviews past events; monitors compliance with policies, standards, principles, and guides; and assesses future reliability for various growth and operational scenarios. NERC provides planning recommendations and operating guidelines, but has no formal authority over electric utilities.

Since most of the transmission infrastructure in the U.S. and Canada is interconnected, bulk power reliability must look at systems larger than a single utility. The territory covered by NERC is far too large to study and manage as a whole, and is divided into ten regions. These NERC regions are: East Central Area Reliability Coordination Agreement (ECAR), Electric Reliability Council of Texas (ERCOT), Florida Reliability Coordinating Council (FRCC), Mid-Atlantic Area Council (MAAC), Mid-Atlantic Interconnected Network (MAIN), Mid-Continent Area Power Pool (MAPP), Northeast Power Coordinating Council (NPCC), Southeastern Electric Reliability Council (SERC), Southwest Power Pool (SPP), and the Western Systems Coordinating Council (WSCC). The geographic territories assigned to the ten NERC regions are shown in Fig. 19.1.

Even though there are ten NERC regions, there are only four major transmission grids in the U.S. and Canada: the area associated with the Western Systems Coordinating Council, the area associated with the Electric Reliability Council of Texas, Quebec, and the Eastern United States. These are usually referred to as the Western Interconnection, the ERCOT Interconnection, the Quebec Interconnection, and the Eastern Interconnection. Each of these grids is highly interconnected within their boundaries, but

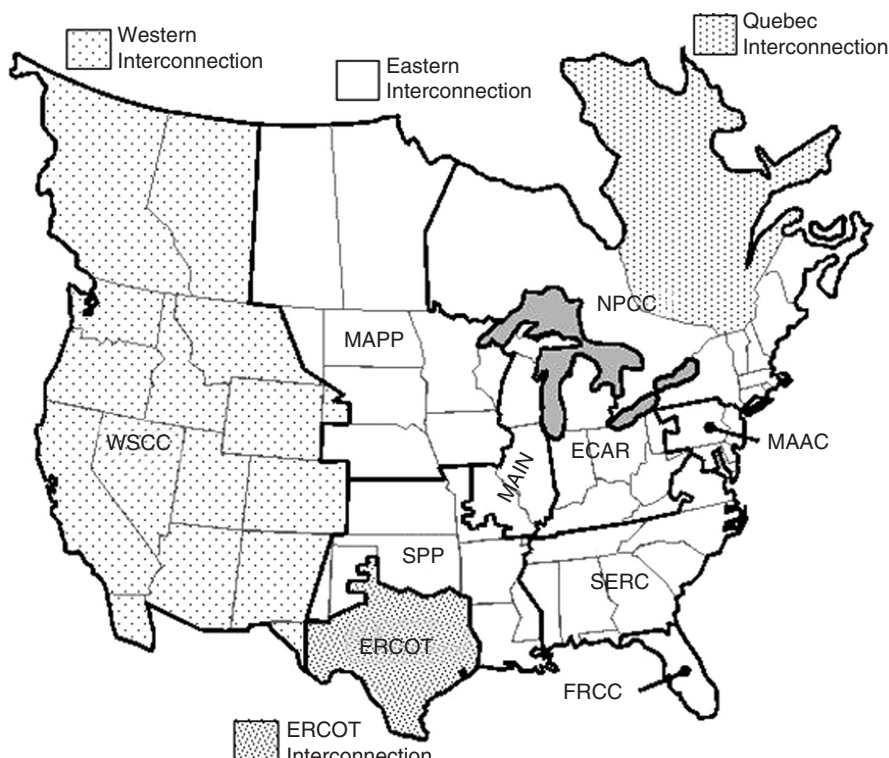


FIGURE 19.1 NERC regions.

only has weak connections to the other grids. The geographic territories associated with these four interconnections are shown in Fig. 19.1.

NERC looks at two aspects of bulk power system reliability: system adequacy and system security. A system must have enough capacity to supply power to its customers (adequacy), and it must be able to continue supplying power to its customers if some unforeseen event disturbs the system (security). Each of these two aspects of reliability is further discussed below.

19.2 System Adequacy Assessment

System adequacy is defined as the ability of a system to supply all of the power demanded by its customers (Billinton and Allan, 1988). Three conditions must be met to ensure system adequacy. First, its available generation capacity must be greater than the demanded load plus system losses. Second, it must be able to transport this power to its customers without overloading any equipment. Third, it must serve its loads within acceptable voltage levels.

System adequacy assessment is probabilistic in nature (Allan et al., 1994; Schilling et al., 1989). Each generator has a probability of being available, P_A , a probability of being available with a reduced capacity, P_R , and a probability of being unavailable, P_U . This allows the probability of all generator state combinations to be computed. A simple two-generator example is shown in Table 19.1. There are nine possible generator state combinations, and the probability of being in a particular combination is the product of the individual generator state probabilities. In general, if there are n generators and x possible states for each generator, the number of possible generator state combinations is:

$$\text{Generator State Combinations} = x^n \quad (19.1)$$

In addition to generator state combinations, loading behavior must be known. Information is found by looking at historical load bus demand in recent years. For the best accuracy, 8760 hour peak demand curves are used for each load bus. These correspond to hourly peak loads for a typical year. To reduce computational and data requirements, it is usually acceptable to reduce each set of 8760-hour load curves to three weekly load curves (168 hours each). These correspond to typical weekly load patterns for winter conditions, spring/autumn conditions, and summer conditions. Weekly load curves can be scaled up or down to represent temperatures that are above or below normal. Sample weekly load curves for a winter peaking load bus are shown in Fig. 19.2.

To perform an adequacy assessment, each generation state combination is compared with all hourly loading conditions. For each combination of generation and loading, a power flow is performed. If the available generation cannot supply the loads or if any constraints are violated, the system is inadequate and certain loads must be shed. After all generation/load combinations are examined, the adequacy assessment is complete.

TABLE 19.1 Generator State Probabilities

Generator State		
Generator 1	Generator 2	Probability
Available	Available	$P_{A1} P_{A2}$
Available	Reduced	$P_{A1} P_{R2}$
Available	Unavailable	$P_{A1} P_{U2}$
Reduced	Available	$P_{R1} P_{A2}$
Reduced	Reduced	$P_{R1} P_{R2}$
Reduced	Unavailable	$P_{R1} P_{U2}$
Unavailable	Available	$P_{U1} P_{A2}$
Unavailable	Reduced	$P_{U1} P_{R2}$
Unavailable	Unavailable	$P_{U1} P_{U2}$

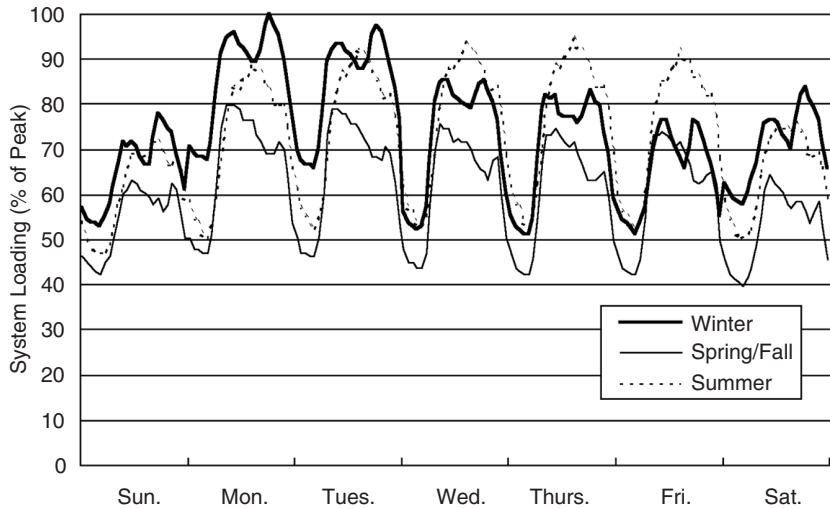


FIGURE 19.2 Weekly load curves by season.

An adequacy assessment produces the following information for each load bus: (1) the combinations of generation and loading that result in load interruptions, and (2) the probability of being in each of these inadequate state combinations. From this information, it is simple to compute the expected number of interruptions for each load bus, the expected number of interruption minutes for each load bus, and the expected amount of unserved energy for each load bus. These load bus results can then be aggregated to produce the following system indices:

- **LOLE** (Loss of Load Expectation)—the expected number of hours per year that the system will have to shed load.
- **EENS** (Expected Energy Not Served)—the expected number of megawatt hours per year that a system will not be able to supply.

System adequacy assessment assumes that the transmission system is available. This may not always be the case. A classic example is the 1965 blackout, which was initiated by the unexpected loss of a transmission line. To address such events, system security assessment is required.

19.3 System Security Assessment

System security is defined as the ability of a power system to supply all of its loads in the event of one or more contingencies (a contingency is an unexpected event such as a system fault or a component outage). This is divided into two separate areas: static security assessment and dynamic security assessment.

Static security assessment determines whether a power system is able to supply peak demand after one or more pieces of equipment (such as a line or a transformer) are disconnected. The system is tested by removing a piece (or multiple pieces) of equipment from the normal power flow model, rerunning the power flow, and determining if all bus voltages are acceptable and all pieces of equipment are loaded below emergency ratings. If an unacceptable voltage or overload violation occurs, load must be shed for this condition and the system is *insecure*. If removing any single component will not result in the loss of load, the system is *N-1 Secure*. If removing any *X* arbitrary components will not result in the loss of load, the system is *N-X Secure*. *N* refers to the number of components on the system and *X* refers to the number of components that can be safely removed.

Performing a static security assessment can be computationally intensive. For example, an N-2 assessment on a modest system with 5000 components (1500 buses, 500 transformers, and 3000 lines) will require more than 25 million power flows to be performed. For this reason, contingency ranking methods are often used. These methods rank each contingency based on its likelihood of resulting in load curtailment. Contingencies are examined in order of their contingency ranking, starting with the most severe. If a prespecified number of contingencies are tested and found to be secure, it is assumed that contingencies with less severe rankings are also secure and do not need to be examined.

Static security assessment is based on steady state power flow solutions. For each contingency, it assumes that the system protection has properly operated and the system has reached a steady state. In fact, the power system may not actually reach a steady state after it has been disturbed. Checking whether a system will reach a steady state after a fault occurs is referred to as *dynamic security assessment* (also referred to as *transient security assessment*).

When a fault occurs, the system is less able to transfer power from synchronous generators to synchronous motors. Since the instantaneous power input has not changed, generators will begin to speed up and motors will begin to slow down (analogous to the chain slipping while riding a bicycle). This increases the rotor angle difference between generators and motors. If this rotor angle exceeds a critical value, the system will become unstable and the machines will not be able to regain synchronism. After the protection system clears the fault, the rotor angle difference will still increase since the power transfer limits of the system are still less than the prefault condition. If the fault is cleared quickly enough, this additional increase will not cause the rotor angle difference to exceed the critical angle and the system will return to a synchronous state (ABB Power, 1997).

An example of a transient stability test is shown in Fig. 19.3. This shows the rotor angle difference between a synchronous generator and a synchronous motor during a fault sequence. When the fault occurs, the rotor angle begins to increase. If the fault is not cleared, the rotor angle quickly exceeds the critical angle. If the fault is cleared at 0.3 sec, the rotor angle still increases beyond the critical value. The system is dynamically stable for this fault if it is cleared in 0.2 sec. The rotor angle will still increase after the fault occurs, but will stabilize below the critical value.

A dynamic security assessment will consist of many transient stability tests that span a broad range of loading conditions, fault locations, and fault types. To reduce the number of tests required, contingency rankings (similar to static security assessment) can be used.

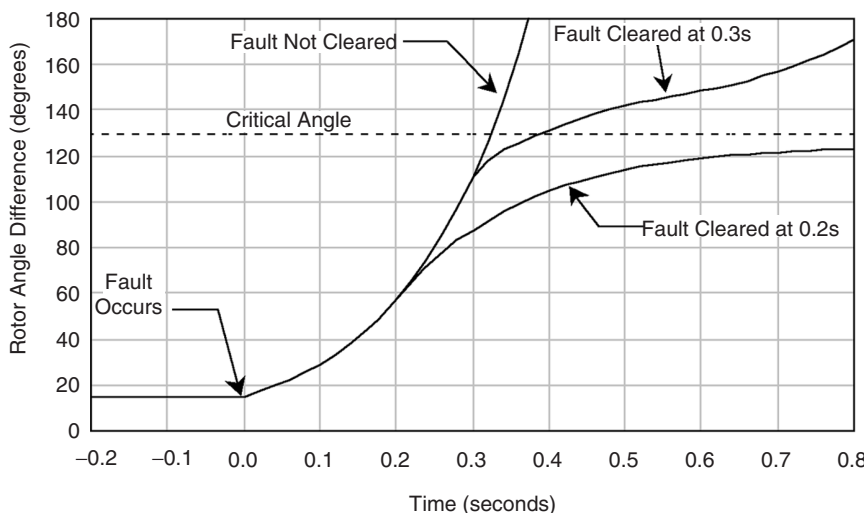


FIGURE 19.3 Dynamic security assessment.

19.4 Probabilistic Security Assessment

Although the “N-1 Criterion” remains popular, it has received much criticism since it treats unlikely events with the same importance as more frequent events. Using the N-1 Criterion, large amounts of money may be spent to reinforce a system against a very rare event. From a reliability perspective, this money *might* be better spent in other areas such as replacing old equipment, decreasing maintenance intervals, adding automation equipment, adding crews, and so on. To make such value judgments, both the impact of each contingency and its probability of occurrence must be considered (Endrenyi, 1978). This is referred to as *probabilistic security assessment*. To do this type of assessment, each piece of equipment needs at least two fundamental pieces of information: the *failure rate* of the equipment (usually denoted λ , in failures per year), and the mean time to repair of the equipment (usually denoted *MTTR*, in hours).

Performing a probabilistic security assessment is similar to a performing a standard static security assessment. First, contingencies are ranked and simulated using a power flow. If a contingency results in the loss of load, information about the number and size of interrupted loads, the frequency of the contingency, and the repair time of the contingency are recorded. This allows quantities such as *EENS* (Expected Energy Not Served) to be easily computed. If contingency i causes kW_i amount of kilowatts to be interrupted, then *EENS* is equal to:

$$EENS = \sum_i kW_i \lambda_i MTTR_i \quad (19.2)$$

It is important to note that this is the *EENS* due to contingencies, and is separate from the *EENS* due to generation unavailability. It is also important to note that this formula assumes that $\lambda_i MTTR_i$ is small when compared to one year. If this is not the case, a component will experience fewer failures per year than its failure rate and the equation must be adjusted accordingly.

19.5 Distribution System Reliability

The majority of customer reliability problems stem from distribution systems. For a typical residential customer with 90 min of interrupted power per year, between 70 and 80 minutes will be attributable to problems occurring on the distribution system that it is connected to (Billinton and Jonnativithula, 1996). This is largely due to radial nature of most distribution systems, the large number of components involved, the sparsity of protection devices and sectionalizing switches, and the proximity of the distribution system to end-use customers.

Since reliability means different things to different people, it is necessary to address the definition of “distribution system reliability” in more detail. In distribution systems, reliability primarily relates to equipment outages and customer interruptions:

- **Outage**—when a piece of *equipment* is deenergized.
- **Momentary interruption**—when a *customer* is deenergized for less than a few minutes.
- **Sustained interruption**—when a *customer* is deenergized for more than a few minutes.

Customers do not, in the strictest sense, experience power outages. Customers experience power interruptions. If power is restored within a few minutes, it is considered a momentary interruption. If not, it is considered a sustained interruption. The precise meaning of “a few minutes” varies from utility to utility, but is typically between 1 and 5 min. The IEEE defines a momentary interruption based on 5 min. (Note: some references classify interruptions into four categories rather than two. Instantaneous interruptions last a few seconds, momentary interruptions last a few minutes, temporary interruptions last a few hours, and sustained interruptions last many hours.)

On a historical note, momentary interruptions used to be considered a “power quality issue” rather than a “reliability issue.” It is now generally agreed that momentary interruptions are an aspect of reliability since (1) momentary interruptions can cause substantial problems to all types of customers,

and (2) many trade-offs must be made between momentary interruptions and sustained interruptions during system planning, operation, and control. It can also be observed that customer voltage sags, typically considered a power quality issue, are slowly becoming a reliability issue for similar reasons.

Distribution system reliability is not dependent solely upon component failure characteristics. It is also dependent upon how the system responds to component failures. To understand this, it is necessary to understand the sequence of events that occurs after a distribution system fault.

19.6 Typical Sequence of Events after an Overhead Distribution Fault

1. The fault causes high currents to flow from the source to the fault location. These high currents may result in voltage sags for certain customers. These sags can occur on all feeders that have a common coupling at the distribution substation.
2. An instantaneous relay trips open the feeder circuit breaker at the substation. This causes the entire feeder to be deenergized. A pause allows the air around the fault to deionize, and then a reclosing relay will close the circuit breaker. If no fault current is detected, the fault has cleared itself and all customers on the feeder have experienced a momentary interruption.
3. If the fault persists, time overcurrent protection devices are allowed to clear the fault. If the fault is on a fused lateral, the fuse will blow and customers on the lateral will be interrupted. If the feeder breaker trips again, the reclosing relay will repeat the reclosing process a preset number of times before locking out. After the feeder breaker locks out, all customers on the feeder will be interrupted.
4. The electric utility will receive trouble calls from customers with interrupted power. It will dispatch a crew to locate the fault and isolate it by opening up surrounding sectionalizing switches. It may also attempt to reconfigure the distribution system in an attempt to restore power to as many customers as possible while the fault is being repaired. Fault isolation can be very fast if switches are motor operated and remotely controlled, but switching usually takes between 15 and 60 min.
5. The crew repairs the faulted equipment and returns the distribution system to its normal operating state.

As can be seen, *a fault on the distribution system will impact many different customers in many different ways*. In general, the same fault will result in voltage sags for some customers, momentary interruptions for other customers, and varying lengths of sustained interruptions for other customers, depending on how the system is switched and how long the fault takes to repair.

Distribution system reliability assessment methods are able to predict distribution system reliability based on system configuration, system operation, and component reliability data (Brown et al., 1996). This ability is becoming increasingly important as the electric industry becomes more competitive, as regulatory agencies begin to regulate reliability, and as customers begin to demand performance guarantees. The most common reliability assessment methods utilize the following process: (1) they simulate a system's response to a contingency, (2) they compute the reliability impact that this contingency has on each customer, (3) the reliability impact is weighted by the probability of the contingency occurring, and (4) steps 1–3 are repeated for all contingencies. Since this process results in the reliability that each customer can expect, new designs can be compared, existing systems can be analyzed, and reliability improvement options can be explored.

19.7 Distribution Reliability Indices

Utilities typically keep track of customer reliability by using reliability indices. These are average customer reliability values for a specific area. This area can be the utility's entire service area, a particular geographic region, a substation service area, a feeder service area, and so on. The most commonly used

reliability indices give each customer equal weight. This means that a large industrial customer and a small residential customer will each have an equal impact on computed indices. The most common of these *customer reliability indices* are: System Average Interruption Frequency Index (SAIFI), System Average Interruption Duration Index (SAIDI), Customer Average Interruption Duration Index (CAIDI), and Average System Availability Index (ASAI) (IEEE Working Group, 1998). Notice that these indices are redundant. If SAIFI and SAIDI are known, both CAIDI and ASAI can be calculated. Formulae for these indices are:

$$SAIFI = \frac{\text{Total Number of Customer Interruptions}}{\text{Total Number of Customers Served}} \quad \text{per year} \quad (19.3)$$

$$SAIDI = \frac{\sum \text{Customer Interruption Durations}}{\text{Total Number of Customers Served}} \quad \text{hours per year} \quad (19.4)$$

$$CAIDI = \frac{\sum \text{Customer Interruption Durations}}{\text{Total Number of Customer Interruptions}} = \frac{SAIDI}{SAIFI} \quad \text{hours per interruption} \quad (19.5)$$

$$ASAI = \frac{\text{Customer Hours Service Availability}}{\text{Customer Hours Service Demand}} = \frac{8760 - SAIDI}{8760} \quad \text{per unit} \quad (19.6)$$

Some less commonly used reliability indices are not based on the total number of customers served. The Customer Average Interruption Frequency Index (CAIFI) and the Customer Total Average Interruption Duration Index (CTAIDI) are based upon the number of customers that have experienced one or more interruptions in the relevant year. The Average System Interruption Frequency Index (ASIFI) and the Average System Interruption Duration Index (ASIDI) are based upon the connected kVA of customers (these are sometimes referred to as load-based indices). Formulae for these indices are:

$$CAIFI = \frac{\text{Total Number of Customer Interruptions}}{\text{Customers Experiencing 1 or more Interruptions}} \quad \text{per year} \quad (19.7)$$

$$CTAIDI = \frac{\sum \text{Customer Interruption Durations}}{\text{Customers Experiencing 1 or more Interruptions}} \quad \text{hours per year} \quad (19.8)$$

$$ASIFI = \frac{\text{Connected kVA Interrupted}}{\text{Total Connected kVA Served}} \quad \text{per year} \quad (19.9)$$

$$ASIDI = \frac{\text{Connected kVA Hours Interrupted}}{\text{Total Connected kVA Served}} \quad \text{hours per year} \quad (19.10)$$

As momentary interruptions become more important, it becomes necessary to keep track of indices related to momentary interruptions. Since the duration of momentary interruptions is of little consequence, a single frequency related index, the Momentary Average Interruption Frequency Index (MAIFI), is all that is needed. MAIFI, like SAIFI, weights each customer equally (there is currently no load-based index for momentary interruptions). The formula for MAIFI is:

$$MAIFI = \frac{\text{Total Number of Customer Momentary Interruptions}}{\text{Total Number of Customers Served}} \quad \text{per year} \quad (19.11)$$

The precise application of MAIFI varies. This variation is best illustrated by an example. Assume that a customer experiences three recloser operations followed by a recloser lockout, all within a period of one minute. Some utilities would not count this event as a momentary interruption since the customer experiences a sustained interruption. Other utilities would count this event as three momentary

interruptions and one sustained interruption. Similarly, if a customer experiences three recloser operations within a period of one minute with power being restored after the last reclosure, some utilities would count the event as three momentary interruptions and other utilities would count the event as a single momentary interruption.

19.8 Storms and Major Events

When electric utilities compute reliability indices, they often exclude interruptions caused by “storms” and “major events.” The definition of a major event varies from utility to utility, but a typical example is when more than 10% of customers experience an interruption during the event. The event starts when the notification of the first interruption is received and ends when all customers are restored service.

In nonstorm conditions, equipment failures are independent events—the failure of one device is completely independent of another device. In contrast, major events are characterized by common-mode failures. This means that a common cause is responsible for all equipment failures. The result is that many components tend to fail at the same time. This puts a strain on utility resources, which can only handle a certain number of concurrent failures (Brown et al., 1997). The most common causes of major events are wind storms, ice storms, and heat waves.

Wind storms refer to linear winds that blow down trees and utility poles. The severity of wind storms is dependent upon sustained wind speed, gust speed, wind direction, and the length of the storm. Severity is also sensitive to vegetation management and the time elapsed since the last wind storm. Since a wind storm will tend to blow over all of the weak trees, a similar storm occurring a few months later may have little impact. A U.S. map showing wind speeds for the worst expected storm in 50 years is shown in Fig. 19.4.

Ice storms refer to ice buildup on conductors. This has four major effects: (1) it places a heavy physical load on the conductors and support structures, (2) it increases the cross-sectional area that is exposed to the wind, (3) ice can break off and cause a conductor to jump into the phase wires located above it, and (4) galloping. Galloping occurs when ice buildup assumes a teardrop shape and acts as an airfoil. During high winds, this can cause conductors to swing wildly and with great force. Ice can also cause problems by accumulating in trees, causing limbs to break off, and causing entire trunks to fall over into power lines.

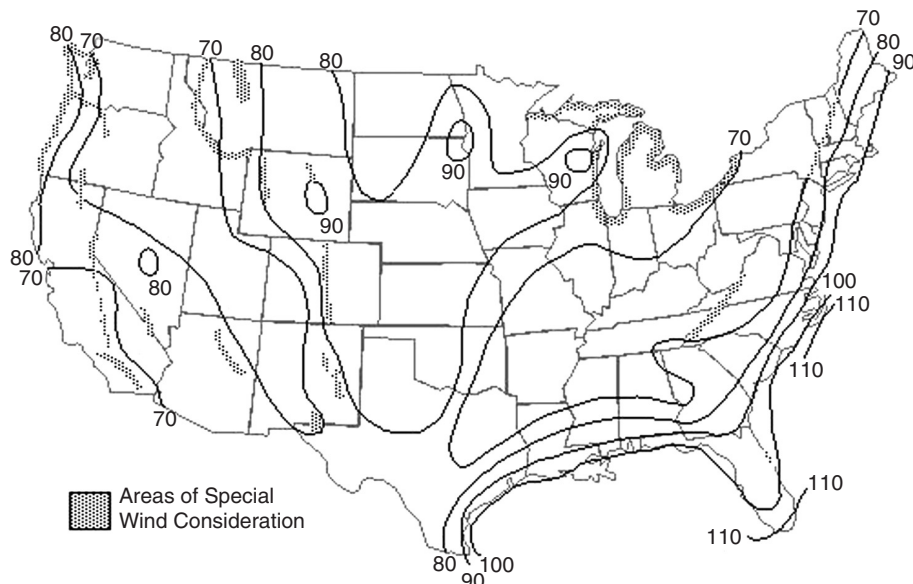


FIGURE 19.4 50-year wind storm (sustained wind speed in mi/hr).

Heat waves are extended periods of exceedingly hot weather. This hot weather causes electricity demand to skyrocket due to air-conditioning loads. At the same time, conductors cannot carry as much electricity since they cannot transfer heat as effectively to their surroundings. This combination of heavy loading and conductor de-rating can cause overhead wires to become overloaded and sag to dangerous levels. Overloaded cables will cause insulation to lose life. In a worst-case scenario, the maximum power transfer capabilities of the system can be approached, resulting in a voltage collapse condition. Humidity exacerbates the impact of heat waves since it causes air conditioners to consume more energy.

19.9 Component Reliability Data

For a reliability model to be accurate, component reliability data must be representative of the system being modeled. Utilities recognize this and are increasing their efforts to keep track of component failure rates, failure modes, repair times, switching times, and other important reliability parameters. Unfortunately, reliability statistics vary widely from utility to utility and from country to country. The range of equipment reliability data that can be found in published literature is shown in Table 19.2.

Because component reliability is very system specific, it is beneficial to calibrate reliability models to historical reliability indices. In this process, component reliability parameters are adjusted until historical reliability indices match computed reliability indices (Brown et al., 1998). The amount that each parameter is adjusted should depend on the confidence of the original value and the sensitivity of the reliability indices to changes in this value. To illustrate, consider an overhead distribution system. A reliability model of this system is created using component reliability data from published literature. Unfortunately, the reliability indices that the model produces do not agree with the historical performance of the system over the past few years. To fix this, the failure rate and repair times of overhead lines (along with other component parameters) can be adjusted until predicted reliability matches historical reliability.

19.10 Utility Reliability Problems

To gain a broader understanding of power system reliability, it is necessary to understand the root causes of system faults and system failures. A description of major failure modes is now provided.

TABLE 19.2 Equipment Reliability Data

Component	Failure Rate (per year)	MTTR (hours)
Substation Equipment		
Power transformers	0.015–0.07	15–480
Circuit breakers	0.003–0.02	6–80
Disconnect switches	0.004–0.16	1.5–12
Air insulated buswork	0.002–0.04	2–13
Overhead Equipment		
Transmission lines ^a	0.003–0.140	4–280
Distribution lines ^a	0.030–0.180	4–110
Switches/fused cutouts	0.004–0.014	1–4
Pole mounted transformer	0.001–0.004	3–8
Underground Equipment		
Cable ^a	0.005–0.04	3–30
Padmount switches	0.001–0.01	1–5
Padmount transformers	0.002–0.003	2–6
Cable terminations/joints	0.0001–0.002	2–4

^aFailure rates for lines and cable are per mile.

19.10.1 Underground Cable

A major reliability concern pertaining to underground cables is electrochemical treeing. Treeing occurs when moisture penetration in the presence of an electric field reduces the dielectric strength of cable insulation. When the dielectric strength is degraded sufficiently, transients caused by lightning or switching can result in dielectric breakdown. Electrochemical treeing usually affects extruded dielectric cable such as cross-linked polyethylene (XLPE) and ethylene-propylene rubber (EPR), and is largely attributed to insulation impurities and bad manufacturing. To reduce failures related to electrochemical treeing, a utility can install surge protection on riser poles (transitions from overhead to underground), can purchase tree-retardant cable, and can test cable reels before accepting them from the manufacturer.

Existing cable can be tested and replaced if problems are found. One way to do this is to apply a DC voltage withstand test (approximately 3 times nominal RMS voltage). Since cables will either pass or not pass this test, information about the state of cable deterioration cannot be determined. Another popular method for cable testing is to inject a small signal into one end and check for reflections that will occur at partial discharge points. Other methods are measuring the power factor over a range of frequencies (dielectric spectroscopy), analyzing physical insulation samples in a lab for polymeric breakdown (degree of polymerization), and using cable indentors to test the hardness of the insulation.

Not all underground cable system failures are due to cable insulation. A substantial percentage occurs at splices, terminations, and joints. Major causes are due to water ingress and poor workmanship. Heat shrink covers can be used to waterproof these junctions and improve reliability.

The last major reliability concern for underground cable is dig-ins. This is when excavation equipment cuts through one or more cables. To prevent dig-ins, utilities should encourage the public to have cable routes identified before initiating site excavation. In extreme cases where high reliability is required, utilities can place cable in concrete-encased duct banks.

19.10.2 Transformer Failures

Transformers are critical links in power systems, and can take a long time to replace if they fail. Through-faults cause extreme physical stress on transformer windings, and are the major cause of transformer failures. Overloads rarely result in transformer failures, but do cause thermal aging of winding insulation.

When a transformer becomes hot, the insulation on the windings slowly breaks down and becomes brittle over time. The rate of thermal breakdown approximately doubles for every 10°C . 10°C is referred to as the “Montsinger Factor” and is a rule of thumb describing the Arrhenius theory of electrolytic dissociation. Because of this exponential relationship, transformer overloads can result in rapid transformer aging. When thermal aging has caused insulation to become sufficiently brittle, the next fault current that passes through the transformer will mechanically shake the windings, a crack will form in the insulation, and an internal transformer fault will result.

Extreme hot-spot temperatures in liquid-filled transformers can also result in failure. This is because the hot spot can cause free bubbles that reduce the dielectric strength of the liquid. Even if free bubbles are not formed, high temperatures will increase internal tank pressure and may result in overflow or tank rupture.

Many transformers are fitted with load tap changers (LTCs) for voltage regulation. These mechanically moving devices have historically been prone to failure and can substantially reduce the reliability of a transformer (Willis, 1997). Manufacturers have addressed this problem and new LTC models using vacuum technology have succeeded in reducing failure rates.

19.10.3 Lightning

A lightning strike occurs when the voltage generated between a cloud and the ground exceeds the dielectric strength of the air. This results in a massive current stroke that usually exceeds 30,000 amps. To make matters worse, most strokes consist of multiple discharges within a fraction of a second. Lightning

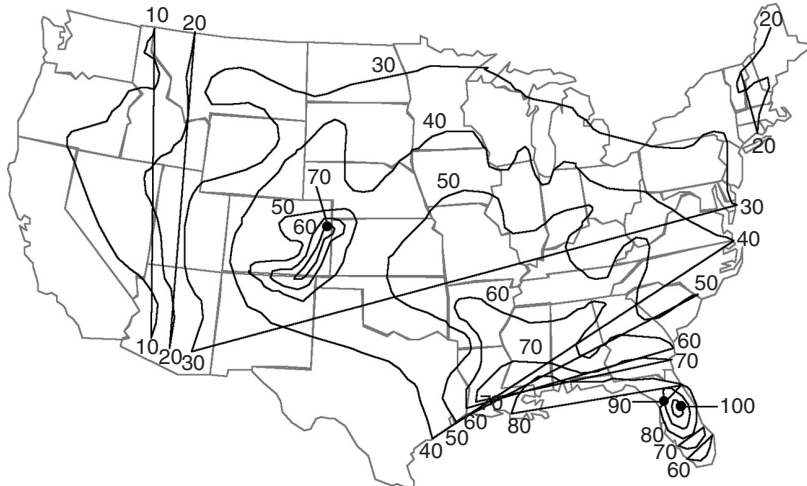


FIGURE 19.5 Number of thunderstorm days per year.

is the major reliability concern for utilities located in high keraunic areas (Burke, 1994). An isokeraunic map for the U.S. is shown in Fig. 19.5.

Lightning can affect power systems through direct strikes (the stroke contacts the power system) or through indirect strikes (the stroke contacts something in close proximity and induces a traveling voltage wave on the power system). Lightning can be protected against by having a high system BIL, by using shield wires, by using surge arrestors to clamp voltages across equipment, and by having a low impedance ground. Direct strikes are virtually impossible to protect against on a distribution system.

19.10.4 Tree Contact

Trees continuously grow, can fall over onto conductors, can drop branches onto conductors, can push conductors together, and can serve as gateway for animals. This is why many utilities spend more on tree trimming than on any other preventative maintenance activity.

When a tree branch bridges two conductors, a fault does not occur immediately. This is because a moist tree branch has a substantial resistance. A small current begins to flow and starts to dry out the wood fibers. After several minutes, the cellulose will carbonize, resistance will be greatly reduced, and a short circuit will occur. Branches brushing against a single phase conductor typically *do not* result in system faults.

Faults due to tree contact can be reduced by using tree wire. This is overhead wire with an insulated jacket similar to cable. Tree wire can be effective, but faults tend to result in conductor burndown since they will not motor (move themselves along the conductor) like faults on bare conductor.

19.10.5 Birds

Birds are the most common cause of animal faults on both transmission systems and air insulated substations. Different types of birds cause different types of problems, but they can generally be classified as nesting birds, roosting birds, raptors, and woodpeckers.

Nesting birds commonly build their homes on transmission towers and in substations. Nesting materials can cause faults, and bird excrement can contaminate insulators. Nesting birds also attract predators such as raccoons, snakes, and cats. These predators can be a worse reliability problem than the birds themselves.

Roosting birds use electrical equipment to rest on or to search for prey. They can be electrocuted by bridging conductors with their wings, and their excrement can contaminate insulators. To prevent birds from roosting, anti-roosting devices can be placed on attractive sites. For locations that cater to thousands of roosting birds, more extreme deterrent methods such as pyrotechnics can be used.

Raptors are birds of prey such as eagles, hawks, ospreys, owls, and vultures. Reliability problems are similar to other roosting and nesting birds, but special consideration may be required since most raptors are protected by the federal government.

Woodpeckers peck holes in wood with their beaks as they search for insects. This does not harm trees (the bark regenerates), but can cause devastating damage to utility poles. This can be prevented by using steel poles, by using repellent, or by tricking a woodpecker into believing that there is already a resident woodpecker (woodpeckers are quite territorial).

19.10.6 Squirrels

Squirrels are a reliability concern for all overhead distribution systems near wooded areas. Squirrels will not typically climb utility poles, but will leap onto them from nearby trees. They cause faults by bridging grounded equipment with phase conductors. Squirrel problems can be mitigated by cutting down nearby access trees or by installing animal guards on insulators.

19.10.7 Snakes

Snakes are major reliability concerns in both substations and underground systems. They can squeeze through very small openings, can climb almost anything, and have the length to easily span phase conductors. Snakes are usually searching for food (birds in substations and mice in underground systems), and removing the food supply can often remove the snake problem. Special “snake fences” are also available.

19.10.8 Insects

It is becoming more common for fire ants to build nests in pad mounted equipment. Their nesting materials can cause short circuits, the ants can eat away at conductor insulation, and they make equipment maintenance a challenge.

19.10.9 Bears, Bison, and Cattle

These large animals do not typically cause short circuits, but degrade the structural integrity of poles by rubbing on guy wires. Bears can also destroy wooden poles by using them as scratching posts, and black bears can climb wooden utility poles. These problems can be addressed by placing fences around poles and guy wire anchors.

19.10.10 Mice, Rats, and Gophers

These rodents cause faults by gnawing through the insulation of underground cable. They are the most common cause of animal-related outages on underground equipment. To make matters worse, they will attract snakes (also a reliability problem). Equipment cabinets should be tightly sealed to prevent these small animals from entering. Ultrasonic devices can also be used to keep rodents away (ultrasonic devices will not keep snakes away).

19.10.11 Vandalism

Vandalism can take many different forms, from people shooting insulators with rifles to professional thieves stealing conductor wire for scrap metal. Addressing these reliability problems will vary greatly from situation to situation.

19.11 Reliability Economics

When a power interruption occurs, both the utility and the interrupted customers are inconvenienced. The utility must spend money to fix the problem, will lose energy sales during the interruption, and may be sued by disgruntled customers. From the customer perspective, batch processes may be ruined, electronic devices may crash, production may be lost, retail sales may be lost, and inventory (such as refrigerated food) may be ruined.

When a customer experiences an interruption, there is an amount of money that it would be willing to pay to have avoided the interruption. This amount is referred to as the customer's incurred cost of poor reliability, and consists of a base cost plus a time dependent cost. The base cost is the same for all interruptions, relates to electronic equipment shutdown and interrupted processes, and is equivalent to the cost of a momentary interruption. The time dependent cost relates to lost production and extended inconvenience, and reflects that customers would prefer interruptions to be shorter rather than longer.

The customer cost of an interruption varies widely from customer to customer and from country to country. Other important factors include the time of year, the day of the week, the time of day, and whether advanced warning is provided. Specific results are well documented by a host of customer surveys (Billinton et al., 1983; Tollefson et al., 1991; Tollefson et al., 1994; IEEE Std. 493–1990). For planning purposes, it is useful to aggregate these results into a few basic customer classes: commercial, industrial, and residential. Since larger customers will have a higher cost of reliability, results are normalized to the peak kW load of each customer. Reliability cost curves for typical U.S. customers are shown in Fig. 19.6.

Average customer cost curves tend to be linear and can be modeled as an initial cost plus a first order, time dependent cost. Specific customer cost curves may be extremely nonlinear. For example, a meat packing warehouse depending upon refrigeration may be unaffected by interruptions lasting many hours. At a certain point, the meat will begin to spoil and severe economic losses will quickly occur. After the meat spoils, additional interruption time will harm this particular customer much more.

19.12 Annual Variations in Reliability

Power system reliability varies from year to year. In a lucky year, a system may have a SAIDI of 30 min. The next year, this exact same system may experience a SAIDI of 8 h. This type of variation is inevitable and must be considered when comparing reliability indices. It is also important to note that the variance of reliability indices will tend to be less for areas serving more customers. Individual customer reliability will tend to be the most volatile, followed by feeder reliability, substation reliability, regional reliability, and so forth.

The importance of annual reliability variance will grow as utilities become subject to performance-based rates and as customer reliability guarantees become more common. These types of contracts

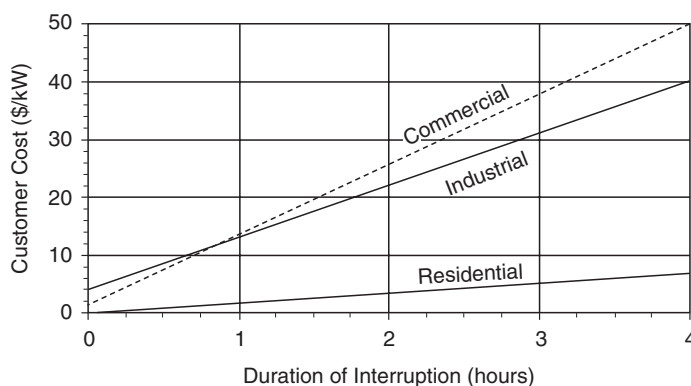


FIGURE 19.6 Typical U.S. customer interruption costs (1999 dollars).

expose utilities to new risks that must be understood and managed. Since performance-based contracts penalize and reward utilities based on reliability, annual variations must be understood for fair contracts to be negotiated and managed.

Contractual issues concerning service reliability are becoming important as the electric industry becomes more competitive. Customers can choose between suppliers, and realize that there is a trade-off between reliability and rates. Some customers will demand poor reliability at low rates, and other customers will demand high reliability at premium rates. To address the wide variation in customer needs, utilities can no longer be suppliers of energy alone, but must become suppliers of both energy and reliability. Power system reliability is now a *bona fide* commodity with explicit value for utilities to supply and explicit value that customers demand.

References

- Allan, R.N., Billinton, R., Breipohl, A.M., and Grigg, C.H., Bibliography on the application of probability methods in power system reliability evaluation, *IEEE Trans. on Power Syst.*, 9, 1, 41–49, Feb. 1994.
- Billinton, R. and Allan, R.N., *Reliability Assessment of Large Electric Power Systems*, Kluwer Academic Publishers, Dordrecht, The Netherlands, 1988.
- Billinton, R. and Allan, R., *Reliability Evaluation of Engineering Systems: Concepts and Techniques* (2nd edition) Plenum Press, New York, 1992.
- Billinton, R. and Jonnavaithula, S., A Test System for Teaching Overall Power System Reliability Assessment, *IEEE Trans. on Power Syst.*, 11, 4, 1670–1676, Nov. 1996.
- Billinton, R., Wacker, G., and Wojczynski, E., Comprehensive bibliography on electrical service interruption costs, *IEEE Trans. on Power Appar. Syst.*, PAS-102, 6, 1831–1837, June 1983.
- Brown, R.E., Gupta, S., Christie, R.D., Venkata, S.S., and Fletcher, R.D., Distribution system reliability analysis using hierarchical Markov modeling, *IEEE Trans. on Power Delivery*, 11, 4, 1929–1934, Oct. 1996.
- Brown, R.E., Gupta, S., Christie, R.D., Venkata, S.S., and Fletcher, R.D., Distribution system reliability: momentary interruptions and storms, *IEEE Trans. on Power Delivery*, 12, 4, 1569–1575, October 1997.
- Brown, R.E. and Ochoa, J.R., Distribution system reliability: default data and model validation, *IEEE Trans. on Power Syst.*, 13, 2, 704–709, May 1998.
- Burke, J.J., *Power Distribution Engineering*, Marcel Dekker, Inc., New York, 1994.
- Electrical Transmission and Distribution Reference Book*, ABB Power T&D Company, Inc., Raleigh, NC, 1997.
- Endrenyi, J., *Reliability in Electric Power Systems*, John Wiley & Sons, Ltd., New York, 1978.
- IEEE Recommended Practice for the Design of Reliable Industrial and Commercial Power Systems*, IEEE Std. 493-1990.
- IEEE Working Group on System Design, *Trial Use Guide for Power Distribution Reliability Indices*, Report P1366, IEEE, 1998.
- Philipson, L. and Willis, H.L., *Understanding Electric Utilities and De-regulation*, Marcel Dekker, Inc., New York, 1999.
- Ramakumar, R., *Engineering Reliability: Fundamentals and Applications*, Prentice-Hall, Inc., Englewood Cliffs, NJ, 1993.
- Schilling, M.T., Billinton, R., Leite da Silva, A.M., and El-Kady, M.A., Bibliography on composite system reliability (1964–1988), *IEEE Trans. on Power Syst.*, 4, 3, 1122–1132, Aug. 1989.
- Tollefson, G., Billinton, R., Wacker, G., Chan, E., and Awuya, J., A Canadian customer survey to assess power system reliability worth, *IEEE Trans. on Power Syst.*, 9, 1, 443–450, Feb. 1994.
- Tollefson, G., Billinton, R., and Wacker, G., Comprehensive bibliography on reliability worth and electric service consumer interruption costs 1980–1990, *IEEE Trans. on Power Syst.*, 6, 4, 1508–1514, Nov. 1991.
- Willis, H.L., *Power Distribution Planning Reference Book*, Marcel Dekker, Inc., New York, 1997.

20

Probabilistic Methods for Planning and Operational Analysis

Gerald T. Heydt
Arizona State University

Peter W. Sauer
*University of Illinois
at Urbana-Champaign*

20.1	Uncertainty in Power System Engineering.....	20-1
20.2	Deterministic Power Flow Studies.....	20-2
20.3	Monte Carlo Power Flow Studies	20-2
20.4	Analytical Probabilistic Power Flow Studies.....	20-4
20.5	Applications for Available Transfer Capability	20-6
20.6	An Example of Stochastic Available Transfer Capability.....	20-7
20.7	An Example of Expected Financial Income from Transmission Tariffs.....	20-8
20.8	Conclusions.....	20-9

20.1 Uncertainty in Power System Engineering

Probabilistic methods are mathematical techniques to formally consider the impact of uncertainty in models, parameters, or data. Typical uncertainties include the future value of loading conditions, fuel prices, weather, and the status of equipment. Methods to consider all possible values of uncertain data or parameters include such techniques as interval analysis, minimum/maximum analysis, and fuzzy mathematics. In many cases, these techniques will produce conservative results because they do not necessarily incorporate the “likelihood” of each value of a parameter in an expected range, or they might be intentionally designed to compute “worse case” scenarios. These techniques are not discussed further here. Instead, this chapter presents two techniques that have been successfully applied to power system planning and operational analysis as noted by the “Application of Probability Methods” subcommittee of the IEEE Power Engineering Society in Rau et al. (1994). They are

- Monte Carlo simulation: analysis in which the system to be studied is subjected to pseudorandom operating conditions, and the results of many analyses are recorded and subsequently statistically studied. The advantage is that no specialized forms or simplifications of the system model are needed.
- Analytical probability methods: analysis in which the system to be studied is represented by functions of several random variables of known distribution.

Rau et al. (1994) also noted that probabilistic load flow methods would be well suited to evaluate loadability limits and transfer capabilities under uncertainties created by industry restructuring. They also noted the needs to include uncertainty analysis in cost/worth studies and security assessment.

This chapter focuses on those two analysis tools and illustrates the differences between the Monte Carlo simulation method and the analytical probability method.

20.2 Deterministic Power Flow Studies

Conventional, deterministic power flow studies (load flow studies) are one of the most widely used analysis tools for both planning and operations (Heydt, 1996). They can imprecisely be described through three features:

- Power flow analysis is the computation of steady-state conditions for a given set of loads P (active power) and Q (reactive power) and a given system configuration (interconnecting lines/transfomers).
- Active-power generation and bus voltage magnitudes are specified at the generator buses.
- Power flow analysis gives a solution of system states, mainly bus voltage phase angles (δ) and magnitudes (V).

Additional complexities such as phase-shifting and tap-changing-under-load (TCUL) transformers and other devices are often added to this basic description. And of course many other “solution” quantities such as generator reactive power output and line power flows are often added.

The main method used for power flow analysis is the Newton–Raphson (NR) method, a method to find the zeros of $f(X) = 0$ where f is a vector-valued function of P and Q summations at each bus (Kirchhoff’s current law in terms of power), and X is the system state vector (primarily δ and V). There is normally a natural weak coupling between real power and voltage magnitude (P and V) as well as reactive power and voltage angle (Q and δ). This weak coupling can be exploited in the NR method to speed up solutions. Figures 20.1 and 20.2 are pictorials of this decoupling.

This decoupling can be utilized to increase the speed of computing exact solutions, and also can be used to create superfast approximate linear solutions. In both cases, the inputs to the power flow solution algorithms shown are deterministic. When there is uncertainty in the input data, this can be considered using the two methods introduced earlier—Monte Carlo and analytical probability. These two methods are discussed next in the context of power flow analysis.

20.3 Monte Carlo Power Flow Studies

In Monte Carlo power flow studies, multiple power flow studies are run using different sets of input data. The various sets of input data are typically obtained from random number generators to correspond to some desired statistical distribution. For example, the true future total load of a power

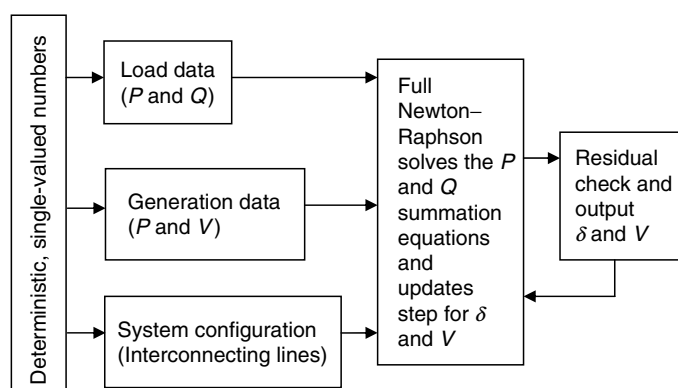


FIGURE 20.1 Conventional Newton–Raphson power flow study.

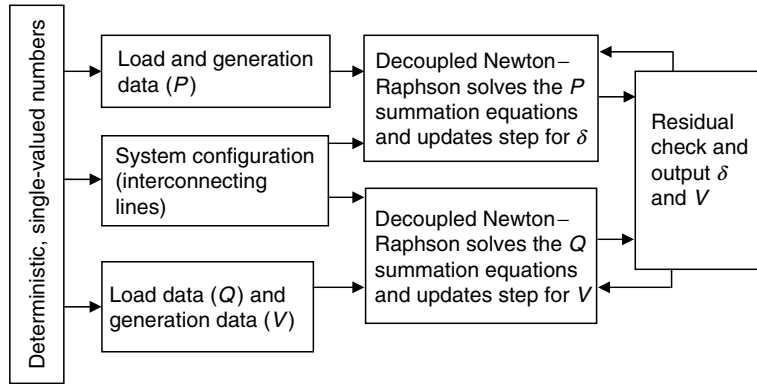


FIGURE 20.2 Decoupled Newton–Raphson power flow study.

system (and its allocation to system buses) might be unknown, but an expected value might be known together with a variance with specified statistical distribution (i.e., uniform or normal). This problem could be a problem with a scalar random variable (random total load at one time instant with known deterministic allocation to system buses), or it could be a problem with a vector of random variables (random total load at one time instant plus random allocation to system buses). In the scalar case, this would require numerous power flow studies using numerous random samples for the total load. In the vector case, this would require numerous power flow studies using numerous random samples for the total load (perhaps one statistical distribution) plus numerous random samples for the factors that allocate the total load to the system buses (perhaps another statistical distribution). This could perhaps be defined more easily by simply considering each system bus load to be a random variable. This would require a decision of which “multivariate” statistical distribution to use (i.e., all bus load values are independent and normally distributed, or all bus loads are fully correlated and normally distributed, or something in between). In most cases, the Monte Carlo power flow studies are done for “variations” from the expected value of the random variables. As such, the expected value of the variation in bus load from the expected value would be zero. The first Monte Carlo power flow study is usually the case where all variations are equal to their expected value (zero). This is also often called the “base case.” Figure 20.3 shows the Monte Carlo simulation method for considering uncertainty in the input data.

The statistical description of the distribution is typically a histogram. This is a plot of the value of the output variable on the horizontal axis and the number of times that value occurs on the vertical axis.

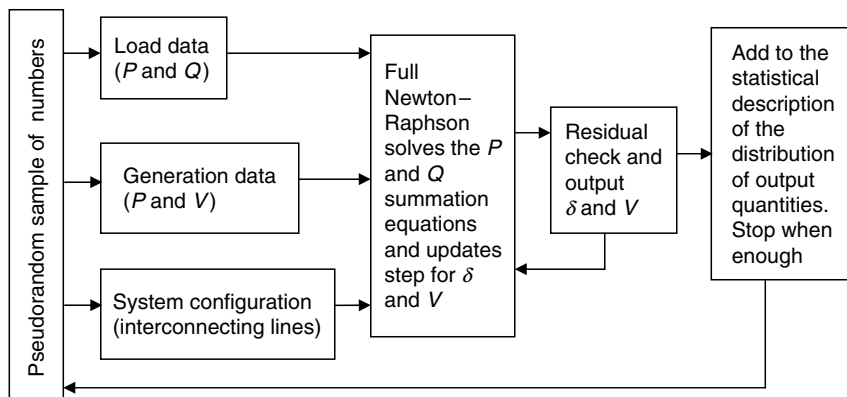


FIGURE 20.3 Monte Carlo power flow study.

The horizontal values are grouped into “ranges” of possible values (i.e., all values from 0.1 to 0.2, 0.2 to 0.3, etc.). These histograms are similar in concept to the probability density function of analytical methods. There are also numerical descriptions (moments) of the statistical distribution that can be computed—i.e., mean, variance, skewness, kurtosis, etc. One problem with the Monte Carlo method is in determining the number of samples that are sufficient to properly represent the variation in the uncertain parameters. For example, are 100 samples sufficient to represent all possible variations in the total system load? How about 1000? One way to look at this is—“The deterministic solution is just one sample, so anything more than one is better than the deterministic solution.” But, what is important in the choice of samples is the specification of what is most likely to represent the most likely possible values of the uncertain data. This normally requires a large number of samples. Another problem with Monte Carlo methods is the large computational burden required to study a large number of samples.

Multiple power flow studies can also be used to compute the variation of system bus voltages (and all other output quantities) throughout the day, week, or year as the load varies. For example, if there was an interest in computing the line flows for every hour of the day for one year (assuming all load and generation data are known for each hour), this would require 8760 power flow studies (one per hour). It is important to realize that although this is not really a Monte Carlo simulation as the variation of the load data is not from a random phenomenon (i.e., daily, weekly, and seasonal variations in load are somewhat predictable), it is computationally the same as running 8760 “samples” and observing the distribution of the output quantities. The “statistical distribution” would give an indication of the percentage of time throughout the year during which a line flow was in a certain range. If there was an interest in considering the uncertainty in the total load variation throughout the year, some mechanism for specifying the “variations” from the base case would need to be given for each hour of everyday. Presumably, these variations would take the form of random samples created from some known statistical distribution. A Monte Carlo simulation of this could easily result in the need for over one million power flow studies. And, if the uncertainty of the data was extended to random samples of load at each bus for each hour, the result could be the need for over one billion power flow studies.

20.4 Analytical Probabilistic Power Flow Studies

Because it is very difficult to perform analytical probability analysis for large nonlinear systems, the most probabilistic power flow studies exploit two properties of power systems that lead to a linear, smaller model. First, the decoupling that was discussed above allows the real power and voltage angle to be completely separated from the reactive power and voltage magnitude in computation. This not only reduces the size of the problem, but also reduces the accuracy and loses voltage information. Second, the fact that “small” changes in bus real power injections result in “small” changes in bus voltage angles leads to a linear approximation as follows:

$$\Delta\delta_{\text{bus}} = T_1 \Delta P_{\text{bus}} \quad (20.1)$$

So, for an initial power flow solution giving the bus voltage angle vector δ_{bus}^0 for an initial bus real power injection vector, P_{bus}^0 , an approximate power flow solution for a problem with $P_{\text{bus}}^1 = P_{\text{bus}}^0 + \Delta P_{\text{bus}}$ is given by $\delta_{\text{bus}}^1 = \delta_{\text{bus}}^0 + T_1 \Delta P_{\text{bus}}$.

It is important to point out that the vector of bus real power injection changes does not include the injection change at the swing (or slack) bus of the power flow study. And, the vector of bus voltage angles does not include an entry for the swing (or slack) bus of the power flow study. This is because the swing (or slack) bus is chosen as the fixed-angle reference for the power flow study and also provides the balance in real power for any specified condition. In this manner, the vector of bus real power injection changes could include a single entry and the result of this injection change would automatically be offset by a nearly equal and opposite injection change at the swing bus.

This linear analysis can be extended to approximate the resulting change in real power line flows as

$$\Delta P_{\text{line}} = T_2 \Delta \delta_{\text{bus}} \quad (20.2)$$

This combination of linear approximations gives the traditional “generation shift distribution factor,” which is also the “power transfer distribution factor” for power transfers from a bus to or from the swing bus (Heydt, 1996):

$$\Delta P_{\text{line}} = T_2 T_1 \Delta P_{\text{bus}} = T \Delta P_{\text{bus}} \quad (20.3)$$

This relationship is the heart of the linear power flow, which enables analytical probabilistic methods. One reason a linear computation is important is that the linear sum of jointly normal random variables is also jointly normal (Papoulis, 1965). This makes the computation of the statistical distribution of the output variables very easy to compute from the specified statistical distribution of the input variables. For example, if there is some uncertainty in the value of the loads, an initial power flow study could be done using the expected value of the loads. This would be a deterministic power flow study. To account for the uncertainty in load, an analytical probabilistic power flow could be done as follows:

Step 1. Specify the statistical distribution of the variation of load (ΔP_{bus})—for a scalar (total load) this might be a zero mean, normal distribution with some specified variance. For a vector of zero-mean jointly normal load variations, the statistical distribution would be specified by also giving the covariance between each load variation. A covariance of zero would mean that the two uncertain jointly normal variations are statistically “independent.” A covariance of ± 1.0 would mean that the two jointly normal variations are fully correlated (linearly related). The covariance matrix C_{load} contains the complete statistical description of all the load variations through the variances (diagonal) and covariances (off diagonal).

Step 2. Compute the statistical distribution of the variation of line real power flows. When the variations in loads are assumed to be zero-mean jointly normal, the complete description of the statistical distribution of the variation of line real power flows is found easily as (Papoulis, 1965)

$$C_{\text{line}} = T_3 C_{\text{load}} T_3^t \quad (20.4)$$

where “t” denotes matrix transposition. The mean value of the variation in line real power flows is taken as zero because the mean value of the bus real power injection variations was assumed zero and the two are assumed to be linearly related. Now, the fact that the variations in line real power flows are not really linearly related to the bus real power injection variations means that these statistical distributions will not be exact. Figure 20.4 shows how the analytic probabilistic power flow study is done.

Stochastic power flow is another term that has been used for analytical probabilistic power flow. Since stochastic processes are statistical processes involving a number of random variables depending on a variable parameter (usually time), this terminology has been adopted as equivalent. One of the first publications on this method was of Borkowska (1974). The subject continues to attract interest (Vorsic et al., 1991).

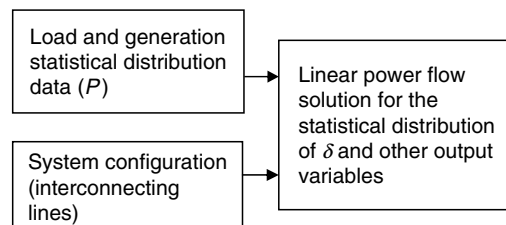


FIGURE 20.4 Analytic probabilistic power flow study.

20.5 Applications for Available Transfer Capability

In order to realize open access to electric power transmission networks and promote generation competition and customer choice, the Federal Energy Regulatory Commission requires that available transfer capability (ATC) be made available on a publicly accessible open access same-time information system (OASIS). The ATC is defined as a measure of the transfer capability, or available “room” in the physical transmission network for transfers of power for further commercial activity, over and above already committed uses (NERC, 1996). The ATC is defined by NERC as the total transfer capability (TTC) minus the transmission reliability margin (TRM), capacity benefit margin (CBM), and existing power flows:

$$\text{ATC} = \text{TTC} - \text{TRM} - \text{CBM} - \text{Existing power flows} \quad (20.5)$$

where the TTC is the total amount of power that can be sent from bus A to bus B within a power network in a reliable manner, the TRM is the amount of transmission transfer capability necessary to ensure network security under uncertainties, and the CBM is the amount of TTC reserved by load serving entities to ensure access to generation from interconnected systems to meet generation reliability requirements. Neglecting TRM and CBM reduces the computation of ATC to

$$\text{ATC} = \text{TTC} - \text{Existing power flows}. \quad (20.6)$$

The ATC between two buses (or groups of buses) determines the maximum additional power that can be transmitted in an interchange schedule between the specified buses. ATC is clearly determined by load flow study results and transmission limits. As an illustration, consider Fig. 20.5 in which 1000 MW is transmitted from bus A to bus B. If the line rating is 1500 MW and if no parallel paths exist from A to B, the ATC from A to B is 500 MW.

In a real power system, the network and the computation of the ATC are much more complicated as parallel flows make the relationship between transfers and flows less obvious. In addition, the ATC is uncertain due to the uncertainty of power system equipment availability and power system loads. An evaluation of the stochastic behavior of the ATC is important to reduce the likelihood of congestion. The ATC is determined by power flow studies subject to transmission system limits. These phenomena are nonlinear in behavior. As discussed above, linearization can be used to estimate line flows in a power flow study model. This section presents a method of finding the stochastic ATC using a linear transformation of line power flows into ATC.

Increasing the transfer power increases the loading in the network. At some point, operational or physical limits to various elements are reached that prevent further increase. The largest value of transfer that causes no limit violations is used to compute the TTC and ATC. Limits are affected by the power injections at both buses A and B. This effect can be found analytically by finding the distribution factors of the lines and other components. In this context, a “distribution factor” refers to the power transfer distribution factor for line $i - j$ and bus k , where an equal and opposite injection is automatically made at the swing bus.

The complexity of the ATC calculation is drastically reduced by linearizing the power flow study problem and considering only thermal transmission limits. The linearization is most accurate when only small deviations from the point of linearization are encountered. The use of thermal limits is justified for short transmission circuits. The transmission system linearization in this case is done using power transfer distribution factors, which are discussed above. Starting with a base case

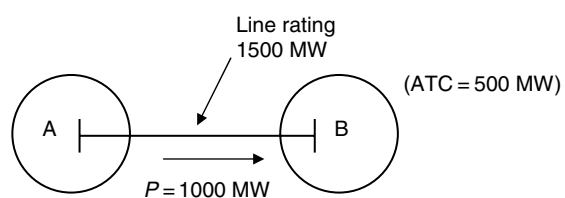


FIGURE 20.5 An example of available transfer capability (ATC).

power flow solution, the addition of a power transfer from bus A to bus B impacts the flow in the line between bus i and bus j as

$$P_{ij}^1 = P_{ij}^0 + (T_{ij,A} - T_{ij,B})P_{AB} \quad (20.7)$$

where P_{AB} is the power transfer from bus A to bus B (assumed to be positive). When $(T_{ij,A} - T_{ij,B})$ is positive, the transfer that results in rated power flow on line $i-j$ is

$$P_{AB,ij} = \left(P_{ij}^{\text{Rated}} - P_{ij}^0 \right) / (T_{ij,A} - T_{ij,B}) \quad (20.8)$$

When $(T_{ij,A} - T_{ij,B})$ is negative, the transfer that results in rated power flow on line $i-j$ is

$$P_{AB,ij} = \left(-P_{ij}^{\text{Rated}} - P_{ij}^0 \right) / (T_{ij,A} - T_{ij,B}) \quad (20.9)$$

Each line will have a value of $P_{AB,ij}$ that represents the maximum value of power transfer from bus A to bus B without overloading line ij . The minimum of all these values would be the ATC for the AB transfer.

Once this minimum is determined, the question is, “What if there is uncertainty in the initial bus and line loadings?” As discussed above, there are at least two ways to incorporate uncertainty in this computation. The first way is the Monte Carlo method that specifies a statistical distribution of the uncertain parameter (perhaps total load) and utilizes pseudorandom number samples to perform brute force repeated ATC solutions. This could involve full nonlinear power flow studies, or faster linear power flow studies. The collection of ATC solutions that come from a large sample of total load values gives the statistical distribution of the ATC, perhaps as a histogram. If the critical line that determines the ATC of the AB transfer does not change with the uncertainty of the initial bus and line loadings, then the possible variation in ATC can be easily computed from the statistical distribution of the initial line flow. For example, if the uncertainty of initial line flows is normally distributed with zero mean and some variance, then the ATC from A to B is also normally distributed with zero mean, as it is a linear function of the initial flow in the critical line. The variance is also directly available because of the linear transformation.

20.6 An Example of Stochastic Available Transfer Capability

The following example illustrates the basic principles of stochastic ATC. The IEEE 14-bus system was studied with the base case bus and line variables as given in Christie (1999) and Pai (1979). For the uncertainty analysis by Monte Carlo methods, the bus loads were generated on the computer using 100 samples from a random number generator. The bus real power loads were assumed to be statistically independent with a normal distribution that had a mean equal to the base case and a standard deviation equal to 10% of the base case. Bus load power factor was maintained at the base case value. A comparison of the Monte Carlo results with the analytical method is given in Table 20.1.

TABLE 20.1 Comparison of Monte Carlo and Analytical Methods for ATC

“From” Bus	“To” Bus	Analytical Mean	Analytical Variance	Monte Carlo Mean	Monte Carlo Variance
1	9	8.5	4.5	7.147	5.008
1	10	4.177	2.3005	4.7766	2.3356
1	11	2.7144	0.7038	2.764	1.1549
2	9	7.8480	4.5208	7.318	5.6584

The Monte Carlo results required 100 full nonlinear power flow studies of ATC, whereas the analytical results required a simple direct multiplication. Additional results for this example are available in Stahlhut et al. (2005).

20.7 An Example of Expected Financial Income from Transmission Tariffs

A second illustration of the two methods for considering uncertainty deals with the estimation of transmission tariff revenue because of unknown future loading. This illustration was reported also in Westendorf (2005) and Stahlhut et al. (2005). The work is presented in three parts. The first includes a study of transmission tariff revenue based on an estimated hourly forecast for one year. This “base case” solution provides the expected revenue for the year for that forecasted loading level. The second part includes a Monte Carlo simulation of possible variations in revenue for a forecast error of known statistical distribution. This is a repeat of the base case solution for 100 different possible cases (per hour) sampled from a normal distribution function—using total load as the random variable. This error in total load was then “distributed” to the individual buses using the base case percentage allocation. The third part included an analytical solution to estimate the expected statistical distribution of the transmission tariff revenue using linear power flow techniques.

This analysis used the IEEE 14-bus test system (Pai, 1979; Christie, 1999) and computed revenue from transmission tariffs using an assumed tariff of \$0.04 per MW-mile for each transmission line. An annual income was also computed by summing the hourly incomes for the year. Because the transmission tariff is a function of the length of each transmission line, an estimate of the transmission line lengths was necessary. The total impedance of a transmission line is dependent on the length of the line. The line length is directly proportional to the transmission line impedance. The method for calculating the lengths of the transmission lines in the IEEE 14-bus test system based on the total line impedance of each line was developed as follows. A power base for the system was assumed to be $S_{\text{base}} = 100$ MVA. Using the nominal voltages, V_{base} , of the transmission lines and the power base of the system, each transmission line reactance value, the length of the line was calculated by assuming a conversion factor of $0.7 \Omega/\text{mile}$. Secondly, lines containing transformers (i.e., lines 8–10) were considered to be zero-length lines.

A load forecast taking into account hourly variations was developed for this investigation by using publicly accessible approximate historical load data for each hour of everyday for the year 2004 from the PJM Web site (PJM, 2005). The integrated hourly load data for the PJM-E area were scaled to match the system load of 259 MW of the IEEE 14-bus test system. Using the hourly load data, power flows were conducted to determine the megawatt flows on the transmission lines allowing the calculation of the each line revenue for the hour. The total revenue generated for each hour was calculated by summing all of the line revenues calculated from the power flows. While standard nonlinear power flow methods were used to compute the Monte Carlo solutions, standard linear power flow methods were used to calculate the analytical solutions.

The Monte Carlo simulations and the analytical methods were compared. Both methods provided results for the distribution of the system revenue generated for each hour. Although an entire year was analyzed, [Table 20.2](#) lists the results from both methods for just 1 day.

Column 1 is the time of day studied. Column 2 is the expected revenue using the Monte Carlo simulation, which created deviations from the base case using a zero-mean random number generator (100 samples per hour). Column 3 shows the revenue from the base case. The fact that these two columns are quite close is due to the fact that the deviations were sampled from a zero-mean number generator and the system behavior is nearly linear for deviations of this size. The standard deviation of the sampled distribution was 3%. This was designed to produce a sample load forecast with expected variations between plus and minus 10% of the base case. Column 4 shows the Monte Carlo sample standard deviation, and Column 5 shows the analytical standard deviation found using the assumed linear nature of the calculation and the assumed normal distribution of the forecast error.

TABLE 20.2 Comparison of Monte Carlo and Analytical Methods for Expected Revenue for 1 Day

Time	Mean Total Revenue (\$)	Base Case Total Revenue (\$)	Simulated Standard Deviation σ_{revenue} (\$)	Analytical Standard Deviation σ_{revenue} (\$)
100	390.66	390.96	12.49	9.96
200	382.23	382.95	11.28	9.76
300	378.27	381.11	12.82	9.72
400	383.13	384.06	12.29	9.79
500	394.60	393.56	13.23	10.03
600	427.99	426.22	14.47	10.83
700	478.56	479.04	14.23	12.13
800	510.09	510.85	16.94	12.91
900	505.21	506.51	14.03	12.81
1000	501.30	501.86	13.83	12.69
1100	497.15	496.49	13.93	12.56
1200	490.09	491.41	12.79	12.43
1300	494.68	490.73	13.83	12.42
1400	488.98	488.53	15.66	12.36
1500	484.86	483.91	15.24	12.25
1600	484.97	484.78	14.77	12.27
1700	502.80	504.46	14.16	12.76
1800	537.99	538.33	17.39	13.59
1900	543.86	544.99	16.76	13.75
2000	536.59	538.02	19.71	13.58
2100	527.99	527.33	14.94	13.32
2200	500.62	502.73	15.19	12.71
2300	464.40	466.21	13.47	11.81
2400	427.75	430.47	14.41	10.93

The error in standard deviations can be attributed to several things. The linear power flow method is an approximation that is used in the analytical method but not in the Monte Carlo simulation method. The Monte Carlo method only used 100 random samples to create the sample standard deviation. These are not a large number of samples and contribute to the discrepancy in the two methods.

20.8 Conclusions

Power system planning will always have a need to consider the uncertainty of future conditions and the impact that these uncertainties have on technical and financial issues. When uncertainties can be assumed small, linear power flow methods that are needed for analytical techniques can significantly reduce computational effort.

References

- Borkowska, B., Probabilistic load flow, IEEE Trans. Power App. Syst., PAS-93(3), 1974, 752–759.
- Christie, R., Power system test archive, 1999, http://www.ee.washington.edu/research/pstca/pf14/pg_tca14bus.htm
- Heydt, G.T., *Computer Analysis Methods for Power Systems*, Macmillan, New York, 1996.
- NERC, Available transfer capability definitions and determination, North American Electric Reliability Council, June 1996.
- Pai, M.A., *Computer Techniques in Power System Analysis*, Tata McGraw Hill, New Delhi, 1979.
- Papoulis, A., *Probability, Random Variables, and Stochastic Processes*, McGraw-Hill Book Co., New York, 1965.
- PJM Interconnection, Hourly load data, 2005, <http://www.pjm.com/markets/jsp/loadhrvr.jsp>.

- Rau, N., Grigg, C.H., and Silverstein, B., Living with uncertainty: R&D trends and needs in applying probability methods to power system planning and operation, IEEE PES Review, November, 1994, 24–25.
- Stahlhut, J., Feng, G., Hedman, K., Westendorf, B., Heydt, G., Sauer, P., and Sheble, G., Uncertain power flows and transmission expansion planning, Accepted for presentation at the 2005 North American Power Symposium, Ames, IA, October 23–25, 2005.
- Vorsic, J., Muzek, V., Skerbinek, G., Stochastic load flow analysis, in *Proceedings of the Electrotechnical Conference*, Vol. 2, May 22–24, 1991, 1445–1448.
- Westendorf, B., Stochastic transmission revenues, MSEE Thesis, University of Illinois at Urbana-Champaign, Urbana, IL, May 2005.

IV

Power Electronics

Mark Nelms

Auburn University

21	Power Semiconductor Devices <i>Kaushik Rajashekara</i>	21-1
	Thyristor and Triac • Gate Turn-Off Thyristor (GTO) • Reverse-Conducting Thyristor (RCT) and Asymmetrical Silicon-Controlled Rectifier (ASCR) • Power Transistor • Power MOSFET • Insulated-Gate Bipolar Transistor (IGBT) • MOS-Controlled Thyristor (MCT)	
22	Uncontrolled and Controlled Rectifiers <i>Mahesh M. Swamy</i>	22-1
	Introduction • Uncontrolled Rectifiers • Controlled Rectifiers • Conclusion	
23	Inverters <i>Michael Giesselmann</i>	23-1
	Introduction and Overview • Fundamental Issues • Single-Phase Inverters • Three-Phase Inverters • Multilevel Inverters • Line Commutated Inverters	
24	Active Filters for Power Conditioning <i>Hirofumi Akagi</i>	24-1
	Harmonic-Producing Loads • Theoretical Approach to Active Filters for Power Conditioning • Integrated Series Active Filters • Practical Applications of Active Filters for Power Conditioning	
25	FACTS Controllers <i>Luis Morán, Juan Dixon, M. José Espinoza, and José Rodríguez</i>	25-1
	Introduction • Shunt Compensators • Series Compensation • Hybrid Compensation • FACTS Controller's Applications • Conclusions	

21

Power Semiconductor Devices

21.1	Thyristor and Triac	21-1
21.2	Gate Turn-Off Thyristor (GTO)	21-3
21.3	Reverse-Conducting Thyristor (RCT) and Asymmetrical Silicon-Controlled Rectifier (ASCR)	21-4
21.4	Power Transistor.....	21-4
21.5	Power MOSFET.....	21-5
21.6	Insulated-Gate Bipolar Transistor (IGBT)	21-5
21.7	MOS-Controlled Thyristor (MCT)	21-7

Kaushik Rajashekara
Delphi Automotive Systems

The modern age of power electronics began with the introduction of thyristors in the late 1950s. Now there are several types of power devices available for high-power and high-frequency applications. The most notable power devices are gate turn-off thyristors, power Darlington transistors, power MOSFETs, and insulated-gate bipolar transistors (IGBTs). Power semiconductor devices are the most important functional elements in all power conversion applications. The power devices are mainly used as switches to convert power from one form to another. They are used in motor control systems, uninterrupted power supplies, high-voltage DC transmission, power supplies, induction heating, and in many other power conversion applications. A review of the basic characteristics of these power devices is presented in this section.

21.1 Thyristor and Triac

The thyristor, also called a silicon-controlled rectifier (SCR), is basically a four-layer three-junction *pnpn* device. It has three terminals: anode, cathode, and gate. The device is turned on by applying a short pulse across the gate and cathode. Once the device turns on, the gate loses its control to turn off the device. The turn-off is achieved by applying a reverse voltage across the anode and cathode. The thyristor symbol and its volt-ampere characteristics are shown in Fig. 21.1. There are basically two classifications of thyristors: converter grade and inverter grade. The difference between a converter-grade and an inverter-grade thyristor is the low turn-off time (on the order of a few microseconds) for the latter. The converter-grade thyristors are slow type and are used in natural commutation (or phase-controlled) applications. Inverter-grade thyristors are used in forced commutation applications such as DC-DC choppers and DC-AC inverters. The inverter-grade thyristors are turned off by forcing the current to zero using an external commutation circuit. This requires additional commutating components, thus resulting in additional losses in the inverter.

Thyristors are highly rugged devices in terms of transient currents, di/dt , and dv/dt capability. The forward voltage drop in thyristors is about 1.5 to 2 V, and even at higher currents of the order of 1000 A, it seldom exceeds 3 V. While the forward voltage determines the on-state power loss of the device at any

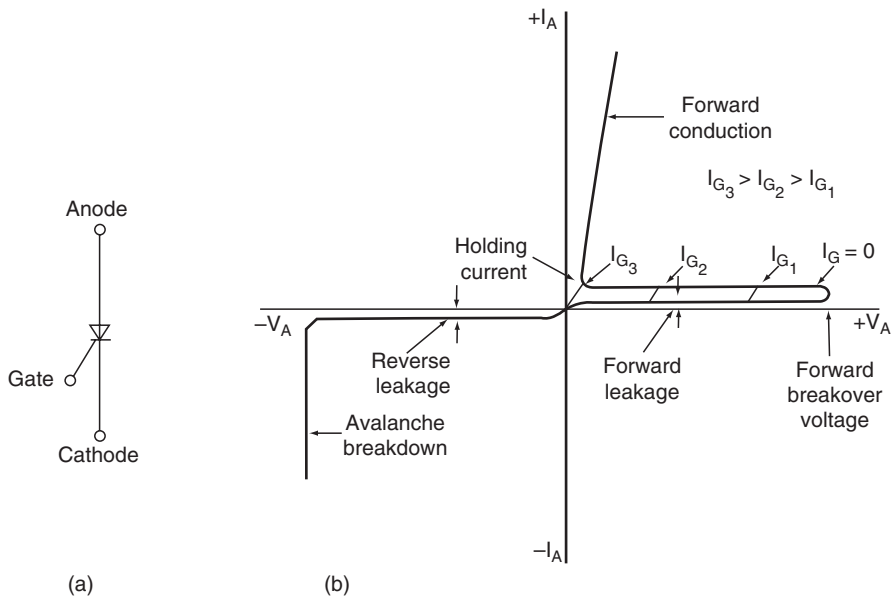


FIGURE 21.1 (a) Thyristor symbol and (b) volt-ampere characteristics. (From B.K. Bose, *Modern Power Electronics: Evaluation, Technology, and Applications*, p. 5. © 1992 IEEE.)

given current, the switching power loss becomes a dominating factor affecting the device junction temperature at high operating frequencies. Because of this, the maximum switching frequencies possible using thyristors are limited in comparison with other power devices considered in this section.

Thyristors have I^2t withstand capability and can be protected by fuses. The nonrepetitive surge current capability for thyristors is about 10 times their rated root mean square (rms) current. They must be protected by snubber networks for dv/dt and di/dt effects. If the specified dv/dt is exceeded, thyristors may start conducting without applying a gate pulse. In DC-to-AC conversion applications, it is necessary to use an antiparallel diode of similar rating across each main thyristor. Thyristors are available up to 6000 V, 3500 A.

A triac is functionally a pair of converter-grade thyristors connected in antiparallel. The triac symbol and volt-ampere characteristics are shown in Fig. 21.2. Because of the integration, the triac has poor

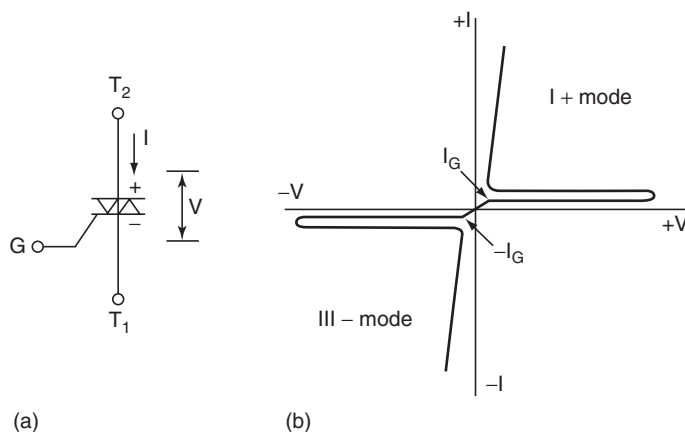


FIGURE 21.2 (a) Triac symbol and (b) volt-ampere characteristics. (From B.K. Bose, *Modern Power Electronics: Evaluation, Technology, and Applications*, p. 5. © 1992 IEEE.)

reapplied dv/dt , poor gate current sensitivity at turn-on, and longer turn-off time. Triacs are mainly used in phase control applications such as in AC regulators for lighting and fan control and in solid-state AC relays.

21.2 Gate Turn-Off Thyristor (GTO)

The GTO is a power switching device that can be turned on by a short pulse of gate current and turned off by a reverse gate pulse. This reverse gate current amplitude is dependent on the anode current to be turned off. Hence there is no need for an external commutation circuit to turn it off. Because turn-off is provided by bypassing carriers directly to the gate circuit, its turn-off time is short, thus giving it more capability for high-frequency operation than thyristors. The GTO symbol and turn-off characteristics are shown in Fig. 21.3.

GTOs have the I^2t withstand capability and hence can be protected by semiconductor fuses. For reliable operation of GTOs, the critical aspects are proper design of the gate turn-off circuit and the snubber circuit. A GTO has a poor turn-off current gain of the order of 4 to 5. For example, a 2000-A peak current GTO may require as high as 500 A of reverse gate current. Also, a GTO has the tendency to latch at temperatures above 125°C. GTOs are available up to about 4500 V, 2500 A.

21.3 Reverse-Conducting Thyristor (RCT) and Asymmetrical Silicon-Controlled Rectifier (ASCR)

Normally in inverter applications, a diode in antiparallel is connected to the thyristor for commutation/freewheeling purposes. In RCTs, the diode is integrated with a fast switching thyristor in a single silicon chip. Thus, the number of power devices could be reduced. This integration brings forth a substantial improvement of the static and dynamic characteristics as well as its overall circuit performance.

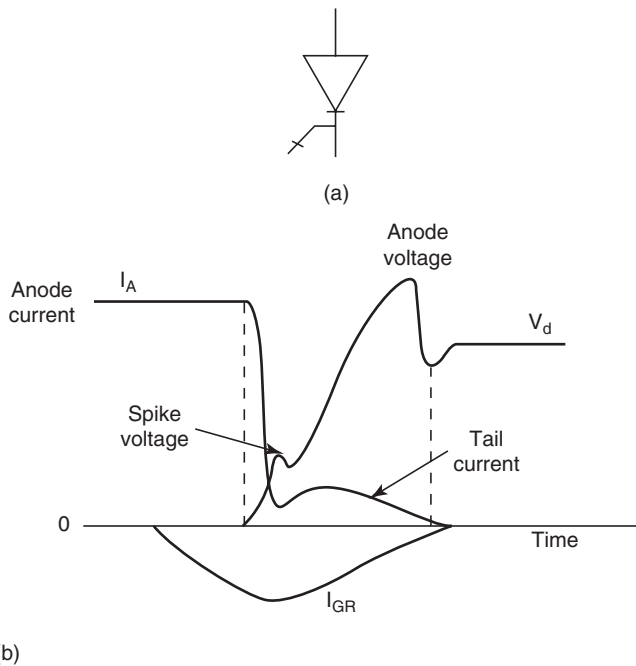


FIGURE 21.3 (a) GTO symbol and (b) turn-off characteristics. (From B.K. Bose, *Modern Power Electronics: Evaluation, Technology, and Applications*, p. 5. © 1992 IEEE.)

The RCTs are designed mainly for specific applications such as traction drives. The antiparallel diode limits the reverse voltage across the thyristor to 1 to 2 V. Also, because of the reverse recovery behavior of the diodes, the thyristor may see very high reapplied dv/dt when the diode recovers from its reverse voltage. This necessitates use of large RC snubber networks to suppress voltage transients. As the range of application of thyristors and diodes extends into higher frequencies, their reverse recovery charge becomes increasingly important. High reverse recovery charge results in high power dissipation during switching.

The ASCR has similar forward blocking capability to an inverter-grade thyristor, but it has a limited reverse blocking (about 20–30 V) capability. It has an on-state voltage drop of about 25% less than an inverter-grade thyristor of a similar rating. The ASCR features a fast turn-off time; thus it can work at a higher frequency than an SCR. Since the turn-off time is down by a factor of nearly 2, the size of the commutating components can be halved. Because of this, the switching losses will also be low.

Gate-assisted turn-off techniques are used to even further reduce the turn-off time of an ASCR. The application of a negative voltage to the gate during turn-off helps to evacuate stored charge in the device and aids the recovery mechanisms. This will, in effect, reduce the turn-off time by a factor of up to 2 over the conventional device.

21.4 Power Transistor

Power transistors are used in applications ranging from a few to several hundred kilowatts and switching frequencies up to about 10 kHz. Power transistors used in power conversion applications are generally *npn* type. The power transistor is turned on by supplying sufficient base current, and this base drive has to be maintained throughout its conduction period. It is turned off by removing the base drive and making the base voltage slightly negative (within $-V_{BE(\max)}$). The saturation voltage of the device is normally 0.5 to 2.5 V and increases as the current increases. Hence, the on-state losses increase more than proportionately with current. The transistor off-state losses are much lower than the on-state losses because the leakage current of the device is of the order of a few milliamperes. Because of relatively larger switching times, the switching loss significantly increases with switching frequency. Power transistors can block only forward voltages. The reverse peak voltage rating of these devices is as low as 5 to 10 V.

Power transistors do not have I^2t withstand capability. In other words, they can absorb only very little energy before breakdown. Therefore, they cannot be protected by semiconductor fuses, and thus an electronic protection method has to be used.

To eliminate high base current requirements, Darlington configurations are commonly used. They are available in monolithic or in isolated packages. The basic Darlington configuration is shown schematically in Fig. 21.4. The Darlington configuration presents a specific advantage in that it can considerably increase the current switched by the transistor for a given base drive. The $V_{CE(sat)}$ for the Darlington is generally more than that of a single transistor of similar rating with corresponding increase in on-state power loss. During switching, the reverse-biased collector junction may show hot-spot breakdown effects that are specified by reverse-bias safe operating area (RBSOA) and forward-bias safe operating area (FBSOA). Modern devices with highly interdigitized emitter base geometry force more uniform current distribution and therefore considerably improve secondary breakdown effects. Normally, a well-designed switching aid network constrains the device operation well within the SOAs.

FIGURE 21.4 A two-stage Darlington transistor with bypass diode. (From B.K. Bose, *Modern Power Electronics: Evaluation, Technology, and Applications*, p. 6. © 1992 IEEE.)

21.5 Power MOSFET

Power MOSFETs are marketed by different manufacturers with differences in internal geometry and with different names such as MegaMOS, HEXFET, SIPMOS, and TMOS. They have unique features that make them potentially attractive for switching applications. They are essentially voltage-driven rather than current-driven devices, unlike bipolar transistors.

The gate of a MOSFET is isolated electrically from the source by a layer of silicon oxide. The gate draws only a minute leakage current on the order of nanoamperes. Hence, the gate drive circuit is simple and power loss in the gate control circuit is practically negligible. Although in steady state the gate draws virtually no current, this is not so under transient conditions. The gate-to-source and gate-to-drain capacitances have to be charged and discharged appropriately to obtain the desired switching speed, and the drive circuit must have a sufficiently low output impedance to supply the required charging and discharging currents. The circuit symbol of a power MOSFET is shown in Fig. 21.5.

Power MOSFETs are majority carrier devices, and there is no minority carrier storage time. Hence, they have exceptionally fast rise and fall times. They are essentially resistive devices when turned on, while bipolar transistors present a more or less constant $V_{CE(\text{sat})}$ over the normal operating range. Power dissipation in MOSFETs is $Id^2 R_{DS(\text{on})}$, and in bipolars it is $I_C V_{CE(\text{sat})}$. At low currents, therefore, a power MOSFET may have a lower conduction loss than a comparable bipolar device, but at higher currents, the conduction loss will exceed that of bipolars. Also, the $R_{DS(\text{on})}$ increases with temperature.

An important feature of a power MOSFET is the absence of a secondary breakdown effect, which is present in a bipolar transistor, and as a result, it has an extremely rugged switching performance. In MOSFETs, $R_{DS(\text{on})}$ increases with temperature, and thus the current is automatically diverted away from the hot spot. The drain body junction appears as an antiparallel diode between source and drain. Thus, power MOSFETs will not support voltage in the reverse direction. Although this inverse diode is relatively fast, it is slow by comparison with the MOSFET. Recent devices have the diode recovery time as low as 100 ns. Since MOSFETs cannot be protected by fuses, an electronic protection technique has to be used.

With the advancement in MOS technology, ruggedized MOSFETs are replacing the conventional MOSFETs. The need to ruggedize power MOSFETs is related to device reliability. If a MOSFET is operating within its specification range at all times, its chances for failing catastrophically are minimal. However, if its absolute maximum rating is exceeded, failure probability increases dramatically. Under actual operating conditions, a MOSFET may be subjected to transients—either externally from the power bus supplying the circuit or from the circuit itself due, for example, to inductive kicks going beyond the absolute maximum ratings. Such conditions are likely in almost every application, and in most cases are beyond a designer's control. Rugged devices are made to be more tolerant for over-voltage transients. Ruggedness is the ability of a MOSFET to operate in an environment of dynamic electrical stresses, without activating any of the parasitic bipolar junction transistors. The rugged device can withstand higher levels of diode recovery dv/dt and static dv/dt .

21.6 Insulated-Gate Bipolar Transistor (IGBT)

The IGBT has the high input impedance and high-speed characteristics of a MOSFET with the conductivity characteristic (low saturation voltage) of a bipolar transistor. The

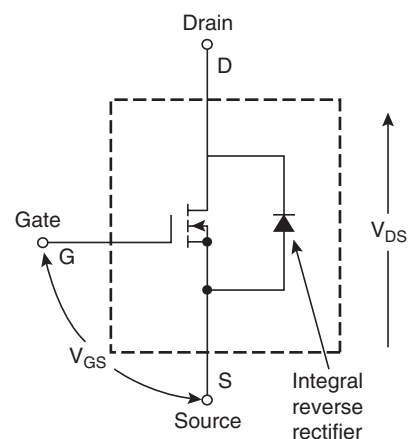


FIGURE 21.5 Power MOSFET circuit symbol. (From B.K. Bose, *Modern Power Electronics: Evaluation, Technology, and Applications*, p. 7. © 1992 IEEE.)

IGBT is turned on by applying a positive voltage between the gate and emitter and, as in the MOSFET, it is turned off by making the gate signal zero or slightly negative. The IGBT has a much lower voltage drop than a MOSFET of similar ratings. The structure of an IGBT is more like a thyristor and MOSFET. For a given IGBT, there is a critical value of collector current that will cause a large enough voltage drop to activate the thyristor. Hence, the device manufacturer specifies the peak allowable collector current that can flow without latch-up occurring. There is also a corresponding gate source voltage that permits this current to flow that should not be exceeded.

Like the power MOSFET, the IGBT does not exhibit the secondary breakdown phenomenon common to bipolar transistors. However, care should be taken not to exceed the maximum power dissipation and specified maximum junction temperature of the device under all conditions for guaranteed reliable operation. The on-state voltage of the IGBT is heavily dependent on the gate voltage. To obtain a low on-state voltage, a sufficiently high gate voltage must be applied.

In general, IGBTs can be classified as punch-through (PT) and nonpunch-through (NPT) structures, as shown in Fig. 21.6. In the PT IGBT, an N^+ buffer layer is normally introduced between the P^+ substrate and the N^- epitaxial layer, so that the whole N^- drift region is depleted when the device is blocking the off-state voltage, and the electrical field shape inside the N^- drift region is close to

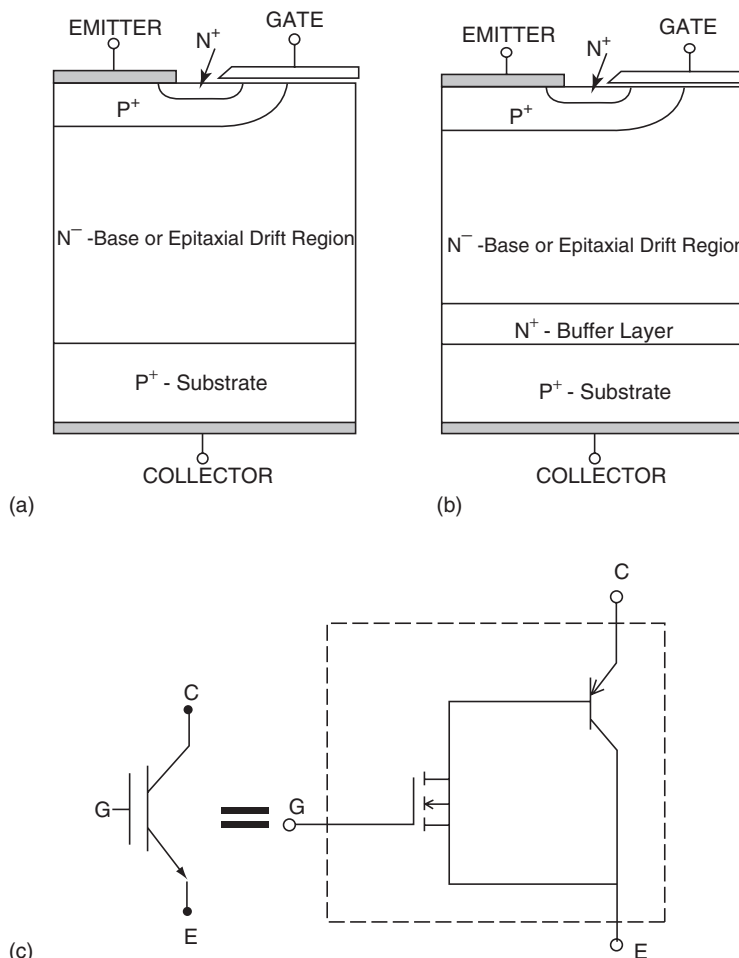


FIGURE 21.6 (a) Nonpunch-through IGBT, (b) punch-through IGBT, (c) IGBT equivalent circuit.

a rectangular shape. Because a shorter N⁻ region can be used in the punch-through IGBT, a better trade-off between the forward voltage drop and turn-off time can be achieved. PT IGBTs are available up to about 1200 V.

High voltage IGBTs are realized through a nonpunch-through process. The devices are built on an N⁻ wafer substrate which serves as the N⁻ base drift region. Experimental NPT IGBTs of up to about 4 KV have been reported in the literature. NPT IGBTs are more robust than PT IGBTs, particularly under short circuit conditions. But NPT IGBTs have a higher forward voltage drop than the PT IGBTs.

The PT IGBTs cannot be as easily paralleled as MOSFETs. The factors that inhibit current sharing of parallel-connected IGBTs are (1) on-state current unbalance, caused by V_{CE(sat)} distribution and main circuit wiring resistance distribution, and (2) current unbalance at turn-on and turn-off, caused by the switching time difference of the parallel connected devices and circuit wiring inductance distribution. The NPT IGBTs can be paralleled because of their positive temperature coefficient property.

21.7 MOS-Controlled Thyristor (MCT)

The MCT is a new type of power semiconductor device that combines the capabilities of thyristor voltage and current with MOS gated turn-on and turn-off. It is a high power, high frequency, low conduction drop and a rugged device, which is more likely to be used in the future for medium and high power applications. A cross-sectional structure of a p-type MCT with its circuit schematic is shown in Fig. 21.7. The MCT has a thyristor type structure with three junctions and PNPN layers between the anode and cathode. In a practical MCT, about 100,000 cells similar to the one shown are paralleled to achieve the desired current rating. MCT is turned on by a negative voltage pulse at the gate with respect to the anode, and is turned off by a positive voltage pulse.

The MCT was announced by the General Electric R & D Center on November 30, 1988. Harris Semiconductor Corporation has developed two generations of p-MCTs. Gen-1 p-MCTs are available at 65 A/1000 V and 75A/600 V with peak controllable current of 120 A. Gen-2 p-MCTs are being developed at similar current and voltage ratings, with much improved turn-on capability and switching speed. The reason for developing a p-MCT is the fact that the current density that can be turned off is 2 or 3 times higher than that of an n-MCT; but n-MCTs are the ones needed for many practical applications. Harris Semiconductor Corporation is in the process of developing n-MCTs, which are expected to be commercially available during the next one to two years.

The advantage of an MCT over IGBT is its low forward voltage drop. N-type MCTs will be expected to have a similar forward voltage drop, but with an improved reverse bias safe operating area and switching speed. MCTs have relatively low switching times and storage time. The MCT is capable of high current densities and blocking voltages in both directions. Since the power gain of an MCT is extremely high, it could be driven directly from logic gates. An MCT has high di/dt (of the order of 2500 A/ μ s) and high dv/dt (of the order of 20,000 V/ μ s) capability.

The MCT, because of its superior characteristics, shows a tremendous possibility

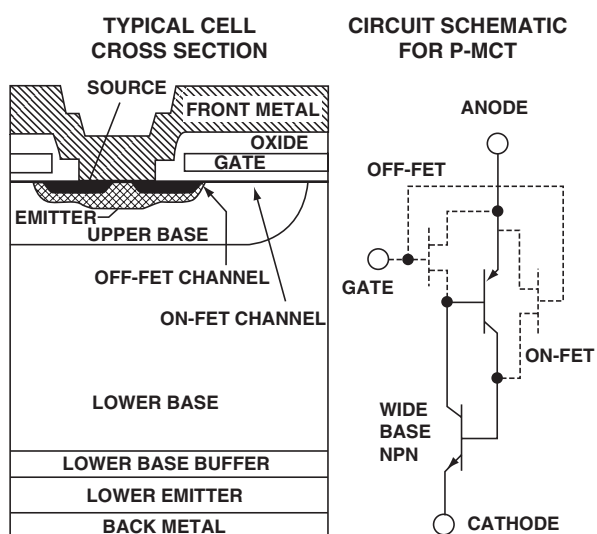


FIGURE 21.7 (From Harris Semiconductor, *User's Guide of MOS Controlled Thyristor*. With permission.)

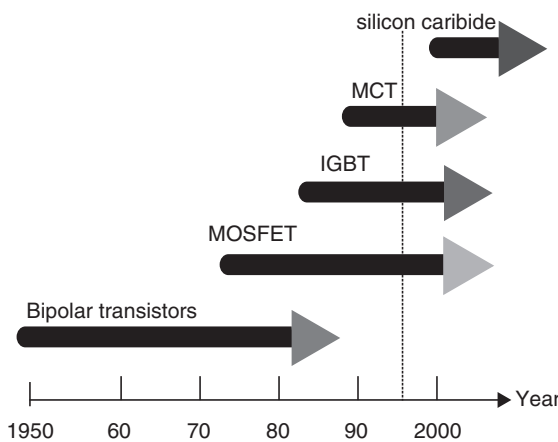


FIGURE 21.8 Current and future power semiconductor devices development direction. (From A.Q. Huang, Recent Developments of Power Semiconductor Devices, *VPEC Seminar Proceedings*, pp. 1–9. With permission.)

for applications such as motor drives, uninterrupted power supplies, static VAR compensators, and high power active power line conditioners.

The current and future power semiconductor devices developmental direction is shown in Fig. 21.8. High-temperature operation capability and low forward voltage drop operation can be obtained if silicon is replaced by silicon carbide material for producing power devices. The silicon carbide has a higher band gap than silicon. Hence, higher breakdown voltage devices could be developed. Silicon carbide devices have excellent switching characteristics and stable blocking voltages at higher temperatures. But the silicon carbide devices are still in the very early stages of development.

References

- B.K. Bose, *Modern Power Electronics: Evaluation, Technology, and Applications*, New York: IEEE Press, 1992.
- Harris Semiconductor, *User's Guide of MOS Controlled Thyristor*.
- A.Q. Huang, Recent Developments of Power Semiconductor Devices, in *VPEC Seminar Proceedings*, September 1995, 1–9.
- N. Mohan and T. Undeland, *Power Electronics: Converters, Applications, and Design*, John Wiley & Sons, New York, 1995.
- J. Wojslawowicz, Ruggedized transistors emerging as power MOSFET standard-bearers, *Power Technics Magazine*, January 1988, 29–32.

Further Information

- B.M. Bird and K.G. King, *An Introduction to Power Electronics*, Wiley-Interscience, New York, 1984.
- R. Sittig and P. Roggwiller, *Semiconductor Devices for Power Conditioning*, Plenum, New York, 1982.
- V.A.K. Temple, Advances in MOS controlled thyristor technology and capability, *Power Conversion*, 544–554, Oct. 1989.
- B.W. Williams, *Power Electronics, Devices, Drivers and Applications*, John Wiley, New York, 1987.

22

Uncontrolled and Controlled Rectifiers

22.1	Introduction.....	22-1
22.2	Uncontrolled Rectifiers	22-2
	Mechanics of Diode Conduction • Single-Phase Half-Wave Rectifier Circuits • Full-Wave Rectifiers • Three-Phase Rectifiers (Half-Wave and Full-Wave) • Average Output Voltage • Influence of Three-Phase Rectification on the Power System • Why VFDs Generate Harmonics • Harmonic Limit Calculations Based on IEEE 519-1992 • Harmonic Mitigating Techniques • Addition of Inductive Impedance • Capacitor-Based Passive Filters • Multi-Pulse Techniques	
22.3	Controlled Rectifiers	22-28
	Gate Circuit Requirements • Single-Phase H-Bridge Rectifier Circuits with Thyristors • Three-Phase Controlled AC to DC Rectifier Systems • Average Output Voltage • HVDC Transmission Systems • Power System Interaction with Three-Phase Thyristor AC to DC Rectifier Systems	
22.4	Conclusion	22-40

Mahesh M. Swamy
Yaskawa Electric America

22.1 Introduction

Rectifiers are electronic circuits that convert bidirectional voltage to unidirectional voltage. This process can be accomplished either by mechanical means like in the case of dc machines employing commutators or by static means employing semiconductor devices. Static means of rectification is more efficient and reliable compared to rotating commutators. In this chapter, we will discuss rectification of electric power for industrial and commercial use. In other words, we will not be discussing small signal rectification that generally involves low power and low voltage signals. Static power rectifiers can be classified into two broad groups. They are (a) uncontrolled rectifiers and (b) controlled rectifiers. Uncontrolled rectifiers make use of power semiconductor diodes, whereas controlled rectifiers make use of thyristors (SCRs), gate turn off thyristors (GTOs), and MOSFET controlled thyristors (MCTs).

Rectifiers, in general, are widely used in power electronics to rectify single-phase as well as three-phase voltages. DC power supplies used in computers, consumer electronics, and a host of other applications typically make use of single-phase rectifiers. Industrial applications include, but are not limited to industrial drives, metal extraction processes, industrial heating, power generation and transmission, etc. Most industrial applications of large power rating typically employ three-phase rectification processes.

Uncontrolled rectifiers in single-phase and in three-phase circuits will be discussed in [Section 22.2](#). [Section 22.3](#) will focus on controlled rectifiers. Application issues regarding uncontrolled and controlled rectifiers will be briefly discussed within each section. [Section 22.4](#) will conclude this chapter.

22.2 Uncontrolled Rectifiers

Simplest uncontrolled rectifier use can be found in single-phase circuits. There are two types of uncontrolled rectification. They are (a) half-wave rectification and (b) full-wave rectification. Half-wave and full-wave rectification techniques have been used in single-phase as well as in three-phase circuits. As mentioned earlier, uncontrolled rectifiers make use of diodes. Diodes are two terminal semiconductor devices that allow flow of current in only one direction. The two terminals of a diode are known as the anode and the cathode.

22.2.1 Mechanics of Diode Conduction

Anode is formed when a pure semiconductor material, typically silicon, is doped with impurities that have fewer valence electrons than silicon [4]. Silicon has an atomic number of 14, which according to Bohr's atomic model means that the K and L shells are completely filled by 10 electrons and the remaining 4 electrons occupy the M shell. The M shell can hold a maximum of 18 electrons. In a silicon crystal, every atom is bound to four other atoms, which are placed at the corners of a regular tetrahedron. The bonding, which involves sharing of a valence electron with a neighboring atom, is known as covalent bonding. When a group-3 element (typically boron, aluminum, gallium, and indium) is doped into the silicon lattice structure, three of the four covalent bonds are made. However, one bonding site is vacant in the silicon lattice structure. This creates vacancies or *holes* in the semiconductor. In the presence of either a thermal field or an electrical field, electrons from a neighboring lattice or from an external agency tend to migrate to fill this vacancy. The vacancy or *hole* can also be said to move toward the approaching electron, thereby creating a mobile hole and hence current flow. Such a semiconductor material is also known as lightly doped semiconductor material or *p type*. Similarly, cathode is formed when silicon is doped with impurities that have higher valence electrons than silicon. This would mean elements belonging to group 5. Typical doping impurities of this group are phosphorus, arsenic, and antimony. When a group 5 element is doped into the silicon lattice structure, it over-satisfies the covalent bonding sites available in the silicon lattice structure, creating excess or loose electrons in the valence shell. In the presence of either a thermal field or an electrical field, these loose electrons easily get detached from the lattice structure and are free to conduct electricity. Such a semiconductor material is also known as heavily doped semiconductor material or *n type*.

The structure of the final doped crystal even after the addition of *acceptor* impurities (group 3) or *donor* impurities (group 5) remains electrically neutral. The available electrons balance the net positive charge and there is no charge imbalance.

When a p-type material is joined with an n-type material, a *p-n* junction is formed. Some loose electrons from the n-type material migrate to fill the holes in the p-type material and some holes in the p-type migrate to meet with the loose electrons in the n-type material. Such a movement causes the p-type structure to develop a slight negative charge and the n-type structure to develop some positive charge. These slight positive and negative charges in the n-type and p-type areas, respectively, prevent further migration of electrons from n-type to p-type and holes from p-type to n-type areas. In other words, an energy barrier is automatically created due to the movement of charges within the crystalline lattice structure. Keep in mind that the combined material is still electrically neutral and no charge imbalance exists.

When a positive potential greater than the barrier potential is applied across the p-n junction, the electrons from the n-type area migrate to combine with the holes in the p-type area and vice-versa. The p-n junction is said to be *forward biased*. Movement of charge particles constitutes current flow. Current is said to flow from the anode to the cathode when the potential at the anode is higher than the potential at the cathode by a minimum threshold voltage also known as the junction barrier voltage. The magnitude of current flow is high when the externally applied positive potential across the p-n junction is high.

When the polarity of the applied voltage across the p-n junction is reversed compared to the case described above, then the flow of current ceases. The holes in the p-type area move away from the n-type

area and the electrons in the n-type area move away from the p-type area. The p-n junction is said to be *reverse biased*. In fact, the holes in the p-type area get attracted to the negative external potential and similarly the electrons in the n-type area get attracted to the positive external potential. This creates a depletion region at the p-n junction and there are almost no charge carriers flowing in the depletion region. This phenomenon brings us to an important observation that a p-n junction can be utilized to force current to flow only in one direction depending on the polarity of the applied voltage across it. Such a semiconductor device is known as a *diode*. Electrical circuits employing diodes to convert ac voltage to unidirectional voltage across a load are known as *rectifiers*. The voltage–current characteristic of a typical power semiconductor diode along with its symbol is shown in Fig. 22.1.

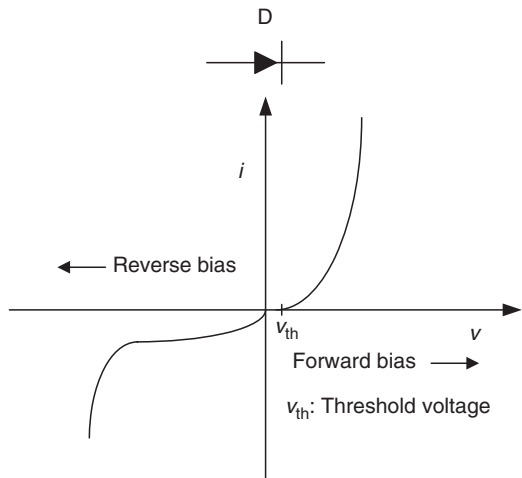


FIGURE 22.1 Typical v – i characteristic of a semiconductor diode and its symbol.

22.2.2 Single-Phase Half-Wave Rectifier Circuits

A single-phase half-wave rectifier circuit employs one diode. A typical circuit, which makes use of a half-wave rectifier, is shown in Fig. 22.2. A single-phase ac source is applied across the primary windings of a transformer. The secondary of the transformer consists of a diode and a resistive load. This is typical since many consumer electronic items including computers utilize single-phase power.

Typically, the primary side is connected to a single-phase ac source, which could be 120 V, 60 Hz, 100 V, 50 Hz, 220 V, 50 Hz, or any other utility source. The secondary side voltage is generally stepped down and rectified to achieve low dc voltage for consumer applications. The secondary voltage, the voltage across the load resistor and the current through it is shown in Fig. 22.3. For a purely resistive load, $V_0 = \sqrt{2}V_{\text{sec}}/\pi$.

When the voltage across the anode–cathode of diode D1 in Fig. 22.2 goes negative, the diode does not conduct and no voltage appears across the load resistor R. The current through R follows the voltage across it. The value of the secondary voltage is chosen to be 24 Vac and the value of R is chosen to be 2Ω . Since, only one-half of the input voltage waveform is allowed to pass onto the output, such a rectifier is known as *half-wave rectifier*. The voltage ripple across the load resistor is rather large and in typical power supplies, such ripples are unacceptable. The current through the load is discontinuous and the current through the secondary of the transformer is unidirectional. The ac component in the secondary of the transformer is balanced by a corresponding ac component in the primary winding. However, the dc component in the secondary does not induce any voltage on the primary side and hence it is not compensated for. This dc current component through the transformer secondary can cause the transformer to saturate and is not advisable for large power applications. In order to smoothen the output voltage across the load resistor R and to make the load current continuous, a smoothing filter circuit comprising of either a large dc capacitor or a combination of a series inductor and shunt dc capacitor is employed. Such a circuit is shown in Fig. 22.4 and the resulting waveforms are shown in Fig. 22.5.

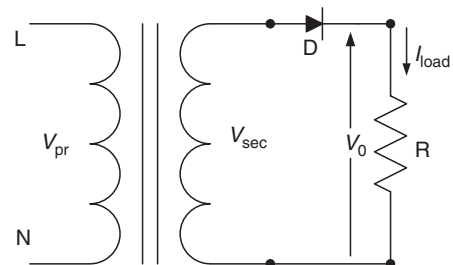


FIGURE 22.2 Electrical schematic of a single-phase half-wave rectifier circuit feeding a resistive load. Average output voltage is V_0 .

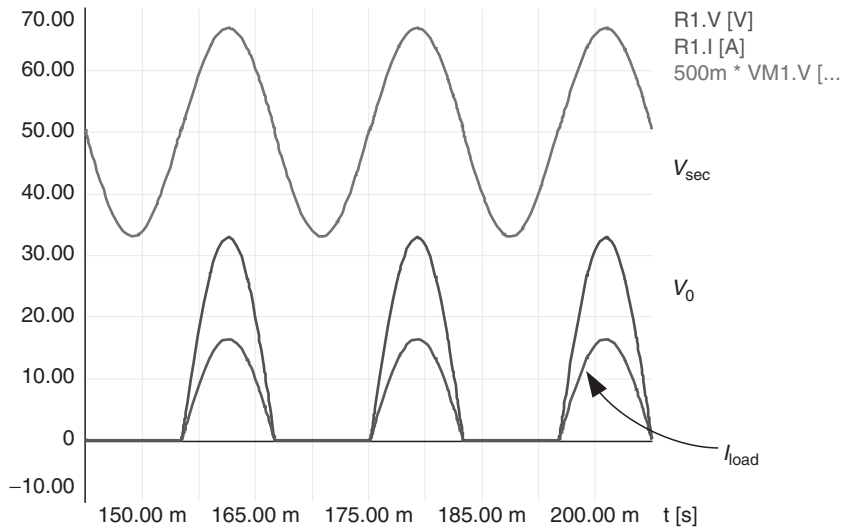


FIGURE 22.3 Typical waveforms at various points in the circuit of Fig. 22.2.

It is interesting to see that the voltage across the load resistor has very little ripple and the current through it is smooth. However, the value of the filter components employed is large and is generally not economically feasible. For example, in order to get a voltage waveform across the load resistor R that has less than 25% peak-to-peak voltage ripple, the value of inductance that had to be used is 3 mH and the value of the capacitor is 20,000 μF . Increasing the value of inductance does reduce the peak-to-peak ripple across the load. However, the voltage drop across the inductor increases and the average voltage across the resistor reduces significantly.

22.2.3 Full-Wave Rectifiers

In order to improve the performance without adding bulky filter components, it is a good practice to employ full-wave rectifiers. The circuit in Fig. 22.2 can be easily modified into a full-wave rectifier. The transformer is changed from a single secondary winding to a center-tapped secondary winding. Two diodes are now employed instead of one. The new circuit is shown in Fig. 22.6.

The waveforms for the circuit of Fig. 22.6 are shown in Fig. 22.7. The voltage across the load resistor is a full-wave rectified voltage. The current has subtle discontinuities but it can be improved by employing smaller size filters. For a purely resistive load, $V_0 = \sqrt{2}V_{\text{sec}}/\pi$.

A typical filter for the circuit of Fig. 22.6 may include only a capacitor. The waveforms are shown in Fig. 22.8. Adding a capacitor filter distorts the secondary voltage due to discontinuous and pulsating current flowing through the secondary windings.

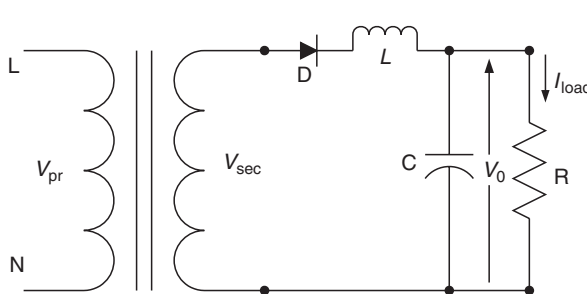


FIGURE 22.4 Modified circuit of Fig. 22.2 employing smoothing filters.

Another way of reducing the size of the filter components is to increase the frequency of the supply. In many power supply applications similar to the one used in computers, a high frequency ac supply is achieved by means of switching. The high frequency ac is then level translated via a ferrite core transformer with multiple secondary windings. The secondary voltages are then rectified employing a simple circuit

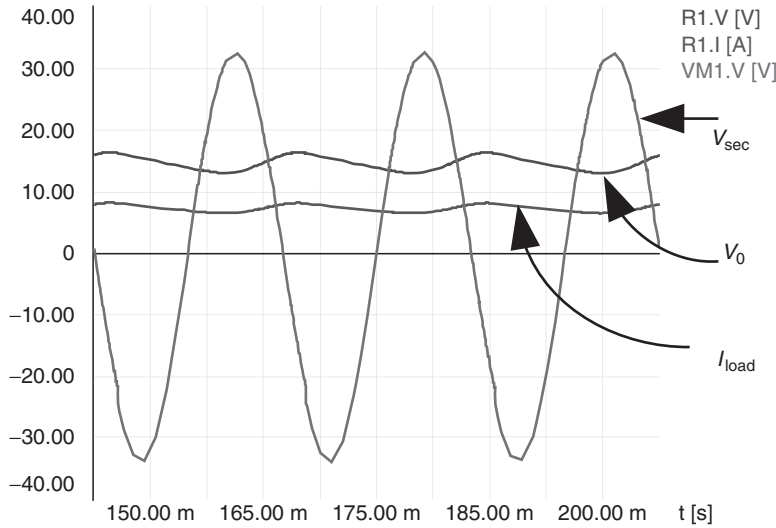


FIGURE 22.5 Voltage across load resistor R and current through it for the circuit in Fig. 22.4.

as that shown in Fig. 22.2 or 22.4 with much smaller filters. The resulting voltage across the load resistor is then maintained to have a peak–peak voltage ripple of less than 1%.

Full-wave rectification can be achieved without the use of center-tap transformers. Such circuits make use of four diodes in single-phase circuits and six diodes in three-phase circuits. The circuit configuration is typically referred to as the *H-bridge* circuit. A single-phase full-wave H-bridge topology is shown in Fig. 22.9. The main difference between the circuit topology shown in Figs. 22.6 and 22.9 is that the H-bridge circuit employs four diodes whereas the topology of Fig. 22.6 utilizes only two diodes. The VA rating of the center tap transformer, however, is higher than that of the transformer needed for H-bridge rectifier. The voltage and current stresses in the diodes in Fig. 22.6 are also greater than that in the diodes of Fig. 22.9.

In order to highlight the basic difference in the two topologies, it will be interesting to compare the component ratings for the same power output. To make the comparison easy, let both topologies employ very large filter inductors such that the current through R is constant and ripple free. Let this current through R be denoted by I_{dc} . Let the power being supplied to the load be denoted by P_{dc} . The output power and the load current are then related by the following expression:

$$P_{dc} = I_{dc}^2 R \quad (22.1)$$

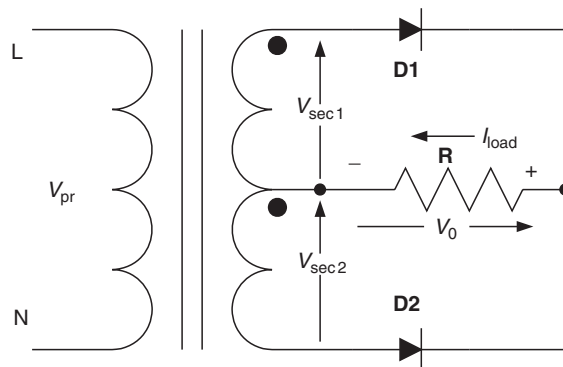


FIGURE 22.6 Electrical schematic of a single-phase full-wave rectifier circuit. Average output voltage is V_0 . For balanced operation, $V_{sec1} = V_{sec2} = V_{sec}$.

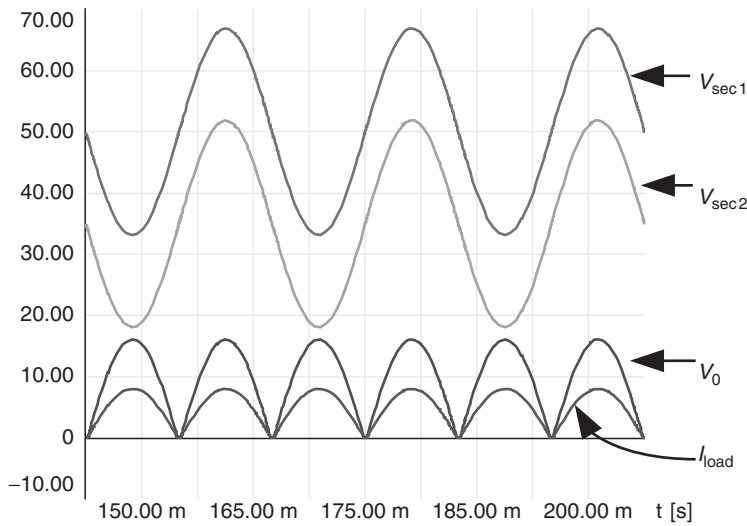


FIGURE 22.7 Typical waveforms at various points in Fig. 22.6. V scale: 1/10 of actual value.

The rms current flowing through the first secondary winding in the topology in Fig. 22.6 will be $I_{dc}/\sqrt{2}$. This is because the current through a secondary winding flows only when the corresponding diode is forward biased. This means that the current through the secondary winding will flow only for one half cycle. If the voltage at the secondary is assumed V , the VA rating of the secondary winding of the transformer in Fig. 22.6 will be given by

$$\begin{aligned} VA_1 &= VI_{dc}/\sqrt{2} \\ VA_2 &= VI_{dc}/\sqrt{2} \\ VA &= VA_1 + VA_2 = \sqrt{2}VI_{dc} \end{aligned} \quad (22.2)$$

This is the secondary-side VA rating for the transformer shown in Fig. 22.6.

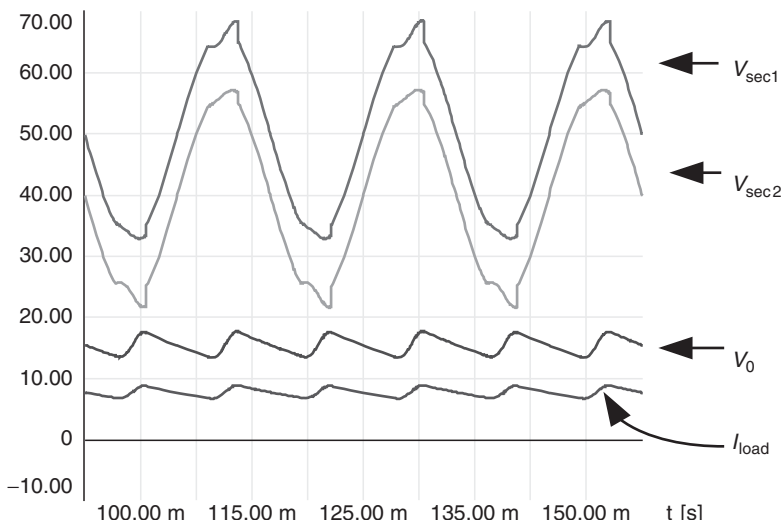


FIGURE 22.8 Voltage across the load resistor and current through it with only capacitor filter. V scale: 1/10 of actual value.

For the isolation transformer shown in Fig. 22.9, let the secondary voltage be V and the load current be of a constant value, I_{dc} . Since, in the topology of Fig. 22.9, the secondary winding carries the current I_{dc} when diodes D1 and D2 conduct and as well as when diodes D3 and D4 conduct, the rms value of the secondary winding current is I_{dc} . Hence, the VA rating of the secondary winding of the transformer shown in Fig. 22.9 is given by $VA = VI_{dc}$, and is less than that needed for the topology of Fig. 22.6. Note that the primary VA rating for both cases remains the same since in both cases, the power being transferred from the source to the load remains the same.

When diode D2 in the circuit of Fig. 22.6 conducts, the secondary voltage of the second winding $V_{sec2} (=V)$ appears at the cathode of diode D1. The voltage being blocked by the diode D1 can thus reach two times the peak secondary voltage ($=2V_{pk}$) (Fig. 22.7). In the topology of Fig. 22.9, when diodes D1 and D2 conduct, the voltage $V_{sec} (=V)$, which is same as V_{sec2} , appears across D3 and D4 in series. This means that the diodes have to withstand only one time the peak of the secondary voltage, V_{pk} . The rms value of the current flowing through the diodes in both topologies is the same. Hence, from the diode voltage rating as well as from the secondary VA rating points of view, the topology of Fig. 22.9 is better than that of Fig. 22.6. Further, the topology in Fig. 22.9 can be directly connected to a single-phase ac source since it does not need a center-tapped transformer. The voltage waveform across the load is similar to that shown in Figs. 22.7 and 22.8.

In many industrial applications, the topology shown in Fig. 22.9 is used along with a dc filter capacitor to smoothen the ripples across the load resistor. The load resistor is simply a representative of a load. It could be an inverter system or a high-frequency resonant link. In any case, the diode rectifier bridge would see a representative load resistor. For the same output power and the same peak-to-peak ripple voltage across the load, the dc filter capacitor in case of single-phase source will need to be much larger compared to that for a three-phase source connected to a six-diode rectifier bridge circuit.

When the rectified power is large, it is advisable to add a dc link inductor. This can reduce the size of the capacitor to some extent and reduce the current ripple through the load. When the rectifier is turned ON initially with the capacitor at zero voltage, large amplitude of charging current will flow into the filter capacitor through a pair of conducting diodes. The diodes D1~D4 should be rated to handle this large surge current. In order to limit the high inrush current, it is a normal practice to add a charging resistor in series with the filter capacitor. The charging resistor limits the inrush current but creates a significant power loss if it is left in the circuit under normal operation. Typically, a contactor is used to short-circuit the charging resistor after the capacitor is charged to a desired level. The resistor is thus electrically non-functional during normal operating conditions. A typical arrangement showing a single-phase full-wave H-bridge rectifier system for an inverter application is shown in Fig. 22.10. The charging current at time of turn-ON is shown in a simulated waveform in Fig. 22.11. Note that the contacts across the soft-charge resistor are closed under normal operation. The contacts across the soft-charge resistor are initiated by various means. The coil for the contacts could be powered from the input ac supply and a timer or it could be powered ON by a logic controller that senses the level of voltage across the dc bus capacitor or senses the rate of change in voltage across the dc bus capacitor. A simulated waveform depicting the inrush with and without a soft-charge resistor is shown in Figs. 22.11a and b, respectively.

The value of soft-charge resistor used is 6Ω . The dc bus capacitor is about $1200 \mu\text{F}$. To show typical operation, at start-up, there is no load and resistor R represents only the bleed-off resistor of approximately $4.7 \text{ k}\Omega$ present across the capacitor. The peak value of the charging current for this case is observed to be approximately 50 A.

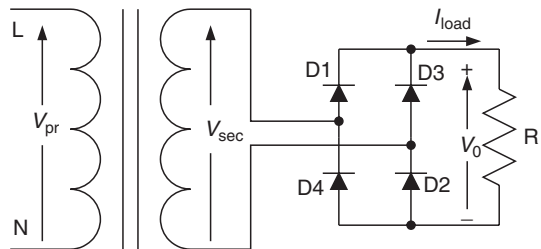


FIGURE 22.9 Schematic representation of a single-phase full-wave H-bridge rectifier.

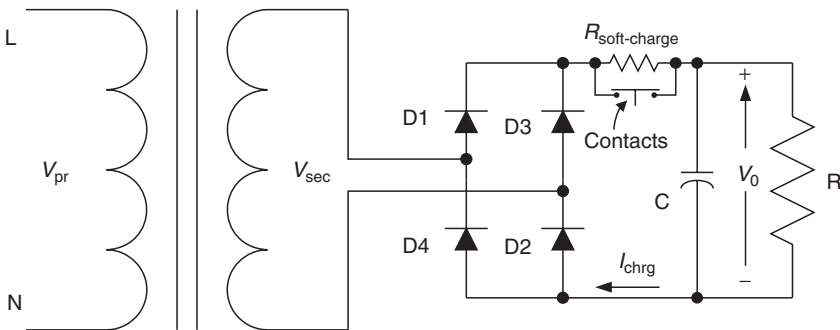


FIGURE 22.10 Single-phase H-bridge circuit with soft-charge resistor–contactor arrangement.

In the case without any soft charge resistor, the current is limited by the system impedance and by the diode forward resistance. The peak current is observed to be about 175 A for the same parameters as assumed for the case with soft charge resistor. Note that the dc bus capacitor gets charged to a value almost twice of the input peak voltage and this is due to the resonance type of condition set in by the input impedance of the ac source that includes the leakage inductance of the input transformer. The high voltage across the dc bus takes a long time to bleed-off through the bleed resistor. The high voltage can damage the inverter IGBTs if the load is an inverter and hence charging the dc bus capacitor without soft charging resistors is not recommended and should always be avoided.

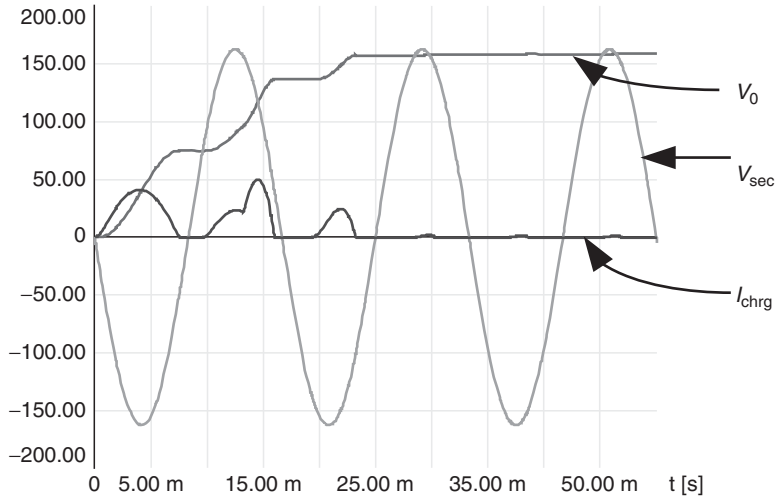
For larger power applications, typically above 1.5 kW, it is advisable to use a higher power supply. In some applications, two of the three-phases of a three-phase power system is used as the source powering the rectifier of Fig. 22.9. The line-line voltage could be either 240 Vac or 480 Vac. Under those circumstances, a load of up to 4 kW can be powered using single-phase supply before adopting a full three-phase H-bridge configuration. Beyond 4 kW, the size of the capacitor becomes too large to achieve a peak-peak voltage ripple of less than 10%. Hence, it is advisable then to employ three-phase rectifier configurations.

22.2.4 Three-Phase Rectifiers (Half-Wave and Full-Wave)

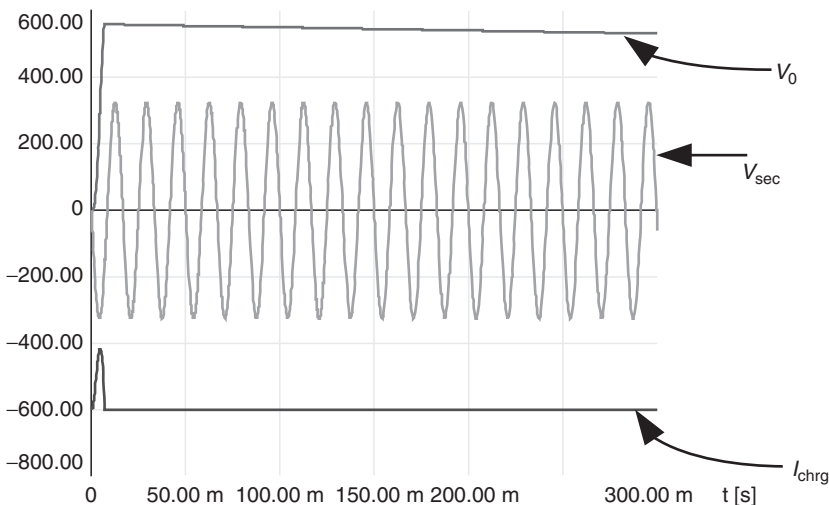
Similar to the single-phase case, there exist half-wave and full-wave three-phase rectifier circuits. Again, similar to the single-phase case, the half-wave rectifier in the three-phase case also has dc components in the source current. The source has to be large enough to handle this. It is thus not advisable to use three-phase half-wave rectifier topology for large power applications. The three-phase half-wave rectifier employs three diodes whereas the full-wave H-bridge configuration employs six diodes. Typical three-phase half-wave and full-wave topologies are shown in Fig. 22.12.

In the half-wave rectifier shown in Fig. 22.12a, the shape of the output voltage and current through the resistive load is dictated by the instantaneous value of the source voltages, A, B, and C. These source voltages are phase shifted in time by 120 electrical degrees, which corresponds to approximately 5.55 ms for a 60 Hz system. This means that if A phase reaches its peak value at time t_1 , B phase will achieve its peak 120 electrical degrees later ($t_1 + 5.55$ ms), and C will achieve its peak 120 electrical degrees later than B ($t_1 + 5.55$ ms + 5.55 ms). Since all three phases are connected to the same output resistor R, the phase that provides the highest instantaneous voltage is the phase that appears across R. In other words, the phase with the highest instantaneous voltage reverse biases the diodes of the other two phases and prevents them from conducting, which consequently prevents those phase voltages from appearing across R. Since a particular phase is connected to only one diode in Fig. 22.12a, only three pulses, each of 120° duration, appear across the load resistor, R. Typical output voltage across R and current through it for the circuit of Fig. 22.12a is shown in Fig. 22.13a.

A similar explanation can be provided to explain the voltage waveform across a purely resistive load in the case of a three-phase full-wave rectifier shown in Fig. 22.12b. The output voltage that appears across



(a)



(b)

FIGURE 22.11 (a) Charging current and voltage across capacitor for the circuit of Fig. 22.10. V scale: 1/2 of actual value. (b) Charging current and voltage across capacitor for no soft-charge resistor. V scale: Actual voltage.

R is the highest instantaneous line-line voltage and not simply the phase voltage. Since there are six such intervals, each of 60 electrical degrees duration in a given cycle, the output voltage waveform will have six humps in one cycle (Fig. 22.13b). Since a phase is connected to two diodes (diode pair), each phase conducts current out and into itself, thereby eliminating dc component in one complete cycle.

The waveform for a three-phase full-wave rectifier with a purely resistive load is shown in Fig. 22.13b. Note that the number of humps in Fig. 22.13a is only three in one ac cycle whereas the number of humps in Fig. 22.13b is six in one ac cycle. Further, the peak-to-peak ripple in the voltage as well as in the current is significantly lower in the full bridge configuration compared to the half-bridge configuration.

In both the configurations shown in Fig. 22.12, the load current does not become discontinuous due to three-phase operation. Comparing this to the single-phase half-wave and full-wave rectifier, the output voltage ripple is much lower in three-phase rectifier systems compared to single-phase rectifier

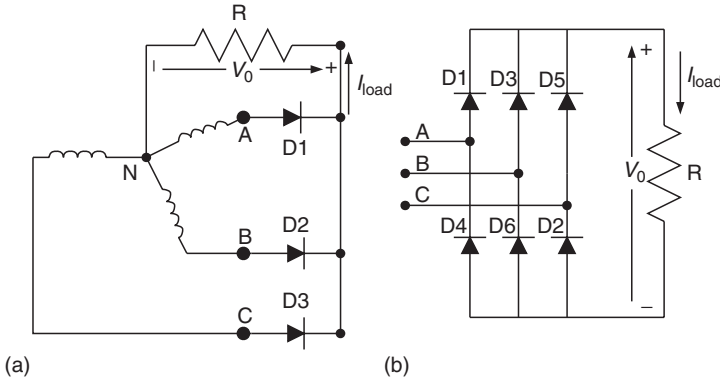


FIGURE 22.12 Schematic representation of three-phase rectifier configurations. (a) Half-wave rectifier needing a neutral point, N, and (b) full-wave rectifier.

systems. Hence, with the use of moderately sized filters, three-phase full-wave rectifiers can be operated at hundred to thousands of kilowatts. The only limitation would be the size of the diodes used and power system harmonics, which will be discussed next. Since there are six humps in the output voltage waveform per electrical cycle, the three-phase full-wave rectifier shown in Fig. 22.12b is also known as a six-pulse rectifier system.

22.2.5 Average Output Voltage

In order to evaluate the average value of the output voltage for the two rectifiers shown in Fig. 22.12, the output voltages in Figs. 22.13a and b have to be integrated over a cycle. For the circuit shown in Fig. 22.12a, the integration yields the following:

$$V_0 = \frac{3}{2\pi} \int_{\pi/6}^{5\pi/6} \sqrt{2} V_{L-N} \sin(wt) d(wt) \quad (22.3)$$

$$V_0 = \frac{3\sqrt{3}\sqrt{2} V_{L-N}}{2\pi}$$

A similar operation can be performed to obtain the average output voltage for the circuit shown in Fig. 22.12b. This yields

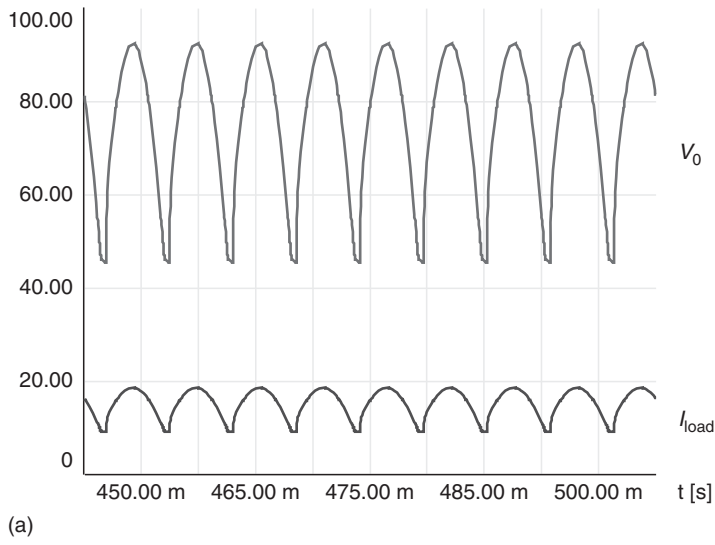
$$V_0 = \frac{3}{\pi} \int_{\pi/3}^{2\pi/3} \sqrt{2} V_{L-L} \sin(wt) d(wt) \quad (22.4)$$

$$V_0 = \frac{3\sqrt{2} V_{L-L}}{\pi} = \frac{3\sqrt{2}\sqrt{3} V_{L-N}}{\pi}$$

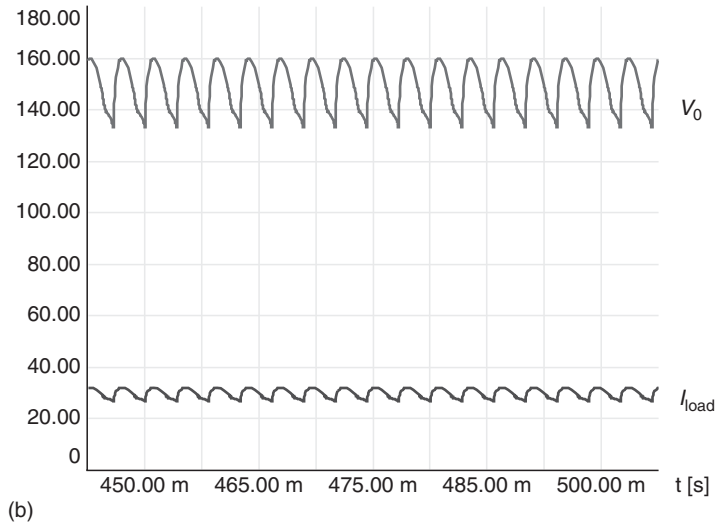
In other words, the average output voltage for the circuit in Fig. 22.12b is twice that for the circuit in Fig. 22.12a.

22.2.6 Influence of Three-Phase Rectification on the Power System

Events over the last several years have focused attention on certain types of loads on the electrical system that result in power quality problems for the user and utility alike. Equipments which have become common place in most facilities including computer power supplies, solid state lighting ballast, adjustable speed drives (ASDs), and uninterruptible power supplies (UPSs) are examples of nonlinear loads. Nonlinear loads are loads in which the current waveform does not have a linear relationship with the voltage waveform. In other words, if the input voltage to the load is sinusoidal and the current is



(a)



(b)

FIGURE 22.13 (a) Typical output voltage across a purely resistive load and current through it for the half-wave rectifier shown in Fig. 22.12a. V scale: 0.5 of actual value. (b) Typical output voltage across a purely resistive load and current through it for the full-wave rectifier shown in Fig. 22.12b. V scale: 0.5 of actual value.

non-sinusoidal then such loads will be classified as nonlinear loads because of the nonlinear relationship between voltage and current. Nonlinear loads generate voltage and current harmonics, which can have adverse effects on equipment that are used to deliver electrical energy to them. Examples of power delivery equipment include power system transformers, feeders, circuit breakers, etc. Power delivery equipments are subject to higher heating losses due to harmonic currents consumed by nonlinear loads to which they are connected. Harmonics can have a detrimental effect on emergency or standby power generators, telephones, and other sensitive electrical equipment. When reactive power compensation in the form of passive power factor improving capacitors is used with nonlinear loads, resonance conditions can occur that may result in even higher levels of harmonic voltage and current distortion thereby causing equipment failure, disruption of power service, and fire hazards in extreme conditions.

The electrical environment has absorbed most of these problems in the past. However, the problem has now reached a magnitude where Europe, the U.S., and other countries have proposed standards to responsibly engineer systems considering the electrical environment. IEEE 519-1992 and IEC 555 have evolved to become a common requirement cited when specifying equipment on newly engineered projects. Various harmonic filtering techniques have been developed to meet these specifications. The present IEEE 519-1992 document establishes acceptable levels of harmonics (voltage and current) that can be introduced into the incoming feeders by commercial and industrial users. Where there may have been little cooperation previously from manufacturers to meet such specifications, the adoption of IEEE 519-1992 and other similar world standards now attracts the attention of everyone.

22.2.7 Why VFDs Generate Harmonics

The current waveform at the inputs of a variable frequency drive (VFD) is not continuous. It has multiple zero-crossings in one electrical cycle. The DC bus capacitor draws charging current only when it is discharged due to the motor load. The charging current flows into the capacitor when the input rectifier is forward biased, which occurs when the instantaneous input voltage is higher than the DC voltage across the DC bus capacitor. The pulsed current drawn by the dc bus capacitor is rich in harmonics because it is discontinuous as seen in Fig. 22.1.

The voltage harmonics generated by VFDs are due to the flat-topping effect caused by weak AC source charging the DC bus capacitor without any intervening impedance. The distorted voltage waveform gives rise to voltage harmonics and this is of a more important concern than current harmonics. The reason is simple. Voltage is shared by all loads and it affects all loads connected in an electrical system. Current distortion has a local effect and pertains to only that circuit that is feeding the nonlinear load. Hence, connecting nonlinear loads like VFDs to a weak ac system requires more careful consideration than otherwise.

The discontinuous, non-sinusoidal current waveform as shown in Fig. 22.1 can be mathematically represented by sinusoidal patterns of different frequencies having a certain amplitude and phase relationship among each other. By adding these components, the original waveform can be reconstructed. The amplitude of the various sinusoidal components that need to be used to reconstruct a given non-sinusoidal waveform is expressed in terms of a mathematical expression called total harmonic distortion. The total harmonic current distortion is defined as

$$\text{THD}_I = \frac{\sqrt{\sum_{n=2}^{n=\infty} I_n^2}}{I_1}$$

I_1 is the rms value of the fundamental component of current; and I_n is the rms value of the n^{th} harmonic component of current.

The reason for doing this is that it is easier to evaluate the heating effect caused by continuous sinusoidal waveforms of different frequencies and corresponding amplitudes than to estimate the heating effects caused by discontinuous non-sinusoidal waveforms.

The order of current harmonics produced by a semiconductor converter during normal operation is termed as characteristic harmonics. In a three-phase, six-pulse converter with no DC bus capacitor, the characteristic harmonics are non-triplet odd harmonics (e.g., 5th, 7th, 11th, etc.). In general, the characteristic harmonics generated by a semiconductor converter are given by

$$h = kq \pm 1 \quad (22.5)$$

h is the order of harmonics, k is any integer, and q is the pulse number of the semiconductor converter (six for a six-pulse converter). When operating a six-pulse rectifier-inverter system with a DC bus

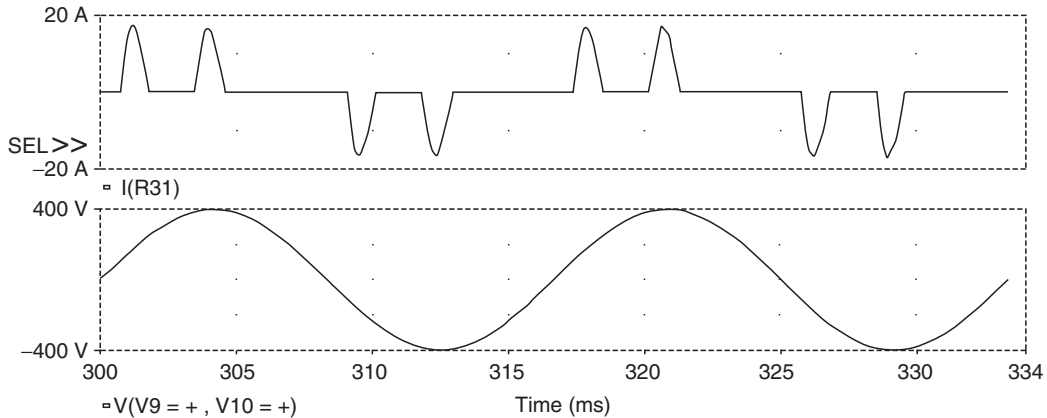


FIGURE 22.14 Typical pulsed current waveform as seen at input of a VFD.

capacitor (voltage source inverter or VSI), harmonics of orders other than those given by the above equation may be observed. Such harmonics are called non-characteristic harmonics. Though of lower magnitude, these also contribute to the overall harmonic distortion of the input current. The per unit value of the characteristic harmonics present in the theoretical current waveform at the input of the semiconductor converter is given by $1/h$ where h is the order of the harmonics. In practice, the observed per unit value of the harmonics is much greater than $1/h$. This is because the theoretical current waveform is a rectangular pattern made up of equal positive and negative halves, each occupying 120 electrical degrees. The pulsed discontinuous waveform observed commonly at the input of a VFD (Fig. 22.14) digresses greatly from the theoretical waveform.

22.2.8 Harmonic Limit Calculations Based on IEEE 519-1992

The IEEE 519-1992 [5] relies strongly on the definition of the point of common coupling or PCC. The PCC from the power utility point of view will usually be the point where power comes into the establishment (i.e., point of metering). However, the IEEE 519-1992 document also suggests that, “within an industrial plant, the point of common coupling (PCC) is the point between the nonlinear load and other loads” [1]. This suggestion is crucial since many plant managers and building supervisors feel that it is equally if not more important to keep the harmonic levels at or below acceptable guidelines within their facility. In view of the many recently reported problems associated with harmonics within industrial plants [2], it is important to recognize the need for mitigating harmonics at the point where the nonlinear load is connected to the power system. This approach would minimize harmonic problems, thereby reducing costly downtime and improving the life of electrical equipment. If harmonic mitigation is accomplished for individual nonlinear loads or a group of nonlinear loads collectively, then the total harmonics at the point of the utility connection will in most cases meet or better the IEEE recommended guidelines. In view of this, it is becoming increasingly common for project engineers and consultants to require nonlinear equipment suppliers to adopt the procedure outlined in IEEE 519-1992 to mitigate the harmonics to acceptable levels at the point of the offending equipment. For this to be interpreted equally by different suppliers, the intended PCC must be identified. If not defined clearly, many suppliers of nonlinear loads would likely adopt the PCC to be at the utility metering point, which would not benefit the plant or the building but rather the utility.

Having established that it is beneficial to adopt the PCC to be the point where the nonlinear load connects to the power system, the next step is to establish the short-circuit ratio. Short-circuit ratio calculations are key in establishing the allowable current harmonic distortion levels. For calculating the short-circuit ratio, the available short-circuit current at the input terminals of the nonlinear load needs to be determined. If the short-circuit value available at the low-voltage side of the utility transformer

TABLE 22.1 Current Distortion Limits for General Distribution Systems

I_{sc}/I_L	(120 V through 69,000 V)						TDD	
	Maximum Harmonic Current Distortion in Percent of I_L							
	Individual Harmonic Order (Odd Harmonics)							
I_{sc}/I_L	<11	11 ≤ h ≤ 17	17 ≤ h ≤ 23	23 ≤ h ≤ 35	35 ≤ h			
<20 ^a	4.0	2.0	1.5	0.6	0.3		5.0	
20 < 50	7.0	3.5	2.5	1.0	0.5		8.0	
50 < 100	10.0	4.5	4.0	1.5	0.7		12.0	
100 < 1000	12.0	5.5	5.0	2.0	1.0		15.0	
>1000	15.0	7.0	6.0	2.5	1.4		20.0	

Even harmonics are limited to 25% of the odd harmonic limits above.

^a All power generation equipment is limited to these values of current distortion, regardless of actual I_{sc}/I_L ; where I_{sc} is the maximum short-circuit current at PCC and I_L is the maximum demand load current (fundamental frequency) at PCC. TDD is total demand distortion and is defined as the harmonic current distortion in percent of maximum demand load current. The maximum demand current interval could be either a 15-min or a 30-min interval.

feeding the establishment (building) is known, and the cable and other series impedances in the electrical circuit between the low-voltage side of the transformer and the input to the nonlinear load are known, then the available short-circuit at the nonlinear load can be calculated. In practice, it is common to assume the same short-circuit current level as at the secondary of the utility transformer feeding the nonlinear load. The next step is to compute the fundamental value of the rated input current into the nonlinear load. In case the nonlinear load is a VFD operating an induction motor, the NEC amp rating for induction motors can be used to obtain this number. NEC amps are fundamental amps that a motor draws when connected directly to the utility supply. An example is presented here to recap the above procedure.

A 100-hp ASD–motor combination connected to a 480-V system being fed from a 1500-kVA, three-phase transformer with an impedance of 4% is required to meet IEEE 519-1992 at its input terminals. The rated current of the transformer is $1500 \times 1000 / (\sqrt{3} \times 480)$, which is calculated to be 1804.2 A. The short-circuit current available at the secondary of the transformer is equal to the rated current divided by the per unit impedance of the transformer. This is calculated to be 45,105.5 A. The short-circuit ratio, which is defined as the ratio of the short-circuit current at the PCC to the fundamental value of the nonlinear current, is computed next. NEC rating for a 100-hp, 460-V induction motor is 124 A. Assuming that the short-circuit current at the VFD input is practically the same as that at the secondary of the utility transformer, the short-circuit ratio is calculated to be: 45,105.5/124 which equals 363.75. On referring to the IEEE 519-1992 Table 22.1 [1], the short-circuit ratio falls in the 100–1000 category. For this ratio, the total demand distortion (TDD) at the point of VFD connection to the power system network is recommended to be 15% or less. For reference, Table 22.1 [1] is reproduced.

22.2.9 Harmonic Mitigating Techniques

Various techniques of improving the input current waveform are discussed below. The intent of all techniques is to make the input current more continuous to reduce the overall current harmonic distortion. The different techniques can be classified into three broad categories:

- a. Passive technique
- b. Active technique
- c. Hybrid technique—combination of passive and active techniques

There are three different options in the passive configuration. They are:

1. Addition of inductive impedance—line reactors or dc link chokes or both
2. Capacitor-based harmonic filters—tuned as well as broad band type
3. Multi-pulse techniques (12-pulse, 18-pulse, etc.)

This chapter will concentrate only on the passive techniques. Each of the mentioned passive options will be briefly discussed with their relative advantages and disadvantages.

22.2.10 Addition of Inductive Impedance

22.2.10.1 Three-Phase Line Reactors

A line reactor makes the current waveform less discontinuous resulting in lower current harmonics. Since the reactor impedance increases with frequency, it offers larger impedance to the flow of higher order harmonic currents.

On knowing the input reactance value, the expected current harmonic distortion can be estimated. A table illustrating the expected input current harmonics for various amounts of input reactance is shown below:

Percent Harmonics vs. Total Line Impedance

Harmonic	3%	4%	5%	6%	7%	8%	9%	10%
5th	40	34	32	30	28	26	24	23
7th	16	13	12	11	10	9	8.3	7.5
11th	7.3	6.3	5.8	5.2	5	4.3	4.2	4
13th	4.9	4.2	3.9	3.6	3.3	3.15	3	2.8
17th	3	2.4	2.2	2.1	0.9	0.7	0.5	0.4
19th	2.2	2	0.8	0.7	0.4	0.3	0.25	0.2
%THID	44.13	37.31	34.96	32.65	30.35	28.04	25.92	24.68
True rms	1.09	1.07	1.06	1.05	1.05	1.04	1.03	1.03

Input reactance is determined by the series combination of impedance of the ac reactor, input transformer (building–plant incoming-feed transformer), and power cable. By adding all the inductive reactance upstream, the effective line impedance can be determined and the expected harmonic current distortion can be estimated from the above chart. The effective impedance value in percent is based on the actual loading and is

$$Z_{\text{eff(pu)}} = \frac{\sqrt{3} \times 2\pi f \times L_T \times I_{\text{act(fnd.)}}}{V_{L-L}} \times 100 \quad (22.6)$$

$I_{\text{act(fnd.)}}$ is the fundamental value of the actual load current and V_{L-L} is the line–line voltage. L_T is the total inductance of all reactance upstream. The effective impedance of the transformer as seen from the nonlinear load is

$$Z_{\text{eff,x-mer}} = \frac{Z_{x-mer} \times I_{\text{act(fnd.)}}}{I_r} \quad (22.7)$$

$Z_{\text{eff,x-mer}}$ is the effective impedance of the transformer as viewed from the nonlinear load end; Z_{x-mer} is the nameplate impedance of the transformer; and I_r is the nameplate rated current of the transformer.

The reactor electrically separates the dc bus voltage from the ac source so that the ac source is not clamped to the dc bus voltage during diode conduction. This feature reduces flat topping of the ac voltage waveform caused by many VFDs when operated with weak ac systems.

However, introducing ac inductance between the diode input terminal and the ac source causes overlap of conduction between outgoing diode and incoming diode in a three-phase diode rectifier system. The overlap phenomenon reduces the average dc bus voltage. This reduction depends on the

duration of the overlap in electrical degrees, which in turn depends on the value of the intervening inductance used and the current amplitude. The duration of overlap in electrical degrees is commonly represented by μ . In order to compute the effect quantitatively, a simple model can be assumed. Assume that the line comprises of inductance L in each phase. Let the dc load current be I_{dc} and let it be assumed that this current does not change during the overlap interval. The current through the incoming diode at start is zero and by the end of the overlap interval, it is I_{dc} . Based on this assumption, the relationship between current and voltage can be expressed as

$$\begin{aligned} v_{ab} &= \sqrt{2}V_{L-L} \sin(wt) = 2L(di/dt) \\ \sqrt{2}V_{L-L} \int_{(\pi/3)}^{(\pi/3)+\mu} \sin(wt) d(t) &= 2L \int_0^{I_{dc}} di \\ I_{dc} &= \frac{\sqrt{2}V_{L-L}[\cos(\pi/3) - \cos(\pi/3 + \mu)]}{2wL} = \frac{\sqrt{2}V_{L-L}[\sin(\pi/3 + \mu/2) \sin(\mu/2)]}{wL} \end{aligned} \quad (22.8)$$

For small values of overlap angle μ , $\sin(\mu/2) = \mu/2$ and $\sin(\pi/3 + (\mu/2)) = \sin(\pi/3)$. Rearranging the above equation yields

$$\mu = \frac{2\sqrt{2}wLI_{dc}}{V_{L-L}\sqrt{3}} \quad (22.9)$$

From the above expression, the following observations can be made:

1. If the inductance L in the form of either external inductance or leakage inductance of transformer or lead length is large, the overlap duration will be large.
2. If the load current I_{dc} is large, the overlap duration is large.

The average output voltage will reduce due to the overlap angle as mentioned before. In order to compute the average output voltage with a certain overlap angle, the limits of integration have to be changed. This exercise yields the following:

$$\begin{aligned} V_0 &= \frac{3}{\pi} \int_{\mu+(\pi/3)}^{\mu+(2\pi/3)} \sqrt{2}V_{L-L} \sin(wt) d(wt) \\ V_0 &= \frac{3\sqrt{2}V_{L-L} \cos(\mu)}{\pi} = \frac{3\sqrt{2}\sqrt{3}V_{L-N} \cos(\mu)}{\pi} \end{aligned} \quad (22.10)$$

Thus, it can be seen that the overlap angle contributes to the reduction in the average value of the output dc bus voltage. Unfortunately, higher values of external inductive reactance increase the overlap angle, which in turn reduces the average output voltage as seen from the above equation.

22.2.10.2 DC Link Choke

Based on the above discussion, it can be noted that any inductor of adequate value placed in between the ac source and the dc bus capacitor of the VFD will help in making the input current waveform more continuous. Hence, a DC link choke, which is electrically present after the diode rectifier bridge and before the dc bus capacitor, can be used to reduce the input current harmonic distortion. The dc link choke appears to perform similar to the three-phase line inductance. However, on analyzing the behavior of the dc link choke, it can be seen that the dc link choke behaves similar to the input ac line inductor only from current distortion point of view but has a completely different influence on the average output voltage.

An important difference is that the DC link choke is after the diode rectifier block and so they do not contribute to the overlap phenomenon discussed earlier with regard to external ac input reactors. Hence,

there is no dc bus voltage reduction similar to the way as experienced when ac input reactors are used. The DC link choke increases the diode conduction duration. There is a critical DC link choke inductance value, which when exceeded will result in complete 60° conduction of a diode pair. Any value of dc link inductance beyond this critical value is of no further importance and thus introducing a very large dc link inductor will have no further benefit. A larger inductance value will only be associated with a higher winding resistance and cause marginally extra voltage drop across the winding resistance, resulting in higher power loss without altering the input current distortion or the average output dc voltage significantly. The critical DC link choke that is needed to achieve complete 60° -conduction is derived next.

It is assumed that the source is ideal with zero impedance. The forward voltage drop across the conducting diodes is also neglected. When no dc link inductance is used, the dc bus charges up to the peak of the input ac line and since the source is assumed ideal and the voltage drop across the diode is neglected, the average dc bus voltage remains at the peak of the input ac line-line voltage even under the loaded condition. This assumption is not true and corrections for this will be made later. The critical inductance is that value which will result in the average dc bus voltage to drop from its peak value to the average three-phase rectified value. The voltage across the dc link inductor absorbs the difference. Mathematically, the following is true:

$$\begin{aligned} L_{\text{cr}} \frac{\Delta i}{\Delta t} &= V_m - V_{3\text{-ph-avg}} = V_m - \frac{3V_m}{\pi} \\ L_{\text{cr}} &= \frac{\pi - 3}{\pi} V_m \frac{\Delta t}{\Delta i} = \frac{\pi - 3}{\pi} V_m \frac{T/6}{I_{\text{dc}}} \end{aligned} \quad (22.11)$$

L_{cr} is the critical value of the DC link choke and I_{dc} is the load current. The change in current Δi in the above equation is the difference from no-load condition to rated-load condition. Hence, Δi is the rated average DC link current that flows continuous for a 60° conduction interval. T is the period of the input AC supply. In Eq. (22.11), it should be pointed out that if continuous current conduction for 60° duration is desired at a lower value of DC load current, a DC link inductor of a large value is required.

From the expression for the critical dc link inductance, it is seen that the value depends on the load condition, frequency of the input ac supply and the peak value of the input ac line-line voltage, V_m . It is also interesting to note that the value of the critical dc link inductor for a 240 V system for the same load is 1/4th the value for a 480 V system.

22.2.11 Capacitor-Based Passive Filters

Passive filters consist of passive components like inductors, capacitors, and resistors arranged in a predetermined fashion either to attenuate the flow of harmonic components through them or to shunt the harmonic component into them. Passive filters can be of many types. Some popular ones are: series passive filters, shunt passive filters, and low-pass broadband passive filters. Series and shunt passive filters are effective only in a narrow proximity of the frequency at which they are tuned. Low-pass broadband passive filters have a broader bandwidth and attenuate a larger range of harmonics above their cutoff frequency.

22.2.11.1 Series Passive Filter

One way to mitigate harmonics generated by nonlinear loads is to introduce a series passive filter (Fig. 22.15) in the incoming power line so that the filter offers high impedance to the flow of harmonics from the source to the nonlinear load. Since the series passive filter is tuned to a particular frequency, it offers high impedance at only its tuned frequency. Depending on the physical property of L and C chosen, typically there exists a narrow band around the tuned frequency where the impedance remains high.

Series passive filters have been used more often in single-phase applications where it is effective in attenuating the 3rd harmonic component. The series pass filter is generally designed to offer low

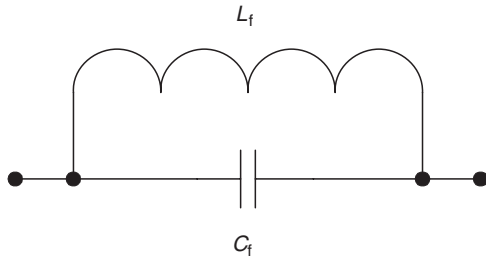


FIGURE 22.15 Single-phase representation of a series filter configuration.

passive filter is placed across the incoming line and is designed to offer very low impedance to current components corresponding to its tuned frequency. Another way of explaining the behavior of a shunt filter is to consider the energy flow from the source to the nonlinear load via the shunt filter. Energy at fundamental frequency flows into the shunt passive filter and the energy at the filter's tuned frequency flows out of the shunt filter since it offers lower impedance for flow of energy at its tuned frequency compared to the source. In other words, the harmonic component needed by the nonlinear load is provided by the shunt filter rather than the ac source.

The fundamental frequency energy component flowing into the shunt filter is the reason for leading VARs and can cause over-voltage at the filter terminals. This can create problems with VFDs that are vulnerable to higher than normal voltage and under light-load condition can encounter over-voltage trips.

Similar to the series tuned filter, the shunt tuned filter is effective only at and around its tuned frequency and only one section of the filter alone is inadequate to provide for all the harmonic energy needed by a typical nonlinear load (VFD). Multiple sections are needed, which makes them bulky and expensive.

The commonly used three-phase shunt filter sections comprise of individual sections tuned for a 5th, 7th, and perhaps a high-pass section typically tuned near the 11th harmonic. Unfortunately, if care is not taken, the shunt filter will try to provide the harmonic energy needed by all nonlinear loads connected across its terminals. In this process, it can be overloaded and be damaged if unprotected. In order to avoid import of harmonics, it is important to use series line reactors, which impede the harmonic energy flow from other sources into the shunt tuned filter sections, as shown in Fig. 22.17. However, the addition of extra line inductance can aggravate the over-voltage condition experienced by inverter drive systems at light-load conditions. The over-voltage tolerance margin would be compromised and the VFD could be more vulnerable to fault out on over-voltage thereby causing nuisance trips. The probability of this occurrence increases if the installation happens to be close to a capacitor-switching utility substation.

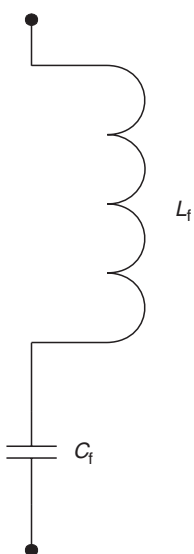


FIGURE 22.16 Single-phase representation of a shunt-tuned filter configuration.

impedance at the fundamental frequency. A major drawback of this approach is that the filter components have to be designed to handle the rated load current. Further, one filter section is not adequate to attenuate the entire harmonic spectrum present in the input current of a nonlinear system. Multiple sections may be needed to achieve this, which makes it bulky and expensive.

22.2.11.2 Shunt Passive Filter

The second and more common approach is to use a shunt passive filter, as shown in Fig. 22.16. The shunt

filter is placed across the incoming line and is designed to offer very low impedance to current components corresponding to its tuned frequency. Another way of explaining the behavior of a shunt filter is to consider the energy flow from the source to the nonlinear load via the shunt filter. Energy at fundamental frequency flows into the shunt passive filter and the energy at the filter's tuned frequency flows out of the shunt filter since it offers lower impedance for flow of energy at its tuned frequency compared to the source. In other words, the harmonic component needed by the nonlinear load is provided by the shunt filter rather than the ac source.

The fundamental frequency energy component flowing into the shunt filter is the reason for leading VARs and can cause over-voltage at the filter terminals. This can create problems with VFDs that are vulnerable to higher than normal voltage and under light-load condition can encounter over-voltage trips.

Similar to the series tuned filter, the shunt tuned filter is effective only at and around its tuned frequency and only one section of the filter alone is inadequate to provide for all the harmonic energy needed by a typical nonlinear load (VFD). Multiple sections are needed, which makes them bulky and expensive.

The commonly used three-phase shunt filter sections comprise of individual sections tuned for a 5th, 7th, and perhaps a high-pass section typically tuned near the 11th harmonic. Unfortunately, if care is not taken, the shunt filter will try to provide the harmonic energy needed by all nonlinear loads connected across its terminals. In this process, it can be overloaded and be damaged if unprotected. In order to avoid import of harmonics, it is important to use series line reactors, which impede the harmonic energy flow from other sources into the shunt tuned filter sections, as shown in Fig. 22.17. However, the addition of extra line inductance can aggravate the over-voltage condition experienced by inverter drive systems at light-load conditions. The over-voltage tolerance margin would be compromised and the VFD could be more vulnerable to fault out on over-voltage thereby causing nuisance trips. The probability of this occurrence increases if the installation happens to be close to a capacitor-switching utility substation.

22.2.11.3 Low-Pass Broadband Filter

The low-pass broadband filter [6] is similar to the circuit configuration of Fig. 22.17. To improve the filtering performance, the inductor L_s is substituted by L_f and there is no series inductor with C_f . By removing L_f from the shunt path, the filter configuration changes from tuned type to broadband type. One advantage of the low-pass broadband harmonic filter is that unlike the shunt and series type filters, the broadband filter need not be configured in multiple stages or sections to offer wide spectrum filtering. In other words, one filter section achieves the performance close to the combined effect of the 5th, 7th, and the high-pass shunt tuned filter section. A typical broadband filter section is shown in Fig. 22.18. The series inductor L_f offers high impedance to limit

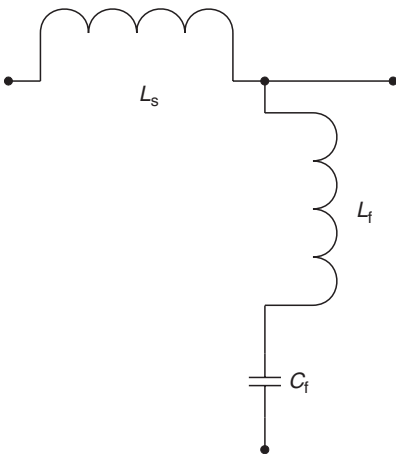


FIGURE 22.17 Shunt tuned filter section with a series inductor to prevent import of harmonics.

number for that converter. Higher the pulse number, lower is the total harmonic distortion since the order of the characteristic harmonics shifts to a higher value. Pulse number is defined as the number of diode-pair conduction intervals that occur in one electrical cycle. In a three-phase, six-diode bridge rectifier, the number of diode-pair conduction intervals is six and such a rectifier is known as a six-pulse rectifier. By using multiple six-pulse diode rectifiers in parallel and phase shifting the input voltage to each rectifier bridge by a suitable value, multi-pulse operation can be achieved.

22.2.12.1 Twelve-Pulse Techniques

A 12-pulse rectifier operation can be achieved by using two six-pulse rectifiers in parallel with one rectifier fed from a power source that is phase shifted with respect to the other rectifier by 30 electrical degrees. The 12-pulse rectifier will have the lowest harmonic order of 11. In other words, the 5th, and the 7th harmonic orders are theoretically nonexistent in a 12-pulse converter. Again, as mentioned in [Section 22.2.7](#), the amplitude of the characteristic harmonic is typically proportional to the inverse of the harmonic order. In other words, the amplitude of the 11th harmonic in a 12-pulse system will be 1/11 of the fundamental component and the amplitude of the 13th harmonic will be 1/13 of the

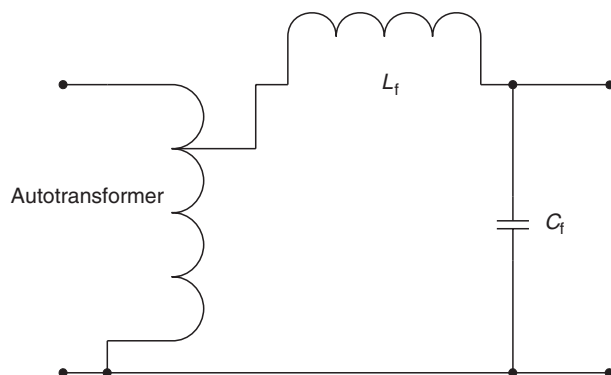


FIGURE 22.18 Broadband filter section with autotransformer.

import and export of harmonics from and to other non-linear loads on the system [2].

However, removing L_f from the shunt branch and moving it to the series branch aggravates the over-voltage problem experienced by VFDs. Autotransformers have been used in the past to address this problem. Since the over-voltage is a function of the load current, the correction offered by auto-transformer works only at one operating point at best and is inadequate to handle a wide range of operating conditions. In addition, the size and cost of the total filter configuration becomes high and less appealing. The leading VAR problem is not resolved and in fact has been found to interfere with power measurement and monitoring systems. These unfavorable features are serious enough to limit the use of such filters for VFD applications.

22.2.12 Multi-Pulse Techniques

As discussed earlier, the characteristic harmonics generated by a semiconductor converter are a function of the pulse number

fundamental component. There are many different ways of achieving the necessary phase shift to realize 12-pulse operation. Some popular methods are:

- Three winding isolation transformer
- Hybrid 12-pulse method
- Autotransformer method

22.2.12.1.1 Three Winding Isolation Transformer Method

A three winding isolation transformer has three different sets of windings. One set of winding is typically called the primary, while the other two sets are called secondary windings. The primary winding can be connected in delta or wye configuration. One set of secondary winding is connected in delta while the other set is connected in wye configuration. This arrangement automatically yields a 30° phase shift between the two sets of secondary windings. A traditional 12-pulse arrangement using a three winding isolation transformer is shown in Fig. 22.19. The realization of 12-pulse operation in the circuit of Fig. 22.19 is discussed next.

The current flowing out of the secondary windings, viewed independently, is similar to that observed in a six-pulse rectifier. However, since the voltages are phase shifted by 30 electrical degrees, the currents are also phase shifted by the same amount. In other words, if i_1 is the fundamental current through one set of secondary windings, and i_2 is the 30° phase-shifted current in the other set of secondary windings, then i_1 and i_2 can be expressed as follows:

$$\begin{aligned} i_1 &= I_m \sin(\omega t) \\ i_2 &= I_m \sin\left(\omega t - \frac{\pi}{6}\right) \end{aligned} \quad (22.12)$$

The 5th harmonic component of the current in one of the secondary windings will be phase shifted with respect to its corresponding phase in the other set. However, it should be noted that the phase shift will get multiplied by the harmonic number as well. The 5th harmonic component in the two sets of windings can be represented as follows:

$$\begin{aligned} i_{5(1)} &= I_{5m} \sin(5 \cdot \omega t) \\ i_{5(2)} &= I_{5m} \sin\left(b5\omega t - \frac{5\pi}{6} - \frac{\pi}{6}\right) = -I_{5m} \sin(5\omega t) \end{aligned} \quad (22.13)$$

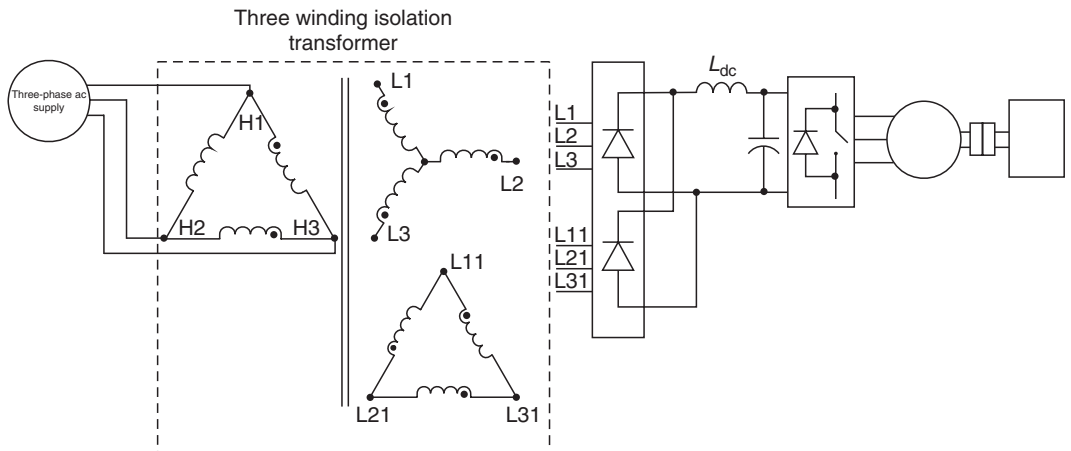


FIGURE 22.19 Typical schematic of a 12-pulse configuration using a three winding isolation transformer. DC link choke improves performance.

Similar expressions can be written for the 7th harmonic currents in each set of the secondary windings. From the above expressions, it can be said that the flux pattern formed by the 5th and 7th harmonic components by one set of secondary windings is theoretically equal and opposite to the 5th and 7th harmonic flux components produced by the second set of secondary windings. Consequently, there are no 5th and 7th harmonic components reflected on to the primary windings and so the 5th and 7th harmonic components do not theoretically exist in the input AC supply feeding the primary windings.

Based on the above explanation, it can be said that in a three winding isolation transformer arrangement, magnetic flux coupling plays an important role in assuring the elimination of low order current harmonics. Any departure from the ideal scenario assumed above will yield sub-optimal flux cancellation and higher total current harmonic distortion. Leakage flux and the primary magnetizing flux create nonideal conditions and are responsible for the existence of noncharacteristic harmonics in the input current of a typical 12-pulse system. Minor winding imbalance between the two sets of secondary windings also contributes to sub-optimal performance.

22.2.12.1.1.1 Advantages Some important advantages of the three winding isolation transformer configuration to achieve 12-pulse operation are listed below:

- Twelve-pulse operation yields low total current harmonic distortion.
- Three winding arrangement yields isolation from the input ac source, which has been seen to offer high impedance to conducted EMI.
- It offers in-built impedance due to leakage inductance of transformer. This smoothes the input current and helps further reduce the total current harmonic distortion.
- It is ideally suited for voltage level translation. If the input is at a high voltage (3.2 or 4.16 kV), and the drive system is rated for 480 V operation, this is ideal to step-down and to achieve the benefits of 12-pulse operation.

22.2.12.1.1.2 Disadvantages In spite of its appeal, the three winding isolation transformer configuration has a few shortcomings listed below:

- Three winding transformer has to be rated for full power operation, which makes it bulky and expensive.
- Leakage inductance of the transformer will cause reduction in the dc bus voltage, which will require the use of taps in the primary winding to compensate for this drop. Addition of taps will increase cost.
- Due to minor winding mismatch, leakage flux, and nontrivial magnetizing current, the total current harmonic distortion can be higher than expected.
- Needs the VFD to be equipped with two six-pulse rectifiers that increases the cost of the VFD.

22.2.12.1.2 Hybrid 12-Pulse Method

One disadvantage of the three winding arrangement mentioned earlier is its size and cost. On re-examining the circuit of Fig. 22.6, it can be noted that one set of winding does not have any phase shift with respect to the primary winding. This is important because it allows one six-pulse rectifier circuit to be directly connected to the ac source via some balancing inductance to match the inductance in front of the other six-pulse rectifier circuit to achieve 12-pulse operation.

The resulting scheme has one six-pulse rectifier powered via a phase-shifting isolation transformer, while the other six-pulse rectifier is fed directly from the ac source via matching impedance. Such a 12-pulse arrangement is called a hybrid 12-pulse configuration and is shown in Fig. 22.20. The phase-shifting transformer feeding one of the two six-pulse rectifiers is sized to handle half the rated power. Similarly, the matching inductor is sized to carry only half the rated current. This arrangement results in the overall size of the transformer and matching inductor combination to be smaller and less expensive than the three winding arrangement.

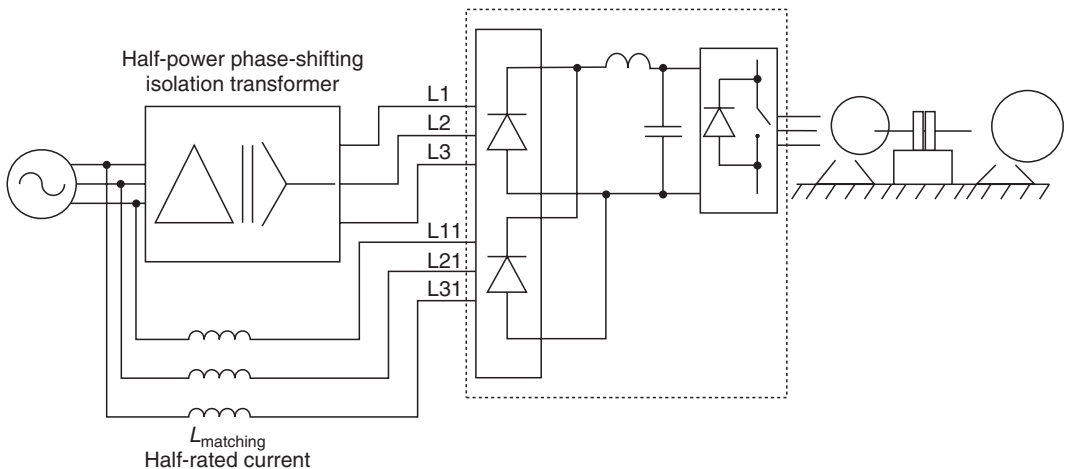


FIGURE 22.20 Schematic of a typical hybrid 12-pulse arrangement.

22.2.12.1.2.1 Advantages

Some important advantages of the hybrid 12-pulse are listed below:

- Size and cost of the hybrid 12-pulse configuration is much less than the 3-winding arrangement.
- Twelve-pulse operation is achieved with low total current harmonic distortion.
- Unlike the 3-winding method, in this method the currents (instead of flux in the core) in the two bridges are combined at the source to cancel the low order harmonics. Leakage flux and winding mismatch problems do not occur.

22.2.12.1.2.2 Disadvantages

The hybrid version also has some important disadvantages that need to be pointed out. They are as follows:

- Impedance mismatch between the leakage inductance and the external matching inductance can never be accomplished for all operating conditions because the leakage inductance is a function of current through the transformer while the external inductance is in the form of self-inductance, which is constant till its rated current value.
- In order to minimize the effect of mismatch, an input ac line inductor may need to be used sometimes to comply with the harmonic levels recommended in IEEE 519 (1992).
- Use of extra inductance ahead of the transformer-inductor combination can cause extra voltage drop that cannot be compensated for.
- Arrangement of Fig. 22.20 cannot be used where level translation is needed.
- Advantage of high impedance to conducted EMI as offered by the three winding arrangement is lost on using the hybrid arrangement of Fig. 22.20.
- Similar to the three winding configuration, this method also requires the VFD to have two six-pulse rectifiers.

It should be pointed out that in spite of the shortcomings listed above this method is gaining in popularity primarily because of size and cost advantage. The transformer leakage inductance and the external matching inductance are matched to perform at rated current so that low harmonic distortion is achieved at rated operating conditions.

22.2.12.1.3 Autotransformer Method

The phase shift necessary to achieve multi-pulse operation can also be achieved by using autotransformers. Autotransformers do not provide any isolation between the input and output but can be used to

provide phase shift. Autotransformers are typically smaller compared to regular isolation transformers because they do not need to process the entire power. Majority of the load current passes directly from the primary to the secondary terminals and only a small amount of VA necessary for the phase shift is processed by the autotransformer. This makes them small, inexpensive, and attractive for use in multi-pulse systems.

Though autotransformers are appealing for multi-pulse applications, they are not well suited for single VFD load. In all ac to dc rectification schemes, the diode pair that has the highest voltage across the input terminals conducts to charge the dc bus. When parallel rectifiers are used as in multi-pulse techniques, it is important to maintain sharing of current among the multi-pulse rectifiers. If current sharing is compromised, then the amplitudes of lower order harmonics between the two rectifiers in a 12-pulse scheme will not cancel completely and this will result in poor harmonic performance. By electrically isolating one rectifier from the other in the two schemes discussed thus far, acceptable 12-pulse performance was possible. However, when autotransformers are employed, such isolation is lost and current from one set of phase-shifted windings can flow into the other set, thereby compromising the equal distribution of current between the phase-shifted sets of windings. One way to force the rectifiers to share correctly is to introduce an inter-phase transformer (IPT) in between the outputs of the two diode-rectifier units as shown in Fig. 22.21. A zero sequence blocking transformer (ZSBTs) in between the rectifier and one of the phase-shifted outputs of the autotransformer also helps in reducing non-characteristic triplen harmonics from flowing into the ac system. The autotransformer of Fig. 22.8 has phase-shifted outputs of $\pm 15^\circ$.

The use of ZSBT and IPT makes the overall system bulky and expensive and the choice of autotransformer less appealing. However, in many cases, the VFD is not equipped with two rectifier units and so none of the 12-pulse schemes can be really used in such cases. In such applications, if multiple VFDs are being employed and they can be paired into approximately equal ratings, then the delta-fork autotransformer shown in Fig. 22.21 can be effectively implemented. Instead of isolating the two diode rectifier units in one VFD, it is possible to use two different VFDs operating two independent loads of approximately equal rating and supplying them power from the phase-shifted outputs of the delta-fork transformer. This type of matched pair possibilities exists in a given system and is ideal for VFDs that do not have two independent six-pulse rectifier units. One such scheme of distributing the load between the phase-shifted outputs of a delta-fork autotransformer is shown in Fig. 22.22. This arrangement has been seen in the field to achieve low total current harmonic distortion even with load imbalance in the neighborhood of 20–25%.

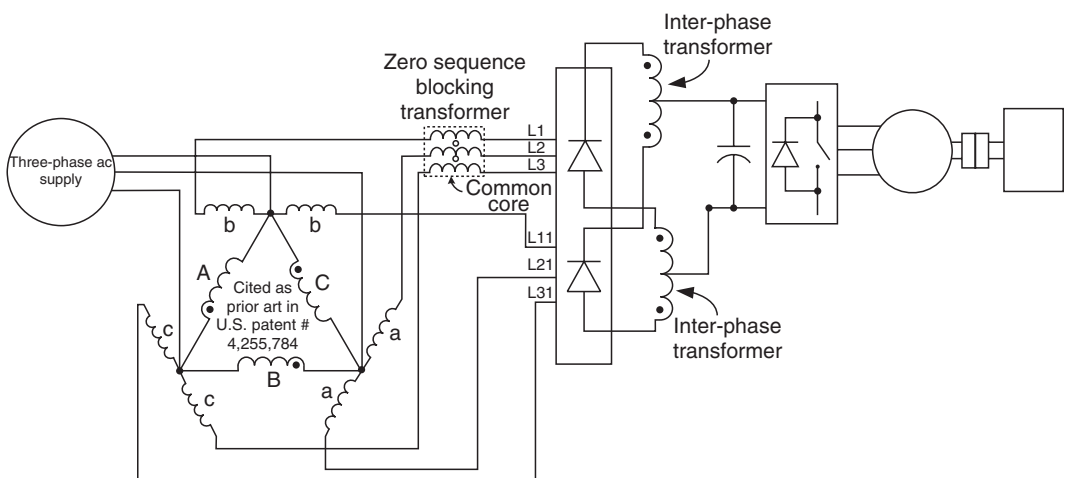


FIGURE 22.21 Delta-fork autotransformer with ZSBT and IPT for 12-pulse applications.

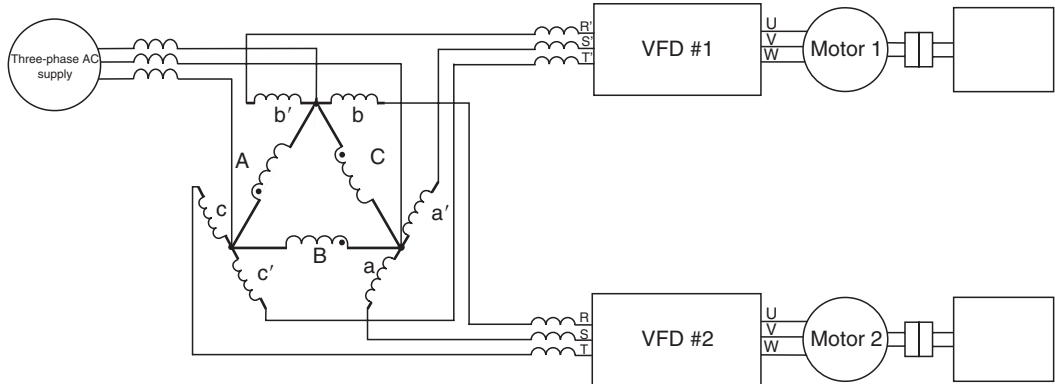


FIGURE 22.22 Use of low cost autotransformer for 12-pulse operation in case of isolated and balanced loads.

22.2.12.1.3.1 Advantages Some important advantages of the autotransformer connection shown in Fig. 22.22 are listed below:

- VFDs do not need to have multiple rectifier units to achieve benefits of 12-pulse operation.
- Size and cost of autotransformer is small and unlike the circuit of Fig. 22.21, there is no need for IPTs and ZSBTs.
- Three-phase input ac reactor in front of each VFD helps in making the current more continuous. These may be replaced by dc link chokes.

22.2.12.1.3.2 Disadvantages The circuit of Fig. 22.22 has a few shortcomings and the reader should be aware of these. They are as follows:

- Better harmonic performance is achieved if the loads are balanced. Since the loads are independent, many times it is not possible to guarantee balance and this may reduce the overall harmonic performance.
- Input ac line inductors or dc link chokes may be necessary to get better harmonic performance.
- VFDs need to be isolated to prevent cross current flow between the two sets of windings and to assure good sharing.

22.2.12.2 Eighteen-Pulse Techniques

Harmonic distortion concerns are serious when the power ratings of the VFD load increase. Large power VFDs are gaining in popularity due to their low cost and impressive reliability. Use of large power VFDs increases the amplitude of low order harmonics that can impact the power system significantly. In many large power installations, current harmonic distortion levels achievable using the 12-pulse technique is insufficient to meet the levels recommended in IEEE 519 (1992). In view of this, lately, quite a lot of interest has been shown in developing the 18-pulse VFD systems to achieve much superior harmonic performance compared to the traditional 12-pulse systems.

The 18-pulse systems have become economically feasible due to the recent advances in autotransformer techniques that help reduce the overall cost and achieve low total current harmonic distortion. As mentioned earlier, when employing autotransformers, care should be taken to force the different rectifier units to share the current properly. The 18-pulse configuration lends itself better in achieving this goal compared to the 12-pulse scheme. Some popular 18-pulse autotransformer techniques are discussed next.

For 18-pulse operation, there is need for three sets of three-phase ac supply that are phase shifted with respect to each other by 20 electrical degrees. Traditionally, this is achieved using a four winding isolation transformer that has one set of primary windings and three sets of secondary windings. One set of secondary winding is in-phase with the primary winding, while the other two sets are phase shifted

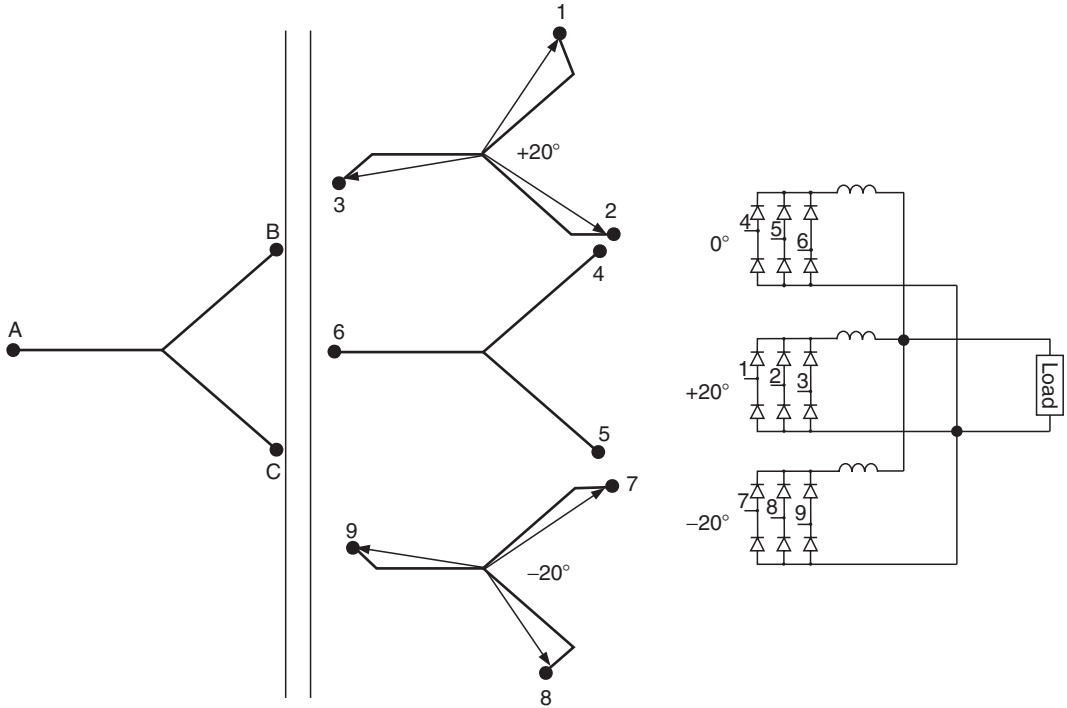


FIGURE 22.23 Schematic representation of 18-pulse converter circuit fed from phase-shifted isolation transformer.

by ± 20 electrical degrees and -20 electrical degrees with the primary. This arrangement yields three phase-shifted supplies that allow 18-pulse operation as shown in Fig. 22.23.

The use of dc link choke as shown in Fig. 22.23 is optional. The leakage inductance of the transformer may be sufficient to smooth the input current and improve the overall current harmonic distortion levels. The primary disadvantage of the scheme shown in Fig. 22.23 is that the phase-shifting isolation transformer is bulky and expensive. A common disadvantage with all 18-pulse schemes is that all of them need three independent three-phase rectifier units. Many VFD manufacturers do not provide this feature and the additional rectifier units needed may have to be provided external to the VFD.

Instead of using $\pm 20^\circ$ phase-shifted outputs from isolation transformer for 18-pulse operation, a nine-phase supply where each phase lags the other by 40 electrical degrees can be used. Some patents that propose this scheme [3] are shown in Fig. 22.24.

Figure 22.24a shows a nine-phase ac supply using wye-fork with a tertiary delta winding to circulate triplen harmonics. The size of the autotransformer is big and there is a need for additional series impedance to smoothen the input ac currents. The rating of the transformer is about 70% of the rating of the load. If the series inductance is not used, then the output dc voltage is about 4.3% higher than that achieved when a standard six-pulse rectifier is used.

Figure 22.24b shows a nine-phase ac supply using delta-fork that does not require additional delta winding. In this configuration, the average dc output voltage is about 14% higher than that obtained using a standard six-pulse rectifier scheme. This can potentially stress the dc bus capacitors and the IGBTs in the inverter section of a VFD. In order to overcome this, additional teaser windings are used as shown. These windings not only add cost and increase the overall rating of the transformer, they also cause imbalance that results in higher than normal circulating currents in the delta windings, which need to be accommodated. The harmonic performance is good but the overall size is large with rated current flow through the teaser windings.

In order to overcome the 14% higher average dc bus voltage observed in the previous configuration, a modification of the configuration was proposed in the patent cited in Fig. 22.24c. The harmonic

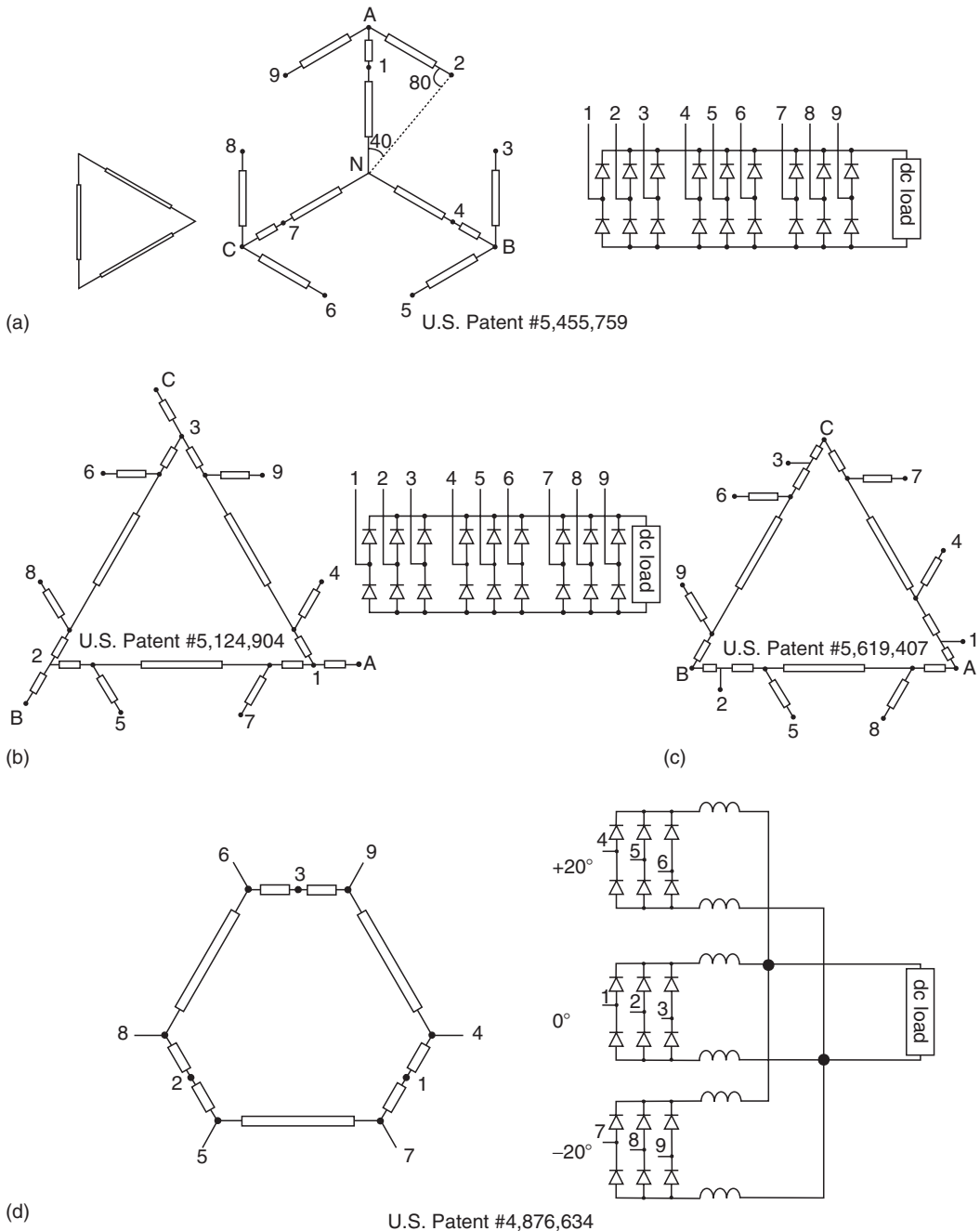


FIGURE 22.24 Autotransformer methods of achieving 18-pulse operation.

performance is equally good and the average dc bus voltage is equal to that observed in six-pulse rectifiers. Similar to the previous configuration, the stub winding currents are high and the teaser winding needs to carry rated load current making the overall transformer big in size and expensive to wind.

In autotransformer configurations using stub or teaser windings shown in Figs 22.24a through c, the overall size and rating of the autotransformer is higher than the optimal value. Use of stub windings typically results in poor utilization of the core and involves more labor to wind the coils. Polygon type of

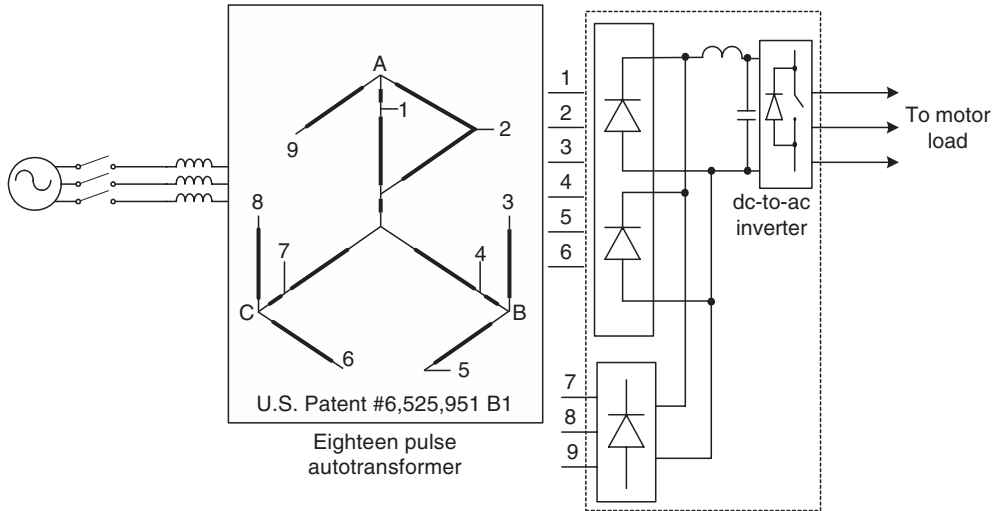


FIGURE 22.25 Schematic of the modified windmill construction of the 18-pulse autotransformer configuration for used with VFDs.

autotransformer is better than stub type autotransformer from size and core utilization points of view. A polygon type autotransformer is shown in Fig. 22.24d. It should be pointed out that the configuration of Fig. 22.24d needs the use of IPTs and input ac inductors to achieve low total current harmonic distortion. The reason is that the outputs are not equally spaced to achieve a nine-phase ac supply as in the previous configurations. The polygon autotransformer of Fig. 22.24d provides $+/-20^\circ$ phase-shifted outputs to achieve 18-pulse operation.

One of the widely used 18-pulse autotransformer configurations is that shown in Fig. 22.25. This configuration is a modified version of the configuration shown in Fig. 22.24a and was proposed by the same author. In the configuration of Fig. 22.25, the delta-connected tertiary winding is included in the wye-fork. This construction is called the windmill construction. Initially the windmill structure was present in each phase and the size of the transformer was still big. The kVA rating was about 60%. By intelligently removing the windmill structure from two of the three phases, it was shown that the performance remained equally good. By adopting the modified structure of Fig. 22.25, the kVA rating of the autotransformer was reduced from 60 to 55%.

In all the 18-pulse autotransformer methods, the change of current from one conducting diode pair to the other is quite sudden. Though the rms current rating may not exceed the current rating of the diode, attention should be given to the di/dt of the current through the diodes. Since the use of autotransformer method of 18-pulse operation is recent, there is not much statistical data available to comment on the di/dt issue with diodes when used in conjunction with 18-pulse autotransformer techniques.

22.2.12.3 Harmonic Mitigation Technique Summary

This section discusses generation of current harmonics by nonlinear loads and the IEEE 519-1992 standard to limit the quantity of these harmonics. A methodology of applying this standard to a practical industrial site has been described. Different harmonic mitigating techniques presently available in the industry have been highlighted. Multi-pulse techniques to achieve low total current harmonic distortion have been discussed. Relative advantage and disadvantage of the techniques presented have also been discussed. Based on the materials presented in this report, the following important conclusions can be drawn:

- a. Passive techniques involving capacitors are associated with circulating current, leading power factor, and high dc bus voltage at light-load condition and hence should be avoided as far as possible. They are also associated with the possibility of causing network resonance and hence if they are installed, care should be taken to monitor resonance conditions and avoid them.

- b. DC link chokes are a better alternative than ac line reactors for harmonic mitigation since they do not cause additional voltage drop if the value is greater than the critical inductance.
- c. To handle transients and surges on the ac line, a combination of small value of ac inductance and dc link choke is preferred.

Multi-pulse techniques offer the best passive solution to handle harmonics. The 18-pulse autotransformer technique and the pseudo 12-pulse technique are attractive for medium power applications, whereas distributing the load on phase-shifted outputs of an autotransformer for small power application is an interesting alternative.

22.2.12.4 Active Harmonic Compensation

Most passive techniques discussed above aim to cure the harmonic problems once nonlinear loads have created them. However, motor-drive manufacturers are developing rectification techniques that do not generate low order harmonics. These drives use active front ends. Instead of using diodes as rectifiers, the active front-end ASDs make use of active switches like IGBTs along with anti-parallel diodes. In such active front-end rectifiers, power flow becomes bi-directional. The input current can be wave shaped and made sinusoidal to have low values of low order harmonics.

Apart from the active front ends, there also exist shunt active filters used for actively introducing a current waveform into the ac network, which when combined with the harmonic current results in an almost perfect sinusoidal waveform.

Interesting and effective combinations of passive tuned and active components have been proposed by many researchers and quite a few of them are reportedly in use in the steel, rail, and power utility industries. Such combination topologies are commonly referred to as Hybrid Structures and have been extensively researched by authors of reference [7].

Most active filter topologies are cost effective in high power ratings but require high initial investment. Hybrid filters also have large bandwidth and good dynamic response. Control is accomplished using digital signal processing (DSP) chips. The hybrid structures also need current and voltage sensors and corresponding analog to digital (A/D) converters. Manufacturers of smaller power equipment like computer power supplies, lighting ballast, etc. have successfully employed active circuits, employing boost converter topologies.

22.3 Controlled Rectifiers

Controlled rectifier circuits make use of controlled switches. One such device is the thyristor. A thyristor is a four-layer (*p-n-p-n*), three-junction device that conducts current only in one direction similar to a diode. The junction marked J3 in Fig. 22.26 is utilized as the control junction and consequently the rectification process can be initiated at will provided the device is favorably biased and the load is of favorable magnitude. The operation of a thyristor can be explained by assuming it to be made up of two transistors connected back-to-back as shown in Fig. 22.26.

Let α_1 and α_2 be the ratio of collector to emitter currents of transistors Q1 and Q2, respectively. In other words,

$$\alpha_1 = \frac{I_{c1}}{I_{e1}}; \quad \alpha_2 = \frac{I_{c2}}{I_{e2}}$$

Also, from Fig. 22.26 $I_{e1} = I_{e2} = I_A$, where I_A is the anode current flowing through the thyristor. From transistor theory, the value of I_{e2} is equal to $I_{c2} + I_{b2} + I_{lkg}$, where I_{lkg} is the leakage current crossing the *n1-p2* junction. From Fig. 22.26, $I_{b2} = I_{c1}$. Hence, the anode current can be rewritten as

$$I_A = I_{c1} + I_{c2} + I_{lkg} \quad (22.14)$$

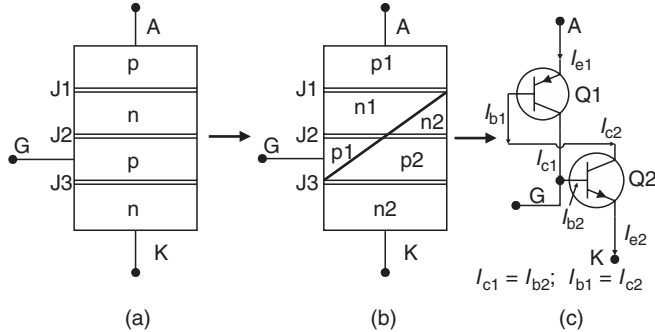


FIGURE 22.26 Virtual representation of a thyristor to explain its operation.

Substituting the collector currents by the product of ratio α and emitter current, the anode current becomes

$$\begin{aligned} I_A &= \alpha_1 I_{e1} + \alpha_2 I_{e2} + I_{lkg} \\ I_A &= (\alpha_1 + \alpha_2) I_A + I_{lkg} \\ I_A &= \frac{I_{lkg}}{1 - (\alpha_1 + \alpha_2)} \end{aligned} \quad (22.15)$$

If the ratio of the collector current to base current (gain) of the transistors is assumed to be β_1 and β_2 , respectively, then the relationship between β_1 , β_2 and α_1 , α_2 can be written as

$$\alpha_1 = \frac{\beta_1}{1 + \beta_1}; \quad \alpha_2 = \frac{\beta_2}{1 + \beta_2} \quad (22.16)$$

Substituting for α_1 and α_2 in the expression for I_A yields the following expression:

$$I_A = \frac{(1 + \beta_1)(1 + \beta_2)I_{lkg}}{1 - \beta_1\beta_2} \quad (22.17)$$

If the values of α_1 and α_2 are low (low gains), then the anode current is low and comparable to the leakage current. Under this condition, the thyristor is said to be in its OFF state. However, if the effective gain of the transistor is such that the product of the gains is close to 1 (i.e., sum of the ratios of α_1 and α_2 are close to 1), then there is a large increase in anode current and the thyristor is said to be in conduction. External circuit conditions can be changed to influence the product of the gains ($\beta_1\beta_2$). Some techniques of achieving this are briefly discussed next.

- Increasing applied voltage: On applying a voltage across the anode to cathode terminals of the thyristor (anode being more positive than the cathode), junctions J1 and J3 in Fig. 22.26 are forward biased while junction J2 is reverse biased. The thyristor does not conduct any current and is said to be in a blocking state. On increasing the applied voltage, minority carriers in junction J2 (i.e., holes in n1, n2 and electrons in p1, p2) start acquiring more energy and hence start to migrate. In this process, these holes could dislodge more holes. Recombination of the electrons and holes also occur, which creates more motion. If the voltage is increased beyond a particular level, the movement of holes and electrons becomes great and junction J2 ceases to exist. The product of the gains of the two transistors in the two-transistor model is said to achieve values close to unity. This method of forcing current to flow through the thyristor is not recommended

since junction J2 gets permanently damaged and the thyristor ceases to block forward voltage. Hence, this method is a destructive method.

- b. High dv/dt : As explained earlier, junction J2 is the forward blocking junction when a forward voltage is applied across anode to cathode of a thyristor. Any p-n junction behaves like a depletion region when it is reverse biased. Since J2 is reverse biased, this junction behaves like a depletion region. Another way of looking at a depletion region is that the boundary of the depletion region has abundant holes and electrons while the region itself is depleted of charged carriers. This characteristic is similar to that of a capacitor. If the voltage across the junction (J2) changes very abruptly, then there will be rapid movement of charged carriers through the depleted region. If the rate of change of voltage across this junction (J2) exceeds a predetermined value, then the movement of charged carriers through the depleted region is so high that junction J2 is again annihilated. After this event, the thyristor is said to have lost its capability to block forward voltage and even a small amount of forward voltage will result in significant current flow, limited only by the load impedance. This method is destructive too and is hence not recommended.
- c. Temperature: Temperature affects the movement of holes and electrons in any semiconductor device. Increasing the temperature of junction J2 will have a very similar effect. More holes and electrons will begin to move causing more dislodging of electrons and holes from the neighboring lattice. If a high temperature is maintained, this could lead to an avalanche breakdown of junction J2 and again render the thyristor useless since it would no longer be able to block forward voltage. Increasing temperature is yet another destructive method of forcing the thyristor to conduct.
- d. Gate current injection: If a positive voltage is applied across the gate to cathode of a thyristor, then junction J3 would be forward biased. Charged carriers will start moving. The movement of charged carriers in junction J3 will attract electrons from n2 region of the thyristor ([Fig. 22.26](#)). Some of these electrons will flow out of the gate terminal but there would be ample electrons that could start crossing junction J2. Since electrons in p2 region of junction J2 are minority carriers, these can cause rapid recombination and help increase movement of minority carriers in junction J2. By steadily increasing the forward biasing potential of junction J3, the depletion width of junction J2 can be controlled. If a forward biasing voltage is applied across anode to cathode of the thyristor with its gate to cathode favorably biased at the same time, then the thyristor can be made to conduct current. This method achieves conduction by increasing the leakage current in a controlled manner. The gain product in the two-transistor equivalent is made to achieve a value of unity in a controlled manner and the thyristor is said to turn ON. This is the only recommended way of turning ON a thyristor. When the gate-cathode junction is sufficiently forward biased, the current through the thyristor depends on the applied voltage across the anode to cathode and the load impedance. The load impedance and the externally applied anode-cathode voltage should be such that the current through the thyristor is greater than a minimum current known as *latching current*, I_L . Under such a condition, the thyristor is said to have *latched ON*. Once it has latched ON, the thyristor remains ON. In other words, even if the forward biasing voltage across the gate-cathode terminals is removed, the thyristor continues to conduct. Junction J2 does not exist during the ON condition. The thyristor reverts to its blocking state only when the current through it falls below a minimum threshold value known as *holding current*, I_h . Typically, holding current is lower than latching current ($I_h < I_L$). There are two ways of achieving this: (i) increase the load impedance to such a value that the thyristor current falls below I_h or (ii) apply reverse-biasing voltage across the anode to cathode of the thyristor. An approximate $v-i$ characteristic of a typical thyristor and its symbol are shown in [Fig. 22.27](#).

Since the thyristor allows flow of current only in one direction like a diode and the instant at which it is turned ON can be controlled, the device is a key component in building a controlled rectifier unit. The diode in all the circuits discussed so far can be replaced with the thyristor. Because of

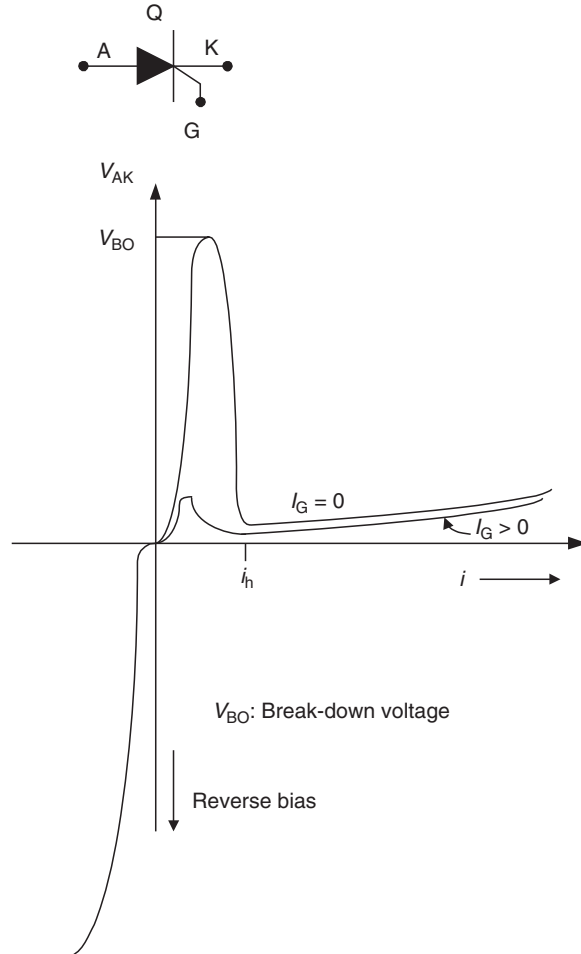


FIGURE 22.27 $v-i$ characteristic of a thyristor along with its symbol.

its controllability, the instant at which the thyristor conducts can be delayed to alter the average and rms output voltages. By doing so, the output voltage and output power from the rectifier can be controlled. Rectifiers that employ thyristors are thus also known as silicon controlled rectifiers or SCR.

A typical single-phase R-L rectifier circuit with one thyristor as the rectifier is shown in Fig. 22.28. The figure also shows the relevant circuit waveforms. The greatest difference between this circuit and its diode counterpart is also shown for comparison. Both circuits conduct beyond π radians due to the presence of the inductor L since the average voltage across an inductor is zero. If the value of the circuit components and the input supply voltage are the same in both cases, the duration for which the current flows into the output R-L load depends on the values of R and L . In the case of the diode circuit it does not depend on anything else while in the case of the thyristor circuit, it also depends on the instant the thyristor is given a gate trigger.

From Fig. 22.28, it is important to note that the energy stored in the inductor during the conduction interval can be controlled in the case of a thyristor in such a manner so as to reduce the conduction interval and thereby alter (reduce) the output power. Both the diode and the thyristor

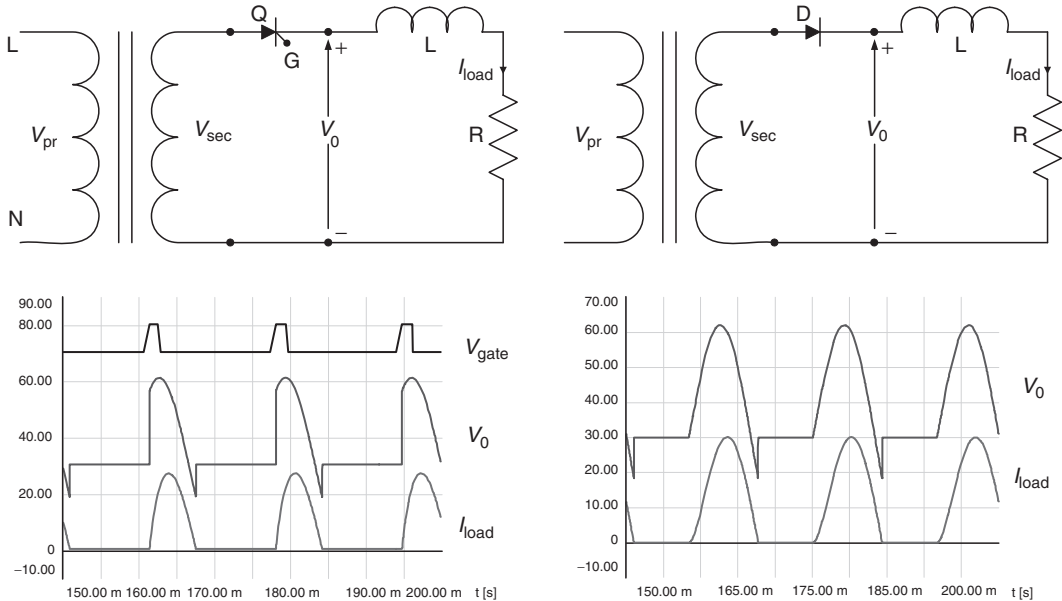


FIGURE 22.28 Comparing a single thyristor rectifier circuit with a single diode rectifier circuit. Note that the thyristor conduction is delayed deliberately to bring out the differences.

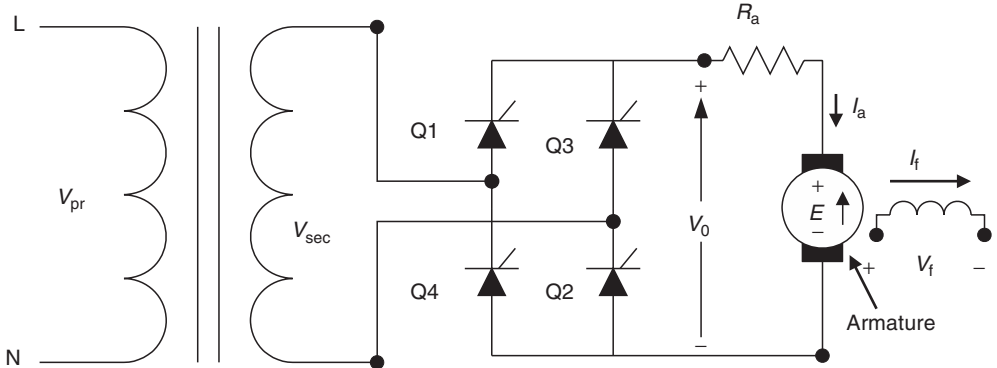
show reverse recovery phenomenon. The thyristor similar to the diode can block reverse voltage applied across it repeatedly, provided the voltage is less than its breakdown voltage.

22.3.1 Gate Circuit Requirements

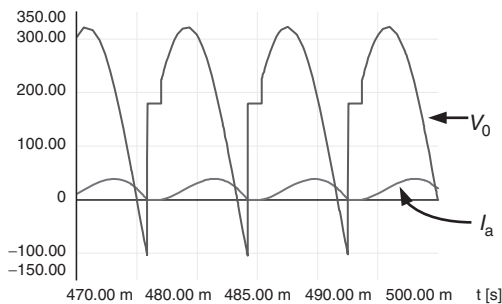
The trigger signal should have voltage amplitude greater than the minimum gate trigger voltage of the thyristor being turned ON. It should not be greater than the maximum gate trigger voltage, either. The gate current should likewise be in between the minimum and maximum values specified by the thyristor manufacturer. Low gate current driver circuits can fail to turn ON the thyristor. The thyristor is a current controlled switch and so the gate circuit should be able to provide the needed turn ON gate current into the thyristor. Unlike the bipolar transistor, the thyristor is not an amplifier and so the gate current requirement does not absolutely depend on the voltage and current rating of the thyristor. Sufficient gate trigger current will turn ON the thyristor and current will flow from the anode to the cathode, provided the thyristor is favorably biased and the load is such that the current flowing is higher than the latching current of the thyristor. In other words, in single-phase AC to DC rectifier circuits, the gate trigger will turn ON the thyristor only if it occurs during the positive part of the ac cycle (Fig. 22.28). Any trigger signal during the negative part of the ac cycle will not turn ON the thyristor and thyristor will remain in the blocking state. Keeping the gate signal ON during the negative part of the ac cycle does not typically damage a thyristor.

22.3.2 Single-Phase H-Bridge Rectifier Circuits with Thyristors

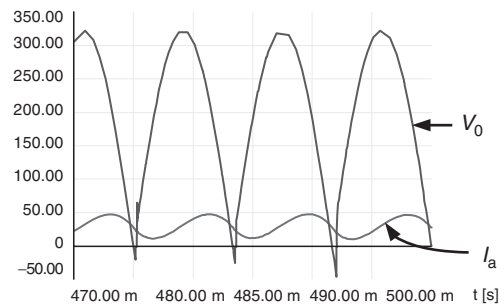
Similar to the diode H-bridge rectifier topology, there exist SCR-based rectifier topologies. Because of their unique ability to be controlled, the output voltage and hence the power can be controlled to desired levels. Since the triggering of the thyristor has to be synchronized with the input sinusoidal voltage in an AC to DC rectifier circuit, soft charging of the filter capacitor can be achieved. In other words, there is no need for employing soft-charge resistor and contactor combination as is required in single-phase and three-phase AC to DC rectifier circuits with dc bus capacitors.



(a) Topological representation



(b) Discontinuous mode of operation



(c) Continuous mode of operation

FIGURE 22.29 Single-phase dc motor control circuit for controlling a separately excited dc motor. R_a indicates equivalent armature resistance and E is the back emf. Typical waveforms are shown in (b) and (c).

In controlled ac to dc rectifier circuits, it is important to discuss control of resistive, inductive, and resistive-inductive load circuits. DC motor control falls into the resistive-inductive load circuit. DC motors are still an important part of the industry. However, the use of dc motor in industrial application is declining rapidly. Control of DC motors is typically achieved by controlled rectifier circuits employing thyristors. Small motors of less than 3-kW (approximately 5 hp) rating can be controlled by single-phase SCR circuits whereas larger ratings require three-phase versions. A typical single-phase H-bridge SCR-based circuit for the control of a DC motor is shown in Fig. 22.29. Typical output waveforms are shown in Fig. 22.30. The current in the load side can be assumed continuous due to the large inductance of the armature of the dc motor.

In Fig. 22.29a, V_f is the field voltage, which is applied externally and generally is independent of the applied armature voltage. Such a dc motor is known as a separately excited motor. I_a is the armature current while I_f is the field current. By altering the instant of turn-ON of the thyristors, the average output voltage can be altered. A DC motor typically generates a back emf that is dependent on speed. In Fig. 22.29b, discontinuous mode of operation is depicted. When the trigger instant is delayed appreciably from the start of the sinusoidal supply voltage waveform, the average output voltage reduces, resulting in discontinuous current flow, which is characterized by zero output current durations as seen in Fig. 22.29b. At the instant the current goes to zero, the output voltage is simply the back emf, E . When current starts flowing again, the input voltage is fed into the output and so the output has portions of the input voltage.

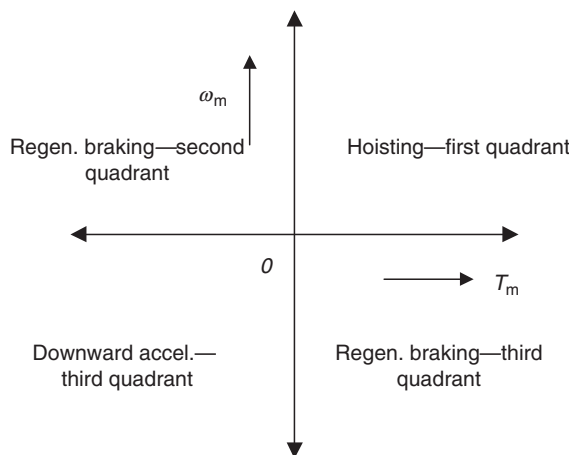


FIGURE 22.30 Four-quadrant operation of a crane or hoist.

On advancing the instant of triggering the thyristors, the output current can be made continuous as seen in Fig. 22.29c. The output voltage increases and since the thyristors conduct for the entire duration, the input wave-shape appears at the output. Since the output voltage can be controlled, the armature current can be effectively controlled. Since the torque produced by a dc motor is directly proportional to the armature current, the torque developed can thus be controlled.

$$T = K\phi I_a \quad (22.18)$$

K is the motor constant and depends on the number of armature conductors, number of poles, and type of winding employed in the dc machine. ϕ is flux produced by the field and is proportional to the field current, I_f . I_a is the armature current. Hence, the torque produced by a dc machine can be rewritten as

$$T = K(K_1 I_f) I_a \quad (22.19)$$

By keeping the field current constant, the torque then becomes directly proportional to the armature current, which is controlled by controlling the output voltage of the AC to DC controlled rectifier. In the circuit shown in Fig. 22.29, it is important to note that the current I_a cannot flow in the opposite direction. Hence, the motor cannot generate negative torque. In order to make the motor run in the opposite direction, the direction of the field has to be changed. Speed control within the base speed can also be accomplished by controlling the armature voltage as is shown below:

$$E = K\phi\omega = K(K_1 I_f)\omega \quad (22.20)$$

ω is the speed of the armature in radians per second. The back emf, E , is the difference between the output dc voltage of the AC to DC controlled rectifier and the drop across the equivalent armature resistance. Hence, E can be rewritten as

$$E = V_a - (I_a R_a); \quad \omega = \frac{V_a - (I_a R_a)}{K K_1 I_f} \quad (22.21)$$

For control of speed above base speed, the field current has to be reduced. Hence, it can be shown that controlling the armature current controls torque and speed below base speed, whereas controlling the field current achieves speed control above base speed. Because of the large inductance of the armature circuit, the current through it can be assumed continuous for practical operating region. The average output voltage of a single-phase AC to DC rectifier circuit for continuous current operation is given by (referring to Fig. 22.29c)

$$V_0 = \frac{1}{\pi} \int_{\alpha}^{\pi+\alpha} (\sqrt{2} V_{\text{rms}}) d(\omega t) = \frac{2\sqrt{2} V_{\text{rms}} \cos(\alpha)}{\pi} \quad (22.22)$$

Equation (22) is derived for continuous current condition. By controlling the triggering angle, α , the average value of the output voltage, V_0 , can be controlled. If armature current control is the main objective (to control output torque), then the controller of Fig. 22.29 can be configured with a feedback loop. The measured current can be compared with a set reference and the error can be used to control the triggering angle, α . Since the output voltage and hence the armature current are not directly proportional to α but to $\cos(\alpha)$, the above method will yield a nonlinear (co-sinusoidal) relationship between the output voltage and control angle, α . However, the error signal $\cos(\alpha)$ instead of α can be chosen to be the control parameter. This would then yield a linear relationship between the output voltage and cosine of control angle, α .

It is important to note from the equation for the output average voltage that the output average voltage can become negative if the triggering angle is greater than 90 electrical degrees. This leads us to the topic of regeneration. AC to DC controlled rectifiers employing thyristors and having large inductance on the DC side can be made to operate in the regeneration mode by simply delaying the trigger angle. This is quite beneficial in hoist applications as explained below.

When a load on a hoist needs to be raised, electrical energy is supplied to the motor. The voltage across the motor is positive and the current through the armature is positive. Positive torque is generated and the load is raised. When the load is being brought down, the motor rotates in the opposite direction, which results in a negative value of back emf. The current through the thyristors cannot go negative, so the motor is still developing positive torque tending to raise the load and prevent it from running away due to the gravitational pull. The negative back emf is supported by advancing the gating angle to be greater than 90 electrical degrees so that the voltage across the armature of the motor is negative but remains slightly more positive than the back emf, the difference causing positive current flow into the motor. The large inductance of the motor helps to maintain the positive direction of current through the armature. From electrical energy flow point of view, the product of current through the motor and the voltage across it is negative meaning that the motor is in regeneration mode.

The kinetic energy due to the motors motion is converted to electrical energy and this produces considerable braking torque. The electrical energy is fed back to the source via the input thyristors. Converting kinetic energy to electrical energy has the desired braking effect and such a conversion is known as regenerative braking.

The above application describes a two-quadrant operation. Cranes and elevators employed in hoist operation are required to operate in all four quadrants (Fig. 22.30). Using only one H-bridge rectifier allows two-quadrant operation—quadrants 1 and 4 or quadrants 2 and 3. For achieving four-quadrant operation, two H-bridge rectifiers are needed, as shown in Fig. 22.31. The four different quadrants of operation are described next for a crane/hoist operation.

In the first quadrant, the motor develops positive torque and motor runs in the positive direction meaning, speed is positive—product of torque and speed is power and so positive electric power is supplied to the motor from the AC to DC rectifier.

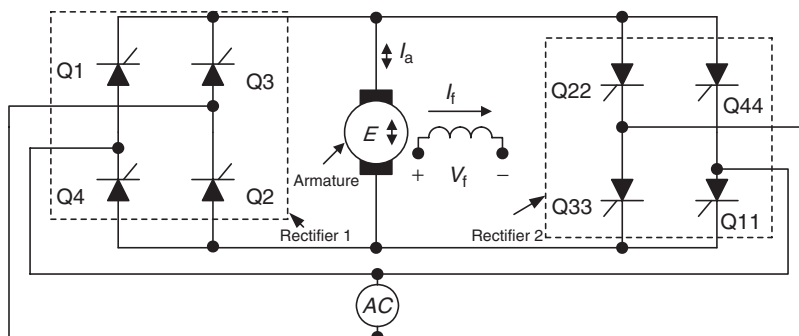


FIGURE 22.31 Two rectifier-bridge arrangements for four-quadrant operation of dc motor.

When the crane with a load is racing upward, close to the end of its travel, the AC to DC controlled rectifier is made to stop powering the motor. The rectifier practically is switched off. The inertia of the load moving upward generates a voltage in the form of a back emf. This voltage is fed into a second rectifier bridge arranged in the opposite direction (Fig. 22.31). The second bridge is turned ON to let the generated voltage across the upwardly mobile motor to flow into the utility thereby converting the inertial motion to electric power. In the second quadrant, speed remains positive but torque becomes negative, since the current through the motor flows in the opposite direction into the second rectifier-bridge arrangement (Fig. 22.31). The product of speed and torque is negative meaning that the motor behaves like a generator during this part of the travel.

Third quadrant of operation occurs at the beginning of the lowering action. Both torque and speed are negative and so the product of torque and speed is positive. Power is applied to the motor to overcome static friction and allows the rotating parts of the mechanism to move the load downward. In this case, the direction of armature current through the motor is opposite to that in quadrant 1 and the electrical power needed by the motor is supplied by the second rectifier-bridge arrangement (Fig. 22.31).

The mechanical load and motor arrangement goes into the fourth quadrant of operation for the larger part of the downward motion. This is the duration during which, the motor resists the tendency of the load to accelerate downward by developing positive torque. Since motion is downward, speed is negative and the product of torque and speed is negative. This means the motor behaves like a generator. Due to the downward motion of the motor, the back emf is negative but the current is positive; and so, from electrical energy flow point of view, the power is negative, meaning that the motor is in regeneration mode.

Since the thyristors cannot conduct in the opposite direction, a new rectifier section arranged in an opposite manner had to be provided to enable the four-quadrant operation needed in cranes and hoists. The method by which unidirectional electrical power was routed to the bi-directional ac utility lines is known as inversion (opposite to rectification). Since no external means of switching OFF the thyristors were employed, the process of inversion is achieved by natural commutation provided by the AC source. Such an inverter is known as line commutated inverter.

22.3.3 Three-Phase Controlled AC to DC Rectifier Systems

The observations made so far for the single-phase controlled AC to DC rectifiers can be easily extended to three-phase versions. An important controlled rectification scheme that was not mentioned in the single-phase case is the semiconverter circuit. In Fig. 22.29, if the thyristors Q2 and Q4 are replaced by diodes (D2 and D4), then the circuit of Fig. 22.29 is converted into a semiconverter circuit. Such a circuit

does not have the potential to provide regeneration capability and hence is of limited use. However, in dual converter applications, especially in three-phase versions, there are a few instances where a semiconverter can be employed to reduce cost. A typical three-phase semiconverter circuit will consist of three thyristors and three diodes arranged in an H-bridge configuration as shown in Fig. 22.32.

Three-phase dual converter schemes similar to the one shown in Fig. 22.31 are still employed to operate large steel mills, hoists, and cranes. However, the advent of vector controlled ac drives has drastically changed the electrical landscape of the modern industry. Most dc motor applications are being rapidly replaced by ac motors with field oriented control schemes. DC motor application in railway traction has also seen significant reduction due to the less expensive and more robust AC motors.

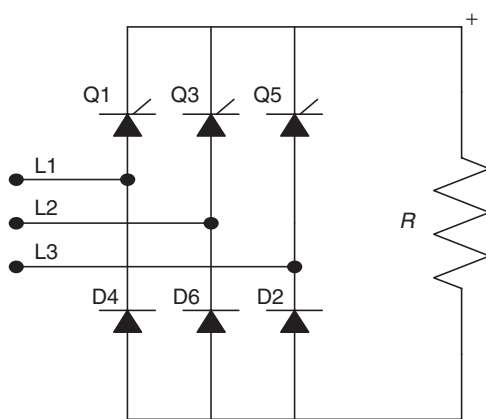


FIGURE 22.32 A typical three-phase semiconverter. Rarely employed in the modern industry.

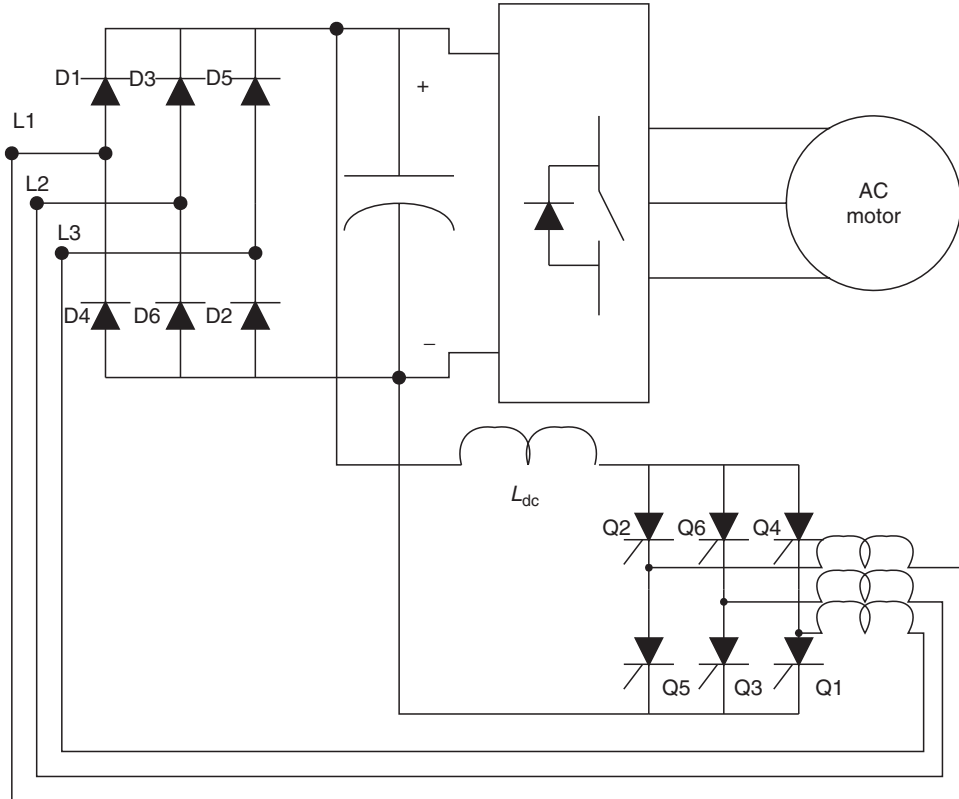


FIGURE 22.33 Use of six-pulse thyristor bridge in the inverter mode to provide regeneration capability to an existing AC drive system.

However, there are still a few important applications where three-phase controlled rectification (inversion) is the most cost-effective solution. One such application is the regenerative converter module that many inverter-drive manufacturers provide as an optional-equipment to customers with overhauling loads. Under normal circumstance, during motoring mode of operation of an ac drive, the regenerative unit does not come into the circuit. However, when the dc bus voltage tends to go higher than a predetermined level due to overhauling of the load, the kinetic energy of the load is converted into electrical energy and is fed back into the ac system via a six-pulse thyristor-based inverter-bridge. One such scheme is shown in Fig. 22.33.

22.3.4 Average Output Voltage

In order to evaluate the average value of the output voltage for a three-phase full-bridge converter, the process of integrating the output voltage similar to the one in Fig. 22.13b has to be undertaken. For the circuit shown in Fig. 22.12b, where the diodes are replaced by thyristors, the integration yields the following:

$$V_0 = \frac{3}{\pi} \int_{\alpha+(\pi/3)}^{\alpha+(2\pi/3)} \sqrt{2} V_{L-L} \sin(wt) d(wt) \quad (22.23)$$

$$V_0 = \frac{3\sqrt{2} V_{L-L} \cos(\alpha)}{\pi} = \frac{3\sqrt{2}\sqrt{3} V_{L-N} \cos(\alpha)}{\pi}$$

The average output voltage for the circuit in Fig. 22.12b with the diodes being replaced by thyristors is only different in the cosine of the triggering angle, α . If the triggering angle is zero, the circuit performs similar to a three-phase diode rectifier and the average output voltages become the same.

22.3.5 HVDC Transmission Systems

One area where it is difficult to replace the use of high voltage, high current carrying thyristors is high voltage DC (HVDC) transmission systems. When large amount of power is to be transported over long distances, or under water, it has been found that HVDC transmission is more economical. HVDC systems are in reality back to back rectifier systems. The sending end rectifier system consists typically of 12- or 24-pulse thyristor bridges whereas the receiving end consists of a similar configuration but in the opposite direction. The receiving end 12- or 24-pulse bridge operates in the inverter mode whereas the sending end operates in the rectifier mode. Twelve-pulse configuration is achieved by cascading two six-pulse bridges in series while 24-pulse configuration needs four six-pulse bridges cascaded in series. Typical advantages of high voltage DC transmission over high voltage AC transmission are listed below:

1. No stability problems due to transmission line length since no reactive power needs to be transmitted.
2. No limitation of cable lengths for underground cable or submarine cable transmission due to the fact that no charging power compensation needs be done.
3. AC power systems can be interconnected employing a DC tie without reference to system frequencies, short-circuit power, etc.
4. High-speed control of DC power transmission is possible because the control angle, α , has a relatively short time constant.
5. Fault isolation between receiving end and sending end can be dynamically achieved due to fast efficient control of the high voltage DC link.
6. Employing simple-control logic can change the energy flow direction very fast. This can help in meeting peak demands at either the sending or the receiving station.
7. High reliability of thyristor converter and inverter stations makes this mode of transmission a viable solution for transmission lengths typically over 500 kms.
8. The right-of-way needed for high voltage DC transmission is much lower than that for AC transmission of the same power capacity.

The advantages of DC transmission over AC transmission should not be misunderstood. DC transmission should not be substituted for AC power transmission. In a power system, it is generally accepted that both AC and DC should be employed to compliment each other. Integration of the two types of transmission enhances the salient features of each other and helps in realizing a power network that ensures high quality and reliability of power supply. A typical rectifier–inverter system employing a 12-pulse scheme is shown in Fig. 22.34.

Typical DC link voltage can be as high as 400–600 kV. Higher voltage systems are also in use. Typical operating power levels are over 1000 MW. There are a few systems transmitting close to 3500 MW of power through two bipolar systems. Most thyristors employed in large HVDC transmission systems are liquid cooled to improve their performance.

22.3.6 Power System Interaction with Three-Phase Thyristor AC to DC Rectifier Systems

Similar to the diode rectifiers, the thyristor-based AC to DC rectifier is associated with low order current harmonics. In addition to current harmonics, there is voltage notching phenomenon occurring at the input terminals of an AC to DC thyristor-based rectifier system. The voltage notching

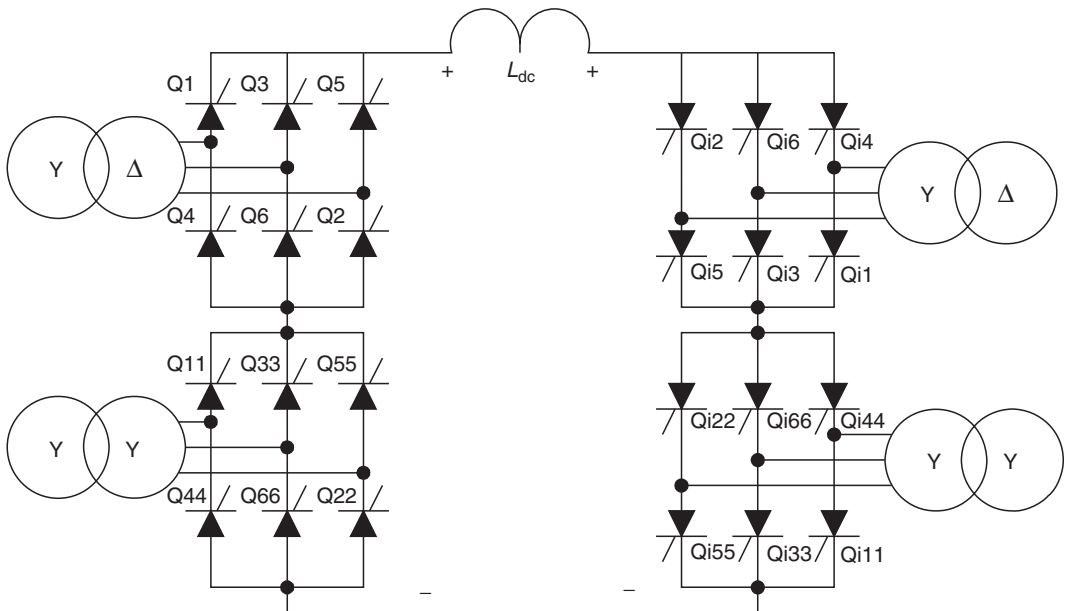


FIGURE 22.34 Schematic representation of a bipolar HVDC system employing 12-pulse rectification/inversion scheme.

is a very serious problem. Since thyristors are generally slower to turn ON and turn OFF compared to power semiconductor diodes, there are nontrivial durations during which an outgoing thyristor and an incoming thyristor remain in conduction thereby creating a short-circuit across the power supply phases feeding the corresponding thyristors. Thyristors used in rectifiers are generally known as phase control type thyristors and have typical turn OFF times of 50–100 μ s. Thyristors employed in inverter circuits typically are faster and have turn OFF times in the 10- to 50- μ s ranges.

Notching can create major disturbances in sensitive electronic equipment that rely on the zero crossing of the voltage for satisfactory operation. Multiple pseudo zero-crossings of the voltage waveform can occur due to the notching effect of thyristor-based rectifier systems. Notching phenomenon can create large magnitudes of currents to flow into power-factor correcting capacitors, thereby potentially causing permanent damage to them. IEEE 519-1992 in the U.S. has strict regulations regarding the depth of the notch as well as the duration of the notch. AC line inductors in series with the supply feeding power to the three-phase bridge help to minimize the notching effect on the power system. The theory behind this phenomenon is discussed next.

When an external inductance is added in front of a three-phase AC to DC rectifier employing thyristors, the duration of commutation increases. In other words, the time duration for which the outgoing thyristor remains in conduction along with the incoming thyristor increases. This overlap duration causes the average output voltage to reduce because during this period, the output voltage is composed of two shorted phases and a healthy phase. The extent of reduction in the output voltage depends on the duration of overlap in electrical degrees. The duration of overlap in electrical degrees is commonly represented by μ . The overlap duration is directly proportional to the value of the external inductance used. If no external line inductor is used, then this duration will depend on the existing inductance of the system including the wiring inductance. In order to compute the factors influencing the overlap duration, a simple model can be assumed. Assume that the line comprises of inductance L in each phase. Let the dc load current be I_{dc} and let it be assumed that this current does not change during the overlap interval. The current in the incoming thyristor is zero at start and by the end of the overlap interval

it increases to I_{dc} . Based on this assumption, the relationship between current and voltage can be expressed as

$$\begin{aligned} v_{ab} &= \sqrt{2}V_{L-L} \sin(\omega t) = 2L(di/dt) \\ \sqrt{2}V_{L-L} \int_{\alpha+(\pi/3)}^{\alpha+(\pi/3)+\mu} \sin(\omega t) d(t) &= 2L \int_0^{I_{dc}} di \\ I_{dc} &= \frac{\sqrt{2}V_{L-L}[\cos(\alpha + \pi/3) - \cos(\alpha + \pi/3 + \mu)]}{2wL} = \frac{\sqrt{2}V_{L-L} \sin(\alpha + \pi/3 + \mu/2) \sin(\mu/2)}{wL} \end{aligned} \quad (22.24)$$

For small values of overlap angle μ , $\sin(\mu/2) = \mu/2$ and $\sin(\alpha + \pi/3 + (\mu/2)) = \sin(\alpha + \pi/3)$. Rearranging the above equation yields

$$\mu = \frac{2wLI_{dc}}{\sqrt{2}V_{L-L} \sin(\alpha + \pi/3)} \quad (22.25)$$

From the above expression, it is interesting to note the following:

1. If the inductance L in the form of either external inductance or leakage inductance of transformer or lead length is large, the overlap duration will be large.
2. If the load current I_{dc} is large, the overlap duration will be large.
3. If the delay angle is small, then the inductance will store more energy and so the duration of overlap will be large. The minimum value of delay angle α is 0° and the maximum value typically is 60° .

The average output voltage will reduce due to the overlap angle as mentioned before. In order to compute the average output voltage with a certain overlap angle, the limits of integration have to be changed. This exercise yields the following:

$$\begin{aligned} V_0 &= \frac{3}{\pi} \int_{\alpha+\mu+(\pi/3)}^{\alpha+\mu+(2\pi/3)} \sqrt{2}V_{L-L} \sin(\omega t) d(\omega t) \\ V_0 &= \frac{3\sqrt{2}V_{L-L} \cos(\alpha + \mu)}{\pi} = \frac{3\sqrt{2}\sqrt{3}V_{L-N} \cos(\alpha + \mu)}{\pi} \end{aligned} \quad (22.26)$$

Thus, it can be seen that the overlap angle has an equivalent effect of advancing the delay angle, thereby reducing the average output voltage. From the discussions in the previous paragraphs on notching, it is interesting to note that adding external inductance increases the duration of the overlap and reduces the average value of the output dc voltage. However, when viewed from the ac source side, the notching effect is conspicuously reduced and in some cases not observable. Since all other electrical equipment in the system will be connected to the line side of the ac inductor (in front of a thyristor-based AC to DC rectifier), these equipments will not be affected by the notching phenomenon of thyristors. The external inductance also helps limit the circulating current between the two thyristors during the overlap duration.

22.4 Conclusion

Uncontrolled and controlled rectifier circuits have been discussed in this chapter. An introduction to the theory of diode and thyristor conduction has been presented to explain the important operating characteristics of these devices. Rectifier topologies employing both, diodes and thyristors, and their relative advantages and disadvantages have been discussed. Use of dual thyristor bridge converter

to achieve four-quadrant operation of a dc motor has been discussed. The topic of high voltage DC (HVDC) transmission has been briefly introduced. Power quality issues relating to diode and thyristor-based rectifier topologies have also been addressed. To probe further into the various topics briefly discussed in this chapter, the reader is encouraged to refer to the references listed below.

References

1. Dewan, S.B. and Straughen, A., *Power Semiconductor Circuits*, John Wiley & Sons, 1975, ISBN 0-471-21180-X.
2. Richard G. Hoft, *Semiconductor Power Electronics*, Van Nostrand Reinhold Electrical/Computer Science and Engineering Series, Van Nostrand Reinhold Company, New York, 1986, ISBN 0-442-22543-1.
3. Sen, P.C., *Principles of Electric Machines and Power Electronics*, John Wiley & Sons, 1997, ISBN 0-471-02295-0.
4. Laughton, M.A. and Say, M.G., Eds., *Electrical Engineer's Reference Book—14th edition*, Butterworths, 1985, ISBN 0-408-00432-0.
5. *IEEE Recommended Practices and Requirements for Harmonic Control in Electrical Power Systems*, IEEE Std. 519-1992.
6. *Passive Harmonic Filter Systems for Variable Frequency Drives*, US Patent 5,444,609 August 1995.
7. Hirofumi Akagi, *State of the Art of Active Filters for Power Conditioning*, Key note Speech KB 1, EPE Conference 2005, Dresden.

23

Inverters

23.1	Introduction and Overview.....	23-1
23.2	Fundamental Issues.....	23-2
23.3	Single-Phase Inverters.....	23-2
23.4	Three-Phase Inverters	23-3
23.5	Multilevel Inverters.....	23-6
23.6	Line Commutated Inverters	23-7

Michael Giesselmann
Texas Tech University

23.1 Introduction and Overview

Inverters are used to create single or polyphase AC voltages from a DC supply. In the class of polyphase inverters, three-phase inverters are by far the largest group. A very large number of inverters are used for adjustable speed motor drives. The typical inverter for this application is a “hard-switched” voltage source inverter producing pulse-width modulated (PWM) signals with a sinusoidal fundamental [11]. Recently research has shown detrimental effects on the windings and the bearings, resulting from unfiltered PWM waveforms and recommend the use of filters [8,21]. A very common application for single-phase inverters are so-called uninterruptable power supplies (UPS) for computers and other critical loads. Here the output waveforms range from square waves to almost ideal sinusoids. UPS designs are classified as either “off-line” or “on-line.” An off-line UPS will connect the load to the utility for most of the time and quickly switch over to the inverter if the utility fails. An on-line UPS will always feed the load from the inverter and switch the supply of the DC bus instead. Since the DC bus is heavily buffered with capacitors, the load sees virtually no disturbance if the power fails.

In addition to the very common hard-switched inverters, active research is being conducted on “soft-switching” techniques. Hard-switched inverters use controllable power semiconductors to connect an output terminal to a stable DC bus. On the other hand, soft switching inverters have an oscillating intermediate circuit and attempt to open and close the power switches under zero-voltage and or zero-current conditions.

A separate class of inverters are the line commutated inverters for multimegawatt power ratings that use thyristors (also called silicon controlled rectifiers [SCRs]). SCRs can only be turned “on” on command. After being turned on, the current in the device must approach zero in order to turn the device off. All other inverters are self-commutated, meaning that the power control devices can be turned on and off. Line-commutated inverters need the presence of a stable utility voltage to function. They are used for DC links between utilities, ultra long distance energy transport, and very large motor drives [1,2,14,16,18]. However, the latter application is more and more taken over by modern hard-switched inverters including multilevel inverters [7,19].

Modern inverters use isolated gate bipolar transistors (IGBTs) as the main power control devices [14]. Besides IGBTs, power MOSFETs are also used especially for lower voltages and power ratings and applications that require high efficiency and high switching frequency. In recent years, IGBTs, MOSFETs and their control and protection circuitry have made remarkable progress. IGBTs are now available with voltage

ratings of 6500 V and current ratings up to 2400 A. MOSFETs have achieved on-state resistances approaching a few milliohms. In addition to the devices, manufacturers today offer customized control circuitry that provides for electrical isolation, proper operation of the devices under normal operating conditions and protection from a variety of fault conditions [14]. In addition, the industry provides good support for specialized passive devices such as capacitors and mechanical components such as low inductance bus-bar assemblies to facilitate the design of reliable inverters. In addition to the aforementioned inverters, a large number of special topologies are used. A good overview is given in Ref. [10].

23.2 Fundamental Issues

Inverters fall in the class of power electronics circuits. The most widely accepted definition of a power electronics circuit is that the circuit is actually processing electric energy rather than information. The actual power level is not very important for the classification of a circuit as a power electronics circuit. One of the most important performance considerations of power electronics circuits like inverters is their energy conversion efficiency. The most important reason for demanding high efficiency is the problem of removing large amounts of heat from the power devices. Of course, the judicious use of energy is also paramount, especially if the inverter is fed from batteries such as in electric cars. For these reasons, inverters operate the power devices, which control the flow of energy, as switches. In the ideal case of a switching event, there would be no power loss in the switch since either the current in the switch is zero (switch open) or the voltage across the switch is zero (switch closed) and the power loss is computed as the product of both. In reality there are two mechanisms that do create some losses, however, which are on-state losses and switching losses [3,12,14,16]. On-state losses are due to the fact that the voltage across the switch in the on state is not zero, but typically in the range of 1–3 V for IGBTs. For power MOSFETs the on-state voltage is often in the same range, but it can be substantially below 0.5 V due to the fact that these devices have a purely resistive conduction channel and no fixed minimum saturation voltage like bipolar junction devices (IGBTs). The switching losses are the second major loss mechanism and are due to the fact that, during the turn on and turn off transition, current is flowing while voltage is present across the device. In order to minimize the switching losses, the individual transitions have to be rapid (tens to hundreds of nanoseconds) and the maximum switching frequency (determining the frequency of transitions) needs to be carefully considered.

In order to avoid audible noise being radiated from motor windings or transformers, many modern inverters operate at switching frequencies substantially above 10 kHz [4,6].

23.3 Single-Phase Inverters

Figure 23.1 shows the basic topology of a full bridge inverter with single-phase output. This configuration is often called an H-bridge due to the arrangement of the power switches and the load. The inverter can deliver and accept both real and reactive power. The inverter has two legs, left and right. Each leg consists of two power control devices (here IGBTs) connected in series. The load is connected between the mid-points of the two-phase legs. Each power control device has a diode connected in antiparallel to it. The diodes provide an alternate path for the load current if the power switches are turned off. For example if the lower IGBT in the left leg is conducting and carrying current towards the negative DC bus, this current would “commutate” into the diode across the upper IGBT of the left leg, if the lower IGBT is turned off. Control of the circuit is accomplished by varying the turn on time of the upper and lower IGBT of each inverter leg, with the provision of never turning on both at the same time, to avoid a short circuit of the DC bus. In fact, modern drivers will not allow this to happen, even if the controller would erroneously command both devices to be turned on. The controller will therefore alternate the turn on commands for the upper and lower switch, i.e., turn the upper switch on and the lower switch off and vice versa. The driver circuit will typically add some additional blanking time (typically 500–1000 ns) during the switch transitions to avoid any overlap in the conduction intervals.

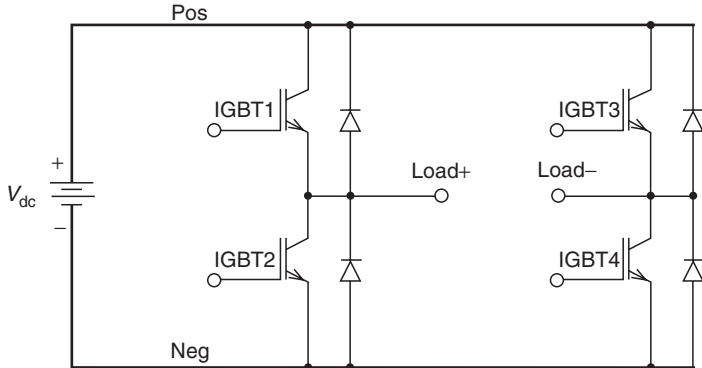


FIGURE 23.1 Topology of a single-phase, full bridge inverter.

The controller will hereby control the duty cycle of the conduction phase of the switches. The average potential of the center-point of each leg will be given by the DC bus voltage multiplied by the duty cycle of the upper switch, if the negative side of the DC bus is used as a reference. If this duty cycle is modulated with a sinusoidal signal with a frequency that is much smaller than the switching frequency, the short-term average of the center-point potential will follow the modulation signal. “Short-term” in this context means a small fraction of the period of the fundamental output frequency to be produced by the inverter. For the single-phase inverter, the modulation of the two legs is inverse of each other such that if the left leg has a large duty cycle for the upper switch, the right leg has a small one, etc. The output voltage is then given by Eq. (23.1) in which m_a is the modulation factor. The boundaries for m_a are for linear modulation—values greater than 1 cause overmodulation and a noticeable increase in output voltage distortion.

$$V_{ac1}(t) = m_a \cdot V_{dc} \cdot \sin(\omega_1 \cdot t) \quad 0 \leq m_a \leq 1 \quad (23.1)$$

This voltage can be filtered using an LC low-pass filter. The voltage on the output of the filter will closely resemble the shape and frequency of the modulation signal. This means that the frequency, wave-shape, and amplitude of the inverter output voltage can all be controlled as long as the switching frequency is at least 25–100 times higher than the fundamental output frequency of the inverter [11]. The actual generation of the PWM signals is mostly done using micro-controllers and digital signal processors (DSPs) [5].

23.4 Three-Phase Inverters

Figure 23.2 shows a three-phase inverter, which is the most commonly used topologies in today’s motor drives. The circuit is basically an extension of the H-bridge style single-phase inverter by an additional leg. The control strategy is similar to the control of the single-phase inverter, except that the reference signals for the different legs have a phase shift of 120° instead of 180° for the single-phase inverter. Due to this phase shift, the odd triplen harmonics (3rd, 9th, 15th, etc.) of the reference waveform for each leg are eliminated from the line-to-line output voltage [14,17]. The even-numbered harmonics are canceled as well if the waveforms are pure AC, which is usually the case. For linear modulation the amplitude of the output voltage is reduced with respect to the input voltage of a three-phase rectifier feeding the DC bus by a factor given by the following equation:

$$\frac{3}{(2\pi)} \cdot \sqrt{3} = 82.7\% \quad (23.2)$$

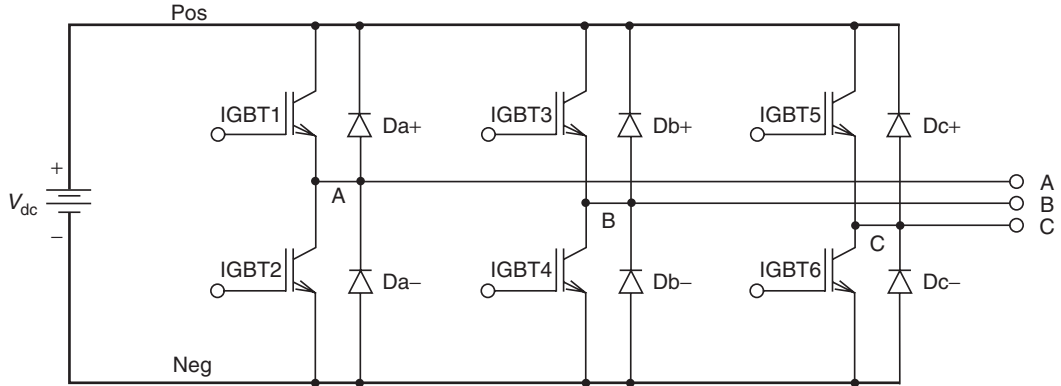


FIGURE 23.2 Topology of a three-phase inverter.

To compensate for this voltage reduction, the fact of the harmonics cancellation is sometimes used to boost the amplitudes of the output voltages by intentionally injecting a 3rd harmonic component into the reference waveform of each phase leg [14].

Figure 23.3 shows the typical output of a three-phase inverter during a startup transient into a typical motor load. This figure was created using circuit simulation. The upper graph shows the PWM waveform between phases A and B whereas the lower graph shows the currents in all three phases. It is obvious that the motor acts a low-pass filter for the applied PWM voltage and the current assumes the wave-shape of the fundamental modulation signal with very small amounts of switching ripple.

Like the single-phase inverter based on the H-bridge topology, the inverter can deliver and accept both real and reactive power. In many cases the DC bus is fed by a diode rectifier from the utility, which

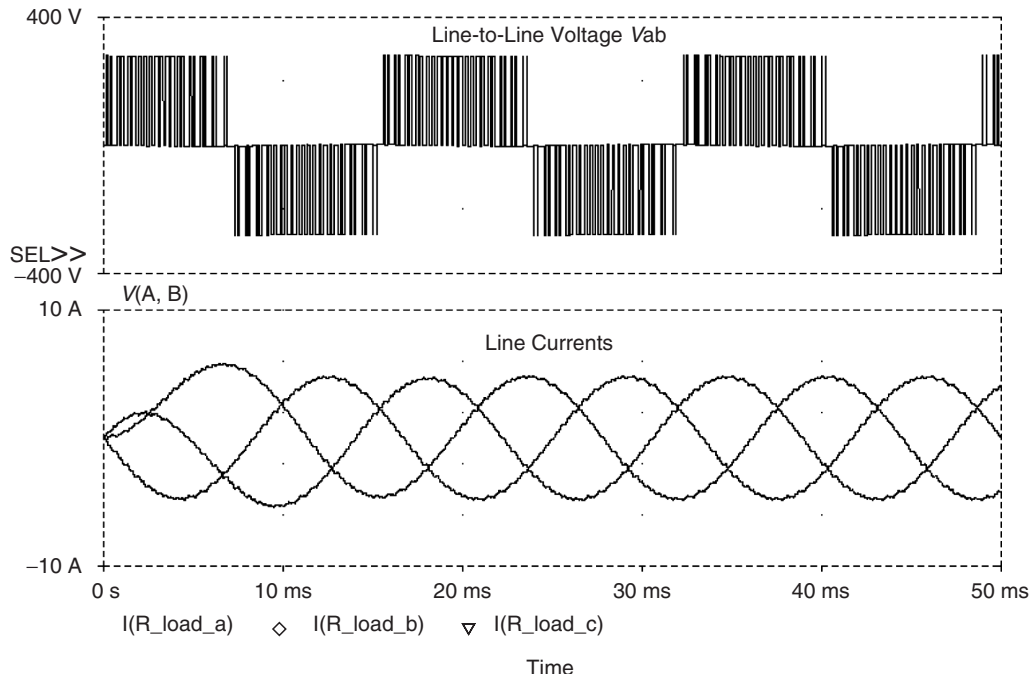


FIGURE 23.3 Typical waveforms of inverter voltages and currents.

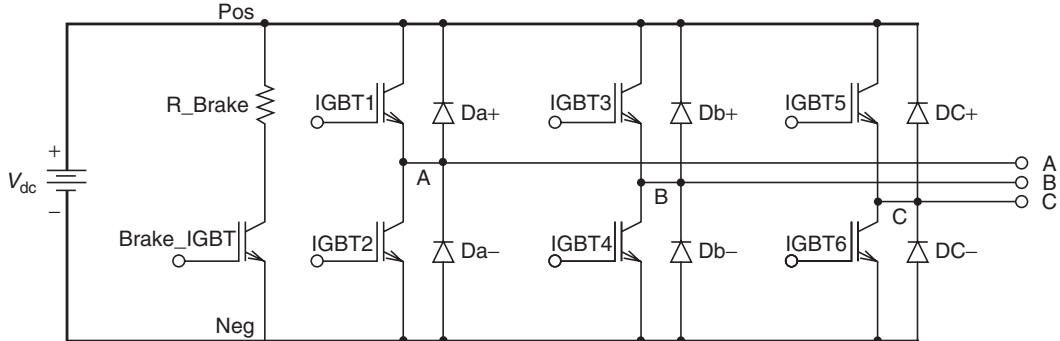


FIGURE 23.4 Topology of a three-phase inverter with brake chopper IGBT.

cannot pass power back to the AC input. The topology of the three-phase rectifier would be the same as shown in Fig. 23.2 with all IGBTs deleted.

A reversal of power flow in an inverter with a rectifier front end would lead to a steady rise of the DC bus voltage beyond permissible levels. If the power flow to the load is only reversing for brief periods of time, such as to brake a motor occasionally, the DC bus voltage could be limited by dissipating the power in a so-called brake resistor. To accommodate a brake resistor, inverter modules with an additional seventh IGBT (called “brake chopper”) are offered. This is shown in Fig. 23.4. For long-term regeneration, the rectifier can be replaced by an additional three-phase converter [14]. This additional converter is often called a controlled synchronous rectifier. The additional converter including its controller is of course much more expensive than a simple rectifier, but with this arrangement bidirectional power flow can be achieved. In addition, the interface towards the utility system can be managed such that the real and reactive power that is drawn from or delivered to the utility can be independently controlled. Also the harmonics content of the current in the utility link can be reduced to almost zero. The topology for an arrangement like this is shown in Fig. 23.5.

The inverter shown in Fig. 23.2 provides a three-phase voltage without a neutral point. A fourth leg can be added to provide a four-wire system with a neutral point. Likewise four-, five-, or n -phase inverters can be realized by simply adding the appropriate number of phase legs.

Like in single-phase inverters, the generation of the PWM control signals is done using modern micro-controllers and DSPs. These digital controllers are typically not only controlling just the inverter, but also through the controlled synthesis of the appropriate voltages, motors and attached loads are controlled for high performance dynamic response. The most commonly used control principle for superior dynamic response is called field-oriented or vector control [5,6,9,13,20].

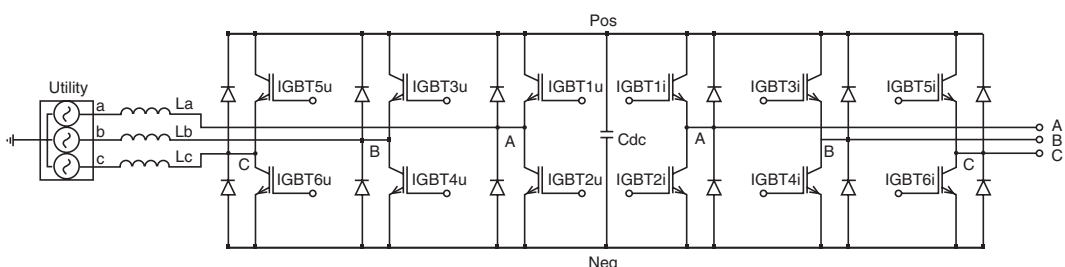


FIGURE 23.5 Topology of a three-phase inverter system for bidirectional power flow.

23.5 Multilevel Inverters

Multilevel inverters are a class of inverters where a DC source with several tabs between the positive and negative terminal is present. The two main advantages of multilevel inverters are the higher voltage capability and the reduced harmonics content of the output waveform due to the multiple DC levels. The higher voltage capability is due to the fact that clamping diodes are used to limit the voltage stress on the IGBTs to the voltage differential between two tabs on the DC bus. Figure 23.6 shows the topology of a three-level, three-phase inverter, which is also called “neutral point clamped” inverter. Here each phase leg consists of four IGBTs in series with additional antiparallel and clamping diodes. The output is again at the center-point of the phase leg. By switching on IGBT pairs 1 and 2, 2 and 3, or 3 and 4, respectively, the output of each phase can be connected to the top DC bus, the center connection of the DC supply, or the negative DC bus. This amounts to three distinct voltage levels for the voltage of each phase, which explains the name of the circuit. It turns out that the resulting line-to-line voltage has five distinct levels in a three-phase inverter.

Another inverter topology which reduces the voltage stress on the IGBTs and enables the synthesis of high-quality output voltage waveforms is shown in Fig. 23.7. This inverter is called an asymmetric cascaded H-bridge inverter because the individual H-bridges have unequal DC bus voltages [22]. For this example, the DC bus voltages of the stages have a ratio of 1:2:4 starting from the top stage. The output of each of the H-bridges can have three distinct values:

- Positive DC bus voltage
- Negative DC bus voltage
- Zero

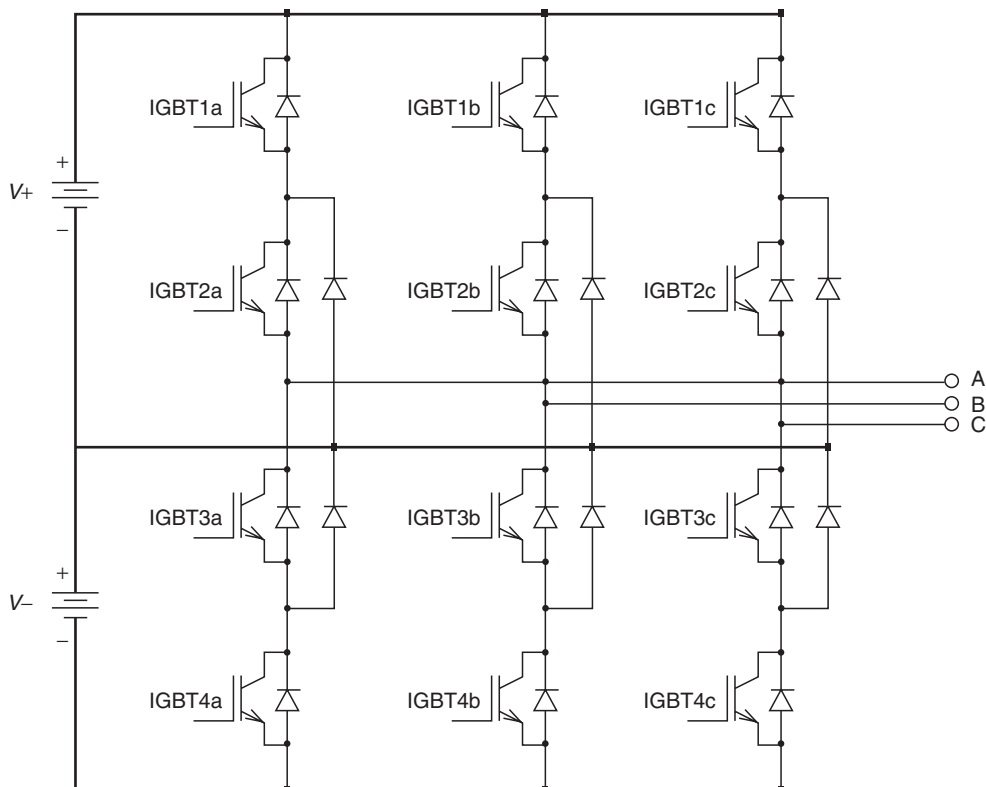


FIGURE 23.6 Topology of a three-level inverter.

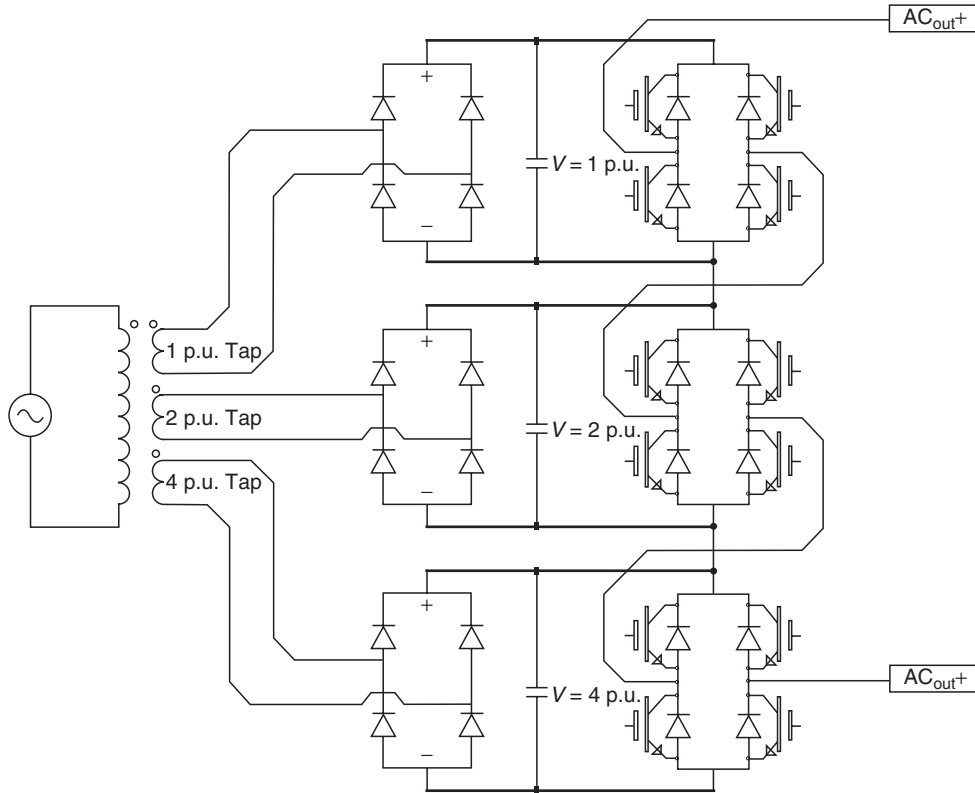


FIGURE 23.7 Topology of a three-stage, asymmetric cascaded H-bridge inverter.

therefore, with the topology shown in Fig. 23.7, the maximum positive and negative output voltage of the entire cascade $1 + 2 + 4 = 7$ times the DC bus voltage of the upper stage. Furthermore, by appropriate selection of the switching states of the individual stages, all intermediate voltage levels including zero can be achieved. Therefore the total number of output levels is 15 for this inverter [22].

Figure 23.8 shows the reference waveforms and PWM output voltages for all three stages as well as the total output voltage of the entire cascade. The waveforms for the H-bridge with 4 p.u. DC bus voltage are shown in the uppermost diagram of Fig. 23.8. It is apparent that this stage is only switching at the fundamental frequency which is appropriate for the high-voltage IGBTs that have to be in this stage. The reference waveform of the H-bridge with 2 p.u. DC bus voltage is derived from the overall sinusoidal reference waveform by subtracting the output voltage of the 4 p.u. stage. In the same manner, the reference voltage for the 1 p.u. stage is obtained by subtracting the combined output of the lower stages from the sinusoidal reference. This last stage is essentially compensating for the difference between the reference and the output of the lower two stages, which provide the bulk of the voltage and power. As shown in Fig. 23.8, each successive stage with lower DC bus voltage has a higher switching frequency. More details about the possible ratios of the DC bus voltages can be found in Ref. [22]. In Ref. [23] the value of multilevel inverters for utility applications is discussed in detail. The advantages of the cascaded H-bridge inverter in this field are its modularity, expandability, and superb output waveform quality.

23.6 Line Commutated Inverters

Figure 23.9 shows the topology of a line commutated inverter. In Fig. 23.9, the SCRs are numbered according to their firing sequence. The circuit can operate both as a rectifier and an inverter. The mode

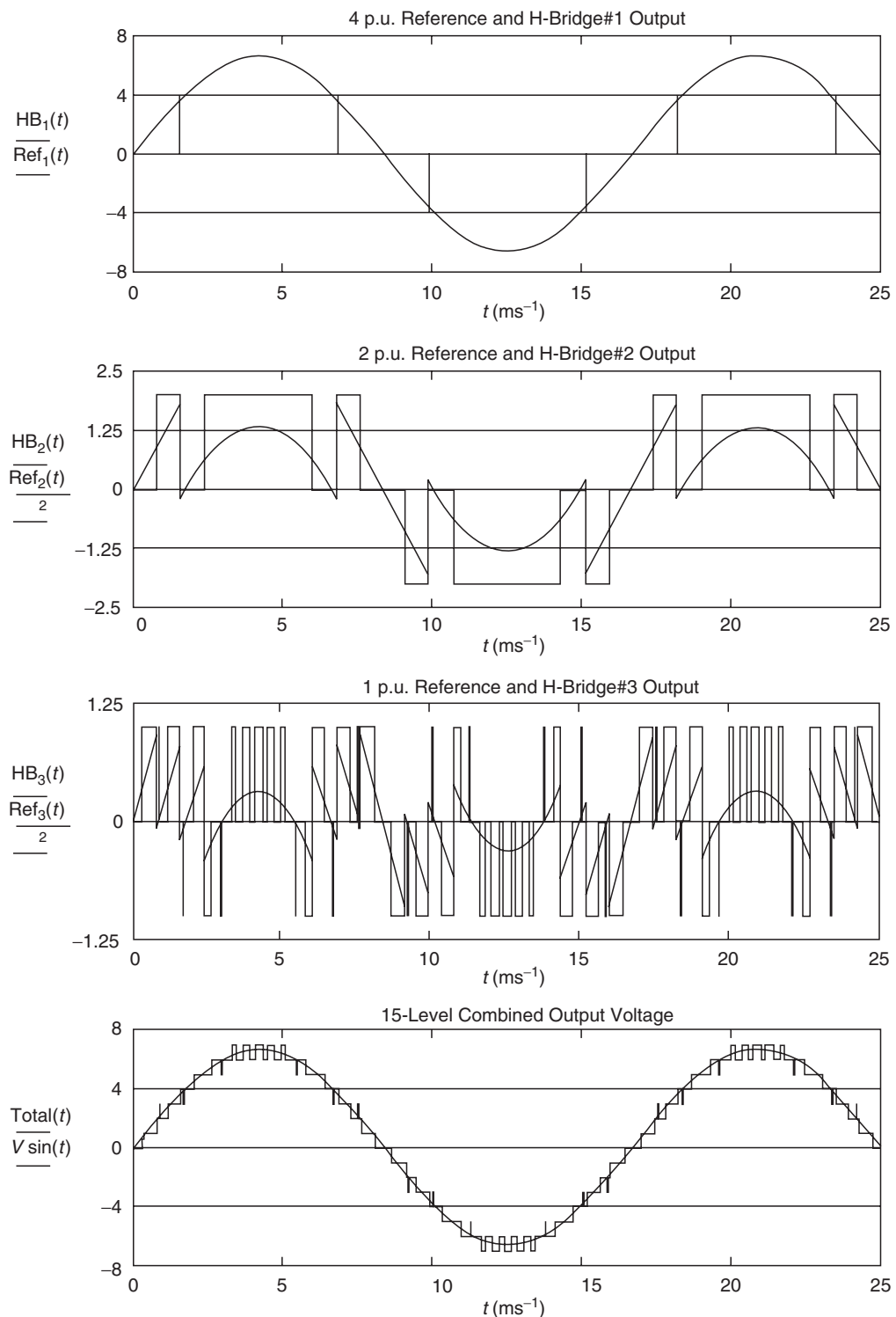


FIGURE 23.8 Switching waveforms for the cascaded H-bridge inverter.

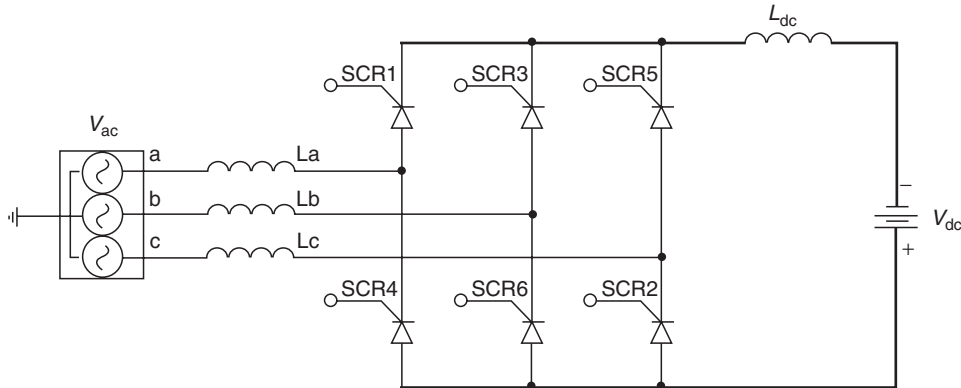


FIGURE 23.9 Line commutated converter in inverter mode.

of operation is controlled by the firing angle of the SCRs in the circuit [1,2,14]. The reference value for the firing angle α is the instant when the voltage across each SCR becomes positive, i.e., when an uncontrolled diode would turn on. This time corresponds to 30° past the positive going zero crossing of each phase. By delaying the turn-on angle α more than 90° past this instant, the polarity of the average DC bus voltage reverses and the circuit enters the inverter mode. The DC source in Fig. 23.9 shows the polarity of the DC voltage for inverter operation. The firing delay angle corresponds to the phase of the utility voltage. The maximum delay angle must be limited to less than 180° , to provide enough time for the next SCR in the sequence to acquire the load current. Equation (23.3) gives the value of the DC output voltage of the converter as a function of the delay angle α and the DC current I_{dc} , which is considered constant:

$$V_{dc} = \frac{3}{\pi} \cdot (\sqrt{2} \cdot V_{LL} \cdot \cos(\alpha) - \omega \cdot L_s \cdot I_{dc}) \quad (23.3)$$

V_{LL} is the rms value of the AC line-to-line voltage, ω is the radian frequency of the AC voltage, and L_s is the value of the inductors L_a , L_b , and L_c in Fig. 23.7. Line commutated inverters have a negative impact on the utility voltage and a relatively low total power factor. Equation (23.4) gives an estimate of the total power factor of the circuit shown in Fig. 23.7 for constant DC current and negligible AC line reactors:

$$PF = \frac{3}{\pi} \cdot \cos(\alpha) \quad (23.4)$$

References

1. Ahmed, A., *Power Electronics for Technology*, Prentice Hall, Upper Saddle River, NJ, 1999, ISBN: 0-13-231069-4.
2. Barton, T.H., *Rectifiers, Cycloconverters, and AC Controllers*, Oxford University Press Inc., New York, 1994, ISBN: 0-19-856163-6.
3. Bird, B.M., King, K.G., Pedder, D.A.G., *An Introduction to Power Electronics*, 2nd edition, John Wiley & Sons, Inc., New York, 1993, ISBN: 0-471-92616-7.
4. Bose, B.K., *Modern Power Electronics, Evolution, Technology, and Applications*, IEEE Press, Piscataway, NJ, 1992, ISBN: 0-87942-282-3.
5. Bose, B.K., *Microcomputer Control of Power Electronics and Drives*, IEEE Press, Piscataway, NJ, 1987, ISBN: 0-87942-219-X.

6. Bose, B.K., *Power Electronics and Variable Frequency Drives*, IEEE Press, Piscataway, NJ, 1996.
7. Brumsickle, W.E., Divan, D.M., Lipo, T.A., Reduced switching stress in high-voltage IGBT inverters via a three-level structure, *IEEE-APEC* 2, 544–550, February 1998.
8. Cash, M.A. and Habetler, T.G., Insulation failure prediction in induction machines using line-neutral voltages, *IEEE Transactions on Industry Applications*, **34**(6), 1234–1239, Nov/Dec 1998.
9. De Donker, R. and Novotny, D.W., The universal field-oriented controller, *Conference Record, IEEE-IAS*, 450–456, 1988.
10. Gottlieb, I.M., *Power Supplies, Switching Regulators, Inverters & Converters*, TAB Books, Inc. Blue Ridge Summit, PA, 1984, ISBN: 0-8306-0665-3.
11. Holtz, J., Pulsewidth modulation—A survey, *IEEE Transactions on Industrial Electronics*, **39**(5), 410–420, 1992.
12. Kassakian, J.G., Schlecht, M.F., Verghese, G.C., *Principles of Power Electronics*, Addison-Wesley Publishing Company, New York, 1991, ISBN: 0-201-09689-7.
13. Lorenz, R.D. and Divan, D.M., Dynamic analysis and experimental evaluation of delta modulators for field oriented induction machines, *IEEE Transactions on Industry Applications*, **26**(2), 296–301, 1990.
14. Mohan, N., Undeland, T., Robbins, W., Eds., *Power Electronics, Converters, Applications, and Design*, 2nd edition, John Wiley & Sons, New York, 1995, ISBN: 0-471-58408-8.
15. Novotny, D.W. and Lipo, T.A., *Vector Control and Dynamics of AC Drives*, Oxford Science Publications, 1996, ISBN: 0-19-856439-2.
16. Rashid, M.H., Ed., *Power Electronics, Circuits, Devices, and Applications*, 2nd edition, Prentice Hall, Englewood Cliffs, NJ, 1993, ISBN: 0-13-678996-X.
17. Shepherd, W. and Zand, P., *Energy Flow and Power Factor in Nonsinusoidal Circuits*, Cambridge University Press, London and New York, 1979, ISBN: 0521-21990-6.
18. Tarter, R.E., *Solid State Power Conversion Handbook*, John Wiley & Sons, Inc., New York, NY, 1993, ISBN: 0-471-57243-8.
19. Tolbert, L.M., Peng, F.Z., and Habetler, T.G., Multilevel converters for large electric drives, *IEEE Transactions on Industry Applications*, **35**(1), 36–44, Jan/Feb 1999.
20. Trzynadlowski, A.M., *The Field Orientation Principle in Control of Induction Motors*, Kluwer Academic, Dordrecht, The Netherlands, 1994, ISBN: 0-7923-9420-8.
21. Von Jouanne, A., Rendusara, D., Enjeti, P., Gray, W., Filtering techniques to minimize the effect of long motor leads on PWM inverter fed AC motor drive systems, *IEEE Transactions on Industry Applications*, 919–926, July/Aug 1996.
22. Song-Manguelle, J. and Rufer, A., Asymmetrical multilevel inverter for large induction machine drives, *Electric Drives & Power Electronics International Conference (EDPE 01)*, 3–5 October, 2001.
23. Rudnick, H., Dixon, J., and Morán, L., Delivering clean and pure power, *IEEE Power & Energy Magazine*, September, October 2003.

24

Active Filters for Power Conditioning

24.1	Harmonic-Producing Loads.....	24-2
	Identified Loads and Unidentified Loads •	
	Harmonic Current Sources and Harmonic Voltage Sources	
24.2	Theoretical Approach to Active Filters for Power Conditioning	24-3
	The Akagi-Nabae Theory • Energy Storage Capacity •	
	Classification of Active Filters • Classification by Objectives:	
	Who is Responsible for Installing Active Filters? •	
	Classification by System Configuration • Classification by Power Circuit • Classification by Control Strategy	
24.3	Integrated Series Active Filters.....	24-11
	System Configuration • Operating Principle • Control Circuit • Experimental Results	
24.4	Practical Applications of Active Filters for Power Conditioning	24-15
	Present Status and Future Trends • Shunt Active Filters for Three-Phase Four-Wire Systems • The 48-MVA Shunt Active Filter for Compensation of Voltage Impact Drop, Variation, and Imbalance	

Hirofumi Akagi
Tokyo Institute of Technology

Much research has been performed on active filters for power conditioning and their practical applications since their basic principles of compensation were proposed around 1970 (Bird et al., 1969; Gyugyi and Stryculla, 1976; Kawahira et al., 1983). In particular, recent remarkable progress in the capacity and switching speed of power semiconductor devices such as insulated-gate bipolar transistors (IGBTs) has spurred interest in active filters for power conditioning. In addition, state-of-the-art power electronics technology has enabled active filters to be put into practical use. More than one thousand sets of active filters consisting of voltage-fed pulse-width-modulation (PWM) inverters using IGBTs or gate-turn-off (GTO) thyristors are operating successfully in Japan.

Active filters for power conditioning provide the following functions:

- reactive-power compensation,
- harmonic compensation, harmonic isolation, harmonic damping, and harmonic termination,
- negative-sequence current/voltage compensation,
- voltage regulation.

The term “active filters” is also used in the field of signal processing. In order to distinguish active filters in power processing from active filters in signal processing, the term “active power filters” often appears in many technical papers or literature. However, the author prefers “active filters for power

conditioning” to “active power filters,” because the term “active power filters” is misleading to either “active filters for power” or “filters for active power.” Therefore, this section takes the term “active filters for power conditioning” or simply uses the term “active filters” as long as no confusion occurs.

24.1 Harmonic-Producing Loads

24.1.1 Identified Loads and Unidentified Loads

Nonlinear loads drawing nonsinusoidal currents from utilities are classified into identified and unidentified loads. High-power diode/thyristor rectifiers, cycloconverters, and arc furnaces are typically characterized as identified harmonic-producing loads because utilities identify the individual nonlinear loads installed by high-power consumers on power distribution systems in many cases. The utilities determine the point of common coupling with high-power consumers who install their own harmonic-producing loads on power distribution systems, and also can determine the amount of harmonic current injected from an individual consumer.

A “single” low-power diode rectifier produces a negligible amount of harmonic current. However, multiple low-power diode rectifiers can inject a large amount of harmonics into power distribution systems. A low-power diode rectifier used as a utility interface in an electric appliance is typically considered as an unidentified harmonic-producing load. Attention should be paid to unidentified harmonic-producing loads as well as identified harmonic-producing loads.

24.1.2 Harmonic Current Sources and Harmonic Voltage Sources

In many cases, a harmonic-producing load can be represented by either a harmonic current source or a harmonic voltage source from a practical point of view. Figure 24.1(a) shows a three-phase diode rectifier with a DC link inductor L_d . When attention is paid to voltage and current harmonics, the rectifier can be

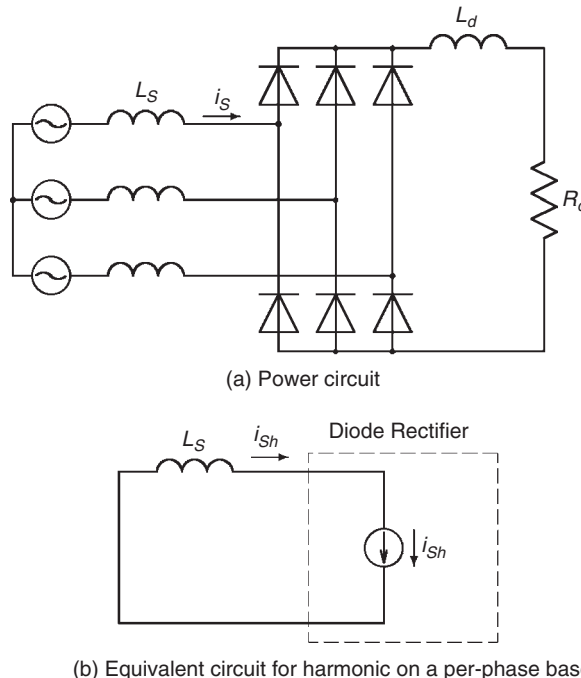
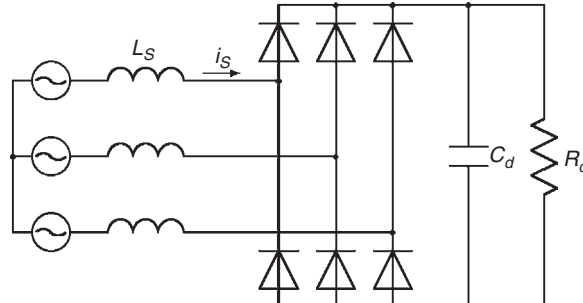
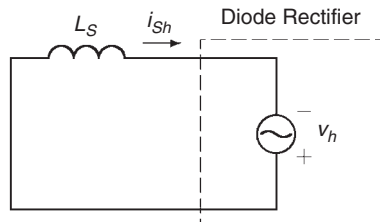


FIGURE 24.1 Diode rectifier with inductive load.



(a) Power circuit



(b) Equivalent circuit for harmonic on a per-phase base

FIGURE 24.2 Diode rectifier with capacitive load.

considered as a harmonic current source shown in Fig. 24.1(b). The reason is that the load impedance is much larger than the supply impedance for harmonic frequency ω_h , as follows:

$$\sqrt{R_L^2 + (\omega_h L_d)^2} \gg \omega_h L_s.$$

Here, L_s is the sum of supply inductance existing upstream of the point of common coupling (PCC) and leakage inductance of a rectifier transformer. Note that the rectifier transformer is disregarded from Fig. 24.1(a). Figure 24.1(b) suggests that the supply harmonic current i_{sh} is independent of L_s .

Figure 24.2(a) shows a three-phase diode rectifier with a DC link capacitor. The rectifier would be characterized as a harmonic voltage source shown in Fig. 24.2(b) if it is seen from its AC terminals. The reason is that the following relation exists:

$$\frac{1}{\omega_h C_d} \ll \omega_h L_s.$$

This implies that i_{sh} is strongly influenced by the inductance value of L_s .

24.2 Theoretical Approach to Active Filters for Power Conditioning

24.2.1 The Akagi-Nabae Theory

The theory of instantaneous power in three-phase circuits is referred to as the “Akagi-Nabae theory” (Akagi et al., 1983; Akagi et al., 1984). Figure 24.3 shows a three-phase three-wire system on the $a-b-c$ coordinates, where no zero-sequence voltage is included in the three-phase three-wire system. Applying

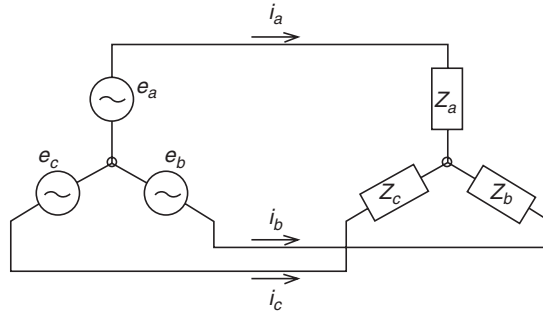


FIGURE 24.3 Three-phase three-wire system.

the theory to Fig. 24.3 can transform the three-phase voltages and currents on the $a-b-c$ coordinates into the two-phase voltages and currents on the $\alpha-\beta$ coordinates, as follows:

$$\begin{bmatrix} e_\alpha \\ e_\beta \end{bmatrix} = \sqrt{\frac{2}{3}} \begin{bmatrix} 1 & -1/2 & -1/2 \\ 0 & \sqrt{3}/2 & -\sqrt{3}/2 \end{bmatrix} \begin{bmatrix} e_a \\ e_b \\ e_c \end{bmatrix} \quad (24.1)$$

$$\begin{bmatrix} i_\alpha \\ i_\beta \end{bmatrix} = \sqrt{\frac{2}{3}} \begin{bmatrix} 1 & -1/2 & -1/2 \\ 0 & \sqrt{3}/2 & -\sqrt{3}/2 \end{bmatrix} \begin{bmatrix} i_a \\ i_b \\ i_c \end{bmatrix}. \quad (24.2)$$

As is well known, the instantaneous real power either on the $a-b-c$ coordinates or on the $\alpha-\beta$ coordinates is defined by

$$p = e_a i_a + e_b i_b + e_c i_c = e_\alpha i_\alpha + e_\beta i_\beta. \quad (24.3)$$

To avoid confusion, p is referred to as three-phase instantaneous real power. According to the theory, the three-phase instantaneous imaginary power, q , is defined by

$$q = e_\alpha i_\beta - e_\beta i_\alpha. \quad (24.4)$$

The combination of the above two equations bears the following basic formulation:

$$\begin{bmatrix} p \\ q \end{bmatrix} = \begin{bmatrix} e_\alpha & e_\beta \\ -e_\beta & e_\alpha \end{bmatrix} \begin{bmatrix} i_\alpha \\ i_\beta \end{bmatrix}. \quad (24.5)$$

Here, $e_\alpha \cdot i_\alpha$ or $e_\beta \cdot i_\beta$ obviously means instantaneous power in the α -phase or the β -phase because either is defined by the product of the instantaneous voltage in one phase and the instantaneous current in the same phase. Therefore, p has a dimension of [W]. Conversely, neither $e_\alpha \cdot i_\beta$ nor $e_\beta \cdot i_\alpha$ means instantaneous power because either is defined by the product of the instantaneous voltage in one phase and the instantaneous current in the other phase. Accordingly, q is quite different from p in dimension and electric property although q looks similar in formulation to p . A common dimension for q should be introduced from both theoretical and practical points of view. A good candidate is [IW], that is, “imaginary watt.”

Equation (24.5) is changed into the following equation:

$$\begin{bmatrix} i_\alpha \\ i_\beta \end{bmatrix} = \begin{bmatrix} e_\alpha & e_\beta \\ -e_\beta & e_\alpha \end{bmatrix} \begin{bmatrix} p \\ q \end{bmatrix} \quad (24.6)$$

Note that the determinant with respect to e_α and e_β in Eq. (24.5) is not zero. The instantaneous currents on the α - β coordinates, i_α and i_β , are divided into two kinds of instantaneous current components, respectively:

$$\begin{bmatrix} i_\alpha \\ i_\beta \end{bmatrix} = \begin{bmatrix} e_\alpha & e_\beta \\ -e_\beta & e_\alpha \end{bmatrix}^{-1} \begin{bmatrix} p \\ 0 \end{bmatrix} + \begin{bmatrix} e_\alpha & e_\beta \\ -e_\beta & e_\alpha \end{bmatrix}^{-1} \begin{bmatrix} 0 \\ q \end{bmatrix} \\ \equiv \begin{bmatrix} i_{\alpha p} \\ i_{\beta p} \end{bmatrix} + \begin{bmatrix} i_{\alpha q} \\ i_{\beta q} \end{bmatrix} \quad (24.7)$$

Let the instantaneous powers in the α -phase and the β -phase be p_α and p_β , respectively. They are given by the conventional definition as follows:

$$\begin{bmatrix} p_\alpha \\ p_\beta \end{bmatrix} = \begin{bmatrix} e_\alpha i_\alpha \\ e_\beta i_\beta \end{bmatrix} = \begin{bmatrix} e_\alpha i_{\alpha p} \\ e_\beta i_{\beta p} \end{bmatrix} + \begin{bmatrix} e_\alpha i_{\alpha q} \\ e_\beta i_{\beta q} \end{bmatrix} \quad (24.8)$$

The three-phase instantaneous real power, p , is given as follows, by using Eqs. (24.7) and (24.8):

$$\begin{aligned} p &= p_\alpha + p_\beta = e_\alpha i_{\alpha p} + e_\beta i_{\beta p} + e_\alpha i_{\alpha q} + e_\beta i_{\beta q} \\ &= \frac{e_\alpha^2}{e_\alpha^2 + e_\beta^2} p + \frac{e_\beta^2}{e_\alpha^2 + e_\beta^2} p + \frac{-e_\alpha e_\beta}{e_\alpha^2 + e_\beta^2} q + \frac{e_\alpha e_\beta}{e_\alpha^2 + e_\beta^2} q \end{aligned} \quad (24.9)$$

The sum of the third and fourth terms on the right-hand side in Eq. (24.9) is always zero. From Eqs. (24.8) and (24.9), the following equations are obtained:

$$p = e_\alpha i_{\alpha p} + e_\beta i_{\beta p} \equiv p_{\alpha p} + p_{\beta p} \quad (24.10)$$

$$0 = e_\alpha i_{\alpha q} + e_\beta i_{\beta q} \equiv p_{\alpha q} + p_{\beta q}. \quad (24.11)$$

Inspection of Eqs. (24.10) and (24.11) leads to the following essential conclusions:

- The sum of the power components, $p_{\alpha p}$ and $p_{\beta p}$, coincides with the three-phase instantaneous real power, p , which is given by Eq. (24.3). Therefore, $p_{\alpha p}$ and $p_{\beta p}$ are referred to as the α -phase and β -phase instantaneous active powers.
- The other power components, $p_{\alpha q}$ and $p_{\beta q}$, cancel each other and make no contribution to the instantaneous power flow from the source to the load. Therefore, $p_{\alpha q}$ and $p_{\beta q}$ are referred to as the α -phase and β -phase instantaneous reactive powers.
- Thus, a shunt active filter without energy storage can achieve instantaneous compensation of the current components, $i_{\alpha q}$ and $i_{\beta q}$ or the power components, $p_{\alpha q}$ and $p_{\beta q}$. In other words, the Akagi-Nabae theory based on Eq. (24.5) exactly reveals what components the active filter without energy storage can eliminate from the α -phase and β -phase instantaneous currents, i_α and i_β or the α -phase and β -phase instantaneous real powers, p_α and p_β .

24.2.2 Energy Storage Capacity

Figure 24.4 shows a system configuration of a shunt active filter for harmonic compensation of a diode rectifier, where the main circuit of the active filter consists of a three-phase voltage-fed PWM inverter and a DC capacitor, C_d . The active filter is controlled to draw the compensating current, i_{AF} , from the utility, so that the compensating current cancels the harmonic current flowing on the AC side of the diode rectifier with a DC link inductor.

Referring to Eq. (24.6) yields the α -phase and β -phase compensating currents,

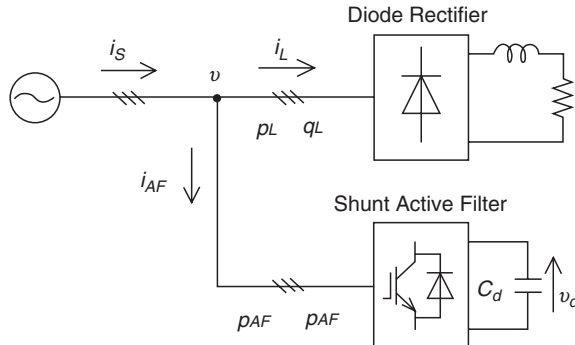


FIGURE 24.4 Shunt active filter.

$$\begin{bmatrix} i_{AF\alpha} \\ i_{AF\beta} \end{bmatrix} = \begin{bmatrix} e_\alpha & e_\beta \\ -e_\beta & e_\alpha \end{bmatrix}^{-1} \begin{bmatrix} p_{AF} \\ q_{AF} \end{bmatrix}. \quad (24.12)$$

Here, p_{AF} and q_{AF} are the three-phase instantaneous real and imaginary power on the AC side of the active filter, and they are usually extracted from p_L and q_L . Note that p_L and q_L are the three-phase instantaneous real and imaginary power on the AC side of a harmonic-producing load. For instance, when the active filter compensates for the harmonic current produced by the load, the following relationships exist:

$$p_{AF} = -\tilde{p}_L, \quad q_{AF} = -\tilde{q}_L. \quad (24.13)$$

Here, \tilde{p}_L and \tilde{q}_L are AC components of p_L and q_L , respectively. Note that the DC components of p_L and q_L correspond to the fundamental current present in i_L and the AC components to the harmonic current. In general, two high-pass filters in the control circuit extract \tilde{p}_L from p_L and \tilde{q}_L from q_L .

The active filter draws p_{AF} from the utility, and delivers it to the DC capacitor if no loss is dissipated in the active filter. Thus, p_{AF} induces voltage fluctuation of the DC capacitor. When the amplitude of p_{AF} is assumed to be constant, the lower the frequency of the AC component, the larger the voltage fluctuation (Akagi et al., 1984; Akagi et al., 1986). If the period of the AC component is one hour, the DC capacitor has to absorb or release electric energy given by integration of p_{AF} with respect to time. Thus, the following relationship exists between the instantaneous voltage across the DC capacitor, v_d and p_{AF} :

$$\frac{1}{2} C_d v_d^2(t) = \frac{1}{2} C_d v_d^2(0) + \int_0^t p_{AF} dt. \quad (24.14)$$

This implies that the active filter needs an extremely large-capacity DC capacitor to suppress the voltage fluctuation coming from achieving “harmonic” compensation of \tilde{p}_L . Hence, the active filter is no longer a harmonic compensator, and thereby it should be referred to as a “DC capacitor-based energy storage system,” although it is impractical at present. In this case, the main purpose of the voltage-fed PWM inverter is to perform an interface between the utility and the bulky DC capacitor.

The active filter seems to “draw” q_{AF} from the utility, as shown in Fig. 24.4. However, q_{AF} makes no contribution to energy transfer in the three-phase circuit. No energy storage, therefore, is required to the active filter, independent of q_{AF} , whenever $p_{AF}=0$.

24.2.3 Classification of Active Filters

Various types of active filters have been proposed in technical literature (Moran, 1989; Grady et al., 1990; Akagi, 1994; Akagi and Fujita, 1995; Fujita and Akagi, 1997; Aredes et al., 1998). Classification of active filters is made from different points of view (Akagi, 1996). Active filters are divided into AC and DC filters. Active DC filters have been designed to compensate for current and/or voltage harmonics on the DC side of thyristor converters for high-voltage DC transmission systems (Watanabe, 1990; Zhang et al., 1993) and on the DC link of a PWM rectifier/inverter for traction systems. Emphasis, however, is put on active AC filter in the following because the term “active filters” refers to active AC filters in most cases.

24.2.4 Classification by Objectives: Who is Responsible for Installing Active Filters?

The objective of “who is responsible for installing active filters” classifies them into the following two groups:

- Active filters installed by *individual consumers* on their own premises in the vicinity of one or more identified harmonic-producing loads.
- Active filters being installed by *electric power utilities* in substations and/or on distribution feeders.

Individual consumers should pay attention to current harmonics produced by their own harmonic-producing loads, and thereby the active filters installed by the individual consumers are aimed at compensating for current harmonics.

Utilities should concern themselves with voltage harmonics, and therefore active filters will be installed by utilities in the near future for the purpose of compensating for voltage harmonics and/or of achieving “harmonic damping” throughout power distribution systems or “harmonic termination” of a radial power distribution feeder. The section titled “Practical Applications of Active Filters for Power Conditioning” describes a shunt active filter intended for installation by electric power utilities on the end bus of a power distribution line.

24.2.5 Classification by System Configuration

24.2.5.1 Shunt Active Filters and Series Active Filters

A standalone shunt active filter shown in Fig. 24.4 is one of the most fundamental system configurations. The active filter is controlled to draw a compensating current, i_{AF} , from the utility, so that it cancels current harmonics on the AC side of a general-purpose diode/thyristor rectifier (Akagi et al., 1990; Peng et al., 1990; Bhattacharya et al., 1998) or a PWM rectifier for traction systems (Krah and Holtz, 1994). Generally, the shunt active filter is suitable for harmonic compensation of a current harmonic source

such as diode/thyristor rectifier with a DC link inductor. The shunt active filter has the capability of damping harmonic resonance between an existing passive filter and the supply impedance.

Figure 24.5 shows a system configuration of a series active filter used alone. The series active filter is connected in series with the utility through a matching transformer, so that it is suitable for harmonic compensation of a voltage harmonic source such as a large-capacity diode rectifier with a DC link capacitor. The series active filter integrated into a diode rectifier with a DC common capacitor is discussed in section V. Table 24.1 shows comparisons between

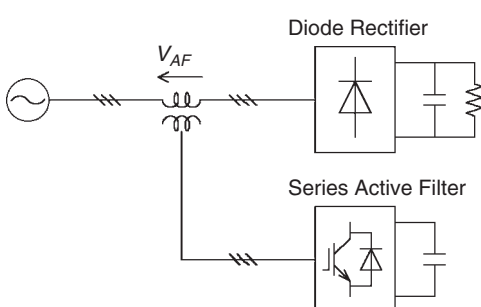


FIGURE 24.5 Series active filter.

TABLE 24.1 Comparison of Shunt Active Filters and Series Active Filters

	Shunt Active Filter	Series Active Filter
System configuration	Figure 24.4	Figure 24.5
Power circuit of active filter	Voltage-fed PWM inverter with current minor loop	Voltage-fed PWM inverter without current minor loop
Active filter acts as	Current source: i_{AF}	Voltage source: v_{AF}
Harmonic-producing load suitable	Diode/thyristor rectifiers with inductive loads, and cycloconverters	Large-capacity diode rectifiers with capacitive loads
Additional function	Reactive power compensation	AC voltage regulation
Present situation	Commercial stage	Laboratory stage

the shunt and series active filters. This concludes that the series active filter has a “dual” relationship in each item with the shunt active filter (Akagi, 1996; Peng, 1998).

24.2.5.2 Hybrid Active/Passive Filters

Figures 24.6, 24.7, and 24.8 show three types of hybrid active/passive filters, the main purpose of which is to reduce initial costs and to improve efficiency. The shunt passive filter consists of one or more tuned LC filters and/or a high-pass filter. [Table 24.2](#) shows comparisons among the three hybrid filters in which the active filters are different in function from the passive filters. Note that the hybrid filters are applicable to any current harmonic source, although a harmonic-producing load is represented by a thyristor rectifier with a DC link in Figs. 24.6, 24.7, and 24.8.

Such a combination of a shunt active filter and a shunt passive filter as shown in Fig. 24.6 has already been applied to harmonic compensation of naturally-commutated twelve-pulse cycloconverters for steel mill drives (Takeda et al., 1987). The passive filters absorbs 11th and 13th harmonic currents while the active filter compensates for 5th and 7th harmonic currents and achieves damping of harmonic resonance between the supply and the passive filter. One of the most important considerations in system design is to avoid competition for compensation between the passive filter and the active filter.

The hybrid active filters, shown in Fig. 24.7 (Peng et al., 1990; Peng et al., 1993; Kawaguchi et al., 1997) and in Fig. 24.8 (Fujita and Akagi, 1991; Balbo et al., 1994; van Zyl et al., 1995), are right now on the commercial stage, not only for harmonic compensation but also for harmonic isolation between supply and load, and for voltage regulation and imbalance compensation. They are considered prospective alternatives to pure active filters used alone. Other combined systems of active filters and passive filters or LC circuits have been proposed in Bhattacharya et al. (1997).

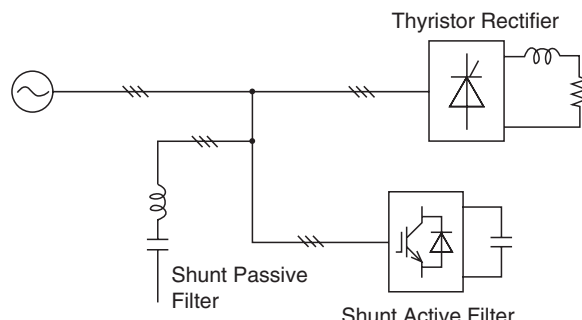


FIGURE 24.6 Combination of shunt active filter and shunt passive filter.

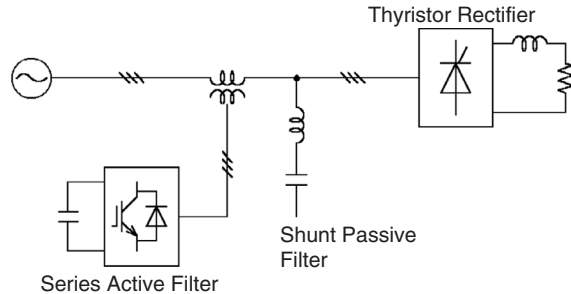


FIGURE 24.7 Combination of series active filter and shunt passive filter.

24.2.6 Classification by Power Circuit

There are two types of power circuits used for active filters; a voltage-fed PWM inverter (Akagi et al., 1986; Takeda et al., 1987) and a current-fed PWM inverter (Kawahira et al., 1983; van Schoor and van Wyk, 1987). These are similar to the power circuits used for AC motor drives. They are, however, different in their behavior because active filters act as nonsinusoidal current or voltage sources. The author prefers the voltage-fed to the current-fed PWM inverter because the voltage-fed PWM inverter is higher in efficiency and lower in initial costs than the current-fed PWM inverter (Akagi, 1994). In fact, almost all active filters that have been put into practical application in Japan have adopted the voltage-fed PWM inverter as the power circuit.

24.2.7 Classification by Control Strategy

The control strategy of active filters has a great impact not only on the compensation objective and required kVA rating of active filters, but also on the filtering characteristics in transient state as well as in steady state (Akagi et al., 1986).

24.2.7.1 Frequency-Domain and Time-Domain

There are mainly two kinds of control strategies for extracting current harmonics or voltage harmonics from the corresponding distorted current or voltage; one is based on the Fourier analysis in the frequency-domain (Grady et al., 1990), and the other is based on the Akagi-Nabae theory in the time-domain. The concept of the Akagi-Nabae theory in the time-domain has been applied to the control strategy of almost all the active filters installed by individual high-power consumers over the last ten years in Japan.

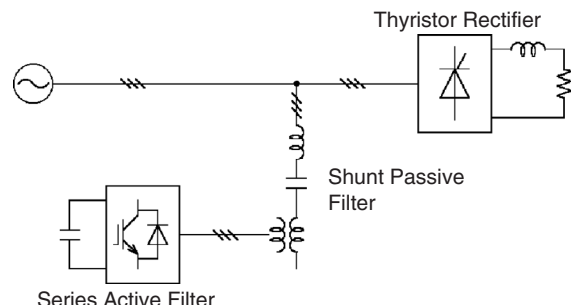


FIGURE 24.8 Series active filter connected in series with shunt passive filter.

TABLE 24.2 Comparison of Hybrid Active/Passive Filters

	Shunt Active Filter Plus Shunt Passive Filter	Series Active Filter Plus Shunt Passive Filter	Series Active Filter Connected in Series with Shunt Passive Filter
System configuration	Figure 24.6	Figure 24.7	Figure 24.8
Power circuit of active filter	<ul style="list-style-type: none"> • Voltage-fed PWM inverter with current minor loop 	<ul style="list-style-type: none"> • Voltage-fed PWM inverter without current minor loop 	<ul style="list-style-type: none"> • Voltage-fed PWM inverter with or without current minor loop
Function of active filter	<ul style="list-style-type: none"> • Harmonic compensation 	<ul style="list-style-type: none"> • Harmonic isolation 	<ul style="list-style-type: none"> • Harmonic isolation or harmonic compensation
Advantages	<ul style="list-style-type: none"> • General shunt active filters applicable • Reactive power • Controllable 	<ul style="list-style-type: none"> • Already existing shunt passive filters applicable • No harmonic current flowing through active filter • Difficult to protect active filter against overcurrent 	<ul style="list-style-type: none"> • Already existing shunt passive filters applicable • Easy protection of active filter • No reactive power control
Problems or issues	<ul style="list-style-type: none"> • Share compensation in frequency domain between active filter and passive filter 	<ul style="list-style-type: none"> • No reactive power control • A few practical applications 	
Present situation	<ul style="list-style-type: none"> • Commercial stage 		<ul style="list-style-type: none"> • Commercial stage

24.2.7.2 Harmonic Detection Methods

Three kinds of harmonic detection methods in the time-domain have been proposed for shunt active filters acting as a current source i_{AF} . Taking into account the polarity of the currents i_S , i_L and i_{AF} in Fig. 24.4 gives

$$\begin{aligned} \text{load-current detection: } & i_{AF} = -i_{Lh} \\ \text{supply-current detection: } & i_{AF} = K_S \cdot i_{Sh} \\ \text{voltage detection: } & i_{AF} = K_V \cdot v_h. \end{aligned}$$

Note that load-current detection is based on feedforward control, while supply-current detection and voltage detection are based on feedback control with gains of K_S and K_V , respectively. Load-current detection and supply-current detection are suitable for shunt active filters installed in the vicinity of one or more harmonic-producing loads by individual consumers. Voltage detection is suitable for shunt active filters that will be dispersed on power distribution systems by utilities, because the shunt active filter based on voltage detection is controlled in such a way to present infinite impedance to the external circuit for the fundamental frequency, and to present a resistor with low resistance of $1/K_V [\Omega]$ for harmonic frequencies (Akagi et al., 1999).

Supply-current detection is the most basic harmonic detection method for series active filters acting as a voltage source v_{AF} . Referring to Fig. 24.5 yields

$$\text{supply current detection: } v_{AF} = G \cdot i_{Sh}.$$

The series active filter based on supply-current detection is controlled in such a way to present zero impedance to the external circuit for the fundamental frequency and to present a resistor with high resistance of $G [\Omega]$ for the harmonic frequencies. The series active filters shown in Fig. 24.5 (Fujita and Akagi, 1997) and Fig. 24.7 (Peng et al., 1990) are based on supply current detection.

24.3 Integrated Series Active Filters

A small-rated series active filter integrated with a large-rated double-series diode rectifier has the following functions (Fujita and Akagi, 1997):

- harmonic compensation of the diode rectifier,
- voltage regulation of the common DC bus,
- damping of harmonic resonance between the communication capacitors connected across individual diodes and the leakage inductors including the AC line inductors,
- reduction of current ripples flowing into the electrolytic capacitor on the common DC bus.

24.3.1 System Configuration

Figure 24.9 shows a harmonic current-free AC/DC power conversion system described below. It consists of a combination of a double-series diode rectifier of 5 kW and a series active filter with a peak voltage and current rating of 0.38 kVA. The AC terminals of a single-phase H-bridge voltage-fed PWM inverter are connected in “series” with a power line through a single-phase matching transformer, so that the combination of the matching transformers and the PWM inverters forms the “series” active filter. For small to medium-power systems, it is economically practical to replace the three single-phase inverters with a single three-phase inverter using six IGBTs. A small-rated high-pass filter for suppression of switching ripples is connected to the AC terminals of each inverter in the experimental system, although it is eliminated from Fig. 24.9 for the sake of simplicity.

The primary windings of the Y- Δ and Δ - Δ connected transformers are connected in “series” with each other, so that the combination of the three-phase transformers and two three-phase diode rectifiers forms the “double-series” diode rectifier, which is characterized as a three-phase twelve-pulse rectifier. The DC terminals of the diode rectifier and the active filter form a common DC bus equipped with an electrolytic capacitor. This results not only in eliminating any electrolytic capacitor from the active filter, but also in reducing current ripples flowing into the electrolytic capacitor across the common DC bus.

Connecting only a commutation capacitor C in parallel with each diode plays an essential role in reducing the required peak voltage rating of the series active filter.

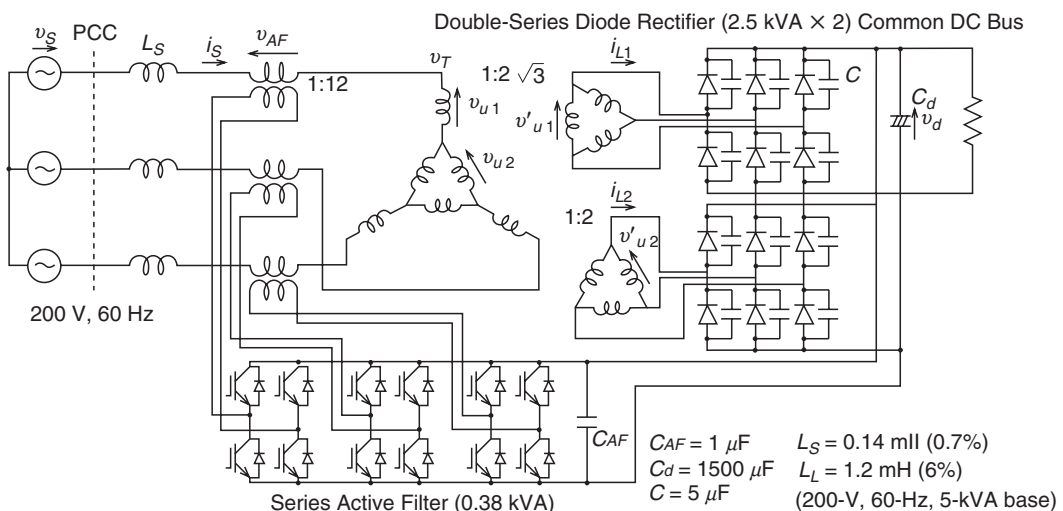


FIGURE 24.9 The harmonic current-free ac/dc power conversion system.

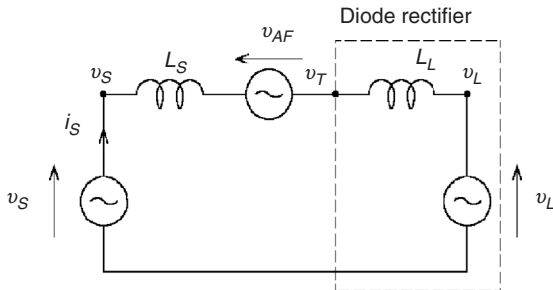


FIGURE 24.10 Single-phase equivalent circuit.

connected to the DC terminal of the diode rectifier, as shown in Fig. 24.9.

The active filter is controlled in such a way as to present zero impedance for the fundamental frequency and to act as a resistor with high resistance of $K [\Omega]$ for harmonic frequencies. The AC voltage of the active filter, which is applied to a power line through the matching transformer, is given by

$$v_{AF}^* = K \cdot i_{Sh} \quad (24.15)$$

where i_{Sh} is a supply harmonic current drawn from the utility. Note that v_{AF} and i_{Sh} are instantaneous values. Figure 24.11 shows an equivalent circuit with respect to current and voltage harmonics in Fig. 24.10. Referring to Fig. 24.11 enables derivation of the following basic equations:

$$I_{Sh} = \frac{V_{Sh} - V_{Lh}}{Z_S + Z_L + K} \quad (24.16)$$

$$V_{AF} = \frac{K}{Z_S + Z_L + K} (V_{Sh} - V_{Lh}) \quad (24.17)$$

where V_{AF} is equal to the harmonic voltage appearing across the resistor K in Fig. 24.10.

If $K \gg Z_S + Z_L$, Eqs. (24.16) and (24.17) are changed into the following simple equations.

$$I_{Sh} \approx 0 \quad (24.18)$$

$$V_{AF} \approx V_{Sh} - V_{Lh}. \quad (24.19)$$

Equation (24.18) implies that an almost purely sinusoidal current is drawn from the utility. As a result, each diode in the diode rectifier continues conducting during a half cycle. Equation (24.19) suggests that the harmonic voltage V_{Lh} , which is produced by the diode rectifier, appears at the primary terminals of the transformers in Fig. 24.9, although it does not appear upstream of the active filter or at the utility-consumer point of common coupling (PCC).

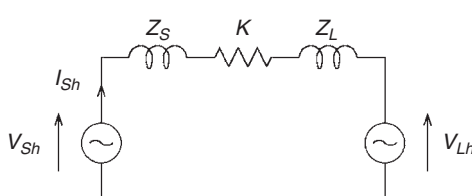


FIGURE 24.11 Single-phase equivalent circuit with respect to harmonics.

24.3.2 Operating Principle

Figure 24.10 shows an equivalent circuit for the power conversion system on a per-phase basis. The series active filter is represented as an AC voltage source v_{AF} , and the double-series diode rectifier as the series connection of a leakage inductor L_L of the transformers with an AC voltage source v_L . The reason for providing the AC voltage source to the equivalent model of the diode rectifier is that the electrolytic capacitor C_d is directly

24.3.3 Control Circuit

Figure 24.12 shows a block diagram of a control circuit based on hybrid analog/digital hardware. The concept of the Akagi-Nabae theory (Akagi, 1983; Akagi, 1984) is applied to the control circuit implementation. The p-q transformation circuit executes the following calculation to convert the three-phase supply current i_{Sv} , i_{Sw} , and i_{Sb} into the instantaneous active current i_p and the instantaneous reactive current i_q .

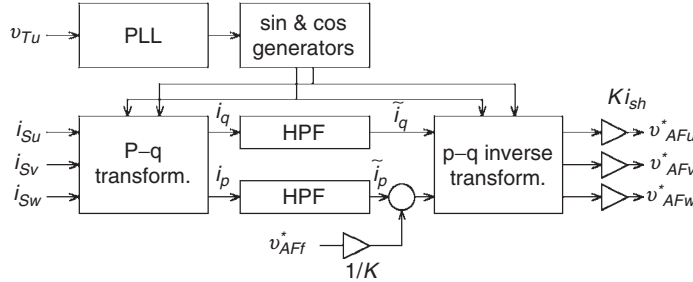


FIGURE 24.12 Control circuit for the series active filter.

$$\begin{bmatrix} i_p \\ i_q \end{bmatrix} = \sqrt{\frac{2}{3}} \begin{bmatrix} \cos \omega t & \sin \omega t \\ -\sin \omega t & \cos \omega t \end{bmatrix} \cdot \begin{bmatrix} 1 & -1/2 & -1/2 \\ 0 & \sqrt{3}/2 & -\sqrt{3}/2 \end{bmatrix} \begin{bmatrix} i_{Su} \\ i_{Sv} \\ i_{Sw} \end{bmatrix}. \quad (24.20)$$

The fundamental components in i_{Su} , i_{Sv} , and i_{Sw} correspond to DC components in i_p and i_q and harmonic components to AC components. Two first-order high-pass-filters (HPFs) with the same cut-off frequency of 10 Hz as each other extract the AC components \tilde{i}_p and \tilde{i}_q from i_p and i_q , respectively. Then, the p-q transformation/inverse transformation of the extracted AC components produces the following supply harmonic currents:

$$\begin{bmatrix} i_{Shu} \\ i_{Shv} \\ i_{Shw} \end{bmatrix} = \sqrt{\frac{2}{3}} \begin{bmatrix} 1 & 0 \\ -1/2 & \sqrt{3}/2 \\ -1/2 & -\sqrt{3}/2 \end{bmatrix} \cdot \begin{bmatrix} \cos \omega t & -\sin \omega t \\ \sin \omega t & \cos \omega t \end{bmatrix} \begin{bmatrix} \tilde{i}_p \\ \tilde{i}_q \end{bmatrix}. \quad (24.21)$$

Each harmonic current is amplified by a gain of K , and then it is applied to the gate control circuit of the active filter as a voltage reference v_{AF}^* in order to regulate the common DC bus voltage, v_{AFe} is divided by the gain of K , and then it is added to \tilde{i}_p .

The PLL (phase locked loop) circuit produces phase information ωt which is a 12-bit digital signal of 60×2^{12} samples per second. Digital signals, $\sin \omega t$ and $\cos \omega t$, are generated from the phase information, and then they are applied to the p-q (inverse) transformation circuits. Multifunction in the transformation circuits is achieved by means of eight multiplying D/A converters. Each voltage reference, v_{AF}^* is compared with two repetitive triangular waveforms of 10 kHz in order to generate the gate signals for the IGBTs. The two triangular waveforms have the same frequency, but one has polarity opposite to the other, so that the equivalent switching frequency of each inverter is 20 kHz, which is twice as high as that of the triangular waveforms.

24.3.4 Experimental Results

In the following experiment, the control gain of the active filter, K , is set to 27Ω , which is equal to 3.3 p.u. on a 3φ 200-V, 15-A, 60-Hz basis. Equation (24.16) suggests that the higher the control gain, the better the performance of the active filter. An extremely high gain, however, may make the control system unstable, and thereby a trade-off between performance and stability exists in determining an optimal control gain. A constant load resistor is connected to the common DC bus, as shown in Fig. 24.9.

Figures 24.13 and 24.14 show experimental waveforms, where a 5-μF commutation capacitor is connected in parallel with each diode used for the double-series diode rectifier. Table 24.3 shows the THD of i_s and the ratio of each harmonic current with respect to the fundamental current contained in i_s . Before starting the active filter, the supply 11th and 13th harmonic currents in Fig. 24.13 are slightly magnified due to resonance between the commutation capacitors C and the AC line and leakage

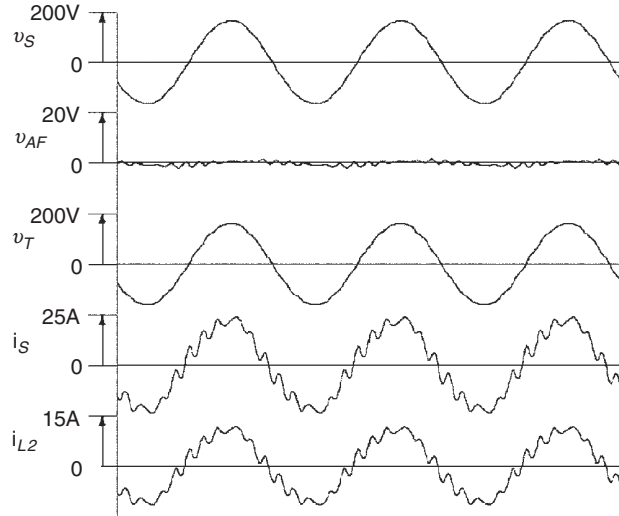


FIGURE 24.13 Experimental waveforms before starting the series active filter.

inductors, L_S and L_L . Nonnegligible amounts of 3rd, 5th, and 7th harmonic currents, which are so-called “non-characteristic current harmonics” for the three-phase twelve-pulse diode rectifier, are drawn from the utility.

Figure 24.14 shows experimental waveforms where the peak voltage of the series active filter is imposed on a limitation of ± 12 V inside the control circuit based on hybrid analog/digital hardware. Note that the limitation of ± 12 V to the peak voltage is equivalent to the use of three single-phase matching transformers with turn ratios of 1:20 under the common DC link voltage of 240 V. After starting the active filter, a sinusoidal current with a leading power factor of 0.96 is drawn because the active filter acts as a high resistor of 27Ω , having the capability of compensating for both voltage harmonics V_{Sh} and V_{Lh} as well as of damping the resonance. As shown in Fig. 24.14, the waveforms of i_S

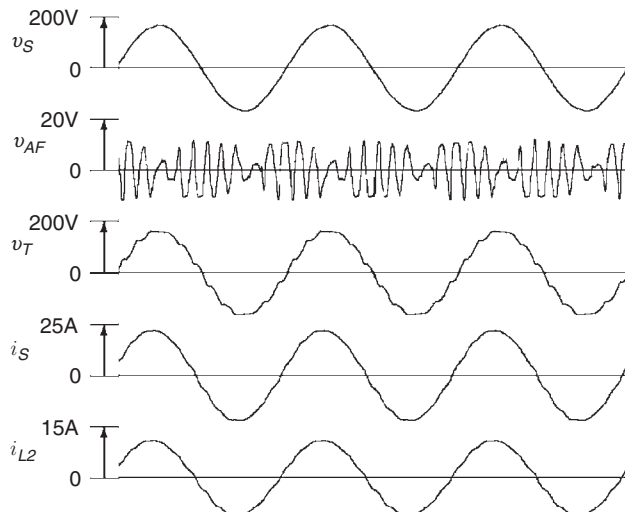


FIGURE 24.14 Experimental waveforms after starting the series active filter.

TABLE 24.3 Supply Current THD and Harmonics Expressed as the Harmonic-to-Fundamental Current Ratio %, Where Commutation Capacitors of 5 μF Are Connected

	THD	3rd	5th	7th	11th	13th
Before (Fig. 24.13)	16.8	5.4	2.5	2.2	12.3	9.5
After (Fig. 24.14)	1.6	0.7	0.2	0.4	0.8	1.0

and v_T are not affected by the voltage limitation, although the peak voltage v_{AF} frequently reaches the saturation or limitation voltage of ± 12 V.

The required peak voltage and current rating of the series active filter in Fig. 24.14 is given by

$$3 \times 12^V / \sqrt{2} \times 15^A = 0.38 \text{ kVA}, \quad (24.22)$$

which is only 7.6% of the kVA-rating of the diode rectifier.

The harmonic current-free AC-to-DC power conversion system has both practical and economical advantages. Hence, it is expected to be used as a utility interface with large industrial inverter-based loads such as multiple adjustable speed drives and uninterruptible power supplies in the range of 1–10 MW.

24.4 Practical Applications of Active Filters for Power Conditioning

24.4.1 Present Status and Future Trends

Shunt active filters have been put into practical applications mainly for harmonic compensation, with or without reactive-power compensation. Table 24.4 shows ratings and application examples of shunt active filters classified by compensation objectives.

Applications of shunt active filters are expanding, not only into industry and electric power utilities but also into office buildings, hospitals, water supply utilities, and rolling stock. At present, voltage-fed PWM inverters using IGBT modules are usually employed as the power circuits of active filters in a range of 10 kVA to 2 MVA, and DC capacitors are used as the energy storage components.

Since a combined system of a series active filter and a shunt passive filter was proposed in 1988 (Peng et al., 1990), much research has been done on hybrid active filters and their practical applications (Bhattacharya et al., 1997; Aredes et al., 1998). The reason is that hybrid active filters are attractive from both practical and economical points of view, in particular, for high-power applications. A hybrid active filter for harmonic damping has been installed at the Yamanashi test line for high-speed magnetically-levitated trains (Kawaguchi et al., 1997). The hybrid filter consists of a combination of a 5-MVA series active filter and a 25-MVA shunt passive filter. The series active filter makes a great contribution to damping of harmonic resonance between the supply inductor and the shunt passive filter.

TABLE 24.4 Shunt Active Filters on Commercial Base in Japan

Objective	Rating	Switching Devices	Applications
Harmonic compensation with or without reactive/negative-sequence current compensation	10 kVA ~ 2 MVA	IGBTs	Diode/thyristor rectifiers and cycloconverters for industrial loads
Voltage flicker compensation	5 MVA ~ 50 MVA	GTO thyristors	Arc furnaces
Voltage regulation	40 MVA ~ 60 MVA	GTO thyristors	Shinkansen (Japanese “bullet” trains)

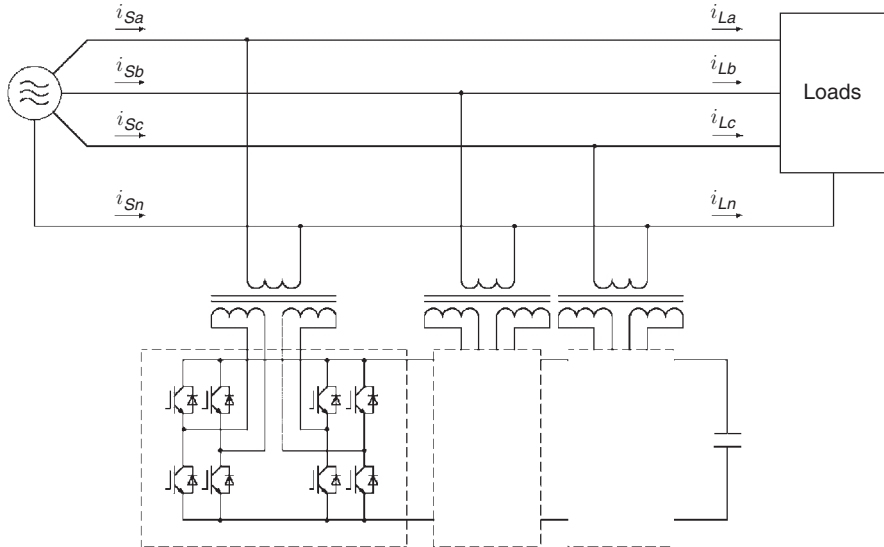


FIGURE 24.15 Shunt active filter for three-phase four-wire system.

24.4.2 Shunt Active Filters for Three-Phase Four-Wire Systems

Figure 24.15 depicts the system configuration of a shunt active filter for a three-phase four-wire system. The 300-kVA active filter developed by Meidensha has been installed in a broadcasting station (Yoshida et al., 1998). Electronic equipment for broadcasting requires single-phase 100-V AC power supply in

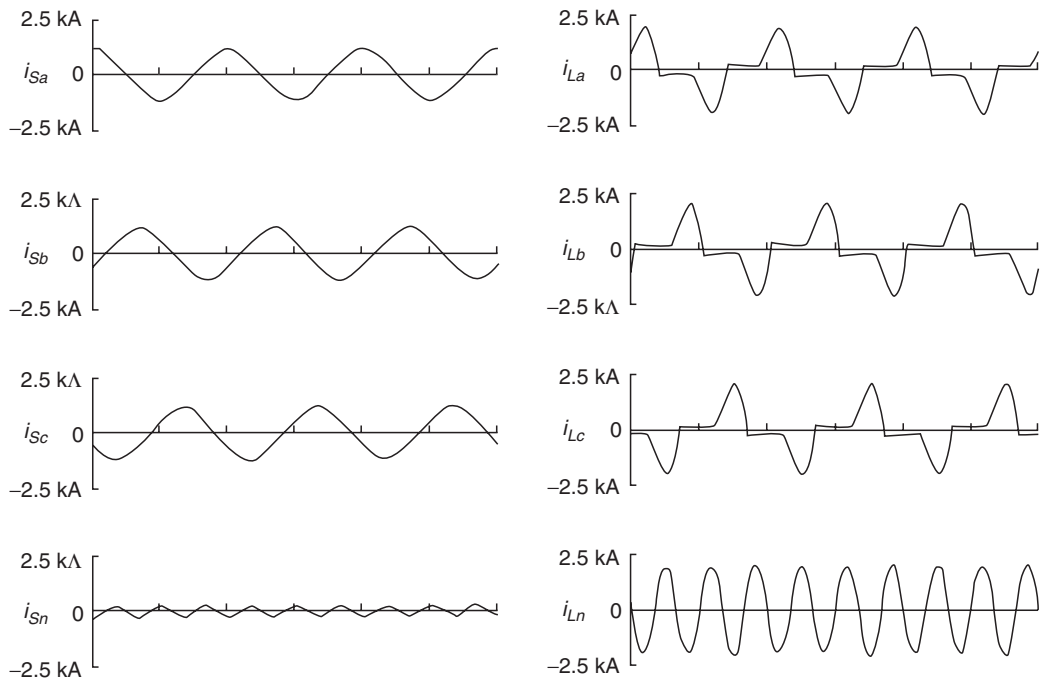


FIGURE 24.16 Actual current waveforms.

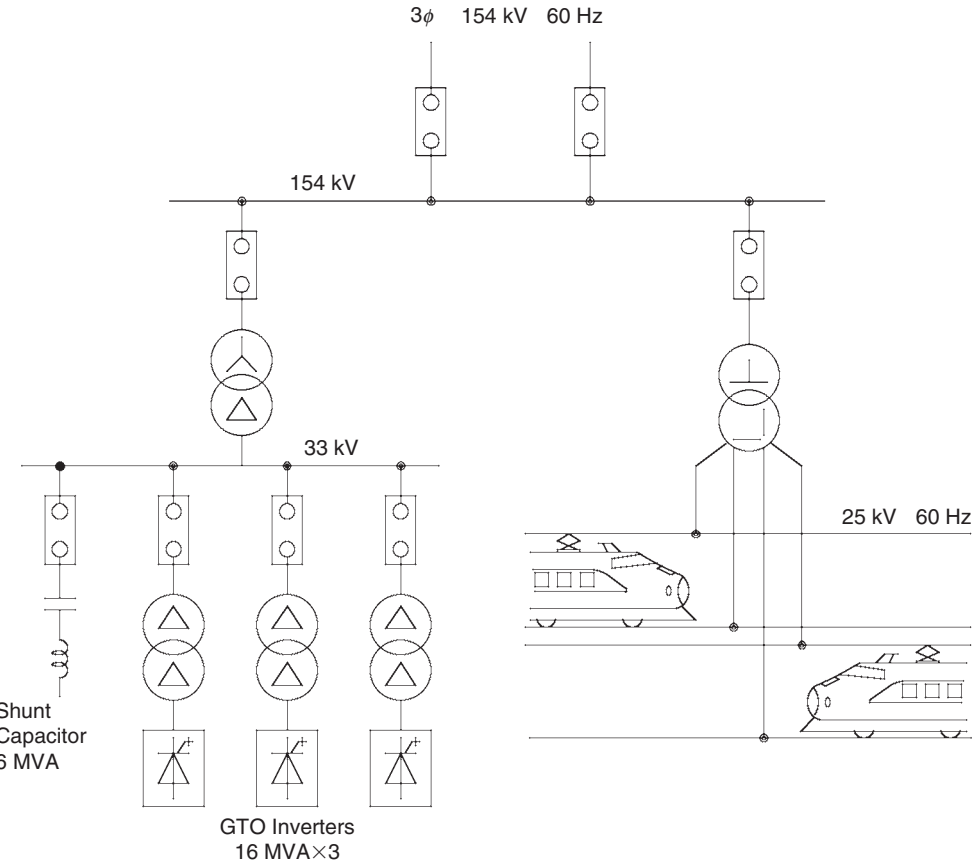


FIGURE 24.17 The 48-MVA shunt active filter installed in the Shintakatsuki substation.

Japan, and therefore the phase-neutral rms voltage is 100 V in Fig. 24.15. A single-phase diode rectifier is used as an AC-to-DC power converter in an electronic device for broadcasting. The single-phase diode rectifier generates an amount of third-harmonic current that flows back to the supply through the neutral line. Unfortunately, the third-harmonic currents injected from all of the diode rectifiers are in phase, thus contributing to a large amount of third-harmonic current flowing in the neutral line. The

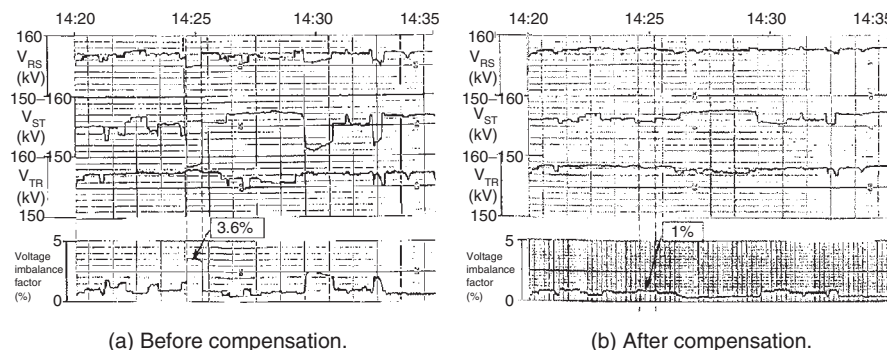


FIGURE 24.18 Installation effect.

current harmonics, which mainly contain the 3rd, 5th, and 7th harmonic frequency components, may cause voltage harmonics at the secondary of a distribution transformer. The induced harmonic voltage may produce a serious effect on other harmonic-sensitive devices connected at the secondary of the transformer.

Figure 24.16 shows actually measured current waveform in Fig. 24.15. The load currents, i_{La} , i_{Lb} , and i_{Lc} , and the neutral current flowing on the load side, i_{Ln} , are distorted waveforms including a large amount of harmonic current, while the supply currents, i_{Sa} , i_{Sb} , and i_{Sc} , and the neutral current flowing on the supply side, i_{Sn} , are almost sinusoidal waveforms with the help of the active filter.

24.4.3 The 48-MVA Shunt Active Filter for Compensation of Voltage Impact Drop, Variation, and Imbalance

Figure 24.17 shows a power system delivering electric power to the Japanese “bullet trains” on the Tokaido Shinkansen. Three shunt active filters for compensation of fluctuating reactive current/negative-sequence current have been installed in the Shintakatsuki substation by the Central Japan Railway Company (Iizuka et al., 1995). The shunt active filters, manufactured by Toshiba, consist of voltage-fed PWM inverters using GTO thyristors, each of which is rated at 16 MVA. A high-speed train with maximum output power of 12 MW draws unbalanced varying active and reactive power from the Scott transformer, the primary of which is connected to the 154-kV utility grid. More than twenty high-speed trains pass per hour during the daytime. This causes voltage impact drop, variation, and imbalance at the terminals of the 154-kV utility system, accompanied by a serious deterioration in the power quality of other consumers connected to the same power system. The purpose of the shunt active filters with a total rating of 48 MVA is to compensate for voltage impact drop, voltage variation, and imbalance at the terminals of the 154-kV power system, and to improve the power quality. The concept of the instantaneous power theory in the time-domain has been applied to the control strategy for the shunt active filter.

Figure 24.18 shows voltage waveforms on the 154-kV bus and the voltage imbalance factor before and after compensation, measured at 14:20–14:30 on July 27, 1994. The shunt active filters are effective not only in compensating for the voltage impact drop and variation, but also in reducing the voltage imbalance factor from 3.6 to 1%. Here, the voltage imbalance factor is the ratio of the negative to positive-sequence component in the three-phase voltages on the 154-kV bus. At present, several active filters in a range of 40 MVA to 60 MVA have been installed in substations along the Tokaido Shinkansen (Takeda et al., 1995).

Acknowledgment

The author would like to thank Meidensha Corporation and Toshiba Corporation for providing helpful and valuable information of the 300-kVA active filter and the 48-MVA active filter.

References

- Akagi, H., New trends in active filters for power conditioning, *IEEE Trans. Ind. Appl.*, 32, 6, 1312–1322, 1996.
- Akagi, H., Trends in active power line conditioners, *IEEE Trans. Power Electronics*, 9, 3, 263–268, 1994.
- Akagi, H., and Fujita, H., A new power line conditioner for harmonic compensation in power systems, *IEEE Trans. Power Deliv.*, 10, 3, 1570–1575, 1995.
- Akagi, H., Fujita, H., and Wada, K., A shunt active filter based on voltage detection for harmonic termination of a radial power distribution line, *IEEE Trans. Ind. Appl.*, 35, 3, 638–645, 1999.
- Akagi, H., Kanazawa, Y., and Nabae, A., Generalized theory of the instantaneous reactive power in three-phase circuits, in *Proceedings of the 1983 International Power Electronics Conference*, Tokyo, Japan, 1983, 1375–1386.
- Akagi, H., Kanazawa, Y., and Nabae, A., Instantaneous reactive power compensators comprising switching devices without energy storage components, *IEEE Trans. Ind. Appl.*, 20, 3, 625–630, 1984.

- Akagi, H., Nabae, A., and Atoh, S., Control strategy of active power filters using multiple voltage-source PWM converters, *IEEE Trans. Ind. Appl.*, 22, 3, 460–465, 1986.
- Akagi, H., Tsukamoto, Y., and Nabae, A., Analysis and design of an active power filter using quad-series voltage-source PWM converters, *IEEE Trans Ind. Appl.*, 26, 1, 93–98, 1990.
- Aredes, M., Heumann, K., and Watanabe, E.H., A universal active power line conditioner, *IEEE Trans. Power Delivery*, 13, 2, 545–551, 1998.
- Balbo, N., Penzo, R., Sella, D., Malesani, L., Mattavelli, P., and Zuccato, A., Simplified hybrid active filters for harmonic compensation in low voltage industrial applications, in *Proceedings of the 1994 IEEE/PES International Conference on Harmonics in Power Systems*, 1994, 263–269.
- Bhattacharya, S., Frank, T.M., Divan, D., and Banerjee, B., Active filter system implementation, *IEEE Industry Applications Magazine*, 4, 5, 47–63, 1998.
- Bhattacharya, S., Cheng, P., and Divan, D., Hybrid solutions for improving passive filter performance in high power applications, *IEEE Trans. Ind. Appl.*, 33, 3, 732–747, 1997.
- Bird, B.M., Marsh, J.F., and McLellan, P.R., Harmonic reduction in multiple converters by triple-frequency current injection, *IEE Proceedings*, 116, 10, 1730–1734, 1969.
- Fujita, H., and Akagi, H., An approach to harmonic current-free AC/DC power conversion for large industrial loads: The integration of a series active filter and a double-series diode rectifier, *IEEE Trans. Ind. Appl.*, 33, 5, 1233–1240, 1997.
- Fujita, H., and Akagi, H., A practical approach to harmonic compensation in power systems—Series connection of passive and active filters, *IEEE Trans. Ind. Appl.*, 27, 6, 1020–1025, 1991.
- Fujita, H., and Akagi, H., The unified power quality conditioner: The integration of series- and shunt-active filters, *IEEE Trans. Power Electronics*, 13, 2, 315–322, 1998.
- Grady, W.M., Samotyj, M.J., and Noyola, A.H., Survey of active power line conditioning methodologies, *IEEE Trans. Power Deliv.*, 5, 3, 1536–1542, 1990.
- Gyugyi, L., and Stryculla, E.C., Active AC power filters, in *Proceedings of the 1976 IEEE/IAS Annual Meeting*, 1976, 529–535.
- Iizuka, A., Kishida, M., Mochinaga, Y., Uzuka, T., Hirakawa, K., Aoyama, F., and Masuyama, T., Self-commutated static var generators at Shintakatsuki substation, in *Proceedings of the 1995 International Power Electronics Conference*, Yokohama, Japan, 1995, 609–614.
- Kawaguchi, I., Ikeda, H., Ogiwara, Y., Syogaki, M., and Morita, H., Novel active filter system composed of inverter bypass circuit for suppression of harmonic resonance at the Yamanashi maglev test line, in *Proceedings of the IEEE-IEE/IAS Power Conversion Conference*, 175–180, 1997.
- Kawahira, H., Nakamura, T., Nakazawa, S., and Nomura, M., Active power filters, in *Proceedings of the 1983 International Power Electronics Conference*, Tokyo, Japan, 1983, 981–992.
- Krah, J.O., and Holtz, J., Total compensation of line-side switching harmonics in converter-fed AC locomotives, in *Proceedings of the 1994 IEEE/IAS Annual Meeting*, 1994, 913–920.
- Lee, T.-N., Pereira, M., Renz, K., and Vaupel, G., Active damping of resonances in power systems, *IEEE Trans. Power Deliv.*, 9, 2, 1001–1008, 1994.
- Moran, S., A line voltage regulator/conditioner for harmonic-sensitive load isolation, in *Proceedings of the 1989 IEEE/IAS Annual Meeting*, 947–951, 1989.
- Peng, F.Z., Application issues of active power filters, *IEEE Industry Application Magazine*, 4, 5, 21–30, 1998.
- Peng, F.Z., Akagi, H., and Nabae, A., Compensation characteristics of the combined system of shunt passive and series active filters, *IEEE Trans. Ind. Appl.*, 29, 1, 144–152, 1993.
- Peng, F.Z., Akagi, H., and Nabae, A., A new approach to harmonic compensation in power systems—A combined system of shunt passive and series active filters, *IEEE Trans. Ind. Appl.*, 26, 6, 983–990, 1990.
- Peng, F.Z., Akagi, H., and Nabae, A., A study of active power filters using quad-series voltage-source PWM converters for harmonic compensation, *IEEE Trans. Power Electronics*, 5, 1, 9–15, 1990.
- Van Schoor, G., and van Wyk, J., A study of a system of a current-fed converters as an active three-phase filter, in *Proceedings of the 1987 IEEE/PELS Power Electronics Specialist Conference*, 482–490, 1987.

- Takeda, M., Murakami, S., Iizuka, A., Kishida, M., Mochinaga, Y., Hase, S., and Mochinaga, H., Development of an SVG series for voltage control over three-phase unbalance caused by railway load, in *Proceedings of the 1995 International Power Electronics Conference*, Yokohama, Japan, 1995, 603–608.
- Takeda, M., Ikeda, K., and Tominaga, Y., Harmonic current compensation with active filter, in *Proceedings of the 1987 IEEE/IAS Annual Meeting*, 808–815, 1987.
- Watanabe, E.H., Series active filter for the DC side of HVDC transmission systems, in *Proceedings of the 1990 International Power Electronics Conference*, Tokyo, Japan, 1024–1030, 1990.
- Yoshida, T., Nakagawa, G., Kitamura, H., and Iwatani, K., Active filters (multi-functional harmonic suppressors) used to protect the quality of power supply from harmonics and reactive power generated in loads, *Meiden Review*, 262, 5, 13–17, 1998 (in Japanese).
- Zhang, W., Asplund, G., Aberg, A., Jonsson, U., and Lööf, O., Active DC filter for HVDC system—A test installation in the Konti-Skan at Lindome converter station, *IEEE Trans. Power Deliv.*, 8, 3, 1599–1605, 1993.
- Van Zyl, A., Enslin, J.H.R., and Spée, R., Converter based solution to power quality problems on radial distribution lines, in *Proceedings of the 1995 IEEE/IAS Annual Meeting*, 2573–2580, 1995.

25

FACTS Controllers

25.1	Introduction.....	25-1
25.2	Shunt Compensators.....	25-3
	Shunt Compensation Principles • Traditional Shunt Compensation • Self-Commutated Shunt Compensators • Comparison between Thyristorized and Self-Commutated Compensators • Superconducting Magnetic Energy Storage	
25.3	Series Compensation.....	25-20
	Series Compensation Principles • Static Synchronous Series Compensator • Thyristor-Controlled Series Compensation	
25.4	Hybrid Compensation	25-31
	Unified Power Flow Controller • Interline Power Flow Controller • Unified Power Quality Conditioner	
25.5	FACTS Controller's Applications	25-34
	500 kV Winnipeg–Minnesota Interconnection (Canada–USA) • Channel Tunnel Rail Link • STATCOM “Voltage Controller” \pm 100 MVar STATCOM at Sullivan Substation (TVA) in Northeastern Tennessee • Unified Power Flow Controller “All Transmission Parameters Controller”: \pm 160 MVA Shunt and \pm 160 MVA Series at Inez Substation (AEP), Northeastern Virginia, USA • Convertible Static Compensator in the New York 345 kV Transmission System	
25.6	Conclusions.....	25-38

Luis Morán

Universidad de Concepción

Juan Dixon

Pontificia Universidad Católica de Chile

M. José Espinoza

Universidad de Concepción

José Rodríguez

Universidad Técnica Federico Santa María

25.1 Introduction

In the last decades power systems have faced new challenges due to deregulation, permanent increase in demand, the implementation of more stringent standard, and lack of investment in new transmission lines. The privatization of utilities has created a new electric power market scenario and a more complicated power system operation. Also, the increased dependence of modern society upon electricity has forced power systems to operate with very high reliability and with almost 100% availability. Moreover, power quality is now becoming a major concern among users and utilities, forcing the development and application of more stringent standards due to the connection of more sophisticated loads. These requirements have obliged to develop new technologies to improve power system operation and controllability. Based in these new technologies two concepts have been created: flexible AC transmission systems (FACTS) and flexible reliable and intelligent electrical energy delivery systems (FRIENDS). In these systems, compensation equipments based in static converters play an important role [1,2].

The FACTS concept was originally created in the 1980s to solve operation problems due to the restrictions on the construction of new transmission lines, to improve power system stability margins,

and to facilitate power exchange between different generation companies and large power users. On the other hand, the FRIENDS concept was created in the 1990s and identifies the operation of utilities with new static compensators and communication systems whose goal is to develop a desirable structure for power delivery systems where distributed generations and distributed energy storage systems are located near the load side. Finally, custom power devices are special applications of FACTS, but oriented to satisfy requirements of power quality at the utility level [5].

The two main objectives of FACTS are to increase the power transfer capability of transmission lines and to maintain the power flow over designated routes. The first objective implies that power flow in a given line should be able to be increased up to the thermal limit by forcing the rated current through the series line impedance. This objective does not mean that the lines would normally be operated at their thermal limit (the transmission losses would be unacceptable), but this option would be available, if needed, to handle severe system contingencies. The second objective implies that, by being able to control the current in a line (for example by changing the effective line impedance) the power flow can be restricted to selected transmission corridors. The achievement of these two basic objectives significantly increases the utilization of existing (and new) transmission assets, and plays a major role in facilitating deregulation [9].

Therefore, the FACTS technology opens up new opportunities for controlling power and enhancing the usable capacity of present transmission systems. The possibility that power through a line can be controlled enables a large potential of increasing the capacity of existing lines. These opportunities arise through the ability of FACTS controllers to adjust the power system electrical parameters including series and shunt impedances, current, voltage, phase angle, and the damping oscillations. The implementation of such equipments requires the development of power electronics-based compensators and controllers. The coordination and overall control of these compensators to provide maximum system benefits and prevent undesirable interactions with different system configurations under normal and contingency conditions present a different technological challenge. This challenge is the development of appropriate system optimization control strategies, communication links, and security protocols.

The IEEE Power Engineering Society (PES) Task Force of the FACTS Working Group defined terms and definitions for FACTS and FACTS controllers. According with this IEEE Working Group, a FACTS controller is a power electronic-based system and other static equipment that provide control of one or more AC transmission system parameters [3].

Different types of FACTS controllers have been developed and implemented, for shunt and/or series compensation. Shunt compensation is used to influence the natural electrical characteristics of the transmission line to increase steady-state transmittable power and to control voltage profile along the line, while series compensation is used to change the transmission line impedance and is highly effective in controlling power flow through the line and in improving system stability. Most of FACTS controllers act over the reactive power flow in order to control voltage profile and to increase power system stability. The concept of VAR compensation using FACTS controllers embraces a wide and diverse field of both transmission system and customer problems, especially related with power quality issues, since most of power quality problems can be attenuated or solved with an adequate control of reactive power [4]. In general, the problem of reactive power compensation is viewed from two aspects: load compensation and voltage support. In load compensation the objectives are to increase the value of the system power factor, to balance the real power drawn from the ac supply, compensate voltage regulation, and to eliminate current harmonic components produced by large and fluctuating nonlinear industrial loads [6]. Voltage support is generally required to reduce voltage fluctuation at a given terminal of a transmission line. Reactive power compensation in transmission systems also improves the stability of the ac system by increasing the maximum active power that can be transmitted. It also helps to maintain a substantially flat voltage profile at all levels of power transmission, it improves HVDC conversion terminal performance, increases transmission efficiency, controls steady-state and temporary overvoltages, and can avoid disastrous blackouts [7,8].

Based on the use of reliable high-speed power electronics, powerful analytical tools, advanced control and microcomputer technologies, static compensators also known as FACTS controllers have been developed and represent a new concept for the operation of power transmission systems. This chapter presents the principles of operation and performance characteristics of different FACTS controllers. Static compensators implemented with thyristors and self-commutated converters are described. New static compensators such as static synchronous compensators (STATCOMs), unified power flow controllers (UPFC), dynamic voltage restorers (DVR), required to compensate modern power transmission and distribution systems are also presented and described [10].

25.2 Shunt Compensators

Shunt compensation is used basically to control the amount of reactive power that flows through the power system. In a linear circuit, the reactive power is defined as the ac component of the instantaneous power, with a frequency equal to 100/120 Hz in a 50 or 60 Hz system. The reactive power generated by the ac power source is stored in a capacitor or a reactor during a quarter of a cycle, and in the next quarter cycle is sent back to the power source. The reactive power oscillates between the ac source and the capacitor or reactor, and also between them, at a frequency equal to two times the rated value (50 or 60 Hz). For this reason it can be compensated using static equipments or VAR generators, avoiding its circulation between the load (inductive or capacitive) and the source, and therefore improving voltage regulation and stability of the power system. Reactive power compensation can be implemented with VAR generators connected in parallel or in series [11].

25.2.1 Shunt Compensation Principles

Figure 25.1 shows the principles and theoretical effects of shunt reactive power compensation in a basic ac system, which comprises a source V_1 , a transmission line, and a typical inductive load. Figure 25.1a shows the system without compensation, and its associated phasor diagram. In the phasor diagram, the phase angle of the current has been related to the load side, which means that the active current I_P is in phase with the load voltage V_2 . Since the load is assumed inductive, it requires reactive power for proper operation, which must be supplied by the source, increasing the current flow from the generator and through the lines. If reactive power is supplied near the load, the line current is minimized, reducing power losses and improving voltage regulation at the load terminals. This can be done with a capacitor, with a voltage source, or with a current source. In Fig. 25.1b, a current-source device is being used to compensate the reactive component of the load current (I_Q). As a result, the system voltage regulation is improved and the reactive current component from the source is almost eliminated.

A current source or a voltage source can be used for reactive shunt compensation. The main advantages of using voltage- or current-source

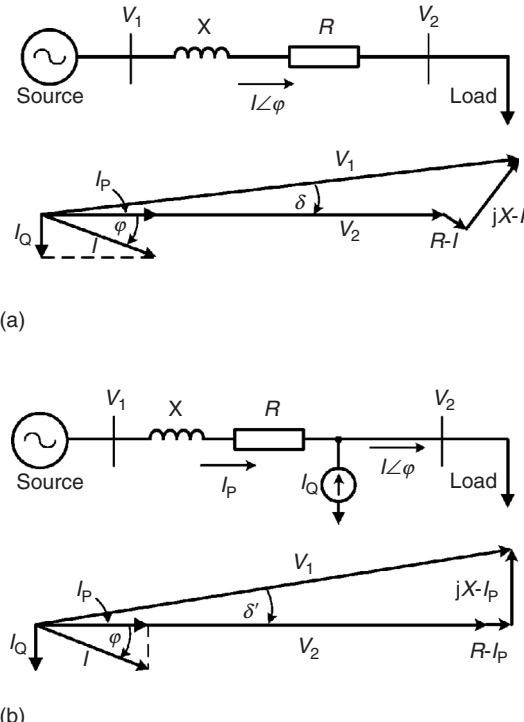


FIGURE 25.1 Principles of shunt compensation in a radial ac system. (a) System phasor diagram without reactive compensation. (b) Shunt compensation of the system with a current source.

VAR generators (instead of inductors or capacitors) are that the reactive power generated is independent of the voltage at the point of connection and can be adjusted in a wide range.

Since shunt compensation is able to change the power flow in the system by varying the value of the applied shunt equivalent impedance, changing the reactive power flow in the system, during and following dynamic disturbances, the transient stability limit can be increased and effective power oscillation damping can be provided. Thereby, the voltage of the transmission line counteracts the accelerating swings of the disturbed machine and therefore damps the power oscillations.

Independent of the source type or system configuration, different requirements have to be taken into consideration for a successful operation of shunt compensators. Some of these requirements are simplicity, controllability, time response, cost, reliability, and harmonic distortion.

25.2.2 Traditional Shunt Compensation

In general, shunt compensators are classified depending on the technology used in their implementation. Rotating and static equipments were commonly used to compensate reactive power and to stabilize power systems. In the last decades, a large number of different static FACTS controllers, using power electronic technologies and digital control schemes have been proposed and developed [11]. There are two approaches to the realization of power electronics-based compensators: the one that employs thyristor-switched capacitors and reactors with tap-changing transformers, and the other group that uses self-commutated static converters. A brief description of the most commonly used shunt compensators is presented below.

25.2.2.1 Fixed or Mechanically Switched Capacitors

Shunt capacitors were first employed for power factor correction in the year 1914 [12]. The leading current drawn by the shunt capacitors compensates the lagging current drawn by the load. The selection of shunt capacitors depends on many factors, the most important of which is the amount of lagging reactive power taken by the load. In the case of widely fluctuating loads, the reactive power also varies over a wide range. Thus, a fixed capacitor bank may often lead to either over-compensation or under-compensation. Variable VAR compensation is achieved using switched capacitors [13]. Depending on the total VAR requirement, capacitor banks are switched into or switched out of the system. The smoothness of control is solely dependent on the number of capacitors switching units used. The switching is usually accomplished using relays and circuit breakers. However, these methods based on mechanical switches and relays have the disadvantage of being sluggish and unreliable. Also, they generate high inrush currents, and require frequent maintenance.

25.2.2.2 Synchronous Condensers

Synchronous condensers have played a major role in voltage and reactive power control for more than 50 years. Functionally, a synchronous condenser is simply a synchronous machine connected to the power system. After the unit is synchronized, the field current is adjusted to either generate or absorb reactive power as required by the ac system. The machine can provide continuous reactive power control when used with the proper automatic exciter circuit. Synchronous condensers have been used at both distribution and transmission voltage levels to improve stability and to maintain voltages within desired limits under varying load conditions and contingency situations. However, synchronous condensers are rarely used today because they require substantial foundations and a significant amount of starting and protective equipment. They also contribute to the short circuit current and they cannot be controlled fast enough to compensate rapid load changes. Moreover, their losses are much higher than those associated with static compensators, and the cost is much higher as well. Their advantage lies in their high temporary overload capability [4].

25.2.2.3 Thyristorized VAR Compensators

As in the case of the synchronous condenser, the aim of achieving fine control over the entire VAR range, has been fulfilled with the development of static compensators but with the advantage of faster response

times [11]. Thyristorized VAR compensators consist of standard reactive power shunt elements (reactors and capacitors) which are controlled to provide rapid and variable reactive power. They can be grouped into two basic categories, the thyristor-switched capacitor (TSC) and the thyristor-controlled reactor (TCR).

25.2.2.3.1 Thyristor-Switched Capacitors

Figure 25.2 shows the basic scheme of a static compensator of the TSC type. First introduced by ASEA in 1971 [12], the shunt capacitor bank is split up into appropriately small steps, which are individually switched in and out using bidirectional thyristor switches. Each single-phase branch consists of two major parts, the capacitor C and the thyristor switches Sw_1 and Sw_2 . In addition, there is a minor component, the inductor L , whose purpose is to limit the rate of rise of the current through the thyristors and to prevent resonance with the network (normally 6% with respect to X_C). The capacitor may be switched with a minimum of transients if the thyristor is turned on at the instant when the capacitor voltage and the network voltage have the same value. Static compensators of the TSC type have the following properties: stepwise control, average delay of one half a cycle (maximum one cycle), and no generation of harmonics since current transient component can be attenuated effectively [12,13].

The current that flows through the capacitor at a given time t is defined by the following expression:

$$i(t) = \frac{V_m}{X_C - X_L} \cos(\omega t + \alpha) - \frac{V_m}{X_C - X_L} \cos \theta \cos(\omega_r t) + \left[\frac{X_C V_m \sin(\alpha)}{\omega_r L (X_C - X_L)} - \frac{V_{C0}}{\omega_r L} \right] \sin(\omega_r t) \quad (25.1)$$

where X_C and X_L are the compensator capacitive and inductive reactances, V_m the source maximum instantaneous voltage, α the voltage phase-shift angle at which the capacitor is connected, ω_r the system resonant frequency ($\omega_r = 1/\sqrt{LC}$), and V_{C0} is the capacitor voltage at $t=0^-$. Expression (25.1) has been obtained assuming that the system equivalent resistance is negligible as compared with the system reactance. This assumption is valid in high-voltage transmission lines. If the capacitor is connected at the moment that the source voltage is maximum and V_{C0} is equal to the source voltage peak value, V_m ($\alpha = \pm 90^\circ$) the current transient component is zero.

Despite the attractive theoretical simplicity of the switched capacitor scheme, its popularity has been hindered by a number of practical disadvantages: the VAR compensation is not continuous, each capacitor bank requires a separate thyristor switch and therefore the construction is not economical, the steady-state voltage across the nonconducting thyristor switch is twice the peak supply voltage, and the thyristor must be rated for or protected by external means against line voltage transients and fault currents.

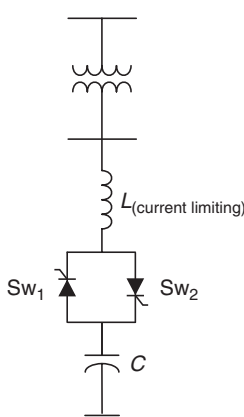


FIGURE 25.2 The thyristor-switched capacitor configuration.

An attractive solution to the disadvantages of using TSC is to replace one of the thyristor switches by a diode. In this case, inrush currents are eliminated when thyristors are fired at the right time, and a more continuous reactive power control can be achieved if the rated power of each capacitor bank is selected following a binary combination, as described in Ref. [14]. This configuration is shown in Fig. 25.3. In this figure, the inductor L_{min} is used to prevent any inrush current produced by a firing pulse out of time.

To connect each branch, a firing pulse is applied at the thyristor gate, but only when the voltage supply reaches its maximum negative value. In this way, a soft connection is obtained [1]. The current will increase starting from zero without distortion, following a sinusoidal waveform, and after the cycle is completed, the capacitor voltage will have the voltage $-V_m$, and the thyristor automatically will block. In this form of operation, both connection and disconnection of the branch will be soft, and without transient component. If the firing pulses and the voltage $-V_m$ are properly adjusted, neither harmonics nor inrush

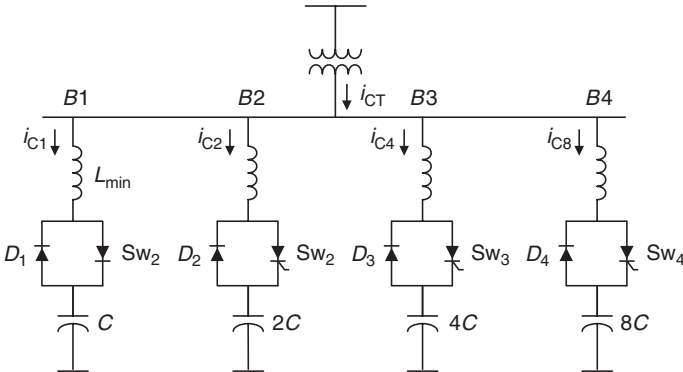


FIGURE 25.3 Binary rated thyristor-diode switched capacitor configuration.

currents are generated, since two important conditions are achieved: dv/dt at $v = -V_m$ is zero, and anode-to-cathode thyristor voltage is equal to zero. Assuming that $v(t) = V_m \sin \omega t$ is the source voltage, V_{C0} the initial capacitor voltage, and $v^{\text{Th}}(t)$ the thyristor anode-to-cathode voltage, the right connection of the branch will be when $v^{\text{Th}}(t) = 0$, that is

$$v^{\text{Th}}(t) = v(t) - V_{C0} = V_m \sin \omega t - V_{C0} \quad (25.2)$$

since $V_{C0} = -V_m$:

$$v^{\text{Th}}(t) = V_m \sin \omega t + V_m = V_m(1 + \sin \omega t) \quad (25.3)$$

then, $v^{\text{Th}}(t) = 0$ when $\sin \omega t = -1 \Rightarrow \omega t = 270^\circ$.

At $\omega t = 270^\circ$, the thyristor is switched on, and the capacitor C begins to discharge. At this point, $\sin(270^\circ) = -\cos(0^\circ)$, and hence $v_C(t)$ for $\omega t \geq 270^\circ$ will be: $V_C(t_0) = -V_m \cos \omega t_0$. The compensating capacitor current starting at t_0 will be:

$$i_c = C \frac{dv_c}{dt} = C \cdot V_m \frac{d}{dt}(-\cos \omega \cdot t_0) = C \cdot V_m \sin \omega \cdot t_0 \quad (25.4)$$

Equation (25.4) shows that the current starts from zero as a sinusoidal waveform without distortion and/or inrush component. If the above switching conditions are satisfied, the inductor L may be minimized or even eliminated.

The experimental oscilloscograms of Fig. 25.4 show how the binary connection of many branches allows an almost continuous compensating current variation. These experimental current waveforms were obtained in a 5 kVar laboratory prototype. The advantages of this topology are that many compensation levels can be implemented with few branches allowing continuous variations without distortion. Moreover, the topology is simpler and more economical as compared with TSC. The main drawback is that it has a time delay of one complete cycle compared with the half cycle of TSC.

25.2.2.3.2 Thyristor-Controlled Reactor

Figure 25.5 shows the power scheme of a static compensator of the TCR type. In most cases, the compensator also includes a fixed capacitor or a filter for low order harmonics, which is not shown in this figure. Each of the three phase branches includes an inductor L , and the thyristor switches Sw_1 and Sw_2 . Reactors may be both switched and phase-angle controlled [15–17].

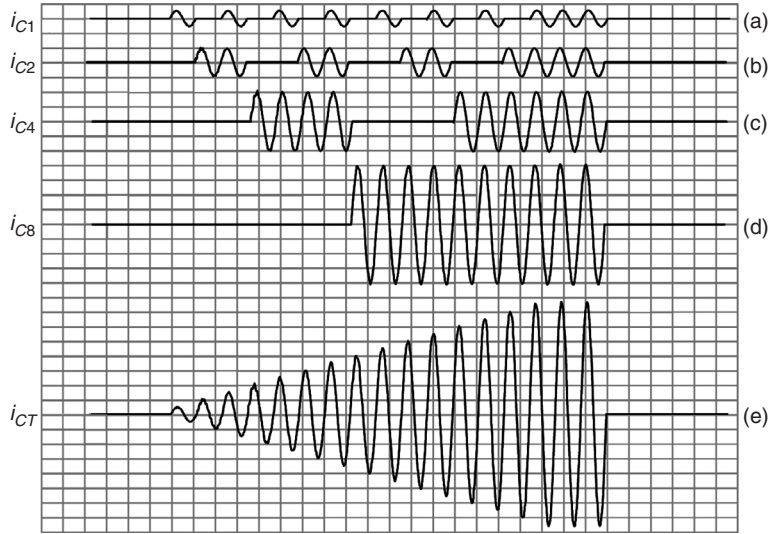


FIGURE 25.4 Experimental compensating phase current of the thyristor-diode switched capacitor: (a) current through B1; (b) current through B2; (c) current through B3; (d) current through B4, and (e) total system compensating current.

When phase-angle control is used, a continuous range of reactive power consumption is obtained. It results, however, in the generation of odd harmonic current components during the control process. Full conduction is achieved with a gating angle of 90° . Partial conduction is obtained with gating angles between 90° and 180° , as shown in Fig. 25.6. By increasing the thyristor gating angle, the fundamental component of the current reactor is reduced. This is equivalent to increase the inductance, reducing the reactive power absorbed by the static compensator.

However, it should be pointed out that the change in the reactor current may only take place at discrete points of time, which means that adjustments cannot be made quicker than once per half cycle. Static compensators of the TCR type are characterized by the ability to perform continuous control, with maximum delay of one-half cycle and practically no transients. The principal disadvantages of this configuration are the generation of low frequency harmonic current components, and higher losses when working in the inductive region (i.e., absorbing reactive power). The relation between the fundamental component of the reactor current and the phase-shift angle α is given by

$$I_1 = \frac{V_{\text{rms}}}{\pi \omega L} (2\pi - 2\alpha + \sin(2\alpha)) \quad (25.5)$$

In a single-phase unit, with balanced phase-shift angles, only odd harmonic components are presented in the reactor current. The amplitude of each harmonic component is defined by

$$I_k = \frac{4V_{\text{rms}}}{\pi X_L} \left[\frac{\sin(k+1)\alpha}{2(k+1)} + \frac{\sin(k-1)\alpha}{2(k-1)} - \cos(\alpha) \frac{\sin(k\alpha)}{k} \right] \quad (25.6)$$

In order to eliminate low frequency current harmonics (3rd, 5th, 7th), delta configurations (for zero sequence harmonics) and passive filters may be used, as shown in Fig. 25.7(a). Twelve pulse configurations are also used as shown in Fig. 25.7(b).

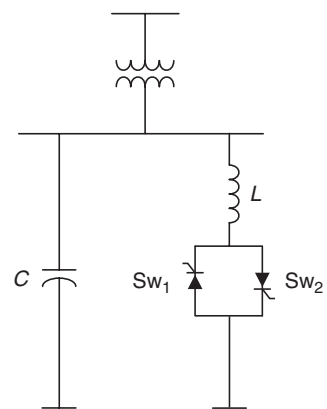


FIGURE 25.5 The thyristor-controlled reactor configuration.

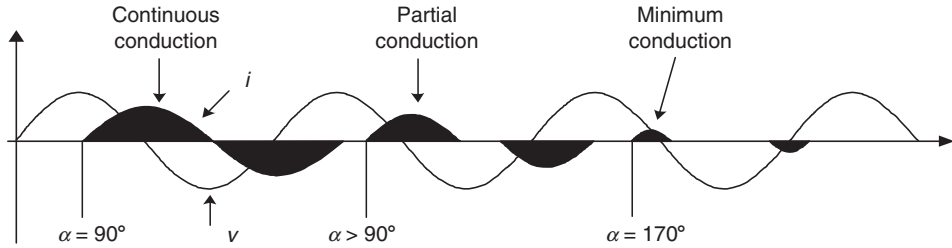


FIGURE 25.6 Simulated voltage and current waveforms in a TCR for different thyristor phase-shift angles, α .

In this case, passive filters are not required, since the 5th and 7th current harmonics are eliminated by the phase-shift introduced by the transformer.

25.2.2.3.3 VAR Compensation Characteristics

One of the main characteristics of static VAR compensators is that the amount of reactive power interchanged with the system depends on the applied voltage, as shown in Fig. 25.8. This figure displays the steady-state $V_T - Q$ characteristics of a combination of fixed capacitor–thyristor-controlled reactor (FC–TCR) compensator. This characteristic shows the amount of reactive power generated or absorbed by the FC–TCR, as a function of the applied voltage. At rated voltage, the FC–TCR presents a linear characteristic, which is limited by the rated power of the capacitor and reactor respectively. Beyond these limits, the $V_T - Q$ characteristic is not linear, which is one of the main disadvantages of this type of VAR compensator.

25.2.2.3.4 Combined Thyristor-Switched Capacitor and Thyristor-Controlled Reactor

Irrespective of the reactive power control range required, any static compensator can be built up from one or both of the above-mentioned schemes (i.e., TSC and TCR), as shown in Fig. 25.9. In those cases where the system with switched capacitors is used, the reactive power is divided into a suitable number of steps and the variation will therefore take place stepwise. Continuous control may be obtained with the addition of a TCR. If it is required to absorb reactive power, the entire capacitor bank is disconnected and the equalizing reactor becomes responsible for the absorption. By coordinating the control between the reactor and the capacitor steps, it is possible to obtain fully stepless control. Static compensators of the combined TSC and TCR type are characterized by a continuous control, practically no transients, low generation of harmonics (because the controlled reactor rating is small compared to the total reactive power), and flexibility in control and operation. An obvious disadvantage of the TSC–TCR as compared

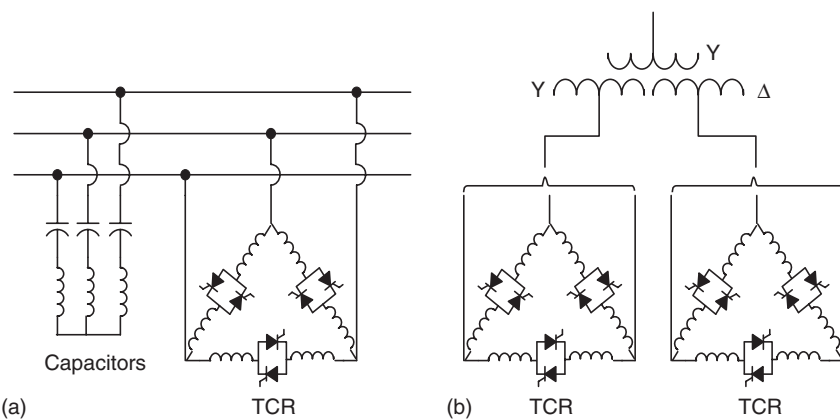


FIGURE 25.7 Fixed capacitor–thyristor-controlled reactor configuration. (a) Six pulse topology. (b) Twelve-pulse topology.

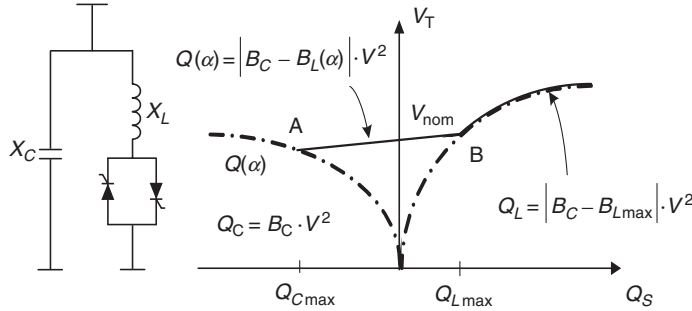


FIGURE 25.8 Voltage–reactive power characteristic of a FC–TCR.

with TCR- and TSC-type compensators is the higher cost. A smaller TCR rating results in some savings, but these savings are more than absorbed by the cost of the capacitor switches and the more complex control system [12].

The voltage–current characteristic of this compensator is shown in Fig. 25.10.

To reduce transient phenomena and harmonic distortion, and to improve the dynamics of the compensator, some researchers have applied self-commutation to TSC and TCR. Some examples of this can be found in Refs. [18,19]. However, best results have been obtained using self-commutated compensators based on conventional two-level and three-level inverters [20].

25.2.3 Self-Commutated Shunt Compensators

The application of self-commutated converters as a means of compensating reactive power has demonstrated to be an effective solution. This technology has been used to implement more sophisticated compensator equipment such as STATCOM, UPFC, and dynamic voltage compensators [3,21]. The STATCOM is based on a solid-state voltage source, implemented with an inverter, and connected in parallel to the power system through a coupling reactor, in analogy with a synchronous machine, generating balanced set of three sinusoidal voltages at the fundamental frequency, with controllable amplitude and phase-shift angle. A STATCOM is a controlled reactive power source. This equipment, however, has no inertia and limited overload capability. Examples of these topologies are shown in Figs. 25.11 and 25.12 [10,21].

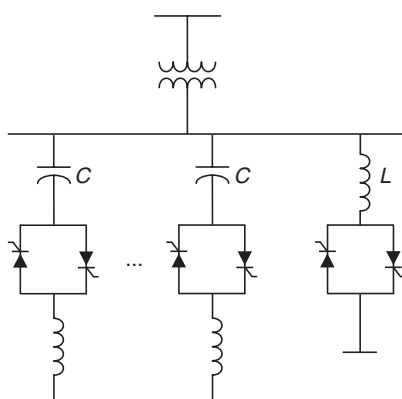


FIGURE 25.9 Combined TSC and TCR configuration.

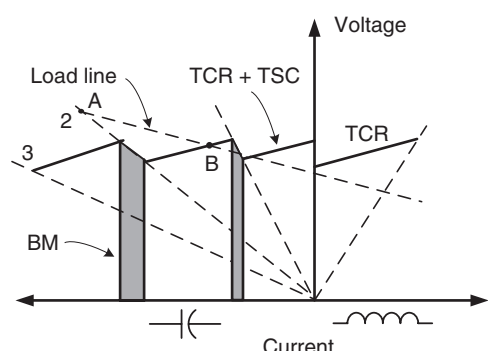


FIGURE 25.10 Steady-state voltage–current characteristic of a combined TSC–TCR compensator.

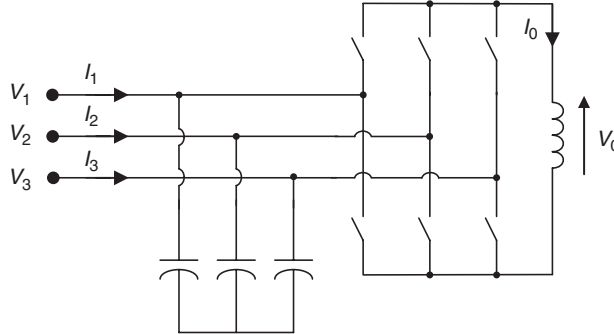


FIGURE 25.11 A VAR compensator topology implemented with a current-source converter.

25.2.3.1 Principles of Operation

With the remarkable progress of gate commutated semiconductor devices, attention has been focused on self-commutated FACTS controllers capable of generating or absorbing reactive power without requiring large banks of capacitors or reactors. Several approaches are possible including current-source and voltage-source converters. The current-source approach shown in Fig. 25.11 uses a reactor supplied with a regulated dc current, while the voltage-source inverter, displayed in Fig. 25.12, uses a capacitor with a regulated dc voltage.

The principal advantages of self-commutated FACTS controllers are the significant reduction of size and the potential reduction in cost achieved from the elimination of a large number of passive components and lower relative capacity requirement for the semiconductor switches [20,21]. Because of its smaller size, self-commutated VAR compensators are well suited for applications where space is a premium.

Self-commutated compensators are used to stabilize transmission systems, improve voltage regulation, correct power factor, and also correct load unbalances [22]. Moreover, they can be used for the implementation of shunt and series compensators. Figure 25.13 shows a shunt STATCOM, implemented with a boost type voltage-source converter. Neglecting the internal power losses of the overall converter, the control of the reactive power is done by adjusting the amplitude of the fundamental component of the output voltage V_{MOD} , which can be modified with the PWM pattern as shown in Fig. 25.14. When V_{MOD} is larger than the voltage V_{COMP} , the VAR compensator generates reactive power (Fig. 25.13b) and when V_{MOD} is smaller than V_{COMP} , the compensator absorbs reactive power (Fig. 25.13c). Its principle of operation is similar to the synchronous machine. The compensation current can be leading or lagging, depending on the relative amplitudes of V_{COMP} and V_{MOD} . The capacitor voltage V_D , connected to the dc link of the converter, is kept equal to a reference value V_{REF} through of a special feedback control loop, which controls the phase-shift angle, δ , between V_{COMP} and V_{MOD} .

The amplitude of the compensator output voltage (V_{MOD}) can be controlled by changing the switching pattern modulation index (Fig. 25.14), or by changing the amplitude of the converter dc voltage V_D . Faster time response is achieved by changing the switching pattern modulation index instead

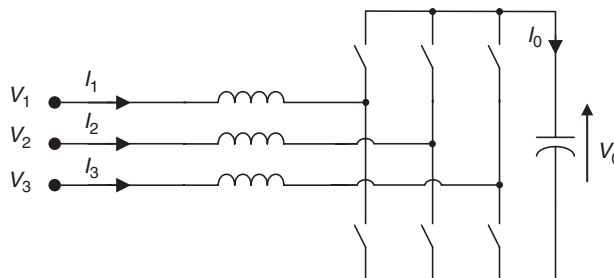


FIGURE 25.12 A VAR compensator topology implemented with a voltage-source converter.

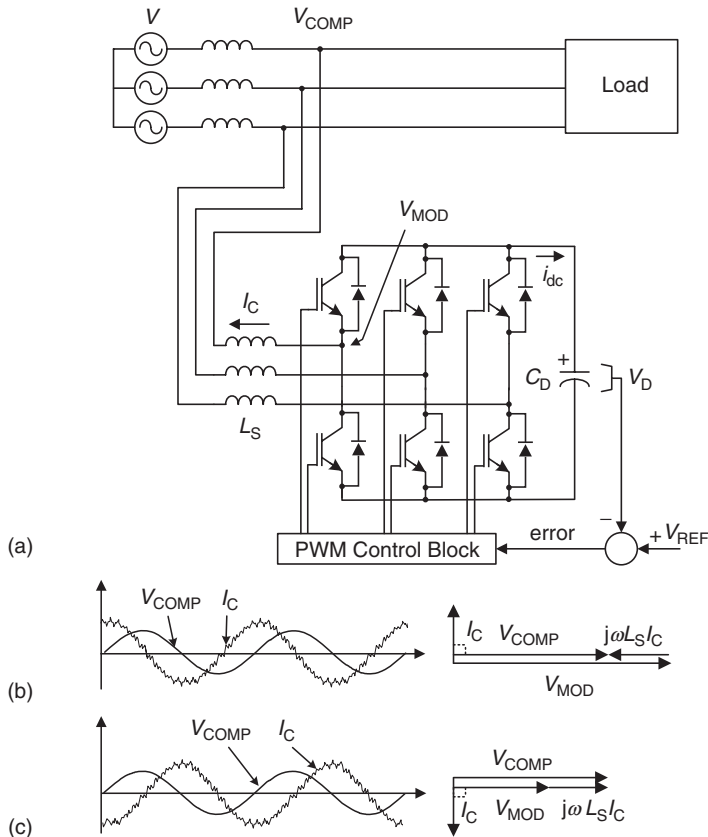


FIGURE 25.13 Simulated current and voltage waveforms of a voltage-source self-commutated shunt VAR compensator. (a) STATCOM topology. (b) Simulated current and voltage waveforms for leading compensation ($V_{MOD} > V_{COMP}$). (c) Simulated current and voltage waveforms for lagging compensation ($V_{MOD} < V_{COMP}$).

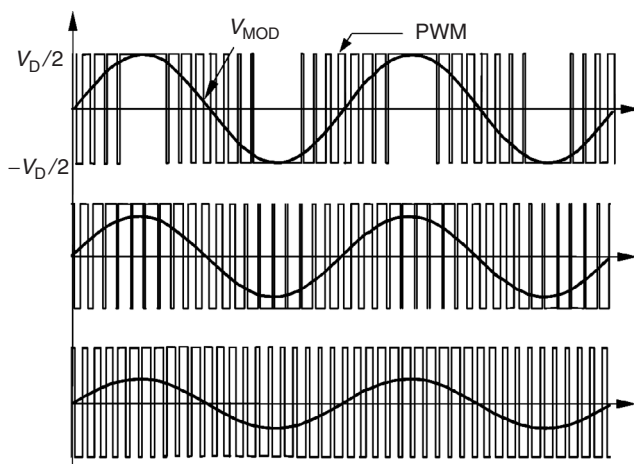


FIGURE 25.14 Simulated compensator output voltage waveform for different modulation index (amplitude of the fundamental voltage component).

of V_D . The converter dc voltage V_D , is changed by adjusting the small amount of active power absorbed by the converter and defined by

$$P = \frac{V_{\text{COMP}} \cdot V_{\text{MOD}}}{X_S} \sin \delta \quad (25.7)$$

where X_S is the converter link reactor, and δ is the phase-shift angle between voltages V_{COMP} and V_{MOD} . To increase the amplitude of V_D a small positive average value of current must circulate through the dc capacitor so that V_D will increase until it reaches the required value. In the same way, if it is necessary to decrease the amplitude of V_D then a small negative average value of current must flow through the dc capacitor. The active power flow of the converter is defined by δ . If δ is positive the converter absorbs active power (increasing V_D), and if δ is negative the converter generates active power, and therefore V_D decreases.

One of the major problems that must be solved when self-commutated converters are used in high-voltage systems is the limited capacity of the gate-controlled semiconductors available in the market (IGBTs and IGCTs). Actual semiconductors can handle a few thousands of amperes and 6 to 10 kV reverse voltage blocking capabilities, which is clearly not enough for high-voltage applications. This problem can be overcome by using more sophisticated converters topologies, as described below.

25.2.3.2 Multilevel Converters

Multilevel converters are being investigated and some topologies are used today as STATCOM. The main advantages of multilevel converters are less harmonic generation and higher voltage capability because of serial connection of bridges or semiconductors. The most popular arrangement today is the three-level neutral-point clamped (NPC) topology.

25.2.3.2.1 Three-Level Neutral-Point Clamped Topology

Figure 25.15 shows a STATCOM implemented with a three-level NPC converter. Three-level converters [23] are becoming the standard topology for medium voltage converter applications, such as machine drives and

active front-end rectifiers. The advantage of three-level converters is that they can reduce the generated harmonic content, for the same switching frequency, since they produce a voltage waveform with more levels than the conventional two-level topology. Another advantage is that they can reduce the semiconductor voltage rating and the associated switching frequency. Three-level converters consist of 12 self-commutated semiconductors such as IGBTs or IGCTs, each of them shunted by a reverse parallel connected power diode, and six diode branches connected between the midpoint of the dc link bus and the midpoint of each pair of switches as shown in Fig. 25.15. By connecting the dc source sequentially to the output terminals, the converter can produce a set of PWM signals in which the frequency, amplitude, and phase of the ac voltage can be modified with adequate control signals.

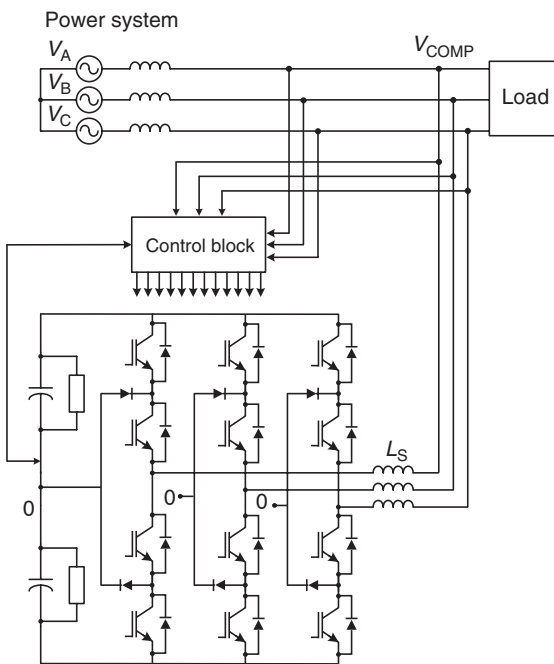


FIGURE 25.15 A STATCOM implemented with a three-level NPC inverter.

25.2.3.2.2 Multilevel Converters with Single-Phase Inverters

Another exciting technology that has been successfully proven uses basic “H” bridges

as shown in Fig. 25.16, connected to line through power transformers. The system uses sinusoidal pulse width modulation (SPWM) with triangular carriers shifted and depending on the number of converters connected in the chain of bridges, the voltage waveform becomes more and more sinusoidal. Figure 25.16(a) shows one phase of this topology implemented with eight “H” bridges and Fig. 25.16(b) shows the voltage waveforms obtained as a function of number of “H” bridges.

An interesting result with this converter is that the ac voltages become modulated by pulse width and by amplitude (PWM and AM). This is because when the pulse modulation changes, the steps of the amplitude also change. The maximum number of steps of the resultant voltage is equal to two times the number of converters plus the zero level. Then, four bridges will result in a nine-level converter per phase.

Figure 25.17 shows the principles of AM operation. When the voltage decreases, some steps disappear, and then the amplitude modulation becomes a discrete function.

25.2.3.2.3 Optimized Multilevel Converter

The number of levels can increase rapidly with few converters when voltage escalation is applied. In a similar way of converter in Fig. 25.16, the topology of Fig. 25.18 has a common dc link with voltage isolation through output transformers, connected in series at the line side. However, the voltages at the line side are scaled in power of three. By using this strategy, the number of voltage steps is maximized and few converters are required to obtain almost sinusoidal voltage waveforms. In the topology of Fig. 25.18, amplitude modulation with 81 levels of voltage is obtained using only four “H” converters per phase (four-stage inverter). In this way, STATCOMs with “harmonic-free” characteristics can be implemented.

It is important to remark that the bridge with the higher voltage is being commutated at the line frequency, which is a major advantage of this topology for high power applications. Another interesting characteristic of this converter, compared with the multilevel strategy with carriers shifted, is that only four “H” bridges per phase are required to get 81 levels of voltage. In the previous multilevel converter with carriers shifted, 40 “H” bridges instead of four are required. For high power applications, probably a less complicated three-stage (three “H” bridges per phase) is enough. In this case, 27 levels or steps of voltage are obtained, which will provide good enough voltage and current waveforms for high-quality operation [26].

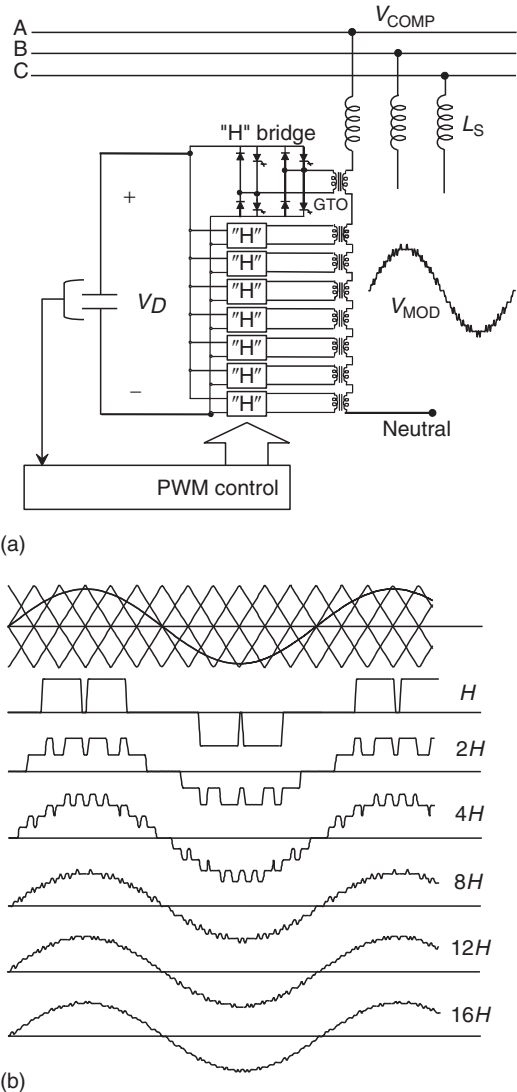


FIGURE 25.16 Multilevel STATCOM implemented with “H” bridge converters and associated voltage waveforms. (a) Multilevel converter with eight “H” bridges per phase and triangular carriers shifted. (b) Voltage waveforms as a function of number of bridges.

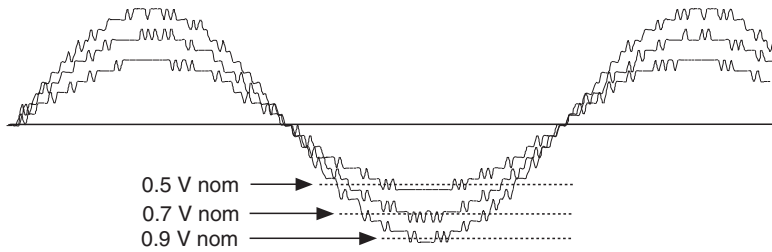


FIGURE 25.17 Amplitude modulation in the voltage waveform topology of Fig. 25.16.

25.2.3.3 STATCOM Design Principles

The principal components of the STATCOM are the PWM converter, the coupling reactor, and the dc capacitor. The converter topology depends on the rated voltage and power, and can be implemented with a voltage- or current-source approach, although most of the STATCOM have been implemented using voltage-source converters. The design of the coupling reactor and dc capacitor is based on the functions they perform. The main purpose of the coupling reactor is to absorb the instantaneous voltage difference that appears between the utility voltage and the converter input voltage. Also, in case of using a voltage-source converter, the reactor helps to reduce the harmonic distortion of the line current, and can contribute to stabilize the converter switching frequency.

25.2.3.3.1 Coupling Reactor Design

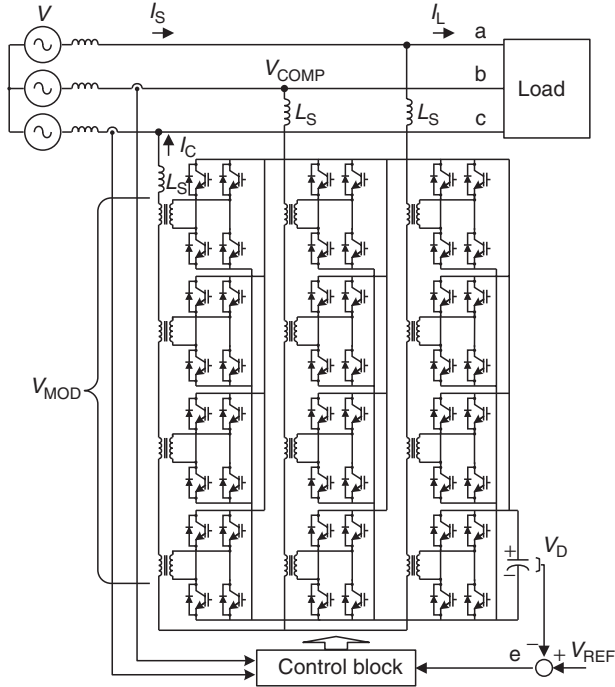
Two criteria have been used to design the coupling reactor. The first one is based in the maximum current harmonic allowed in the input current and the second one is related with the control scheme implemented in the current loop. In the first case, the reactor value is given by expression

$$X_L = \frac{1}{THD_i} \sqrt{\sum_{k=1}^{\infty} \frac{(V_{ak})^2}{k^2}} \quad (25.8)$$

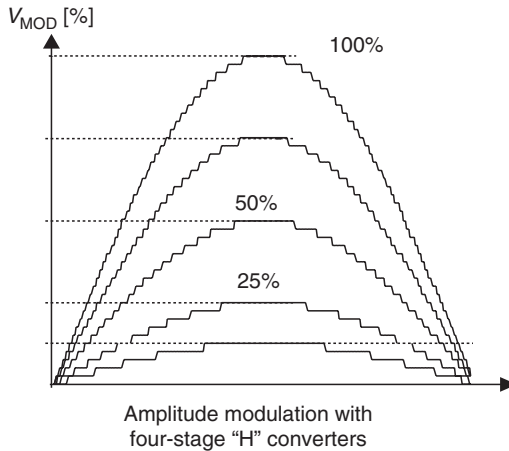
where THD_i is the maximum harmonic distortion allowed in the converter input current (normally 5%), V_{ak} the converter input voltage harmonic component, and k the order of the harmonic component. The converter input voltage, V_{ak} , depends on the PWM technique implemented in the converter.

In case a current control loop is implemented, the reactor value must be rated in order to allow intersections between the current reference and the converter input current. The block diagram of a typical current control scheme used in STATCOM is shown in Fig. 25.19. The principal advantage of this current control scheme is that it forces the converter to operate with constant switching frequency. The constant switching frequency is achieved by comparing the current error signal with a triangular reference waveform. The purpose of introducing the triangular waveform is to stabilize the inverter switching frequency by forcing it to be constant and equal to the frequency of the triangular reference.

The current control method can be explained by considering the hysteresis technique plus the addition of a fixed frequency triangular waveform inside the imaginary hysteresis window (Fig. 25.20). If the current reference, i_s^* , is higher than the generated current, i_s , the error waveform is positive and when compared with the triangular waveform it results in a positive pulse. This pulse will then turn on an inverter bottom switch that will increase the corresponding output line current. In the same way, if i_s^* is lower than i_s , the error waveform is negative and the gating signals are adjusted so that the line current decreases (a top switch is turned on). The slope of the error signal is chosen to be always smaller than the slope of the triangular waveform in order to ensure that an intersection between the two signals exists. Thus, the current error signal is forced to remain between the maximum and the minimum of the triangular waveform and as a result, the line current follows the reference closely. Moreover, since



(a)



(b)

FIGURE 25.18 Optimized STATCOM using "H" bridges converters. (a) Four-stage, 81-level STATCOM, using "H" bridges scaled in power of three; (b) converter output voltage using amplitude modulation.

the error between i_s^* and i_s is always kept within the positive and negative peaks of the triangular waveform, the system has an inherent overcurrent protection. However, a large variation in the reference current will generate a large error signal, which can be higher than the amplitude of the triangular waveform. In this case there will not be an intersection between the error and the triangular waveform, thus the switching pattern will not change until the error is reduced and a new intersection occurs.

The minimum amplitude of the triangular waveform is determined by the maximum slope of the error, which is in turn fixed by the maximum slope of the line current. The maximum slope of the line

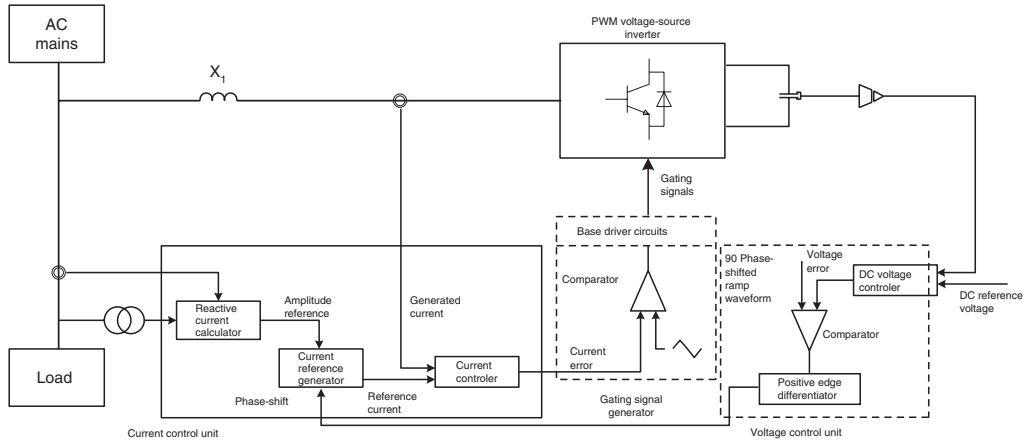


FIGURE 25.19 The block diagram of a current controlled STATCOM.

current is determined by the maximum instantaneous voltage drop across the coupling reactor and the value of the inductance. Reducing the amplitude of the triangular waveform below this value will generate multiple crossing between the current error and the triangular signals thus disturbing the operation of the inverter. The value of the coupling reactor inductance is obtained from expression

$$L = \Delta V_{\text{reactor}} \frac{1}{4A_{\text{triangular}} f_t} \quad (25.9)$$

where $\Delta V_{\text{reactor}}$ is the maximum expected voltage drop across the coupling reactor, $A_{\text{triangular}}$ the amplitude of the triangular control waveform, and f_t the triangular waveform frequency (equals to the converter switching frequency).

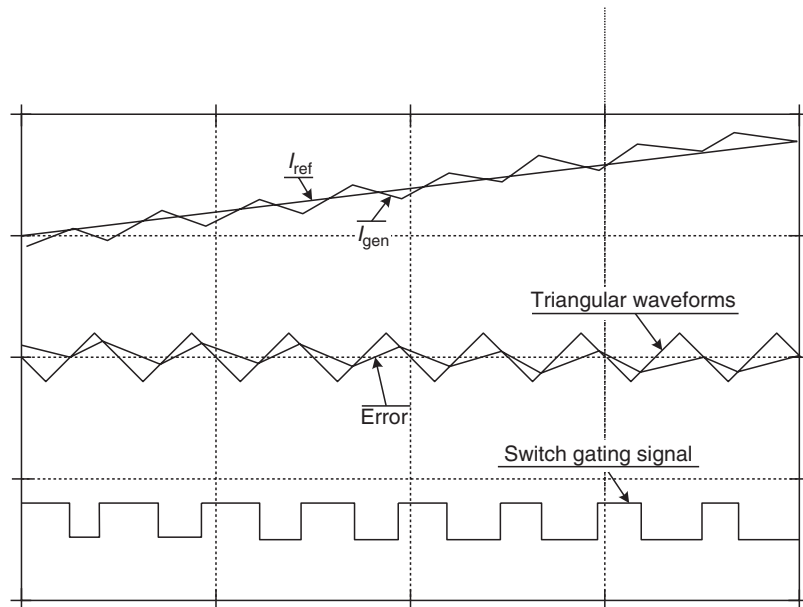


FIGURE 25.20 Principles of operation of the fixed switching frequency current control technique.

25.2.3.3.2 DC Capacitor Design

The function of the dc capacitor is to maintain a dc voltage constant and equal to the reference value imposed by the control scheme. In theory, the dc capacitor is not used as an energy storage element, although it may be necessary to compensate active power in case of outage, especially in industrial applications. Two design criteria are used to calculate the capacitance value. The first is related with the maximum voltage harmonic distortion factor allowed in the dc voltage, and the second one with the maximum voltage fluctuation that can be tolerated in the dc voltage in case of load rejection or a step increase in the load power. In the first case the capacitance is obtained with expression (25.9), and in the second one (maximum voltage fluctuation) with expression (25.10). If the dc capacitor is designed with the constraint that with rated leading VAR compensation, the ripple factor for V_D is less than a given value, the capacitance is defined by expression

$$X_C = \frac{R_V V_D}{\left\{ \sum_k \frac{I_{ck}^2}{k^2} \right\}^{1/2}} \quad (25.10)$$

where R_V is the maximum voltage ripple factor across the dc capacitor and I_{ck} the capacitor current harmonic component.

Independently of the STATCOM control scheme, an overvoltage is created when the converter line currents are forced to reduce their amplitude, or when they are forced to change from a 90° leading to a 90° lagging phase-shift. On the other hand, an undervoltage is generated when the line currents are forced to increase their amplitude, or when they are forced to change from a 90° lagging to a 90° leading phase-shift. These dc voltage fluctuations are created because transiently the dc capacitor supplies (or absorbs) the extra power required by the system. The amplitude of this voltage fluctuation depends on the instant at which the transient occurs and on the amount of change in the line current amplitude. The maximum overvoltage is generated when one of the line currents is forced to change from 1 per unit leading to 1 per unit lagging, and can be calculated using expression

$$V_{D\max} = \frac{1}{C} \int_{\theta/\omega} i_c(t) dt + V_{D0} \quad (25.11)$$

where $V_{D\max}$ is the maximum overvoltage across the dc capacitor, V_{D0} is the steady-state dc voltage, and i_c is the instantaneous capacitor current. The dc current $i_c(t)$ is defined by the product of the converter line currents with the respective switching functions. The principal design constraint for C is to keep the voltage fluctuation below a defined value, ΔV , that is

$$C = \frac{1}{\Delta V} \int_t i_c(t) dt \quad (25.12)$$

Comparing the two design criteria, the second one provides a larger value of C , which contributes to increase the STATCOM stability, making its operation safer.

25.2.3.4 Semiconductor Devices Used for Self-Commutated STATCOMs and FACTS Controllers

Three are the most relevant devices for applications in self-commutated STATCOMs or other FACTS controllers: thyristors, insulated gate bipolar transistors (IGBTs), and integrated gate controlled thyristors (IGCTs). This field of application requires that the semiconductor must be able to block high voltages in the kV range. High-voltage IGBTs required to apply self-commutated converters in FACTS controllers reach now the level of 6.5 kV, allowing for the construction of circuits with a power of several MVA. Also

IGCTs are reaching levels higher than 6 kV. Perhaps, the most important development in semiconductors for high-voltage applications is the light triggered thyristor (LTT). This device is the most important for ultrahigh power applications. Recently, LTT devices have been developed with a capability of up to 13.5 kV and a current of up to 6 kA. These new devices reduce the number of elements in series and in parallel, reducing consequently the number of gate and protection circuits. With these elements, it is possible to reduce cost and increase rated power in FACTS installations of up to several hundreds of MVARs [24].

25.2.4 Comparison between Thyristorized and Self-Commutated Compensators

Thyristorized and self-commutated FACTS controllers are very similar in their functional compensation capability, but the basic operating principles, as shown, are fundamentally different. A STATCOM functions as a shunt-connected synchronous voltage source whereas a thyristorized compensator operates as a shunt-connected, controlled reactive admittance. This difference accounts for the STATCOM's superior functional characteristics, better performance, and greater application flexibility.

In the linear operating range of the V - I characteristic, the functional compensation capability of the STATCOM and Static VAR Compensator (SVC) is similar. Concerning the nonlinear operating range, the STATCOM is able to control its output current over the rated maximum capacitive or inductive range independently of the ac system voltage, whereas the maximum attainable compensating current of the SVC decreases linearly with ac voltage. Thus, the STATCOM is more effective than the SVC in providing voltage support under large system disturbances during which the voltage excursions would be well outside of the linear operating range of the compensator. The ability of the STATCOM to maintain full capacitive output current at low system voltage also makes it more effective than the SVC in improving the transient stability limit. The attainable response time and the bandwidth of the closed voltage regulation loop of the STATCOM are also significantly better than those of the SVC.

Table 25.1 summarizes the comparative merits of the main types of shunt FACTS compensation. The significant advantages of self-commutated compensators make them an interesting alternative to improve compensation characteristics and also to increase the performance of ac power systems.

TABLE 25.1 Comparison of Basic Types of Shunt Compensators

	Static Compensator			
	Synchronous Condenser	TCR (with Shunt Capacitors if Necessary)	TSC (with TCR if Necessary)	Self-Commutated Compensator
Accuracy of compensation	Good	Very good	Good, very good with TCR	Excellent
Control flexibility	Good	Very good	Good, very good with TCR	Excellent
Reactive power capability	Leading/lagging	Lagging/leading indirect	Leading/lagging indirect	Leading/lagging
Control	Continuous	Continuous	Discontinuous (continuous with TCR)	Continuous
Response time	Slow	Fast, 0.5 to 2 cycles	Fast, 0.5 to 2 cycles	Very fast but depends on the control system and switching frequency
Harmonics	Very good	Very high (large-size filters are needed)	Good, filters are necessary with TCR	Good, but depends on switching pattern
Losses	Moderate	Good, but increase in lagging mode	Good, but increase in leading mode	Very good, but increase with switching frequency
Phase balancing ability	Limited	Good	Limited	Very good with 1- ϕ units, limited with 3- ϕ units
Cost	High	Moderate	Moderate	Low to moderate

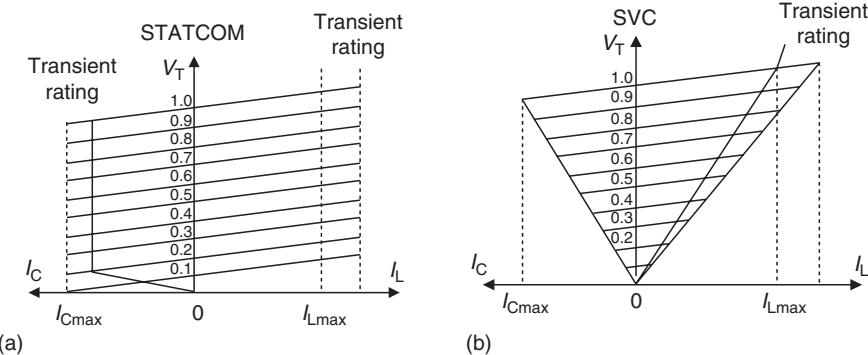


FIGURE 25.21 Voltage–current characteristics of shunt VAR compensators. (a) Compensator implemented with self-commutated converter (STATCOM). (b) Compensator implemented with back to back thyristors.

As compared with thyristor-controlled capacitor and reactor banks, self-commutated VAR compensators have the following advantages:

1. They can provide both leading and lagging reactive power, thus enabling a considerable saving in capacitors and reactors. This in turn reduces the possibility of resonances at some critical operating conditions.
2. Since the time response of self-commutated converter can be faster than the fundamental power network cycle, reactive power can be controlled continuously and precisely.
3. High frequency modulation of self-commutated converter results in a low harmonic content of the supply current, thus reducing the size of passive filter components.
4. They do not generate inrush current.
5. The dynamic performance under voltage variations and transients is improved.
6. Self-commutated VAR compensators are capable of generating 1 p.u. reactive current even when the line voltages are very low. This ability to support the power system is better than that obtained with thyristor-controlled VAR compensators because the current in shunt capacitors and reactors is proportional to the voltage.
7. Self-commutated compensators with appropriate control can also act as active line harmonic filters, DVR, or UPFC.

Figure 25.21 shows the voltage/current characteristic of a self-commutated VAR compensator compared with that of thyristor-controlled SVC. This figure illustrates that the self-commutated compensator offers better voltage support and improved transient stability margin by providing more reactive power at lower voltages. Because no large capacitors and reactors are used to generate reactive power, the self-commutated compensator provides faster time response and better stability to variations in system impedances.

25.2.5 Superconducting Magnetic Energy Storage

The principal limitation of STATCOM is that it cannot provide active power, since they have limited energy storage components (dc capacitor or reactor). This limitation is overcome, if the traditional electrolytic capacitor used in the dc link is replaced by an SMES, as shown in Fig. 25.22. This device is capable to store and instantaneously discharge large quantities of power [27,28]. It stores energy in the magnetic field created by the flow of dc current in a coil of superconducting material that has been cryogenically cooled. These systems have been in use for several years to improve power quality and to provide a premium-quality service for individual customers vulnerable to voltage fluctuations. The SMES recharges within minutes and can repeat the charge/discharge sequence thousands of times

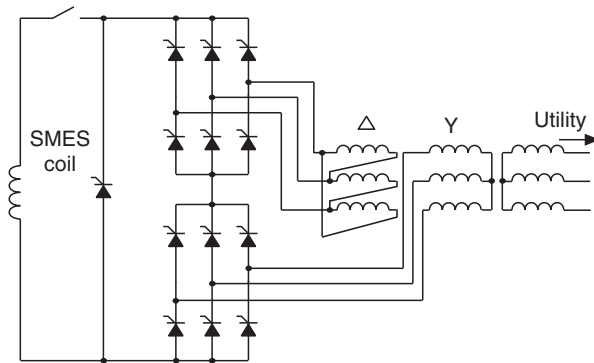


FIGURE 25.22 SMES implemented with a 12-pulse thyristor converter.

without any degradation of the magnet. Recharge time can be accelerated to meet specific requirements, depending on system capacity. It is claimed that SMES is 97–98% efficient and it is much better at providing reactive power on demand. Figure 25.23 shows a different SMES topology using three-level converters.

The first commercial application of SMES was in 1981 [28] along the 500-kV Pacific Intertie, which interconnects California and the Northwest. The device's purpose was to demonstrate the feasibility of SMES to improve transmission capacity by damping inter-area modal oscillations. Since that time, many studies have been performed and prototypes developed for installing SMES to enhance transmission line capacity and performance. A major cost driver for SMES is the amount of stored energy. Previous studies have shown that SMES can substantially increase transmission line capacity when utilities apply relatively small amounts of stored energy and a large power rating (greater than 50 MW).

Another interesting application of SMES for frequency stabilization is in combination with static synchronous series compensator (SSSC) [29].

25.3 Series Compensation

FACTS controllers can also be of the series type. Typical series compensators use capacitors to reduce the equivalent reactance of a power line at rated frequency, thus increasing the voltage at the load terminals. The connection of a series compensator generates reactive power that, in a self-regulated manner, balances a fraction of the line's reactance.

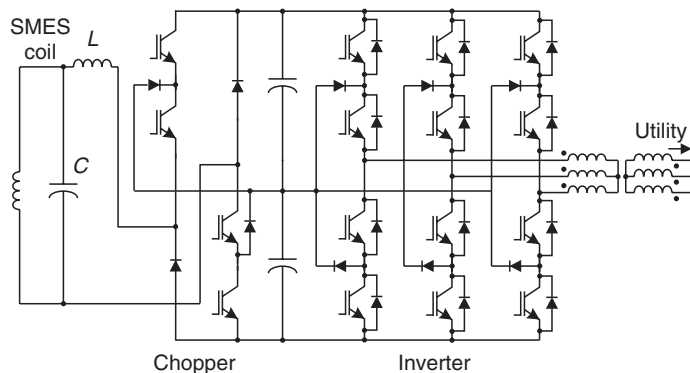


FIGURE 25.23 SMES implemented with a three-level converter.

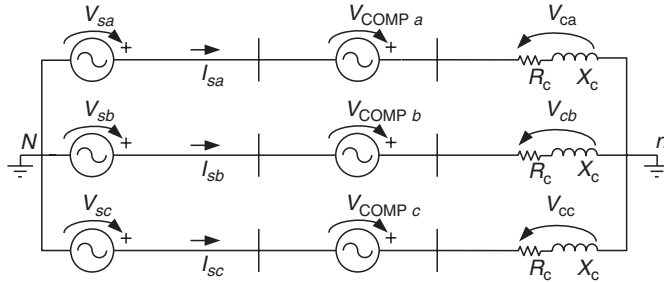


FIGURE 25.24 Three-phase equivalent circuit of a series compensated system.

25.3.1 Series Compensation Principles

Like shunt compensation, series compensation may also be implemented with current- or voltage-source converters. In this type of compensation, the compensator injects a voltage in series with the load, eliminating voltage unbalance at the load terminals, and supplying the voltage component required to operate with rated, balanced, and constant value. Figure 25.24 shows the principle of series compensation.

Figure 25.25 shows a radial power system, with the reference angle in V_2 , and the results obtained with the series compensation using a voltage source, which has been adjusted to have unity power factor operation at V_2 . However, the compensation strategy is different when compared with shunt compensation. In this case, the voltage V_{COMP} has been added between the line and the load to change the angle of V_2 , which becomes the voltage at the load terminals. With the appropriate magnitude and phase-shift adjustment of V_{COMP} , unity power factor can be reached at V_2 . As can be seen from the phasor diagram of Fig. 25.25b, V_{COMP} generates a voltage phasor with opposite direction to the voltage drop in the line inductance. In this type of compensation, the load current cannot be changed, which means that the compensator voltage must be adjusted to reach the required voltage at the load terminals. Moreover, the amount of apparent power interchanged with the series compensator in this case depends on the V_{COMP} phase and magnitude. Real and reactive power can be generated from the series compensator, depending on the load and the system requirements. In most cases, series compensation is used to control voltage at the load terminal, so that only reactive power needs to be exchanged. In this case, series capacitors represent a good alternative.

Series compensation with capacitors is the most common strategy. Series capacitors are connected with a transmission line as shown in Fig. 25.26, which means that all the equipment must be installed on a platform that is fully insulated for the system voltage (both the terminals are at the line voltage). On this platform, the capacitor is located together with overvoltage protection circuits. The overvoltage protection is a key design factor as the capacitor bank has to withstand the throughput

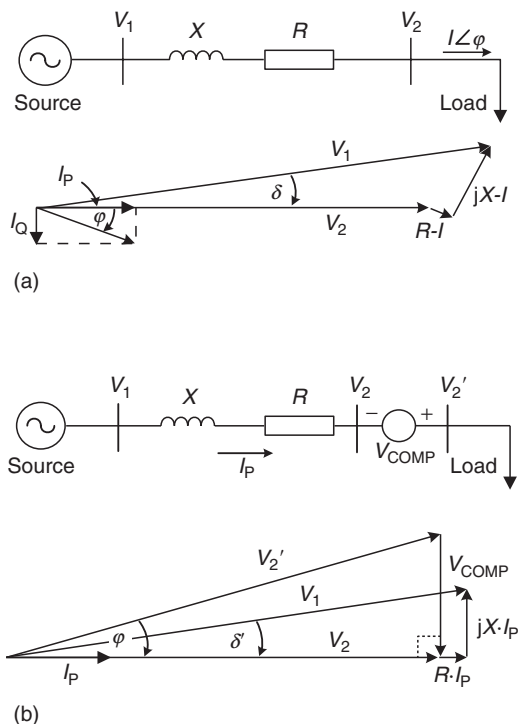


FIGURE 25.25 Principles of series compensation.
(a) The radial system without compensation. (b) Series compensation with a voltage source.

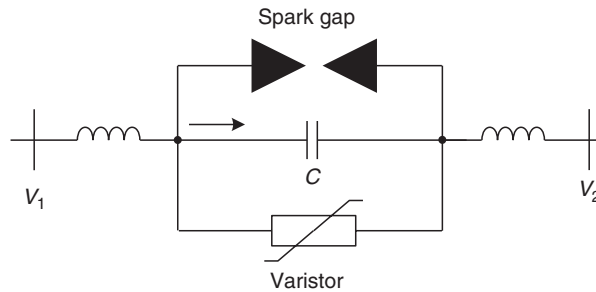


FIGURE 25.26 Series capacitor compensator and associated protection system.

fault current, even at a severe fault. The primary overvoltage protection typically involves nonlinear metal-oxide varistors, a spark gap, and a fast bypass switch.

Series compensation is used basically to improve voltage regulation in transmission and distribution power systems. Different compensation equipments using power electronics have been developed to operate as series compensators, as described below.

25.3.2 Static Synchronous Series Compensator

A voltage-source converter can also be used as a series compensator as shown in Fig. 25.27. The SSSC injects a voltage in series to the line, 90° phase-shifted with the load current, operating as a controllable series capacitor. The basic difference, as compared with series capacitor, is that the voltage injected by an SSSC is not related to the line current and can be independently controlled [3]. If the phase-shift angle between the injected voltage and the line current is not 90° , active power flows through or from the static compensator. In this case, an energy storage element must be included. This element normally is connected in the dc bus, and modifies the compensator control scheme.

In case of medium voltage application, the SSSC is also known as voltage dynamic restorer, and is used to compensate voltage sag, swells, and unbalance. The principle of operation is similar to the SSSC,

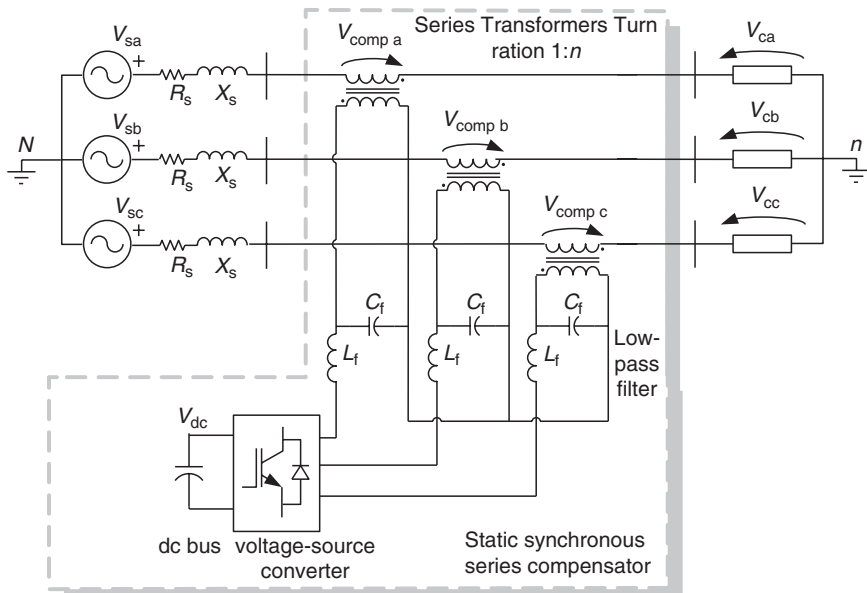


FIGURE 25.27 Static synchronous series compensator (SSSC).

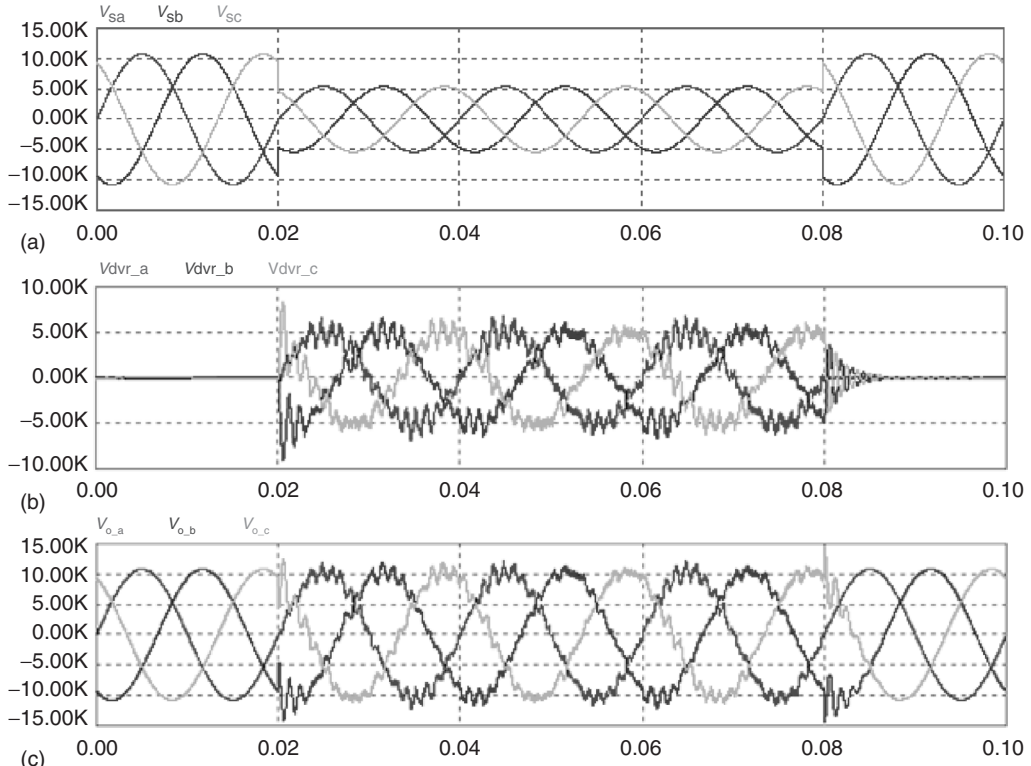


FIGURE 25.28 Voltage waveforms using series compensation. (a) Source voltage. (b) Series compensator voltage. (c) Compensated voltage at the load terminals.

but the main difference is that a DVR can compensate active power, since it may be implemented with an energy storage element in the dc bus.

When voltage sags or swells are present at the load terminals, the SSSC responds by injecting three ac voltages in series with the incoming three-phase network voltages, compensating for the difference between faulted and prefault voltages (Fig. 25.28). Each phase of the injected voltages can be controlled separately (their magnitude and angle). Active and reactive power required to generate these voltages is supplied by the voltage-source converter, fed from a dc link as shown in Fig. 25.28. In order to be able to mitigate voltage sag, the SSSC must present fast control response (Fig. 25.28).

Voltage fluctuation at the load terminals can be in magnitude or in phase (or both) as shown in Fig. 25.29. When the power supply conditions remain normal the SSSC operate in low-loss standby mode, with the converter side of the booster transformer shorted. Since no voltage-source converter (VSC) modulation takes place, the SSSC produces only conduction losses. In case active power needs to be compensated, an energy storage element must be supplied. This energy storage element is normally connected to the dc bus (supper capacitors, batteries), or the other alternative is to keep the dc capacitor loaded at rated voltage through a noncontrolled rectifier connected to the power line, as shown in Fig. 25.30. This is the typical power circuit configuration of a DVR.

25.3.2.1 Compensation Strategies

The magnitude of the compensated voltage can be obtained from the equivalent circuit shown in Fig. 25.24, and the phasor diagram shown in Fig. 25.20, and is equal to

$$\dot{V}_{compj} = \dot{V}_{cj} - \dot{V}_{sj} \quad (25.13)$$

$$V_{compj}\angle\beta = V_{cj}\angle\alpha - V_{sj}\angle\delta \quad (25.14)$$

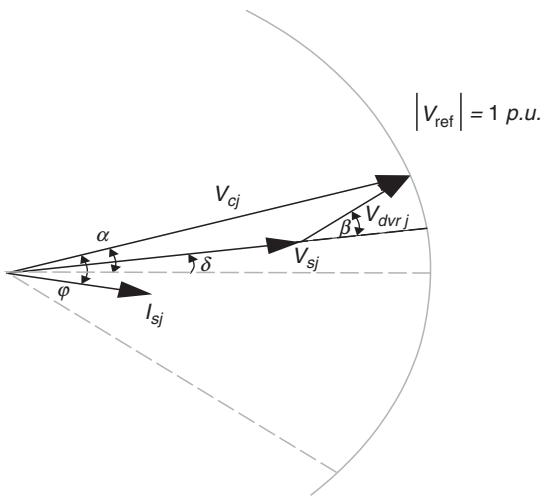


FIGURE 25.29 Phasor diagram for series voltage compensation.

compensated voltage is generated in phase with the load voltage as shown in Fig. 25.31. In this case the compensator does not correct the phase-shift introduced at the voltage terminals.

The active and reactive power delivered by the series compensator is given by

$$P_{\text{comp}j} = V_{\text{comp}j} \cdot I_{sj} \cdot \cos(\varphi) \quad (25.17)$$

$$Q_{\text{comp}j} = V_{\text{comp}j} \cdot I_{sj} \cdot \sin(\varphi) \quad (25.18)$$

The in-phase compensation strategy requires the injection of both active and reactive power due to the angle between the compensation voltage and the system current (φ). The active power is taken from the energy storage unit, which defines the ride-through capability of the static series compensator (SSSC or DVR).

Using complex variables

$$\begin{aligned} V_{\text{comp}j} \angle \beta &= V_{cj}(\cos \alpha + j \sin \alpha) \\ &- V_{sj}(\cos \delta + j \sin \delta) \end{aligned} \quad (25.15)$$

The magnitude of the voltage component that must be generated is equal to

$$|V_{\text{comp}}| = \sqrt{V_{cj}^2 + V_{sj}^2 - 2 \cdot V_{cj} \cdot V_{sj} \cdot \cos(\alpha - \delta)} \quad (25.16)$$

From this expression, different compensation strategies are derived.

25.3.2.1.1 Boosting or In-Phase Compensation

The first compensation strategy is called boosting or in-phase compensation, since the

compensator does not correct the phase-shift introduced at the voltage terminals.

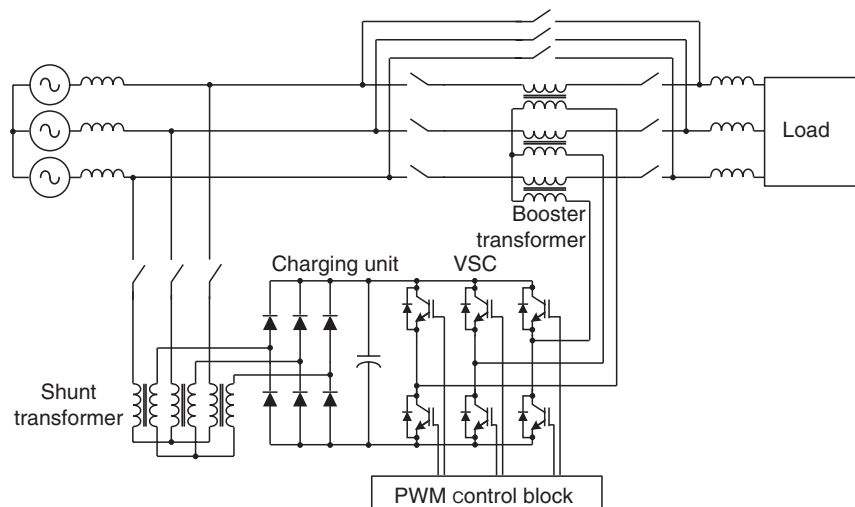


FIGURE 25.30 Power circuit topology of a dynamic voltage restorer (DVR).

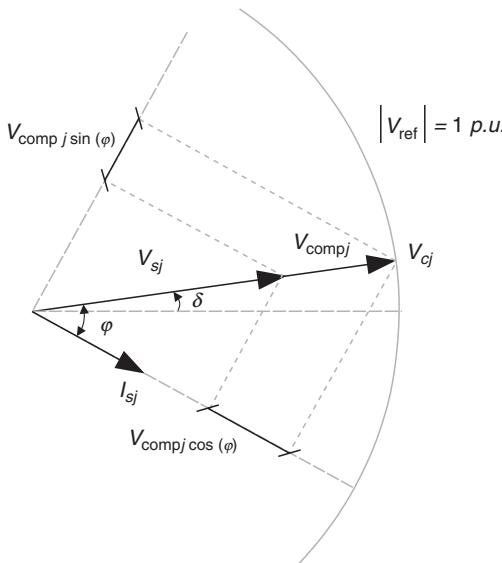


FIGURE 25.31 Phasor diagram of the compensated voltage scheme.

The active power injected by the series compensator, $P_{\text{comp}j}$, is minimum when the load power factor is equal to 1 (Eq. [25.21]).

25.3.2.2 Reference Signal Generation

The reference signal is used by the power converter control scheme to generate the required output voltage necessary to keep the load voltage at a given value. Different methods can be used, and the differences are based on the simplicity of implementation, number of calculations, and execution time.

25.3.2.2.1 Pythagoras Method

Based on the Pythagoras theorem, it is possible to generate the signal required to compensate the system voltage drop at the load terminals. This scheme is based on the synchronization of the compensator control signals with the system voltage. The equation used is

$$\sin^2 \theta + \cos^2 \theta = 1 \quad (25.22)$$

The block diagram for the generation of the compensation voltage reference signal for single-phase application is shown in Fig. 25.33.

One of the problems that must be taken into consideration during the generation of the compensated voltage reference signal is the sign, which must indicate if the voltage perturbation is a sag or a swell. The type of perturbation defines the polarity of the compensated voltage. If the perturbation is a sag, the compensated voltage must be in phase with the system voltage, but, if the perturbation is a swell, the compensated voltage must be phase-shifted 180° with

25.3.2.1.2 Minimum Power Injection

Unlike the boosting method, the minimum power injection strategy defines an optimal angle for which the compensation voltage V_{comp} is 90° phase-shift with the system current, canceling the injection of active power from the series compensator. The limiting factor to compensate the sag only with reactive power is the load power factor. Figure 25.32 illustrates the phasor diagram of the compensation voltage with minimum power injection.

The active power delivered by the series compensator can be obtained from Fig. 25.32.

$$P_{\text{comp}j} = P_{sj} - P_{cj} \quad (25.19)$$

$$P_{\text{comp}j} = (V_{cj} \cdot I_{sj} \cdot \cos(\varphi)) - (V_{sj} \cdot I_{sj} \cdot \cos(\varphi - \alpha + \delta_j)) \quad (25.20)$$

$$P_{\text{comp}j} = \cos(\varphi_c) - V_{sj} \cdot \cos(\varphi_s) \quad (25.21)$$

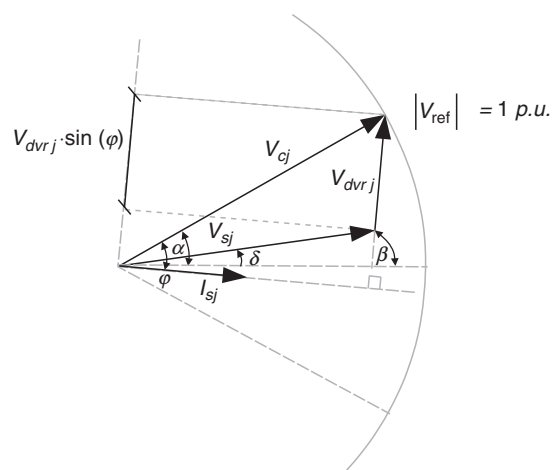


FIGURE 25.32 Phasor diagram of the minimum power injection method.

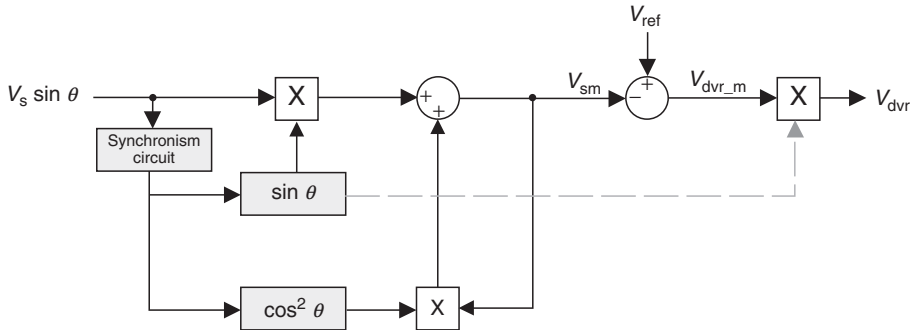


FIGURE 25.33 The block diagram of the Pitagoras algorithm.

respect to the equivalent system voltage. The synchronization circuit used to generate the $\sin \theta$ signal defines the control scheme time response. Different circuits and methods can be used to synchronize the reference signal with the system voltage: zero voltage detector, fast Fourier transform, or phase locked loop. The fastest algorithm is the zero crossing detection, with a time response equal to half a cycle of the system frequency. The Pitagoras method allows the generation of a positive reference signal in case of sag and a negative signal in case of a swell.

25.3.2.2.2 Synchronous Reference Frame

The synchronous reference frame method uses the transformation from the stationary reference frame abc to a dq axes, which are synchronized with the system voltage. The advantage of transforming the voltages from abc to dq is that sinusoidal signals generate continuous signals in dq axis, allowing the use of linear control algorithms. The block diagram of the synchronous reference frame algorithm is shown in Fig. 25.34. This scheme generates dc error signals, which are easier to process as compared with the Pitagoras algorithm. Since the system voltages are line to line, in order to transform them in phase to neutral, they must be multiplied by $1/(1-a^2)$ term.

Another alternative to go from abc to dq axis is to use $\alpha\beta$ transformation, as shown in Fig. 25.35. In this case, the phase-shift angle θ , used to synchronize the dq axis, is obtained from Eq. (25.22).

The principal disadvantage of the indirect algorithm is the presence of a second order harmonic in V_α and V_β , used to calculate θ . The amplitude of this second order harmonic depends on the voltage unbalance in the abc reference frame. The use of a passive low-pass filter to eliminate the second order harmonic introduces a significant time delay, affecting the transient response of the SSSC. Simulated waveforms showing the characteristics of synchronous reference frame method are shown in Figs. 25.36 and 25.37, for a balance and unbalance voltage perturbation.

25.3.2.2.3 Sequence Components in Synchronous Reference Frame

Another alternative to generate the reference signal is to use sequence components. From the line voltages in abc frame, the negative, zero, and positive sequence voltage components are calculated:

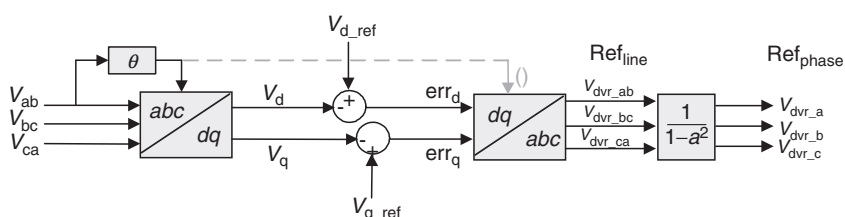


FIGURE 25.34 The block diagram of the synchronous reference frame direct algorithm.

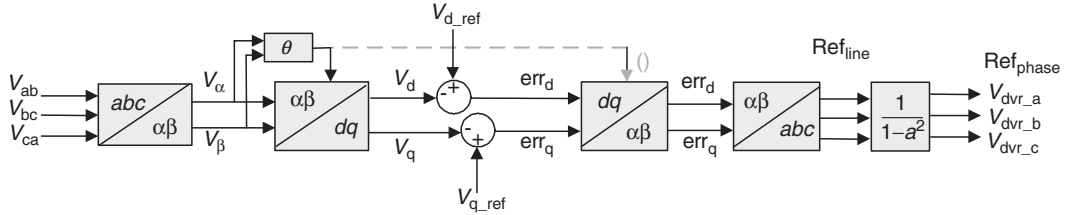


FIGURE 25.35 The block diagram of the synchronous reference frame indirect algorithm.

$$\begin{bmatrix} V_{ab}^0 \\ V_{ab}^1 \\ V_{ab}^2 \end{bmatrix} = \frac{1}{3} \begin{bmatrix} 1 & 1 & 1 \\ 1 & a & a^2 \\ 1 & a^2 & a \end{bmatrix} * \begin{bmatrix} V_{ab} \\ V_{bc} \\ V_{ca} \end{bmatrix} \quad (25.23)$$

The block diagram used to generate the reference signals with the sequence components algorithm is shown in Fig. 25.38. The reference voltage signals are phase to neutral, and are calculated from the line to line voltages. By transforming the sequence components from abc to dq reference frame, dc quantities are obtained.

If the voltage perturbation is balanced, the reference signals have only positive sequence component, but if the perturbation is unbalanced, positive and negative sequence components are obtained as shown in Fig. 25.39.

25.3.2.3 Power Circuit Design

The power circuit topology of the SSSC is composed by the three-phase PWM voltage-source inverter, the second order resonant LC filters, the coupling transformers, and the secondary ripple frequency (Fig. 25.27). The main design characteristics for each of the power components are described below.

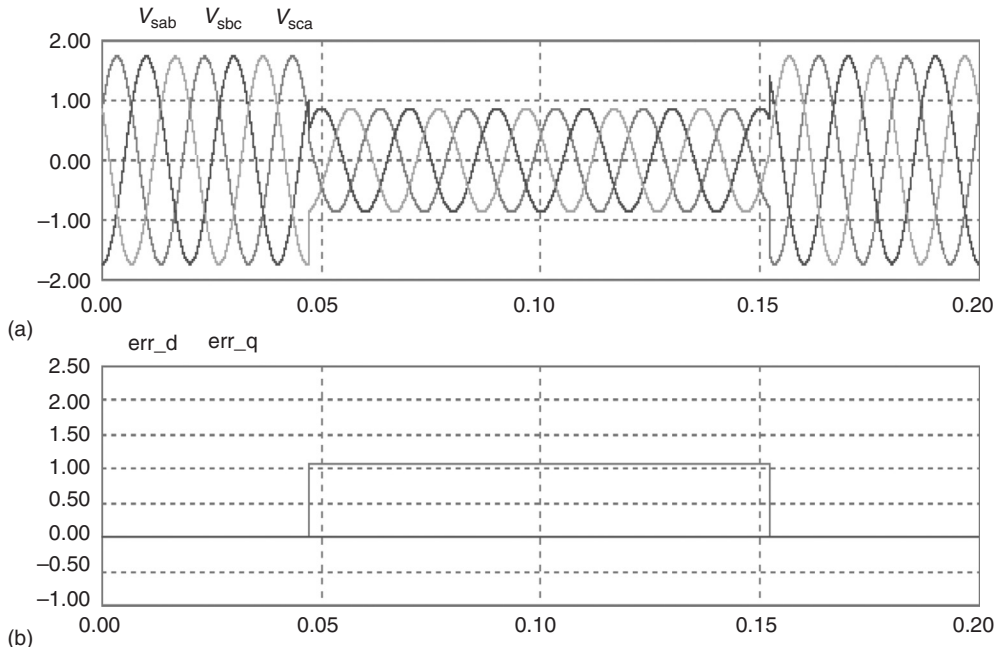


FIGURE 25.36 Simulated voltage waveforms for a balance sag. (a) Line to line system voltage in abc reference frame. (b) Voltage signals in dq axes.

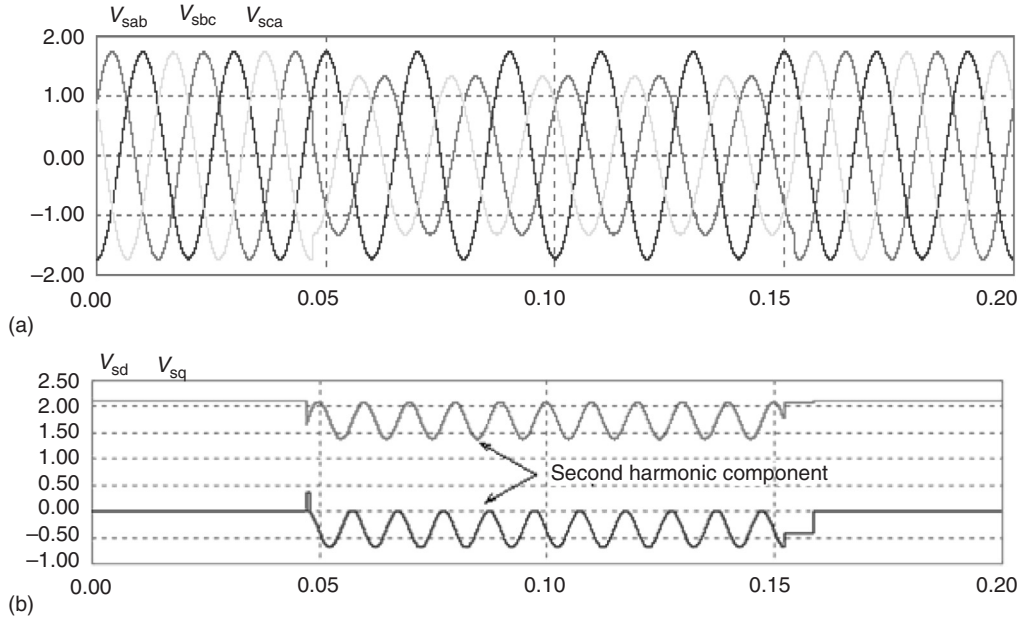


FIGURE 25.37 Simulated voltage waveforms for an unbalance sag. (a) Line to line system voltage in *abc* reference frame. (b) Voltage signals in *dq* axes.

25.3.2.3.1 PWM Voltage-Source Inverter

The rated apparent power required by the inverter can be obtained by calculating the apparent power generated in the primary of the series transformer. The voltage reflected across the primary winding of the coupling transformer is defined by the following expression:

$$V_{\text{series}} = \sqrt{K_2^2(V_1 + V_2)^2} \quad (25.24)$$

where V_{series} is the rms voltage across the primary winding of the coupling transformer, and K_2 is equal to 1. The fundamental component of the primary voltage depends on the amplitude of the negative and positive sequence component of the source-voltage defined by the system voltage regulation and unbalance. The transformer primary current depends on the load.

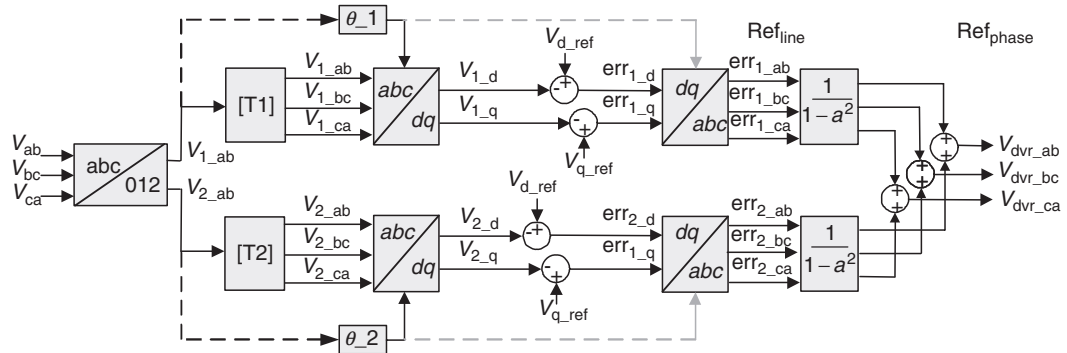


FIGURE 25.38 The block diagram of the sequence components algorithm.

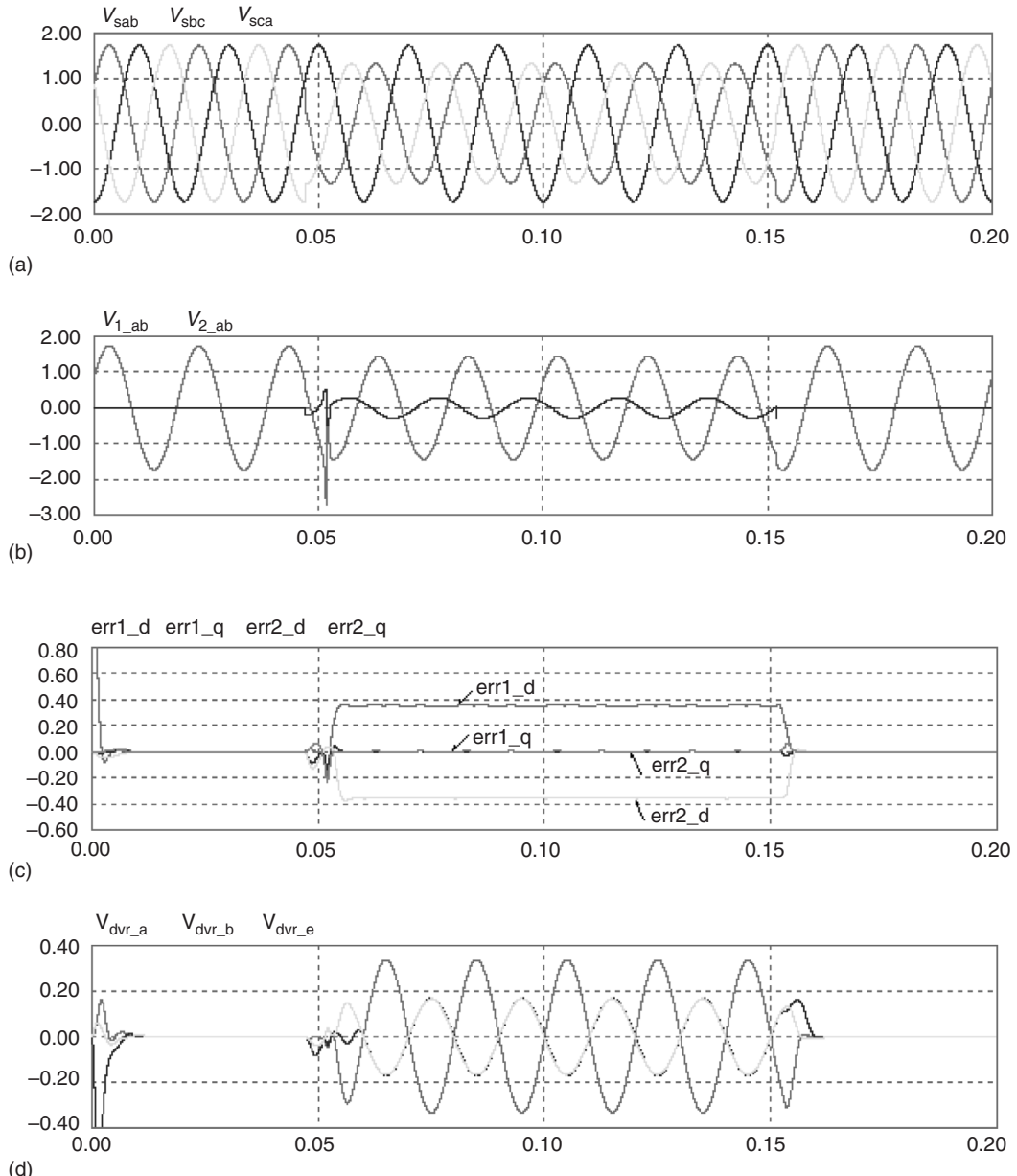


FIGURE 25.39 Simulated waveforms for an unbalance voltage sag. (a) Unbalanced line to line system voltage in abc reference frame. (b) Positive and negative voltage sequence components in abc reference. (c) Positive and negative sequence reference signal voltages in dq reference frame. (d) Positive and negative sequence reference signal voltages in abc reference frame.

25.3.2.3.2 Coupling Transformer

The primary windings of the coupling transformers are connected in series to the power system, and as such, they behave as current transformers. The total apparent power required by each series transformer is one-third the total apparent power of the inverter. The turn ratio of the coupling transformer is specified according with the inverter dc bus voltage. The correct value of the turn ratio a must be specified according with the overall SSSC performance. The turn ratio of the coupling transformer

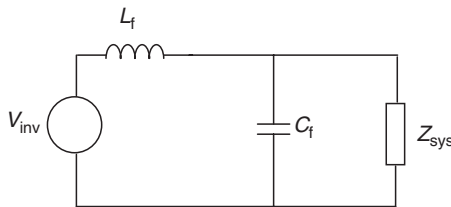


FIGURE 25.40 The single-phase equivalent circuit of the inverter ripple filter.

must be optimized through the simulation of the overall SSSC, since it depends on the values of different related parameters. In general, the transformer turn ratio must be high in order to reduce the amplitude of the inverter output current and to reduce the voltage induced across the primary winding. Also, the selection of the transformer turn ratio influences the performance of the ripple filter connected at the output of the PWM inverter.

25.3.2.3.3 Secondary Ripple Filter

It is important to note that the design of the secondary ripple filter depends mainly on the coupling transformer turn ratio and on the frequency of the triangular waveform used to generate the inverter gating signals. The ripple filter connected at the output of the inverter avoids the induction of the high frequency ripple voltage generated by the PWM inverter switching pattern at the terminals of the primary windings of the coupling transformers. In this way, the voltage applied in series to the power system corresponds to the components required to compensate voltage unbalance and regulation. The single-phase equivalent circuit of the ripple filter is shown in Fig. 25.40.

The voltage reflected to the primary winding of the series transformer has the same waveform as the voltage across the filter capacitor. For low frequency components, the inverter output voltage must be almost equal to the voltage across C_f . However, for high frequency components, most of the inverter output voltage must drop across L_f , in which case the voltage at the capacitor terminals is almost zero. Moreover, C_f and L_f must be selected in order to not exceed the burden of the series transformer. The ripple filter must be designed for the carrier frequency of the PWM voltage-source inverter. To calculate C_f and L_f the system equivalent impedance at the carrier frequency, Z_{sys} , reflected to the secondary must be known. This impedance is equal to

$$Z_{sys(\text{secondary})} = a^2 Z_{sys(\text{primary})} \quad (25.25)$$

For the carrier frequency, the following design criteria must be satisfied:

1. $X_{Cf} \ll X_{Lf}$ to ensure that at the carrier frequency most of the inverter output voltage will drop across L_f .
2. X_{Cf} and $X_{Lf} \ll Z_{sys}$ to ensure that the voltage divider is between L_f and C_f .

25.3.3 Thyristor-Controlled Series Compensation

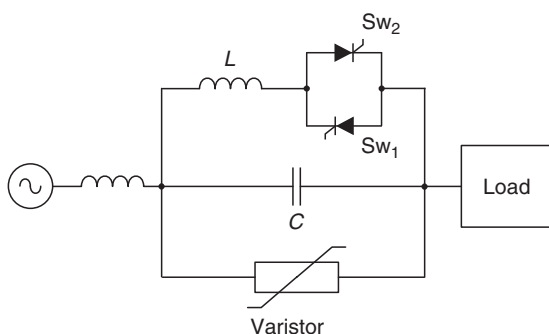


FIGURE 25.41 Power circuit topology of a thyristor-controlled series compensator.

Figure 25.41 shows a single line diagram of a thyristor-controlled series compensator (TCSC). TCSC provides a proven technology that addresses specific dynamic problems in transmission systems. TCSCs are an excellent tool to introduce if increased damping is required when interconnecting large electrical systems. Additionally, they can overcome the problem of subsynchronous resonance (SSR), a phenomenon that involves an interaction between large thermal generating units and series compensated transmission systems.

There are two bearing principles of the TCSC concept. First, the TCSC provides

electromechanical damping between large electrical systems by changing the reactance of a specific interconnecting power line, i.e., the TCSC will provide a variable capacitive reactance. Second, the TCSC shall change its apparent impedance (as seen by the line current) for subsynchronous frequencies such that a prospective SSR is avoided. Both these objectives are achieved with the TCSC using control algorithms that operate concurrently. The controls will function on the thyristor circuit (in parallel to the main capacitor bank) such that controlled charges are added to the main capacitor, making it a variable capacitor at fundamental frequency but a “virtual inductor” at subsynchronous frequencies.

For power oscillation damping, the TCSC scheme introduces a component of modulation of the effective reactance of the power transmission corridor. By suitable system control, this modulation of the reactance is made to counteract the oscillations of the active power transfer, in order to damp these out.

25.4 Hybrid Compensation

Static synchronous VAR compensators (STATCOM) and SSSC or DVR can be integrated to get a system capable of controlling the power flow of a transmission line during steady-state conditions and providing dynamic voltage compensation and short circuit current limitation during system disturbances [31].

25.4.1 Unified Power Flow Controller

The UPFC, shown in Fig. 25.42, consists of two switching converters operated from a common dc link provided by a dc capacitor, one connected in series with the line and the other in parallel. This arrangement functions as an ideal ac to ac power converter in which the real power can freely flow in either direction between the ac terminals of the two inverters, and each one can independently generate (or absorb) reactive power at its own ac output terminal. The series converter of the UPFC injects via series transformer, an ac voltage with controllable magnitude and phase angle in series with the transmission line. The shunt converter supplies or absorbs the real power demanded by the series converter through the common dc link. The inverter connected in series provides the main function of the UPFC by injecting an ac voltage V_{pq} with controllable magnitude ($0 \leq V_{pq} \leq V_{pq\max}$) and phase angle ρ ($0 \leq \rho \leq 360^\circ$), at the power frequency, in series with the line via a transformer. The transmission

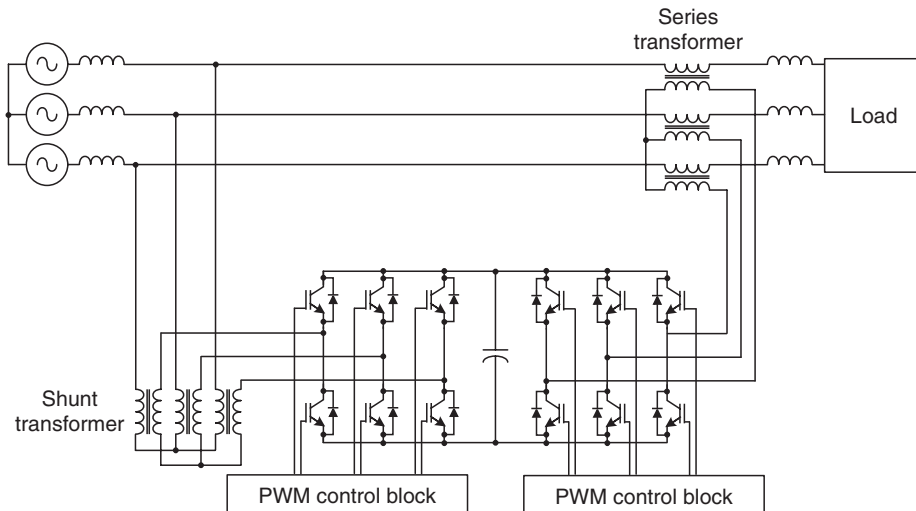


FIGURE 25.42 UPFC power circuit topology.

line current flows through the series voltage source resulting in real and reactive power exchange between the UPFC and the ac system. The real power exchanged at the ac terminal, i.e., the terminal of the coupling transformer, is converted by the inverter into dc power, which appears at the dc link as positive or negative real power demand. The reactive power exchanged at the ac terminal is generated internally by the inverter.

The basic function of the inverter connected in parallel (inverter 1) is to supply or absorb the real power demanded by the inverter connected in series to the ac system (inverter 2), at the common dc link. Inverter 1 can also generate or absorb controllable reactive power, if it is desired, and thereby it can provide independent shunt reactive compensation for the line. It is important to note that whereas there is a closed “direct” path for the real power negotiated by the action of series voltage injection through inverter 1 and back to the line, the corresponding reactive power exchanged is supplied or absorbed locally by inverter 2 and therefore it does not flow through the line. Thus, inverter 1 can be operated at a unity power factor or be controlled to have a reactive power exchange with the line independently of the reactive power exchanged by inverter 2. This means that there is no continuous reactive power flow through the UPFC.

25.4.2 Interline Power Flow Controller

An interline power flow controller (IPFC), shown in Fig. 25.43, consists of two series voltage-source converters whose dc capacitors are coupled, allowing active power to circulate between different power lines [33]. The IPFC addresses the problem of compensating a number of transmission lines at a given substation. Series capacitive compensators are used to increase the transmittable active power over a given line but they are unable to control the reactive power flow in, and thus the proper load balancing of the line. With the IPFC active power can be transferred between different lines, and therefore it is possible to

1. equalize both active and reactive power flows between different lines,
2. reduce the burden of the overloaded lines by active power transfer,

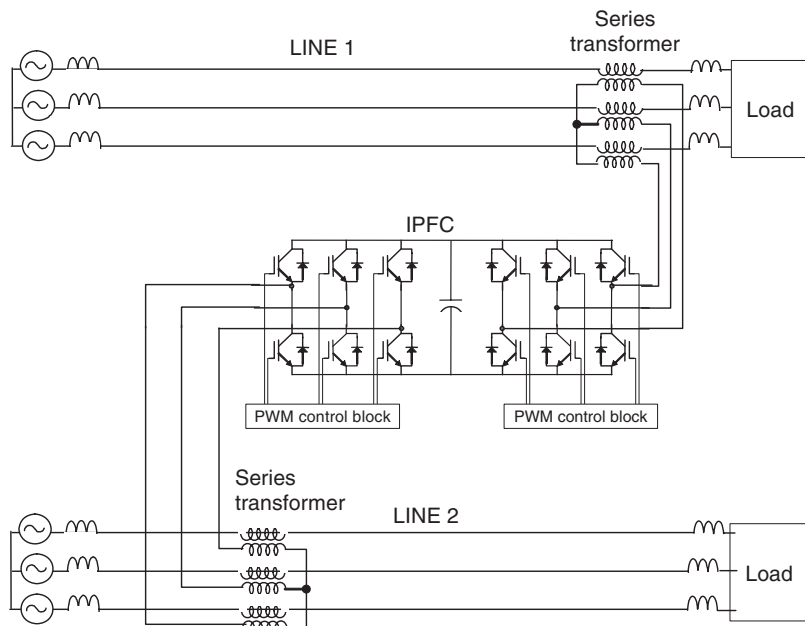


FIGURE 25.43 IPFC power circuit topology.

3. compensate against resistive line voltage drops and the corresponding reactive power demand, and
4. increase the effectiveness of the overall compensating system for dynamic disturbances.

In the IPFC the converters do not only provide series reactive compensation but can also be controlled to supply active power to a common dc link from its own transmission line. Like this, active power can be provided from the overloaded lines for active power compensation in other lines. This scheme requires a rigorous maintenance of the overall power balance at the common dc terminal by appropriate control action, allowing that underloaded lines provide appropriate active power transfer to the overloaded ones. When operating below its rated capacity, the IPFC is in regulation mode, allowing the regulation of the active and reactive power flows on one line, and the active power flow on the other line. In addition, the net active power generation by the two coupled converters is zero, neglecting power losses.

25.4.3 Unified Power Quality Conditioner

Unlike the previous alternatives, the unified power quality conditioner (UPQC), shown in Fig. 25.44, has two main objectives. First, to provide a near sinusoidal and constant voltage to a critical load regardless of the variations (sag, swells, distortion) of the voltage at the ac main terminals in the point of common coupling (PCC). Second, compensate the reactive and/or distorted current taken by the load achieving a near sinusoidal and unity power factor at the PCC. For these reasons, the UPQC is more oriented for load compensation in industrial power distribution systems.

The UPQC consists of two PWM converters operated from a common dc voltage link, which must be kept constant. One converter connected in series with the line and the other connected in parallel [31]. The series converter task is to achieve the first objective (clean load voltage) and the parallel converter the second one (sinusoidal current at the system terminals).

The ac voltages of the two converters can be generated with an arbitrary amplitude and phase, thus providing four degrees of freedom. On the other hand, the objectives of achieving a given power factor at the system terminals, a given rms load voltage, and a constant dc link voltage leave one degree of freedom. From the control point of view, this extra degree of freedom could be used to set a given phase-shift between the load voltage and the system voltage. This arbitrary phase angle forces active power to circulate through the dc link of the UPQC. This approach extends the compensating capabilities of the UPQC as compared to null active power circulating through the dc link.

Figure 25.45(a) shows the general phasor diagram of the UPQC connected to a load with $\cos \phi$ power factor, a system power factor $\cos \theta$, a phase-shift angle α between the load and system voltages, a voltage

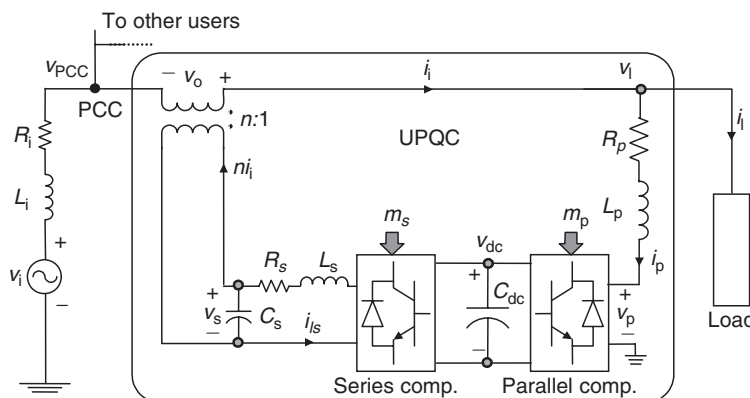


FIGURE 25.44 UPQC power circuit topology.

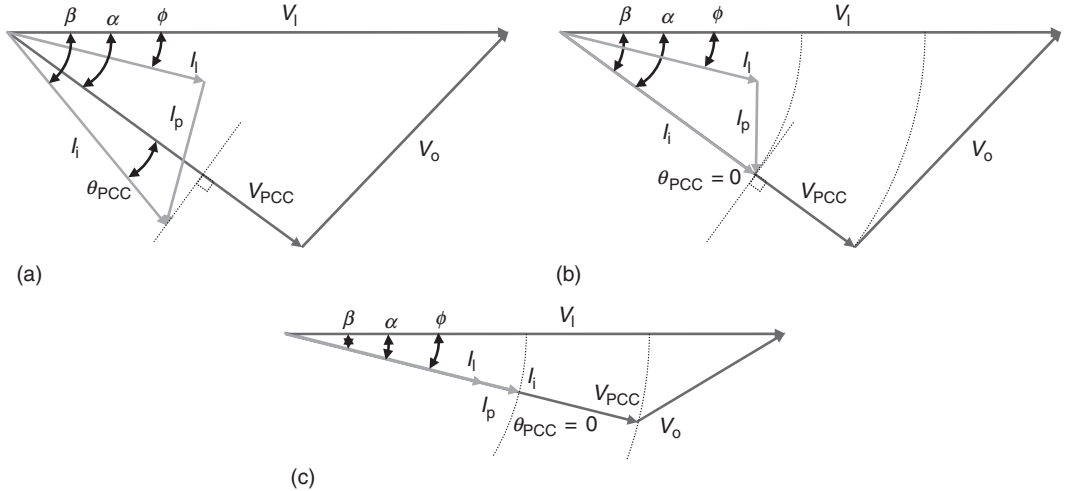


FIGURE 25.45 UPQC phasor's diagrams. (a) For a general application. (b) For unity power load power factor. (c) For unity system power factor.

system V_{PCC} ($V_{PCC} < V_I$), and rated voltage V_I at the load side. Figure 25.45(b) shows that with the UPFC unity power factor can be achieved at the PCC ($\theta_{PCC} = 0$). Finally, Fig. 25.45(c) shows that in the case of unity power factor at the PCC, the current I_p can be minimized, therefore the losses at the UPFC are reduced. This operating condition can be achieved if the currents I_i , I_l , and I_p are in phase, which is achieved for an $\alpha \neq 0$ (unless no sag/swell is present). It is important to note in this case that the active power flowing through the dc link is not zero since the phase-shift angle between the series injected voltage V_0 and the supply current I_i is not 90° .

25.5 FACTS Controller's Applications

The implementation of high-performance FACTS controllers enables power grid owners to increase existing transmission network capacity while maintaining or improving the operating margins necessary for grid stability. As a result, more power can reach consumers with a minimum impact on the environment, after substantially shorter project implementation times, and at lower investment costs—all compared to the alternative of building new transmission lines or power generation facilities. Some of the examples of high-performance power system controllers that have been installed and are operating in power systems are described below. Some of these projects have been sponsored by the Electric Power Research Institute (EPRI), based on a research program implemented to develop and promote FACTS.

25.5.1 500 kV Winnipeg–Minnesota Interconnection (Canada–USA) [33]

Northern States Power Co. (NSP) of Minnesota is operating an SVC in its 500 kV power transmission network between Winnipeg and Minnesota. This device is located at Forbes substation, in the state of Minnesota, and is shown in Fig. 25.46. The purpose is to increase the power interchange capability on existing transmission lines. This solution was chosen instead of building a new line as it was found superior with respect to increased advantage utilization as well as reduced environmental impact. With the SVC in operation, the power transmission capability was increased in about 200 MW.

The system has a dynamic range of 450 MVA inductive to 1000 MVA capacitive at 500 kV, making it one of the largest of its kind in the world. It consists of an SVC and two 500 kV, 300 MVA mechanically

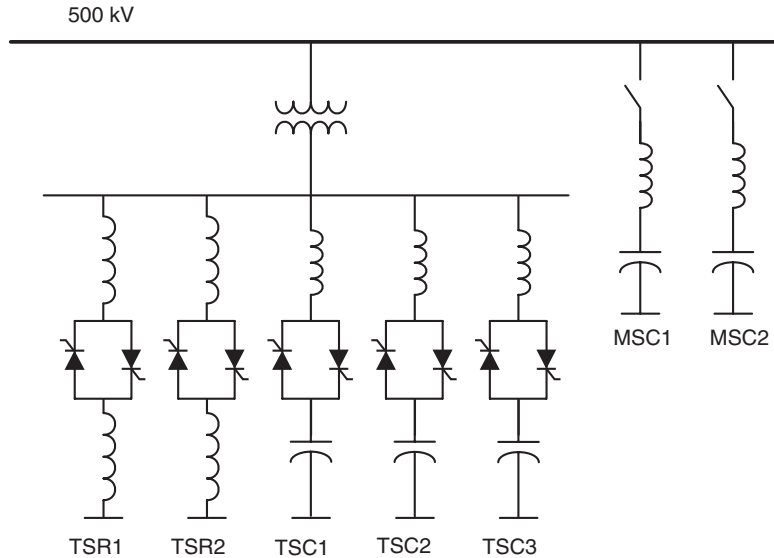


FIGURE 25.46 SVC at the Forbes substation.

switched capacitor banks (MSC). The large inductive capability of the SVC is required to control the overvoltage during loss of power from the incoming HVDC at the northern end of the 500 kV line.

The SVC consists of two thyristor-switched reactors (TSR) and three TSC. Additionally, the SVC has been designed to withstand brief (<200 ms) overvoltages up to 150% of rated voltage. Without the SVC, power transmission capacity of the NSP network would be severely limited, either due to excessive voltage fluctuations following certain fault situations in the underlying 345 kV system, or due to severe overvoltages at loss of feeding power from HVDC lines coming from Manitoba.

25.5.2 Channel Tunnel Rail Link [31]

Today, it is possible to travel between London and Paris in just over two hours, at a maximum speed of 300 km/h. The railway power system is designed for power loads in the range of 10 MW. The traction feeding system is a modern 50-Hz, 2–25-kV supply incorporating an autotransformer scheme to keep the voltage drop along the traction lines low. Power step-down from the grid is direct, via transformers connected between two phases. A major feature of this power system, shown in Fig. 25.47, is the SVC support. The primary purpose of VAR is to balance the unsymmetrical load and to support the railway voltage in the case of a feeder station trip—when two sections have to be fed from one station. The second purpose of the SVCs is to ensure a low tariff for the active power by maintaining unity power factor during normal operation. Finally, the SVCs alleviate harmonic pollution by filtering the harmonics from the traction load.

Harmonic compensation is important because strict limits apply to the traction system's contribution to the harmonic level at the supergrid connection points. The SVCs for voltage support only are connected on the traction side of the interconnecting power transformers. The supergrid transformers for the traction supply have two series-connected medium-voltage windings, each with its midpoint grounded. This results in two voltages, 180° apart, between the winding terminals and ground. The SVCs are connected across these windings; consequently, there are identical single-phase SVCs connected feeder to ground and catenary to ground. The traction load of up to 120 MW is connected between two phases. Without compensation, this would result in an approximately 2% negative phase sequence voltage. To counteract the unbalanced load, a load balancer (an asymmetrically controlled SVC) has been

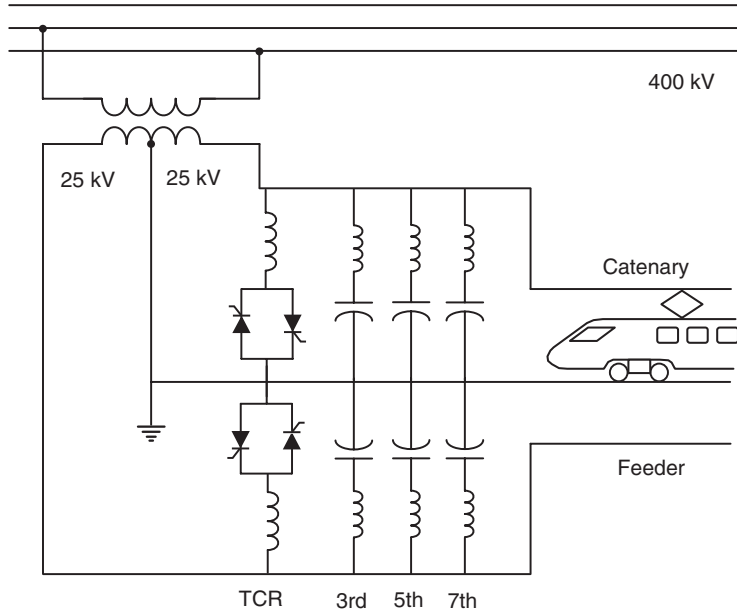


FIGURE 25.47 VAR compensation system for the channel tunnel.

installed in the Sellinge substation. This has a three-phase connection to the grid. The load balancer transfers active power between the phases in order to create a balanced load (as seen by the supergrid).

25.5.3 STATCOM “Voltage Controller” ± 100 MVar STATCOM at Sullivan Substation (TVA) in Northeastern Tennessee [25]

The Sullivan substation is supplied by a 500 kV bulk power network and by four 161 kV lines that are interconnected through a 1200 MVA transformer bank. Seven distributors and one large industrial customer are served from this substation. The STATCOM, shown in Fig. 25.48, is implemented with a

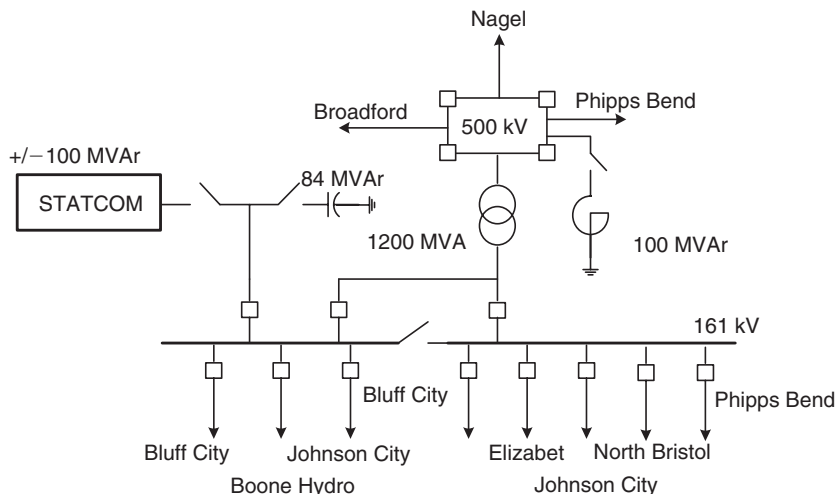


FIGURE 25.48 The 100 MVA STATCOM at Sullivan substation.

48 pulse, two-level voltage-source inverter that combines eight six pulse three-phase inverter bridges, each with a nominal rating of 12.5 MVA, a single step-down transformer having a wye and delta secondary to couple the inverter to the 161 kV transmission line, and a closed-loop liquid cooling system that contains a pumping skid and a fan-cooled, liquid to air heat exchanger unit, a central control system with operator interface. The STATCOM system is housed in one building that is a standard commercial design with metal walls and roof and measured 27.4×15.2 m.

The STATCOM regulates the 161 kV bus voltage during daily load increases to minimize the activation of the tap changing mechanism on the transformer bank, which interconnects the two power systems. The use of this VAR compensator to regulate the bus voltage has resulted in the reduction of the use tap changer from about 250 times per month to two to five times per month. Tap changing mechanisms are prone to failure, and the estimated cost of each failure is about \$1 million. Without the STATCOM, the transmission company would be compelled either to install a second transformer bank or to construct a fifth 161 kV line into the area; both are costly alternatives.

25.5.4 Unified Power Flow Controller “All Transmission Parameters Controller”: ± 160 MVA Shunt and ± 160 MVA Series at Inez Substation (AEP), Northeastern Virginia, USA [25]

The Inez load area has a power demand of approximately 2000 MW and is served by a long and heavily loaded 138 kV transmission lines. This means that, during normal power delivery, there is a very small voltage stability margin for system contingencies. Single contingency outages in the area will adversely affect the underlying 138 kV system, and in certain cases, a second contingency would be intolerable, resulting in a wide-area blackout. A reliable power supply to the Inez area requires effective voltage support and added real power supply facilities. System studies have identified a reinforcement plan that includes, among other things, the following system upgrades:

- (a) Construction of a new double-circuit high-capacity 138-kV transmission line from Big Sandy to Inez substation
- (b) Installation of FACTS controller to provide dynamic voltage support at the Inez substation and to ensure full utilization of the new high-capacity transmission line

The UPFC satisfies all these needs, providing independent dynamic control of transmission voltage as well as real and reactive power flow. The UPFC installation (see Fig. 25.49) comprises two identical three-phase 48-pulse, 160 MVA voltage-source inverters couple to two sets of dc capacitor banks. The two inverters are interfaced with the ac system via two transformers, a set of magnetically coupled windings configured to construct a 48-pulse sinusoidal waveshape. With this arrangement, the following operation modes are possible.

Inverter 1 (connected in parallel) can operate as a STATCOM, with either one of the two main shunt transformers, while inverter 2 (connected in series) operates as an SSSC. Alternatively, inverter 2 can be connected to the spare shunt transformer and operates as an additional STATCOM. With the later configuration, a formidable shunt reactive capability of ± 320 MVA would be available, necessary for voltage support at some transmission contingencies in the Inez area. The expected benefits of the installed UPFC are the following:

- (a) Dynamic voltage support at the Inez substation to prevent voltage collapse under double transmission contingency conditions
- (b) Flexible and independent control of real and reactive power flow on the new high capacity (950 MVA thermal rating) of the 138 kV transmission line
- (c) Reduction of real power losses by more than 24 MW, which is equivalent to a reduction of CO₂ emissions by about 85,000 tons per year
- (d) More than 100 MW increase in the power transfer and excellent voltage support at the Inez bus

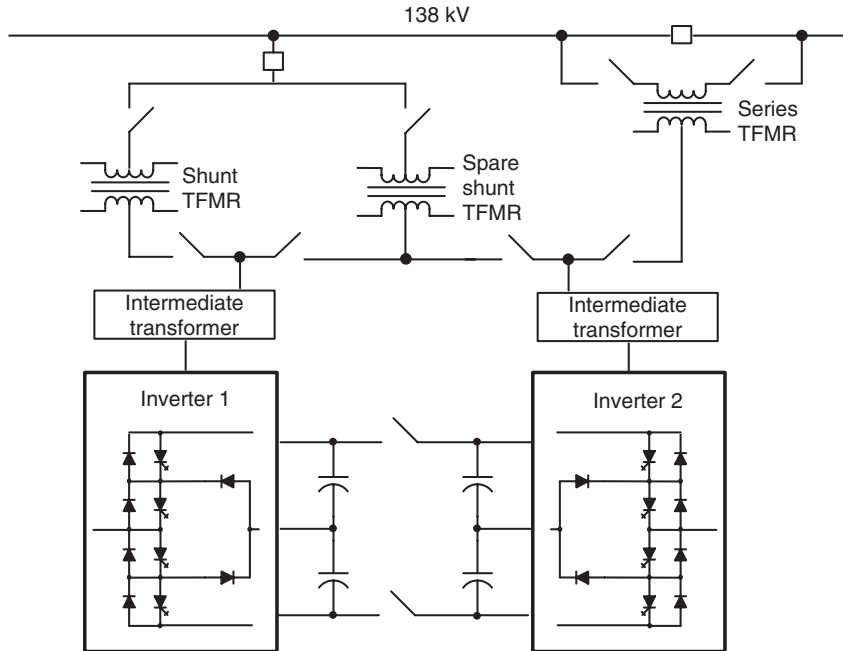


FIGURE 25.49 Inverter pole assembly of UPFC at Inez substation.

25.5.5 Convertible Static Compensator in the New York 345 kV Transmission System [35]

Convertible Static Compensator (CSC), a versatile and reconfigurable device based on FACTS technology, was designed, developed, tested, and commissioned in the New York 345 kV transmission system. The CSC, shown in Fig. 25.50, consists of two 100 MVA voltage-source converters which can be reconfigured and operated as either STATCOM, SSSC, UPFC, or IPFC. The CSC installation at the New York Power Authority's (NYPA) Marcy 345 kV substation consists of a 200 MVA shunt transformer with two identical secondary windings, and two 100 MVA series coupling transformers for series devices in two 345 kV lines. The CSC provides voltage control on the 345 kV Marcy bus, improved power flow transfers, and superior power flow control on the two 345 kV lines leaving the Marcy substation: Marcy–New Scotland line and Marcy–Coopers Corner line.

Each voltage-source inverter of Fig. 25.50 has 12 three-level NPC poles connected to a common dc bus. Inverter pole outputs are connected to an intermediate transformer, which synthesize the three-phase near-sinusoidal 48-pulse waveform that is coupled into the transmission system.

25.6 Conclusions

The principles of operation and the actual technological development of different FACTS controllers have been presented and analyzed. Starting from the principles of active, reactive, and voltage compensation, including classical solutions using phase-controlled semiconductors has been reviewed. The introduction of self-commutated topologies based on IGBT and IGCT semiconductors produced a dramatic improvement in the performance of FACTS controllers, since they have a faster dynamic behavior, they can control more variables, and introduce less pollution to power systems. The introduction of new self-commutated topologies at even higher voltage levels will increase the impact of FACTS controllers in future applications.

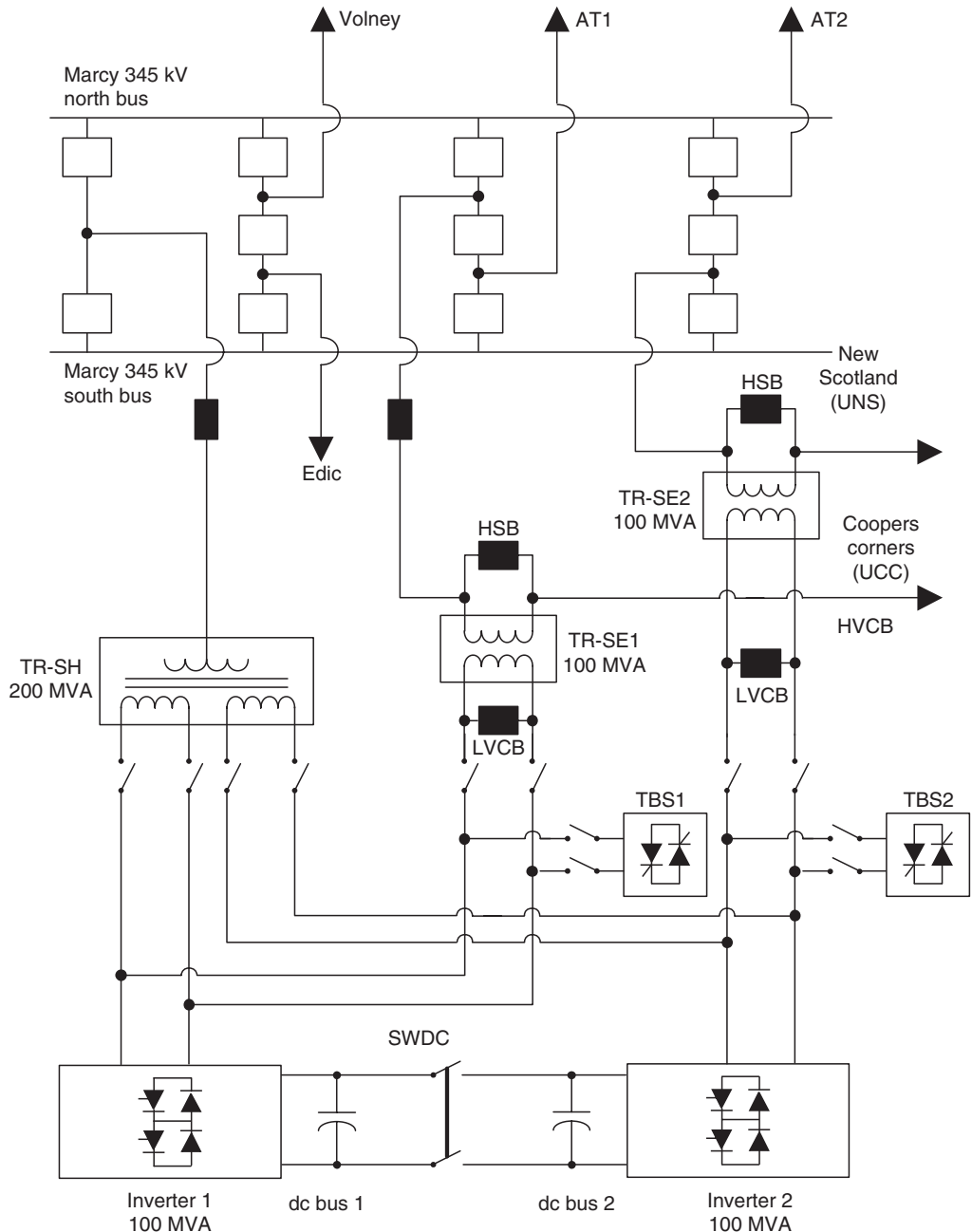


FIGURE 25.50 One-line diagram of 2×100 MVA CSC.

Some relevant examples of FACTS controllers have been described, where it can be observed that modern compensators improve power systems performance, helping to increase reliability and the quality of power delivered to the customers. These examples show that static power compensators will be used on a much wider scale in the future as grid performance and reliability becomes an even more important factor. Having better grid controllability will allow utilities to reduce investment in the transmission lines themselves. The combination of modern control with real-time information and power electronic

technologies will move them very close to their physical limits. Besides, the development of faster and more powerful semiconductor valves will increase in the near future the applicability of FACTS controllers to higher limits.

Acknowledgment

The authors would like to thank Fondecyt (the Chilean Research Council) for the financial support given through the Projects #105 0067 and #105 0958. The support obtained from Universidad de Concepción, Pontificia Universidad Católica de Chile, and Universidad Federico Santa María is also acknowledged.

References

1. K. Stahlkopf and M. Wilhelm, Tighter controls for busier systems, *IEEE Spectrum*, 1997, 34(4), 48–52.
2. R. Grünbaum, Å. Petersson, and B. Thorvaldsson, FACTS, improving the performance of electrical grids, *ABB Rev.*, March 2003, 11–18.
3. N. Hingorani and L. Gyugyi, *Understanding FACTS, Concepts and Technology of Flexible AC Transmission Systems*, IEEE Press, New York, 2000.
4. T. Miller, *Reactive Power Control in Electric Systems*, John Wiley & Sons, Chichester, 1982.
5. E. Wanner, R. Mathys, and M. Hausler, Compensation systems for industry, *Brown Boveri Rev.*, 1983, 70, 330–340.
6. G. Bonnard, The problems posed by electrical power supply to industrial installations, *Proc. IEE Part B*, 1985, 132, 335–340.
7. A. Hammad and B. Roesle, New roles for static VAR compensators in transmission systems, *Brown Boveri Rev.*, 1986, 73, 314–320.
8. N. Grudinin and I. Roytelman, Heading off emergencies in large electric grids, *IEEE Spectrum*, 1997, 34(4), 43–47.
9. C. Taylor, Improving grid behavior, *IEEE Spectrum*, 1999, 36(6), 40–45.
10. R. Grünbaum, M. Noroozian, and B. Thorvaldsson, FACTS—Powerful systems for flexible power transmission, *ABB Rev.*, May 1999, 4–17.
11. Canadian Electrical Association, *Static Compensators for Reactive Power Control*, Cantext Publications, Canada, 1984.
12. H. Frank and S. Ivner, Thyristor-controlled shunt compensation in power networks, *ASEA J.*, 1981, 54, 121–127.
13. H. Frank and B. Landstrom, Power factor correction with thyristor-controlled capacitors, *ASEA J.*, 1971, 45(6), 180–184.
14. J. Dixon, Y. del Valle, M. Orchard, M. Ortúzar, L. Morán, and C. Maffrand, A full compensating system for general loads, based on a combination of thyristor binary compensator, and a PWM-IGBT active power filter, *IEEE Trans. Industrial Electron.*, 2003, 50(5), 982–989.
15. S. Torseng, Shunt-connected reactors and capacitors controlled by thyristors, *IEE Proc. Part C*, 1981, 128(6), 366–373.
16. L. Gyugyi, Reactive power generation and control by thyristor circuits, *IEEE Trans. Industry Applic.*, 1979, IA-15(5), 521–532.
17. L. Gyugyi, R. Otto, and T. Putman, Principles and applications of static, thyristor-controlled shunt compensators, *IEEE Trans. PAS*, 1980, PAS-97(5), 1935–1945.
18. A. Chakravorti and A. Emanuel, A current regulated switched capacitor static volt ampere reactive compensator, *IEEE Trans. Industry Applic.*, 1994, 30(4), 986–997.
19. H. Jin, G. Goós, and L. Lopes, An efficient switched-reactor-based static var compensator, *IEEE Trans. Industry Applic.*, 1994, 30(4), 997–1005.
20. Y. Sumi, Y. Harumoto, T. Hasegawa, M. Yano, K. Ikeda, and T. Mansura, New static var control using force-commutated inverters, *IEEE Trans. PAS*, 1981, PAS-100(9), 4216–4223.

21. L. Morán, P. Ziogas, and G. Joos, Analysis and design of a synchronous solid-state VAR compensator, *IEEE Trans. Industry Applic.*, 1989, IA-25(4), 598–608.
22. J. Dixon, J. García, and L. Morán, Control system for a three-phase active power filter which simultaneously compensates power factor and unbalanced loads, *IEEE Trans. Industrial Electron.*, 1995, 42(6), 636–641.
23. J. Lai and F. Peng, Multilevel converters a new breed of power converters, *IEEE Trans. Industrial Applic.*, 1996, IA-32(3), 509–517.
24. L. Lorenz, Power Semiconductors: State of the Art and Future Developments. Keynote Speech at the International Power Electronics Conference, IPEC Niigata, 2005, Japan, April 2005, CD ROM.
25. A. Edris, FACTS technology development: an update, *IEEE Power Engng Rev.*, March 2000, 4–9.
26. S. Bhattacharya, B. Fardanesh, B. Shperling, S. Zelingher, Convertible Static Compensator: Voltage Source Converter Based FACTS Application in the New York 345 kV Transmission System, International Power Electronics Conference, IPEC 2005, April 2005. Niigata, Japan, pp. 2286–2294.
27. M. Superczynski, Analysis of the Power Conditioning System for a Superconducting Magnetic Energy Storage Unit, Master's Thesis, Virginia Polytechnic Institute and State University, August 2000.
28. Reassessment of Superconducting Magnetic Energy Storage (SMES) Transmission System Benefits, Report number 01006795, March 2002.
29. I. Ngamroo, Robust frequency stabilization by coordinated superconducting magnetic energy storage with static synchronous series compensator, *Int. J. Emerging Electric Power Systems*, 2005, 3(1), pp. 16–25.
30. C. Sepúlveda, J. Espinoza, and R. Ortega, Analysis and Design of a Linear Control Strategy for Three-phase UPQCs, Conf. Rec. IECON'04, Busan, Korea, November 3–6, 2004.
31. R. Grünbaum, Å. Petersson, and B. Thorvaldsson, FACTS improving the performance of electrical grids, ABB Review Special Report on Power Technologies, 2003, pp. 13–18.
32. J. Dixon and L. Morán, A clean four-quadrant sinusoidal power rectifier, using multistage converters for subway applications, *IEEE Trans. Industrial Electron.*, 2005, 52(3), pp. 653–661.
33. X. Wei, J. Chow, B. Fardanesh, and A. Edris, A Dispatch Strategy for an Interline Power Flow Controller Operating At Rated Capacity, PSCE 2004, 2004 IEEE/PES Power Systems Conference and Exposition, New York, October, pp. 10–13, 2004.
34. C. Luongo, Superconducting storage systems: an overview, *IEEE Trans. Magnetics*, 1996, 32(4), 2214–2223.
35. K. Sen, Recent Developments in Electric Power Transmission Technology, The Carnegie Mellon Electricity Industry Center, EPP Conference Room, April 15, 2003 (http://wpweb2.tepper.cmu.edu/ceic/SeminarPDFs/Sen_CEIC_Seminar_4_15_03.pdf).

